Combating antimicrobial resistance by targeting underexplored pathways

Dissertation

zur Erlangung des Grades
des Doktors der Naturwissenschaften
der Naturwissenschaftlich-Technischen Fakultät
der Universität des Saarlandes

von

M.Sc. Daan Willocx

Saarbrücken
2024

Tag des Kolloquiums:	11. Juni 2024
Dekan:	Prof. Dr.-Ing. Michael Vielhaber
Berichterstatter:	Professorin Dr. Anna K. H. Hirsch
	Professor Dr. Uli Kazmaier
Akad. Mitglied:	Priv.-Doz. Dr. Matthias Engel
Vorsitz:	Prof. Dr. Claus-Michael Lehr

Die vorliegende Arbeit wurde von Oktober 2020 bis April 2024 unter Anleitung von Frau Prof. Dr. Anna K. H. Hirsch in der Fachrichtung Medizinische Chemie der Naturwissenschaftlich-Technischen Fakultät der Universität des Saarlandes, sowie am Helmholtz-Institut für Pharmazeutische Forschung Saarland (HIPS) in der Abteilung Drug Design and Optimization (DDOP) angefertigt.

“Ik moet just niks”

W. van Aert.

Acknowledgments

First, I would to express my gratitude towards Prof. Dr. Anna K. H. Hirsch for providing me the opportunity to complete my PhD in her research group. Her supervision and guidance were decisive for the successful completion of this project. Additionally, I would like to commend her for establishing the MepAnti project. A groundbreaking project with the aim to tackle antimicrobial resistance by targeting the MEP pathway.

Next, I would like to express my gratitude towards Prof. Dr. Uli Kazmaier and Dr. Matthias Engel for being part of my thesis committee meetings and providing me with valuable insights during our committee meetings.

I would like to express my gratitude towards Dr. Charles Mowbray and Dr. Zhizhou Fang for being my supervisor during my internships at DND*i* and Merck KGaA, respectively.

I am deeply grateful to Dr. Eleonora Diamanti for her supervision throughout the first two years of my PhD and her continued support until this day. In this regard, I would also like to thank Dr. Mostafa Hamed for taking over supervision and providing me with great advice. This project would not have been possible without the guidance and advice of these amazing supervisors!

Next, I would like to thank everyone involved in the MepAnti project for his or her outstanding collaborations and dedication throughout my PhD journey. The productive meetings and shared efforts have truly enriched this research endeavor. A special thanks goes Victor Gawriljuk, Camilla Ornago, Lucia D'Auria, Antoine Lacour, Thibaut Quennesson, Maria Braun Cornejo, Gabriella Ines Bianchino, Bruna Schuck, Vidhisha Sonawane, Patricia Bravo, and Lorenzo Bizzarri for making this project an experience I will always cherish. I sincerely hope that our paths will cross again in the future.

I am thankful to all those who have contributed to the completion of this thesis. Many thanks to Lorenzo Bizzari, Dr. Andreas Kany and Dr. Alaa Alhayek for developing the LC-MS based IspD assay. Thank you to Dr. Jörg Haupenthal, Simone Amann, Jeannine Jung, Jannine Seelbach and Tabea Wittmann for organizing and performing biological assays. My appreciation goes to Samira Speicher and Mostafa Hamed to keep the chemistry lab running. I am deeply grateful to Angeliki Vgenopoulou for her contributions to the project as an intern.

I would like to extend my sincere gratitude to all colleagues and staff members on the second floor for their contributions to creating a welcoming and hospitable working environment. Especially Ahmed Amin, Angeliki Vgenopoulou, Antoine Lacour, Danica Walsh, Dominik Kolling, Gabriele Bianchi, Gwenaëlle Jézéquel, Hugo Scherer, Ioulia Exapicheidou, Milica Selaković, and Života Selaković, your camaraderie, support, and positive energy have made every day a pleasure. Thank you for fostering a sense of community and making our workplace a place where friendships flourish.

I want to extend my heartfelt appreciation to my flatmate, Antoine Lacour, for all the unforgettable moments we have shared together, especially during the challenges of COVID-19. From finding secondhand furniture in the streets of Saarbrücken to enjoying a cold beer after a long day, your friendship has been a source of joy and comfort. Thank you for not only being an incredible roommate but also for navigating through the ups and downs of this past year with resilience and valuable advice. Your presence has truly made this living experience memorable.

I would like to express my sincere gratitude to all my friends and family residing in Belgium for their unwavering support, flexibility, and patience throughout my time living in Germany. Your encouragement and willingness to adapt to the distance have been invaluable to me. Without your support, this journey would not have been possible. Thank you for always being there for me, no matter the distance.

Deep appreciation goes to Loran Snoeks, for her incredible patience, unwavering support, and constant presence by my side throughout this journey.

Curriculum Vitae

Education

❖ Marie Skłodowska-Curie Research Fellow (PhD student)

[14/10/2020 – **Current**]

Thesis title: Combating antimicrobial resistance by targeting underexplored pathways

Description: During the initial phase of the PhD, biophysical techniques, including surface plasmon resonance and thermal shift assay, were used to identify small molecule and fragment hits. Later, a structure-activity relationship study was conducted for the most promising hits. Publication of these results is forthcoming.

Research group**:** Drug Design and Optimisation led by Prof. Dr. Anna K. H. Hirsch at Helmholtz-Institut für Pharmazeutische Forschung Saarland, Germany

❖ Master of Chemistry

[23/09/2018 – 30/06/2020]

Thesis title: Rhodium-catalyzed transannulation of 4,5-fused 1,2,3-triazoles toward the synthesis of various *N*-heterocyclic compounds

Description: I initially optimized the reaction conditions, followed by exploration of the reaction's scope. This research was subsequently published in *The Journal of Organic Chemistry (*DOI: https://doi.org/10.1021/acs.joc.2c01456)

Research group: Laboratory of Organic Synthesis led by Prof. Dr. Wim Dehaen at KULeuven, Belgium

❖ Bachelor of Chemistry

[13/09/2015 – 30/06/2018]

UHasselt, Belgium

Research experience

❖ Internship at Merck KGaA, Germany

[01/05/2022 – 30/06/2022]

Description: Internship within the Drug Metabolism and Pharmacokinetics (DMPK) department, with a primary focus on conducting Caco-2 permeability assays. Engaged in hands-on experimentation, data collection, and analysis under the guidance of experienced researchers. Gained practical insights into the assessment of drug absorption and permeability.

Internship at Drugs for Neglected Diseases Initiative, Switzerland

[30/09/2021 – 11/11/2021]

Description: Internship focused on gaining insights into the operations of a non-profit drug research and development organization. I contributed to the establishment of a comprehensive database aimed at facilitating research efforts. Engaged in tasks such as data collection, organization, and analysis.

❖ Internship at Johnson & Johnson Innovative Medicine, Belgium

[31/01/2019 – 29/06/2019]

Description: Internship focused on gaining practical experience in the design and synthesis of pharmacologically active compounds. Engaged in hands-on activities including molecular design, synthesis, purification, and characterization of compounds. Developed proficiency in laboratory techniques and gained insights into the process of drug discovery and development

Publications

D. Willocx, E. Diamanti, A. K. H. Hirsch, IspD as an anti-infective drug target: Unveiling the History, Catalytic Mechanism, and Structural Marvels of the Enzyme; Manuscript in preparation.

Contribution see Introduction

D. Willocx, L. Bizzarri, A. Alhayek, P. Bravo, B. Illarionov, K. Rox, J. Lohse, M. Fischer, A. M. Kany, H. Hahne, M. Rottmann, M. Witschel, M. M. Hamed, E. Diamanti, A. K. H. Hirsch; Targeting Plasmodium falciparum IspD in the Methyl-D-Erythritol Phosphate Pathway: Urea-Based Compounds with Nanomolar Potency on target with low micromolar whole-cell activity; Uploaded to ChemRxiv (doi:10.26434/chemrxiv-2024-15kb) and under revision at *Journal of Medicinal Chemistry* (ACS) on 05/04/2024.

Contribution see Chapter 1

D. Willocx, F. Borel, L. D'Auria, E. Diamanti, M. M. Hamed, A. K. H. Hirsch; Discovery of fragment by X-ray crystallographic screening targeting the CTP binding site of *Pseudomonas aeruginosa* IspD; Manuscript in preparation.

Contributions see Chapter 2

D. Willocx, F. F. Lillich, E. Proschak, A. Tsarenko, D. J. Slotboom, M. M. Hamed, A. K. H. Hirsch; Oxaprozine Derivatives as Anti-Gram-Positive Agents Targeting Bacterial Energy-Coupling Factor Transporters; Manuscript in preparation.

Contributions see Chapter 3

Summary

Antimicrobial resistance (AMR) is widely considered one of the greatest threats to public health in the 21st century. To turn the tide in the fight against it, anti-infectives with unpreceded mechanisms of action are desperately needed. Within this study, we address this challenge by investigating two underexplored drug targets found across a spectrum of pathogens, including *Plasmodium falciparum*, *Pseudomonas aeruginosa*, and *Streptococcus pneumoniae*.

The first target is the third enzyme of the Methyl-*D*-Erythritol Phosphate (MEP) pathway namely, IspD. The pathway is essential in many pathogens for the biosynthesis of the universal isoprenoid precursors isopentenyl diphosphate (IDP) and dimethylallyl diphosphate (DMADP) but is absent in human cells. Our endeavors encompass a comprehensive review of existing literature on the enzyme and its inhibitors, various screenings, and optimization of identified hits.

Our second target is the energy-coupling factor (ECF) transporters, a class of transmembrane proteins essential for the uptake of various water-soluble vitamins and metal cations. These transmembrane proteins are common among Gram-positive pathogens, including *S. pneumoniae* and *Staphylococcus aureus*, but are absent in human cells. Our efforts entail a screening campaign followed by optimization of the identified hit compound.

In summary, we expanded the arsenal of inhibitors of two un(der)explored targets that could potentially play a pivotal role in combating AMR in the near future by providing access to resistance-breaking antibiotics with an unprecedented mode of action. Furthermore, with the review, we aimed to facilitate research conducted on IspD.

Zusammenfassung

Die antimikrobielle Resistenz (AMR) gilt weithin als eine der größten Bedrohungen für die öffentliche Gesundheit im 21. Jahrhundert. Um das Blatt im Kampf gegen die Resistenz zu wenden, werden Antiinfektiva mit bisher unbekannten Wirkmechanismen dringend benötigt. In dieser Studie widmen wir uns dieser Herausforderung, indem wir zwei bisher wenig erforschte Angriffspunkte für Medikamente untersuchen, die in einem breiten Spektrum von Krankheitserregern vorkommen, darunter *Plasmodium falciparum*, *Pseudomonas aeruginosa*, *Enterococcus faecalis* und *Streptococcus pneumoniae*.

Das erste Zielprotein, auf das sich diese Arbeit konzentrierte, ist das dritte Enzym des Methyl-*D*-Erythritolphosphat(MEP)-Wegs, nämlich IspD. Dieser Stoffwechselweg ist in vielen Krankheitserregern für die Biosynthese der universellen Isoprenoid-Vorstufen Isopentenyl-Diphosphat (IDP) und Dimethylallyl-Diphosphat (DMADP) unerlässlich und fehlt vor allem in menschlichen Zellen. Unsere Bemühungen umfassen eine umfassende Betrachtung der vorhandenen Literatur über das Enzym und seine Inhibitoren, verschiedene Screenings und die Optimierung der identifizierten Hits.

Unser zweites Zielprotein sind die Energy-Coupling-Factor (ECF)-Transporter, eine Klasse von Transmembranproteinen, die für die Aufnahme verschiedener wasserlöslicher Vitamine und Metallkationen wichtig sind. Diese Transmembranproteine sind in einer Untergruppe von Gram-positiven Krankheitserregern, einschließlich *Streptococcus pneumoniae* und *S. aureus*, vorhanden, fehlen aber in menschlichen Zellen. Unsere Bemühungen umfassen eine Screening_Kampagne einer hauseigenen Substanzbibliothek und die anschließende Optimierung eines der identifizierten Treffer.

Zusammenfassend lässt sich sagen, dass wir das Arsenal an Hemmstoffen für zwei un(ter)erforschteTargets erweitert haben, die in naher Zukunft eine entscheidende Rolle bei der Bekämpfung von AMR spielen könnten. Darüber hinaus wollten wir mit dem Übersichtsartikel die Forschung zu IspD erleichtern.

List of abbreviations

^{1}H-STD-NMR	^{1}H saturation–transfer difference nuclear magnetic resonance;
ABC	ATP-binding cassette
AMR	antimicrobial resistance
At	*Arabidopsis thaliana*
AUC0-t	area under the concentration-time curve from time zero to time t
BITZ	2-phenyl benzo[d]isothiazol-3(2H)-one
Bs	*Bacillus subtilis*
CDP-ME	4-diphosphocytidyl-2-*C*-methylerythritol
Cl_obs	clearance (based on observed last time point with measurable concentration)
CTP	cytidine triphosphate
CuAAC,	copper-catalyzed azide-alkyne cycloaddition
DB	domiphenbromide
DDA	data-dependent acquisition
DIA	data-independent acquisition
DCM	dichloromethane
DMADP	dimethylallyl diphosphate
DMF	*N*,*N*-dimethylformamide
DMSO	dimethyl sulfoxide
DXP	1-deoxyxylulose 5- phosphate
Ec	*Escherichia coli*
Eq	equivalents
ESI	electron spray ionization
FA	formic acid
EC_{50}	fifty percent inhibitory concentrations
ECF	energy-coupling factor
GAP	glyceraldehyde-3-phosphate
HESI	heated electrospray ionization
HTS	high-throughput screening
HPLC	high-pressure liquid chromatography
Hs	*Homo sapiens*
IC_{50}	Half-maximal inhibitory concentration
IDP	isopentenyl diphosphate
IspD	4-diphosphocytidyl-2*C*-methyl-D-erythritol synthase
IV	intravenous
K_m	Michaelis constant
Kp	*Klebsiella pneumoniae*
LCMS	liquid chromatography–mass spectrometry
MEP	2-*C*-methylerythritol-*D*-erythritol-4-phosphate
MIC	minimum inhibitory concentration
MOA	mode of action
MOI	mode of inhibition
MRT	mean residence time
Ms	*Mycobacterium smegmatis*
Mt	*Mycobacterium tuberculosis*
MVA	mevalonate pathway
MWD	multiple wave detector
n.a.	no activity
NBS	*N*-bromosuccinimide
ND	not detected
NMR	nuclear magnetic resonance
Pa	*Pseudomonas aeruginosa*
Pf	*Plasmodium falciparum*
PPi	inorganic diphosphate
PK	pharmacokinetic

Pv	*Plasmodium vivax*
SAR	structure–activity relationship
SD	standard deviation
Vz_obs	volume of distribution associated with the terminal phase

Table of contents

1. Introduction

1.1 Introduction: IspD as an Anti-infective Drug Target: Unveiling the History, Catalytic Mechanism, and Structural Marvels of the Enzyme.

Daan Willocx, Eleonora Diamanti, Anna K. H. Hirsch

Contributions: Eleonora Diamanti and Anna K. H. Hirsch defined, supervised and edited the project. Daan Willocx wrote the manuscript.

All authors have given approval to the final version of the manuscript.

This chapter will be submitted to the *Journal of Medicinal Chemistry* (ACS) without or with minor modifications.

IspD as an Anti-infective Drug Target: Unveiling the History, Catalytic Mechanism, and Structural Marvels of the Enzyme

Daan Willocx[†,¶], Eleonora Diamanti[†], Anna K. H. Hirsch[*,†,‡,¶]

[†]Helmholtz Institute for Pharmaceutical Research (HIPS) – Helmholtz Centre for Infection Research (HZI), Saar-land University, Campus E8.1, 66123 Saarbrücken, Germany

[‡]Helmholtz International Lab for Anti-Infectives, Saarland University, Campus E8.1, 66123 Saarbrücken, Germany

[¶] Saarland University, Department of Pharmacy, Campus E8.1, 66123 Saarbrücken, Germany

ABSTRACT: Antimicrobial resistance (AMR) and herbicide resistance pose urgent threats to society, necessitating novel anti-infectives and herbicides exploiting untapped modes of action like inhibition of IspD, the third enzyme in the MEP pathway. The MEP-pathway is essential for a wide variety of human pathogens, including *Pseudomonas aeruginosa*, *Mycobacterium tuberculosis*, and *Plasmodium falciparum,* as well as plants. Within the current perspective, we focused our attention on the third enzyme in this pathway, IspD, offering a comprehensive summary of the reported modes of inhibition and common trends with the goal to inspire future research dedicated to this underexplored target. In addition, we included an overview of the history, catalytic mechanism and structure of the enzyme to facilitate access to this attractive target.

Both herbicides and anti-infectives are indispensable pillars of modern civilization based on their revolutionary impact. While anti-infectives allow safe and effective treatment of infectious diseases, herbicides made harvests more reliable and enhanced crop yields, of particular importance in light of a growing population.[1,2] Despite their accomplishments, both are prone to resistance development, which has become increasingly problematic in recent years. For example, in 2019 alone, an estimated 4.95 million deaths were attributed to antimicrobial resistance.[3] Hence, new anti-infectives and herbicides with new modes of action (MOA) are urgently needed.[4] In this regard, the 2-*C*-methylerythritol-D-erythritol-4-phosphate (MEP) pathway is a rich source of attractive targets (Scheme 1). The pathway ensures the biosynthesis of the essential isoprenoid precursors isopentenyl diphosphate (IDP) and dimethylallyl diphosphate (DMAPP) and is constituted by seven enzymes.[5] Previous works demonstrated the dependency of plants and many human pathogens on the MEP pathway, including *Mycobacterium tuberculosis* (*Mt*), *Plasmodium* parasites, and *Pseudomonas aeruginosa* (*Pa*) (Table 1).[6-10] Importantly, the pathway is absent in human cells, reducing the risk of off-target-based side effects.[11-14] We have previously analyzed the druggability of the MEP enzymes *in silico* by utilizing DoGSiteScorer, a web-based tool designed to identify and characterize potential binding pockets and subpockets.[11,15] The evaluation supports the potential druggability of all substrate- and cofactor-binding pockets of the MEP pathway enzymes. Targeting these active sites is, however, challenging as most are highly polar as a consequence of the hydrophilic phosphorylated intermediates. Nonetheless, most enzymes feature allosteric pockets with a more favorable hydrophobic character. For example, targeting the allosteric pocket in *Arabidopsis thaliana* IspD (*At*IspD) led to a new class of inhibitors with nanomolar activity.[14] In this perspective, we will focus on the third enzyme in the MEP pathway, namely 4-diphosphocytidyl-2*C*-methyl-D-erythritol synthase (IspD). The enzyme is encoded on the *ygbp* gene and catalyzes the conversion of MEP and CTP towards 4-diphosphocytidyl-2*C*-methyl-D-erythritol (CDP-ME) and diphosphate.[16] Regardless of the wide-spread occurrence of the MEP pathway, only a handful of IspD homologues have confirmed to be inhibited by small-molecule inhibitors, again highlighting the underexplored nature of this attractive target. In the following, the discovery, mechanism and structure of IspD are discussed as well as all known inhibitors and their binding mode. We aim to provide a deeper understanding about the target in general and inspiration for the design of future generations of inhibitors.

Discovery of the MEP pathway. The isoprenoids are one of the largest classes of natural products comprising over 50,000 structurally diverse members. All of them share IDP and DMAPP as common precursors, which are linked

Table 1. Prevalence of the MEP pathway.

Gram-positive	Gram-negative
Nocardia terpenica	*Chlamydia pneumoniae*
Bacillus anthracis	*Pseudomonas aeruginosa*
Clostridium difficile	*Klebsiella pneumoniae*
Listeria monocytogenes	*Haemophilus influenzae*
Bacillus subtilis	*Vibrio cholerae*

Scheme 1. Overview of the MEP pathway.

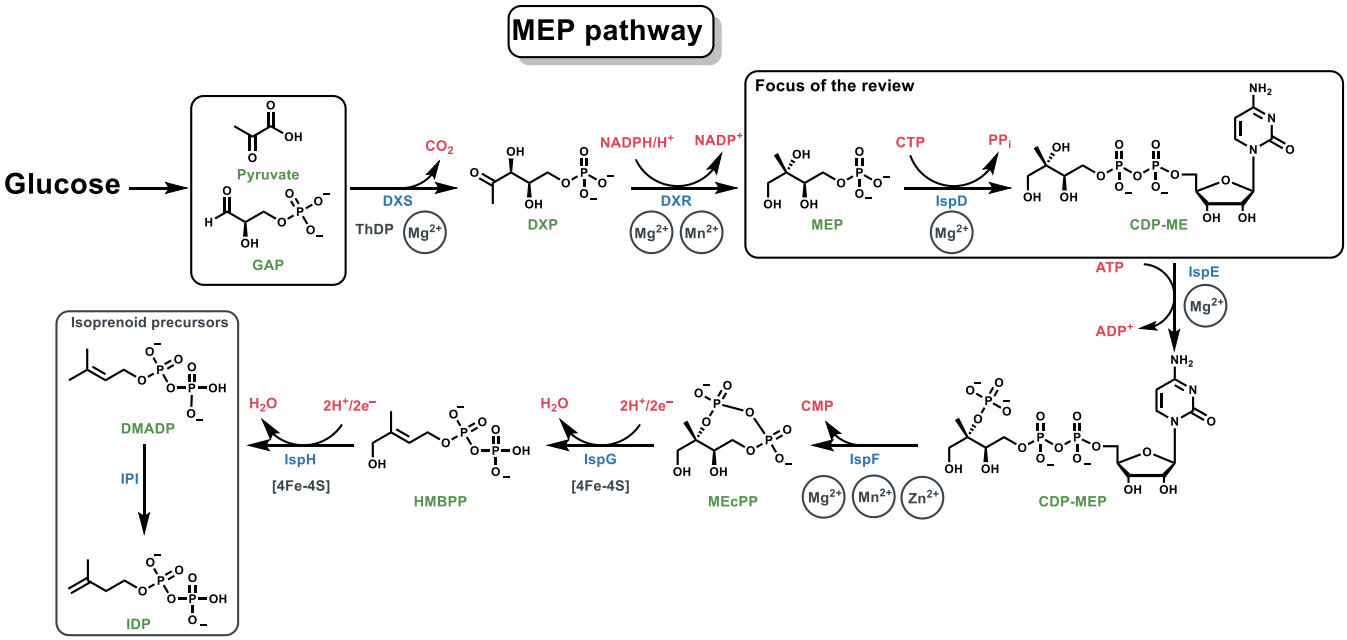

together *via* condensation reactions. Functionalization of the linked precursors with moieties such as alcohols, aldehydes, and esters, leads to great diversity within this class of biomolecules.[17, 18] Until the mid-1990's, there was a consensus among scientists that the mevalonate pathway (MVA) was the only biosynthetic pathway for organisms to produce DMAPP and IDP. Conflicting results in ^{13}C-labeling experiments concerning isoprenoids biosynthesis however, hinted at the existence of an additional pathway. The MEP pathway was later independently discovered by the research groups of Rohmer and Arigoni.[13,19] By using ^{13}C-labeled glucose in isotopic feeding experiments, two alternative starting molecules could be identified, namely, glyceraldehyde-3-phosphate (GAP) and pyruvate.[20] The assignment of pyruvate and GAP as precursors led to the identification of the first intermediate in the new pathway, the unbranched 1-deoxyxylulose 5- phosphate (DXP). Only three years after the initial discovery, the third enzyme in this cascade was uncovered by Kuzuyama *et al.*[21] At that point in time, only the first two enzymes, DXS and DXR, and their substrates DXP and MEP were known. The other enzymes were discovered by the same group using *Escherichia coli* (*Ec*) transformants. Their experiments led to the identification of an enzyme exhibiting the ability of transforming MEP in the presence of CTP, towards an unknown product. After characterization, the product could be identified as CDP-ME.[21] Shortly after the discovery of *Ec*IspD, Rohdich F. *et al.* isolated the first plant-based IspD from *A. thaliana*.[22] In the years following, the whole pathway was characterized, leading to the discovery of in total seven enzymes that catalyze what is now known as the MEP pathway of isoprenoid precursor biosynthesis.

Target validation of the enzymes of the MEP pathway. The MEP pathway enzymes have been thoroughly studied during the years after their discovery. It became clear that disruptions in the MEP pathway enzymes resulted in lethality for various organisms, including *Escherichia coli* (*Ec*) and *M. tuberculosis*.[6, 23, 24] The MEP pathway and its products were also found to be essential during the whole life cycle of *Plasmodium* parasites. Interestingly, within these parasites, the pathway takes place in the apicoplast, a non-photosynthetic plastid-like organelle of prokaryotic origin, instead of the cytosol. [25-29] Although plants use the MVA and MEP pathway simultaneously, both turned out to be essential for their survival. Each of them take place in different compartments, with the MVA pathway happening in the cytosol and the MEP pathway in the plastids. Even though both pathways afford identical isoprenoid precursors, these in turn lead to structurally divers isoprenoids. For example, the MEP pathway isoprenoid precursors are used for the production of chlorophyll and carotenoids, while most sterols originated from MVA-derived precursors.[17] The combination of all these discoveries highlight the unique therapeutic and herbicidal features of targeting the MEP pathway

The catalytic mechanism of IspD. Two theoretical mechanisms for cytidyl transferases have been proposed. The first starts with the formation of a highly reactive metaphosphate intermediate at the α-phosphate from CTP. Next, the intermediate undergoes a nucleophilic attack from the 4-phosphate from MEP directed at the α-phosphate of CTP affording CDP-ME and releasing diphosphate (Scheme 2). The second mechanism starts with the nucleophilic attack of the 4-phosphate of MEP onto the α-phosphate of CTP, resulting in an unstable

Scheme 2. Representation of the proposed reaction mechanisms catalyzed by IspD leading to the formation of 4-diphosphocytidyl-2*C*-methyl-D-erythritol (CDP-ME).

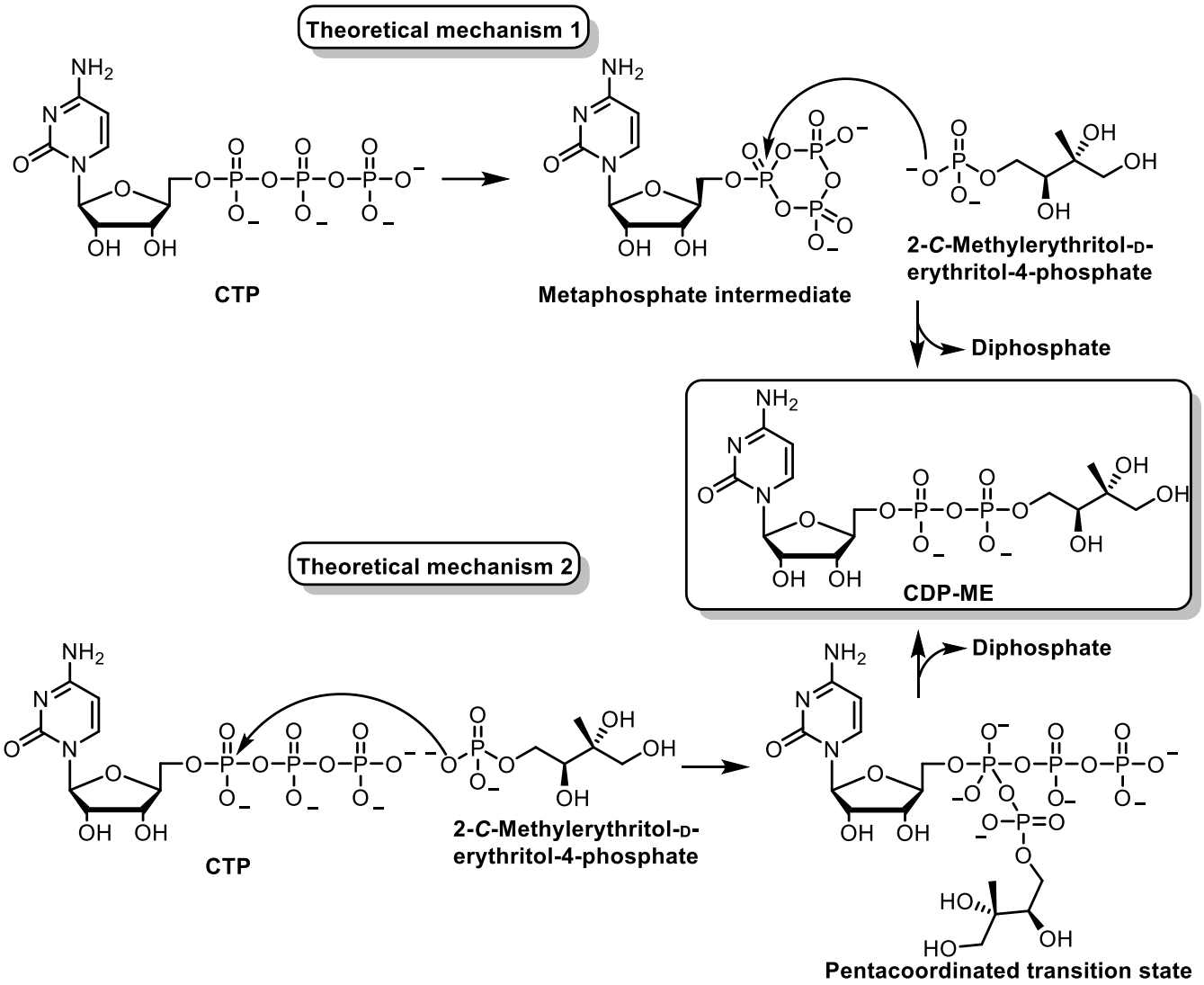

pentacoordinated negatively charged transition state, which subsequently collapses in CDP-ME with the release of diphosphate (Scheme 2). Experimental data has yet to be acquired to unambiguously confirm the correct mechanism. Neverteless, current crystallographic data on *apo*-IspD and the IspD–CTP complexes suggest that the protein surface rearranges upon CTP binding meaning that there are plenty positively charged amino acid side chains present that stabilize the pentavalent transition stage besides the metal. Furthermore, the α-phosphate of CTP is displaced to be in the proximity of MEP to undergo nucleophilic attack, favoring the second reaction mechanism.[30] Further studies to unravel the sequence of the mechanism were performed by pulse-chase experiments by Richard *et al*. In these experiments, when ^{14}C-labeled CTP was used, the ratio overwhelmingly shifted toward radiolabeled CDP-ME, on the other hand, when ^{14}C-labeled MEP was used, this amplification was not observed. Both observations point towards a sequential mechanism in which CTP must bind to the enzyme before MEP. Observations pointing in the same direction were found by Seemann and coworkers after performing bisubstrate kinetic analysis, finding the dissociation constant of MEP from the IspD-CTP complex to be 20 μM, which is 13 times lower than the dissociation constant for the MEP–IspD complex (265 μM).[31] Further investigations towards the catalytic mechanism uncovered a clear preference for CTP as nucleotide 5-triphosphate. Other nucleotide 5-triphosphates such as adenosine triphosphate, guanosine triphosphate, and uridine triphosphate, exhibited either significantly reduced turnover or no turnover at all. The selectivity is attributed to the compact pocket in which the nucleotide base resides during the catalytic action. As co-factor, the divalent Mg^{2+} cation yields the highest activity although the use of Mn^{2+} and Co^{2+} also led to formation of CDP-ME. Conversely, the use of other divalent cations such as, Cu^{2+}, Ni^{2+}, Ca^{2+}, Fe^{2+}, or Zn^{2+}, rendered IspD inactive.[32] Michaelis constants (K_m)

for both MEP and CTP of several IspD homologues demonstrate similar values for all homologues, with the only inconsistency being the K_m value for MEP of *At*IspD (Table 2).

Table 2. Overview of Michaelis constants (K_m) of several IspD homologues.

Homologue	K_m [CTP] (μM)	K_m [MEP] (μM)
*Pf*IspD[a]	59 ± 4	61
*Pv*IspD[b]	110 ± 6	/
*Mt*IspD[c]	126 ± 18	92 ± 8
*Ec*IspD[d]	84 ± 9	40 ± 7
*At*IspD[e]	114	500
*Bs*IspD[f]	133 ± 29	125 ± 19

[a]*Plasmodium falciparum* IspD[33,34]; [b]*P. vivax* IspD[33]; [c]*Mycobacterium tuberculosis* IspD[35]; [d]*Escherichia coli* IspD[31]; [e] *Arabidopsis thaliana* IspD[22]; [f]*Bacillus subtilis* IspD[36].

The Overall Structure of IspD. The structure of IspD consists of a homodimer, of which, each monomer comprises two structurally different subdomains. The first and largest of these subdomains features an alternating pattern of beta strands and alpha helical segments resembling a Rossmann-like fold with a unique connectivity pattern between both secondary protein structures (Figure 2, green). The Rossmann fold is a tertiary protein structure commonly found in proteins binding nucleotides.[37] The second, and smaller subdomain, resembles a so-called β-arm, which has a hook-like structure (Figure 2, blue). The subdomain acts as an attachment point to connect both dimers; furthermore, it also plays a significant role in the enzymatic activity as it contains the MEP binding site.[30] Sequence-based comparison between several pathogenic bacterial species including *Salmonella typhi*, *Vibrio cholera*, *Haemophilus infuenzae*, *P. aeruginosa*, and *M. tuberculosis*, revealed a high conservation of the overall structure.[38] Even when monomer structures of *Ec*IspD are compared with its plant-based homologue from *A. thaliana*, significant similarity was observed. However, in this example, care has to be taken as the same comparison between homodimers displays significant differences.[7] Furthermore, there is more than one case where the general structure of IspD differs making drug discovery programs even more challenging. For example, *P. falciparum* IspD (*Pf*IspD) contains over three times more amino acids than its *E. coli* homologue. The structure of *Pf*IspD has not been elucidated to date, however, some homology models have been constructed using *Ec*IspD as template.[39-41] Another exception of the general structure is the occasionally observed IspDF in which, IspD and IspF are covalently linked to one other.[42] The enzyme cluster catalyzes two non-consecutive steps within the MEP pathway, which is rarely observed for bifunctional proteins and has comparable activity with its monofunctional counterpart.[43] Comparison of the active site of crystalized *Campylobacter jejuni* IspDF with *Ec*IspD demonstrated remarkable similarity between both.[44]

Active-site structure. Valuable insights about the amino acids constituting the active site were obtained from

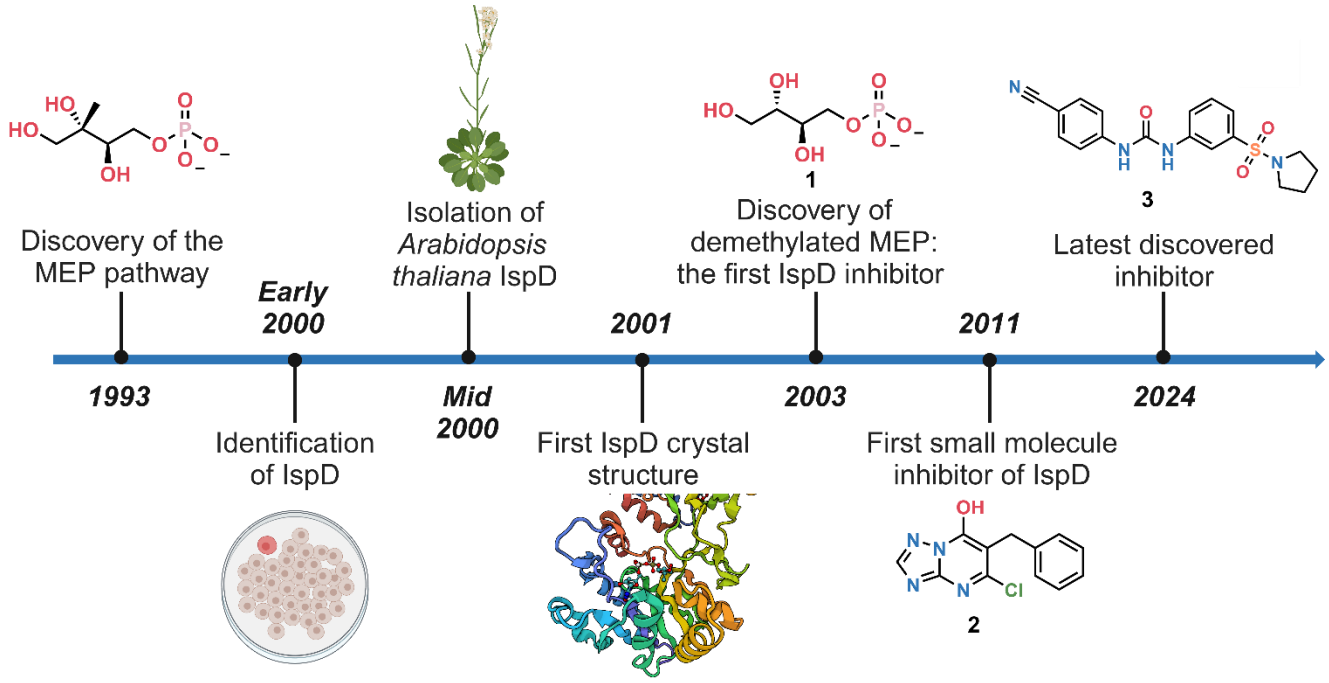

Figure 1. IspD research from initial discovery to different homologues, mechanism and inhibitors. **1**[54], **2** [14], **3**[71]

co-crystal structures of *Ec*IspD in complex with both CTP and CDP-ME (PDB accession codes IDs 1I52 and 1INI respectively).[30] When bound to the protein, the negatively charged phosphates of CTP are stabilized by coordination with the Mg^{2+} ion. Both α and γ-phosphates form a hydrogen bonding network with Arg-20. Furthermore, the α-phosphate is in direct contact with Lys-27. These interactions play a key role in the mechanism as they both prime CTP for nucleophilic attack by MEP and stabilize the postulated pentacoordinate transition state (Figure 3, middle). These residues were found to be highly conserved in serval pathogenic bacterial species including *S. typhi*, *V. cholera*, *H. infuenzae*, *P. aeruginosa,* and *M. tuberculosis*, emphasizing their importance. On the other hand, one of the hydroxy groups of the ribose forms hydrogen bonds with the backbone carbonyl of Pro-13 and backbone amide Ala-107, while the other hydroxyl forms a hydrogen bond with the backbone amide of Gly-16. Lastly, the cytidine is positioned in a tight pocked formed by hydrogen bonds between Ala-14, Ala-15, Gly-82, Asp-83, and Ser-88 (Figure 3, top). The size of the pocket sterically constrains the use of larger nucleotide bases hence, explaining the clear preference for CTP over all other nucleotide-5-triphospates. Interestingly, most interactions formed between CTP and the protein diminish when CDP-ME is formed, facilitating the release of the product (Figure 3). The interactions formed between MEP and the protein are more difficult to trace, as no co-crystal structure of IspD in complex with MEP has been solved to date. An explanation for this could be the proposed sequential mechanism by which CTP should bind to IspD before MEP could bind. Based on the co-crystal structure of IspD in complex with CDP-ME, MEP seems to form hydrogen bonds with Arg-157 and Lys-213 (Figure 3, bottom).[30] All these highly polar interactions make the IspD active site the most polar among all MEP pathway enzymes. Later reported crystal structures of *At*IspD (PDB accession code 1W77)[7] *M. tuberculosis* IspD (*Mt*IspD) (PDB accession code 2XWN)[42], *M. smegmatis* IspD (*Ms*IspD) (PDB accession code 2XWM)[42], and *B. subtilis* IspD (BsIspD) (PDB accession code *apo* structure 5DDT, CTP-Mg^{2+} complex 5HS2)[36] demonstrated highly similar active sites.[7] As with the general structure, sequence comparison between various pathogenic bacteria demonstrated great conservation of the amino acids lining the active site of IspD, even for *Pf*IspD.[30,42]

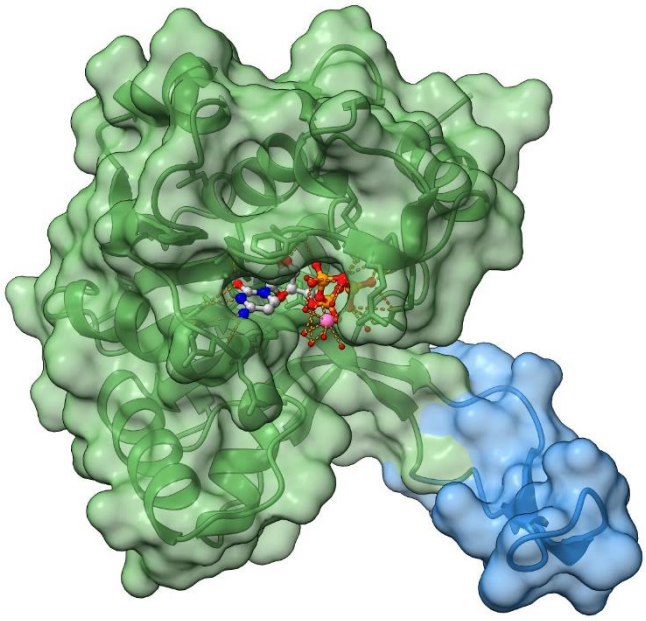

Figure 2. Crystal structure of *Ec*IpsD with CTP in the active site (PDB accession code 1I52). Visual representation of the two subunits. Green: larger subunit (residues 1–136 and 160–236); Blue: smaller subunit (residues 137–159).

Allosteric pocket. Besides the active site, IspD is also believed to have a targetable allosteric pocket in close proximity of the active site. This pocket is rather flexible, not visible in the *apo*-protein, and it only opens upon binding of an inhibitor. Looking at the allosteric pocket in *At*IspD, we can see that it is much less hydrophilic, making it a more appealing for future drug development. At this point in time, only inhibitors for *At*IspD have been confirmed targeting this pocket, but it is assumed that it is also present in most other IspD homologues. [12, 14, 45, 46]

Human IspD. Despite the absence of the MEP pathway in humans, recent research suggests that the human homologue of IspD (*Hs*IspD) is an essential enzyme for dystroglycan *O*-mannosylation. Defects or deficiency in dystroglycan *O*-mannosylation lead to muscular dystrophy, severe brain abnormalities, and in some cases to the Walker–Warburg syndrome.[47,48] Analysis of the crystal structure of *Hs*IspD demonstrated strong similarity with the active site of *Ec*IspD, and in extension the whole larger subdomain. Significantly less conservation is observed for the small subdomain, especially the sequential motifs are completely different. At this point in time, it is unclear if the enzymatic reaction of *Hs*IspD takes place in the active site or if there is a newly formed active site on the smaller subdomain.[49]

Strategies to identify IspD inhibitors. Three distinct methodologies have been employed to investigate potential IspD inhibitors. The most commonly used method employs the use of an enzymatic assay to test large compound libraries on their ability to inhibit a certain homolog of IspD.[40,50, 51] The main advantage of this method is the ability to screen large libraries of both small molecules and fragments quickly and straightforward. Disadvantages include, potential side targets and/or poor penetration once hits discovered this way are moved to a whole-cell assay.

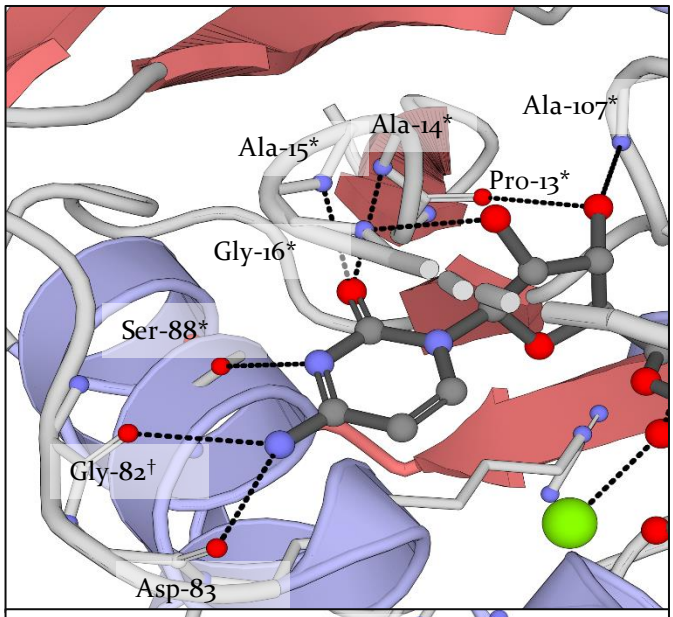
Ala-107*
Ala-14*
Ala-15*
Pro-13*
Gly-16*
Ser-88*
Gly-82†
Asp-83

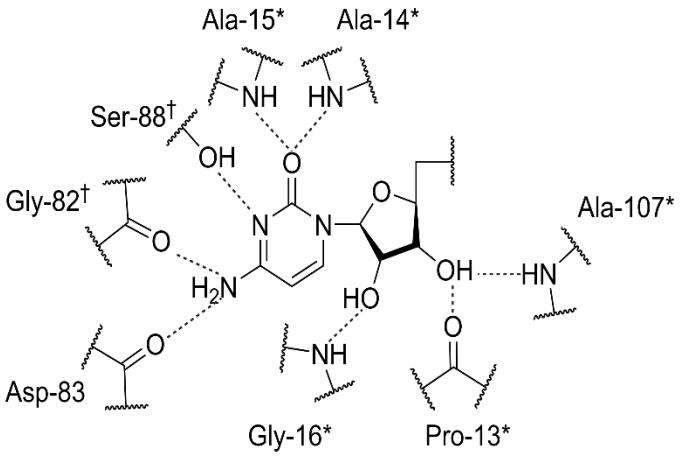
Ala-15*
Ala-14*
Ser-88†
Gly-82†
Ala-107*
Asp-83
Gly-16*
Pro-13*

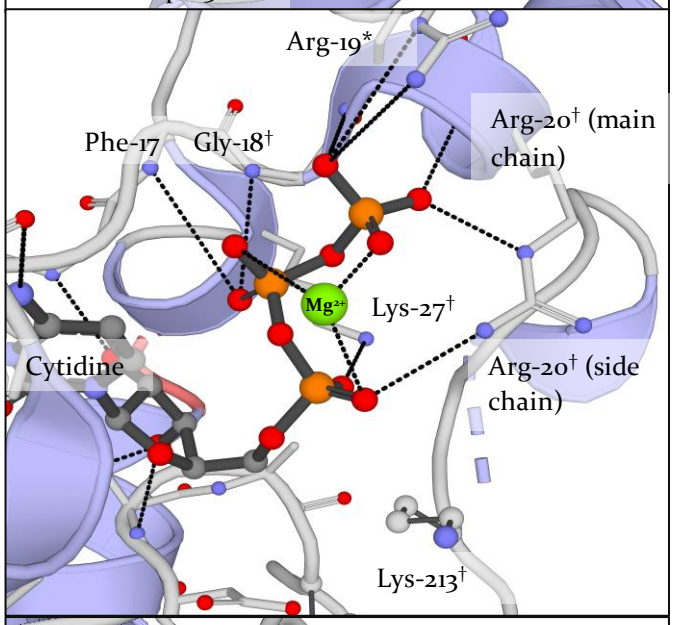
Arg-19*
Arg-20† (main chain)
Phe-17
Gly-18†
Mg2+
Lys-27†
Cytidine
Arg-20† (side chain)
Lys-213†

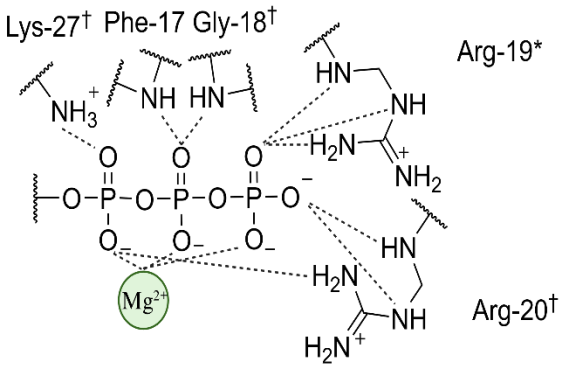
Lys-27† Phe-17 Gly-18†
Arg-19*
Mg2+
Arg-20†

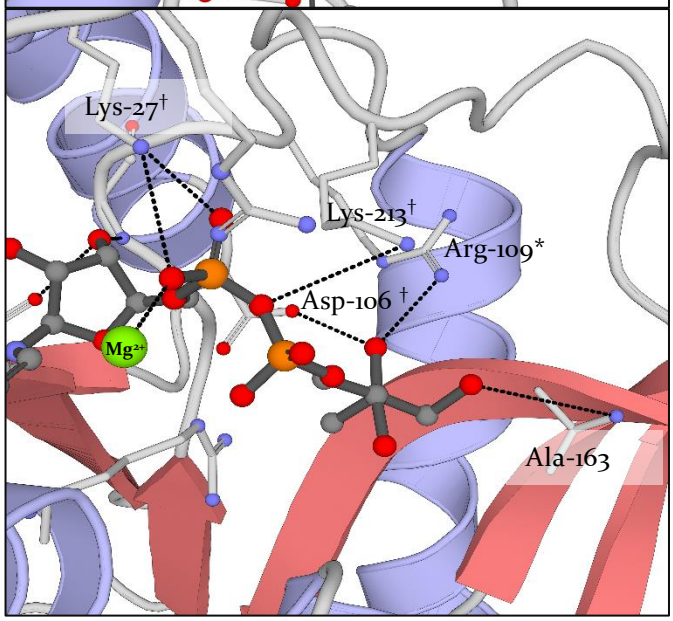
Lys-27†
Lys-213†
Arg-109*
Asp-106 †
Mg2+
Ala-163

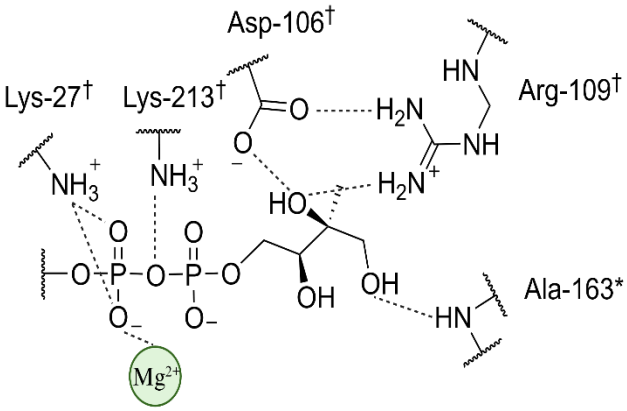
Asp-106†
Lys-27†
Lys-213†
Arg-109†
Ala-163*
Mg2+

Figure 3. Co-crystal structure of cytidine and CDP-ME in the active site of *Escherichia coli* IspD (PDB accession code 1INI and 1I52); Highly conserved residues (*); Strictly conserved (†); Top: overview of the interactions of the cytidine present in both crystal structures; middle: summary of the interactions of the triphosphate tail of CTP; bottom: Interactions of the phosphate and MEP part of CDP-ME. Highly conserved residues (*): Pro-13, Ala-14, Ala-15, Gly-16, Arg-19, Ser-88, Ala-107, Ala-163.Strictly conserved residues (†):Gly-18, Arg-20, Lys-27, Gly-82, Asp-106, Arg-109, Thr-140, Arg-157,Thr-165, Lys-213. Not conserved residues: Phe-17, Asp-83.

In the second method, a rescue assay is employed. In this experimental setup, the target organism is cultivated in two distinct media. Both of these media contain the potential inhibitor being tested, however, one of the media also includes IDP. If the potential inhibitor specifically targets the MEP pathway, the expectation is that growth inhibition will occur in the medium that lacks IDP. In contrast, in the medium that is supplemented with IDP, growth inhibition should be either absent or only partial.[52] Screenings performed this way lead to inhibitors selective for the MEP pathway that are able to penetrate and reach the target. Despite the clear advantage in selectivity for MEP pathway enzymes, these screenings are work-intensive and require the cultivation of potentially dangerous pathogens. In addition, further research is needed to pin point the targeted enzyme within the MEP pathway.

Lastly, modification of one of the substrates can also yield potential inhibitors. This technique is mostly limited to MEP due to the wide spread occurrence of CTP.[53] Unfortunately, MEP mimics have an elaborate synthesis due to their high polarity, phosphate group, and the many chiral centers.[31, 54-56]

Table 3. Assessment of 5 against various resistant *Plasmodium falciparum* strains.

***Plasmodium falciparum* strain**	**Whole-cell growth inhibition EC_{50} (μM)**
3D7 (control)	0.9 ± 0.1
D6 (mefloquine-resistant)	0.8 ± 0.1
7G8 (chloroquine-resistant)	1.0 ± 0.3
IPC 5202 (artemisinin-resistant	1.4 ± 0.2

Ideally a combination of the first two techniques is used in succession to benefit from the swiftness of the enzymatic assay at first and later the selectivity of the rescue assay can help to determine the most ideal hit to further optimize. To further facilitate this process, one can always use virtual techniques to preliminary filter compound libraries to select the most interesting compounds to screen.[57] Molecular docking studies can also be used to have some preliminary filtering of compound libraries.

IspD inhibitors. Based on the crystal structures just described, it is clear that IspD constitutes a rather challenging target due to the high polarity, solvent-exposure and flexibility of the protein. Nevertheless, many groups focused on the discovery of selective IspD inhibitors over the years because it is an attractive target to combat AMR. Nonetheless, there is still a lack of IspD inhibitors that efficiently target the various homologues and feature good whole-cell activity as well as pharmacokinetic properties. Fortunately, the reported IspD inhibitors display a wide range of modes of inhibition, which will inspire the design of future inhibitors. We will present the inhibitors categorized based on their mode of inhibition.

Competitive inhibitors. Competitive inhibitors for both substrates are known. While CTP-competitive

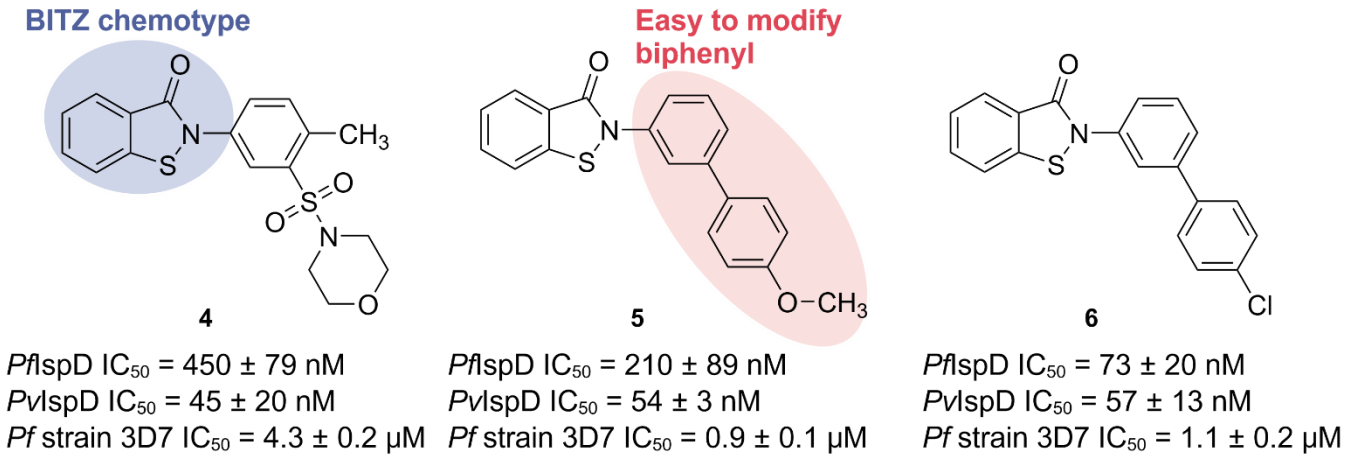

Figure 4. Overview of BITZ compounds and their IC_{50} values against *Plasmodium falciparum* (*Pf*) and *P. vivax* IspD, and growth inhibition against the *Pf* strain 3D7.;

Scheme 3. Presumed covalent mechanism of BITZ.

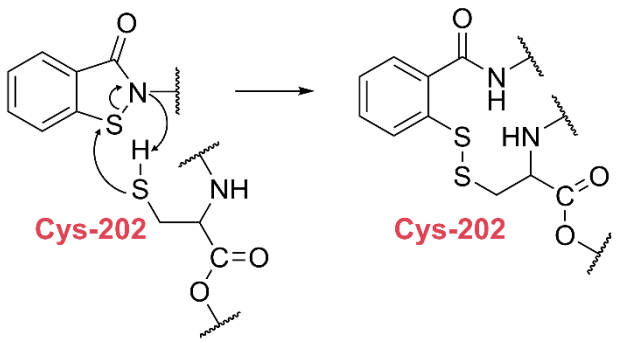

inhibitors are drug-like small molecules, MEP-competitive inhibitors mimic the substrate. Interestingly, these mimics undergo the catalytic reaction, yielding the corresponding derivative of CDP-ME which, in most cases, led to inhibition of downstream enzymes or afforded nonfunctional versions of IDP and DMAPP.

BITZ chemical class. By a combined approach of cheminformatics and high-throughput enzymatic screening, Hale and coworkers, discovered a sub micromolar *Pf*IspD inhibitor starting from a commercial compound library of 500,000 compounds (BioFocus DPI).[57] During the workflow, similarity searches and scaffold-hopping were used to isolate interesting compounds from the library, resulting in a selection of around 10,000 compounds that were experimentally screened against *Pf*IspD. During this screen, the 2-phenyl benzo[*d*]isothiazol-3(2*H*)-one (BITZ) chemotype was repeatedly noticed. Initial hit **4**, exhibited an IC_{50} value of 450 ± 79 nM on *Pf*IspD and 45 ± 20 nM on *P. vivax* (*Pv*) IspD (Figure 4). Additionally, **4** also demonstrated low micromolar activity (Strain 3D7 EC_{50} = 4.3 ± 0.2 µM) in a whole-cell assay. A follow-up SAR was performed around the BITZ chemotype. As first step in the SAR, the sulfonyl-morpholine was replaced by a biphenyl group allowing for easier modification on both rings (Figure 4). Optimization led to compound **6,** for which they managed to enhance potency against *Pf*IspD (IC_{50} = 73 ± 20 nM) while retaining low nanomolar activity on *Pv*IspD. As a result, the two homologues likely feature a similar binding pocket. Besides good enzymatic activity, BITZ compounds also exhibit growth inhibition against the 3D7 strain of *P.falciparum* with EC_{50} values ranging from low micromolar to high nanomolar (Figure 4). Furthermore, when **5** was tested against several *P. falciparum* strains resistant to the most commonly used malaria treatments, similar results were obtained (Table 3).To verify that the growth inhibition is a result of tackling the MEP pathway, and in particular IspD, early ring-stage cultures of *P. falciparum* were treated with **5** at five times the IC_{50} value. Metabolic profiling of these cultures revealed a significant decrease in downstream MEP metabolites and normal

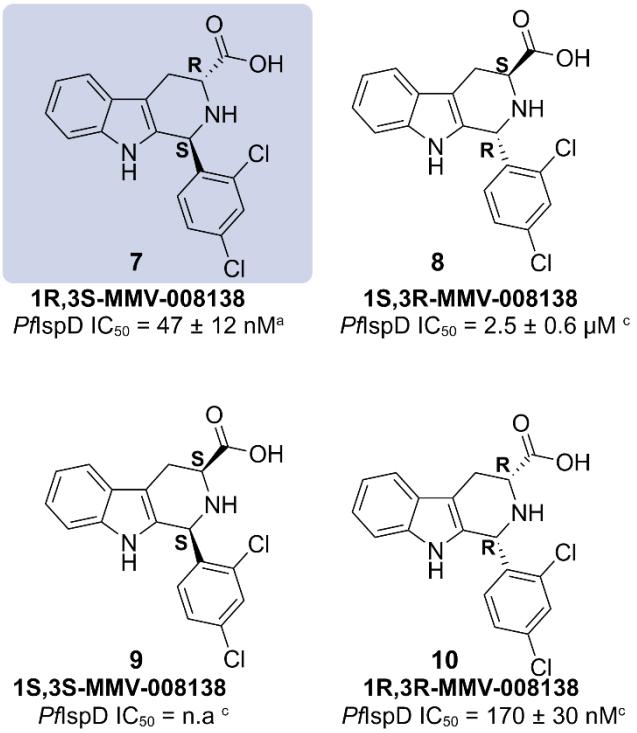

Figure 5. Overview of the enantiomers of **MMV-008138** and their IC_{50}'s against *Plasmodium falciparum* (*Pf*) IspD; a[33]; b[51]; c [34].

levels of upstream metabolites, hence validating IspD as a target. Despite these encouraging results, it became apparent that IspD was not the only target as IDP supplementation during rescue experiments did not lead to survival of the parasite. To elucidate the binding mode of this compound class, a homology model was constructed based on a previously published *Ec*IspD crystal structure (PDB accession code 1I52)[30]. Docking of compound **5** into the homology model afforded the best result when **5** was present inside the CTP binding site. In this pose, the isothiazolidin-3-one moiety was observed to be in close proximity of Cys-202. This observation led to the proposal that BITZ operates through a covalent mechanism wherein the thiol of Cys-202 reacts with the sulfur atom in the isothiazolidin-3-one moiety leading to ring opening and affording a disulfide bond between IspD and BITZ (Scheme 3). To confirm their proposal, both time- and dose-dependent inhibition kinetics were studied. Results from both experiments pointed towards a covalent inhibition mechanism. To further corroborate this hypothesis, a mutant was constructed, wherein Cys-202 was replaced by an alanine. This replacement led to a six-fold decrease in sensitivity of **5** (*Pf*IspD-[Cys202Ala] IC_{50} = 470 ± 39 nM *vs* *Pf*IspD IC_{50} = 210 ± 89 nM). Lastly, the BITZ compounds proven inactive against *Ec*IspD, in which Cys-202 is not conserved.

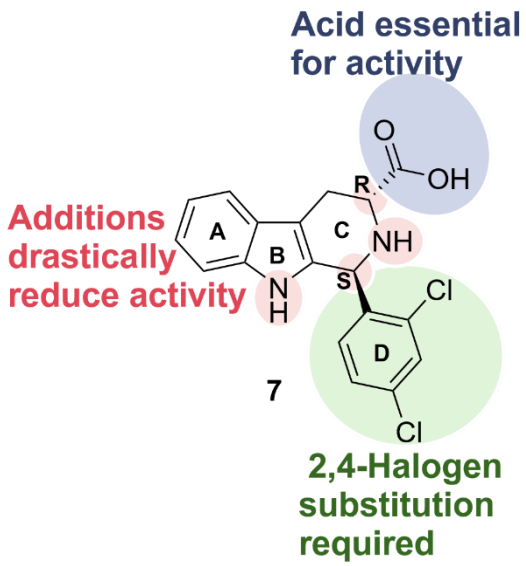

Figure 6. Overview of the structural features key for the activity of the **MMV-008138** chemotype.

MMV-08138. By far the most explored IspD inhibitor to date is **MMV-08138**, which was identified through a phenotypic IDP rescue screening of the malaria box compounds (Figure 5). Screening was conducted in this way to ensure hit selectivity for the MEP pathway enzymes. **MMV-08138** proved to be capable of inhibiting 95% of growth at 5 µM when IDP was absent from the medium, on the contrary, IDP supplementation compromised the majority of the growth inhibition.[52] During screening efforts, the racemic mixture was used and only after enantiomeric separation, the activity could be attributed to the 1*R*,3*S* conformer (**7**) (*Pf*IspD IC_{50} = 47 ± 12 nM, Figure 5). Interestingly, the other conformers were either significantly less or even inactive. On account of the phenotypic character of the screening, the targeted enzyme within the MEP pathway had to be elucidated before optimization could commence. To do so, the authors generated **MMV-08138**-resistant strains by exposing susceptible parasites to the inhibitor until a resistant strain emerged. This experiment was repeated three times, once with the racemic mixture of **MMV-08138** at lethal dose, once with the 1*R*,3*S* conformer (**7**) at IC_{75} concentration and lastly the resistant strain grown at IC_{75} concentration was exposed to a lethal dose. Next, the whole genome of the three resistant strains was sequenced and compared to the parent and reference strains. This comparison gave rise to the discovery of a mutation in the gene encoding for IspD for all three resistant strains. Two unique mutations were identified; the first being an exchange from glutamate to glutamine at position 688 [Glu688Gln]; the second a conversion of a leucine to isoleucine at position 244 [Leu244Ile].[34] To fully confirm that these modifications were responsible for the resistance towards **7**, both IspD variants were expressed

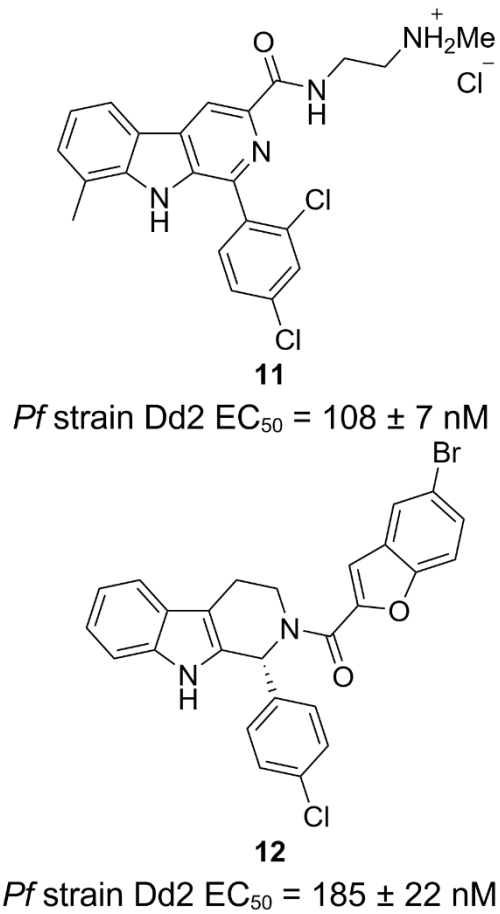

Figure 7. New chemical classes derived from the **MMV-008138** chemotype demonstrating promising growth inhibition of *Plasmodium falciparum* (*Pf*) strain Dd2; **11**[52]; **12**[53].

and purified. Activity determination of **7** against the purified enzymes led to IC_{50} values of 100 ± 24 nM for *Pf*IspD-[Glu688Gln] and 320 ± 165 nM for *Pf*IspD-[Leu244Ile], compared to an IC_{50} value of 47 ± 12 nM for wild-type IspD. Additional metabolic profiling of *P. falciparum* parasites, treated with **7** displayed significantly reduced levels of downstream MEP pathway metabolites in comparison with control parasites and parasites treated with chloroquine or artemisinin.[33] Both findings consolidate inhibition of IspD as mode of inhibition (MOI). With the target known, the binding mode could be elucidated by determining enzymatic kinetics at varying substrate and inhibitor concentrations. Analysis pointed in the direction of noncompetitive and competitive inhibition towards MEP and CTP, respectively. This finding suggests that **7** binds within the CTP binding pocket. To get an idea of which interactions might play a role, **7** was docked into the active side of a homology model based on the *Ec*IspD structure (PDB accession code 1I52). The prediction showed that an array of four hydrogen bonds between the carboxylic acid and Thr-664, Arg-208,

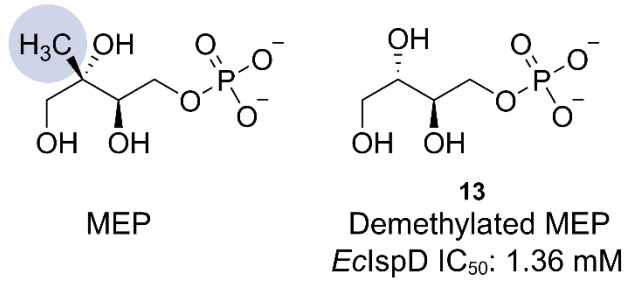

Figure 8. 2-*C*-Methyl-D-erythritol 4-phosphate (MEP) and demethylated MEP.

and Lys-215 would presumably be the key interaction for the activity. Lastly, the spectrum of **7** was explored against other IspD homologues. Interestingly, **7** demonstrated specific inhibition for *plasmodial* species with great activity towards *Pv*IpsD (IC_{50} = 310 ± 80 nM), while being inactive towards both *Ec*IspD and *Mt*IspD. [33] Until today, multiple SAR studies have been conducted on the **MMV-0008138** chemotype, although, none of them led to an improvement in potency. Nonetheless, these studies exposed some of the structural features that are key for the activity. For example, a 2,4-halogen substitution pattern at the D-ring and the carboxyl group, although replacement with methyl amide retained most of the activity (Figure 6). Furthermore, it was seen that any extensions to the nitrogen atoms or chiral centers led to a complete loss of activity, presumably due to conformational changes imposed by additions at these site (Figure 6).[58-60] Due to the promising nature of the **MMV-0008138** chemotype, several structure similarity searches have been run on the libraries constituting the Malaria Box. This led to the discovery of two new classes, closely resembling **MMV-0008138**, with promising antimalarial activities. Unfortunately, IDP rescue assays conducted for both new classes revealed that IspD is no longer the primary target for these new classes (**11, 12**; Figure 7).[61, 62]

MEP derivatives. The following inhibitors structurally mimic MEP with the aim of achieving a potentially double MOI. On the one hand, the analogues could compete with MEP, on the other hand, they could lead to the synthesis

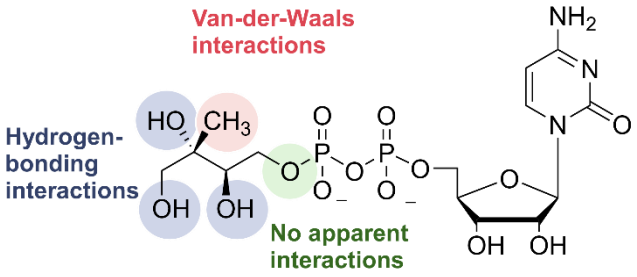

Figure 9. Overview of the interactions of 4-diphosphocytidyl-2*C*-methyl-D-erythritol (CDP-ME)

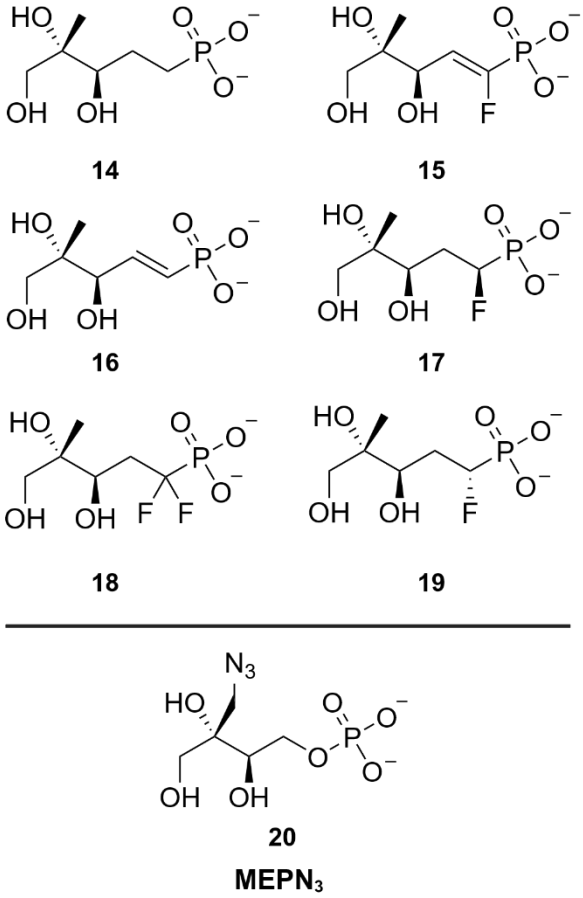

Figure 10. Top: Overview fluoroalkyl phosphonyl analogues of 2-*C*-Methyl-D-erythritol 4-phosphate (MEP); Bottom: $MEPN_3$ analog of MEP.

of analogues of MEP pathway metabolites, or even IDP and DMADP, which are unable to undergo any further conversion to isoprenoids. This approach not only leads to accumulation of purposeless metabolites/products, but could also induce metabolic stress as a consequence of the energetic cost of the MEP pathway. Due to its advantages, several attempts by various research groups were undertaken to find such MEP mimics.

Demethylated MEP. The most straightforward MEP mimic discovered today is demethylated MEP (Figure 8). This analogue has an IC_{50} value of 1.36 mM against *Ec*IspD, displaying, turnover of the compound, albeit with slower kinetics then the natural substrate, towards demethylated CDP-ME was observed.[54]

Fluoroalkyl phosphonyl analogues. Based on previously reported IspD co-crystal structures with CDP-ME, Bartee *et al.* evaluated the best position to modify MEP. The ideal position was found to be the oxygen atom linking the methylerythritol part and the phosphonates as this does not make any obvious interactions with the protein interface (Figure 9).[55–63] Modification of the

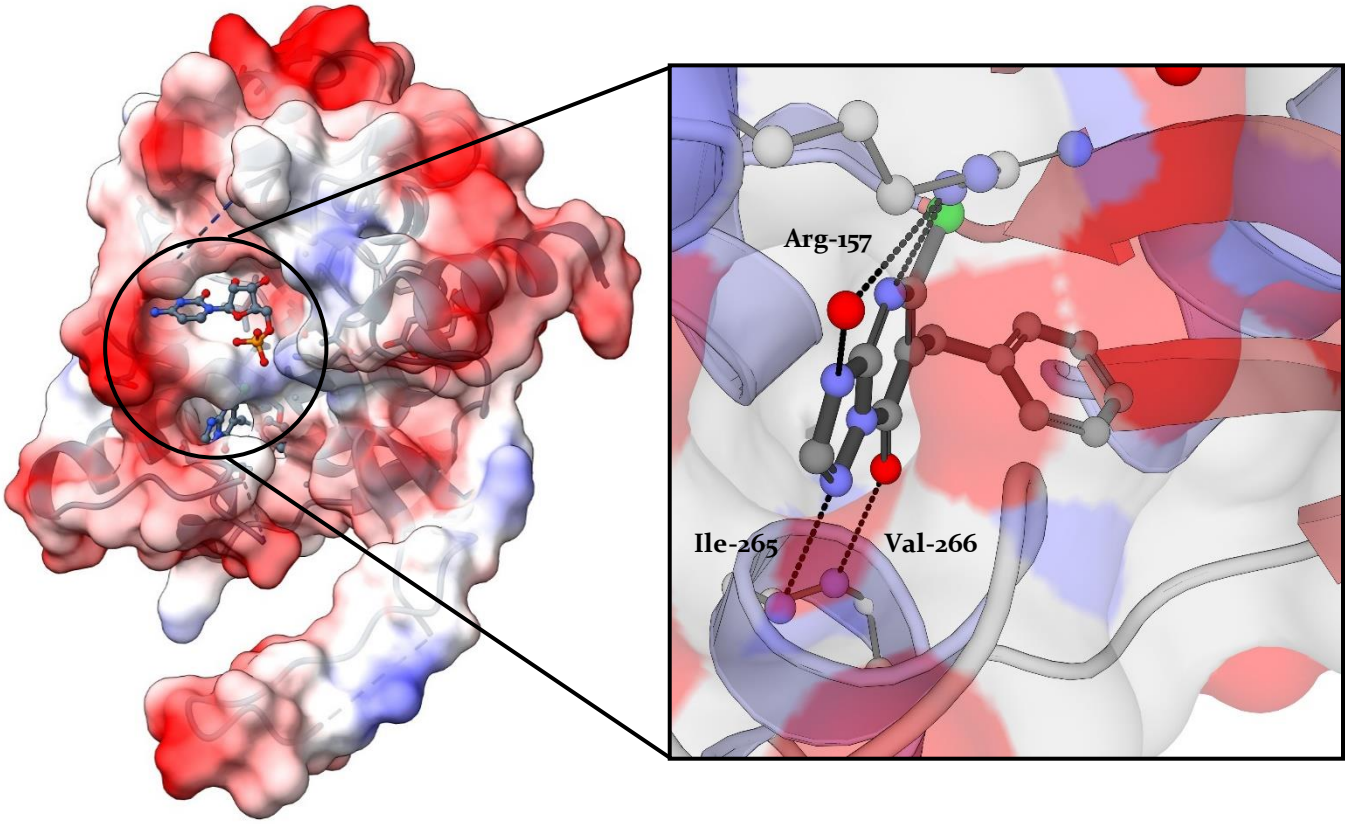

Figure 11. Crystal structure of *Arabidopsis thaliana* IspD with **21** in the allosteric pocket.

hydroxyl moieties would cause a loss of hydrogen-bonding interactions, while replacement of the methyl group would lose van der Waals interactions (Figure 9). In total, six derivatives in which the oxygen atom was replaced by a carbon atom were synthesized (Figure 10). The ability of these derivatives to serve as substrate was confirmed by LC-MS detection of the corresponding CDP-ME analogues. Despite their ability as substrates, the analogues have significantly lower catalytic efficiencies (k_{cat}/K_m) in comparison with MEP. The authors postulated that the major factor influencing the catalytic efficient was the change in reactivity resulting from swapping the oxygen with a carbon resulting in a decreased of turnover (k_{cat}) and that there was only a minor loss in affinity of the modified substrates towards the protein (K_m). The influence of the analogues on MEP turnover was determined for *Ec*, *Pf* and *Mt*IspD. It became clear that the derivatives containing saturated linkers performed the best within these experiments, with compound **19** outperforming the rest. IC_{50} values for **19** were determined against *Ec* and *Pf*IspD being 0.7 ± 0.1 and 1.3 ± 0.7 mM,< respectively.

MEPN$_3$. Lastly, Baatarkhuu *et al.* reasoned that the introduction of an azide function would give rise to an interesting starting point for fragment-based drug discovery. With this idea in mind, the introduction of the azide was performed at the 2*C*-methylene, to not interfere with any of the hydrogen-bond forming hydroxyl groups. The resulting compound (**20**, Figure 9), named MEPN$_3$, exhibits an excellent IC_{50} value of 41.5 ± 3.8 μM against *Ec*IspD. Determination of the MOI of this new inhibitor was done with steady-state inhibition kinetics. This gave rise to the discovery that **20** is able to bind to both substrate binding sites, albeit with a preference for the MEP binding pocket. Furthermore, **20** favors the free enzyme above the enzyme-substrate complex. Docking studies performed on a co-crystal structure of *Ec*IspD in complex with CDP-ME (PDB accession code 1I52) further substantiated this MOI. As with the previous inhibitors mimicking MEP, it was found that MEPN$_3$ could still serve

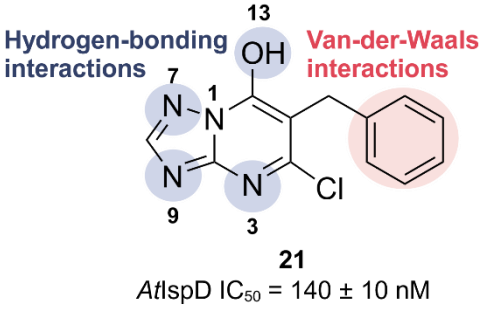

Figure 12. Initial hit of the azolopyridine class with the points of interaction highlighted

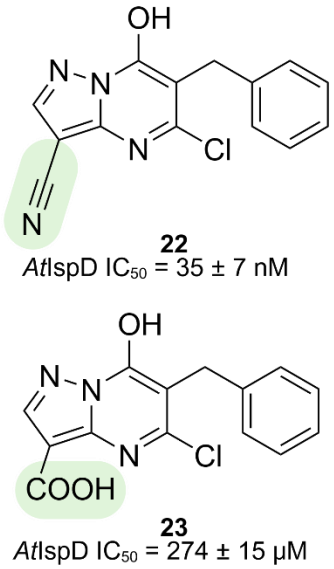

Figure 13. Initial hit of the azolopyridine class with the points of interaction highlighted.

as a substrate, resulting in the formation of CDP-MEPN$_3$. The docking study also revealed enough space within the binding pocket to extend **20** with the formation of a triazole, which would allow further optimization of this compound class, which is yet to be reported.[31]

Allosteric inhibitors of IspD. As mentioned before, IspD features an allosteric site with a more favorable lipophilic character (Figure 11). At the moment, all reported allosteric IspD inhibitors target *At*IspD.

Azolopyridines. Azolopyridines were discovered during a HTS of over 100,000 compounds, to find compounds targeting *At*IspD at BASF. Compound **21**, endowed with an IC$_{50}$ value of 140 ± 10 nM against *At*IspD, caught the interest of Witschel and co-workers. Elucidation of the co-crystal structure of *At*IspD in complex with **21** (PBD accession code 2YC3) uncovered that the compound occupies the allosteric pocket instead of the active site (Figure 11 and 12). Within this allosteric pocket, the phenyl ring fits tightly into a hydrophobic pocket in which it makes a multitude of lipophilic interactions. In addition, **21** forms four hydrogen bonds: between N3 and Arg-157, between the deprotonated hydroxyl and the backbone NH of Ile-265, between N9 and Ile-265 and lastly between N7 and a highly localized water molecule at the entrance of the pocket. Witschel *et al.* tried to enhance the potency by displacing this highly ordered water molecule at the entrance of the allosteric pocket through the addition of a nitrile or carboxylic acid at the N9 position, respectively (Figure 13). Both moieties succeeded in displacing the water molecule and by doing so gained an extra hydrogen bond with the protein (PDB accession code 2YC5; nitrile, 2YMC; carboxylic acid). Despite this, only in the case of the nitrile an increase in potency (**22**, *At*IspD IC$_{50}$ = 35 ± 7 nM) was noticed. In the case of the carboxylic acid (**23**, *At*IspD IC$_{50}$ = 274 ± 15 μM), the gain in potency is negligible in comparison with the energy cost needed for the desolvation of the carboxylate moiety upon binding. Further modifications were directed at the phenyl ring, but even the smallest increase in volume led to reduced activity.[14] A more detailed description of the allosteric inhibition mechanism can be found below. Further development of the *in vivo* herbicidal activity of the azolopyridines was performed by Clough *et al.*that obtained promising results , although, it became apparent that IspD was no longer the *in vivo* target of these new derivatives.[64]

Pseudilines and derived compound classes. The following compound class contains four "generations" of lead molecules discovered and optimized by different research groups. The main structural motif of this class is a direct link between a highly halogenated phenyl ring and a 5-membered heterocycle (Figure 14). The first generation of this class was discovered by BASF during a HTS-campaign using a spectrophotometric *At*IspD inhibtion assay. This led to the discovery of several hits exhibiting IC$_{50}$ values below 25 μM, among which, pseudilines 24 (*At*IspD IC$_{50}$ = 13 ± 2 μM) and 25 (*At*IspD IC$_{50}$ = 12 ± 1 μM) displayed the best activity (Figure 14). Pseudilines are a class of highly halogenated natural products with antibiotic properties originally isolated from seawater derived bacteria in 1966 by Burkholder and coworkers.[65,66] A handful of additional pseudiline derivatives were synthesized, but despite these efforts, no improvement in activity was achieved. A co-crystal structure was acquired, from which it became apparent that the pseudilines bind in the same allosteric pocked as the azolopyridines, demonstrating the flexible character of this pocket (PDB accession code 4NAL; 24; 4NAN; 25). The main interaction seen in the binding pocket is a bivalent chelation of the pseudilin hydroxyl and pyrrole nitrogen atom to a Cd^{2+} cation. The tetrahedral coordination of the Cd^{2+} cation is completed by interactions with the Gln-238 side chain and

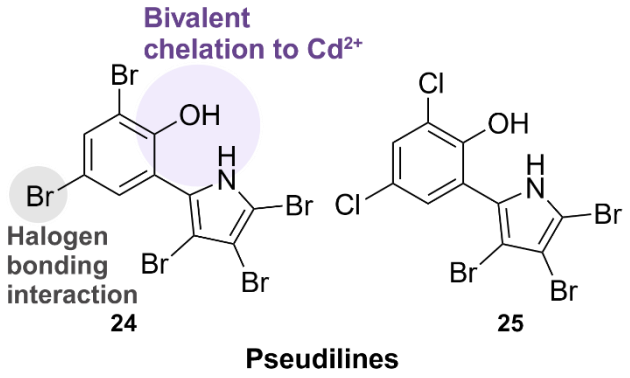

Figure 14. Summary of the interactions between the Pseudilines, *Arabidopsis thaliana* IspD. and Cd^{2+}

Table 4. Summary of the activity of the pseudilines.

#	*At*IspD IC_{50} (μM)		*Pv*IspD IC_{50} (μM)	
	W/O $CdSO_4$	40 μM $CdSO_4$	W/O $CdSO_4$	40 μM $CdSO_4$
24	13 ± 2	1.4 ± 0.2	48 ± 9	57 ± 12
25	12 ± 1	2.2 ± 0.2	56 ± 8	41 ± 7

Data shown for both *Arabidopsis thaliana* IspD and *Plasmodium vivax* IspD without and within the presence of 40 μM $CdSO_4$.

a water molecule present in the binding pocket. The presence of the Cd^{2+} in the crystal structure results from the use of $CdSO_4$ during crystallization.[46] Bivalent metal ions are frequently added to protein crystallization conditions to promote crystallization.[67] Further interactions to the protein include a halogen-bonding interaction between the halogen atom in *para* position of the hydroxyl and the carbonyl oxygen atom of Val-239. The interactions formed with Cd^{2+} cation in the crystal structure prompted Kunfermann *et al.* to repeat activity measurements in the presence of 40 μM of $CdSO_4$. This addition led to a 10-fold increase in activity for both hits (Table 4). Further profiling of the pseudilines led to the detection of micromolar activity against *Pv*IspD.

A second screening, also performed at BASF, with compounds having similar chemical structure as pseudilins **24** and **25**, gave rise to the discovery of compound **28** (*At*IspD IC_{50} = 418 ± 75 μM) (Figure 15). While the general scaffold remains similar, the pyrrole is replaced by an isoxazole and, consequently, the ability to make bivalent coordination was lost and hence also the benefit from the addition of bivalent metal ions. The authors again reverted to co-crystallization to elucidate the MOI (PDB accession code: 5MRM). Similar to the pseudilins, the halogen in *para*position forms a halogen-bonding interaction with carbonyl oxygen of Val-239. In this case, also the halogen in the *ortho* position is capable of forming a halogen bond with the carbonyl oxygen atom of Glu-267 (Figure 15). This interaction proved to be essential, as replacement of the halogen by hydrogen resulted in a ten-fold loss in activity. The hydroxyl forms hydrogen-bonding interactions with the side chain hydroxyl group of Ser-264 and an ordered water molecule present in the pocket. The CF_3 moiety on the isoxazole ring is positioned in a small pocket in which it forms a multitude of interactions, contributing greatly to the activity. Lastly, some π-stacking interactions of the phenyl ring with the methyl groups of Val-266 and the carboxyl side chain of Gln-238 were seen to contribute to the overall affinity of the compound.

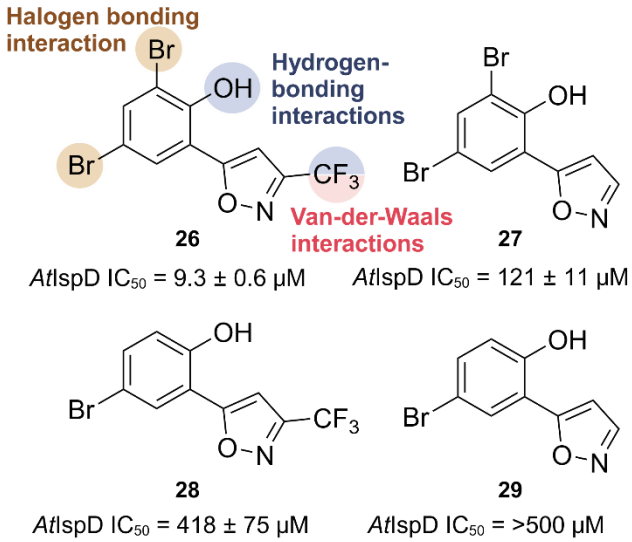

Figure 15. Summary of the interactions between the isoxazole and *Arabidopsis thaliana* IspD, some derivatives and their activity against At*IspD*

Interestingly, although the azolopyridines, pseudilines and the isoxazoles bind in the same allosteric pocket, different conformational changes are imposed by the different classes, which, in turn, lead to unique allosteric mechanisms. While binding of azolopyridines leads to a protrusion of Asp-262 into the MEP pocket, preventing MEP from binding. Engagement of pseudilins on the one hand blocks the CTP ribose binding site by displacement of Arg-157 and on the other hand causes steric and electrostatic repulsions in the MEP binding pocket by displacement of Asp-261. The allosteric mechanism of the isoxazoles is to a degree in between both mechanisms, Arg-157 stays in place while both Asp-261 and Asp-262 protrude into the active site and cause electrostatic repulsions, hindering both substrates from binding. A complete overview of all residues affected by binding of the inhibitors inside the allosteric pocket, as well as graphical representation, can be found elsewhere.[45]

Interestingly, Wang *et al.* tried to further enhance the activity by replacing the isoxazole ring by a pyrazole. A wide variety of substitution patterns with this scaffold was explored, although, this did not lead to any significant improvement over the isoxazole. Docking studies using the *At*IspD-isoxazole complex (PDB accession code 5MRM)[45] as a template revealed that this new class has similar interactions with the protein as the isoxazoles. Furthermore, predictions show that the NH is not participating in any interaction with the protein.[68]

Lastly, Zhang and coworkers combined the scaffolds of **24** and Diuron, a commercial herbicide, to further expand the scope of the pseudilines towards algae. Ultimately their efforts resulted in several compounds exhibiting promising

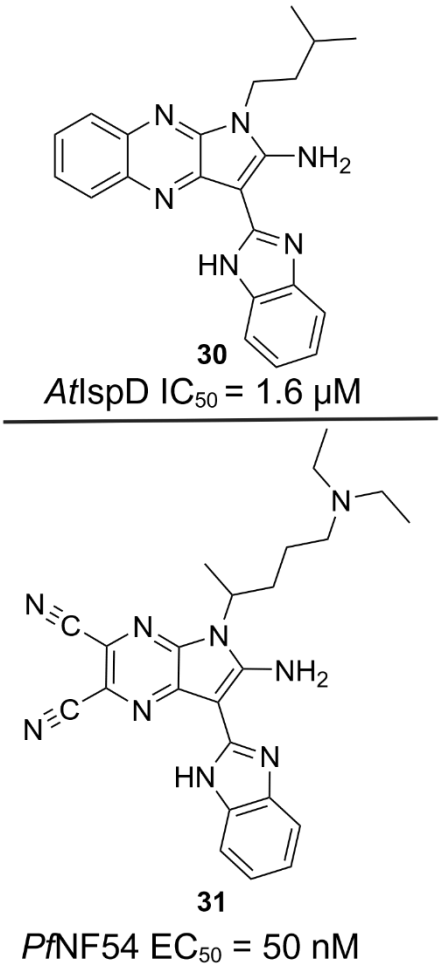

Figure 16. Top: Initial pyrrolopyrazine, *Arabidopsis thaliana* (*At*); Bottom: pyrrolopyrazine derivatives, *Plasmodium falciparum* (*Pf*).

anti-cyanobacterial activity, of which, one compounds also demonstrates moderate inhibition of *Ec*IspD (91% inhibition at 100 µM). Interestingly, these derivatives display very low or even no inhibitory activity towards *At*IspD.[69]

Inhibitors with unknown MOI. In the following, we will highlight IspD inhibitors for which the MOI is still unknown.

Pyrrolopyrazines. The first class of compounds discussed here are the pyrrolopyrazines.[70] This class was discovered at BASF during a HTS aiming to find inhibitors of *At*IspD. The initial hit **30** was found to have an IC_{50} value of 1.6 µM for *At*IspD (Figure 16). Many derivatives were synthesized and tested but none showed any improvements over **30**. The compound class was later tested against asexual blood stages of the *Pf*NF54 strain, wherein it showed excellent potency (EC_{50} ≈ 200 nM). Further optimization led to an array of analogues with low nanomolar activity on *Pf*NF54, while also featuring good

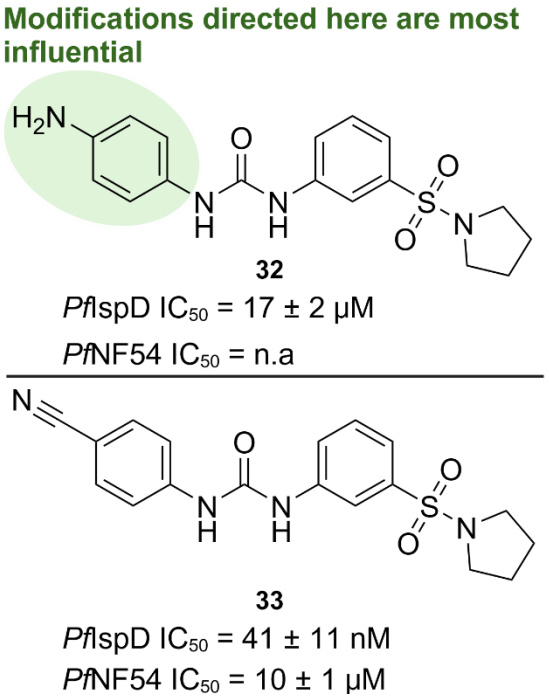

Figure 17. Top: initial hit urea class; below: promising urea compound; Activities against both *Plasmodium falciparum* (*Pf*) IspD and *Pf*NF54 strain are displayed.

selectivity and low toxicity. In addition, their lead compound (**31**), demonstrated excellent activity against liver schizont stage in the *P. berghei* mouse model. The discrepancy in activity between *At* and *Pf* led the authors to believe that there are additional or different enzymes being targeted by the pyrrolopyrazines. A wide array of computational studies were performed to elucidate those targets, which ended up pointing towards kinases, and more specifically, *Pf*PK5. Inhibitory activity of the lead compound for this enzyme was seen at a concentration of 30 µM but further experiments have to be performed to unambiguously assign *Pf*PK5 as the cellular target of the pyrrolopyrazines.

Urea class. The next class was discovered during an HTS campaign targeting *Pv*IspD after which all hits were concomitantly tested against *Pf*IspD and *Pf*NF54 cells.[71] The initial hit compound **32** had an IC_{50} value of 17 ± 2 µM on *Pf*IspD but was lacking whole-cell activity. We next optimized the activity of the compound class with a focus on retaining the straightforward synthesizable urea linker. The SAR study resulted in a 400-fold increase in activity on *Pf*IspD and activity in a whole-cell assay (Figure 17). During the SAR study, we noticed that modifications directed at the Western ring had the highest impact on the potency. Especially electron-withdrawing moieties at the *para* position had the most influence on the increase in potency. With optimized compounds in hand, we tried to elucidate the MOI by kinetic characterization in the presence of

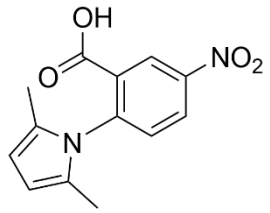

34

*Pf*IspD IC_{50} = 271 ± 24 μM

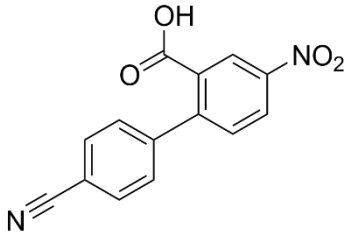

35

*Pf*IspD IC_{50} = 151 ± 17 μM

Figure 18. Structures of the initial hit and optimized compound of the biphenyl carboxylic acid, *Plasmodium falciparum* (*Pf*).

different inhibitor concentrations. We noticed that compound **33** was not competing with any of the substrates, hint ing towards allosteric inhibition. Follow-up experiments are required to confirm this hypothesis, but this could imply that the urea class would be the first inhibitor targeting the allosteric pocket of an IspD homolog other than *At*IspD. Lastly, the initial ADME profiles of some selected derivatives were measured showing promising results. The *in vivo* pharmacokinetic profiles of the most promising compounds in mice were highly encouraging for further optimization of the compound class.

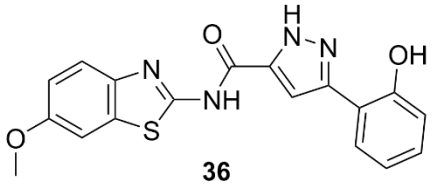

36

*At*IspD IC_{50} = 1.8 μM

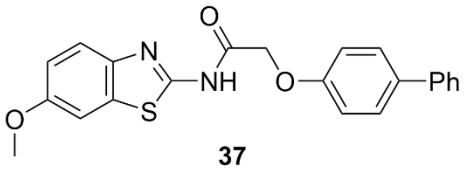

37

*At*IspD IC_{50} = 6.3 μM

Figure 19. Structures of the initial hits of the aminobenzothiazole compound class, *Arabidopsis thaliana* (*At*)

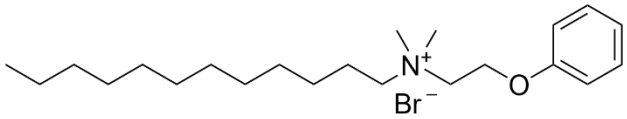

38

*Mt*IspD IC_{50} = 800 nM

MIC *Mt* strains (μg/mL)
H37Rv : 8
MDR-TB : 8
XDR-TB : 16

Figure 20. Domiphenbromide, Minimum inhibitory concentration (MIC), *Mycobacterium tuberculosis* (*Mt*)

Biphenyl carboxylic acid. The next inhibitor was discovered during an HTS campaign using a proprietary library from BASF.[39] The authors selected compound **34** bacause of its low micromolar activity against *Pf*IspD and its fragment-like size, allowing plenty chemical modifications to be made (Figure 18). Besides enhancing the potency and physicochemical properties, the SAR of this fragment also focused on finding a replacement for the pyrrole, as this motif might be problematic in a drug development program. The SAR resulted in compound **35**, which features a good balance between improved potency and physicochemical properties. Furthermore, the pyrrole was replaced with a benzonitrile moiety (Figure 18). To elucidate the binding mode of the fragment, the authors resorted to buildingt a homology model based on an *Ec*IspD crystal structure (PDB accession code 1I52). After docking the fragment, it became apparent that the majority of the activity was due to the formation of two hydrogen bonds between the carboxylic acid and Lys-207 and Ile-205. Another hydrogen bond was seen between the terminal nitro group and Arg-429. This predicted binding mode within the active site of the protein was not experimentally confirmed.

Aminobenzothiazoles. The aminobenzothiazoles (**36** and **37**) were also discovered during screenings at BASF aiming to find *At*IspD inhibitors (Figure 19).[72] This compound class has low micromolar activity against *At*IspD, although no further optimization of this class was done until this date.

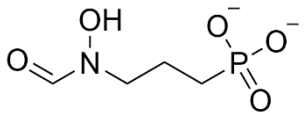

39

*Ec*IspD IC_{50} = 20.4 ± 3.3 mM

*Ec*DXR IC_{50} = 0.81 ± 0.27 μM

Figure 21. Structure of fosmidomycin with its inhibitory activities against both IspD and DXR originating from *Escherichia coli* (*Ec*).

Domiphenbromide. Domiphenbromide (DB, **38**) was found to inhibit *Mt*IspD by Peng *et al.* (Figure 20). The compound was found by utilizing an HTS campaign on a small proprietary library of 3200 compounds. In addition, DB exhibited growth inhibition on various strains of *Mt*, although, its target(s) in the cell still has (have) to be experimentally confirmed. [35] Recently, Biosca *et al.* reported on the ability of DB to be a fast-acting antimalarial, although, additional experiments have to be performed to confirm the MOI.[73]

Fosmidomycin. Lastly, Zhang B. *et al.* found that fosmidomycin (**42**), a known inhibitor of the second enzyme of the MEP pathway DXR (*Ec*DXR IC_{50} = 0.81 ± 0.27), also inhibits *Ec*IspD with an IC_{50} value of 20.4 ± 3.3 mM (Figure 21).[50]

Conclusions

Despite all previous efforts, there is still only a small number of IspD inhibitors described in the literature. Furthermore, the existing inhibitors only target a handful of IspD homologues, while IspD is found wide-spread among human pathogens and plants. As described above, IspD can be inhibited with a wide array of MOI's ranging from competitive over covalent to allosteric inhibition. Taking this all into account, there is still a lot of untapped potential.

Future research towards IspD inhibitors should preferably be aimed at the allosteric site of IspD due to the hydrophilic character of the active site, making it challenging to balance the polarity of inhibitors between achieving high affinity for the target and not jeopardizing its ability to cross membranes. Targeting the more lipophilic allosteric pocket, as demonstrated by Witschel and coworkers, should allow for the development of more balanced inhibitors with a more favorable polarity.

In summary, due to its widespread occurrence and absence in human cells, IspD has the potential to play a key role in the quest towards novel anti-infectives and herbicides with a unique mode of action. Especially for the development of broad-spectrum anti-infectives there is a lot of promise due to the overwhelming structural similarities between the different IspD homologues of various pathogens.

AUTHOR INFORMATION

Corresponding Author

***Anna K. H. Hirsch** – *Helmholtz Institute for Pharmaceutical Research (HIPS)-Helmholtz Centre for Infection Research (HZI), Saarland University, Campus E 8.1, 66123 Saarbrücken, Germany;*
Email: Anna.hirsch@helmholtz-hips.de

Present Addresses

†If an author's address is different than the one given in the affiliation line, this information may be included here.

Author Contributions

E.D. and A. K. H. H. defined, supervised and edited the project. D.W. wrote the manuscript. The manuscript was written through contributions of all authors. / All authors have given approval to the final version of the manuscript.

Funding Sources

This project has received funding from the European Union's Horizon 2020 research and innovation programme under the Marie Skłodowska-Curie grant agreement N° 860816 MepAnti.

Notes

The authors declare no competing financial interest.
All figures were created with BioRender.com

ABBREVIATIONS

AMR, antimicrobial resistance; *At*, *arabidopsis thaliana*; *Bs*, *bacillus subtilis*; DXP, 1-deoxyxylulose 5- phosphate; DMAPP, dimethylallyl diphosphate; DB, domiphenbromide; CDP-ME, 4-diphosphocytidyl-2C-methyl-D-erythritol; IspD, 4-diphosphocytidyl-2C-methyl-D-erythritol synthase; *Ec*, *escherichia coli*; GAP, glyceraldehyde-3-phosphate; HTS, high throughput screen; Hs, homo sapiens; IDP, isopentenyl diphosphate; MEP, methylerythritol-D-erythritol-4-phosphate; MVA, mevalonate pathway; K_m, Michaelis constants; MIC, minimum inhibitory concentration; MOI, mode of inhibition; MOA, modes of action; *Ms*; *mycobacterium smegmatis*; *Mt*, *Mycobacterium tuberculosis*; BITZ, 2-phenyl benzo[d]isothiazol-3(2H)-one; *Pf*, *plasmodium falciparum*; *Pv*, *plasmodium vivax*; *Pa*, *pseudomonas aeruginosa*.

REFERENCES

(1) Frei, A.; Verderosa, A. D.; Elliott, A. G.; Zuegg, J.; Blaskovich, M. A. T. Metals to combat antimicrobial resistance. *Nature Reviews Chemistry* **2023**, *7* (3), 202-224. DOI: 10.1038/s41570-023-00463-4.
(2) Menne, H.; Köcher, H. HRAC Classification of Herbicides and Resistance Development. In *Modern Crop Protection Compounds*, 2011; pp 5-28.
(3) Murray, C. J. L.; Ikuta, K. S.; Sharara, F.; Swetschinski, L.; Robles Aguilar, G.; Gray, A.; Han, C.; Bisignano, C.; Rao, P.; Wool, E.; et al. Global burden of bacterial antimicrobial resistance in 2019: a systematic analysis. *The Lancet* **2022**, *399* (10325), 629-655. DOI: 10.1016/S0140-6736(21)02724-0 (acccessed 2023/08/14).
(4) O'Neill, J. *Tackling drug-resistant infections globally: final report and recommendations*; Government of the United Kingdom, 2016.
(5) Hunter, W. N. The Non-mevalonate Pathway of Isoprenoid Precursor Biosynthesis *. *Journal of Biological Chemistry* **2007**, *282* (30), 21573-21577. DOI: 10.1074/jbc.R700005200 (acccessed 2023/09/14).
(6) Eoh, H.; Brennan, P. J.; Crick, D. C. The Mycobacterium tuberculosis MEP (2C-methyl-d-erythritol 4-phosphate) pathway as a new drug target. *Tuberculosis* **2009**, *89* (1), 1-11. DOI: 10.1016/j.tube.2008.07.004 (acccessed 2022-04-29T13:50:02).
(7) Gabrielsen, M.; Kaiser, J.; Rohdich, F.; Eisenreich, W.; Laupitz, R.; Bacher, A.; Bond, C. S.; Hunter, W. N. The crystal structure of a plant 2C-methyl-D-erythritol 4-phosphate cytidylyltransferase exhibits a distinct quaternary structure compared to bacterial homologues and a possible role in feedback regulation for cytidine monophosphate.

FEBS Journal **2006**, *273* (5), 1065-1073. DOI: 10.1111/j.1742-4658.2006.05133.x (acccessed 2023-06-23T11:26:03).
(8) Steinbacher, S.; Kaiser, J.; Eisenreich, W.; Huber, R.; Bacher, A.; Rohdich, F. Structural Basis of Fosmidomycin Action Revealed by the Complex with 2-C-Methyl-d-erythritol 4-phosphate Synthase (IspC): IMPLICATIONS FOR THE CATALYTIC MECHANISM AND ANTI-MALARIA DRUG DEVELOPMENT *. *Journal of Biological Chemistry* **2003**, *278* (20), 18401-18407. DOI: 10.1074/jbc.M300993200 (acccessed 2023/08/22).
(9) Parish, T.; Stoker Neil, G. glnE Is an Essential Gene inMycobacterium tuberculosis. *Journal of Bacteriology* **2000**, *182* (20), 5715-5720. DOI: 10.1128/jb.182.20.5715-5720.2000 (acccessed 2023/08/22).
(10) Heuston, S.; Begley, M.; Gahan, C. G. M.; Hill, C. Isoprenoid biosynthesis in bacterial pathogens. *Microbiology 158* (6), 1389. DOI: https://doi.org/10.1099/mic.0.051599-0.
(11) Masini, T.; Kroezen, B. S.; Hirsch, A. K. H. Druggability of the enzymes of the non-mevalonate-pathway. *Drug Discovery Today* **2013**, *18* (23), 1256-1262. DOI: https://doi.org/10.1016/j.drudis.2013.07.003.
(12) Wang, X.; Dowd, C. S. The Methylerythritol Phosphate Pathway: Promising Drug Targets in the Fight against Tuberculosis. *ACS Infect. Dis.* **2018**, *4* (3), 278-290, Review. DOI: 10.1021/acsinfecdis.7b00176.
(13) Frank, A.; Groll, M. The Methylerythritol Phosphate Pathway to Isoprenoids. *Chemical Reviews* **2017**, *117* (8), 5675-5703. DOI: 10.1021/acs.chemrev.6b00537 (acccessed 2022-04-28T08:51:47).
(14) Witschel, M. C.; Höffken, H. W.; Seet, M.; Parra, L.; Mietzner, T.; Thater, F.; Niggeweg, R.; Röhl, F.; Illarionov, B.; Rohdich, F.; et al. Inhibitors of the Herbicidal Target IspD: Allosteric Site Binding. *Angewandte Chemie International Edition* **2011**, *50* (34), 7931-7935. DOI: 10.1002/anie.201102281 (acccessed 2022-04-26T13:52:01).
(15) Volkamer, A.; Kuhn, D.; Rippmann, F.; Rarey, M. DoGSiteScorer: a web server for automatic binding site prediction, analysis and druggability assessment. *Bioinformatics* **2012**, *28* (15), 2074-2075. DOI: 10.1093/bioinformatics/bts310 (acccessed 8/22/2023).
(16) Eisenreich, W.; Rohdich, F.; Bacher, A. Deoxyxylulose phosphate pathway to terpenoids. *Trends in Plant Science* **2001**, *6* (2), 78-84. DOI: https://doi.org/10.1016/S1360-1385(00)01812-4.
(17) Eisenreich, W.; Bacher, A.; Arigoni, D.; Rohdich, F. Biosynthesis of isoprenoids via the non-mevalonate pathway. *Cellular and Molecular Life Sciences* **2004**, *61* (12). DOI: 10.1007/s00018-004-3381-z (acccessed 2022-04-29T13:39:34).
(18) Gershenzon, J.; Dudareva, N. The function of terpene natural products in the natural world. *Nature Chemical Biology* **2007**, *3* (7), 408-414. DOI: 10.1038/nchembio.2007.5.
(19) Rohmer, M.; Knani, M.; Simonin, P.; Sutter, B.; Sahm, H. Isoprenoid biosynthesis in bacteria: a novel pathway for the early steps leading to isopentenyl diphosphate. *Biochemical Journal* **1993**, *295* (2), 517-524. DOI: 10.1042/bj2950517 (acccessed 2023-08-07T13:56:27).
(20) Rohmer, M.; Seemann, M.; Horbach, S.; Bringer-Meyer, S.; Sahm, H. Glyceraldehyde 3-Phosphate and Pyruvate as Precursors of Isoprenic Units in an Alternative Non-mevalonate Pathway for Terpenoid Biosynthesis. *Journal of the American Chemical Society* **1996**, *118* (11), 2564-2566. DOI: 10.1021/ja9538344 (acccessed 2023-08-07T14:40:29).
(21) Kuzuyama, T.; Takagi, M.; Kaneda, K.; Dairi, T.; Seto, H. Formation of 4-(cytidine 5′-diphospho)-2-C-methyl-d-erythritol from 2-C-methyl-d-erythritol 4-phosphate by 2-C-methyl-d-erythritol 4-phosphate cytidylyltransferase, a new enzyme in the nonmevalonate pathway. *Tetrahedron Letters* **2000**, *41* (5), 703-706. DOI: https://doi.org/10.1016/S0040-4039(99)02143-7.
(22) Rohdich, F.; Wungsintaweekul, J.; Eisenreich, W.; Richter, G.; Schuhr, C. A.; Hecht, S.; Zenk, M. H.; Bacher, A. Biosynthesis of terpenoids: 4-Diphosphocytidyl-2C-methyl-d-erythritol synthase of Arabidopsis thaliana. *Proceedings of the National Academy of Sciences* **2000**, *97* (12), 6451-6456. DOI: 10.1073/pnas.97.12.6451 (acccessed 2023/08/08).
(23) Eoh, H.; Brown Amanda, C.; Buetow, L.; Hunter William, N.; Parish, T.; Kaur, D.; Brennan Patrick, J.; Crick Dean, C. Characterization of the Mycobacterium tuberculosis 4-Diphosphocytidyl-2-C-Methyl-d-Erythritol Synthase: Potential for Drug Development. *Journal of Bacteriology* **2007**, *189* (24), 8922-8927. DOI: 10.1128/jb.00925-07 (acccessed 2023/11/15).
(24) Freiberg, C.; Wieland, B.; Spaltmann, F.; Ehlert, K.; Brotz, H.; Labischinski, H. Identification of novel essential Escherichia coli genes conserved among pathogenic bacteria. *Journal of molecular microbiology and biotechnology* **2001**, *3* (3), 483-489.
(25) Sparr, C.; Purkayastha, N.; Kolesinska, B.; Gengenbacher, M.; Amulic, B.; Matuschewski, K.; Seebach, D.; Kamena, F. Improved Efficacy of Fosmidomycin against Plasmodium and Mycobacterium Species by Combination with the Cell-Penetrating Peptide Octaarginine. *Antimicrobial Agents and Chemotherapy* **2013**, *57* (10), 4689-4698. DOI: 10.1128/aac.00427-13 (acccessed 2023/11/15).
(26) Cassera, M. B.; Gozzo, F. C.; D'Alexandri, F. L.; Merino, E. F.; del Portillo, H. A.; Peres, V. J.; Almeida, I. C.; Eberlin, M. N.; Wunderlich, G.; Wiesner, J.; et al. The Methylerythritol Phosphate Pathway Is Functionally Active in All Intraerythrocytic Stages of Plasmodium falciparum*. *Journal of Biological Chemistry* **2004**, *279* (50), 51749-51759. DOI: 10.1074/jbc.M408360200 (acccessed 2023/11/15).
(27) Yeh, E.; DeRisi, J. L. Chemical Rescue of Malaria Parasites Lacking an Apicoplast Defines Organelle Function in Blood-Stage Plasmodium falciparum. *PLOS Biology* **2011**, *9* (8), e1001138. DOI: 10.1371/journal.pbio.1001138.
(28) Wiley Jessica, D.; Merino Emilio, F.; Krai Priscilla, M.; McLean Kyle, J.; Tripathi Abhai, K.; Vega-Rodríguez, J.; Jacobs-Lorena, M.; Klemba, M.; Cassera Maria, B. Isoprenoid Precursor Biosynthesis Is the Essential Metabolic Role of the Apicoplast during Gametocytogenesis in Plasmodium falciparum. *Eukaryotic Cell* **2015**, *14* (2), 128-139. DOI: 10.1128/ec.00198-14 (acccessed 2023/11/15).
(29) Saggu, G. S.; Pala, Z. R.; Garg, S.; Saxena, V. New Insight into Isoprenoids Biosynthesis Process and Future Prospects for Drug Designing in Plasmodium. *Front. Microbiol.* **2016**, *7*, 14, Article. DOI: 10.3389/fmicb.2016.01421.
(30) Richard, S. B.; Bowman, M. E.; Kwiatkowski, W.; Kang, I.; Chow, C.; Lillo, A. M.; Cane, D. E.; Noel, J. P. Structure of 4-diphosphocytidyl-2-C- methylerythritol synthetase involved in mevalonate-independent isoprenoid biosynthesis. *Nature Structural Biology* **2001**, *8* (7), 641-648. DOI: 10.1038/89691.
(31) Baatarkhuu, Z.; Chaignon, P.; Borel, F.; Ferrer, J.-L.; Wagner, A.; Seemann, M. Synthesis and Kinetic evaluation of an azido analogue of methylerythritol phosphate: a Novel Inhibitor of E. coli YgbP/IspD. *Sci Rep* **2018**, *8* (1). DOI: 10.1038/s41598-018-35586-y (acccessed 2022-04-26T13:56:53).
(32) Rohdich, F.; Wungsintaweekul, J.; Fellermeier, M.; Sagner, S.; Herz, S.; Kis, K.; Eisenreich, W.; Bacher, A.; Zenk, M. H. Cytidine 5′-triphosphate-dependent biosynthesis of isoprenoids: YgbP protein of *Escherichia coli* catalyzes the formation of 4-diphosphocytidyl-2-*C*-methylerythritol. *Proceedings of the National Academy of Sciences* **1999**, *96* (21), 11758-11763. DOI: 10.1073/pnas.96.21.11758 (acccessed 2023-08-08T09:10:39).
(33) Imlay, L. S.; Armstrong, C. M.; Masters, M. C.; Li, T.; Price, K. E.; Edwards, R. L.; Mann, K. M.; Li, L. X.; Stallings, C. L.; Berry, N. G.; et al. Plasmodium IspD (2-C-Methyl-d-erythritol 4-Phosphate Cytidyltransferase), an Essential and Druggable Antimalarial Target. *ACS Infect. Dis.* **2015**, *1* (4), 157-167. DOI: 10.1021/id5000047s.
(34) Wu, W.; Herrera, Z.; Ebert, D.; Baska, K.; Cho, S. H.; Derisi, J. L.; Yeh, E. A Chemical Rescue Screen Identifies a Plasmodium falciparum Apicoplast Inhibitor Targeting MEP Isoprenoid Precursor Biosynthesis. *Antimicrobial Agents and Chemotherapy* **2015**, *59* (1), 356-364. DOI: 10.1128/aac.03342-14 (acccessed 2022-04-26T14:03:06).
(35) Gao, P.; Yang, Y.; Xiao, C.; Liu, Y.; Gan, M.; Guan, Y.; Hao, X.; Meng, J.; Zhou, S.; Chen, X.; et al. Identification and validation of a novel lead compound targeting 4-diphosphocytidyl-2-C-methylerythritol synthetase (IspD) of mycobacteria. *European Journal of Pharmacology* **2012**, *694* (1), 45-52. DOI: https://doi.org/10.1016/j.ejphar.2012.08.012.
(36) Jin, Y.; Liu, Z.; Li, Y.; Liu, W.; Tao, Y.; Wang, G. A structural and functional study on the 2-C-methyl-d-erythritol-4-phosphate

cytidyltransferase (IspD) from Bacillus subtilis. *Sci Rep* **2016**, *6* (1), 36379. DOI: 10.1038/srep36379.
(37) Shin, W.-H.; Kihara, D. 55 Years of the Rossmann Fold. In *Protein Supersecondary Structures: Methods and Protocols*, Kister, A. E. Ed.; Springer New York, 2019; pp 1-13.
(38) Kemp, L. E.; Bond, C. S.; Hunter, W. N. Structure of a tetragonal crystal form ofEscherichia coli2-C-methyl-<scp>D</scp>-erythritol 4-phosphate cytidylyltransferase. *Acta Crystallographica Section D Biological Crystallography* **2003**, *59* (3), 607-610. DOI: 10.1107/s090744490202365x (acccessed 2023-06-23T11:27:14).
(39) Diamanti, E.; Hamed, M. M.; Lacour, A.; Bravo, P.; Illarionov, B.; Fischer, M.; Rottmann, M.; Witschel, M.; Hirsch, A. K. H. Targeting the IspD Enzyme in the MEP Pathway: Identification of a Novel Fragment Class. *ChemMedChem* **2022**. DOI: 10.1002/cmdc.202100679 (acccessed 2022-04-26T14:15:43).
(40) Price, K. E.; Armstrong, C. M.; Imlay, L. S.; Hodge, D. M.; Pidathala, C.; Roberts, N. J.; Park, J.; Mikati, M.; Sharma, R.; Lawrenson, A. S.; et al. Molecular Mechanism of Action of Antimalarial Benzoisothiazolones: Species-Selective Inhibitors of the Plasmodium spp. MEP Pathway enzyme, IspD. *Sci Rep* **2016**, *6* (1), 36777. DOI: 10.1038/srep36777 (acccessed 2022-04-26T13:53:46).
(41) Imlay, L. S.; Armstrong, C. M.; Masters, M. C.; Li, T.; Price, K. E.; Edwards, R. L.; Mann, K. M.; Li, L. X.; Stallings, C. L.; Berry, N. G.; et al. Plasmodium IspD (2-C-Methyl-<scp>d</scp>-erythritol 4-Phosphate Cytidyltransferase), an Essential and Druggable Antimalarial Target. *ACS Infectious Diseases* **2015**, *1* (4), 157-167. DOI: 10.1021/id5000047s (acccessed 2022-04-26T14:03:47).
(42) Bjorkelid, C.; Bergfors, T.; Henriksson, L. M.; Stern, A. L.; Unge, T.; Mowbray, S. L.; Jones, T. A. Structural and functional studies of mycobacterial IspD enzymes. *Acta Crystallographica Section D* **2011**, *67* (5), 403-414.
(43) Gabrielsen, M.; Rohdich, F.; Eisenreich, W.; Gräwert, T.; Hecht, S.; Bacher, A.; Hunter, W. N. Biosynthesis of isoprenoids. *European Journal of Biochemistry* **2004**, *271* (14), 3028-3035. DOI: https://doi.org/10.1111/j.1432-1033.2004.04234.x (acccessed 2023/08/11).
(44) Gabrielsen, M.; Bond, C. S.; Hallyburton, I.; Hecht, S.; Bacher, A.; Eisenreich, W.; Rohdich, F.; Hunter, W. N. Hexameric Assembly of the Bifunctional Methylerythritol 2,4-Cyclodiphosphate Synthase and Protein-Protein Associations in the Deoxy-xylulose-dependent Pathway of Isoprenoid Precursor Biosynthesis *. *Journal of Biological Chemistry* **2004**, *279* (50), 52753-52761. DOI: 10.1074/jbc.M408895200 (acccessed 2023/08/11).
(45) Schwab, A.; Illarionov, B.; Frank, A.; Kunfermann, A.; Seet, M.; Bacher, A.; Witschel, M. C.; Fischer, M.; Groll, M.; Diederich, F. Mechanism of Allosteric Inhibition of the Enzyme IspD by Three Different Classes of Ligands. *ACS Chemical Biology* **2017**, *12* (8), 2132-2138. DOI: 10.1021/acschembio.7b00004 (acccessed 2022-04-26T14:08:10).
(46) Kunfermann, A.; Witschel, M.; Illarionov, B.; Martin, R.; Rottmann, M.; Höffken, H. W.; Seet, M.; Eisenreich, W.; Knölker, H.-J.; Fischer, M.; et al. Pseudilins: Halogenated, Allosteric Inhibitors of the Non-Mevalonate Pathway Enzyme IspD. *Angewandte Chemie International Edition* **2014**, *53* (8), 2235-2239. DOI: 10.1002/anie.201309557 (acccessed 2022-04-26T14:10:02).
(47) van Tol, W.; van Scherpenzeel, M.; Alsady, M.; Riemersma, M.; Hermans, E.; Kragt, E.; Tasca, G.; Kamsteeg, E.-J.; Pennings, M.; van Beusekom, E.; et al. Cytidine Diphosphate-Ribitol Analysis for Diagnostics and Treatment Monitoring of Cytidine Diphosphate-l-Ribitol Pyrophosphorylase A Muscular Dystrophy. *Clinical Chemistry* **2019**, *65* (10), 1295-1306. DOI: 10.1373/clinchem.2019.305391 (acccessed 8/14/2023).
(48) Willer, T.; Lee, H.; Lommel, M.; Yoshida-Moriguchi, T.; de Bernabe, D. B. V.; Venzke, D.; Cirak, S.; Schachter, H.; Vajsar, J.; Voit, T.; et al. ISPD loss-of-function mutations disrupt dystroglycan O-mannosylation and cause Walker-Warburg syndrome. *Nature Genetics* **2012**, *44* (5), 575-580. DOI: 10.1038/ng.2252.
(49) Riemersma, M.; Froese, D. S.; van Tol, W.; Engelke, U. F.; Kopec, J.; van Scherpenzeel, M.; Ashikov, A.; Krojer, T.; von Delft, F.; Tessari, M. Human ISPD is a cytidyltransferase required for dystroglycan O-mannosylation. *Chemistry & biology* **2015**, *22* (12), 1643-1652.
(50) Zhang, B.; Watts, K. M.; Hodge, D.; Kemp, L. M.; Hunstad, D. A.; Hicks, L. M.; Odom, A. R. A Second Target of the Antimalarial and Antibacterial Agent Fosmidomycin Revealed by Cellular Metabolic Profiling. *Biochemistry* **2011**, *50* (17), 3570-3577. DOI: 10.1021/bi200113y.
(51) Illarionova, V.; Kaiser, J.; Ostrozhenkova, E.; Bacher, A.; Fischer, M.; Eisenreich, W.; Rohdich, F. Nonmevalonate Terpene Biosynthesis Enzymes as Antiinfective Drug Targets: Substrate Synthesis and High-Throughput Screening Methods. *The Journal of Organic Chemistry* **2006**, *71* (23), 8824-8834. DOI: 10.1021/jo0614660.
(52) Bowman, J. D.; Merino, E. F.; Brooks, C. F.; Striepen, B.; Carlier, P. R.; Cassera, M. B. Antiapicoplast and Gametocytocidal Screening To Identify the Mechanisms of Action of Compounds within the Malaria Box. *Antimicrobial Agents and Chemotherapy* **2014**, *58* (2), 811-819. DOI: doi:10.1128/aac.01500-13.
(53) Bakovic, M.; Fullerton, M. D.; Michel, V. Metabolic and molecular aspects of ethanolamine phospholipid biosynthesis: the role of CTP:phosphoethanolamine cytidylyltransferase (Pcyt2). *Biochemistry and Cell Biology* **2007**, *85* (3), 283-300. DOI: 10.1139/O07-006 (acccessed 2024/01/04).
(54) Lillo, A. M.; Tetzlaff, C. N.; Sangari, F. J.; Cane, D. E. Functional expression and characterization of eryA, the erythritol kinase of Brucella abortus, and enzymatic synthesis of l-Erythritol-4-phosphate. *Bioorganic & Medicinal Chemistry Letters* **2003**, *13* (4), 737-739. DOI: https://doi.org/10.1016/S0960-894X(02)01032-6.
(55) Bartee, D.; Wheadon, M. J.; Freel Meyers, C. L. Synthesis and Evaluation of Fluoroalkyl Phosphonyl Analogues of 2-C-Methylerythritol Phosphate as Substrates and Inhibitors of IspD from Human Pathogens. *The Journal of Organic Chemistry* **2018**, *83* (17), 9580-9591. DOI: 10.1021/acs.joc.8b00686.
(56) Richard, S. B.; Bowman, M. E.; Kwiatkowski, W.; Kang, I.; Chow, C.; Lillo, A. M.; Cane, D. E.; Noel, J. P. *Nature Structural Biology* **2001**, *8* (7), 641-648. DOI: 10.1038/89691 (acccessed 2022-04-28T09:35:40).
(57) Price, K. E.; Armstrong, C. M.; Imlay, L. S.; Hodge, D. M.; Pidathala, C.; Roberts, N. J.; Park, J.; Mikati, M.; Sharma, R.; Lawrenson, A. S.; et al. Molecular Mechanism of Action of Antimalarial Benzoisothiazolones: Species-Selective Inhibitors of the Plasmodium spp. MEP Pathway enzyme, IspD. *Sci Rep* **2016**, *6*, 12, Article. DOI: 10.1038/srep36777.
(58) Cagašová, K.; Ghavami, M.; Yao, Z.-K.; Carlier, P. R. Questioning the γ-gauche effect: stereoassignment of 1,3-disubstituted-tetrahydro-β-carbolines using ¹H–¹H coupling constants. *Organic & Biomolecular Chemistry* **2019**, *17* (27), 6687-6698. DOI: 10.1039/c9ob01139k (acccessed 2023-06-28T09:21:35).
(59) Yao, Z.-K.; Krai, P. M.; Merino, E. F.; Simpson, M. E.; Slebodnick, C.; Cassera, M. B.; Carlier, P. R. Determination of the active stereoisomer of the MEP pathway-targeting antimalarial agent MMV008138, and initial structure–activity studies. *Bioorganic & Medicinal Chemistry Letters* **2015**, *25* (7), 1515-1519. DOI: https://doi.org/10.1016/j.bmcl.2015.02.020.
(60) Ding, S.; Ghavami, M.; Butler, J. H.; Merino, E. F.; Slebodnick, C.; Cassera, M. B.; Carlier, P. R. Probing the B- & C-rings of the antimalarial tetrahydro-β-carboline MMV008138 for steric and conformational constraints. *Bioorganic & Medicinal Chemistry Letters* **2020**, *30* (22), 127520. DOI: https://doi.org/10.1016/j.bmcl.2020.127520.
(61) Mathew, J.; Ding, S.; Kunz, K. A.; Stacy, E. E.; Butler, J. H.; Haney, R. S.; Merino, E. F.; Butschek, G. J.; Rizopoulos, Z.; Totrov, M.; et al. Malaria Box-Inspired Discovery of N-Aminoalkyl-β-carboline-3-carboxamides, a Novel Orally Active Class of Antimalarials. *ACS Medicinal Chemistry Letters* **2022**, *13* (3), 365-370. DOI: 10.1021/acsmedchemlett.1c00663 (acccessed 2023-06-16T14:00:08).
(62) Almolhim, H.; Ding, S.; Butler, J. H.; Bremers, E. K.; Butschek, G. J.; Slebodnick, C.; Merino, E. F.; Rizopoulos, Z.; Totrov, M.; Cassera, M. B.; et al. Enantiopure Benzofuran-2-carboxamides of 1-Aryltetrahydro-β-carbolines Are Potent Antimalarials In Vitro. *ACS Medicinal Chemistry Letters* **2022**, *13* (3), 371-376. DOI: 10.1021/acsmedchemlett.1c00697.
(63) Richard, S. B.; Lillo, A. M.; Tetzlaff, C. N.; Bowman, M. E.; Noel, J. P.; Cane, D. E. Kinetic Analysis of Escherichia coli 2-C-Methyl-

<scp>d</scp>-erythritol-4-phosphate Cytidyltransferase, Wild Type and Mutants, Reveals Roles of Active Site Amino Acids. *Biochemistry* **2004**, *43* (38), 12189-12197. DOI: 10.1021/bi0487241 (acccessed 2023-06-23T11:23:26).

(64) Clough, J. M.; Dale, R. P.; Elsdon, B.; Hawkes, T. R.; Hogg, B. V.; Howell, A.; Kloer, D. P.; Lecoq, K.; Mclachlan, M. M.; Milnes, P. J.; et al. Synthesis and evaluation of hydroxyazolopyrimidines as herbicides; the generation of amitrole in planta. *Pest Management Science* **2016**, *72* (12), 2254-2272. DOI: 10.1002/ps.4264 (acccessed 2022-04-26T13:53:54).

(65) Burkholder Paul, R.; Pfister Robert, M.; Leitz Frederick, H. Production of a Pyrrole Antibiotic by a Marine Bacterium. *Applied Microbiology* **1966**, *14* (4), 649-653. DOI: 10.1128/am.14.4.649-653.1966 (acccessed 2023/08/03).

(66) Lovell, F. M. The Structure of a Bromine-Rich Marine Antibiotic. *J. Am. Chem. Soc* **1966**, *88*, 4510.

(67) Hegde, R. P.; Pavithra, G. C.; Dey, D.; Almo, S. C.; Ramakumar, S.; Ramagopal, U. A. Can the propensity of protein crystallization be increased by using systematic screening with metals? *Protein Science* **2017**, *26* (9), 1704-1713. DOI: 10.1002/pro.3214 (acccessed 2023-08-03T15:05:10).

(68) Wang, J.; Zhou, Y.; Wang, X.; Duan, L.; Duan, J.; Li, W.; Zhang, A. Synthesis and Evaluation of Halogenated 5-(2-Hydroxyphenyl)pyrazoles as Pseudilin Analogues Targeting the Enzyme IspD in the Methylerythritol Phosphate Pathway. *Journal of Agricultural and Food Chemistry* **2020**, *68* (10), 3071-3078. DOI: 10.1021/acs.jafc.9b08057 (acccessed 2022-04-26T14:11:45).

(69) Wang, J.; Wu, W.; Zhou, Y.; Han, M.; Zhou, X.; Sun, Y.; Zhang, A. Design, synthesis and activity evaluation of pseudilin analogs against cyanobacteria as IspD inhibitors. *Pesticide Biochemistry and Physiology* **2024**, *199*, 105769. DOI: https://doi.org/10.1016/j.pestbp.2024.105769.

(70) Reker, D.; Seet, M.; Pillong, M.; Koch, C. P.; Schneider, P.; Witschel, M. C.; Rottmann, M.; Freymond, C.; Brun, R.; Schweizer, B.; et al. Deorphaning Pyrrolopyrazines as Potent Multi-Target Antimalarial Agents. *Angewandte Chemie International Edition* **2014**, *53* (27), 7079-7084. DOI: 10.1002/anie.201311162 (acccessed 2022-04-26T14:12:29).

(71) Willocx, D.; Bizzarri, L.; Alhayek, A.; Bravo, P.; Illarionov, B.; Rox, K.; Lohse, J.; Fischer, M.; Kany, A. M.; Hahne, H.; et al. Targeting Plasmodium falciparum IspD in the Methyl-D-Erythritol Phosphate Pathway: Urea-Based Compounds with Nanomolar Potency on target with low micromolar whole-cell activity. *ChemRxiv.* **2024**. DOI: doi:10.26434/chemrxiv-2024-15kb1.

(72) Witschel, M.; Röhl, F.; Niggeweg, R.; Newton, T. In search of new herbicidal inhibitors of the non-mevalonate pathway. *Pest Management Science* **2013**, *69* (5), 559-563. DOI: 10.1002/ps.3479 (acccessed 2022-04-26T13:49:32).

(73) Biosca, A.; Ramírez, M.; Gomez-Gomez, A.; Lafuente, A.; Iglesias, V.; Pozo, O. J.; Imperial, S.; Fernàndez-Busquets, X. Characterization of Domiphen Bromide as a New Fast-Acting Antiplasmodial Agent Inhibiting the Apicoplastidic Methyl Erythritol Phosphate Pathway. *Pharmaceutics* **2022**, *14* (7), 1320. DOI: 10.3390/pharmaceutics14071320 (acccessed 2023-08-07T11:20:22).

2. Aims of the Thesis

With the emergence of resistance by pathogens against a growing array of anti-infectives, there is an urgent need to identify unused drug targets. Within this work, we aimed to tackle this challenge by focusing our attention on finding inhibitors for both IspD within the MEP pathway and the energy-coupling factor (ECF) transporters. The MEP pathway enjoys a widespread occurrence spanning from the *Plasmodium* parasites and *Mycobacterium tuberculosis* (*Mt*) to Gram-negative pathogens such as *Pseudomonas aeruginosa* and *Klebsiella pneumoniae,* and Gram-positive pathognes for instance *Clostridium difficile* and *Bacillus anthracis*. The ECF transporters on the other hand, are predominately found in Gram-positive pathogens such as *Streptococcus pneumoniae* and *Staphylococcus aureus*. Moreover, both targets are not present in human cells, reducing the risk of off-target side effects.

Within the initial chapters of this thesis, we sought to address the lack of IspD inhibitors. Previous work performed in collaboration with BASF and the University of Hamburg yielded an initial hit, demonstrating promising activity against IspD originating from *P. falciparum*. A structure–activity relationship (SAR) study around the hit compound led to the identification of a handful of frontrunner compounds for which we determined the ADMET profile and even some *in vivo* properties. Moreover, we included in this work an MS-based enzymatic assay for direct IspD activity determination that we employed to determine the mode of inhibition of the compound class. These results are outlined in Chapter 1

A second IspD hit was discovered during a crystallographic screening conducted against IspD originating from *P. aeruginosa* by collaborators at the Commissariat à l´énergie atomique et aux énergies alternatives, France. We validated the hit with the help of ^{1}H-STD-NMR spectroscopy and initiated preliminary fragment growing efforts. The inhibitory activity of these derivatives was evaluated in the MS-based enzymatic assay against IspD originating from a range of Gram-negative pathogens and *Mt*. Results of this work are outlined in Chapter 2.

Chapter 3 covers our efforts concerning discovery and optimization of inhibitors targeting the ECF transporter. Once the initial hit was identified, we commenced a systematic SAR study to optimize each part of the initial hit sequentially. Having identified the most effective arrangement, we determined the activity of our frontrunner compound in a proteoliposome-based assay and screened its potency against a panel of relevant Gram-positive pathogens.

3. Results

3.1 Chapter 1: Targeting *Plasmodium falciparum* IspD in the Methyl-*D*-Erythritol Phosphate Pathway: Urea-Based Compounds with Nanomolar Potency on target with low micromolar whole-cell activity

Daan Willocx, Lorenzo Bizzarri, Alaa Alhayek, Patricia Bravo, Boris Illarionov, Katharina Rox, Jonas Lohse, Markus Fischer, Andreas M. Kany, Hannes Hahne, Matthias Rottmann, Matthias Witschel, Mostafa M. Hamed, Eleonora Diamanti, Anna K. H. Hirsch

Contributions: Daan Willocx, Eleonora Diamanti, Mostafa M. Hamed, Matthias Witschel, and Anna K. H. Hirsch conceived the project; Synthesis and characterization of the compounds was performed by Daan Willocx, Eleonora Diamanti, Mostafa M. Hamed and Matthias Witschel; HTS and biological evaluation of derivatives against *Pf*IspD was performed by Boris Illarionov and Markus Fischer; Evaluation of the potency against *Pf*NF54 was performed by Patricia Bravo and Matthias Rottmann; Development of the LC-MS based IspD assay and kinetic characterization was performed by Alaa Alhayek, Lorenzo Bizzarri and Andreas M. Kany; ADMET and PK profiling experiments were executed by Andreas M. Kany and Katharina Rox; Daan Willocx wrote the manuscript with contributions from all authors. Anna K. H. Hirsch coordinated the project.

All authors have given approval to the final version of the manuscript.

This chapter is currently under review at the *Journal of Medicinal Chemistry* (ACS)

Targeting *Plasmodium falciparum* IspD in the Methyl-*D*-Erythritol Phosphate Pathway: Urea-Based Compounds with Nanomolar Potency on target with low micromolar whole-cell activity

Daan Willocx,[†,¶,‡] Lorenzo Bizzarri,[ψ,#,¶] Alaa Alhayek,[ψ,†] Patricia Bravo,[§,∥] Boris Illarionov,[⊥] Katharina Rox,[∫,∂] Jonas Lohse,[#] Markus Fischer,[⊥] Andreas M. Kany,[†] Hannes Hahne,[#] Matthias Rottmann,[§,∥] Matthias Witschel[¦], Mostafa M. Hamed,[†] Eleonora Diamanti,[†] Anna K. H. Hirsch*[,†,¶]

[†]Helmholtz Institute for Pharmaceutical Research (HIPS), Helmholtz Centre for Infection Research (HZI), Saarland University, Campus E8.1, 66123 Saarbrücken, Germany

¶Saarland University, Department of Pharmacy, Campus E8.1, 66123 Saarbrücken, Germany

[#]OmicScouts GmbH, Lise-Meitner-Straße 30, 85354 Freising, Germany

[§]Swiss Tropical and Public Health Institute, Kreuzstrasse 2, 4123 Allschwil, Switzerland

[∫]Helmholtz Centre for Infection Research (HZI), Department of Chemical Biology, Inhoffenstraße 7, 38124 Braunschweig, Germany

[∂]German Center for Infection Research (DZIF), Partner site Hannover-Braunschweig, Inhoffenstraße 7, 38124 Braunschweig, Germany

[∥]Universität Basel, Petersplatz 1, 4003 Basel, Switzerland

[⊥]Hamburg School of Food Science, University of Hamburg, Grindelallee 117, 20146 Hamburg, Germany

[¦]BASF-SE, Carl-Bosch-Strasse 38, 67056 Ludwigshafen, Germany

ABSTRACT: The methyl-*D*-erythritol phosphate (MEP) pathway has emerged as an interesting target in the fight against antimicrobial resistance. The pathway is essential in many human pathogens, including *Plasmodium falciparum* (*Pf*), but is absent in human cells, reducing the risk of off-target side effects. In the present study, we conducted a high-throughput screening on the third enzyme of the pathway, IspD, and discovered a new chemical class for which we ran a structure–activity relationship investigation, resulting in low-nanomolar inhibitors of *Pf*IspD. In addition, we determined the whole-cell activity (*Pf*NF54 IC_{50} = 3.4 ± 1.0 μM), mode of inhibition, metabolic, and plasma stability of the new compound class. *In vivo* pharmacokinetic profiling of a selection of compounds demonstrated promising behavior for future development. Lastly, we disclosed a new MS-based enzymatic assay for direct IspD activity determination, circumventing the need for auxiliary enzymes. We used this assay to investigate the mode of inhibition of our new compound class. In summary, we have identified a readily synthesizable compound class, demonstrating excellent activity and a promising profile, positioning it as a valuable tool compound for advancing research on IspD.

Since the commercialization of penicillin in the 1940s, Sir Alexander Fleming warned the public about the dangers of antimicrobial resistance (AMR) resulting from over-and misuse of anti-infectives. Now, decades later, his warnings are more relevant than ever with AMR reaching alarming levels.[1, 2] A recent example of newly developed resistance is the discovery of artemisinin-resistant strains of *Plasmodium falciparum* (*Pf*), one of the parasites that causes malaria, in Africa, Southeast Asia, the Pacific islands, and Latin America. Artemisinin-based treatments have been the 'gold standard' for malaria treatments for many years and resistance will have disastrous effects for malaria-prone regions.[3] The 2-*C*-methylerythritol-D-erythritol-4-phosphate (MEP) pathway, needed for the biosynthesis of the isoprenoid precursors isopentenyl diphosphate (IDP) and dimethylallyl diphosphate (DMADP), is an essential biosynthetic pathway in most Gram-negative bacteria, *Mycobacterium tuberculosis* and the *Plasmodium parasites*. Furthermore, the MEP pathway is absent in human cells, mitigating the risk of off-target side effects, hence making it a source of promising drug targets.[4, 5] Validation of the MEP pathway enzymes as drug target is based on fosmidomycin, an inhibitor of the second protein, IspC or DXR, of the MEP pathway. Currently in second-phase clinical trials as a combination treatment for malaria.[6] Within the present study, we focused on targeting the third enzyme in the MEP pathway, known as, IspD, MEP cytidyltransferase, or *ygbp*. IspD catalyzes the formation of 4-diphosphocytidyl-2-*C*-methylerythritol (CDP-ME) from MEP and cytidine triphosphate (CTP) in

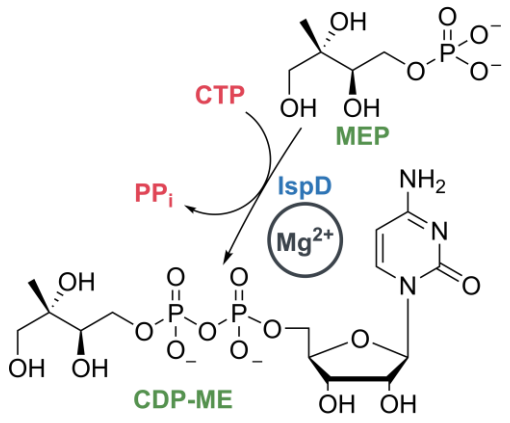

Scheme 1. Reaction catalyzed by IspD starting from MEP and CTP affording CDP-ME. Mg^{2+} is the suspected cofactor in the reaction.

the presence of Mg^{2+}, releasing inorganic diphosphate (PP_i) (Scheme 1).[7] Previously reported inhibitors targeting *Pf*IspD can be subdivided into three chemical classes, namely, benzoisothiazolones **1**, identified by a combined approach of cheminformatics and high-throughput enzymatic screening, MMV008138 **2** recognized through phenotypic screening of the library of GlaxoSmithKline and lastly, a biphenyl carboxylic acid fragment **3** recently discovered by our group in collaboration with BASF (Figure 1). Despite the potential of IspD as a drug target, the number of IspD inhibitors reported is rather low, furthermore, the reported inhibitors are rather elaborated to synthesize or lack whole-cell activity. [5, 8-12] A possible cause might be the lack of a crystal structure of *Pf*IspD available in the Protein Data Bank (PDB). Here, we report the structure–activity relationship (SAR) study of a new urea-based compound class targeting *Pf*IspD with low nanomolar activity *in vitro*. Its synthesis is straightforward, in one step from the corresponding aniline and isocyanate. A high-throughput screening (HTS) approach on *Plasmodium vivax* IspD and subsequent confirmation of hits concomitantly on *Pf*IspD and *Pf*NF54 led to the discovery of the initial hit (**4**, Figure 2) endowed with an IC_{50} of 17 ± 2 µM against *Pf*IspD but lacking whole-cell activity. Synthesis of a total of 33 derivatives shed a light on

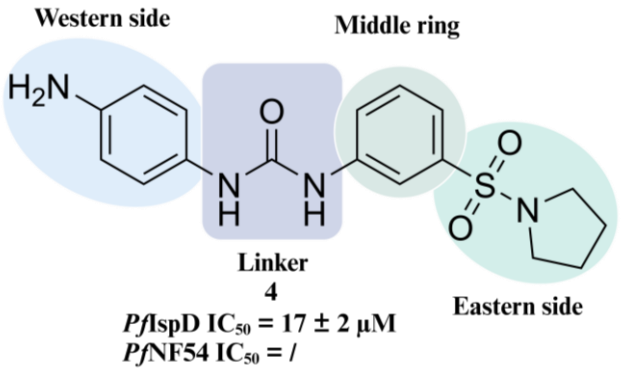

Figure 2. Initial hit compound (**4**) with an overview of the performed SAR study.

the SAR of this newly discovered class reaching IC_{50} values as low as 41 nM and establishing whole-cell activity in low micromolar range. Throughout our study, we made efforts to maintain the easily synthesizable core of the urea class, ensuring the molecule's accessibility, given that antimalarials are predominantly utilized in low and middle-income countries.

RESULTS

SAR Exploration. We commenced exploration of the initial hit by synthesizing derivatives with diverse moieties on the Western side phenyl ring (Figure 2). Compounds **4**–**18** were synthesized as depicted in Scheme 2. Depending on commercial availability, we either generated isocyanates *in situ* by reacting the respective amine with triphosgene or purchased them. Nucleophilic addition between 3-(pyrrolidin-1-ylsulfonyl)aniline and the respective isocyanate afforded the desired compounds. At first, we directed modifications towards the primary amine and replaced it by moieties with different electronic effects (**5**–**11**) (Table 1). We observed that more electron-withdrawing substituents, such as a nitro (**8**) or nitrile group (**10**), had a pronounced effect on the potency, resulting in a factor 400 increase (*e.g.*, **8**, *Pf*IspD IC_{50} = 41 ± 7 nM). While substituents with a less distinct electron-withdrawing effect, such as the trifluoromethyl (**11**) and the

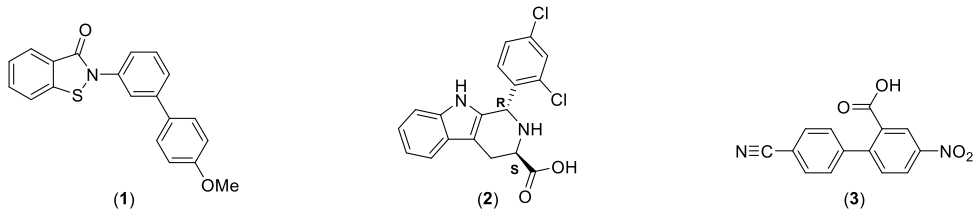

Class	Benzoisothiazolones	MMV-08138	Biphenyl carboxylic acid
***Pf* IspD IC$_{50}$ =**	210 nM	7.1 nM	151 µM
EC$_{50}$=	920 nM[a]	110 nM[b]	No data

Figure 1. Currently known classes of inhibitors showing enzymatic activity against *Pf*IspD. EC_{50} values were measured against different strains of *Plasmodium falciparum*. [a]: strain = 3D7; [b]: strain = W2; Benzoisothiazolones [8] (**1**), MMV-08138[9-12] (**2**), Biphenylcarboxilic acid[5] (**3**).

Table 1. ***In vitro*** **and whole-cell activities for compounds 4–18**

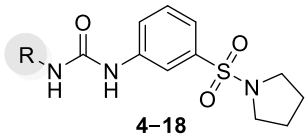

#	Structure, R=	*Pf*IspD (IC_{50} nM)[a]	*Pf*NF54 (IC_{50} μM)[b]	#	Structure, R=	*Pf*IspD (IC_{50} nM)[a]	*Pf*NF54 (IC_{50} μM)[b]
4	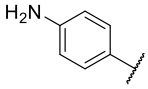	17000 ± 2000	n.a.	**12**	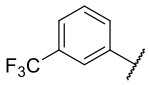	415 ± 60	5.0 ± 0.1
5	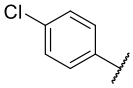	130 ± 12	38 ± 2	**13**	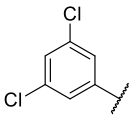	135 ± 30	7.4 ± 0.6
6	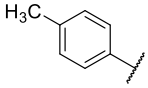	370 ± 80	37 ± 1	**14**	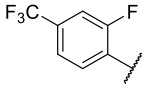	135 ± 30	8.7 ± 1.0
7	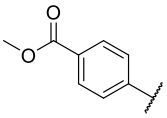	170 ± 20	n.a.	**15**	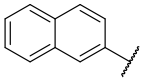	n.a.	23 ± 3
8	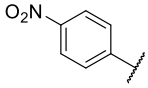	41 ± 7	8.5 ± 1.2	**16**	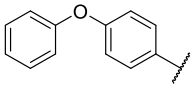	>1000	7.4 ± 1.0
9	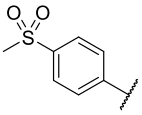	330 ± 40	17 ± 1	**17**	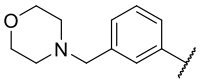	>1000	6.5 ± 0.8
10	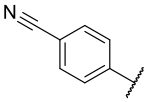	41 ± 11	10 ± 1	**18**	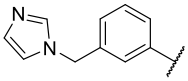	>1000	17 ± 3
11	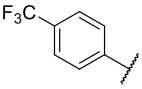	91 ± 19	4.2 ± 0.5				

[a]Assays were performed in replicate as independent experiments ($n \geq 2$); values are shown as mean ± SD. [b]Assays were performed in replicate as independent experiments ($n = 2$); values are shown as mean ± SD. n.a. indicates the absence of activity

chloride (**5**), had a smaller effect on the potency (*e.g*, **11**, *Pf*IspD IC_{50} = 91 ± 19 nM). Lastly, weak donating groups, such as the methyl (**6**), had an even smaller increase in potency (*e.g*, **6**, *Pf*IspD IC_{50} = 370 ± 80 nM), but were still significantly better than the initial hit compound **4**. The reduced increase in potency of **9** (*Pf*IspD IC_{50} = 330 ± 40 nM) could possibly be attributed to the size of the substituent as will be seen later. In addition, low micromolar activity in the whole-cell assay was noted for these derivatives. Next, we explored various substitution patterns on the phenyl ring (**12–14**). Placement of trifluoromethyl in *meta* position (**12**, *Pf*IspD IC_{50} = 415 ± 60 nM) did not improve upon its *para*-substituted counterpart (**11**, *Pf*IspD IC_{50} = 91 ± 19 nM). Furthermore, having multiple substituents (**13–14**) did also not lead to improvements in *Pf*IspD activity over the mono-substituted derivatives. To determine whether there was still room for growth on the Western side, we synthesized analogues **15–18** using the general synthetic route depicted in Scheme 2. Growth in this direction resulted in a significant loss in activity, which we interpret as a lack of space for further expansions. For the remainder of the SAR,

Scheme 2. General synthetic procedure followed for the synthesis of 4–18[a]

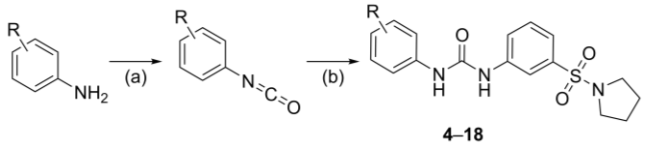

[a]Reagents and conditions: (a) triphosgene, Et_3N, DCM, 0 °C to room temperature, 3 h, used as such in the next reaction step; (b) 3-(pyrrolidin-1-ylsulfonyl)aniline, DMF, room temperature, overnight, 8–95% yield.

we decided to select **8** as scaffold and continued derivatization from its structure. Next, we focused on the urea linker itself (Table 2). Both positions of the urea bond were methylated successively as depicted in Scheme S1. To ensure selective methylation, **19** was synthesized by first transforming 3-(pyrrolidin-1-ylsulfonyl)aniline into the corresponding isocyanate with triphosgene, followed by addition of deprotonated *N*-methyl-4-nitroaniline to the reaction mixture. On the other hand, **20** was synthesized *via* two steps. First, a reductive amination between 3-(pyrrolidin-1-ylsulfonyl)aniline and paraformaldehyde resulted in *N*-methyl-3-(pyrrolidin-1-ylsulfonyl)aniline to which 1-isocyanato-4-nitrobenzene was added, resulting in a nucleophilic addition affording **20**. Unfortunately, methylation of either site of the urea bond led to complete loss of activity. A possible explanation for this observation could be the loss of hydrogen bonding interactions or conformational changes imposed by the methylation. Next we explored the possibility of replacing the urea with a thiourea (**21**) by employing an isothiocyanate in the synthesis instead of an isocyanate. This modification resulted as well in a decrease in activity (**21**, *Pf*lspD IC_{50} = 395 ± 60 nM) in comparison with its urea counterpart (**8**, *Pf*lspD IC_{50} = 41 ± 7 nM). Subsequent, modifications explored the Eastern side of the molecule (Figure 2). For the synthesis of these derivatives (**22–26**), we used the

Scheme 3. Synthesis of compounds 30–36[a]

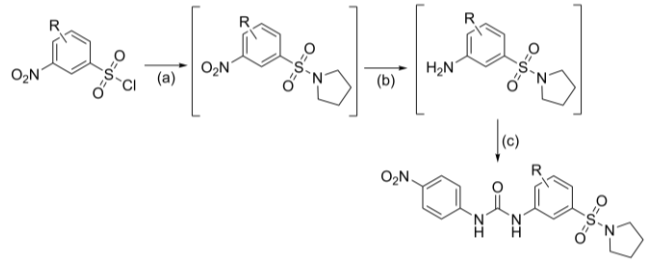

[a]Reagents and reactions conditions: (a) respective 3-nitrobenzenesulfonyl chloride, pyrrolidine, triethylamine, acetonitrile, 0 °C, 5 min; (b) Fe powder, NH_4Cl (166 mM in water), EtOH, 80 °C, 2.5 h; (c) 1-isocyanato-4-nitrobenzene, DMF, room temperature, 4 h, 5–37% yield over three steps.

same synthetic procedure as depicted in scheme 2 with the only difference that the amine was varied instead of the isocyanate. Initially, we replaced the pyrrolidine with more flexible dimethyl (**22**) and diethyl (**23**) amine groups (Table 2). These derivatives did not manage to enhance activity

Table 4 *In vitro* and whole-cell activities for compounds 19–26.

#	Structure, R=	*Pf*lspD (IC_{50} nM)[a]	*Pf*NF54 (IC_{50} µM)[b]
19	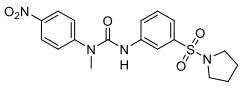	>1000	n.a.
20	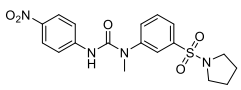	>1000	8 ± 2.0
21	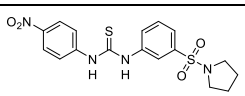	395 ± 60	15 ± 1.0
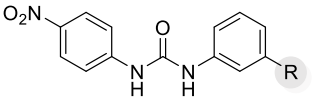 **22–26**			
#	**Structure, R=**	***Pf*lspD (IC_{50} nM)[a]**	***Pf*NF54 (IC_{50} µM)[b]**
22		180 ± 20	n.a.
23	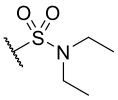	230 ± 25	3.4 ± 1.0
24	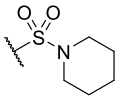	225 ± 20	16 ± 0.6
25	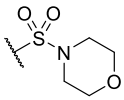	600 ± 110	8.1 ± 0.1
26	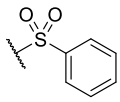	47 ± 7	9.6 ± 0.3

[a]Assays were performed in replicate as independent experiments ($n \geq 2$); values are shown as mean ± SD. [b]Assays were performed in replicate as independent experiments ($n = 2$); values are shown as mean ± SD. n.a. indicates the absence of activity.

(**22**, *Pf*lspD IC_{50} = 180 ± 20 nM) over the pyrrolidine-containing parent compound (**8**, *Pf*lspD IC_{50} = 41 ± 7 nM) (Table 2).

Table 4 ***In vitro*** **and whole-cell activities for compounds 27–36**

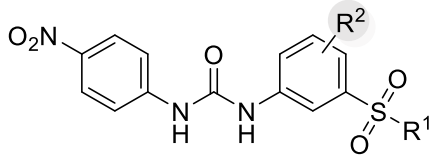

25–34

#	Structure, R¹=	Structure, R²=	*Pf*IspD (IC_{50} µM)[a]	*Pf*NF54 (IC_{50} µM)[b]	#	Structure, R¹=	Structure, R²=	*Pf*IspD (IC_{50} µM)[a]	*Pf*NF54 (IC_{50} µM)[b]
25		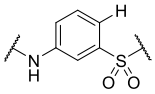	0.6 ± 0.1	8.1 ± 0.1	**32**		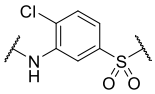	2.1 ± 0.3	16.9 ± 3.2
27		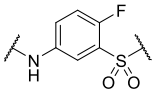	0.4 ± 0.1	7.3 ± 1.3	**33**		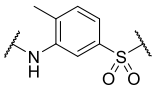	3.6 ± 0.4	11.0 ± 1.7
28		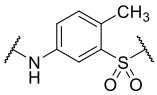	2.4 ± 0.3	2.7 ± 0.2	**34**		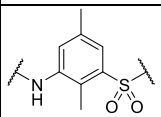	>10	15.3 ± 0.5
29		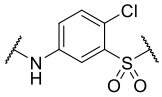	>10	6.9 ± 0.2	**35**		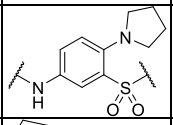	>10	9.7 ± 0.8
30		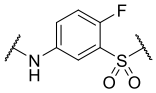	>10	6.3 ± 1.4	**36**		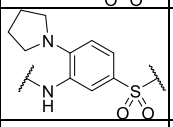	>10	18.0 ± 2.6
31		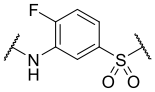	>10	18.4 ± 1.4					

[a]Assays were performed in replicate as independent experiments ($n \geq 2$); values are shown as mean ± SD. [b]Assays were per-formed in replicate as independent experiments ($n \geq 2$); values are shown as mean ± SD. n.a. indicates the absence of activity.

Ring expansion towards piperidine and morpholine likewise failed to increase activity (**24–25**). On the other hand, when we substituted the pyrrolidine with a phenyl ring, the activity could be retained (**26**). Lastly, we explored a handful of compounds containing modifications on the middle ring (Table 3). Initially, these compounds were synthesized containing a morpholine (**27–29**) instead of a pyrrolidine, as anilines of these derivatives were commercially available. Interestingly, compound **27** (*Pf*IspD IC_{50} = 395 ± 3.5 nM) showed enhanced activity over parent compound **25** (*Pf*IspD IC_{50} = 600 ± 110 nM). Consequently, we decided to construct derivatives containing the pyrrolidine (**30–36**). A three-step synthesis led to compounds **30–36** (Scheme 2). As a first step, a nucleophilic substitution reaction took place between pyrrolidine and the respective 3-nitrobenzenesulfonyl chloride. Next, the nitro group was reduced to the amine, which was then reacted with 1-isocyanato-4-nitrobenzene, affording the desired urea compounds (Table 3). After examination of these compounds in our *in vitro* assays, we could not observe any increase in potency over **8**, even not for the derivative containing the 4-fluoro moiety (**30**), which previously triggered a rise in potency. In summary, modifications directed at the Western side of the molecule are most influential towards the activity of the compound class. Positioning electron-withdrawing substituents at the *para* position induced the most notable changes, enabling compounds **8** and **10** to reach IC_{50} values of 41 nM. Other substituents or further expansions at this position did not achieve such an increase in potency. In addition, an unsubstituted urea linker is detrimental for the activity of the compound class. Attempts to modify the middle ring turned out to be futile as any placement of a moiety led to a decrease in activity. On the Eastern side of the molecule, a pyrrolidine or phenyl ring led to the highest *in vitro* activity. Overall, compounds **8**, **10** and **26** are seen as frontrunners of the urea class, exhibiting the best *in vitro* activity, while also showing modest activity in the whole-cell assay. Interestingly, compound **26** constitutes a potential starting point to further explore the urea class by

placing substituents on the phenyl ring or by growing in this direction.

LC-MS based activity assay. To gain an idea on the mode of inhibition of our new compound class, we intended to do a characterization of the enzyme kinetics under a range of inhibitor concentrations. Our intention was to perform this experiment without the influence of auxiliary enzymes inherent to the photometric assay used for IC_{50} determinations.[13] To achieve this goal, we sought to uncover a way to measure the progress of the enzymatic reaction without relying on any secondary reactions. In our exploration, we encountered the work of Li *et al.*, who successfully profiled and quantified MEP metabolites in leaves using liquid chromatography–tandem mass spectrometry.[14] With this information in hand, we sought to develop an IspD activity assay based on the LC-MS detection and quantification of both substrate and product. Initial experiments revealed a significantly more pronounced signal for CDP-ME compared to MEP, with the latter often indistinguishable from background noise.

Table 5. Comparison of Michaelis constants.

	K_m^{CTP} (µM)	K_m^{MEP} (µM)
Our results[a]	58 ± 9	46 ± 3
Wu *et al.*[12]	Not reported	61
Imlay *et al*[10]	59 ± 4	Not reported
Ghavami *et al*[16]	9 ± 3	12 ± 3

[a]Assays were performed in replicate as independent experiments (n = 2); values are shown as mean ± SD

An explanation for this observation might be the difference in ease of ionization, with CDP-ME being more readily ionizable then MEP. Furthermore, we observed identical fragmentation for MEP and the MEP part of CDP-ME, resulting in an overestimation of the MEP concentration. Hence, we decided to continue the assay development relying on the quantification of the product, CDP-ME. Calibration curves measured for CDP-ME demonstrated a linear progression for a wide concentration range showing an R2 of 0.99 (Figure S1). Finally, an internal standard was chosen, initially several unreactive ATP derivatives, such as adenylyl-imidodiphosphate and adenosine-5'-[(α,β)-methyleno]triphosphate were tested, but those exhibited long elution times of 20 to 30 minutes. Ultimately, we chose 4-methyl-1-oxo-1-(p-tolylamino)pentane-2-sulfonic acid as our internal standard, as its elution time was in the range of that of CDP-ME and showed consisted results.[15] To demonstrate the potential of our new assay, we determined the Michaelis constant (K_m) of both substrates and obtained similar results as previously published (Table 4).[10,12,16] To our knowledge, this is the only reported IspD assay that is not dependent on auxiliary enzymes.

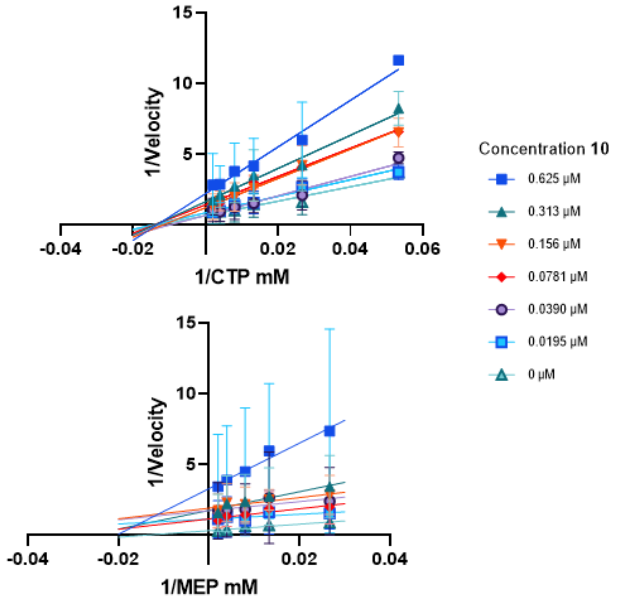

Figure 3. The inhibition of *Pf*IspD by **10** is characterized as non-competitive with CTP, while uncompetitive with MEP. Lineweaver-Burk plots of both substrates at varying concentrations of **10**. Above: CTP was varied; below: MEP concentration was varied.

Mode of inhibition. Next, we measured the influence of **10** on the enzymatic kinetics of both substrates at different concentrations, ranging from 19.5 nM to 625 nM. The results, plotted in Lineweaver—Burk plots, hint towards a non-competitive inhibition of **10** towards CTP and uncompetitive towards MEP (Figure 3, Figure S2 and Figure S3). This finding indicates that compound **10** binds to *Pf*IspD in a manner independent of CTP binding to the active site. In this way, it influences the catalytic activity of the enzyme without affecting CTP binding. This highlights an allosteric inhibition mechanism of the enzyme, which, has been observed before for *Arabidopsis thaliana* IspD by Witschel and coworkers but has never been observed previously for *Pf*IspD.[17] On the other hand, compound **10** selectively targets the *Pf*IspD-MEP complex, influencing the catalytic activity of the enzyme as well as the substrate binding. These findings elucidate the selectivity of compound **10** against both substrates, revealing distinct modulatory effects dependent on the substrate specificity of *Pf*IspD.

Table 6. *In vitro* metabolic and plasma stability of compounds 5, 8, 10 and 26

Model system		5	8	10	26
Mouse Liver S9	$T_{1/2}$ [min][a]	23 ± 3	11 ± 3	20 ± 5	23 ± 3
	Cl_{int} [µl/min/mg][a]	31 ± 4	66 ± 20	36 ± 10	31 ± 4
Human Liver S9	$T_{1/2}$ (min][a]	91 ± 19	53 ± 11	69 ± 12	>120
	Cl_{int} [µl/min/mg][a]	8 ± 2	14 ± 3	10 ± 2	<5
Mouse Plasma	$T_{1/2}$ (min][a]	>150	>150	>150	>150
	% at 2.5 h[a]	>100	>100	>100	>100
Human Plasma	$T_{1/2}$ [min][a]	>150	>150	>150	>150
	% at 2.5 h[a]	>100	>100	>100	>100
HepG2 cytotoxicity	CC_{50} [µM][a]	29 ± 7	62 ± 15	40 ± 5	>100

[a]Assays were performed in duplicate as independent experiments (n = 2); values are shown as mean ± SD

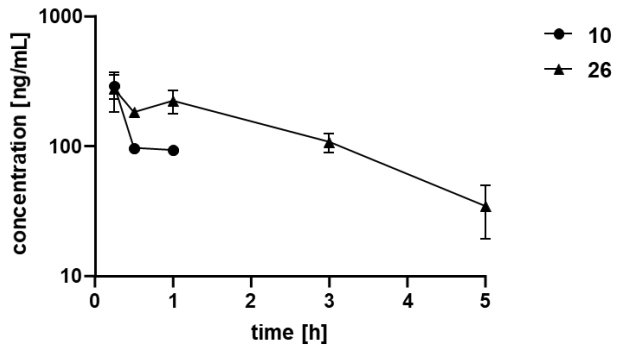

Figure 5. PK plasma profile over time of **10** and **26** at 1 mg/kg IV.

Metabolic and Plasma Stability. To gain an initial understanding of selected ADMET properties of the urea class, the metabolic and plasma stability of selected compounds (**5**, **8**, **10** and **26**), was determined in liver S9 fractions and plasma of both mouse and human (Table 5). Clearance in mouse S9 liver fraction was high to moderate, with compounds **5**, **6** and **26** showing lower clearance than **8** and **37**. In human S9, clearance showed a similar trend with generally lower turnover. No metabolism during 120 min was observed in human S9 fractions for **26**. Regarding plasma stability, all selected compounds showed complete stability in both species (Table 5). Lastly, we also assessed the cytotoxicity towards HepG2 cells. No significant cytotoxicity was observed for **26** up to 100 µM, while the other compounds showed an IC_{50} range of 29–62 µM.

Pharmacokinetic (PK) profiling. As several compounds exhibited promising initial ADMET properties, we embarked on *in vivo* PK studies with compounds **10** and **26**. We administered both compounds in a cassette format *via* the intravenous (IV) route at 1 mg/kg. Whereas compound **10** exhibited a short half-life of only 0.5 h, **26** had a half-life of around 1.6 h suggesting additional clearance mechanisms *in vivo* for compound **10** compared to **26** as the latter had a lower observed plasma clearance compared to **10**. Furthermore, both compounds had a similar volume of distribution of around 2.5–2.9 L/kg, suggesting that compounds might also distribute into tissue (Table 6). Moreover, **26** was still detectable until 5 hours and had higher exposure levels (Figure 5). When looking at terminal organ concentrations, **26** was found at around 203 ng/g tissue in liver, whereas **10** was not detected. This demonstrated that **26** had already favorable PK properties for further development.

Table 7. *In vivo* PK data for compound 10 and 26.

In vivo PK[a]	10	26
$T_{1/2}$ [h]	0.05 ± 0.1	1.55 ± 0.5
C_0 [ng/mL]	912.6 ± 400.2	433.1 ± 256.6
AUC_{0-t} [ng/mL*h]	246.4 ± 63.3	717.4 ± 135.9
MRT [h]	0.6 ± 0.2	2.24 ± 0.7
Vz_obs [L/kg]	2.5 ± 0.8	2.9 ± 1.2
Cl_obs [mL/min/kg]	53.0 ± 8.5	20.9 ± 2.0
Liver ng/g	ND	202.6 ± 45.8

[a]Assays were performed in replicate as independent experiments (n = 2 animals); values are shown as mean ± SD. AUC_{0-t} = area under the concentration-time curve from time zero to time t; MRT = mean residence time; Vz_obs = observed volume of distribution; Cl_obs = observed clearance (based on observed last time point with measurable concentration); ND = not detected

DISCUSSION

With our SAR, we accomplished a 400-fold increase in inhibitory activity of IspD, while also achieving activity in a whole-cell assay (Figure 6). Modifications directed to the Western side of the molecule were most impactful towards the increase in potency, and achieving whole-cell activity. Furthermore, trying to grow at this side of the molecule indicated that there is no space in the binding pocket to further expand in this direction. Adjustments directed at the urea linker, taught us that an unsubstituted urea bond is key for the activity. From there on, modifications directed to the middle ring and Eastern side of the scaffold did not result in further enhancement of the potency. Development of the new LC-MS based activity assay allowed us to gain an idea of the mode of inhibition of this new compound class without the use of auxilary enzymes. Ulitimately, this led to the confirmation of non-competitive inhibition of **10** towards CTP and uncompetitive towards MEP. Therefore, the whole SAR could potentially teach us something about the structure of the allosteric pocket of *Pf*IspD. Structural information of the allosteric pocket could facilitate future research towards *Pf*IspD inhibitors. Especially as the active site of IspD appears to be challenging to target due to its very polar character and solvent-exposure. Lastly, the metabolic clearance and plasma stability experiments demonstrated moderate to good values for some of the representative compounds of the urea class, which were confirmed by *in vivo* PK studies, revealing compound **26** with the best PK properties.

CONCLUSIONS

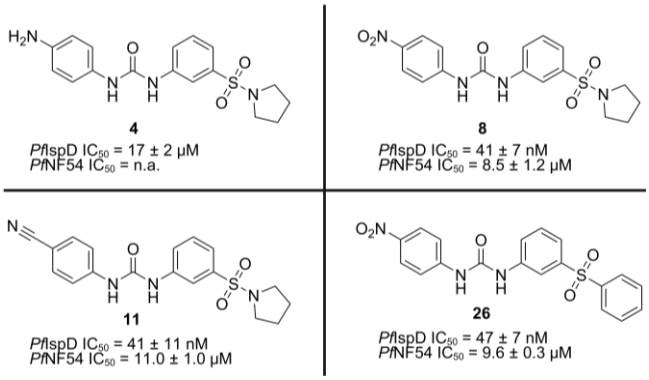

Figure 6. Initial hit compound and the best performing urea class derivatives. n.a. no activity.

In summary, through a HTS campaign, we discovered a new hit compound with an IC_{50} value in the low micromolar range against *Pf*IspD. Conducting SAR around this new chemical entity led to a 400-fold increase in *in vitro* potency and achieved whole-cell activity (Figure 6). The *in vitro* activity of the urea class is on par with other *Pf*IspD inhibitors, with the added benefit of a straightforward synthesis. Utilizing our newly developed LC-MS based IspD assay, we gained insights on the mode of inhibition of our new chemical class, which points towards an allosteric inhibition mechanism. Lastly, initial ADMET and PK studies confirmed the potential of the new class for further development. Overall, due to its potent inhibitory activity, ease to synthesize, interesting mode of inhibition, and good ADMET profile, the urea class has a great potential for further development in the anti-infective field.

EXPERIMENTAL SECTION

General. Purity of all compounds used in biochemical assays was ≥ 95%. Be aware, in contact with water, triphosgene is converted to the extremely toxic phosgene gas. Starting materials and solvents were purchased from commercial suppliers, and used without further purification. All chemical yields refer to purified compounds and were not optimized. Column chromatography was performed using the automated flash chromatography system CombiFlash®Rf (Teledyne Isco) equipped with RediSepRf silica columns. Preparative RP-HPLC was performed either using an UltiMate 3000 Semi-Preparative System (Thermo Fisher Scientific) equipped with nucleodur®C18 Gravity (250 mm × 16 mm, 5 µm) column or using a Pure C-850 Flash/Prep (Buchi) equipped with Nucleodur C18 HTec (250 mm x 40 mm, particle size 5 µm). Low resolution mass spectrometry and purity control of final compounds was carried out using an Ultimate 3000-MSQ LCMS system (Thermo Fisher Scientific) consisting of a pump, an autosampler, MWD detector and an ESI quadrupole mass spectrometer. ^{1}H and ^{13}C NMR spectra were recorded as indicated on a Bruker Avance Neo 500 MHz (^{1}H, 500 MHz; ^{13}C, 126 MHz) with prodigy cryoprobe system. Chemical shifts were recorded as δ values in ppm units and referenced against the residual solvent peak (DMSO-d_6, δ= 2.50, 39.52 and acetone-d_6: δ=2.05, 29.84, CD_3OD: δ= 3.27, 47.6). Splitting patterns describe apparent multiplicities and are designated as s (singlet), br s (broad singlet), d (doublet), dd (doublet of doublet), t (triplet), q (quartet), m (multiplet). Coupling constants (J) are given in Hertz (Hz). High-resolution mass spectra were recorded on a ThermoFisher Scientific (TF, Dreieich, Germany) Q Exactive Focus system equipped with heated electrospray ionization (HESI)-II source. For the LC-MS based IspD assay, a TF UltiMate 3000 binary RSLC UHPLC (Thermo Fisher, Dreieich, Germany) equipped with a degasser, a binary pump, an autosampler, and a thermostated column compartment and a MWD, coupled to a TF TSQ Quantum Access Max mass spectrometer with heated electrospray ionization source (HESI-II) was used. The separation was performed with a SeQuant ZIC-HILIC 5 µM polymeric HPLC column (100 * 2.1 mm) with a precolumn at flow rate of 0.225 µL/min with a mobile phase composed of 50 mM ammonium acetate pH 8.5 (elute A), ACN (eluent B) under the following conditions: 0 – 30 sec 80% B, 30 – 105 sec 70% B, 105 – 135 sec 70–40% B, 135 – 300 sec hold, and 300 - 420 sec 80% B

with 225 µL/min flow rate and a total run time of 7 min. The divert valve was set to 0.49 min. The injection volume was 5 µL. The temperature of the autosampler was set to 6 °C. The following MS settings were used: electrospray ionization (ESI); negative mode for CDP-ME and MEP; collision gas pressure: 1.5 Torr; spray voltage: 10 V. The mass spectrometer was operated in the SRM mode with the following masses: 520.116 (fragment: 322.135 - 322.145) m/z for CDP-ME (tube lens offset 93 V and collision energy 23 eV); 215.006 (fragment: 79.395 - 79.405, 97.395 - 97.405) m/z for MEP (tube lens offset 94 V and collision energy 23 and 47 eV, respectively); 284.07 (fragment: 106.19, 177.03 - 150.15) m/z for 4-methyl-1-oxo-1-(p-tolylamino)pentane-2-sulfonic acid (tube lens offset 28 and 21 respectively V and collision energy 28 and 21 eV, respectively) with a scan width of 0.010 m/z and a scan time of 0.1 s, respectively. Observed retention times were as follows: CDP-ME, MEP, and 4-methyl-1-oxo-1-(p-tolylamino)pentane-2-sulfonic acid 4.90, 4.72, and 1.04 min, respectively (Figure S4). MS-peak areas were determined using TF Xcalibur Software then CDP-ME and MEP peak areas were normalized by the internal standard peak area. All PK plasma samples were analyzed via HPLC-MS/MS using an Agilent 1290 Infinity II HPLC system coupled to an AB Sciex QTrap 6500plus mass spectrometer. HPLC conditions were as follows: column: Agilent Zorbax Eclipse Plus C18, 50x2.1 mm, 1.8 µm; temperature: 30 °C; injection volume: 5 µL; flow rate: 700 µL/min; solvent A: water + 0.1% formic acid; solvent B: acetonitrile + 0.1% formic acid; gradient for 10 and 26: 99% A at 0 min, 99% - 0% A from 0.1 min to 4.0 min, 0 % A until 4.5 min. Mass spectrometric conditions were as follows: Scan type: Q1 and Q3 masses for glipizide, **10** and **26** can be found in Table S1; peak areas of each sample and of the corresponding internal standard were analyzed using Multi-Quant 3.0 software (AB Sciex).

Chemistry.

General procedure 1 (GP-1) for the synthesis of analogues 5–12. To a flask containing 3-(pyrrolidin-1-ylsulfonyl)aniline (1 equiv), and DMF (150 equiv, unless otherwise stated), the respective isocyanate (1 equiv) was added at 0 °C. The resulting mixture was stirred at room temperature overnight, after which, water was added, and the resulting mixture was extracted with EtOAc (3x, 20mL). The combined organic layers were washed with saturated aqueous NaCl solution, dried over $MgSO_4$, filtered, concentrated *in vacuo*, and purified.

General procedure 2 (GP-2) for the synthesis of analogues 13–18. To a flask that contains triphosgene (0.5 equiv) in DCM (150 equiv, unless otherwise stated) at 0 °C under argon atmosphere, a solution of DCM (150 equiv, unless otherwise stated) containing the respective amine (1.2 equiv) and trimethylamine (1.2 equiv) was added and resulting mixture was stirred at room temperature for 3 h. Next, a flask was charged with 3-(pyrrolidin-1-ylsulfonyl)aniline (1 equiv), NaH 60% (1.2 equiv) and DMF (150 equiv), the resulting mixture was stirred for 1 h under argon atmosphere, after which, the solution was added dropwise to the flask containing the triphosgene reaction mixture and the resulting solution was stirred at room temperature overnight. Water (20 mL) was added and the mixture was extracted with EtOAc (3x, 20mL), washed with saturated aqueous NaCl solution, dried over $MgSO_4$, filtered, concentrated *in vacuo*, and purified.

General procedure 3 (GP-3) for the synthesis of analogues 22–29. To a flask containing 1-isocyanato-4-nitrobenzene and DMF (150 equiv, unless otherwise stated), the respective aniline (1 equiv) was added at room temperature. The resulting mixture was stirred at room temperature overnight, after which, water was added and the resulting mixture was extracted with EtOAc (3x, 20mL). The combined organic layers were washed with saturated aqueous NaCl solution, dried over $MgSO_4$, filtered, concentrated *in vacuo*, and purified.

General procedure 4 (GP-4) for the synthesis of analogues 30–34. To a flask containing acetonitrile (100 equiv), trimethylamine (2 equiv), and pyrrolidine (1 equiv) at 0 °C, the respective 3-nitrobenzenesulfonyl chloride (1 equiv) was added. Next the resulting solution was stirred for 5 min at 0 °C, after which, the solvent was evaporated. To the residue, EtOH (140 equiv), an aqueous solution of NH_4Cl at a concentration of 166 mM (0,50 equiv), and Fe powder (5 equiv) were added, the resulting reaction mixture was stirred at 80 °C for 2,5 h. Next, the organic solvent was evaporated *in vacuo*, water (20 mL) was added, and the solution was extracted with EtOAc (3x, 20mL). The combined organic layers were dried over $MgSO_4$, filtered, and concentrated *in vacuo*. Subsequent, the residue was solubilised with DMF (45 equiv), and 1-isocyanato-4-nitrobenzene (1.5 equiv) was added. The resulting reaction mixture was stirred at room temperature for 1 h, after which, DMF was removed on reduced pressure and the residue was purified.

1-(4-Aminophenyl)-3-(3-(pyrrolidin-1-ylsulfonyl)phenyl)urea (**4**) A mixture of 1-(4-nitrophenyl)-3-(3-(pyrrolidin-1-ylsulfonyl)phenyl)urea (**8**) (0.15 g, 0.4 mmol), Fe (0.11 mg, 1.9 mmol), and ammonium chloride (0.01 g, 0.2 mmol) was dissolved in an ethanol/water (2:1) mixture. The mixture was heated to 100°C for 2 hours. Excess ethanol was evaporated *in vacuo*, and the remaining residue was washed with water (3x, 20 mL), and then filtered. The obtained solid was then purified using preparative HPLC affording **4** as a white powder (0.1 g, 72% yield).

^{1}H NMR (500 MHz, DMSO-d_6) δ 10.60 (s, 1H), 10.51 (s, 1H), 8.22 (d, J = 9.1, 2H), 8.08 (s, 1H), 7.82 (d, J = 9.1, 2H), 7.75 (d, J = 7.9, 1H), 7.61 (t, J = 7.8, 1H), 7.56 (d, J = 7.8, 1H), 3.17 (t, J = 6.6, 4H), 1.66 (t, J = 6.6, 4H). ^{13}C NMR (126 MHz, DMSO-d_6) δ 179.7, 145.8, 142.6, 140, 136.2, 129.7, 127.5, 124.5, 123.3, 122.2, 121.8, 47.9, 24.8. HR-MS (ESI) calculated for $C_{17}H_{21}N_4O_3S$ $[M + H]^+$: 361.1256, found: 361.1327

1-(4-Chlorophenyl)-3-(3-(pyrrolidin-1-ylsulfonyl)phenyl)urea (**5**). According to **GP-1**, using 1-chloro-4-isocyanatobenzene (0.08 g, 0.49 mmol), affording after purification by flash chromatography (CH_2Cl_2/MeOH, 10/0 → 9.5/0.5), and washing with MeOH, **5** was afforded as a white powder (22 mg, 11% yield). ^{1}H NMR (500 MHz, DMSO-d_6) δ 9.1 (s, 2H), 8.1 (t, J = 2.0, 1H), 7.7–7.6 (m, 1H), 7.6–7.5 (m, 3H), 7.4 (d, J = 7.7, 1H), 7.4–7.3 (m, 2H), 3.2–3.1 (m, 4H), 1.7–1.6 (m, 4H). ^{13}C NMR (126 MHz, DMSO-d_6) δ 152.9, 141, 138.9, 137, 130.3, 129.1, 126.1, 122.7, 120.8, 120.5, 116.9, 48.3, 25.2. HR-MS (ESI) calculated for $C_{17}H_{19}ClN_3O_3S$ [M+H]$^+$, 380.0757, found: 380.0822. HPLC purity: 98%.

1-(3-(Pyrrolidin-1-ylsulfonyl)phenyl)-3-(p-tolyl)urea (**6**).According to **GP-1**, using *p*-tolyl isocyanate (0.06 mL, 0.48 mmol), afforded after purification by flash chromatography (cyclohexane/EtoAc = 1:1) **6** as white solid (0.15 g, 95% yield). ^{1}H NMR (500 MHz, DMSO-d_6) δ 9.0 (s, 1H), 8.7 (s, 1H), 8.1 (t, J = 2.0, 1H), 7.6–7.5 (m, 1H), 7.5 (t, J = 7.9, 1H), 7.4–7.3 (m, 3H), 7.1 (d, J = 8.3, 2H), 3.2–3.1 (m, 4H), 2.3 (s, 3H), 1.7–1.6 (m, 4H). ^{13}C NMR (126 MHz, DMSO-d_6) δ 153, 137.2, 137, 131.5, 130.2, 129.7, 122.5, 120.6, 119.1, 116.7, 48.3, 25.2, 20.8. HR-MS (ESI) calculated for $C_{18}H_{22}N_3O_3S$ [M + H]$^+$, 360.1304, found: 360.1361. HPLC purity: 99%.

Methyl4-(3-(3-(pyrrolidin-1-ylsulfonyl)phenyl)ureido)benzoate (**7**). According to **GP-1**, using methyl 4-isocyanatobenzoate (0.088 g, 0.5 mmol), and CH_2Cl_2 (10 mL), to afford after filtration of the precipitate, **7** as a white solid (0.15 g, 75% yield). ^{1}H NMR (500 MHz, DMSO-d_6) δ 9.2 (br s, 2H), 8.1 (t, J = 1.8 Hz, 1H), 7.9 (d, J = 8.7 Hz, 2H), 7.7–7.6 (m, 3H), 7.6 (t, J = 7.9 Hz, 1H), 7.4 (d, J = 7.6 Hz, 1H), 3.8 (s, 3H), 3.2–3.1 (m, 4H), 1.7–1.6 (m, 4H). ^{13}C NMR (126 MHz, DMSO-d_6) δ 166.4, 152.7, 144.5, 140.7, 137.1, 130.9, 130.4, 123.2, 122.8, 121.1, 118.1, 117.1, 52.3, 48.3, 25.2. HR-MS (ESI) calculated for $C_{19}H_{22}N_3O_5S$ [M + H]$^+$: 404.1202, found: 404.1275. HPLC purity: 98%

1-(4-Nitrophenyl)-3-(3-(pyrrolidin-1-ylsulfonyl)phenyl)urea (**8**). According to **GP-1**, using 1-isocyanato-4-nitrobenzene (0.1 g, 0.61 mmol), to afford after purification by flash chromatography (CH_2Cl_2/MeOH, 10/0 → 9.5/0.5), **8** as a yellow powder (0.02 g, 8% yield). ^{1}H NMR (500 MHz, DMSO-d_6) δ 9.6 (br s, 1H), 9.4 (br s, 1H), 8.2 (br d, J = 8.9 Hz, 2H), 8.1 (br s, 1H), 7.7 (br d, J = 8.4 Hz, 2H), 7.7 (br d, J = 7.6 Hz, 1H), 7.6 (br t, J = 7.9 Hz, 1H), 7.4 (br d, J = 7.6 Hz, 1H), 3.2–3.1 (m, 4H), 1.7 (br s, 4H). ^{13}C NMR (126 MHz, DMSO-d_6) δ 152.1, 146.1, 141.2, 140, 136.6, 129.9, 125.1, 122.5, 120.9, 117.9, 117.8, 116.8, 47.9, 24.7. HR-MS (ESI) calculated for $C_{17}H_{19}N_4O_5S$ [M + H]$^+$: 391.0998, found: 391.1066. HPLC purity: 100%.

1-(4-(Methylsulfonyl)phenyl)-3-(3-(pyrrolidin-1-ylsulfonyl)phenyl)urea (**9**). According to **GP-1**, using 1-isocyanato-4-(methylsulfonyl)benzene (0.99 g, 0.5 mmol) and, DCM (10 mL), to afford after filtration of the precipitate **9** as a white powder (0.15 g, 70% yield). ^{1}H NMR (500 MHz, DMSO-d_6) δ 9.29 (br s, 2H), 8.1–8.0 (m, 1H), 7.8 (d, J = 8.9 Hz, 2H), 7.7 (d, J = 8.9 Hz, 2H), 7.7 – 7.6 (m, 1H), 7.5 (t, J = 7.9 Hz, 1H), 7.4 (d, J = 7.8 Hz, 1H), 3.2–3.1 (m, 7H), 1.7–1.6 (m, 4H). ^{13}C NMR (126 MHz, DMSO-d_6) δ 152.7, 144.7, 140.6, 137.1, 133.9, 130.4, 128.8, 122.9, 121.2, 118.5, 117.2, 48.3, 44.4, 25.2. HR-MS (ESI) calculated for $C_{18}H_{22}N_3O_5S_2$ [M + H]$^+$: 424.0923, found: 424.0997. HPLC purity: 99%.

1-(4-Cyanophenyl)-3-(3-(pyrrolidin-1-ylsulfonyl)phenyl)urea (**10**). According to **GP-1**, using 4-isocyanatobenzonitrile (0.1 g, 0.69 mmol), to afford after purification by flash chromatography (CH_2Cl_2/MeOH, 10/0 → 9.5/0.5) and recrystallization with CH_2Cl_2, and diethyl ether, **10** as a yellow powder (0.075 g, 29 % yield). ^{1}H NMR (500 MHz, DMSO-d_6) δ 9.3 (br s, 2H), 8.1 (t, J = 1.8 Hz, 1H), 7.8–7.7 (m, 2H), 7.7–7.6 (m, 2H), 7.7–7.6 (m, 1H), 7.6 (t, J = 7.9 Hz, 1H), 7.4 (d, J = 7.8 Hz, 1H), 3.2–3.1 (m, 4H), 1.7–1.64 (m, 4H). ^{13}C NMR (126 MHz, DMSO-d_6) δ 152.6, 144.4, 140.6, 137.1, 133.8, 130.4, 123, 121.3, 119.7, 118.8, 117.2, 104.1, 49.1, 48.3, 25.2. HR-MS (ESI) calculated for $C_{18}H_{19}N_4O_3S$ [M + H]$^+$: 371.1010, found: 371.1157. HPLC purity: 98%.

1-(3-(Pyrrolidin-1-ylsulfonyl)phenyl)-3-(4-(trifluoromethyl)phenyl)urea (**11**). According to **GP-1**, using 1-isocyanato-4-(trifluoromethyl)benzene (0.09 g, 0.5 mmol), and DCM (10 mL), to afford after filtration of the precipitate, **11** as an off-white powder (0.09 g, 0.213 mmol, 43% yield). ^{1}H NMR (500 MHz, DMSO-d_6) δ 9.2 (s, 1H), 8.1 (t, J = 1.8 Hz, 1H), 7.7–7.6 (m, 1H), 7.6–7.5 (m, 1H), 7.5 (t, J = 7.9 Hz, 1H), 7.4 (d, J = 7.8 Hz, 1H), 3.2–3.1 (m, 1H), 1.7–1.6 (m, 1H). ^{13}C NMR (126 MHz, DMSO-d_6) δ 152.8, 143.6, 140.7, 137.1, 130.4, 126.7 – 126.5 (m), 122.9, 121.1, 118.7, 117.1, 48.3, 25.2. ^{19}F NMR (470 MHz DMSO-d_6) δ -60.1. HR-MS (ESI) calculated for $C_{18}H_{19}F_3N_3O_3S$ [M + H]$^+$: 414.1021, found: 414.1087. HPLC purity: 99%.

1-(3-(Pyrrolidin-1-ylsulfonyl)phenyl)-3-(3-(trifluoromethyl)phenyl)urea (**12**). According to **GP-1**, using 1-isocyanato-3-(trifluoromethyl)benzene (0.07 g , 0.35 mmol), to afford after purification by flash chromatography (EtOAc/petroleum ether, 3/7 → 5/5), recrystallization using MeOH, and washing with CH_2Cl_2 (3x, 5 mL), **12** as a white crystalline powder (0.01 g, 8% yield). ^{1}H NMR (500 MHz, CD_3OD) δ 8.1 (t, J = 1.9 Hz, 1H), 7.9 (s, 1H), 7.7 (ddd, J = 8.0, 2.2, 1.2 Hz, 1H), 7.6 (dd, J = 8.2, 1.6 Hz, 1H), 7.6–7.5 (m, 1H), 7.5–7.4 (m, 2H), 7.3–7.2 (m, 1H), 3.3–3.2 (m, 4H), 1.8–1.7 (m, 4H). ^{13}C NMR (126 MHz, CD_3OD) δ 153.3, 140.2, 140, 137.2, 129.4 (d, J = 4.4), 125.3, 123.1, 122.7, 122, 121.1, 118.8, 117.4, 115.2, 47.8, 24.8. ^{19}F NMR (470 MHz DMSO-d_6) δ -61.3. HR-MS (ESI) calculated for $C_{18}H_{19}F_3N_3O_3S$ [M + H]$^+$: 414.1021, found: 414.1088. HPLC purity: 98%.

1-(3,5-Dichlorophenyl)-3-(3-(pyrrolidin-1-ylsulfonyl)phenyl)urea (**13**). According to **GP-2**, using 1,3-dichloro-5-isocyanatobenzene (0.09 g, 0.48 mmol) to afford **13** after evaporation of the solvent as white solid (0.14 g, 77%). ^{1}H NMR (500 MHz, DMSO-d_6) δ 9.4–9.1 (m, 2H), 8.1 (t, J = 1.8 Hz, 1H), 7.7–7.6 (m, 1H), 7.6–7.5 (m, 3H), 7.4 (d, J = 7.8 Hz, 1H), 7.2 (t, J = 1.8 Hz, 1H), 3.2–3.1 (m, 4H), 1.7–1.6 (m, 4H). ^{13}C NMR (126 MHz, DMSO-d_6) δ 152.7, 142.5, 140.6, 137.1, 134.6, 130.4, 123, 121.7, 121.2, 117.2, 117.1, 48.3, 25.2. HR-MS (ESI) calculated for $C_{17}H_{18}Cl_2N_3O_3S$ [M + H]$^+$: 414.0368, found: 414.0430. HPLC purity: 99%

1-(2-Fluoro-4-(trifluoromethyl)phenyl)-3-(3-(pyrrolidin-1-ylsulfonyl)phenyl)urea (**14**). According to **GP-2**, 2-fluoro-4-

(trifluoromethyl)aniline (0.14 g, 0.79 mmol), to afford after purification by flash chromatography (cyclohexane/EtoAc = 1:1), **14** as white powder (0.04 g, 15 % yield). ^{1}H NMR (500 MHz, DMSO-d_6) δ 9.6 (br s, 1H), 9.0 (br s, 1H), 8.4 (t, J = 8.3 Hz, 1H), 8.1 (s, 1H), 7.8–7.7 (m, 1H), 7.6–7.5 (m, 3H), 7.5–7.4 (m, 1H), 3.2–3.1 (m, 4H), 1.7–1.6 (m, 4H). ^{13}C NMR (126 MHz, DMSO-d_6) δ 151.9, 151.7, 145.0, 139.7, 136.5, 129.9, 122.1, 121.9–121.6, 120.7, 120.1, 116.2, 47.7, 24.5. ^{19}F NMR (470 MHz DMSO-d_6) δ -60.2, -127.7. HR-MS (ESI) calculated for $C_{18}H_{18}F_4N_3O_3S$ [M + H]$^+$: 432.0927, found : 432.0995. HPLC purity: 99%.

1-(Naphthalen-2-yl)-3-(3-(pyrrolidin-1-ylsulfonyl)phenyl)urea (**15**). According to **GP-2**, naphtalen-2-amine (0.1 g, 0.70 mmol), to afford after washing with MeOH (5x, 5mL), **15** as an off-white solid (0.02 g, 8% yield). ^{1}H NMR (500 MHz, DMSO-d_6) δ 9.2 (s, 1 H), 9.0 (s, 1 H), 8.2 (s, 1 H), 8.1 (s, 1 H), 7.9 (br d, J=8.85, 2 H), 7.8 (br d, J = 9.77, 1 H), 7.6 (d, J=8.06, 1 H), 7.6 (t, J=7.93, 1 H), 7.5 (dd, J = 8.77, 2.06, 1 H), 7.5 (t, J=7.48, 1 H), 7.4–7.3 (m, 2 H), 3.2–3.1 (m, 4 H), 1.7–1.6 (m, 4 H). ^{13}C NMR (126 MHz, DMSO-d_6) δ 152.7–152.8, 152.7, 140.7, 138.9–142.1, 137.2, 136.7, 133.8, 130, 129.4, 128.6, 127.6, 127.2, 126.6, 124.3, 122.3, 120.5, 120, 116.5, 114, 48, 24. HR-MS (ESI) calculated for $C_{21}H_{22}N_3O_3S$ [M + H]$^+$: 396,1304, found: 396.1364. HPLC purity: 99%.

1-(4-Phenoxyphenyl)-3-(3-(pyrrolidin-1-ylsulfonyl)phenyl)urea **16**. According to **GP-2**, using 4-phenoxyaniline (0.17 g, 0.94 mmol), to afford after purification with flash chromatography (cyclohexane/EtOAc = 7:3) **16** as a white solid (0.18 g, 44%). ^{1}H NMR (500 MHz, DMSO-d_6) δ 9.1 (s, 1H), 8.8 (s, 1H), 8.1 (t, J = 2.0, 1H), 7.6 (ddd, J = 8.2, 2.3, 1.0, 1H), 7.5 (t, J = 7.9, 1H), 7.5–7.4 (m, 2H), 7.4–7.3 (m, 3H), 7.1 (t, J = 7.5, 1H), 7.0 (m, 4H), 3.2–3.1 (m, 4H), 1.7–1.6 (m, 4H). ^{13}C NMR (126 MHz, DMSO-d_6) δ 158.1, 153.1, 151.4, 141.2, 137, 135.8, 130.4, 130.3, 123.3, 122.6, 120.9, 120.7, 120.2, 118.1, 116.8, 48.3, 25.2. HR-MS (ESI) calculated for $C_{23}H_{24}N_3O_4S$ [M + H]$^+$: 438.1409, found: 438.1474. HPLC purity: 99%.

1-(3-(Morpholinomethyl)phenyl)-3-(3-(pyrrolidin-1-ylsulfonyl)phenyl)urea (**17**). According to **GP-2**, 3-(morpholinomethyl)aniline (0.1 g, 0.52 mmol), to afford after washing with MeOH (5x, 5 mL), **17** as a yellow crystalline powder (0.09 g, 31% yield). ^{1}H NMR (500 MHz, DMSO-d_6) δ 9.1 (s, 1 H), 8.8 (s, 1 H), 8.1 (t, J =1.91, 1 H), 7.6 (dd, J =8.16, 1.14, 1 H), 7.5 (t, J=7.93, 1 H), 7.4 (s, 1 H), 7.4 – 7.3 (m, 2 H), 7.3–7.2 (m, 1 H), 7.0–6.9 (m, 1 H), 3.6 (t, J=4.50, 4 H), 3.4 (s, 2 H), 3.2–3.1 (m, 4 H), 2.4 (br s, 4 H), 1.7 –1.6 (m, 4 H). ^{13}C NMR (126 MHz, DMSO-d_6) δ 152.4, 140.6, 139.3, 138.6, 136.5, 129.8, 128.6, 122.8, 122.1, 120.2, 118.8, 117.2, 116.3, 66.2, 62.5, 53.2, 47.8, 24.7. HR-MS (ESI) calculated for $C_{22}H_{29}N_4O_4S$ [M + H]$^+$: 445,1831 , found: 445,1899. HPLC purity: 98%.

1-(3-((1H-Imidazol-1-yl)methyl)phenyl)-3-(3-(pyrrolidin-1-ylsulfonyl)phenyl)urea (**18**). According to **GP-2**, using 3-((1*H*-imidazol-1-yl)methyl)aniline (0.1 g, 0.58 mmol), to afford after washing with MeOH (5x, 5 mL), **18** as a white solid (0.01 g, 4% yield). ^{1}H NMR (500 MHz, DMSO-d_6) δ 9.2 (br s, 1H), 8.9 (br s, 1H), 8.1 (s, 1H), 7.8 (s, 1H), 7.6–7.5 (m, 1H), 7.5 (t, J = 7.9 Hz, 1H), 7.4–7.3 (m, 2H), 7.4–7.3 (m, 1H), 7.3 (t, J = 7.9 Hz, 1H), 7.2–7.1 (m, 1H), 6.9 (s, 1H), 6.9–6.8 (m, 1H), 5.2 (s, 2H), 3.1 (br t, J = 6.6 Hz, 4H), 1.7–1.6 (m, 4H). ^{13}C NMR (126 MHz, DMSO-d_6) δ 152.4, 140.5, 139.7, 138.4, 136.4, 129.7, 129, 122, 120.9, 120.1, 117.6, 117.1, 116.1, 49.4, 47.7, 24.6. HR-MS (ESI) calculated for $C_{21}H_{24}N_5O_3S$ [M + H]$^+$: 426,1522 , found: 426.1582. HPLC purity: 98%.

1-Methyl-1-(4-nitrophenyl)-3-(3-(pyrrolidin-1-ylsulfonyl)phenyl)urea (**19**). To a flask containing triphosgene (0.08 g, 0.27 mmol), and DCM (2 mL) at 0 °C under argon atmosphere, a solution containing 3-((1*H*-imidazol-1-yl)methyl)aniline (0.13 g, 0.89 mmol), trimethylamine (247 mL, 1.78 mmol), and DCM (2 mL), was added. The resulting solution was stirred at room temperature for 2 h. To a different flask, *N*-methyl-4-nitroaniline (0.13 g, 0.89 mmol), sodium hydride (0.03 mg, 1.19 mmol), and DMF (2.5 mL) were added, the resulting solution was stirred at room temperature for two hours, after which, it was added dropwise to the solution containing triphosgene. The resulting mixture was stirred at room temperature for 1 h, next water was added and the mixture was extracted with EtOAc (5x, 20 mL). The combined organic layers were washed with saturated aqueous NaCl solution, dried over $MgSO_4$, filtered, concentrated *in vacuo*, and purified by column chromatography, (CH_2Cl_2/MeOH, 10/0 → 9.5/0.5), and recrystallization (CH_2Cl_2/ diethyl ether), to afford **19** as a yellow solid (0.12 g, 32% yield). ^{1}H NMR (500 MHz, DMSO-d_6) δ 9.2 (s, 1H), 8.3–8.2 (m, 1H), 8.0 (t, J = 1.9 Hz, 1H), 7.8 (dd, J = 8.1, 1.4 Hz, 1H), 7.7–7.6 (m, 1H), 7.5 (t, J = 8.0 Hz, 1H), 7.4 (d, J = 7.8 Hz, 1H), 3.4 (s, 1H), 3.2–3.1 (m, 1H), 1.7–1.6 (m, 1H). ^{13}C NMR (126 MHz, DMSO-d_6) δ 154.7, 150.6, 143.9, 141.1, 136.7, 130, 125.4, 124.9, 124.3, 121.5, 118.8, 48.3, 37.4, 25.2. HR-MS (ESI) calculated for: $C_{18}H_{21}N_4O_5S$ [M + H]$^+$: 405.1154, found: 405.1214. HPLC purity: 99%.

1-Methyl-3-(4-nitrophenyl)-1-(3-(pyrrolidin-1-ylsulfonyl)phenyl)urea (**20**). A flask was charged with 3-(pyrrolidin-1-ylsulfonyl)aniline (0.1 g, 0.44 mmol), paraformaldehyde (0.09 g), and MeOH (5 mL). The resulting solution was stirred at room temperature for 2.5 h, after which, $NaBH_4$ (0.03 g, 0.88 mmol) was added. The resulting mixture was stirred at 60 °C for 16 h, next, water (20 mL) was added, and the mixture was extracted with EtOAc (5x, 20 mL). The combined organic layers were washed with saturated aqueous NaCl solution, dried over $MgSO_4$, filtered, concentrated *in vacuo,* and purified by flash chromatography (EtOAc/petrolium benzyne 3/7 → 6/4) affording *N*-methyl-3-(pyrrolidin-1-ylsulfonyl)aniline (0.06 g, 0.25 mmol, 57% yield) which was added to a flask containing 1-isocyanato-4-nitrobenzene (0.07 g, 0.28 mmol), and DMF (5 mL). The solution was stirred at room temperature overnight, next, water (20 mL) was added, and the resulting mixture was extracted with EtOAc (5x, 20 mL). The combined organic layers were washed with saturated aqueous NaCl solution, dried over $MgSO_4$, filtered, concentrated *in vacuo*, purified by flash chromatography (CH_2Cl_2/MeOH, 10/0 → 9.5/0.5), and recrystallized (MeOH, CH_2Cl_2 and diethyl ether) to afford **20** as an off-white solid (0.02 g, 12% yield). ^{1}H NMR (500

MHz, DMSO-d_6) δ 9.2 (br s, 1H), 8.2 (d, J = 9.2 Hz, 2H), 7.8–7.6 (m, 6H), 3.4 (s, 3H), 3.2–3.1 (m, 4H), 1.7–1.6 (m, 4H) ^{13}C NMR (126 MHz, DMSO-d_6) δ 154.5, 147.4, 144.9, 141.6, 137.2, 130.7 (d, J = 10.9), 125.1, 124.9, 119.1, 48.3, 38.1, 25.1. HR-MS (ESI) calculated for: $C_{18}H_{21}N_4O_5S$ [M + H]$^+$: 405.1154, found: 405.1215. HPLC purity: 100%.

1-(4-Nitrophenyl)-3-(3-(pyrrolidin-1-ylsulfonyl)phenyl)thiourea (**21**). To 3-(pyrrolidin-1-ylsulfonyl)aniline (0.03 g, 0.11 mmol) dissolved in DCM (5 mL) was added 1-isothiocyanato-4-nitrobenzene (0.02 g, 0.11 mmol) at 0 °C. The reaction was then stirred at room temperature for 2 days. The reaction was quenched by the addition of saturated aqueous solution of $NaHCO_3$ (20 mL), and extracted with DCM. The organic solvent was dried over $MgSO_4$, filtered, and then removed *in vacuo* and the reaction was purified using preparative HPLC affording **21** (0.02 g, 35% yield). ^{1}H NMR (500 MHz, DMSO-d_6) δ 9.0 (s, 1H), 7.9 (t, J = 1.8 Hz, 1H), 7.8 (d, J = 8.5 Hz, 2H), 7.8 (dd, J = 8.2, 1.3 Hz, 1H), 7.6 (d, J = 8.4 Hz, 2H), 7.5 (t, J = 8.0 Hz, 1H), 7.4–7.3 (m, 1H), 3.2–3.1 (m, 4H), 1.7–1.62 (m, 4H). ^{13}C NMR (126 MHz, DMSO-d_6) δ 153.7, 145.4, 140.5, 136, 129.5, 127.3, 126.5, 123.9, 121, 118.4, 80.1, 75.1, 47.9, 24.7. HR-MS (ESI) calculated for $C_{17}H_{19}N_4O_4S_2$ [M + H]$^+$: 407.0770, found: 407.0839. HPLC purity: 95%.

N,N-Dimethyl-3-(3-(4-nitrophenyl)ureido)benzenesulfonamide (**22**). According to **GP-3** using, 3-amino-*N,N*-dimethylbenzenesulfonamide (0.1 g, 0.5 mmol), and DCM (10 mL), to afford after filtration of the precipitate, **22** as a white solid (0.09 g, 49% yield). ^{1}H NMR (500 MHz, DMSO-d_6) δ 9.6–9.3 (m, 2H), 8.2–8.1 (m, 2H), 8.1 (t, J = 1.8 Hz, 1H), 7.8–7.7 (m, 2H), 7.6 (dd, J = 7.9, 1.5 Hz, 1H), 7.6 (t, J = 7.9 Hz, 1H), 7.4 (d, J = 7.8 Hz, 1H), 2.7–2.6 (m, 6H). ^{13}C NMR (126 MHz, DMSO-d_6) δ 152.5, 146.6, 141.7, 140.5, 135.7, 130.4, 125.6, 123.2, 121.7, 118.3, 117.5, 38.1. HR-MS (ESI) calculated for $C_{15}H_{17}N_4O_5S$ [M + H]$^+$: 365.0841, found: 365.0915. HPLC purity: 99%.

N,N-diethyl-3-(3-(4-nitrophenyl)ureido)benzenesulfonamide (**23**). According to **GP-3** using, 3-amino-*N,N*-diethylbenzenesulfonamide (0.114 g, 0.5 mmol), and DCM (10 mL), to afford after filtration of the precipitate, **23** as a yellow solid (0.11 g, 58% yield). ^{1}H NMR (500 MHz, DMSO-d_6) δ 9.4 (br s, 2H), 8.2–8.1 (m, J = 9.2 Hz, 2H), 8.1–8.0 (m, 1H), 7.8–7.7 (m, 2H), 7.6 (dd, J = 8.2, 1.0 Hz, 1H), 7.5 (t, J = 7.9 Hz, 1H), 7.4 (d, J = 7.8 Hz, 1H), 3.2 (q, J = 7.2 Hz, 4H), 1.1 (t, J = 7.2 Hz, 6H) ^{13}C NMR (126 MHz, DMSO-d_6) δ 152.5, 146.6, 141.7, 140.8, 140.5, 130.4, 125.6, 122.7, 120.8, 118.3, 116.7, 42.3, 14.6. HR-MS (ESI) calculated for $C_{17}H_{21}N_4O_5S$ [M + H]$^+$: 393.1154, found: 393.1221. HPLC purity: 99%.

1-(4-Nitrophenyl)-3-(3-(piperidin-1-ylsulfonyl)phenyl)urea (**24**). According to **GP-3** using, 3-(piperidin-1-ylsulfonyl)aniline (0.120 g, 0.5 mmol), and DCM (10 mL), to afford after filtration of the precipitate, **24** as an off-white solid (0.112 g, 55% yield). ^{1}H NMR (500 MHz, DMSO-d_6) δ 9.6–9.3 (m, 2H), 8.2–8.1 (m, 2H), 8.1–8.0 (m, 1H), 7.8–7.7 (m, 2H), 7.7 (dd, J = 7.9, 1.6 Hz, 1H), 7.6 (t, J = 7.9 Hz, 1H), 7.4–7.3 (m, 1H), 2.9–2.8 (m, 4H), 1.6–1.5 (m, 4H), 1.4–1.3 (m, 2H) ^{13}C NMR (126 MHz, DMSO-d_6) δ 152.5, 146.5, 141.7, 140.5, 136.6, 130.4, 125.6, 123.1, 121.6, 118.3, 117.3, 47.1, 25.2, 23.3. HR-MS (ESI) calculated for $C_{18}H_{21}N_4O_5S$ [M + H]$^+$: 405.1154, found: 405.1213. HPLC purity: 99%.

1-(3-(Morpholinosulfonyl)phenyl)-3-(4-nitrophenyl)urea (**25**). According to **GP-3** using, 3-orpholinosulfonyl)aniline (0.12 g, 0.5 mmol), and CH_2Cl_2 (5 mL), to afford after filtration of the precipitate, **25** as a white powder (0.06 g, 31% yield). ^{1}H NMR (500 MHz, DMSO-d_6) δ 9.6–9.3 (m, 2H), 8.2–8.1 (m, 2H), 8.1–8.0 (m, 1H), 7.8– 7.7 (m, 2H), 7.7–7.6 (m, 1H), 7.6–7.5 (m, 1H), 7.4 (d, J = 7.6 Hz, 1H), 3.7–3.6 (m, 4H), 2.9–2.8 (m, 4H). ^{13}C NMR (126 MHz, DMSO-d_6) δ 152.6, 141.7, 140.6, 135.4, 130.5, 125.6, 123.5, 121.8, 118.3, 117.5, 65.8, 46.4. HR-MS (ESI) calculated for $C_{17}H_{19}N_4O_6S$ [M + H]$^+$: 407.0947, found: 407.1006. HPLC purity: 99%.

1-(4-Nitrophenyl)-3-(3-(phenylsulfonyl)phenyl)urea (**26**). According to **GP-3** 3-(pyrrolidin-1-ylsulfonyl)aniline (0.16 g, 0.69 mmol) to afford after purification by flash chromatography (CH_2Cl_2/MeOH, 10/0 → 9.5/0.5), and washing the residue with MeOH, and CH_2Cl_2, **26** as a yellow powder (0.08 g, 28% yield). ^{1}H NMR (500 MHz, DMSO-d_6) δ 9.7–9.6 (m, 1H), 9.5–9.4 (m, 1H), 8.3 –8.2 (m, 1H), 8.2–8.1 (m, 2H), 8.0–7.9 (m, 2H), 7.8–7.7 (m, 3H), 7.7–7.5 (m, 5H). ^{13}C NMR (126 MHz, DMSO-d_6) δ 152.5, 146.5, 142.1, 141.8, 141.5, 140.8, 134.3, 130.9, 130.3, 127.8, 125.6, 123.8, 121.5, 118.5, 118.3, 117. HR-MS (ESI) calculated for: $C_{19}H_{16}N_3O_5S$ [M + H]$^+$: 398.0732, found: 398.0800. HPLC purity: 98%.

1-(4-Fluoro-3-(morpholinosulfonyl)phenyl)-3-(4-nitrophenyl)urea (**27**). According to **GP-3** using, 4-fluoro-3-(morpholinosulfonyl)aniline (0.08 g, 0.46 mmol), to afford after purification by flash chromatography (CH_2Cl_2/MeOH, 10/0 → 9.5/0.5), and washing the residue with MeOH, **27** as a yellow powder (0.05 g, 23 % yield). ^{1}H NMR (500 MHz, DMSO-d_6) δ 9.5 (br s, 1H), 9.3 (br s, 1H), 8.2–8.1 (m, 2H), 8.1 (dd, J = 6.0, 2.7 Hz, 1H), 7.8–7.7 (m, 3H), 7.5 (t, J = 9.5 Hz, 1H), 3.7–3.6 (m, 4H), 3.1–3.0 (m, 4H). ^{13}C NMR (126 MHz, DMSO-d_6) δ 154.9, 152.9, 152.5, 146.5, 141.7, 136.4, 126, 125.6, 123.7, 120.6, 118.7, 118.5, 118.3, 66, 46. ^{19}F NMR(470 MHz DMSO-d_6) δ -116.4. HR-MS (ESI) calculated for: $C_{17}H_{18}FN_4O_6S$ [M + H]$^+$: 425.0853, found: 425.0913. HPLC purity: 96%.

1-(4-Chloro-3-(morpholinosulfonyl)phenyl)-3-(4-nitrophenyl)urea (**28**). According to **GP-3** using, 4-chloro-3-(morpholinosulfonyl)aniline (0.1 g, 0.36 mmol), to afford after filtration, and washing (MeOH, CH_2Cl_2 and diethyl ether), **28** as yellow solid (0.01g, 7% yield. ^{1}H NMR (500 MHz, DMSO-d_6) δ 9.7–9.4 (m, 2H), 8.2 (d, J = 2.4 Hz, 1H), 8.3–8.2 (m, 2H), 7.8–7.7 (m, 3H), 7.7– 7.6 (m, 1H), 3.7–3.6 (m, 4H), 3.2–3.1 (m, 4H). ^{13}C NMR (126 MHz, DMSO-d_6) δ 151.96, 145.98, 141.33, 138.69, 134.93, 132.74, 125.12, 123.85, 123.31, 120.89, 117.90, 65.72, 45.74. HR-MS (ESI) calculated for: $C_{17}H_{18}ClN_4O_6S$ [M + H]$^+$: 441.0557, found: 441.0623. HPLC purity: 99%

1-(4-Methyl-3-(morpholinosulfonyl)phenyl)-3-(4-nitrophenyl)urea (**29**). According to **GP-3** using, 4-methyl-3-(morpholinosulfonyl)aniline (0.1 g, 39 mmol), affording after purification by flash chromatography (CH_2Cl_2/MeOH, 10/0 → 9,5/0,5), and recrystallization

(MeOH, CH_2Cl_2, and diethyl ether), **29** as a white solid (0.02 g, 9% yield). ^{1}H NMR (500 MHz, DMSO-d_6) δ 9.5 (br s, 1H), 9.28 (br s, 1H), 8.3–8.2 (m, 2H), 8.1 (d, J = 2.4 Hz, 1H), 7.8–7.7 (m, 2H), 7.6 (dd, J = 8.2, 2.3 Hz, 1H), 7.4 (d, J = 8.4 Hz, 1H), 3.7–3.6 (m, 4H), 3.4 (s, 9H), 3.1–3.0 (m, 4H). ^{13}C NMR (126 MHz, DMSO-d_6) δ 152.5, 146.7, 141.6, 137.9, 135.2, 134, 131.3, 125.7, 123.5, 119.8, 118.2, 66, 45.8, 20.2. HR-MS (ESI) calculated for: $C_{18}H_{21}N_4O_6S$ [M + H]$^+$: 421.1104, found: 421.1174. HPLC purity: 99%.

1-(4-Fluoro-3-(pyrrolidin-1-ylsulfonyl)phenyl)-3-(4-nitrophenyl)urea (**30**). According to **GP-4** using, 1-((2-fluoro-5-nitrophenyl)sulfonyl)pyrrolidine (0.1 g, 0.42 mmol), to afford after purification by preparative RP-HPLC **30** as an orange solid (0.01 g, 6% yield). ^{1}H NMR (500 MHz, DMSO-d_6): δ 10.2–9.8 (m, 1H), 8.8–8.6 (m, 1H), 8.2 (d, J = 9.2 Hz, 2H), 7.8 (d, J = 2.3 Hz, 1H), 7.7 (d, J = 9.2 Hz, 2H), 7.7 (d, J = 2.3 Hz, 1H), 7.0 (d, J = 9.0 Hz, 1H), 3.5–3.4 (m, 4H), 1.9–1.8 (m, 4H). ^{13}C NMR (126 MHz, DMSO-d_6): δ 153.1, 150.7, 146.6, 140.7, 129.3, 127.1, 124.9, 123.4, 117.3, 115.2, 49.8, 24.9. ^{19}F NMR (470 MHz DMSO-d_6) δ -73.5. HR-MS (ESI) calculated for: $C_{17}H_{17}FN_4O_5S$ [M + H]$^+$: 409.0904, found: 409.0967. HPLC purity: 96%.

1-(2-Fluoro-5-(pyrrolidin-1-ylsulfonyl)phenyl)-3-(4-nitrophenyl)urea (**31**) According to **GP-4** using, 4-fluoro-3-nitrobenzenesulfonyl chloride (0.1 g, 0.42 mmol), to afford after purification by preparative RP-HPLC **31** as a gray solid (0.01 g, 5% yield). ^{1}H NMR (500 MHz, DMSO-d_6): δ 9.6 (br s, 1H), 9.2 (br s, 1H), 8.2 (d, J = 2.4 Hz, 1H), 8.2 (d, J = 9.2 Hz, 2H), 7.7 (d, J = 9.2 Hz, 2H), 7.7 (dd, J = 9.2, 2.3 Hz, 1H), 7.3 (d, J = 9.2 Hz, 1H), 3.4–3.3 (m, 4H), 2.0–1.9 (m, 4H). ^{13}C NMR (126 MHz, DMSO-d_6): δ 152.1, 146.2, 144.9, 141.0, 130.3, 128.4, 125.0, 120.7, 120.0, 117.5, 51.8, 25.1. ^{19}F NMR (470 MHz DMSO-d_6) δ -115.9. HR-MS (ESI) calculated for: $C_{17}H_{17}FN_4O_5S$ [M + H]$^+$: 409.0904, found: 409.0967. HPLC purity: 98.

1-(2-Chloro-5-(pyrrolidin-1-ylsulfonyl)phenyl)-3-(4-nitrophenyl)urea (**32**). According to **GP-4** using, 4-chloro-3-nitrobenzenesulfonyl chloride (0.15 g, 0.59 mmol), to afford after purification by preparative RP-HPLC **32** as a yellow solid (0.02 g, 7% yield). ^{1}H NMR (500 MHz, DMSO-d_6): δ 10.3–10.1 (m, 1H), 8.9–8.7 (m, 1H), 8.7 (d, J = 2.0 Hz, 1H), 8.2 (d, J = 9.2 Hz, 2H), 7.8 (d, J = 8.4 Hz, 1H), 7.7 (d, J = 9.2 Hz, 2H), 7.5 (dd, J = 8.4, 2.0 Hz, 1H), 3.2–3.1 (m, 4H), 1.7–1.6 (m, 4H). ^{13}C NMR (126 MHz, DMSO-d_6): δ 152.1, 146.0, 142.0, 136.7, 135.9, 130.8, 126.8, 125.7, 122.5, 119.8, 118.0, 118.3, 48.4, 25.2. HR-MS (ESI) calculated for: $C_{17}H_{17}ClN_4O_5S$ [M + H]$^+$: 425.0608, found: 425.0686. HPLC purity: 97%.

1-(2-Methyl-5-(pyrrolidin-1-ylsulfonyl)phenyl)-3-(4-nitrophenyl)urea (**33**). According to **GP-4** using, 4-methyl-3-nitrobenzenesulfonyl chloride (0.15 g, 0.59 mmol), to afford after purification by preparative RP-HPLC **33** as a yellow solid (0.07 g, 28% yield). ^{1}H NMR (500 MHz, DMSO-d_6): δ 10.0–9.7 (m, 1H), 8.4 (d, J = 1.7 Hz, 1H), 8.2 (d, J = 9.2 Hz, 2H), 7.7 (d, J = 9.2 Hz, 2H), 7.5 (d, J = 7.9 Hz, 1H), 7.4 (dd, J = 8.7, 2.0 Hz, 1H), 3.2–3.1 (m, 4H), 2.4 (s, 3H), 1.7–1.6 (m, 4H). ^{13}C NMR (126 MHz, DMSO-d_6): δ 151.9, 145.9, 141.0, 137.4, 133.7, 132.5, 130.9, 125.1, 125.0, 121.4, 118.8, 117.8, 117.4, 47.6, 24.5, 17.8. HR-MS (ESI) calculated for: $C_{18}H_{20}N_4O_5S$ [M + H]$^+$: 405.1154, found: 405.1219. HPLC purity: 98%.

1-(2,5-Dimethyl-3-(pyrrolidin-1-ylsulfonyl)phenyl)-3-(4-nitrophenyl)urea (**34**). According to **GP-4** using, 2,5-dimethyl-3-nitrobenzenesulfonyl chloride (0.15 g, 0.60 mmol), to afford after purification by preparative RP-HPLC **34** as a yellow solid (0.09 g, 37% yield). ^{1}H NMR (500 MHz, DMSO-d_6): δ 9.9–9.7 (m, 1H), 8.5–8.2 (m, 1H), 8.2 (d, J = 9.2 Hz, 2H), 7.8–7.7 (m, 1H), 7.7 (d, J = 9.2 Hz, 2H), 7.5–7.4 (m, 1H), 3.2 (m, 4H), 2.4 (s, 3H), 2.4 (s, 3H), 1.9–1.8 (m, 4H). ^{13}C NMR (126 MHz, DMSO-d_6): δ 152.4, 146.5, 141.2, 138.7, 137.6, 135.6, 128.3, 126.2, 125.4, 125.0, 117.6, 47.4, 25.2, 20.9, 14.1. HR-MS (ESI) calculated for: $C_{19}H_{22}N_4O_5S$ [M + H]$^+$: 419.1311, found: 419.1373. HPLC purity: 100%.

1-(4-Nitrophenyl)-3-(4-(pyrrolidin-1-yl)-3-(pyrrolidin-1-ylsulfonyl)phenyl)urea (**35**). To a flask containing acetonitrile (1.5 mL), trimethylamine (0.12 g, 1.17 mmol), and pyrrolidine (0.04 g, 0.59 mmol) at room temperature, 2-chloro-5-nitrobenzenesulfonyl chloride (0.15 g, 0.59 mmol) was added. Next the resulting solution was stirred at room temperature for 5 min, after which, the solvent was evaporated. To the residue, EtOH (5.4 mL, 0.1 mmol), an aqueous solution of NH_4Cl at a concentration of 166 mM in water (2.0 mL, 0.34 mmol), and Fe powder (0.19 g, 3.44 mmol) were added, the resulting reaction mixture was stirred at 80 °C for 2,5 h. Next, the organic solvent was evaporated *in vacuo*, water (20 mL) was added, and the solution was extracted with EtOAc (3x, 20 mL). The combined organic layers were dried over $MgSO_4$, filtered, and concentrated *in vacuo*. Subsequent, the residue was solubilized with DMF (2 mL), and 1-isocyanato-4-nitrobenzene (0.14 g, 0.86 mmol) was added. The resulting reaction mixture was stirred at room temperature for 1 h, after which, DMF was removed on reduced pressure, and the residue was purified using preparative RP-HPLC to yield **35** as a yellow solid (0.01 g, 13% yield). ^{1}H NMR (500 MHz, DMSO-d_6): δ 9.6–9.3 (m, 1H), 9.3–9.0 (m, 1H), 8.2 (d, J = 9.2 Hz, 2H), 8.0 (d, J = 2.6 Hz, 1H), 7.7 (d, J = 9.2 Hz, 1H), 7.6 (dd, J = 8.9, 2.6 Hz, 1H), 7.4 (d, J = 8.9 Hz, 1H), 3.3–3.2 (m, 4H), 3.2–3.1 (m, 4H), 1.9–1.8 (m, 4H), 1.8–1.7 (m, 4H). ^{13}C NMR (126 MHz, DMSO-d_6): δ 152.0, 146.3, 144.3, 141.0, 134.1, 133.6, 125.1, 123.8, 123.4, 120.8, 117.6, 53.6, 47.7, 25.4, 24.2. HR-MS (ESI) calculated for: $C_{21}H_{25}N_5O_5S$ [M + H]$^+$: 460.1576, found: 460.1653. HPLC purity: 99%.

1-(4-Nitrophenyl)-3-(2-(pyrrolidin-1-yl)-5-(pyrrolidin-1-ylsulfonyl)phenyl)urea (**36**). To a flask containing acetonitrile (1.5 mL), trimethylamine (0.12 g, 1.17 mmol), and pyrrolidine (0.04 g, 0.59 mmol) at room temperature, 4-chloro-3-nitrobenzenesulfonyl chloride (0.15 g, 0.59 mmol) was added. Next the resulting solution was stirred at room temperature for 5 min, after which, the solvent was evaporated. To the residue, EtOH (5.4 mL, 0.1 mmol), an aqueous solution of NH_4Cl at a concentration of 166 mM in water (2.0 mL, 0.34 mmol), and Fe powder (0.19 g, 3.44 mmol) were added, the resulting reaction mixture was stirred at 80 °C for 2.5 h. Next, the organic solvent was evaporated *in vacuo*, water (20 mL) was added, and the solution was extracted with EtOAc (3x). The combined

organic layers were dried over $MgSO_4$, filtered, and concentrated *in vacuo*. Subsequently, the residue was solubilized with DMF (2 mL) and 1-isocyanato-4-nitrobenzene (0.14 g, 0.86 mmol) was added. The resulting reaction mixture was stirred at room temperature for 1 h, after which, DMF was removed on reduced pressure and the residue was purified using preparative RP-HPLC to yield **36** as a yellow solid (0.02 g, 9% yield) ^{1}H NMR (500 MHz, DMSO-d_6): δ 9.8 (br s, 1H), 8.2 (br s, 1H), 8.2 (d, J = 9.2 Hz, 2H), 7.8 (d, J = 2.1 Hz, 1H), 7.7 (d, J = 9.3 Hz, 2H), 7.4 (dd, J = 8.7, 2.3 Hz, 1H), 7.0 (d, J = 8.9 Hz, 1H), 3.3 (m, 4H), 3.1–3.0 (m, 4H), 2.0–1.9 (m, 4H), 1.7–1.6 (m, 4H). ^{13}C NMR (126 MHz, DMSO-d_6): δ 152.9, 147.4, 146.7, 141.1, 126.0, 125.7, 125.3, 125.2, 124.5, 117.6, 115.8, 50.2, 47.9, 25.0, 24.7. HR-MS (ESI) calculated for: $C_{21}H_{25}N_5O_5S$ [M + H]$^+$: 460.1576, found: 460.1652. HPLC purity: 97%.

Photometric *in vitro* assay. Dilution series (1:2) of inhibitors in DMSO covered the concentration range of approximately 200–0.01 µM. After finishing the dilution series, the final volume of compound solution in DMSO per well was 3 µL. For the IspD assay, 30 µL aliquots of a solution containing 100 mM Tris-HCl, pH 7.6, 0.02% NaN_3, 1 mM MEP and 1 mM CTP were added to microplate wells preloaded with 3 µL of DMSO containing test compounds. The reaction was started by addition of 27 µL aliquots of buffer: 100 mM Tris-HCl, pH 7.6, containing 10 mM $MgCl_2$, 60 mM KCl, 10 mM dithiothreitol, 0.02% NaN_3, 1 mM NADH, 2 mM phosphoenolpyruvate, 2 mM ATP, 1 U mL^{-1} pyruvate kinase, 1 U mL^{-1} lactate dehydrogenase, 1.5 U mL^{-1} *E. coli* IspE, 0.01 µM *Pf*IspD. The reaction was monitored photometrically (340 nm) at room temperature for 30 – 60 min on a plate reader (Spectramax M2, Molecular Devices, Biberach an der Riss, Germany). Initial rates were estimated using Softmax Pro 6.1 software (Molecular Devices, Biberach an der Riss, Germany). IC_{50} values were determined with a nonlinear regression method using the program Dynafit.[19]

Whole-cell assay. *Pf*NF54 wild type parasites cultured in RPMI 1640 medium supplemented with 25 mM HEPES, 24 mM sodium bicarbonate (pH 7.3), 0.36 mM hypoxanthine, 100 µg/mL neomycin and 0.5% Albumax II were used to test for compound activity on parasite multiplication using a [^3H]-hypoxanthine incorporation assay.[20] Compounds were dissolved in DMSO (10 mM), diluted in hypoxanthine-free culture medium and titrated in duplicate over a 64-fold range (6 step twofold dilutions) in 96 well plates. 100 µL Asexual parasite culture (prepared in hypoxanthine-free medium) were added to each well and mixed with the compound to obtain a final haematocrit of 1.25% and a final parasitemia of 0.3%. After incubation for 48 h, 0.25 µCi of [^3H]-hypoxanthine was added per well and plates were incubated for an additional 24 h. Parasites were then harvested onto glass-fiber filters using a Microbeta FilterMate cell harvester (Perkin Elmer, Waltham, US), and radioactivity was counted using a MicroBeta2 liquid scintillation counter (Perkin Elmer, Waltham, US). The results were recorded and expressed as a percentage of the untreated controls. Fifty percent inhibitory concentrations (EC_{50}) were estimated by linear interpolation.[21]

LC-MS based *in vitro* assay.
Dilution series (1:2) of inhibitors in DMSO covered the concentration range of approximately 200–0.01 µM. After finishing the dilution series, the final volume of compound solution in DMSO per well was 2.0 µL. During the assay, the following buffer was used: 100 mM Tris-HCl pH 7.6, 1 mM DTT. To start the assay, aliquots of buffer (49 µL) containing: 306.1 µM CTP, 2.0 mM $MgCl_2$ and 0.1 µM PfIspD, were added to a 96-well plate (Nunc V). Next 2 µL of the inhibitor dilutions (in DMSO) are added and the plate is allowed to incubate at 37 °C for 10 min. Then another 49 µL of buffer containing 306.1 µM MEP was added to start the reaction. The plates were incubated at 37 °C for 40 min, after which, the protein was denaturated by heating up the plate to 95 °C for 5 min. The plate was then centrifuged at 4000 rpm at 4 °C for 5 min to precipitate all solids present in the solution. To another 96-well plate, 190 µL of ice cold 3:1:1 ACN, isopropanol, water mixture was added. Thereafter, 10 µL of each of the supernatants from the assay plate were added. The plate was centrifuged again at 4000 rpm at 4 °C for 5 min, after which, 50 µL of the supernatant was transferred to a plate capable to measured in the MS and covered with a silicon cover. LC-MS conditions and data analysis methods we used were described above.

Determination of enzyme kinetics.

A volume of 80 µL Buffer A containing 100mM Tris-HCl pH 7.6, 1 mM DTT, 1 mM $MgCl_2$, 50 nM *Pf*IspD were added to well A1 96-well plate while 50 µL were added to the rest of the wells. A volume of 20 µL of 10mM CTP was added to the first well, then a serial dilution was conducted by moving 50 µL. To start the reaction, we then added on buffer A 50 µL of Buffer B containing 100mM Tris-HCl pH 7.6, 1 mM DTT, and 1 mM MEP. The assay plate was incubated at 37 °C for 40 min, after which, the protein was denaturated by heating up the plate to 95 °C for 5 min. The plate was then centrifuged at 4000 rpm at 4 °C for 5 min to precipitate the protein. To another 96-well plate, 190 µL of ice cold 3:1:1 ACN, isopropanol, water mixture was added containing 100 nM 4-methyl-1-oxo-1-(p-tolylamino)pentane-2-sulfonic acid, adenylyl-imidodiphosphate and adenosine-5'-[(α,β)-methyleno]triphosphate as internal standard.[15] Thereafter, 10 µL of each of the supernatants from the assay plate were added to the plate containing the mixture with our internal standard. The plate was centrifuged again at 4000 rpm at 4 °C for 5 min, after which, 50 µL of the supernatant was transferred to an LC-MS plate and closed with a silicon cover. LC-MS conditions and data analysis methods we used were described above. The peak area for each conditions were used to calculate the Michaelis–Menten

kinetic parameters using Graphpad Prism v 9. Measurements were performed in duplicates, repeated at least two times from two to three independent experiments.

Determination of mode of inhibition of 10

Dilution series (1:2) of inhibitors in DMSO covered the concentration range of approximately 200–0.01 µM. After finishing the dilution series, the final volume of compound solution in DMSO per well was 2.0 µL. During the assay, the following buffer was used: 100 mM Tris-HCl pH 7.6, 1 mM DTT. To study the inhibition mode against CTP, aliquots of buffer (49 µL) containing: 0, 37.5, 75, 125, 250, 500 µM CTP, 2.0 mM $MgCl_2$ and 0.1 µM PfIspD, were added to a 96-well plate (Nunc V). Next 2 µL of the inhibitor dilutions (in DMSO) are added and the assay plate was incubated at 37 °C for 10 min. Then another 49 µL of buffer containing 500 µM MEP was added to start the reaction. To study the Mode of inhibition toward MEP, similar steps were followed as in case of CTP with using 0, 37.5, 75, 125, 250, 500 µM MEP and 500 µM CTP The assay plate was incubated at 37 °C for 40 min, after which, the protein was denaturated by heating up the plate to 95 °C for 5 min. The assay plate was then centrifuged at 4000 rpm at 4 °C for 5 min to precipitate the protein. To another 96-well plate, 190 µL of ice cold 3:1:1 ACN, isopropanol, water mixture was added containing 100 nM 4-methyl-1-oxo-1-(p-tolylamino)pentane-2-sulfonic acid as internal standard.[15] Thereafter, 10 µL of each of the supernatants from the assay plate were added to the plate containing the mixture with our internal standard. The plate was centrifuged again at 4000 rpm at 4 °C for 5 min, after which, 50 µL of the supernatant was transferred to an LC-MS plate and closed with a silicon cover. LC-MS conditions and data analysis methods we used were described above.

Metabolic Stability in Liver S9 Fractions. For the evaluation of combined phase I and phase II metabolic stability, the compound (1 µM) was incubated with 1 mg/mL pooled mouse liver S9 fraction (Xenotech, Kansas City, USA) or human liver S9 fraction (Corning, USA), 2 mM NADPH, 1 mM UDPGA, 10 mM $MgCl_2$, 5 mM GSH and 0.1 mM PAPS at 37 °C for 240 min. The metabolic stability of testosterone, verapamil and ketoconazole were determined in parallel to confirm the enzymatic activity of mouse S9 fractions, for human S9 testosterone, diclofenac and propranolol were used. The incubation was stopped after defined time points by precipitation of aliquots of S9 enzymes with 2 volumes of cold acetonitrile containing internal standard (150 nM diphenhydramine). Samples were stored on ice until the end of the incubation and precipitated protein was removed by centrifugation (4 °C, 15 min, 4,000 g). Concentration of the remaining test compound at the different time points was analyzed by HPLC-MS/MS (TSQ Quantum Access MAX, Thermo Fisher, Dreieich, Germany) and used to determine half-life (t1/2).

Stability in Mouse and Human Plasma. To determine stability in mouse plasma, the compound (1 µM) was incubated with pooled CD-1 mouse or human plasma (Neo Biotech, Nanterre, France). Samples were taken at defined time points by mixing aliquots with 4 volumes of acetonitrile containing internal standard (125 nM diphenhydramine). Samples were stored on ice until the end of the incubation and precipitated protein was removed by centrifugation (4 °C, 15 min, 4,000 g, 2 centrifugation steps). Concentration of the remaining test compound at the different time points was analyzed by HPLC-MS/MS (TSQ Quantum Access MAX, Thermo Fisher, Dreieich, Germany). The plasma stability of procain, propantheline and diltiazem were determined in parallel to confirm the enzymatic activity.

Pharmacokinetic (PK) studies. For pharmacokinetic experiments, outbred male CD-1 mice (Charles River, Germany), 4 weeks old, were used. The animal studies were conducted in accordance with the recommendations of the European Community (Directive 2010/63/EU, 1st January 2013). All animal procedures were performed in strict accordance with the German regulations of the Society for Laboratory Animal Science (GV-SOLAS) and the European Health Law of the Federation of Laboratory Animal Science Associations (FELASA). Animals were excluded from further analysis if sacrifice was necessary according to the humane endpoints established by the ethical board. All expriments were approved by the ethical board of the Niedersächsisches Landesamt für Verbraucherschutz und Lebensmittelsicherheit, Oldenburg, Germany. Compounds **10** and **26** were administered at 1 mg/kg intravenously in a cassette format (n=2). At the time points 0.25, 0.5, 1, and 3 post administration, up to 25 µL of blood were collected from the lateral tail vein. At 5 h post administration, mice were euthanized to collect blood from the heart as well as to remove spleen and liver aseptically. Whole blood was collected into Eppendorf tubes coated with 0.5 M EDTA and immediately spun down at 15870 x g for 10 min at 4 °C. Then, plasma was transferred into a new Eppendorf tube spleen and liver were homogenized using a Polytron tissue homogenizer. Spleen, liver and plasma samples were stored at -80 °C until analysis. First, a calibration curve was prepared by spiking different concentrations of **10** and **26** into mouse plasma, homogenized spleen or homogenized liver from CD-1 mice. Glipizide was used as an internal standard. In addition, quality control samples (QCs) were prepared for **10** and **26** in the same matrices. For **10** and **26** the same extraction procedure was used: 7.5 µL of a plasma sample (calibration samples, QCs or PK samples) was extracted with 22.5 µL of acetonitrile containing 12.5 ng/mL of glipizide as an internal standard for 5 min at 2000 rpm on an Eppendorf MixMate® vortex mixer. Then samples were spun down at 13.000 rpm for 10 min. Supernatants were transferred to standard HPLC-glass vials. For liver and

spleen, 20 µl of a sample (calibration samples, QCs or PK samples) were extracted with 10 µl water containing 10 % formic acid, and 22.5 µl acetonitrile with 12.5 ng/mL of glipizide as internal standard. Samples were extracted for 5 min at 800 rpm on an Eppendorf MixMate® vortex mixer and spun down for 5 min at 4000 rpm. Peaks of PK samples were quantified using the calibration curve. The accuracy of the calibration curve was determined using QCs independently prepared on different days (Table S1). PK parameters were determined using a non-compartmental analysis with PKSolver.[22]

ASSOCIATED CONTENT

Supporting Information. "This material is available free of charge via the Internet at http://pubs.acs.org."
Further details about cell extract, affinity matrix and sample preparations for the target fishing experiments as well as data analysis. Supplementary reaction and characterization data of all final compounds.

AUTHOR INFORMATION

Corresponding Author

*__Anna K. H. Hirsch__ – *Helmholtz Institute for Pharmaceutical Research (HIPS), Helmholtz Centre for Infection Research (HZI), Saarland University, Campus E8.1, 66123 Saarbrücken, Germany;*
Email: Anna.hirsch@helmholtz-hips.de

Present Addresses

†If an author's address is different than the one given in the affiliation line, this information may be included here.

Author Contributions

ψ Second authors with equal contribution. D.W., E.D., M.M.H., M.W., and A.K.H.H. coordinated the project; Synthesis and characterization of the compounds was performed by D.W., E.D., M.M.H., and M.W.; HTS and biological evaluation of derivatives against *Pf*IspD was performed by B.I. and M.F.; Evaluation of the potency against *Pf*NF54 was performed by P.B. and M.R.; Development of the LC-MS based IspD assay and kinetic characterization was performed by A.A. and L.B.; ADMET and PK profiling experiments were executed by A.K. and K.R.; D.W. wrote the manuscript. The manuscript was written through contributions of all authors. All authors have given approval to the final version of the manuscript.

Funding Sources

This project has received funding from the European Union's Horizon 2020 research and innovation programme under the Marie Skłodowska-Curie grant agreement No 860816. MepAnti

Notes

The authors declare no competing financial interest.
Figure 2, scheme 1 and the graphical abstract were created with BioRender.com

ACKNOWLEDGMENT

D.W. Thank you Simone Amann, Jeannine Jung and Jannine Seelbach for the great work. K.R. receives funding from the German Center for Infection Research (DZIF, TTU 09.719). K.R. thanks Andrea Ahlers, Kimberley Vivien Sander, Janine Schreiber and Jennifer Wolf for excellent technical assistance.

ABBREVIATIONS

AMR, antimicrobial resistance; AUC0-t, area under the concentration-time curve from time zero to time t; CDP-ME, 4-diphosphocytidyl-2-*C*-methylerythritol; Cl_obs, clearance (based on observed last time point with measurable concentration); CTP, cytidine triphosphate; CuAAC, copper-catalyzed azide-alkyne cycloaddition; DDA, data-dependent acquisition; DIA, data-independent acquisition; DCM, dichloromethane; DMADP, dimethylallyl diphosphate; DMF, *N,N*-dimethylformamide; DMSO, dimethyl sulfoxide; Eq, equivalents; ESI, electron spray ionization; FA, formic acid; EC_{50}, fifty percent inhibitory concentrations; HESI, heated electrospray ionization; HTS, high throughput screening; HPLC, high pressure liquid chromatography; IDP, isopentenyl diphosphate; IV, intravenous; *Km*, Michaelis constant; LCMS, liquid chromatography–mass spectrometry; MEP, 2-*C*-methylerythritol-*D*-erythritol-4-phosphate; MRT, mean residence time; MWD, multiple wave detector; n.a., no activity; ND, not detected; NMR, nuclear magnetic resonance; *Pf, plasmodium falciparum*; PPi, inorganic diphosphate; PK, pharmacokinetic; SAR, structure–activity relationship; SD, standard deviation Vz_obs, Volume of distribution associated with the terminal phase;

REFERENCES

(1) Dadgostar, P. Antimicrobial Resistance: Implications and Costs. *Infect Drug Resist*. **2019**, *Volume 12*, 3903-3910.

(2) Cassini, A.; Högberg, L. D.; Plachouras, D.; Quattrocchi, A.; Hoxha, A.; Simonsen, G. S.; Colomb-Cotinat, M.; Kretzsch-mar, M. E.; Devleesschauwer, B.; Cecchini, M.; Ouakrim, D. A.; Oliveira, T. C.; Struelens, M. J.; Suetens C.; Monnet, D. L. Attributable deaths and disability-adjusted life-years caused by infections with antibiotic-resistant bacteria in the EU and the European Economic Area in 2015: a population-level modelling analysis. *Lancet Infect. Dis*. **2019**, *19* (1), 56-66.

(3) Kozlov, M. Resistance to front-line malaria drugs confirmed in Africa. *Nature* **2021**, *597*, 604.

(4) Masini, T.; Kroezen, B. S.; Hirsch, A. K. H. Druggability of the enzymes of the non-mevalonate-pathway. *Drug Discovery Today* **2013**, *18* (23), 1256-1262.

(5) Diamanti, E.; Hamed, M. M.; Lacour, A.; Bravo, P.; Illarionov, B.; Fischer, M.; Rottmann, M.; Witschel, M.; Hirsch, A. K. H. Targeting the IspD Enzyme in the MEP Pathway: Identification of a Novel Fragment Class. *ChemMedChem* **2022** *17*, e202100

(6) Mombo-Ngoma, G.; Remppis, J.; Sievers, M.; Zoleko Manego, R.; Endamne, L.; Kabwende, L.; Veletzky, L.; Nguyen, T. T.; Groger, M.; Lötsch, F.; Mischlinger, J.; Flohr, L.; Kim, J.; Cattaneo, C.; Hutchinson, D.; Duparc S.; Moehrle, J.; Velavan, T. P.; Lell B.; Ramharter, M.; Adegnika, A. A.; Benjamin Mord-müller, B.; Kremsner, P. G. Efficacy and Safety of Fosmidomycin–Piperaquine as Nonartemisinin-Based Combination Therapy for Uncomplicated Falciparum Malaria: A Single-Arm, Age De-escalation Proof-of-Concept Study in Gabon. *Clinical Infectious Diseases*, **2018**, *66* (12), 1823-1830.

(7) Frank, A.; Groll, M. The Methylerythritol Phosphate Pathway to Isoprenoids. *Chemical Reviews*. **2017**, *117* (8), 5675-5703.

(8) Price, K. E.; Armstrong, C. M.; Imlay, L. S.; Hodge, D. M.; Pidathala, C.; Roberts, N. J.; Park, J.; Mikati, M.; Sharma, R.; Lawrenson, A. S.; Tolia, N. H.; Berry, N. G.; O'Neill, P.M.; John, A.R.O. Molecular Mechanism of Action of Antimalarial Benzo-isothiazolones: Species-Selective Inhibitors of the Plasmodium spp. MEP Pathway enzyme, IspD. *Sci Rep*. **2016**, *6*, 12.

(9) Mathew, J.; Ding, S.; Kunz, K. A.; Stacy, E. E.; Butler, J. H.; Haney, R. S.; Merino, E. F.; Butschek, G. J.; Rizopoulos, Z.; Totrov, M.; Cassera, M. B.; Carlier, P. R Malaria Box-Inspired Discovery of N-Aminoalkyl-β-carboline-3-carboxamides, a Novel Orally Active Class of Antimalarials. *ACS Med. Chem. Lett*. **2022**, *13* (3), 365-370.

(10) Imlay, L. S.; Armstrong, C. M.; Masters, M. C.; Li, T.; Price, K. E.; Edwards, R. L.; Mann, K. M.; Li, L. X.; Stallings, C. L.; Berry, N. G.; O'Neill, P. M.; Odom A. R. Plasmodium IspD (2-C-Methyl-d-erythritol 4-Phosphate Cytidyltransferase), an Essential and Druggable Antimalarial Target. *ACS Infect. Dis*. **2015**, *1* (4), 157-167.

(11) Ding, S.; Ghavami, M.; Butler, J. H.; Merino, E. F.; Slebodnick, C.; Cassera, M. B.; Carlier, P. R. Probing the B- & C-rings of the antimalarial tetrahydro-β-carboline MMV008138 for steric and conformational constraints. *Bioorganic Med. Chem. Lett*. **2020**, *30* (22), 127520.

(12) Wu, W.; Herrera, Z.; Ebert, D.; Baska, K.; Cho, S. H.; Derisi, J. L.; Yeh, E. A. Chemical Rescue Screen Identifies a Plasmodium falciparum Apicoplast Inhibitor Targeting MEP Isoprenoid Precursor Biosynthesis. *Antimicrobial Agents and Chemo-therapy* **2015**, *59* (1), 356-364.

(13) Honold, A.; Lettl, C.; Schindele, F.; Illarionov, B.; Haas, R.; Witschel, M.; Bacher, A.; Fischer M.; Inhibitors of the Bifunctional 2-*C*-Methyl-D-erythritol 4-Phosphate Cytidylyl Transferase/2-*C*-Methyl-D-erythritol-2,4-cyclopyrophosphate Synthase (IspDF) of *Helicobacter pylori*. *Helv. Chim. Acta*, **2019**, *102*, e1800228.

(14) Ziku L.; Sharkey, T. D.; Metabolic profiling of the methylerythritol phosphate pathway reveals the source of post-illumination isoprene burst from leaves. *Plant, Cell and Environment*, **2013**, *36*, 429–437.

(15) Konstantinović, J.; Kany, A. M.; Alhayek, A.; Abdelsamie, A.; Sikandar, A.; Voos, K.; Yao, Y.; Andreas, A.; Shafiei, R.; Loretz, B.; Schönauer, E.; Bals, R.; Brandstetter, H.; Hartmann, R. W.; Ducho, C.; Lehr, C.; Beisswenger, C.; Müller, R.; Rox, K.; Haupenthal, J.; Hirsch, A. K. H.; Inhibitors of the Elastase LasB for the Treatment of Pseudomonas aeruginosa Lung Infections. *ACS Cent. Sci*. **2023**, *9*, 12, 2205–2215

(16) Ghavami, M.; Merino, F. E.; Yao, Z.; Elahi, R.; Simpson, M. E.; Fernández-Murga, M. L.; Butler, J. H.; Casasanta, M. A.; Krai, P. M; Totrov, M. M.; Slade, D. J.; Carlier, P. R.; and Cassera, M. B. Biological Studies and Target Engagement of the 2-C-Methyl-d-Erythritol 4-Phosphate Cytidylyltransferase (IspD)-Targeting Antimalarial Agent (1R,3S)-MMV008138 and Analogs. *ACS Infect. Dis*. **2018**, *4*, 4, 549–559

(17) Witschel, M.C., Höffken, H.W., Seet, M., Parra, L., Mietzner, T., Thater, F., Niggeweg, R., Röhl, F., Illarionov, B., Rohdich, F., Kaiser, J., Fischer, M., Bacher, A. and Diederich, F., Inhibitors of the Herbicidal Target IspD: Allosteric Site Binding. *Angew. Chem. Int. Ed*., **2011**, *50*: 7931-7935. https://doi.org/10.1002/anie.201102281

(18) Aebersol, R.; Mann, M.; Mass-spectrometric exploration of proteome structure and function, *Nature*, **2016** Sep *15;537*(7620):347-55.

(19) Kuzmic, P. Program DYNAFIT for the analysis of enzyme kinetic data: application to HIV proteinase, *Anal. Biochem*. **1996**, *237*, 260-273.

(20) Snyder, C.; Chollet, J.; Santo-Tomas, J.; Scheurer, C.; Wittlin, S. In vitro and in vivo interaction of synthetic peroxide RBx11160 (OZ277) with piperaquine in Plasmodium models, *Exp Parasitol* **2007**, *115*(3), 296-300.

(21) Huber, W., and Koella, J.C. A comparison of three methods of estimating EC50 in studies of drug resistance of malaria parasites. *Acta Trop*., **1993**, 55(4), 257-261.

(22) Zhang, Y.; Huo, M.; Zhou, J.; Xie, S.; PKSolver: An add-in program for pharmacokinetic and pharmacodynamic data analysis in Microsoft Excel, *Comput. Methods Programs Biomed*.**2010**, *3*, 306-314.

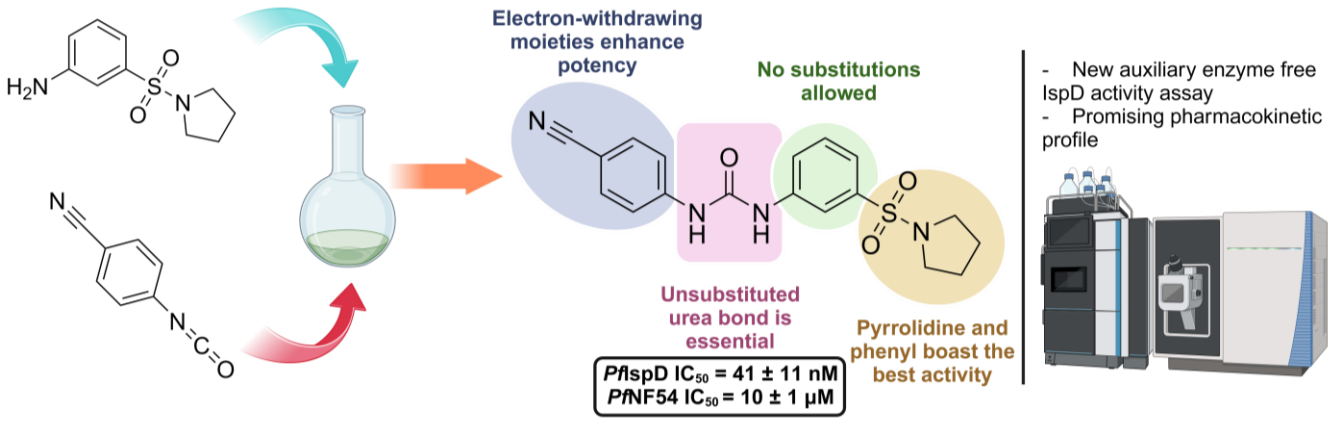
Electron-withdrawing moieties enhance potency
No substitutions allowed
Unsubstituted urea bond is essential
Pyrrolidine and phenyl boast the best activity
PfIspD IC50 = 41 ± 11 nM
PfNF54 IC50 = 10 ± 1 µM
- New auxiliary enzyme free IspD activity assay
- Promising pharmacokinetic profile

Targeting *Plasmodium falciparum* IspD in the Methyl-*D*-Erythritol Phosphate Pathway: Urea-Based Compounds with Nanomolar Potency on target with low micromolar whole-cell activity

Daan Willocx,[†,¶,‡] Lorenzo Bizzarri,[ψ,#,¶] Alaa Alhayek,[ψ,†] Patricia Bravo,[§,∥] Boris Illarionov,[⊥] Katharina Rox,[∫,∂] Jonas Lohse,[#] Markus Fischer,[⊥] Andreas M. Kany,[†] Hannes Hahne,[#] Matthias Rottmann,[§,∥] Matthias Witschel[¦], Mostafa M. Hamed,[†] Eleonora Diamanti,[†] Anna K. H. Hirsch*[,†,¶]

[†]Helmholtz Institute for Pharmaceutical Research (HIPS), Helmholtz Centre for Infection Research (HZI), Saarland University, Campus E8.1, 66123 Saarbrücken, Germany

¶Saarland University, Department of Pharmacy, Campus E8.1, 66123 Saarbrücken, Germany

[#]OmicScouts GmbH, Lise-Meitner-Straße 30, 85354 Freising, Germany

[§]Swiss Tropical and Public Health Institute, Kreuzstrasse 2, 4123 Allschwil, Switzerland

[∫]Helmholtz Centre for Infection Research (HZI), Department of Chemical Biology, Inhoffenstraße 7, 38124 Braunschweig, Germany

[∂]German Center for Infection Research (DZIF), Partner site Hannover-Braunschweig, Inhoffenstraße 7, 38124 Braunschweig, Germany

[∥]Universität Basel, Petersplatz 1, 4003 Basel, Switzerland

[⊥]Hamburg School of Food Science, University of Hamburg, Grindelallee 117, 20146 Hamburg, Germany

[¦]BASF-SE, Carl-Bosch-Strasse 38, 67056 Ludwigshafen, Germany

Table of Contents

S1. Activities of selected compounds against auxiliary enzymes

Table S1. Activities of selected compounds against auxiliary enzymes

#	Structure, R=	*Pf*IspD (IC_{50} nM)[a]	EcIspE (IC_{50} µM)[a]	PK-LDH (IC_{50} µM)[a]
7	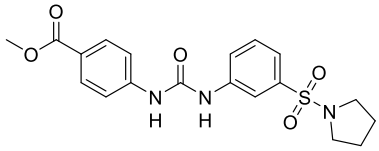	170 ± 20	>500	242 ± 72
9	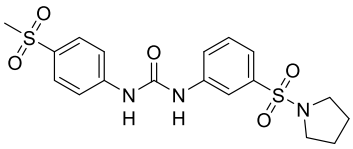	330 ± 40	>500	>500
11	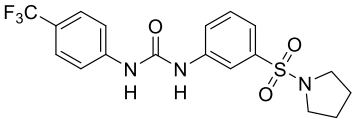	91 ± 19	73 ± 15	73±15
24	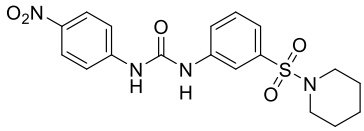	225 ± 20	49 ± 7	>500
25	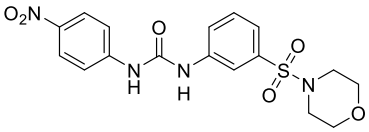	600 ± 110	>500	104 ± 19
27	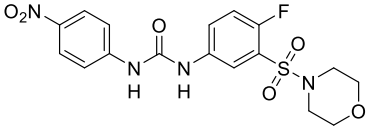	400 ± 100	75 ± 11	>500

[a]Assays were performed in replicate as independent experiments (n = 2); values are shown as mean ± SD.

S2. Calibration curve for CDP-ME

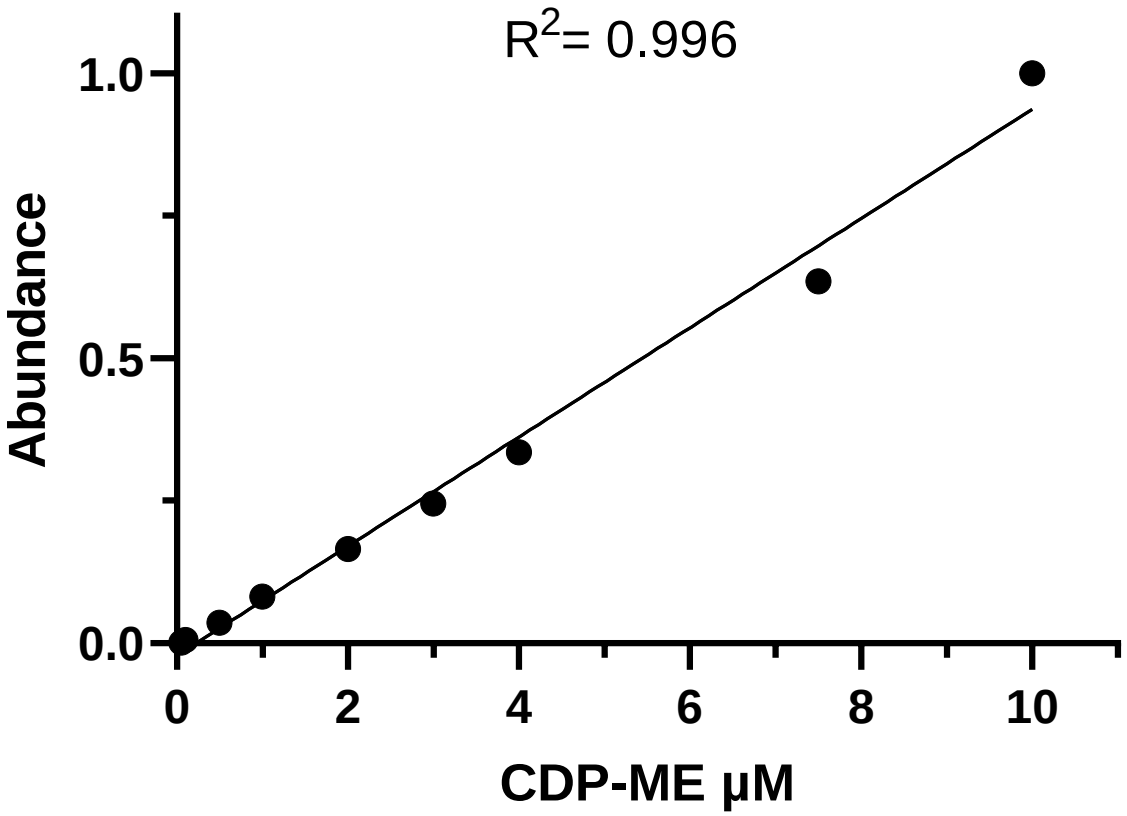

Figure S1. Calibration curve for CDP-ME detection. Concentrations ranging from 50 nM to 10 µM. The calculated area under the curve was converted to values ranging for 0 to 1.

S3. Determination kinetic parameters concerning CTP.

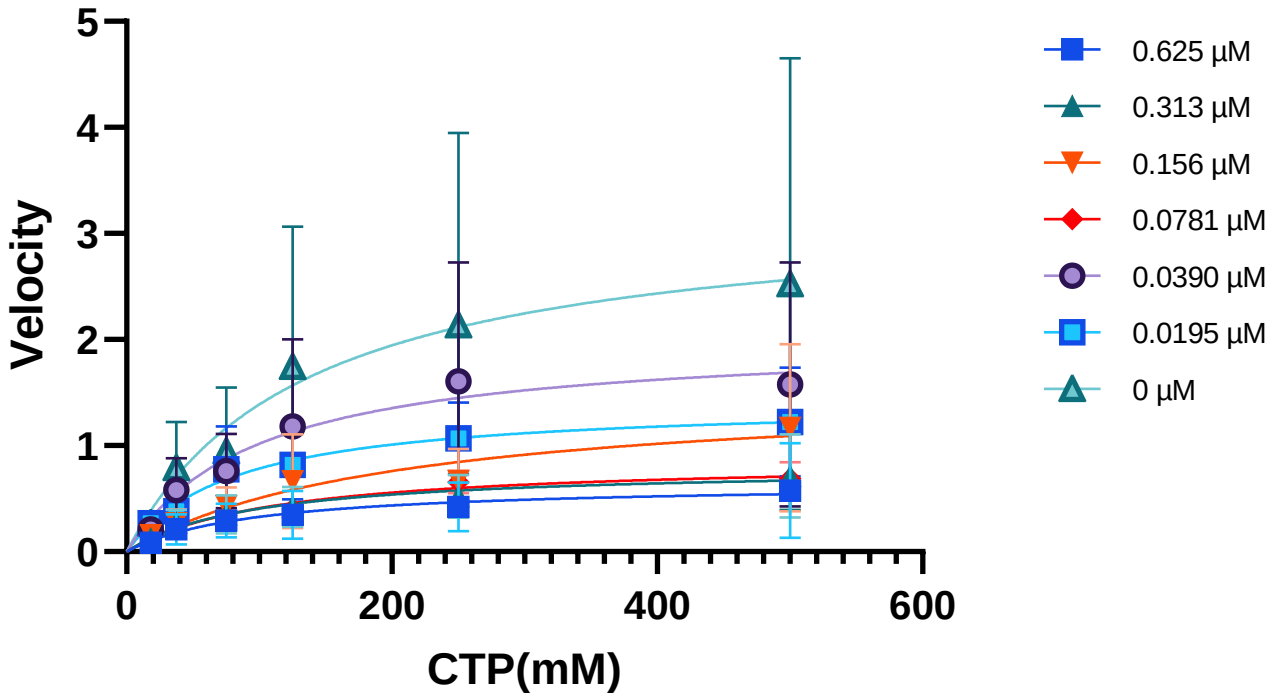

Figure S2. Kinetic parameters were determined concerning the CTP substrate. Each data point reflects the mean ± SD obtained from a minimum of two-independent experiments.

Table S2. Kinetic parameters at different concentrations of compound 10 and at varying CTP concentrations.

Compound 10 (µM)	0.625	0.313	0.156	0.0781	0.0390	0.0195	0.000
V_{max}	0.6496	0.8006	1.537	0.8674	2.021	1.418	3.253
K_m	97.89	97.23	204.4	111.7	98.52	80.79	134.4

S4. Determination kinetic parameters concerning MEP.

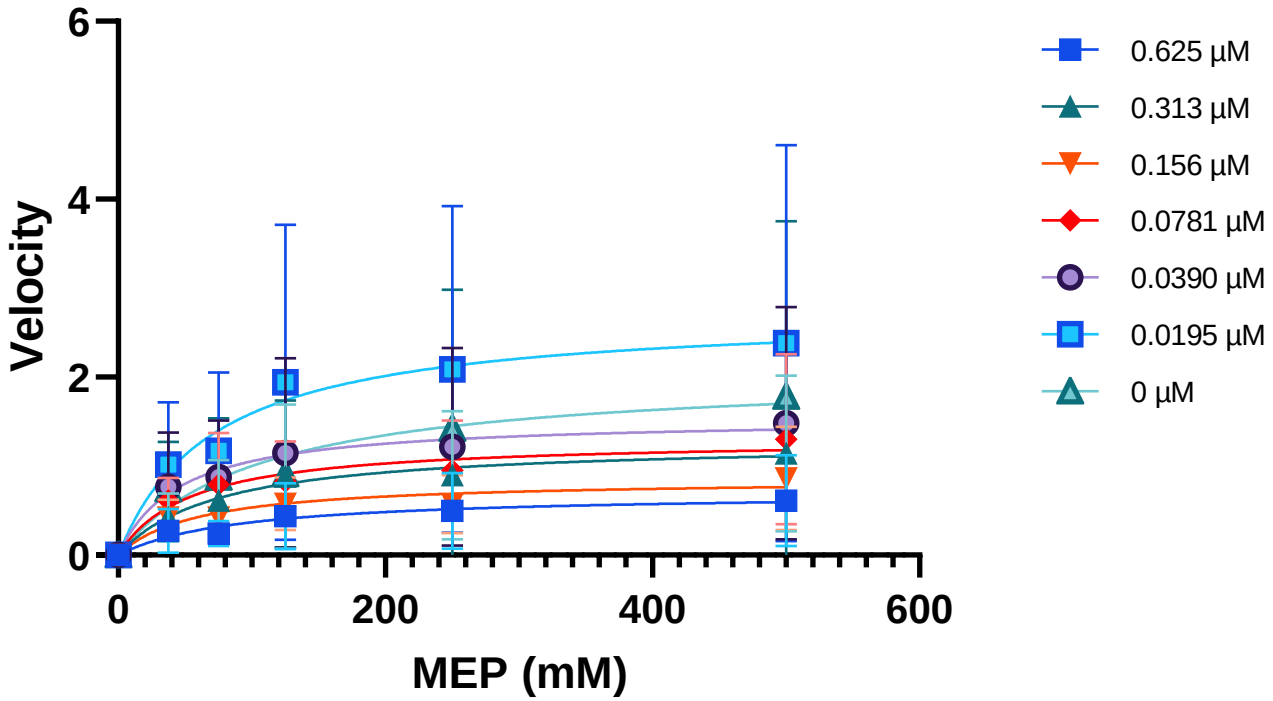

Figure S3. Kinetic parameters were determined concerning the CTP substrate. Each data point reflects the mean ± SD obtained from a minimum of two-independent experiments.

Table S3. Kinetic parameters at different concentrations of compound 10 and at varying MEP concentrations

Compound 10 (µM)	0.625	0.313	0.156	0.0781	0.0390	0.0195	0.000
V_{max}	0.7037	1.277	0.8556	1.305	1.541	2.734	2.064
K_m	90.58	74.61	59.79	53.57	46.05	71.50	106.2

S5. LC-MS chromatograms of MEP, 4-methyl-1-oxo-1-(p-tolylamino)pentane-2-sulfonic acid and CDP-ME respectively

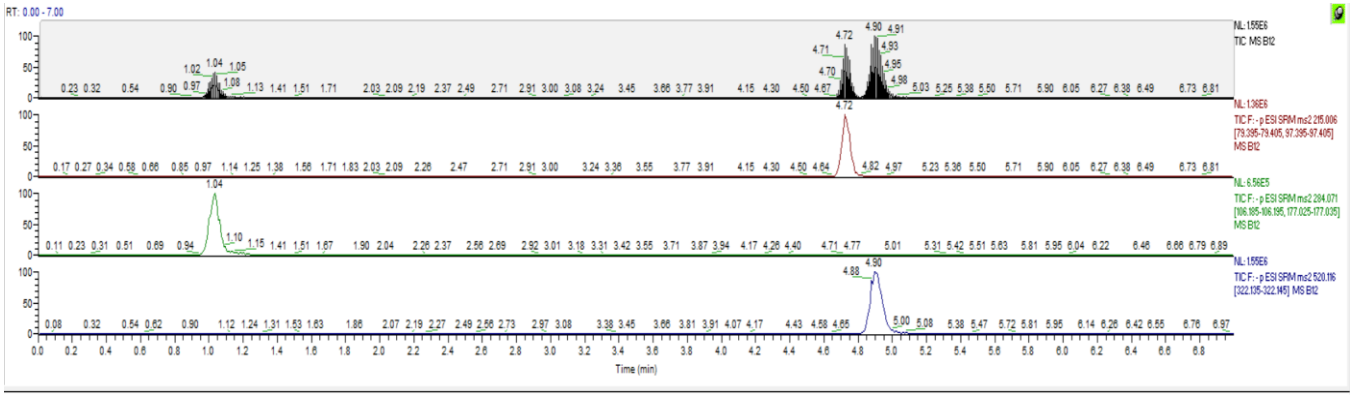

Figure S4. LC-MS chromatogram of MEP (second, red), 4-methyl-1-oxo-1-(p-tolylamino)pentane-2-sulfonic acid (third, green) and CDP-ME (fourth, blue) respectively.

S6. Q1 and Q3 masses for glipizide, 10 and 26

Table S8. Q1 and Q3 masses for glipizide, **10** and **26**

ID	Q1 Mass [Da]	Q3 Mass [Da]	time [msec]	CE [volts]	CXP [volts]	DP [volts]
10	371.022	355.0	30	15	20	101
	371.022	253.0	30	25	28	101
10	392.998	23.2	30	69	10	96
		353.9	30	13	20	96
		252.2	30	19	22	96
26	395.952	136.9	30	-16	-11	-40
		231.9	30	-34	-21	-40
glipizide	443.936	319.100	150	-26	-21	-66
glipizide	443.936	170.100	150	-40	-7	-66

S7. Supplementary reaction schemes

Scheme S2. Synthetic routes for the synthesis of 19 and 20[a]

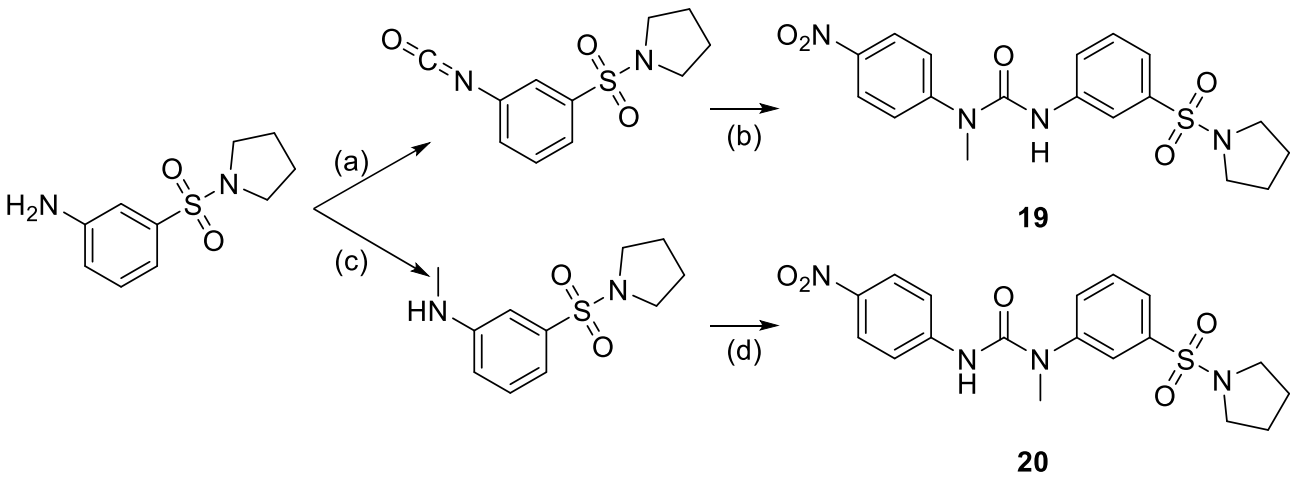

[a]Reagents and reactions conditions: (a) triphosgene, Et_3N, DCM, 0 °C to rt, 3 h, used as such in the next reaction step; (b) *N*-methyl-4-nitroaniline, NaH, DMF, room temperature for 1 h. 32% overall yield; (c) paraformaldehyde, $NaBH_4$, MeOH, at room temperature for 2.5 h to 60 °C for 16 h, 57% yield; (d) 1-isocyanato-4-nitrobenzene, DMF, room temperature for 16 h, 12% yield.

Scheme S3. Synthetic routes for the synthesis of 21[a]

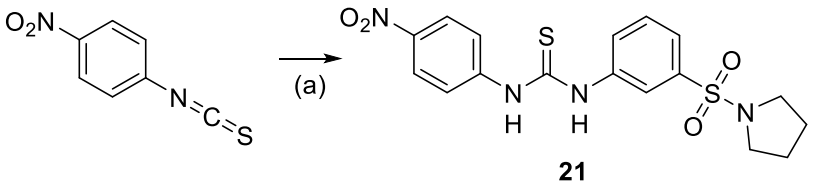

[a]Reagents and reactions conditions:) (e) 3-(pyrrolidin-1-ylsulfonyl)aniline, DMF, room temperature, 48h, 35% yield.

Scheme S4. General reaction scheme for the synthesis of 22-26[a]

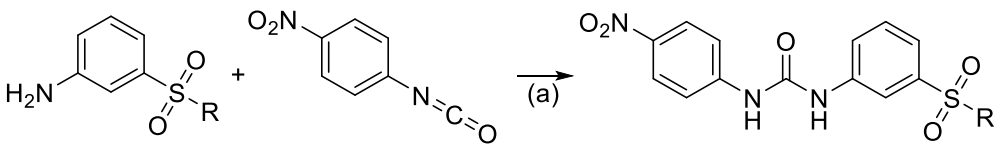

[a]Reagents and reactions conditions: (a) 1-isocyanato-4-nitrobenzene, DMF, room temperature, overnight, 28−58% yield.

Scheme S5. General reaction scheme for the synthesis of compounds 27−29[a].

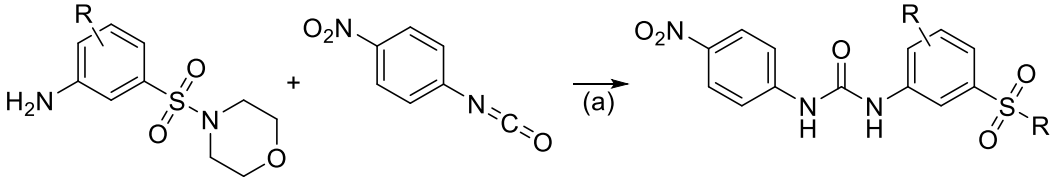

[a]Reagents and reactions conditions: 1-isocyanato-4-nitrobenzene, DMF, room temperature, overnight. 7−23% yield.

S8. ^{1}H NMR and ^{13}C NMR spectra as well as LC-MS and purity traces of Compounds 1−37

4

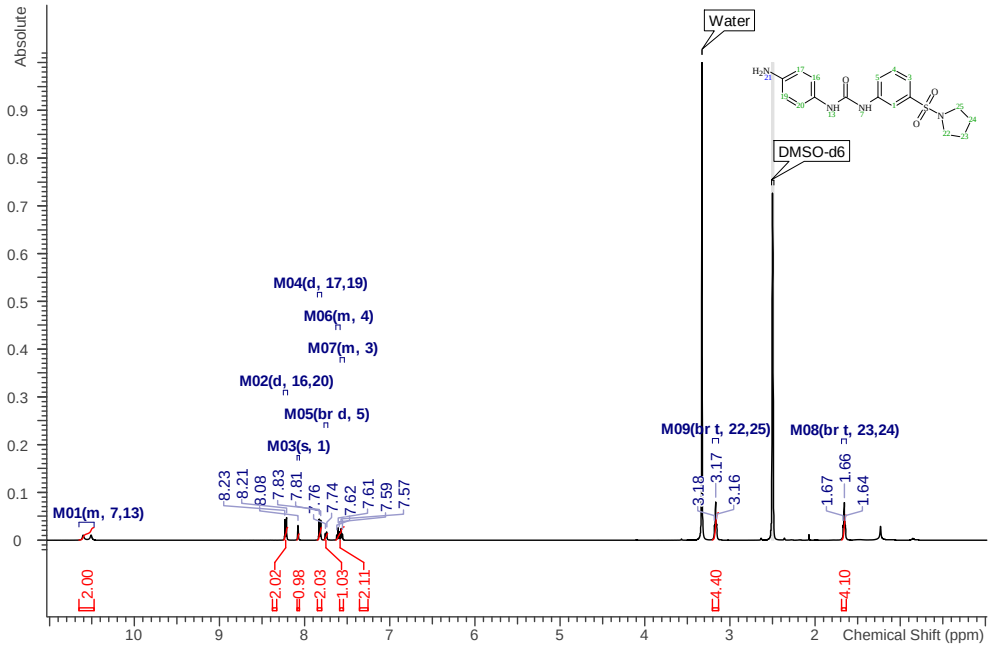

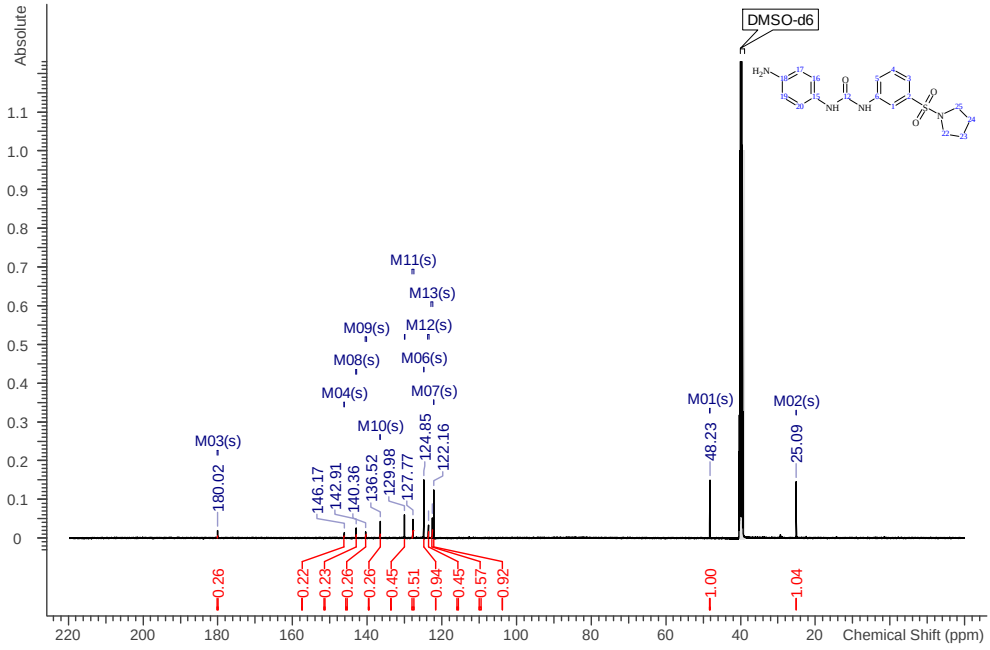

5

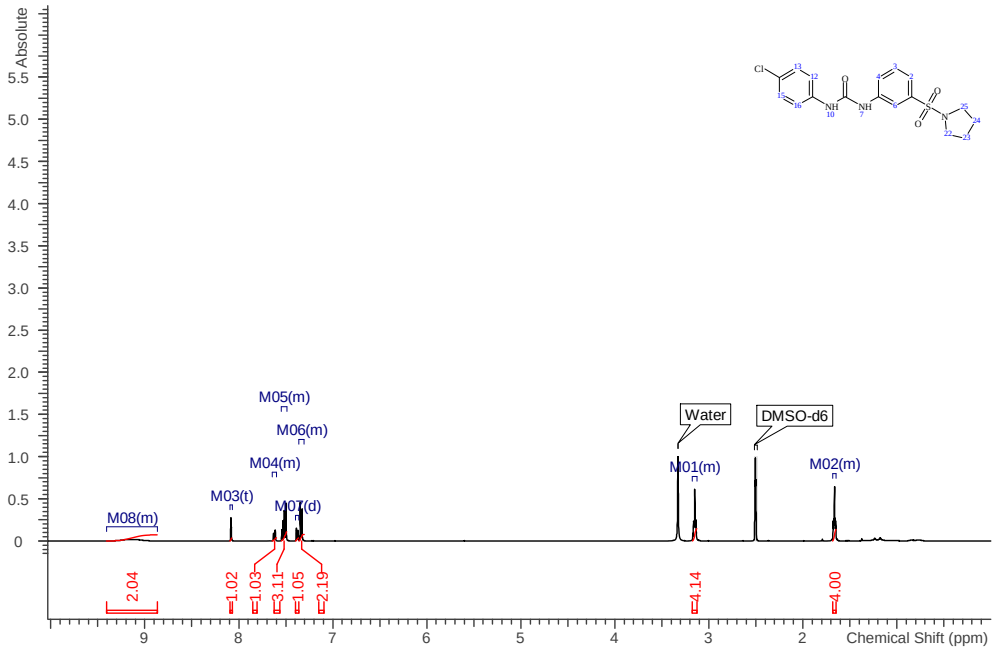
Absolute
Water
DMSO-d6
M01(m)
M02(m)
M03(t)
M04(m)
M05(m)
M06(m)
M07(d)
M08(m)
2.04
1.02
1.03
3.11
1.05
2.19
4.14
4.00
Chemical Shift (ppm)

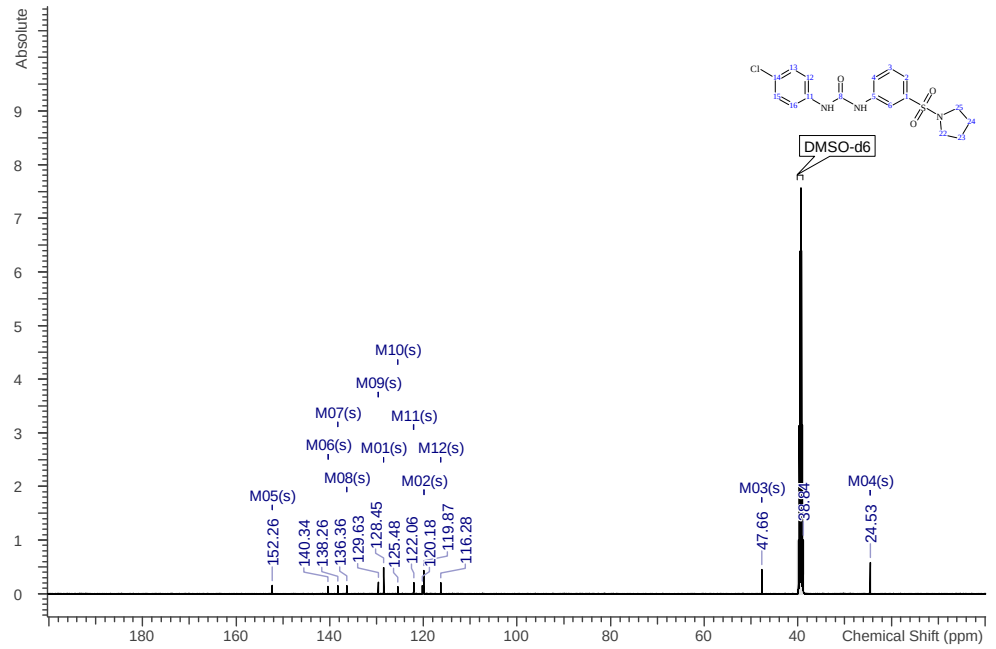
Absolute
DMSO-d6
M01(s)
M02(s)
M03(s)
M04(s)
M05(s)
M06(s)
M07(s)
M08(s)
M09(s)
M10(s)
M11(s)
M12(s)
152.26
140.34
138.26
136.36
129.63
128.45
125.48
122.06
120.18
119.87
116.28
47.66
39.52
39.24
24.53
Chemical Shift (ppm)

6

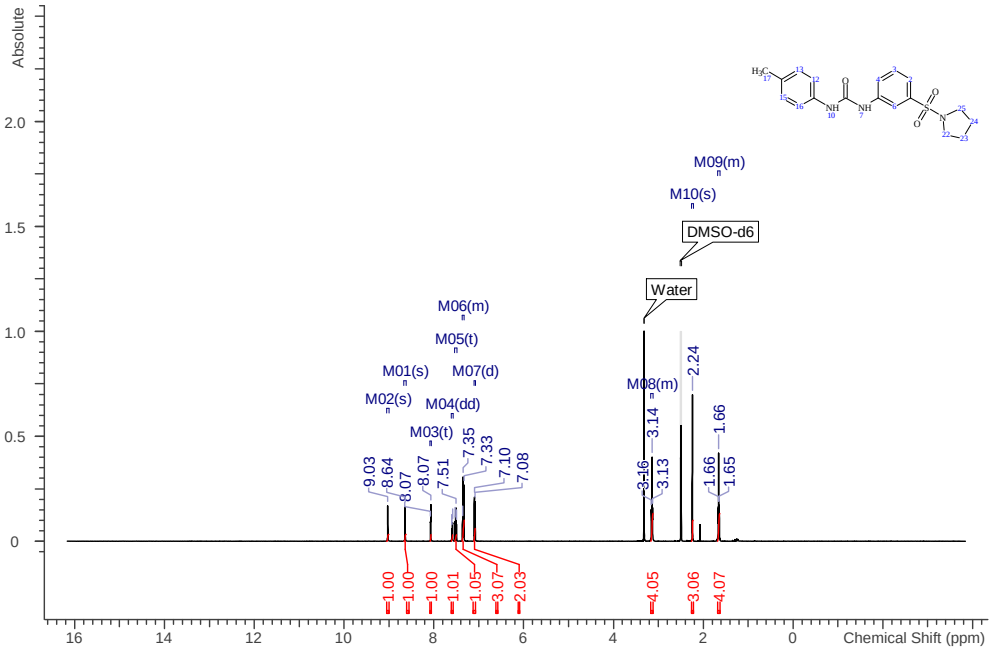
Absolute
Chemical Shift (ppm)
DMSO-d6
Water
M09(m)
M10(s)
M06(m)
M05(t)
M01(s)
M07(d)
M02(s)
M04(dd)
M03(t)
M08(m)
9.03
8.64
8.07
8.07
7.51
7.35
7.33
7.10
7.08
3.16
3.14
3.13
2.24
1.66
1.66
1.65
1.00
1.00
1.00
1.01
1.05
3.07
2.03
4.05
3.06
4.07

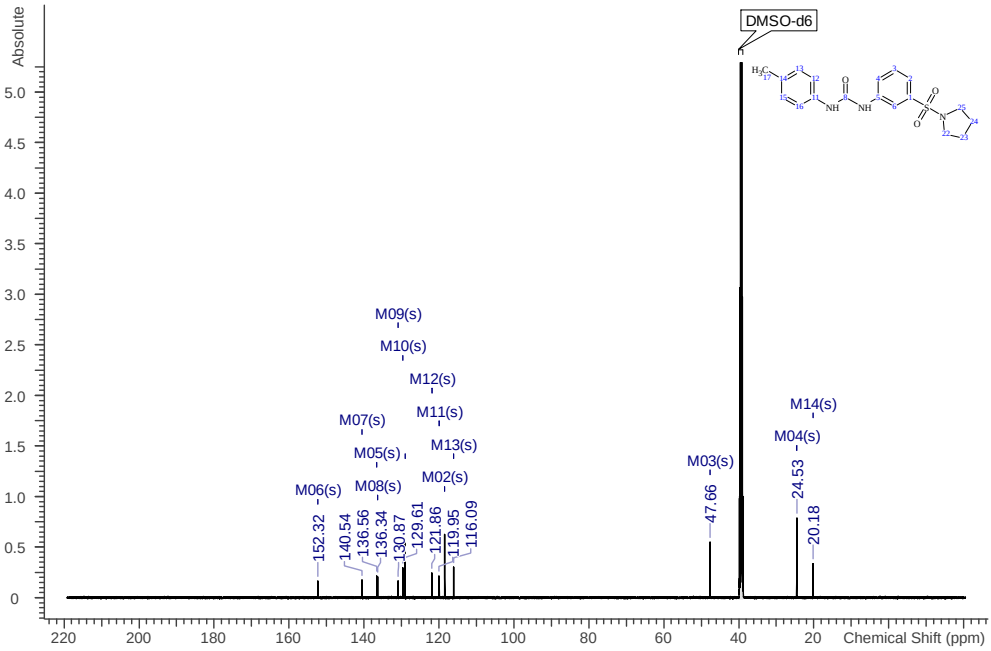
Absolute
Chemical Shift (ppm)
DMSO-d6
M09(s)
M10(s)
M12(s)
M11(s)
M07(s)
M13(s)
M05(s)
M02(s)
M06(s)
M08(s)
M03(s)
M14(s)
M04(s)
152.32
140.54
136.56
136.34
130.87
129.61
121.86
119.95
116.09
47.66
24.53
20.18

7

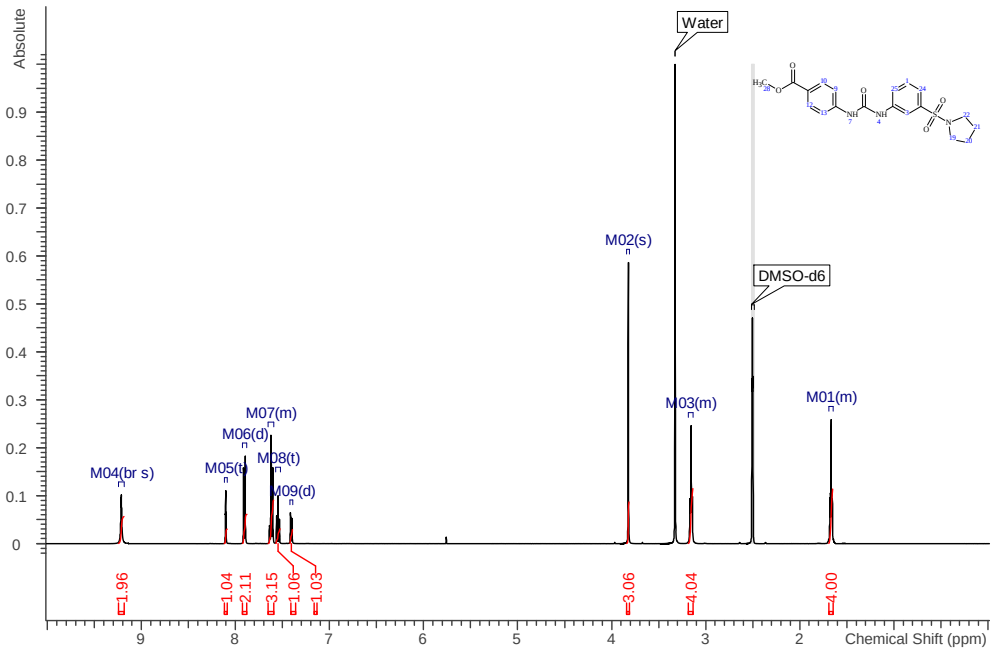
Absolute
Water
DMSO-d6
M02(s)
M03(m)
M01(m)
M07(m)
M06(d)
M08(t)
M05(t)
M04(br s)
M09(d)
1.96
1.04
2.11
3.15
1.06
1.03
3.06
4.04
4.00
Chemical Shift (ppm)

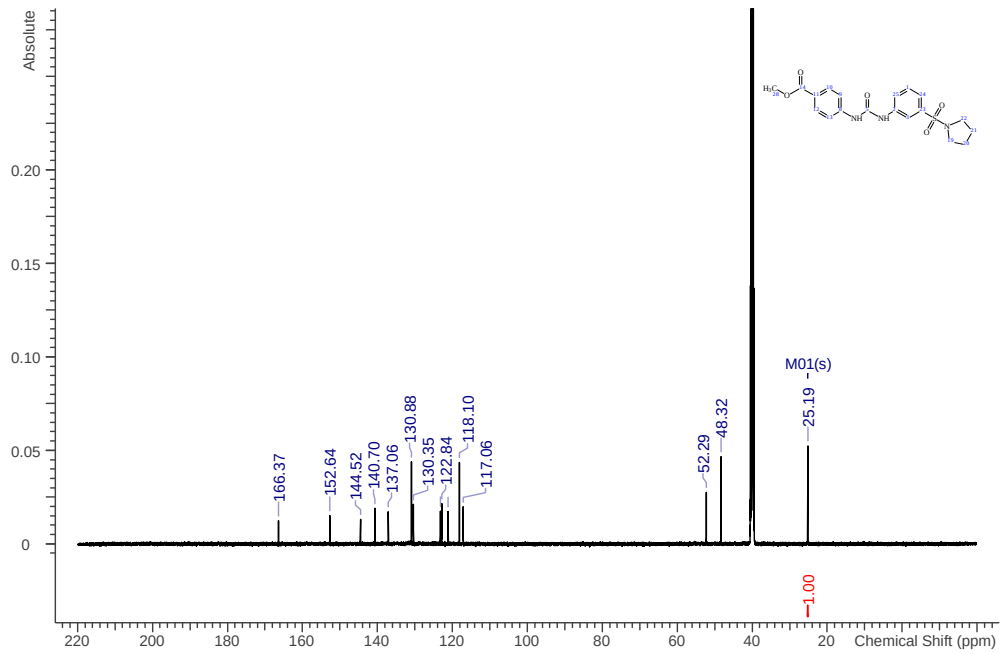
Absolute
M01(s)
166.37
152.64
144.52
140.70
137.06
130.88
130.35
122.84
118.10
117.06
52.29
48.32
25.19
1.00
Chemical Shift (ppm)

8

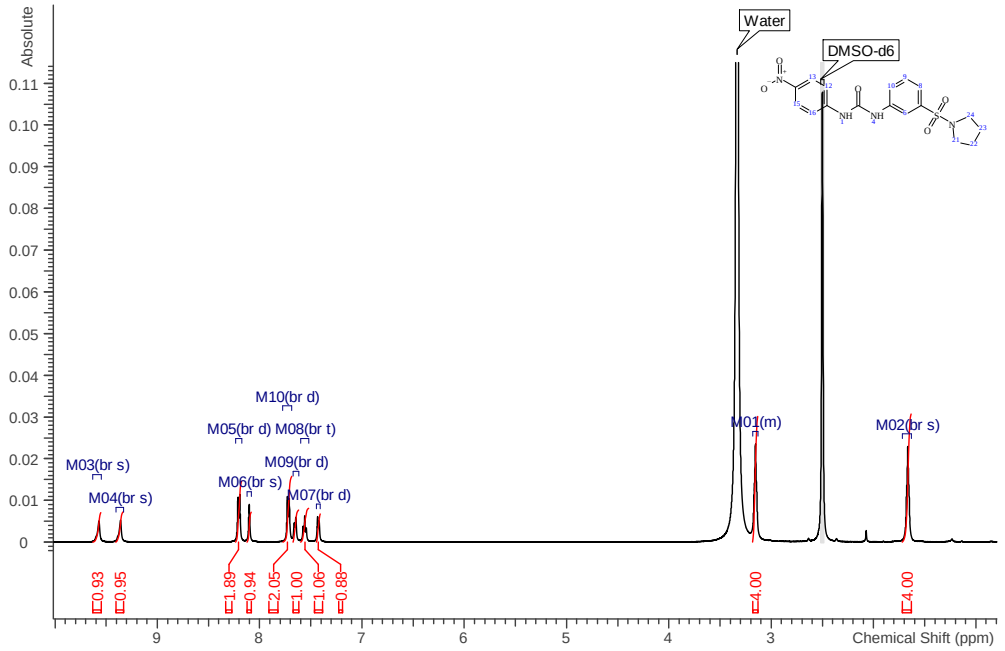
Absolute
Water
DMSO-d6
M01(m)
M02(br s)
M03(br s)
M04(br s)
M05(br d)
M06(br s)
M07(br d)
M08(br t)
M09(br d)
M10(br d)
0.93
0.95
1.89
0.94
2.05
1.00
1.06
0.88
4.00
4.00
Chemical Shift (ppm)

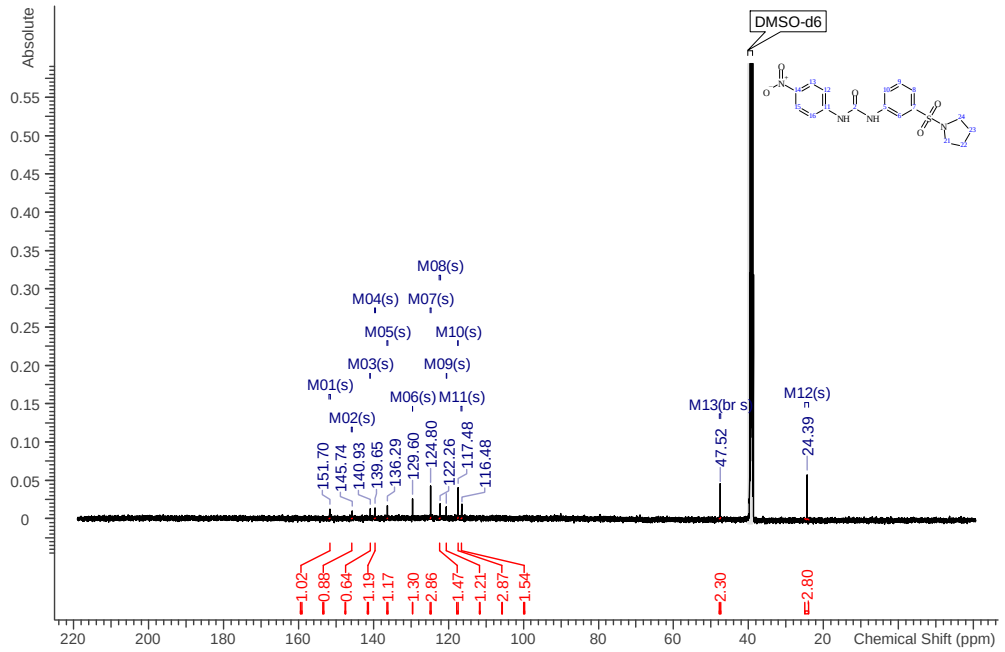
Absolute
DMSO-d6
M01(s)
M02(s)
M03(s)
M04(s)
M05(s)
M06(s)
M07(s)
M08(s)
M09(s)
M10(s)
M11(s)
M12(s)
M13(br s
151.70
145.74
140.93
139.65
136.29
129.60
124.80
122.26
117.48
116.48
47.52
24.39
1.02
0.88
0.64
1.19
1.17
1.30
2.86
1.47
1.21
2.87
1.54
2.30
2.80
Chemical Shift (ppm)

9

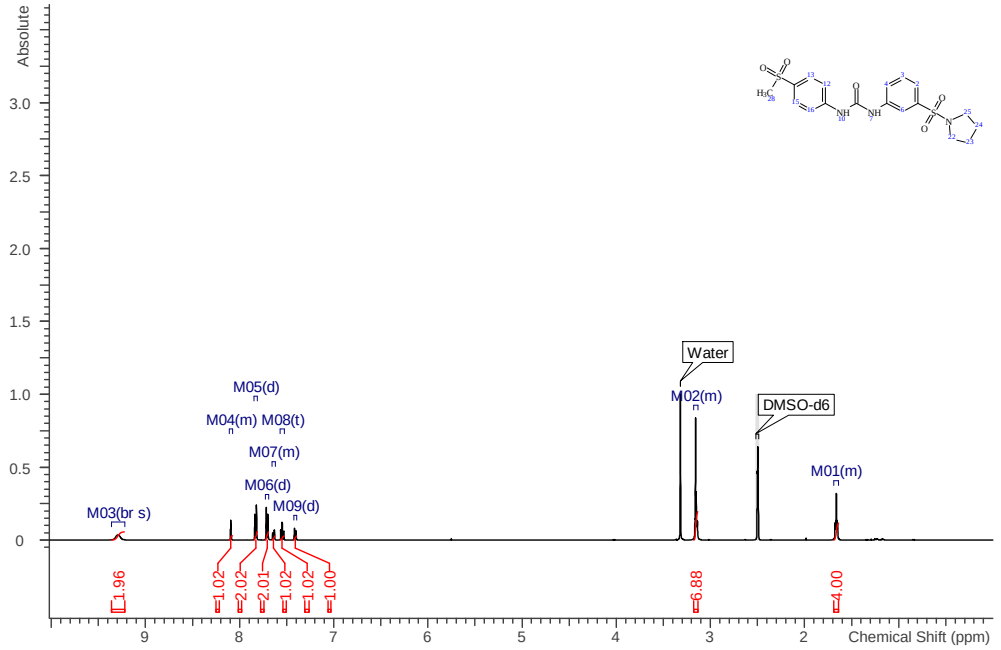
Absolute
Water
DMSO-d6
M01(m)
M02(m)
M03(br s)
M04(m)
M05(d)
M06(d)
M07(m)
M08(t)
M09(d)
1.96
1.02
2.02
2.01
1.02
1.02
1.00
6.88
4.00
Chemical Shift (ppm)

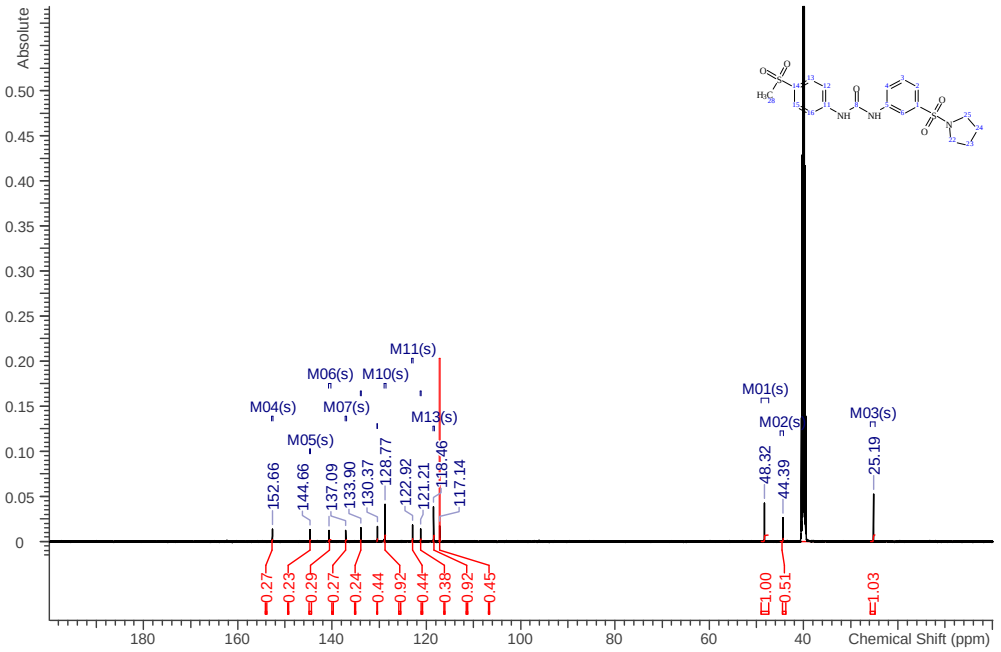
Absolute
M01(s)
M02(s)
M03(s)
M04(s)
M05(s)
M06(s)
M07(s)
M10(s)
M11(s)
M13(s)
48.32
44.39
25.19
152.66
144.66
137.09
133.90
130.37
128.77
122.92
121.21
118.46
117.14
0.27
0.23
0.29
0.27
0.24
0.44
0.92
0.44
0.38
0.92
0.45
1.00
0.51
1.03
Chemical Shift (ppm)

10

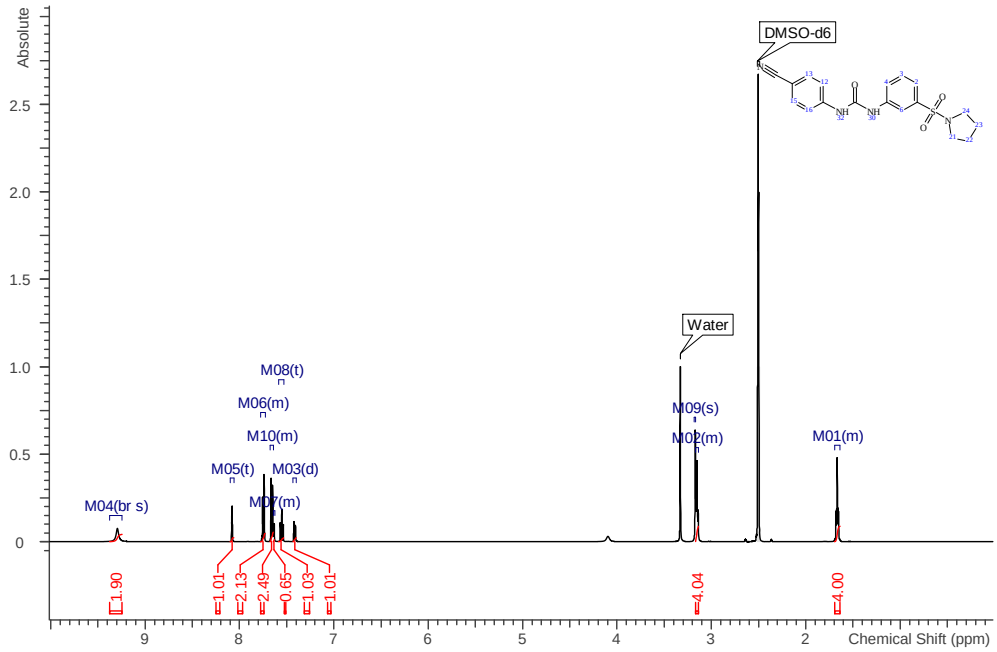
Absolute
DMSO-d6
Water
M08(t)
M06(m)
M10(m)
M05(t)
M03(d)
M04(br s)
M07(m)
M09(s)
M02(m)
M01(m)
1.90
1.01
2.13
2.49
0.65
1.03
1.01
4.04
4.00
Chemical Shift (ppm)

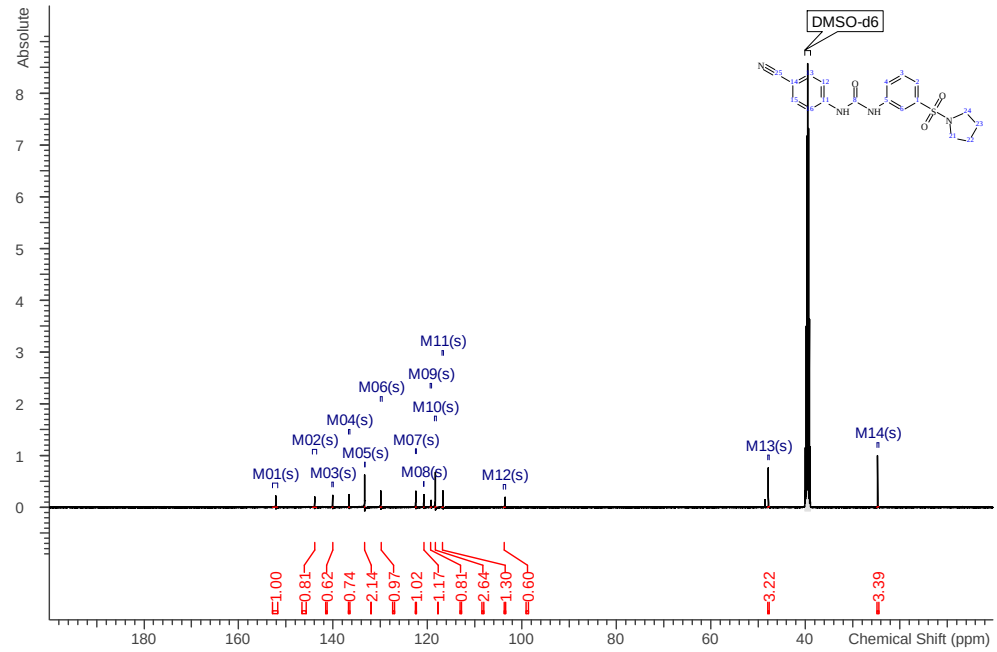
Absolute
DMSO-d6
M11(s)
M09(s)
M06(s)
M10(s)
M04(s)
M02(s)
M07(s)
M05(s)
M01(s)
M03(s)
M08(s)
M12(s)
M13(s)
M14(s)
1.00
0.81
0.62
0.74
2.14
0.97
1.02
1.17
0.81
2.64
1.30
0.60
3.22
3.39
Chemical Shift (ppm)

11

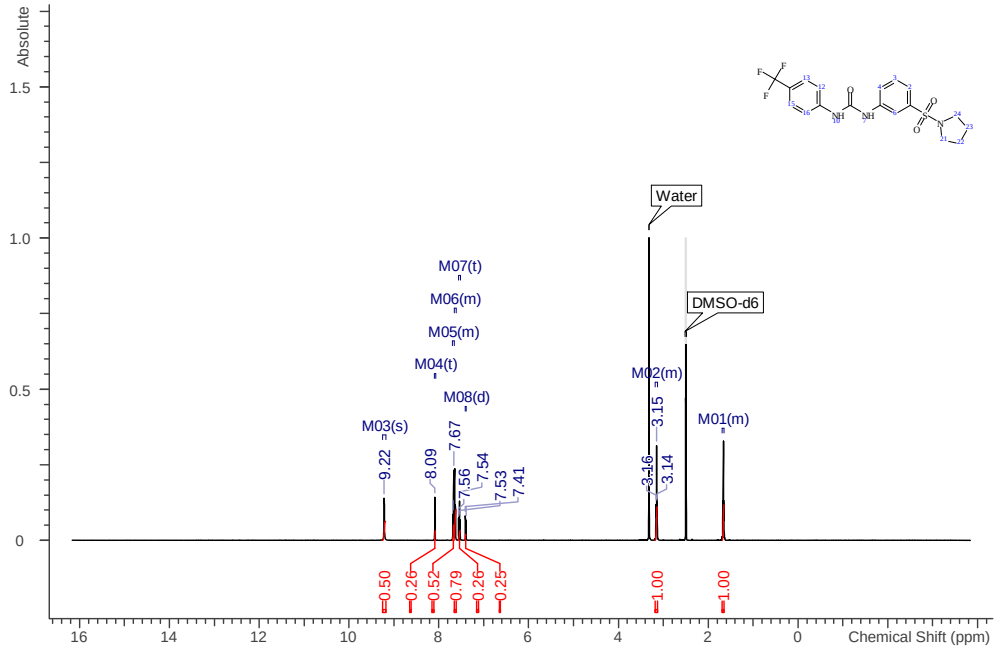
Absolute
Water
DMSO-d6
M07(t)
M06(m)
M05(m)
M04(t)
M08(d)
M03(s)
M02(m)
M01(m)
9.22
8.09
7.67
7.56
7.54
7.53
7.41
3.16
3.15
3.14
0.50
0.26
0.52
0.79
0.26
0.25
1.00
1.00
Chemical Shift (ppm)

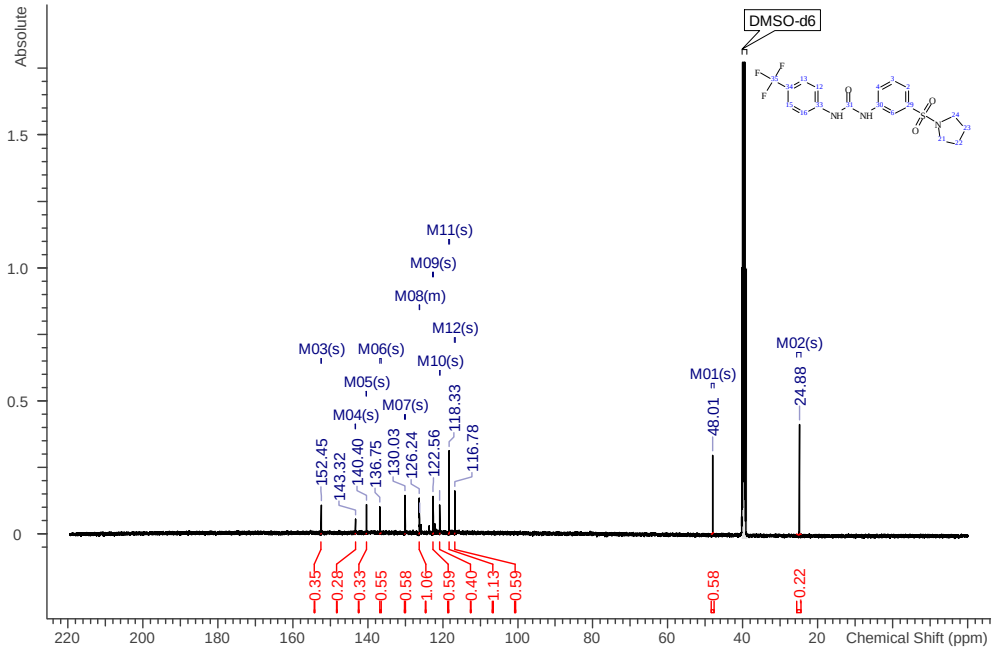
Absolute
DMSO-d6
M11(s)
M09(s)
M08(m)
M12(s)
M03(s)
M06(s)
M10(s)
M05(s)
M04(s)
M07(s)
M01(s)
M02(s)
152.45
143.32
140.40
136.75
130.03
126.24
122.56
118.33
116.78
48.01
24.88
0.35
0.28
0.33
0.55
0.58
1.06
0.59
0.40
1.13
0.59
0.58
0.22
Chemical Shift (ppm)

12

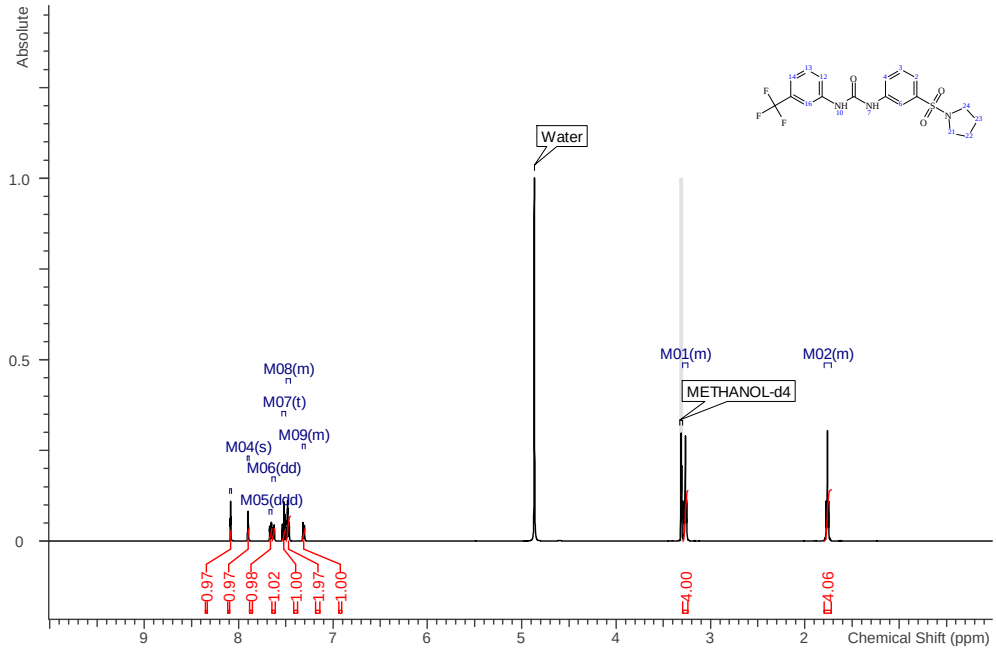
Absolute
Water
M01(m)
M02(m)
METHANOL-d4
M08(m)
M07(t)
M09(m)
M04(s)
M06(dd)
M05(ddd)
0.97
0.97
0.98
1.02
1.00
1.97
1.00
4.00
4.06
Chemical Shift (ppm)

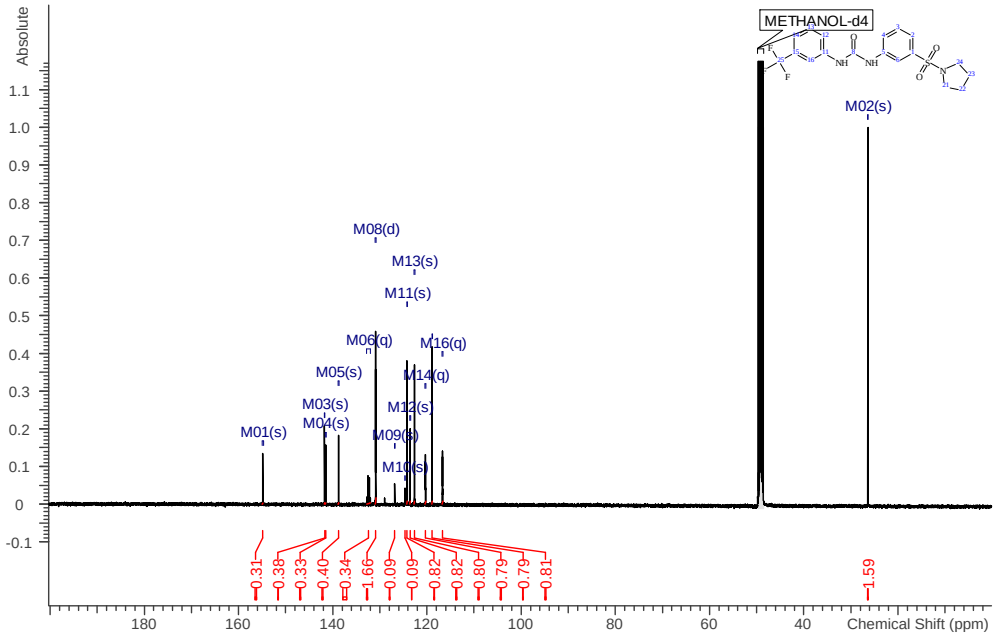
Absolute
METHANOL-d4
M02(s)
M08(d)
M13(s)
M11(s)
M06(q)
M16(q)
M05(s)
M14(q)
M03(s)
M12(s)
M04(s)
M01(s)
M09(s)
M10(s)
0.31
0.38
0.33
0.40
0.34
1.66
0.09
0.09
0.82
0.82
0.80
0.79
0.79
0.81
1.59
Chemical Shift (ppm)

13

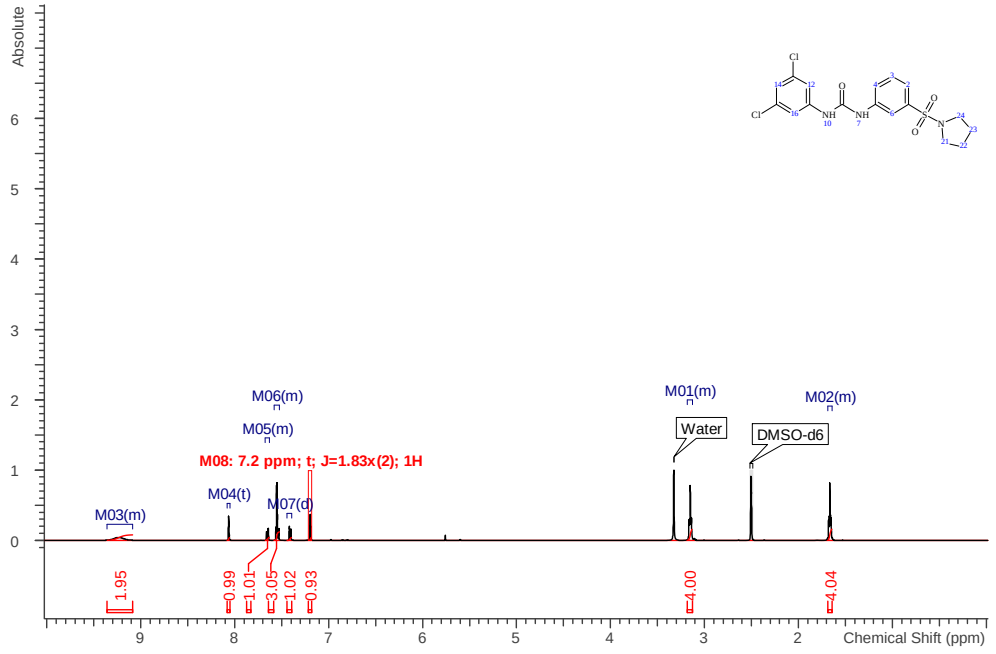
Absolute
M06(m)
M05(m)
M08: 7.2 ppm; t; J=1.83x(2); 1H
M04(t)
M07(d)
M03(m)
M01(m)
Water
DMSO-d6
M02(m)
1.95
0.99
1.01
3.05
1.02
0.93
4.00
4.04
Chemical Shift (ppm)

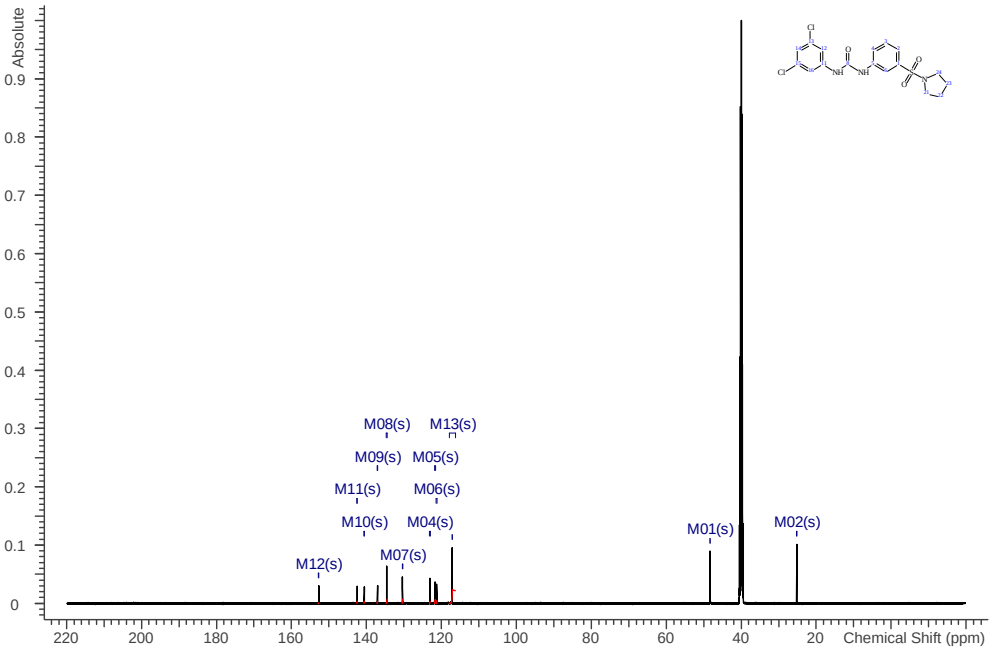
Absolute
M08(s)
M13(s)
M09(s)
M05(s)
M11(s)
M06(s)
M10(s)
M04(s)
M07(s)
M12(s)
M01(s)
M02(s)
Chemical Shift (ppm)

14

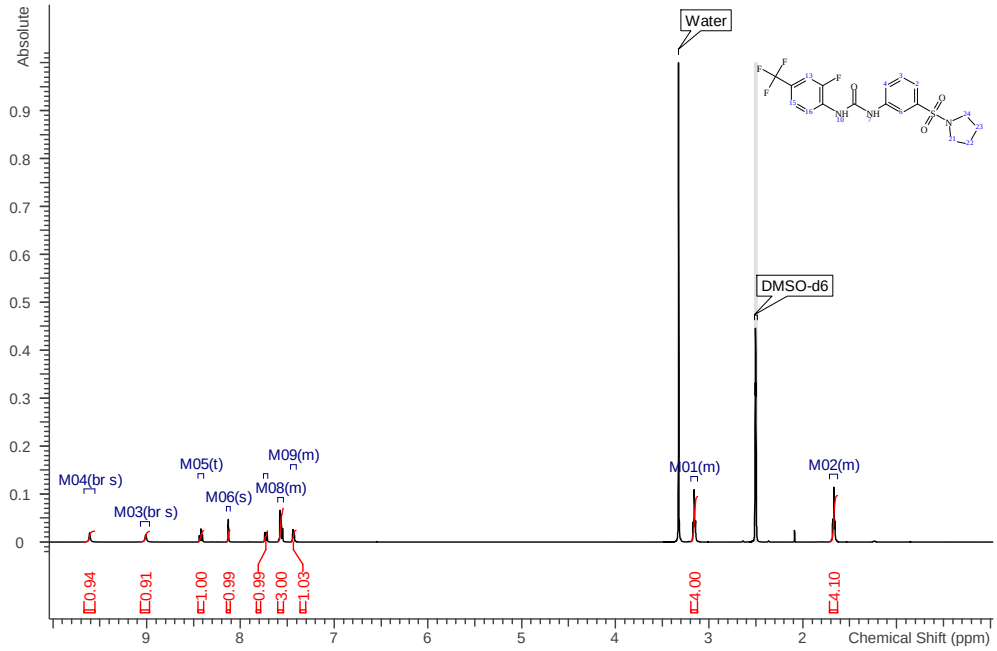
Absolute
Water
DMSO-d6
M04(br s)
M03(br s)
M05(t)
M06(s)
M09(m)
M08(m)
M01(m)
M02(m)
0.94
0.91
1.00
0.99
0.99
3.00
1.03
4.00
4.10
Chemical Shift (ppm)

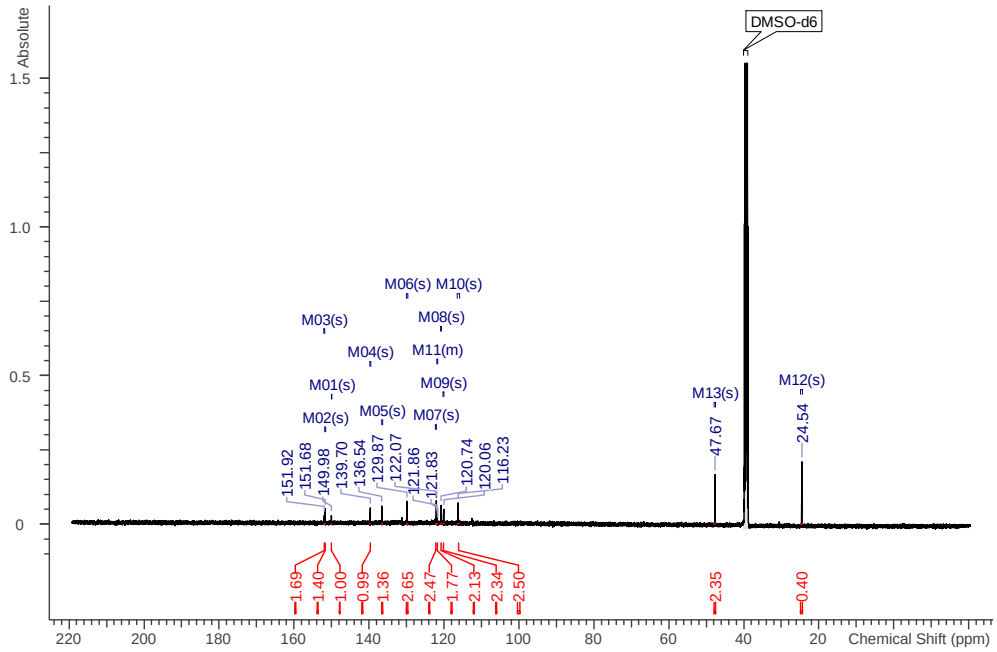
Absolute
DMSO-d6
M06(s) M10(s)
M03(s)
M08(s)
M04(s)
M11(m)
M01(s)
M09(s)
M02(s)
M05(s)
M07(s)
M13(s)
M12(s)
151.92
151.68
149.98
139.70
136.54
129.87
122.07
121.86
121.83
120.74
120.06
116.23
47.67
24.54
1.69
1.40
1.00
0.99
1.36
2.65
2.47
1.77
2.13
2.34
2.50
2.35
0.40
Chemical Shift (ppm)

15

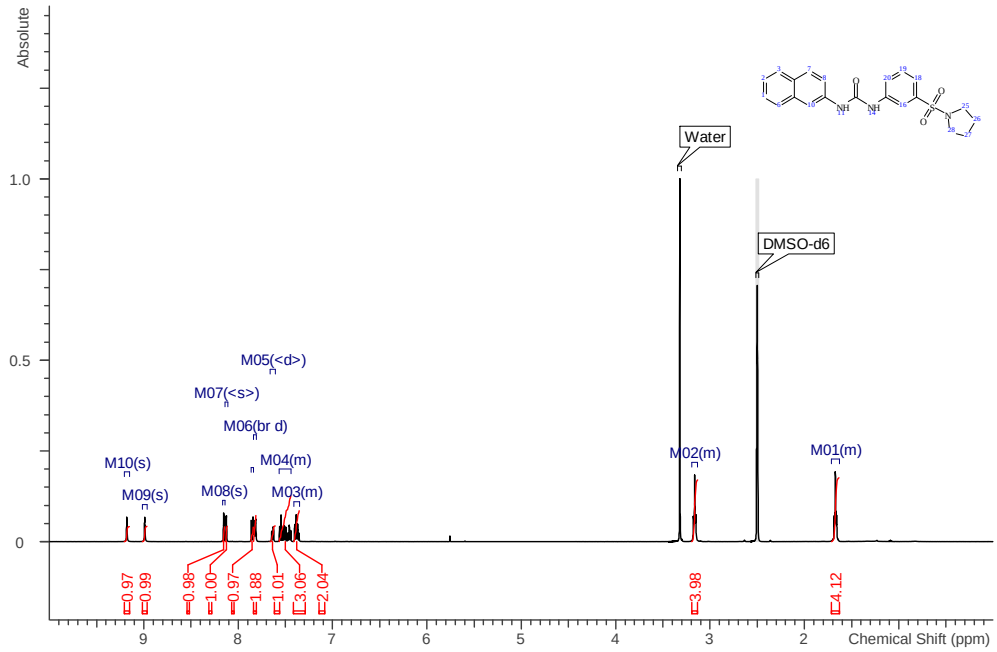
Absolute
1.0
0.5
0
Water
DMSO-d6
M05(<d>)
M07(<s>)
M06(br d)
M04(m)
M10(s)
M09(s)
M08(s)
M03(m)
M02(m)
M01(m)
0.97
0.99
0.98
1.00
0.97
1.88
1.01
3.06
2.04
3.98
4.12
9
8
7
6
5
4
3
2
Chemical Shift (ppm)

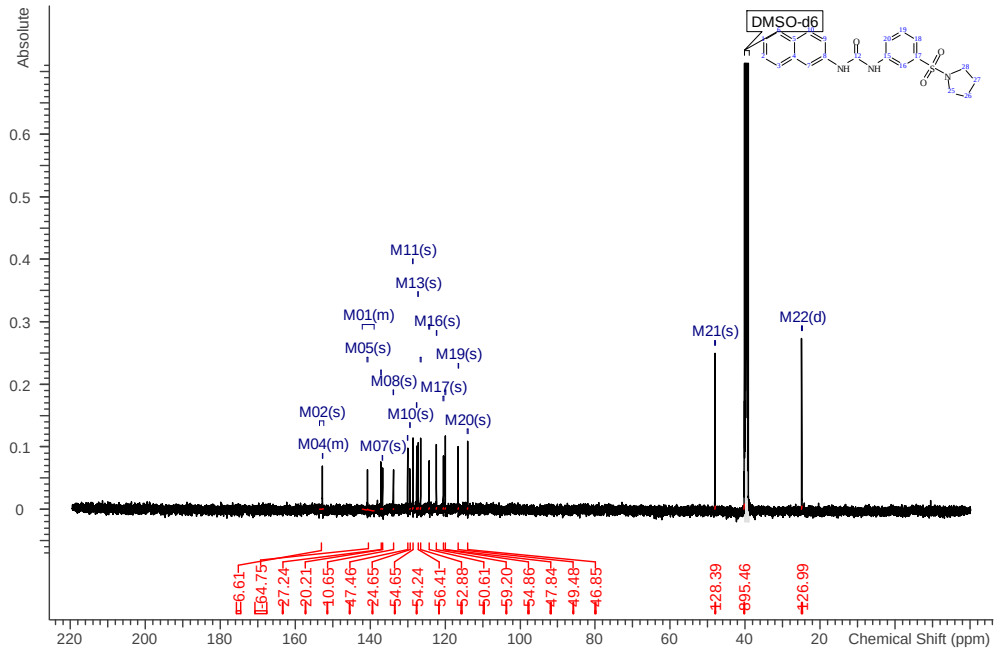
Absolute
0.6
0.5
0.4
0.3
0.2
0.1
0
DMSO-d6
M11(s)
M13(s)
M01(m)
M16(s)
M05(s)
M19(s)
M08(s)
M17(s)
M02(s)
M10(s)
M20(s)
M04(m)
M07(s)
M21(s)
M22(d)
6.61
34.75
27.24
20.21
10.65
47.46
24.65
54.65
54.24
56.41
52.88
50.61
59.20
54.86
47.84
49.48
46.85
28.39
95.46
26.99
220
200
180
160
140
120
100
80
60
40
20
Chemical Shift (ppm)

16

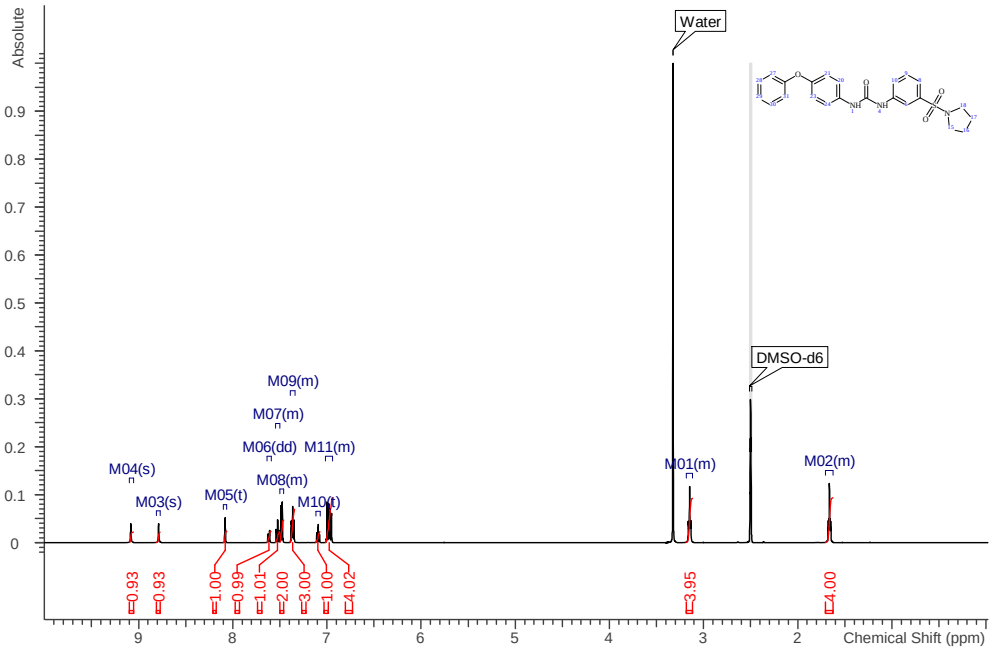
Absolute
Water
DMSO-d6
M01(m)
M02(m)
M03(s)
M04(s)
M05(t)
M06(dd)
M07(m)
M08(m)
M09(m)
M10(t)
M11(m)
0.93
0.93
1.00
0.99
1.01
2.00
3.00
1.00
4.02
3.95
4.00
Chemical Shift (ppm)

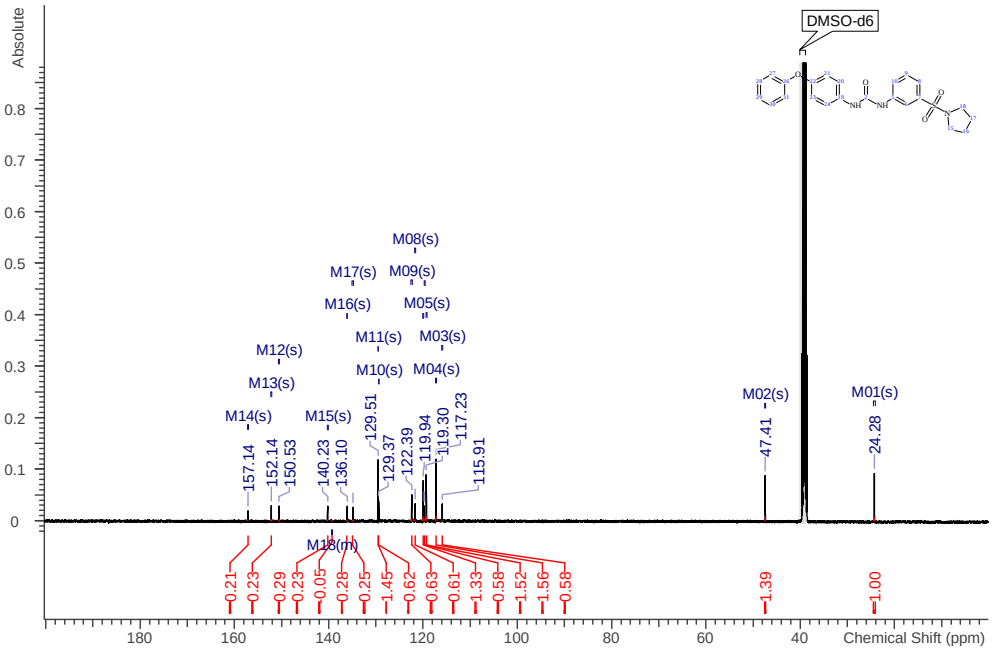
Absolute
DMSO-d6
M01(s)
M02(s)
M03(s)
M04(s)
M05(s)
M08(s)
M09(s)
M10(s)
M11(s)
M12(s)
M13(s)
M14(s)
M15(s)
M16(s)
M17(s)
M18(m)
157.14
152.14
150.53
140.23
136.10
129.51
129.37
122.39
119.94
119.30
117.23
115.91
47.41
24.28
0.21
0.23
0.29
0.23
0.05
0.28
0.25
1.45
0.62
0.63
0.61
1.33
0.58
1.52
1.56
0.58
1.39
1.00
Chemical Shift (ppm)

17

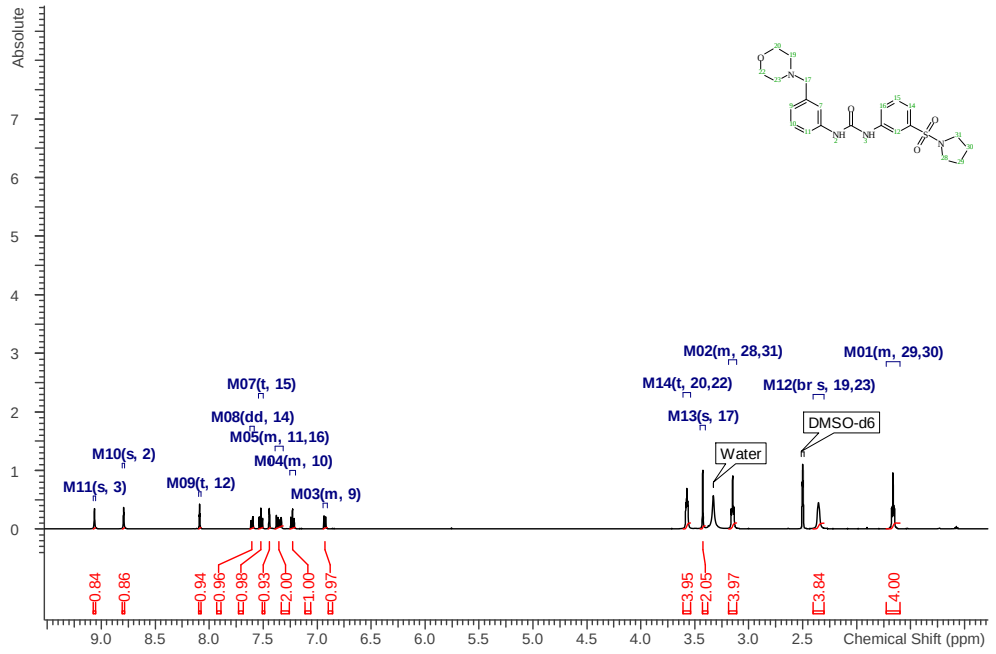
Absolute
M11(s, 3)
M10(s, 2)
M09(t, 12)
M07(t, 15)
M08(dd, 14)
M05(m, 11,16)
M04(m, 10)
M03(m, 9)
M02(m, 28,31)
M14(t, 20,22)
M13(s, 17)
M12(br s, 19,23)
M01(m, 29,30)
Water
DMSO-d6
0.84
0.86
0.94
0.96
0.98
0.93
2.00
1.00
0.97
3.95
2.05
3.97
3.84
4.00
Chemical Shift (ppm)

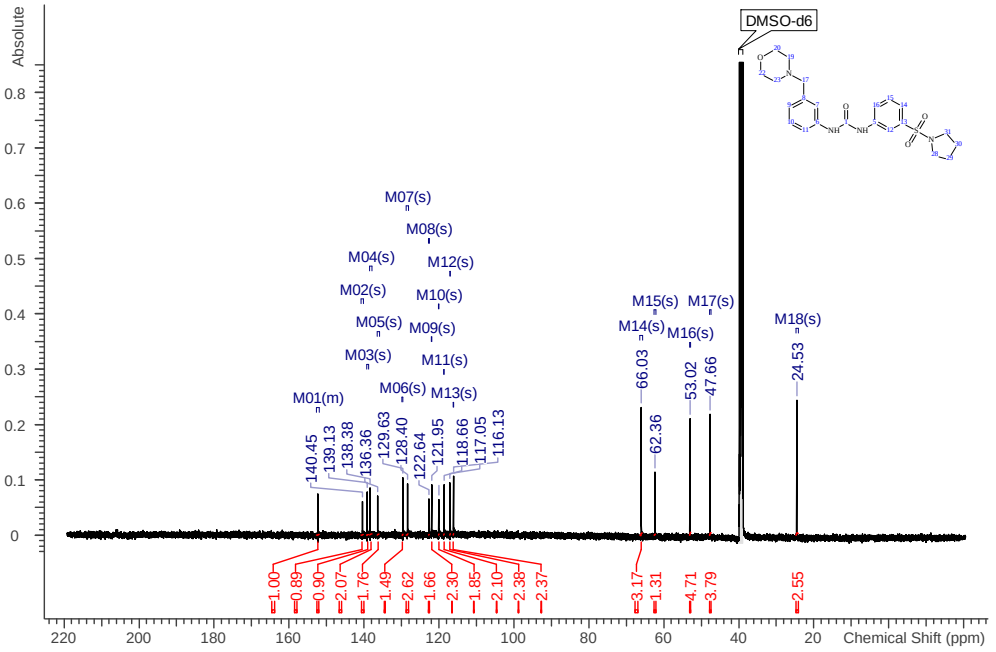
Absolute
DMSO-d6
M07(s)
M08(s)
M04(s)
M12(s)
M02(s)
M10(s)
M05(s)
M09(s)
M03(s)
M11(s)
M06(s)
M13(s)
M01(m)
M15(s)
M17(s)
M14(s)
M16(s)
M18(s)
140.45
139.13
138.38
136.36
129.63
128.40
122.64
121.95
118.66
117.05
116.13
66.03
62.36
53.02
47.66
24.53
1.00
0.89
0.90
2.07
1.76
1.49
2.62
1.66
2.30
1.85
2.10
2.38
2.37
3.17
1.31
4.71
3.79
2.55
Chemical Shift (ppm)

18

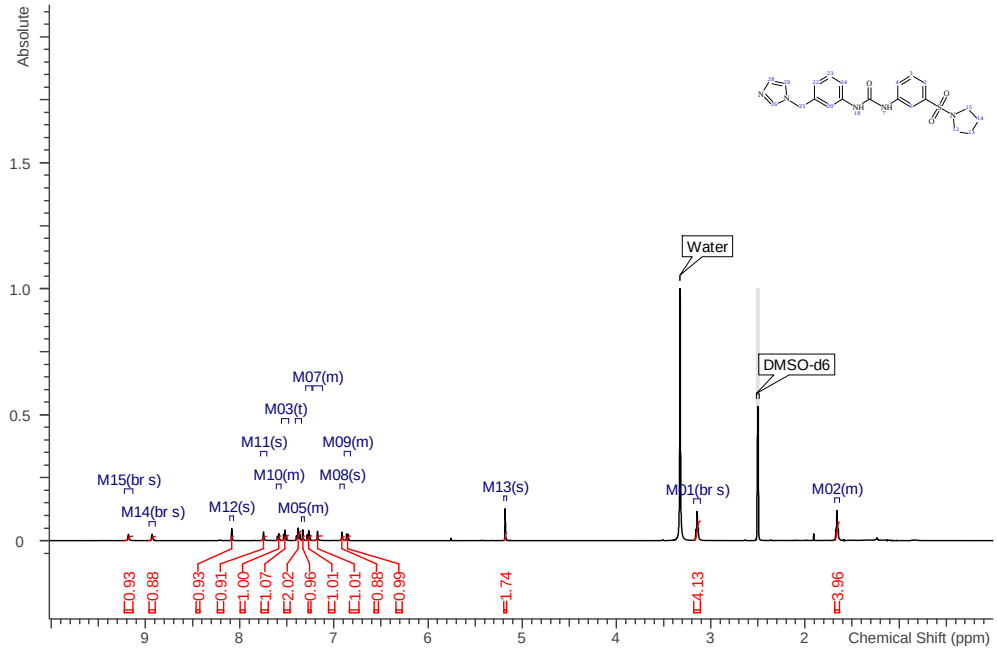
Absolute
Water
DMSO-d6
M07(m)
M03(t)
M11(s)
M09(m)
M15(br s)
M10(m)
M08(s)
M13(s)
M01(br s)
M02(m)
M14(br s)
M12(s)
M05(m)
0.93
0.88
0.93
0.91
1.00
1.07
2.02
0.96
1.01
1.01
0.88
0.99
1.74
4.13
3.96
Chemical Shift (ppm)

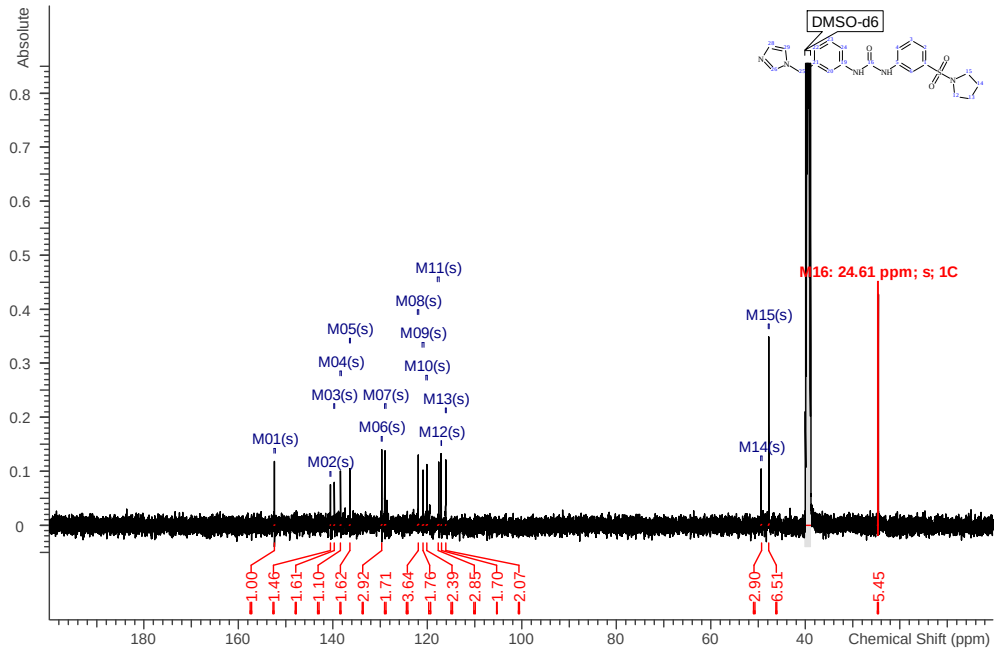
Absolute
DMSO-d6
M16: 24.61 ppm; s; 1C
M11(s)
M08(s)
M05(s)
M09(s)
M04(s)
M10(s)
M03(s)
M07(s)
M13(s)
M06(s)
M12(s)
M01(s)
M02(s)
M15(s)
M14(s)
1.00
1.46
1.61
1.10
1.62
2.92
1.71
3.64
1.76
2.39
2.85
1.70
2.07
2.90
6.51
5.45
Chemical Shift (ppm)

19

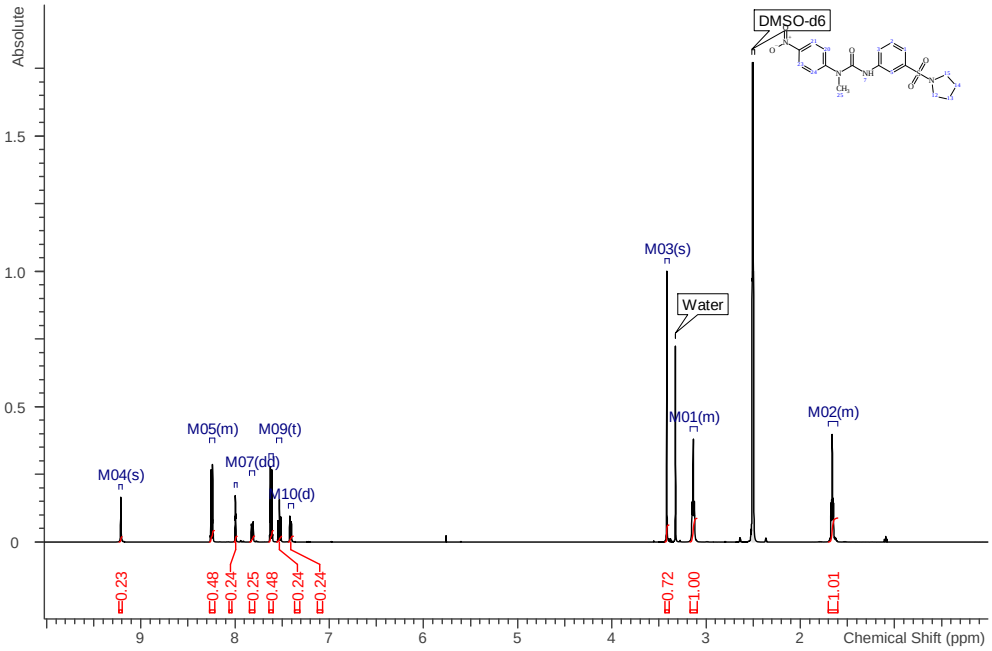
Absolute
DMSO-d6
Water
M03(s)
M01(m)
M02(m)
M05(m)
M09(t)
M07(dd)
M04(s)
M10(d)
0.23
0.48
0.24
0.25
0.48
0.24
0.24
0.72
1.00
1.01
Chemical Shift (ppm)

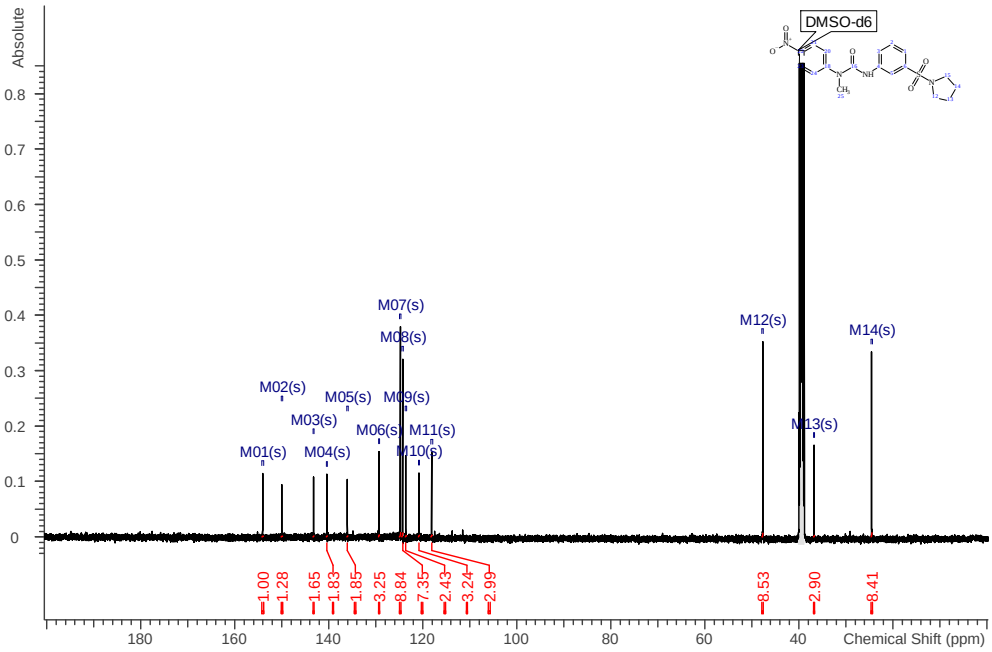
Absolute
DMSO-d6
M07(s)
M08(s)
M12(s)
M14(s)
M02(s)
M05(s)
M09(s)
M03(s)
M06(s)
M11(s)
M13(s)
M01(s)
M04(s)
M10(s)
1.00
1.28
1.65
1.83
1.85
3.25
8.84
7.35
2.43
3.24
2.99
8.53
2.90
8.41
Chemical Shift (ppm)

20

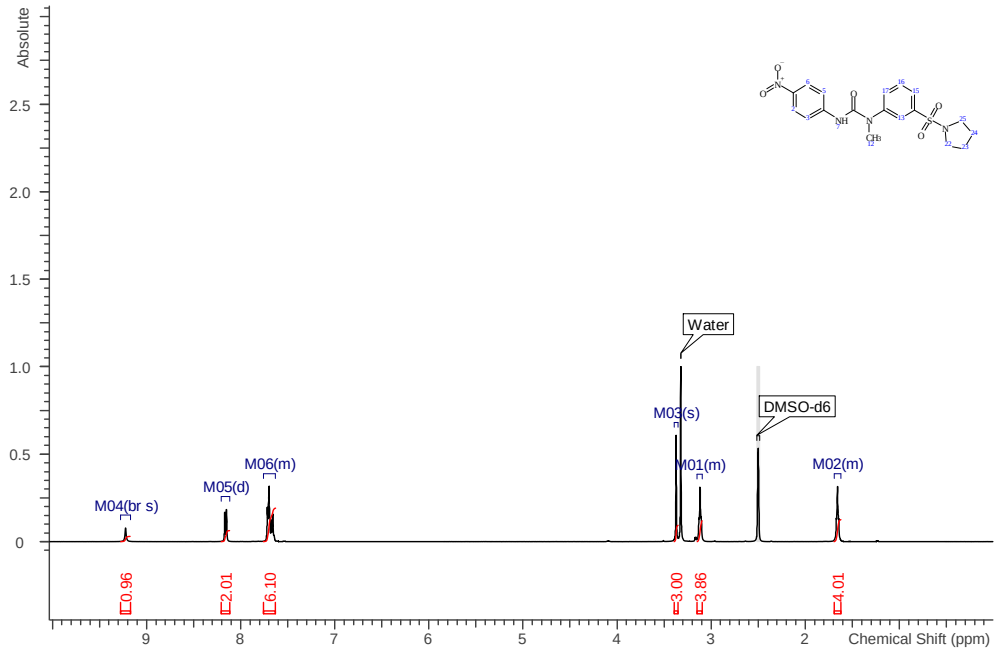
Absolute
Water
DMSO-d6
M01(m)
M02(m)
M03(s)
M04(br s)
M05(d)
M06(m)
0.96
2.01
6.10
3.00
3.86
4.01
Chemical Shift (ppm)

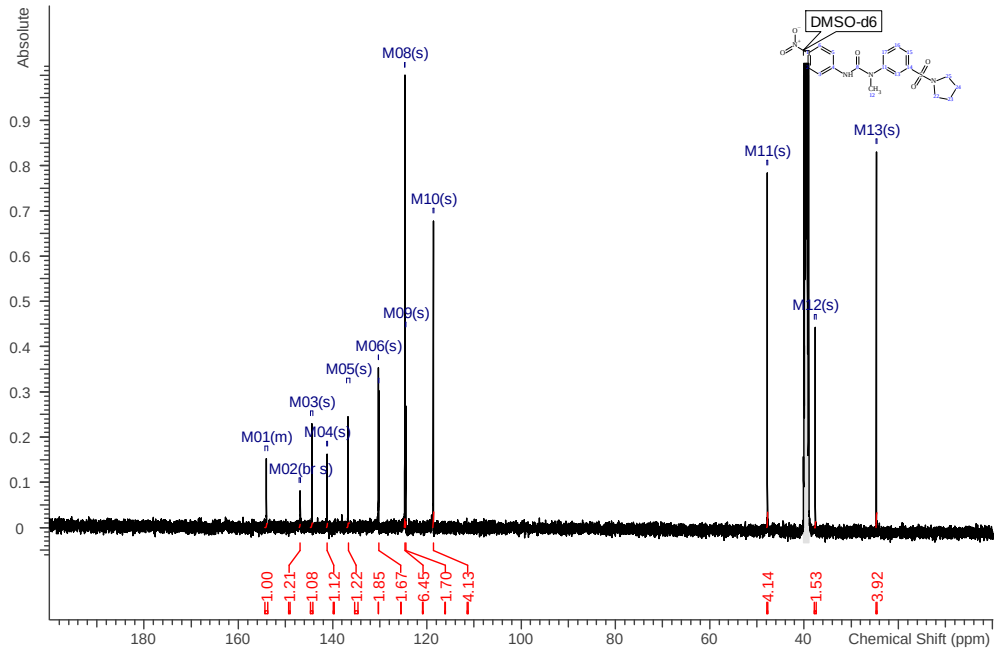
Absolute
DMSO-d6
M01(m)
M02(br s)
M03(s)
M04(s)
M05(s)
M06(s)
M08(s)
M09(s)
M10(s)
M11(s)
M12(s)
M13(s)
1.00
1.21
1.08
1.12
1.22
1.85
1.67
6.45
1.70
4.13
4.14
1.53
3.92
Chemical Shift (ppm)

21

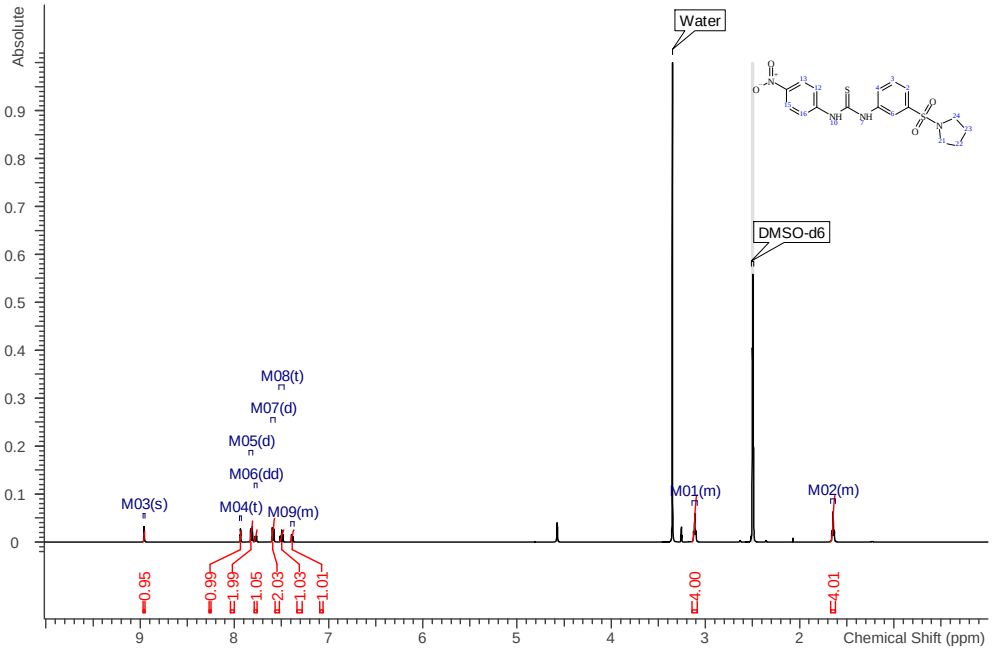
Absolute
Water
DMSO-d6
M08(t)
M07(d)
M05(d)
M06(dd)
M03(s)
M04(t)
M09(m)
M01(m)
M02(m)
0.95
0.99
1.99
1.05
2.03
1.03
1.01
4.00
4.01
Chemical Shift (ppm)

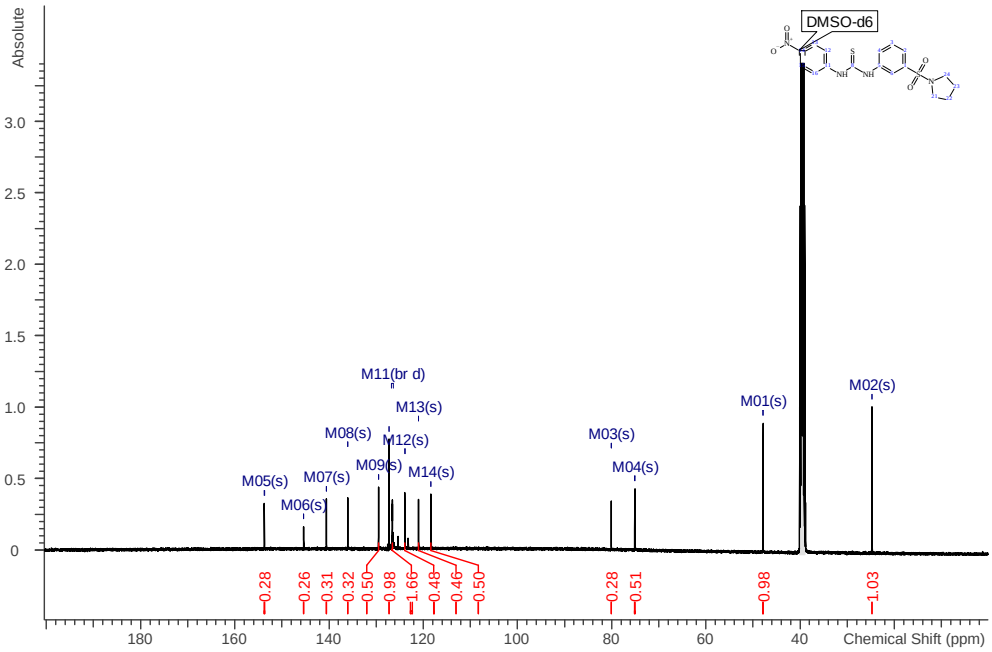
Absolute
DMSO-d6
M11(br d)
M13(s)
M08(s)
M12(s)
M09(s)
M14(s)
M05(s)
M07(s)
M06(s)
M03(s)
M04(s)
M01(s)
M02(s)
0.28
0.26
0.31
0.32
0.50
0.98
1.66
0.48
0.46
0.50
0.28
0.51
0.98
1.03
Chemical Shift (ppm)

22

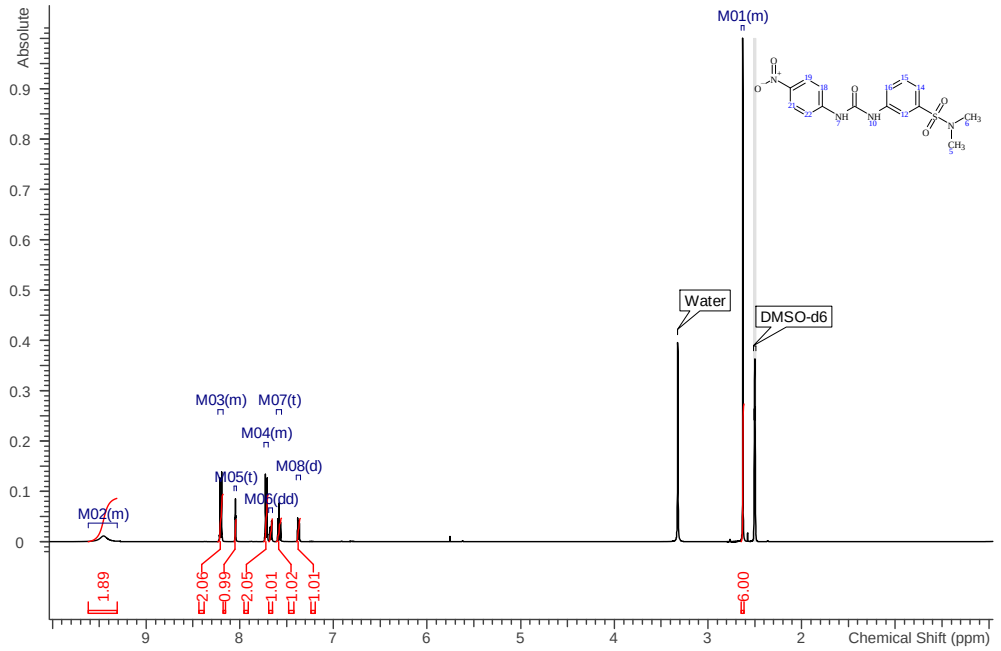
Absolute
M01(m)
Water
DMSO-d6
M03(m)
M07(t)
M04(m)
M08(d)
M05(t)
M06(dd)
M02(m)
1.89
2.06
0.99
2.05
1.01
1.02
1.01
6.00
Chemical Shift (ppm)

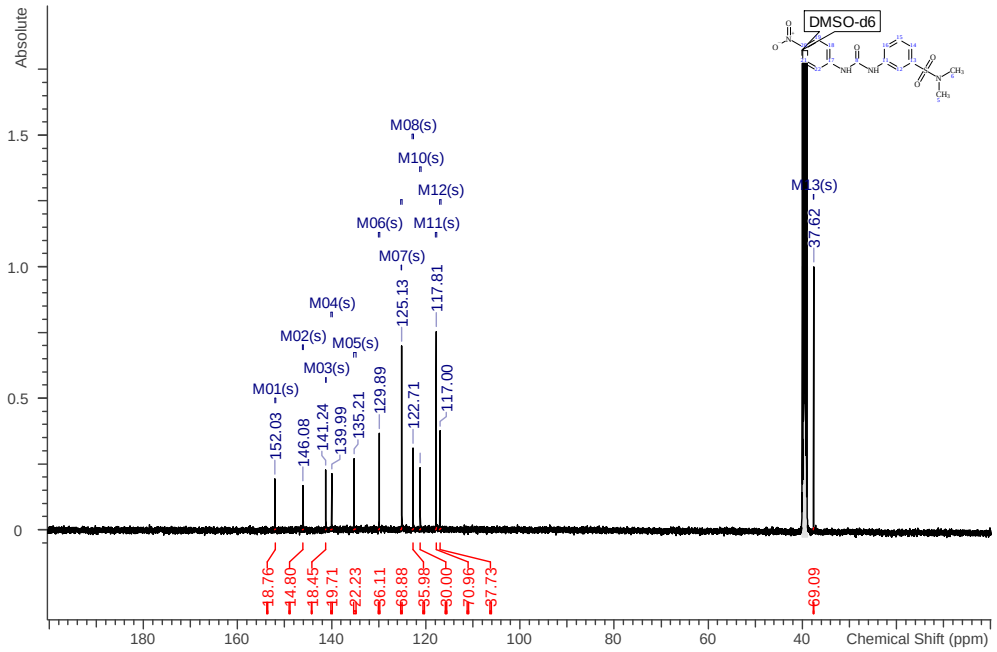
Absolute
DMSO-d6
M08(s)
M10(s)
M12(s)
M13(s)
M06(s)
M11(s)
M07(s)
M04(s)
M02(s)
M05(s)
M03(s)
M01(s)
152.03
146.08
141.24
139.99
135.21
129.89
125.13
122.71
117.81
117.00
37.62
18.76
14.80
18.45
19.71
22.23
36.11
68.88
35.98
30.00
70.96
37.73
69.09
Chemical Shift (ppm)

23

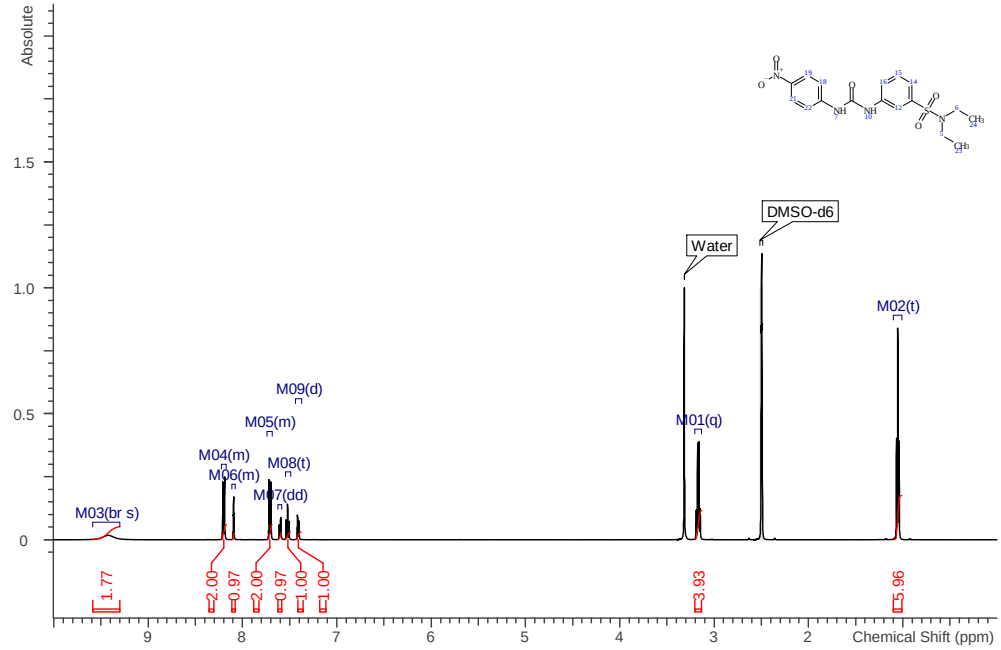
Absolute
Water
DMSO-d6
M02(t)
M01(q)
M09(d)
M05(m)
M04(m)
M06(m)
M08(t)
M07(dd)
M03(br s)
1.77
2.00
0.97
2.00
0.97
1.00
1.00
3.93
5.96
Chemical Shift (ppm)

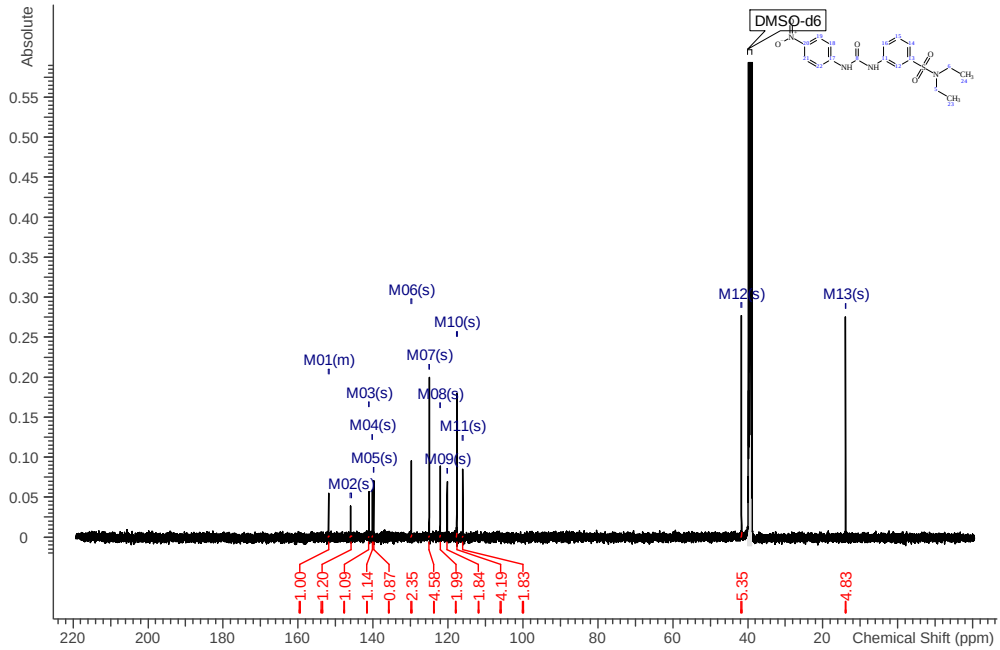
Absolute
DMSO-d6
M06(s)
M10(s)
M01(m)
M07(s)
M03(s)
M08(s)
M04(s)
M11(s)
M05(s)
M09(s)
M02(s)
M12(s)
M13(s)
1.00
1.20
1.09
1.14
0.87
2.35
4.58
1.99
1.84
4.19
1.83
5.35
4.83
Chemical Shift (ppm)

24

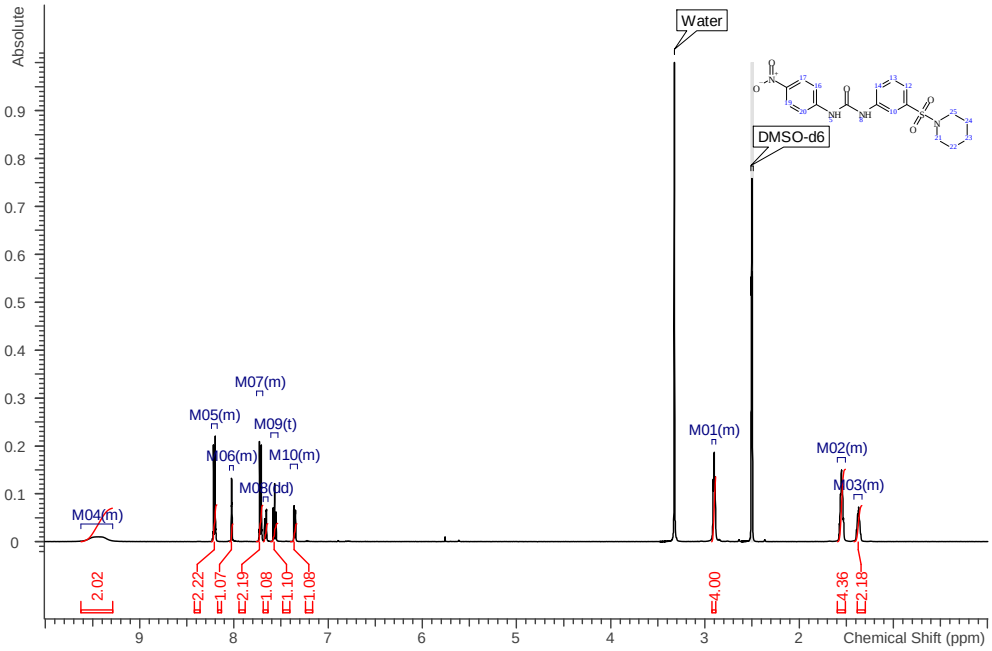
Absolute
Water
DMSO-d6
M01(m)
M02(m)
M03(m)
M04(m)
M05(m)
M06(m)
M07(m)
M08(dd)
M09(t)
M10(m)
2.02
2.22
1.07
2.19
1.08
1.10
1.08
4.00
4.36
2.18
Chemical Shift (ppm)

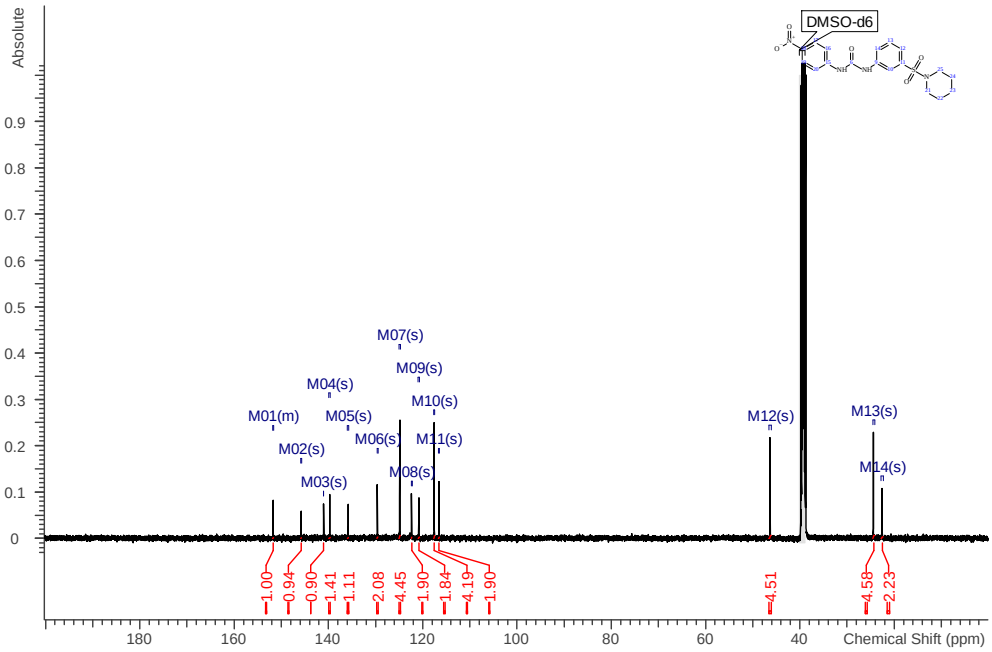
Absolute
DMSO-d6
M01(m)
M02(s)
M03(s)
M04(s)
M05(s)
M06(s)
M07(s)
M08(s)
M09(s)
M10(s)
M11(s)
M12(s)
M13(s)
M14(s)
1.00
0.94
0.90
1.41
1.11
2.08
4.45
1.90
1.84
4.19
1.90
4.51
4.58
2.23
Chemical Shift (ppm)

25

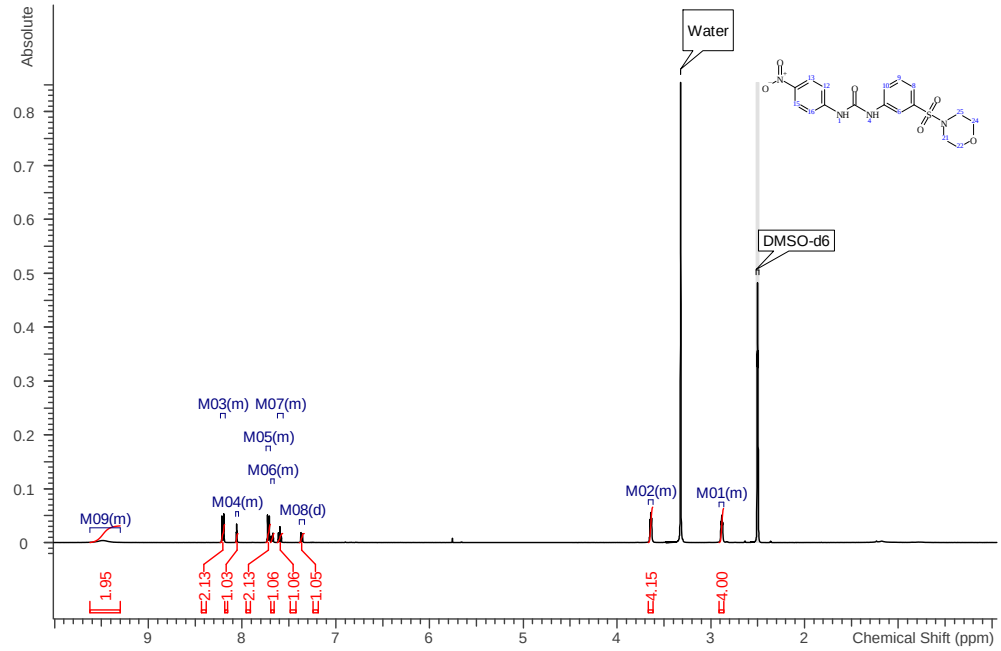
Absolute
Water
DMSO-d6
M03(m) M07(m)
M05(m)
M06(m)
M04(m)
M08(d)
M09(m)
M02(m)
M01(m)
1.95
2.13
1.03
2.13
1.06
1.06
1.05
4.15
4.00
Chemical Shift (ppm)

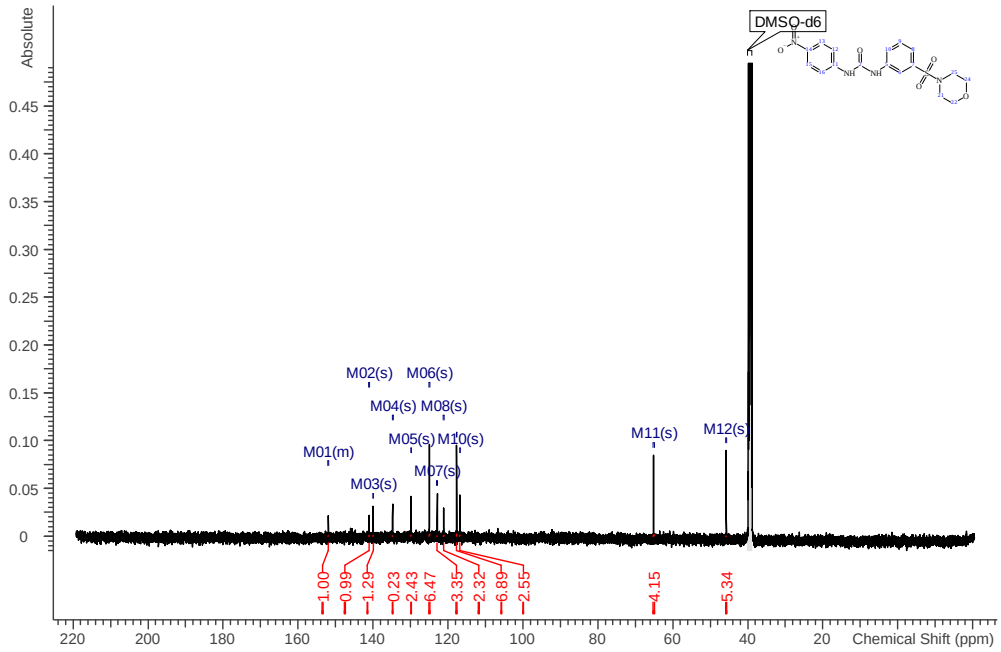
Absolute
DMSO-d6
M02(s) M06(s)
M04(s) M08(s)
M05(s) M10(s)
M01(m)
M07(s)
M03(s)
M11(s)
M12(s)
1.00
0.99
1.29
0.23
2.43
6.47
3.35
2.32
6.89
2.55
4.15
5.34
Chemical Shift (ppm)

26

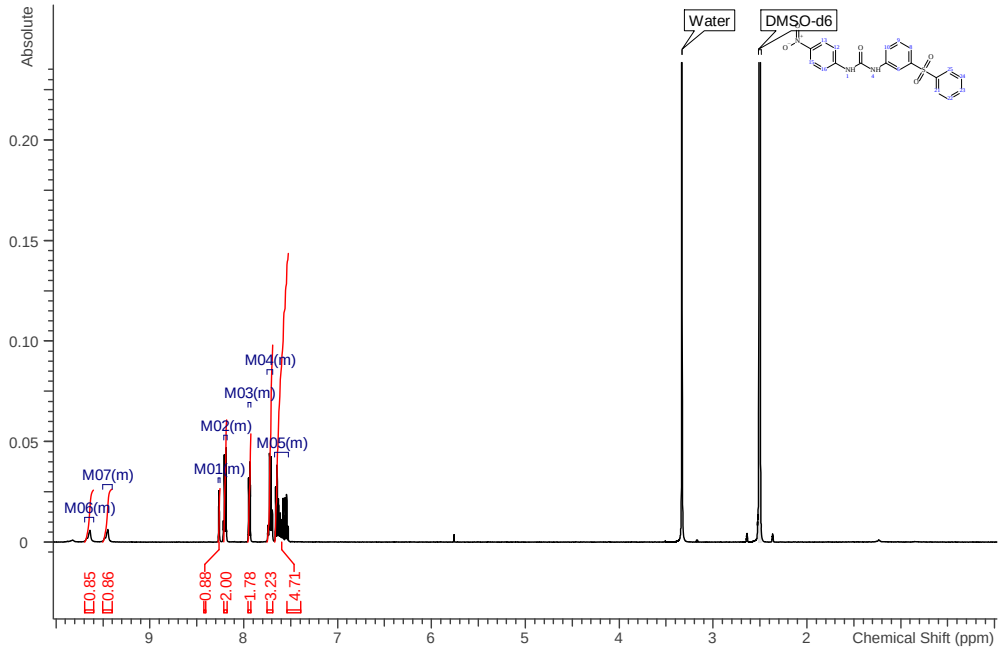
Absolute
Water
DMSO-d6
M04(m)
M03(m)
M02(m)
M05(m)
M01(m)
M07(m)
M06(m)
0.85
0.86
0.88
2.00
1.78
3.23
4.71
Chemical Shift (ppm)

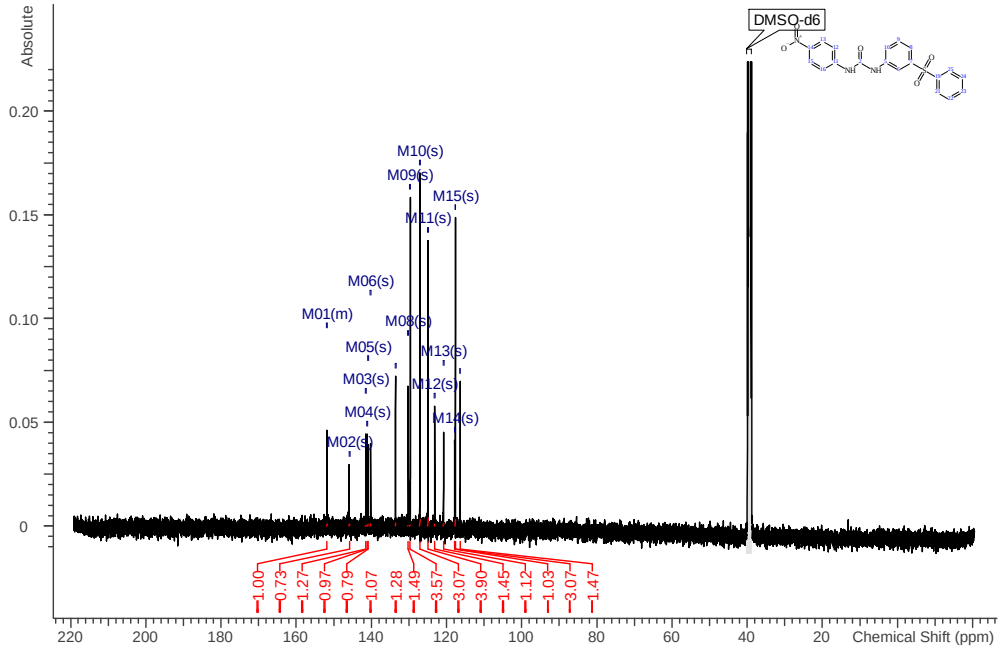
Absolute
DMSO-d6
M10(s)
M09(s)
M15(s)
M11(s)
M06(s)
M01(m)
M08(s)
M05(s)
M13(s)
M03(s)
M12(s)
M04(s)
M14(s)
M02(s)
1.00
0.73
1.27
0.97
0.79
1.07
1.28
1.49
3.57
3.07
3.90
1.45
1.12
1.03
3.07
1.47
Chemical Shift (ppm)

27

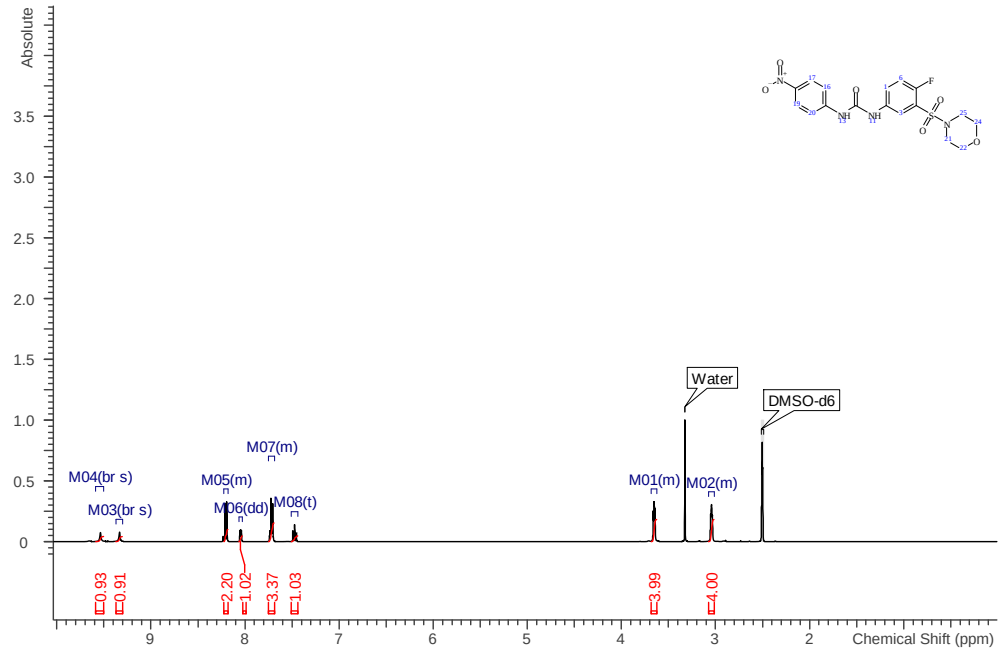
Absolute
Water
DMSO-d6
M04(br s)
M03(br s)
M05(m)
M06(dd)
M07(m)
M08(t)
M01(m)
M02(m)
0.93
0.91
2.20
1.02
3.37
1.03
3.99
4.00
Chemical Shift (ppm)

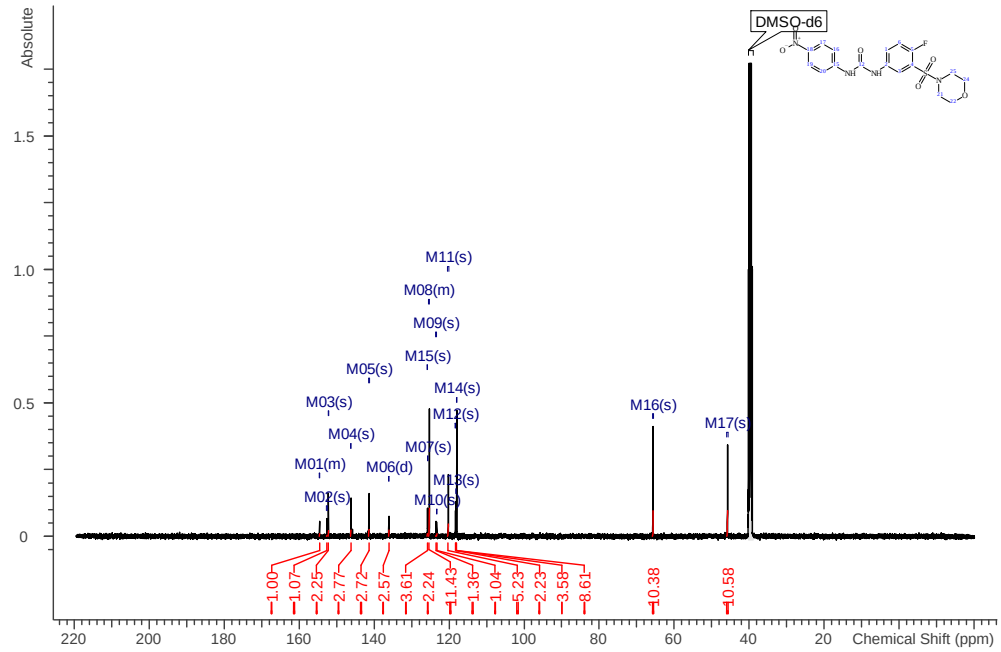
Absolute
DMSO-d6
M11(s)
M08(m)
M09(s)
M15(s)
M05(s)
M14(s)
M03(s)
M12(s)
M04(s)
M07(s)
M01(m)
M06(d)
M13(s)
M02(s)
M10(s)
M16(s)
M17(s)
1.00
1.07
2.25
2.77
2.72
2.57
3.61
2.24
11.43
1.36
1.04
5.23
2.23
3.58
8.61
10.38
10.58
Chemical Shift (ppm)

28

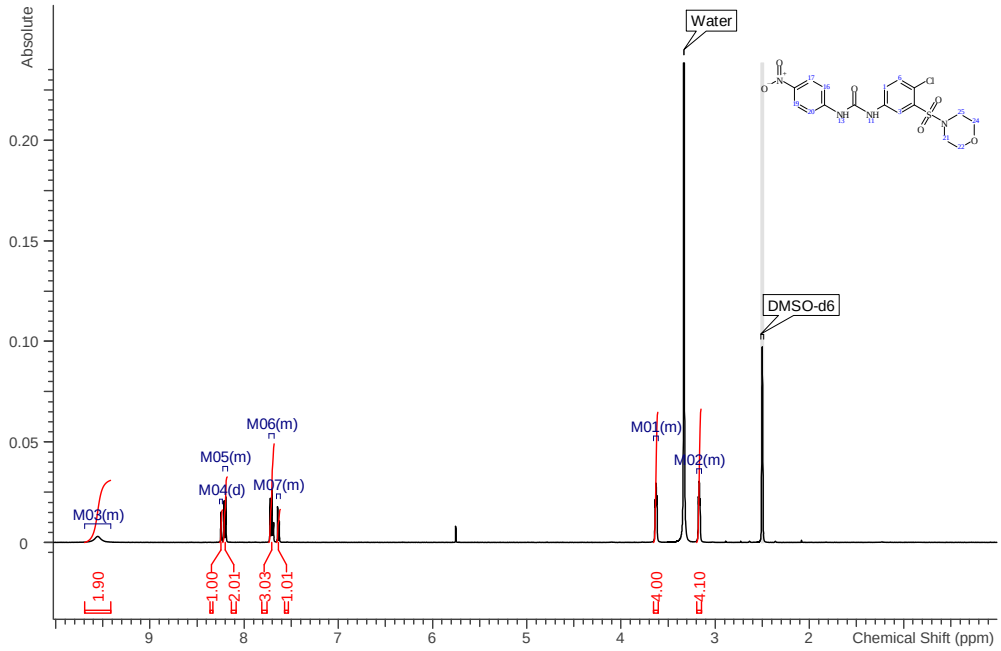
Absolute
Water
DMSO-d6
M01(m)
M02(m)
M03(m)
M04(d)
M05(m)
M06(m)
M07(m)
1.90
1.00
2.01
3.03
1.01
4.00
4.10
Chemical Shift (ppm)

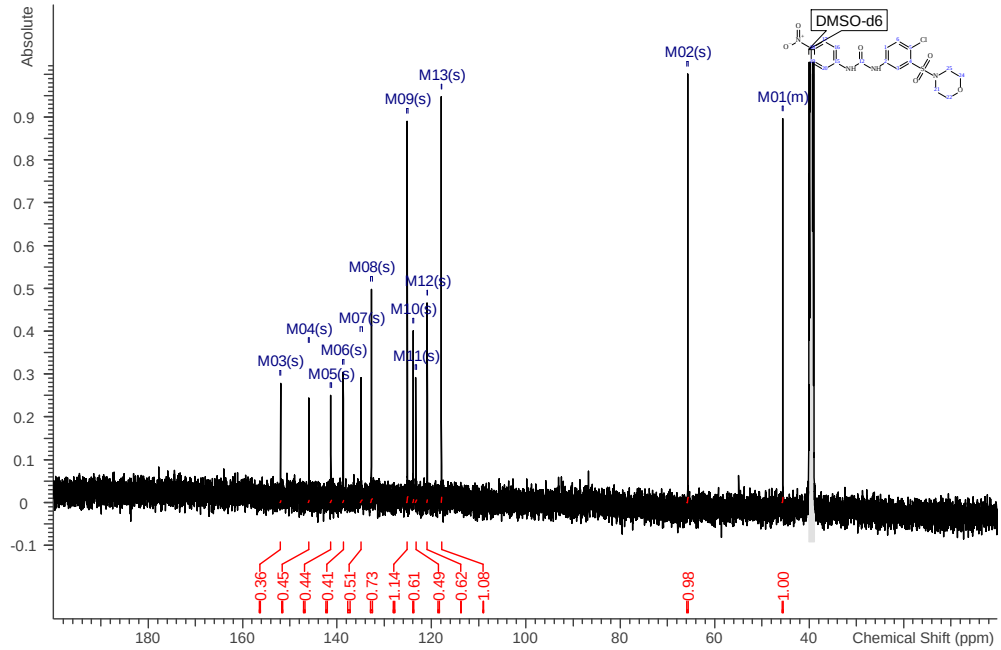
Absolute
DMSO-d6
M01(m)
M02(s)
M03(s)
M04(s)
M05(s)
M06(s)
M07(s)
M08(s)
M09(s)
M10(s)
M11(s)
M12(s)
M13(s)
0.36
0.45
0.44
0.41
0.51
0.73
1.14
0.61
0.49
0.62
1.08
0.98
1.00
Chemical Shift (ppm)

29

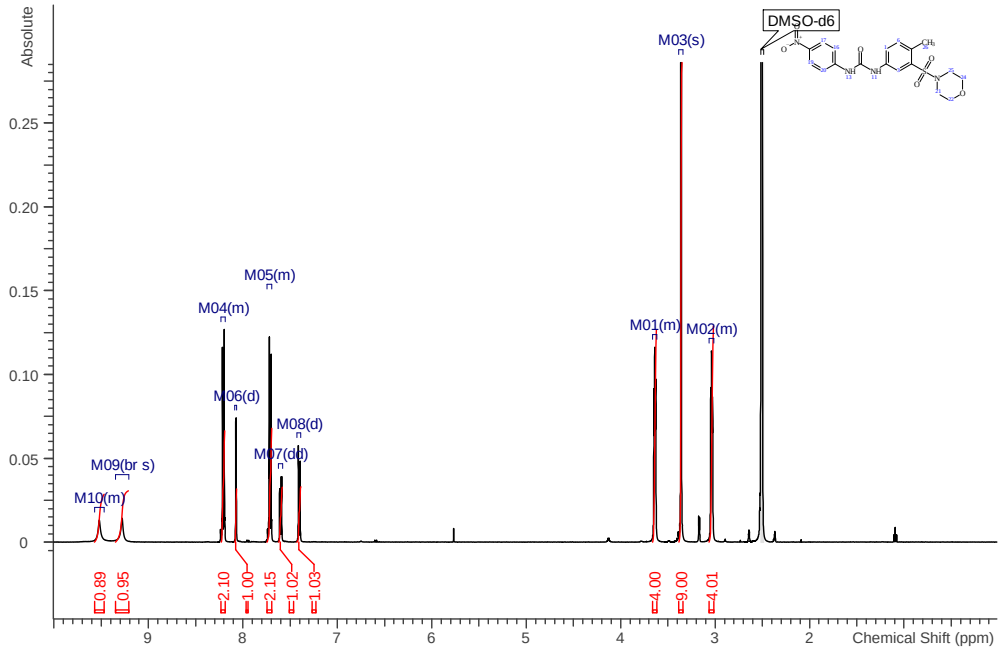
Absolute
DMSO-d6
M03(s)
M05(m)
M04(m)
M01(m)
M02(m)
M06(d)
M08(d)
M07(dd)
M09(br s)
M10(m)
0.89
0.95
2.10
1.00
2.15
1.02
1.03
4.00
9.00
4.01
Chemical Shift (ppm)

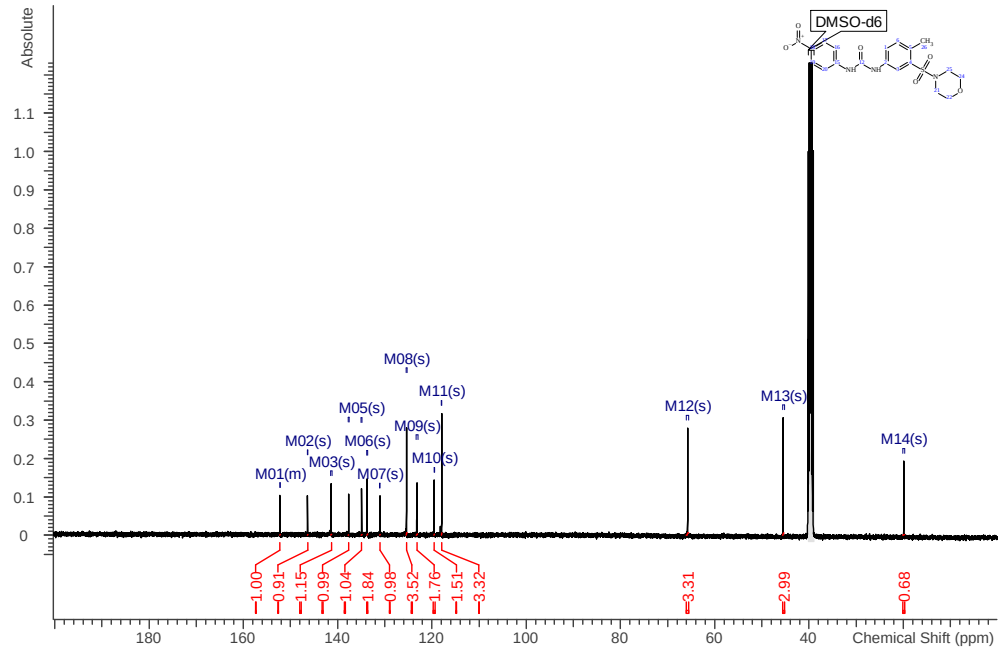
Absolute
DMSO-d6
M08(s)
M11(s)
M05(s)
M09(s)
M02(s)
M06(s)
M03(s)
M10(s)
M01(m)
M07(s)
M12(s)
M13(s)
M14(s)
1.00
0.91
1.15
0.99
1.04
1.84
0.98
3.52
1.76
1.51
3.32
3.31
2.99
0.68
Chemical Shift (ppm)

30

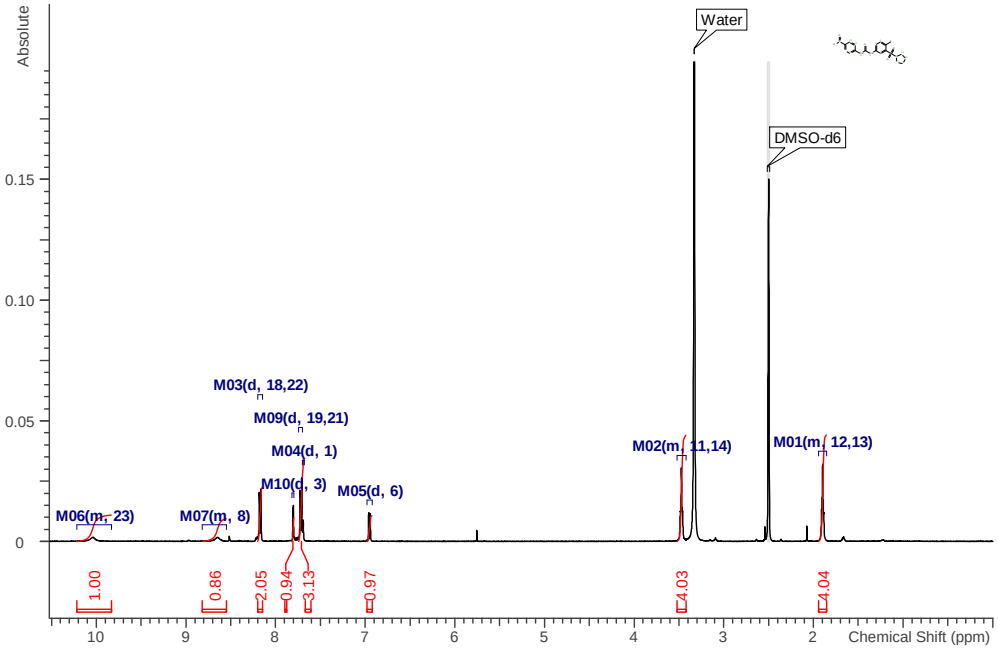
Absolute
Water
DMSO-d6
M03(d, 18,22)
M09(d, 19,21)
M04(d, 1)
M10(d, 3)
M05(d, 6)
M06(m, 23)
M07(m, 8)
M02(m, 11,14)
M01(m, 12,13)
1.00
0.86
2.05
0.94
3.13
0.97
4.03
4.04
Chemical Shift (ppm)

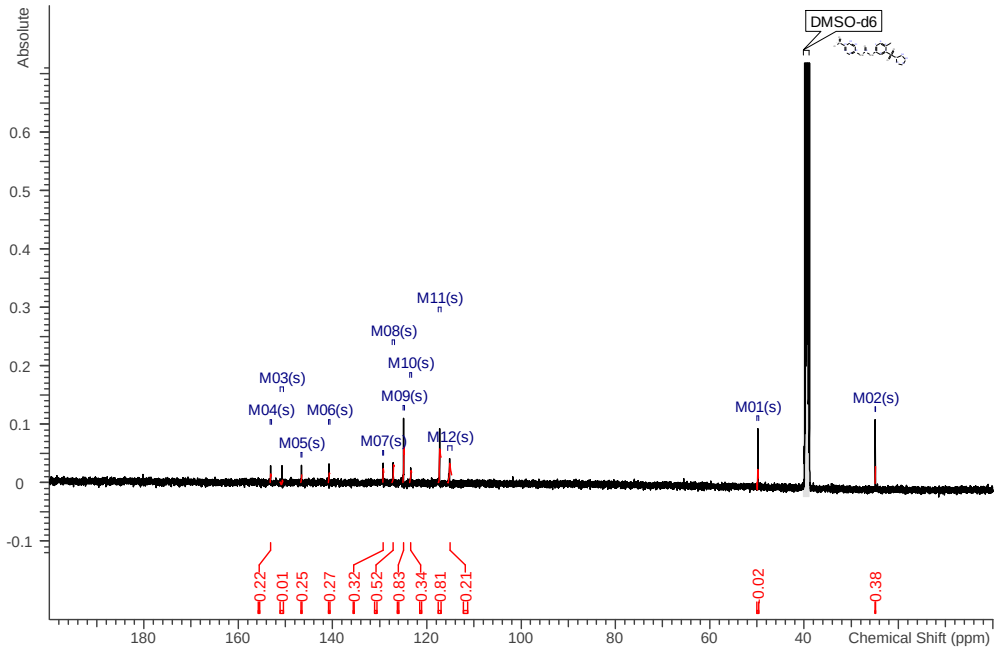
Absolute
DMSO-d6
M11(s)
M08(s)
M10(s)
M03(s)
M09(s)
M04(s)
M06(s)
M05(s)
M07(s)
M12(s)
M01(s)
M02(s)
0.22
0.01
0.25
0.27
0.32
0.52
0.83
0.34
0.81
0.21
0.02
0.38
Chemical Shift (ppm)

31

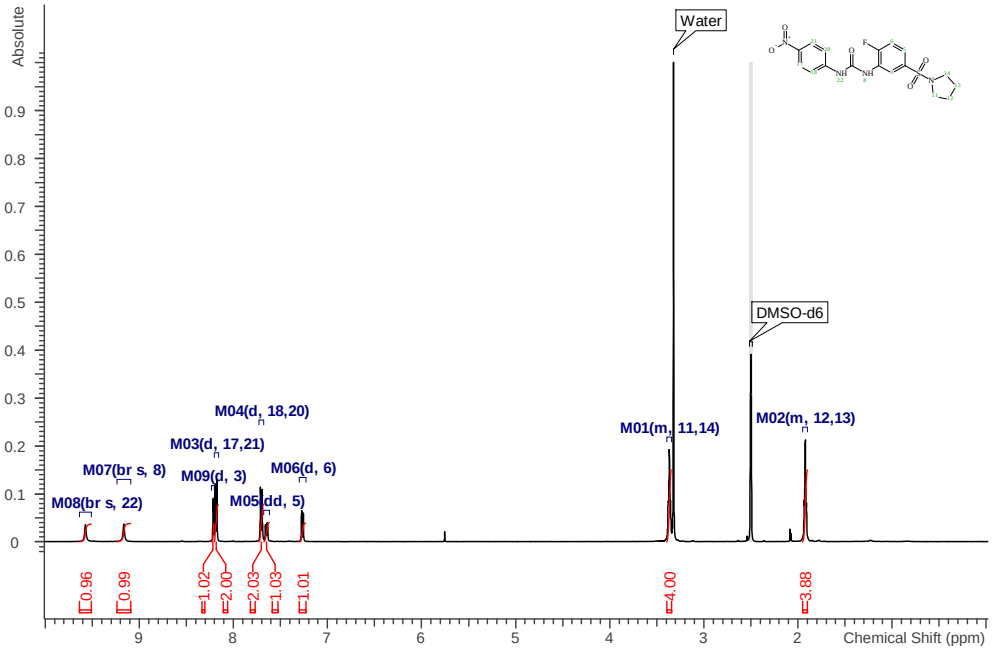
Absolute
Water
DMSO-d6
M01(m, 11,14)
M02(m, 12,13)
M03(d, 17,21)
M04(d, 18,20)
M05(dd, 5)
M06(d, 6)
M07(br s, 8)
M08(br s, 22)
M09(d, 3)
0.96
0.99
1.02
2.00
2.03
1.03
1.01
4.00
3.88
Chemical Shift (ppm)

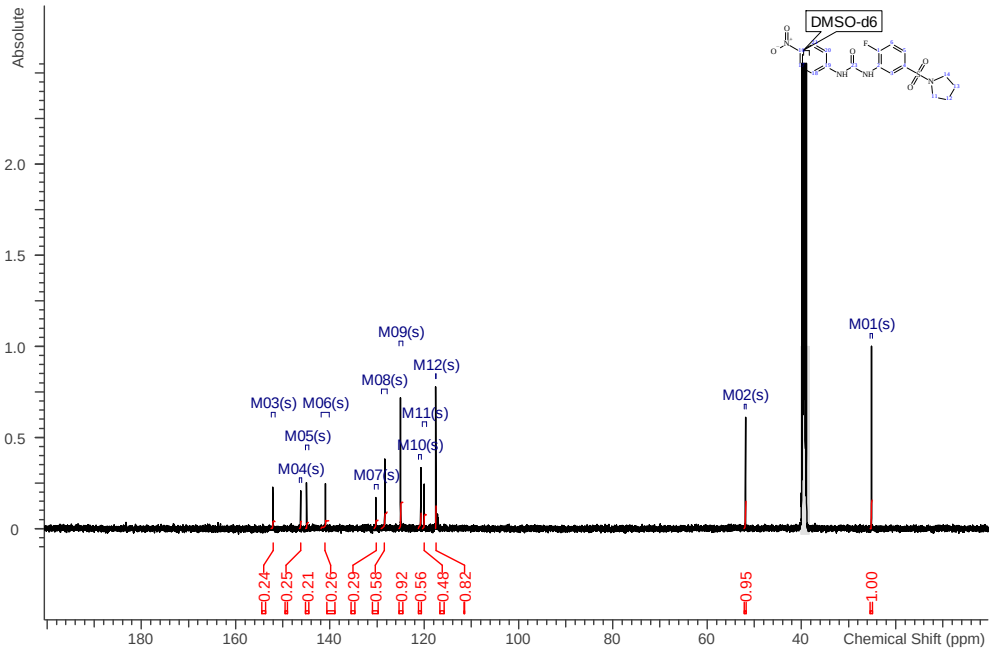
Absolute
DMSO-d6
M01(s)
M02(s)
M03(s)
M04(s)
M05(s)
M06(s)
M07(s)
M08(s)
M09(s)
M10(s)
M11(s)
M12(s)
0.24
0.25
0.21
0.26
0.29
0.58
0.92
0.56
0.48
0.82
0.95
1.00
Chemical Shift (ppm)

32

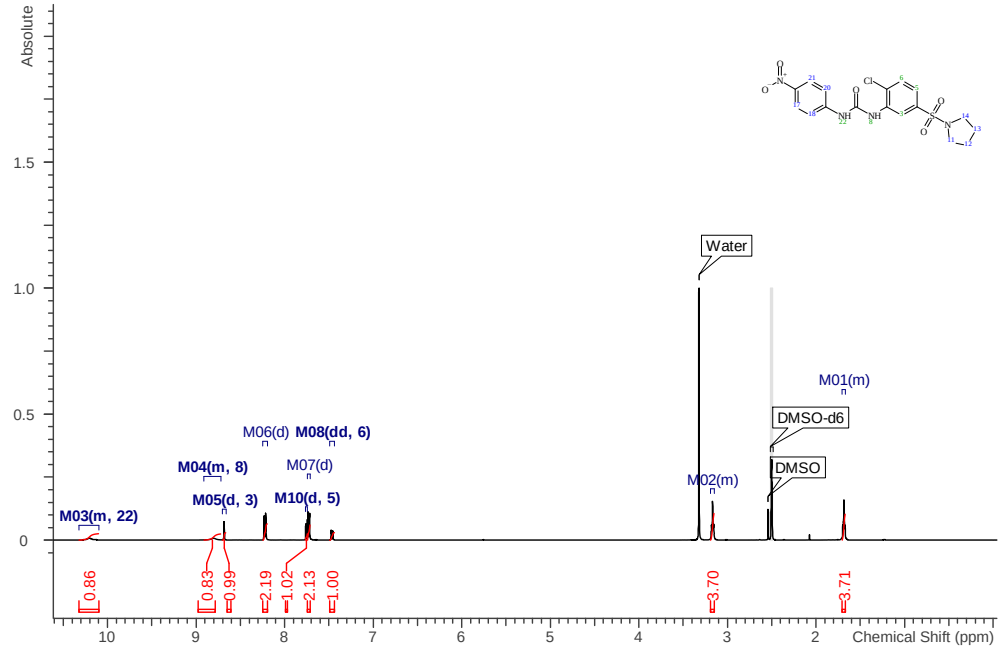
Absolute
Water
M01(m)
DMSO-d6
DMSO
M02(m)
M06(d)
M08(dd, 6)
M04(m, 8)
M07(d)
M05(d, 3)
M10(d, 5)
M03(m, 22)
0.86
0.83
0.99
2.19
1.02
2.13
1.00
3.70
3.71
Chemical Shift (ppm)

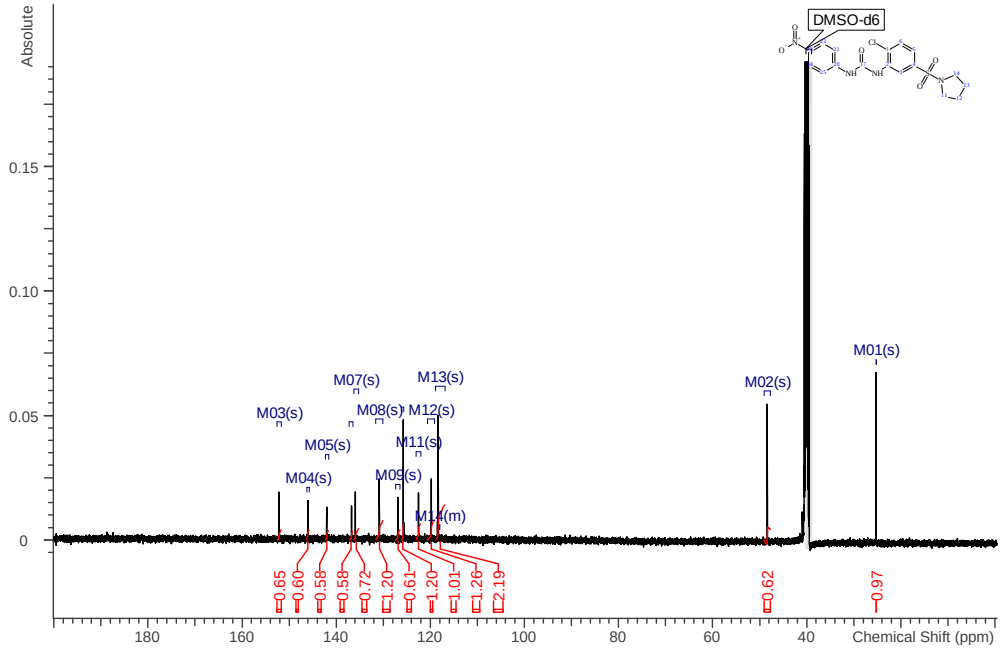
Absolute
DMSO-d6
M01(s)
M02(s)
M07(s)
M13(s)
M03(s)
M08(s)
M12(s)
M05(s)
M11(s)
M04(s)
M09(s)
M14(m)
0.65
0.60
0.58
0.58
0.72
1.20
0.61
1.20
1.01
1.26
2.19
0.62
0.97
Chemical Shift (ppm)

33

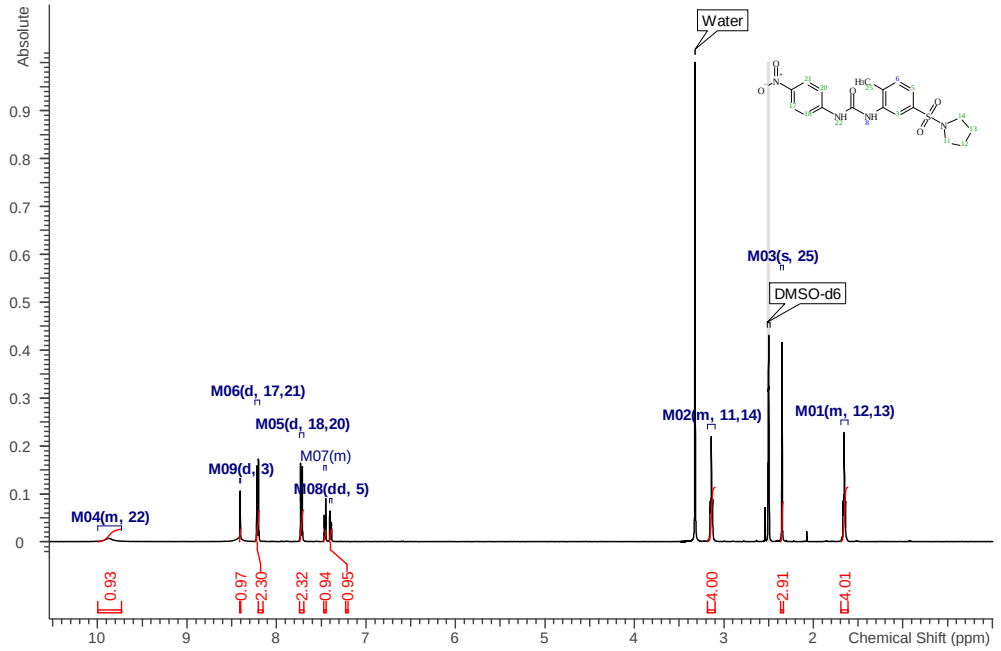
Absolute
Water
DMSO-d6
M03(s, 25)
M06(d, 17,21)
M05(d, 18,20)
M07(m)
M09(d, 3)
M08(dd, 5)
M04(m, 22)
M02(m, 11,14)
M01(m, 12,13)
0.93
0.97
2.30
2.32
0.94
0.95
4.00
2.91
4.01
Chemical Shift (ppm)

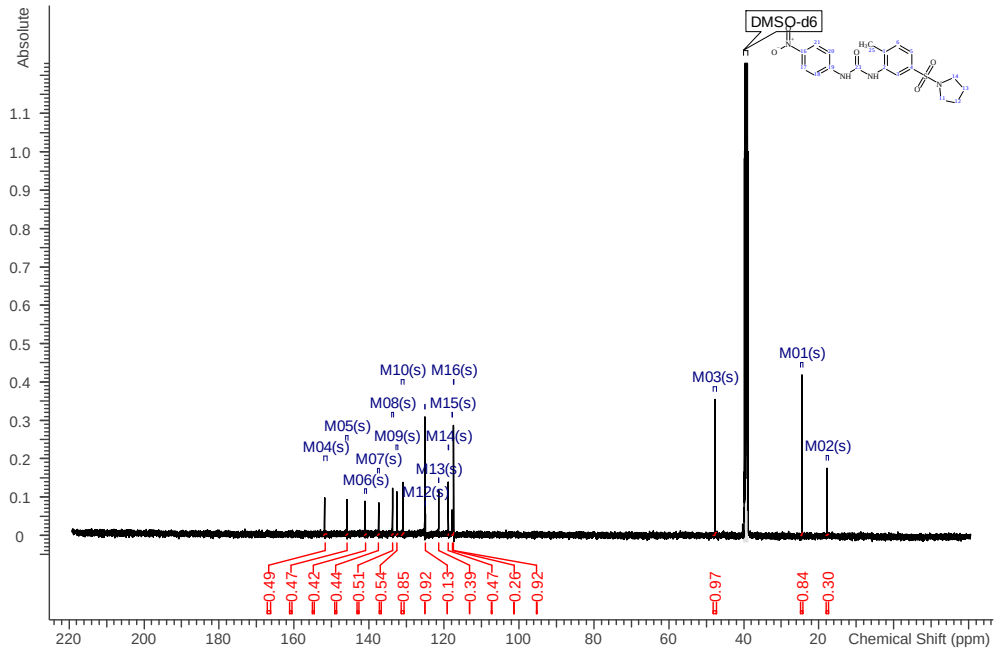
Absolute
DMSO-d6
M10(s)
M16(s)
M08(s)
M15(s)
M05(s)
M09(s)
M14(s)
M04(s)
M07(s)
M13(s)
M06(s)
M12(s)
M03(s)
M01(s)
M02(s)
0.49
0.47
0.42
0.44
0.51
0.54
0.85
0.92
0.13
0.39
0.47
0.26
0.92
0.97
0.84
0.30
Chemical Shift (ppm)

34

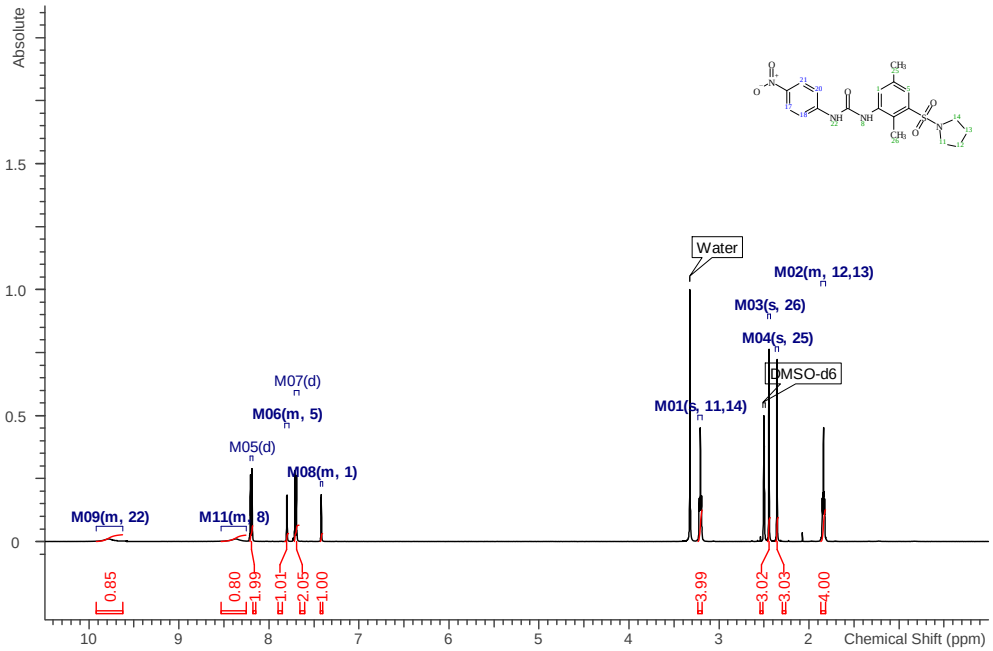
Absolute
1.5
1.0
0.5
0
Water
M02(m, 12,13)
M03(s, 26)
M04(s, 25)
DMSO-d6
M01(s, 11,14)
M07(d)
M06(m, 5)
M05(d)
M08(m, 1)
M09(m, 22)
M11(m, 8)
0.85
0.80
1.99
1.01
2.05
1.00
3.99
3.02
3.03
4.00
10
9
8
7
6
5
4
3
2
Chemical Shift (ppm)

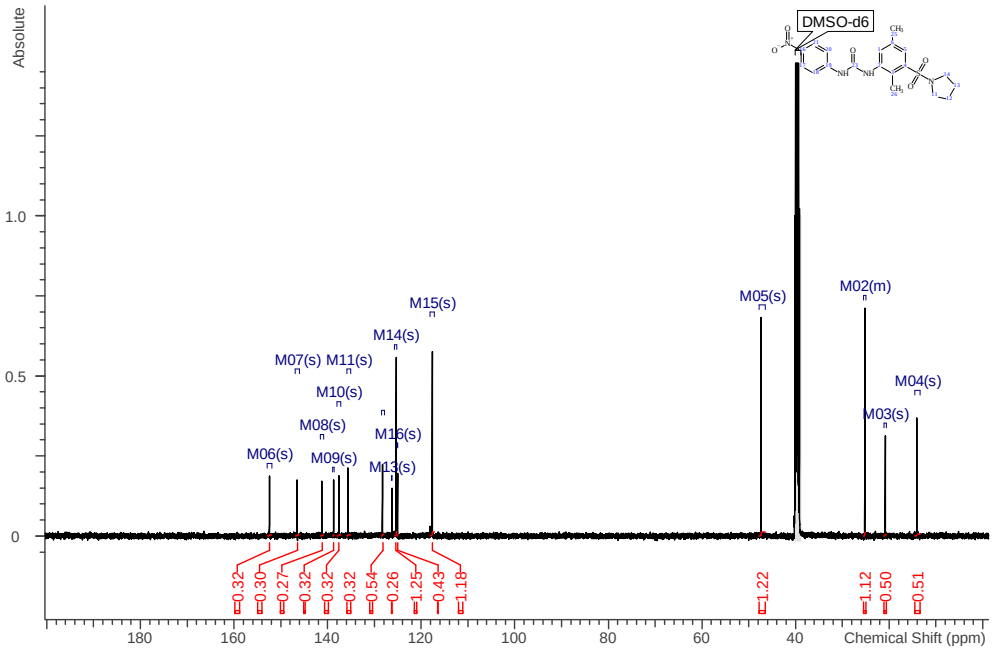
Absolute
1.0
0.5
0
DMSO-d6
M05(s)
M02(m)
M15(s)
M14(s)
M07(s)
M11(s)
M10(s)
M08(s)
M16(s)
M06(s)
M09(s)
M13(s)
M04(s)
M03(s)
0.32
0.30
0.27
0.32
0.32
0.54
0.26
1.25
0.43
1.18
1.22
1.12
0.50
0.51
180
160
140
120
100
80
60
40
Chemical Shift (ppm)

35

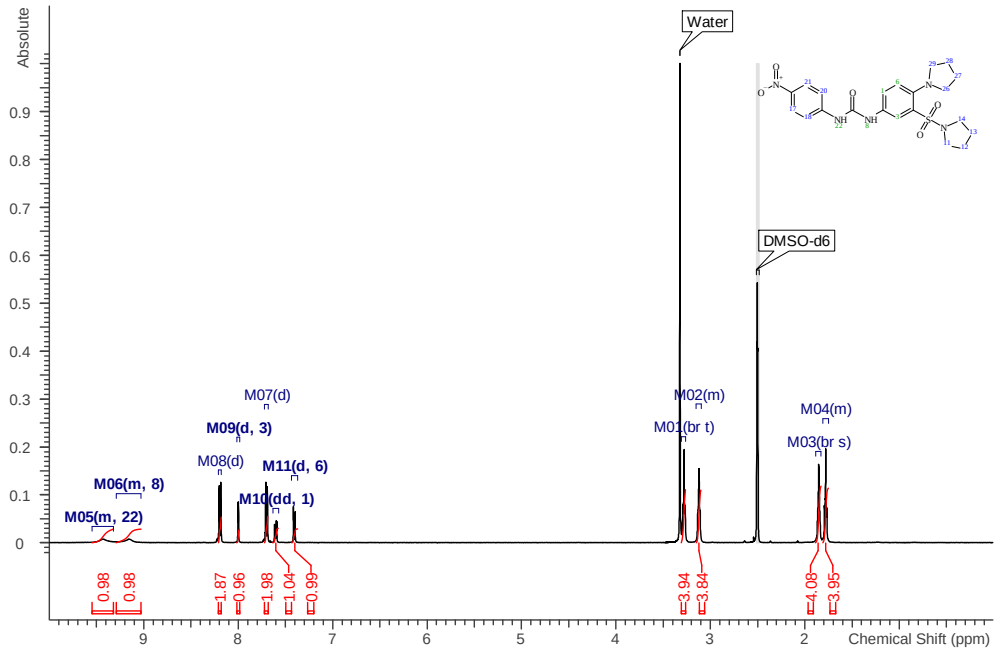
Absolute
Water
DMSO-d6
M07(d)
M09(d, 3)
M08(d)
M11(d, 6)
M06(m, 8)
M10(dd, 1)
M05(m, 22)
M02(m)
M01(br t)
M04(m)
M03(br s)
0.98
0.98
1.87
0.96
1.98
1.04
0.99
3.94
3.84
4.08
3.95
Chemical Shift (ppm)

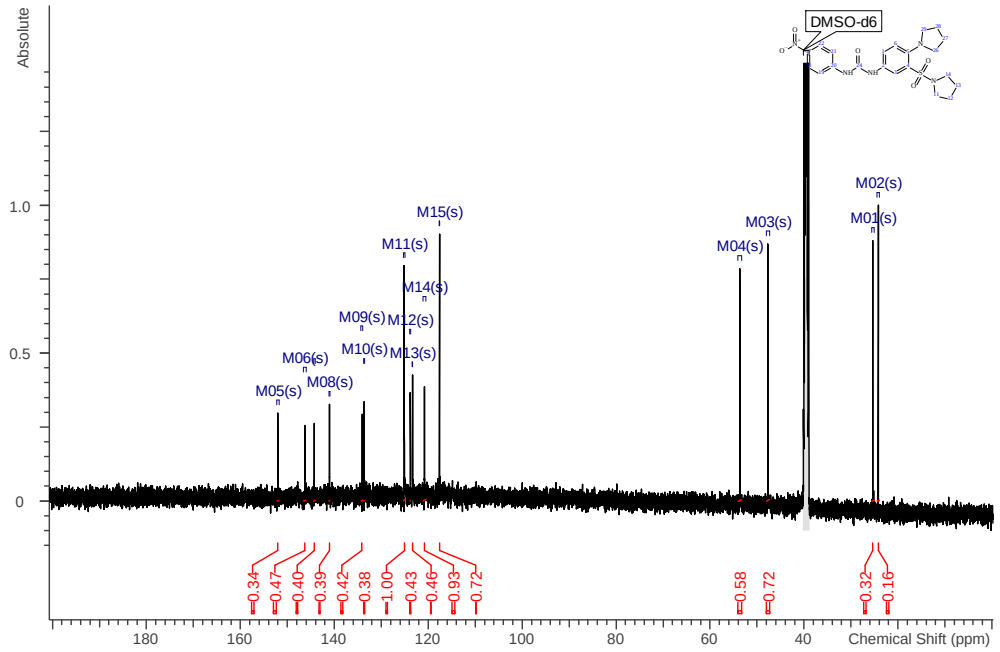
Absolute
DMSO-d6
M15(s)
M11(s)
M14(s)
M09(s)
M12(s)
M10(s)
M13(s)
M06(s)
M08(s)
M05(s)
M02(s)
M01(s)
M03(s)
M04(s)
0.34
0.47
0.40
0.39
0.42
0.38
1.00
0.43
0.46
0.93
0.72
0.58
0.72
0.32
0.16
Chemical Shift (ppm)

36

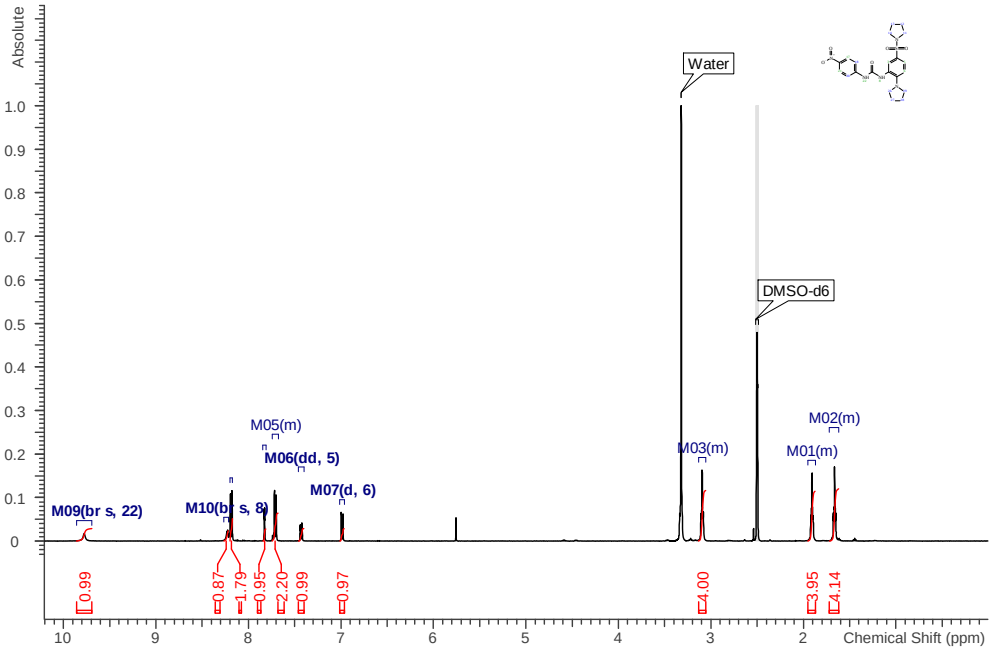
Absolute
Water
DMSO-d6
M09(br s, 22)
M10(br s, 8)
M05(m)
M06(dd, 5)
M07(d, 6)
M03(m)
M02(m)
M01(m)
0.99
0.87
1.79
0.95
2.20
0.99
0.97
4.00
3.95
4.14
Chemical Shift (ppm)

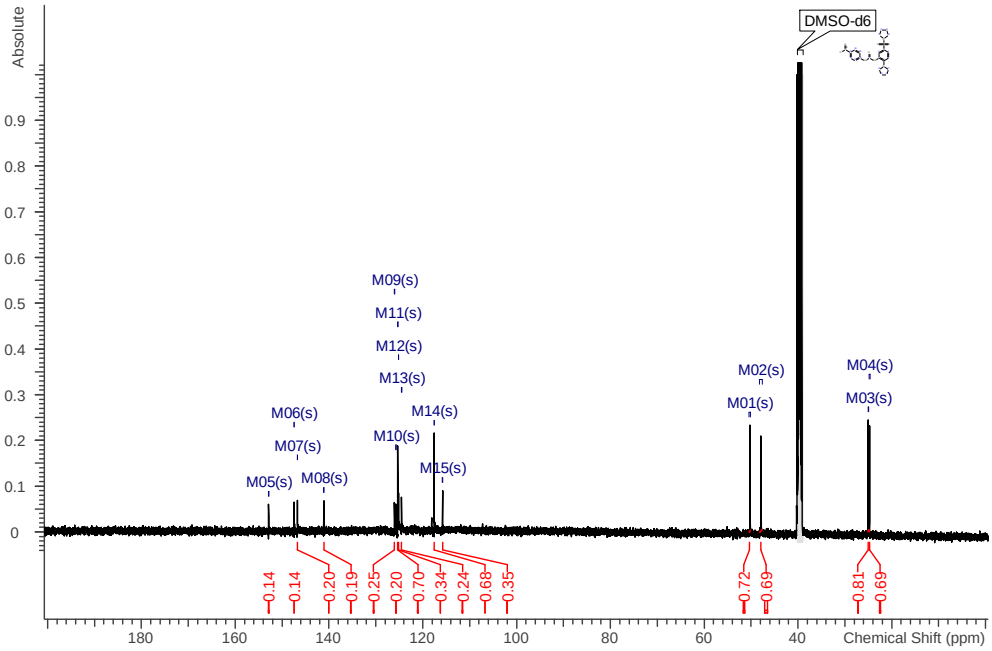
Absolute
DMSO-d6
M09(s)
M11(s)
M12(s)
M13(s)
M14(s)
M10(s)
M15(s)
M06(s)
M07(s)
M05(s)
M08(s)
M02(s)
M01(s)
M04(s)
M03(s)
0.14
0.14
0.20
0.19
0.25
0.20
0.70
0.34
0.24
0.68
0.35
0.72
0.69
0.81
0.69
Chemical Shift (ppm)

4

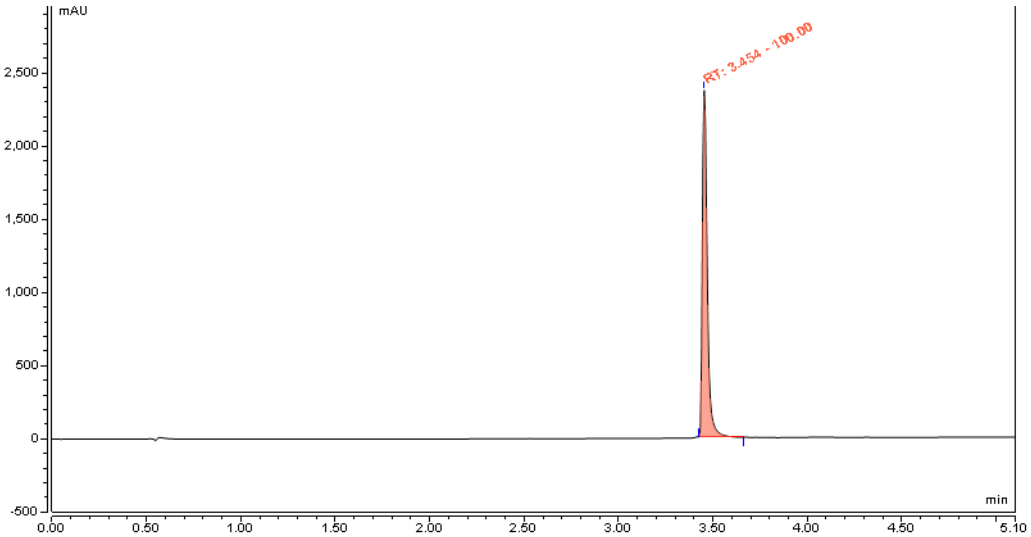
mAU
2,500
2,000
1,500
1,000
500
0
-500
RT: 3.454 - 100.00
min
0.00
0.50
1.00
1.50
2.00
2.50
3.00
3.50
4.00
4.50
5.10

5

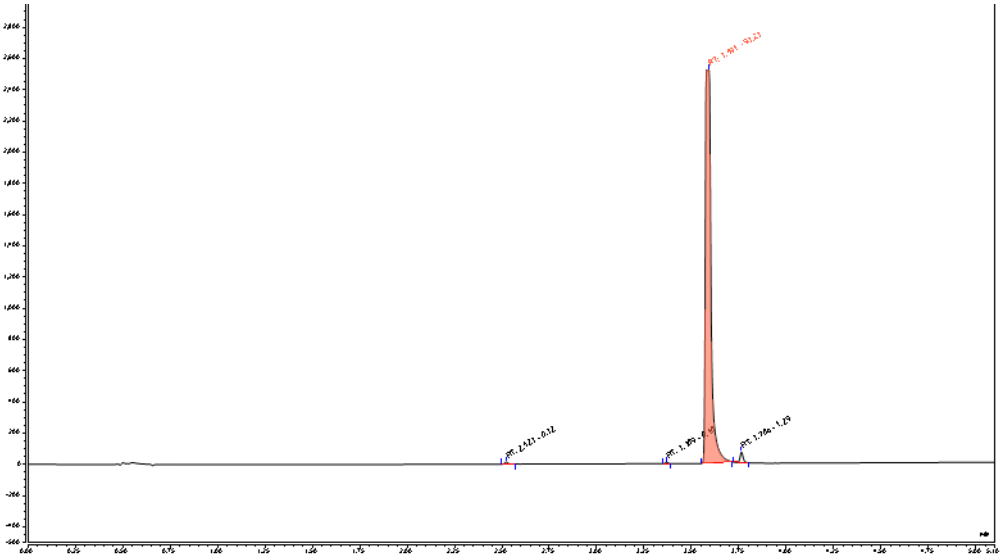

6

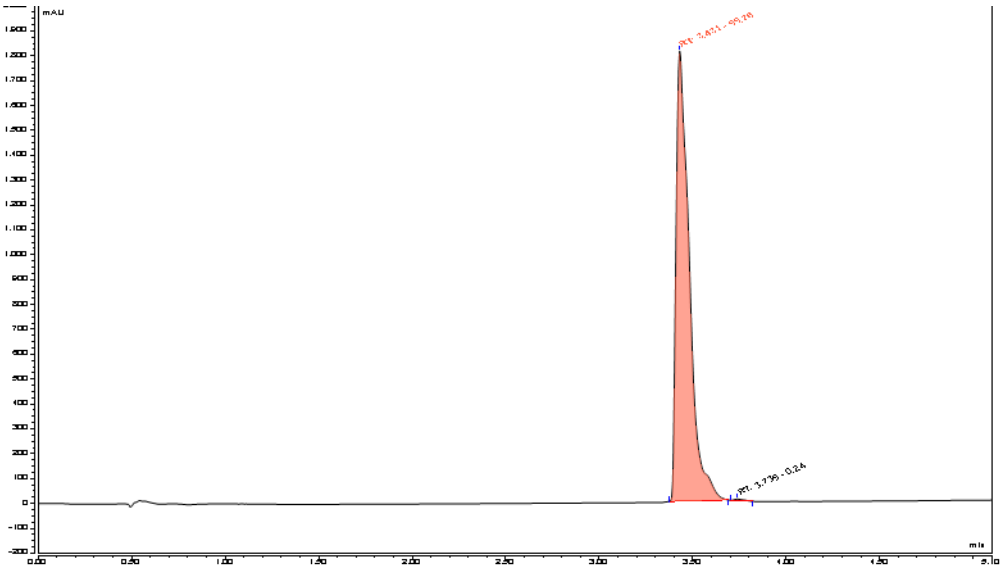
mAU
RT 3.821 - 99.76
RT 3.799 - 0.24
min

7

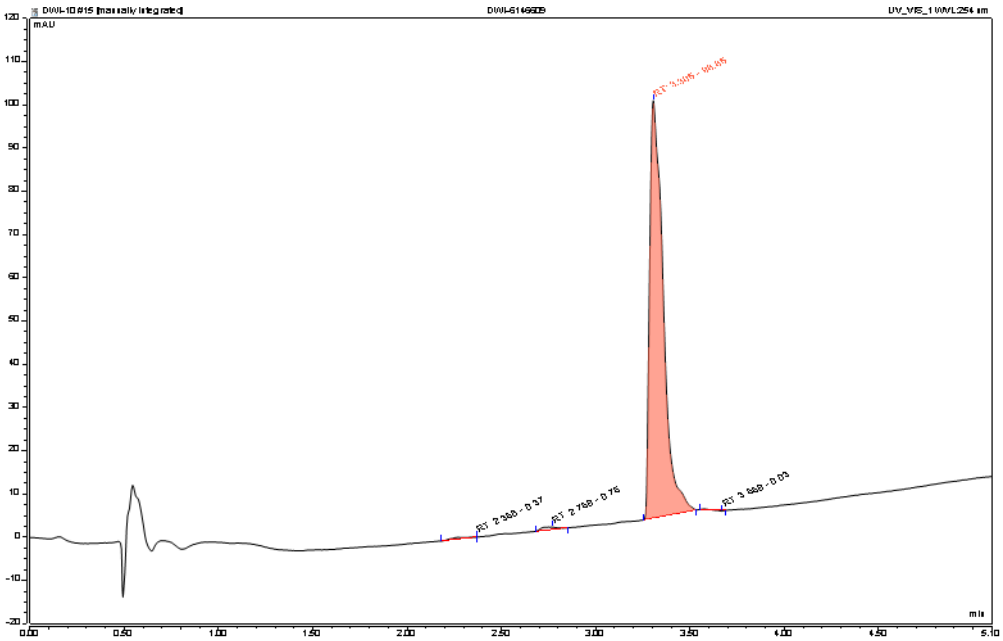
mAU
RT 3.395 - 99.05
RT 2.388 - 0.37
RT 2.768 - 0.75
RT 3.868 - 0.03
min

8

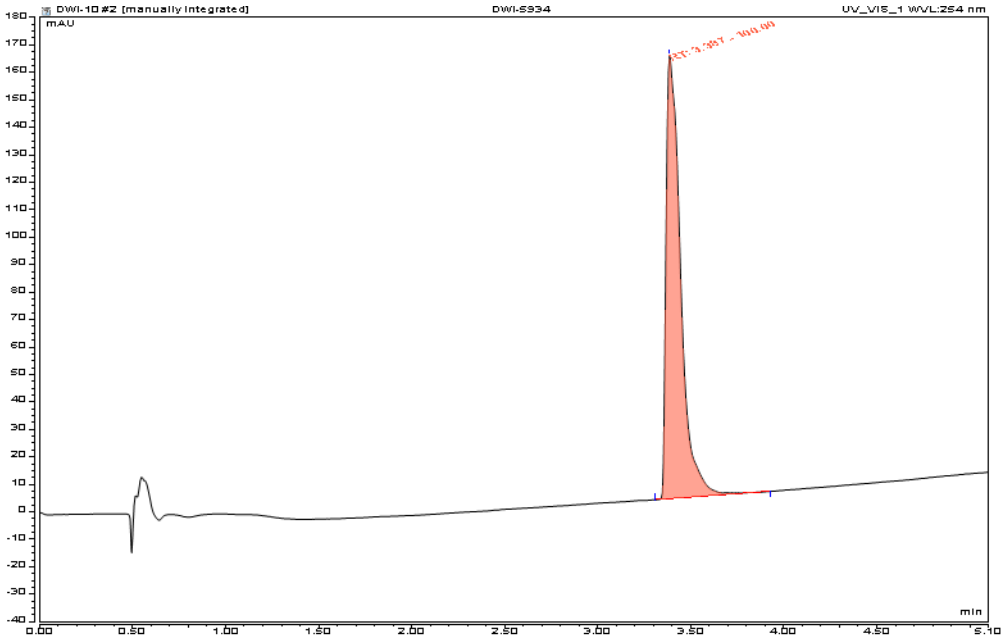
DWI-10 #2 [manually integrated]
DWI-5934
UV_VIS_1 WVL:254 nm
mAU
min

9

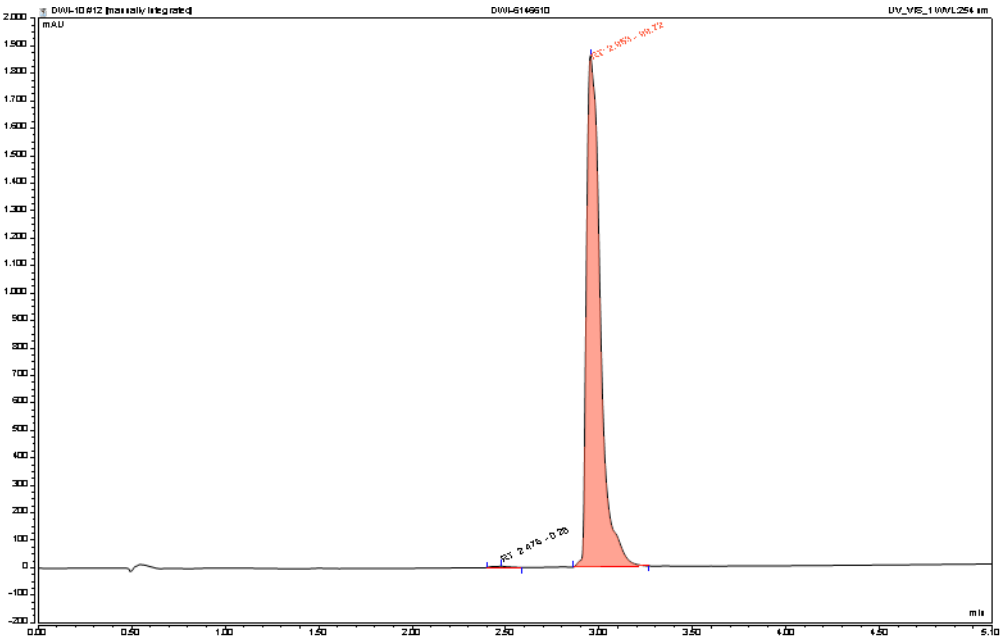
DWI-10 #12 [manually integrated]
DWI-6146610
UV_VIS_1 WVL:254 nm
mAU
min

10

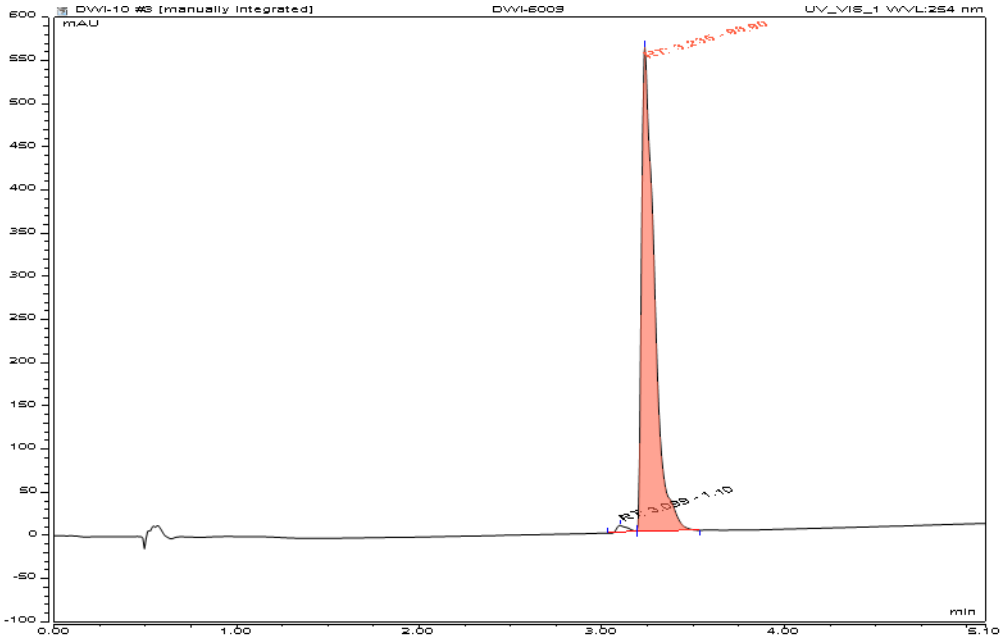
DWI-10 #3 [manually integrated]
DWI-6009
UV_VIS_1 WVL:254 nm
mAU
RT: 3.235 - 99.90
RT: 3.059 - 1.10
min

11

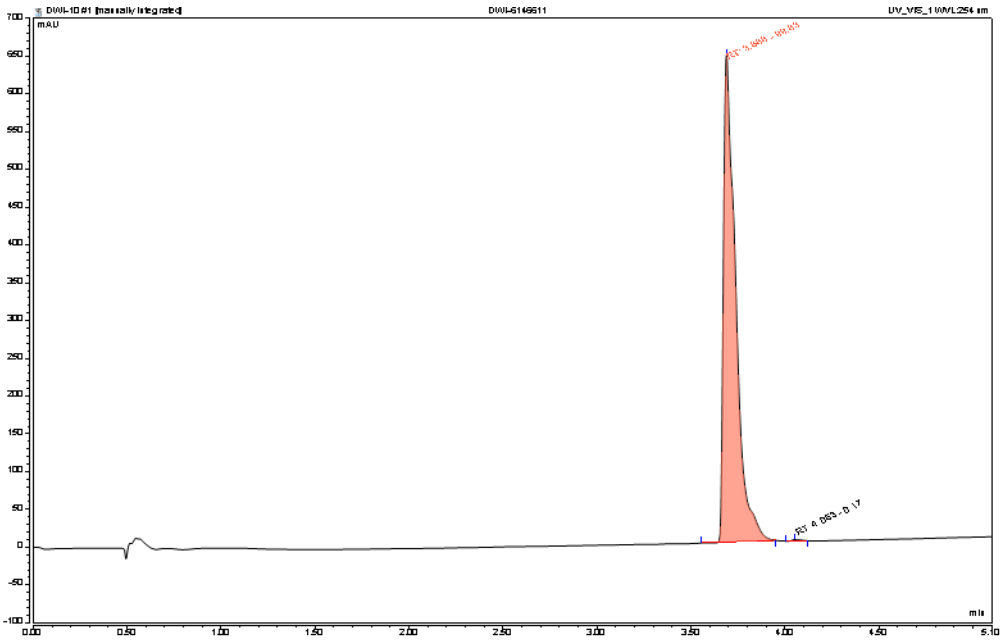
mAU
min

12

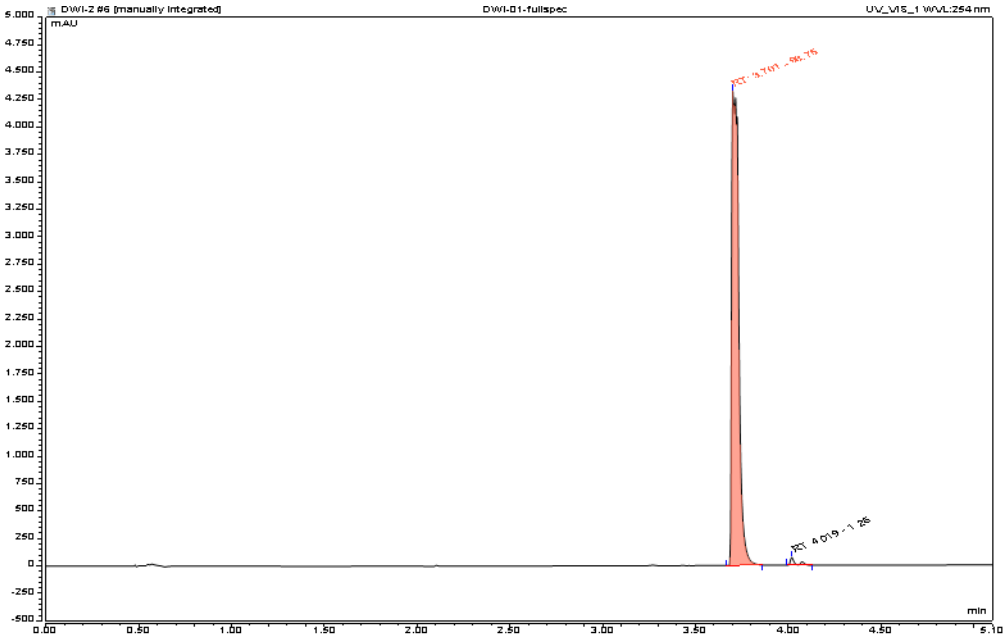
DWI-2 #6 [manually integrated]
DWI-01-fullspec
UV_VIS_1 WVL:254 nm
mAU
min

13

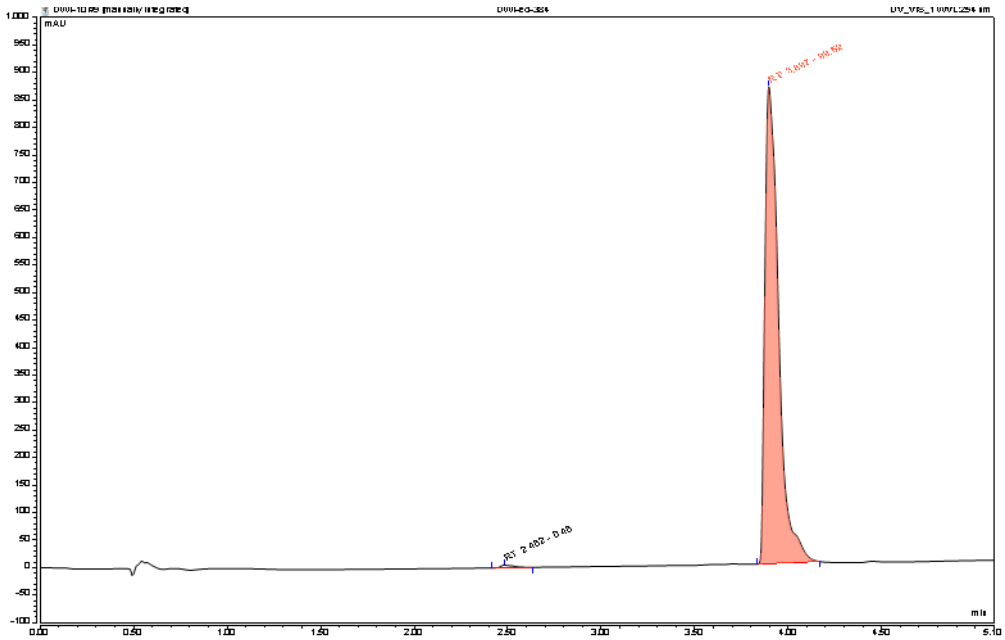
mAU
min

14

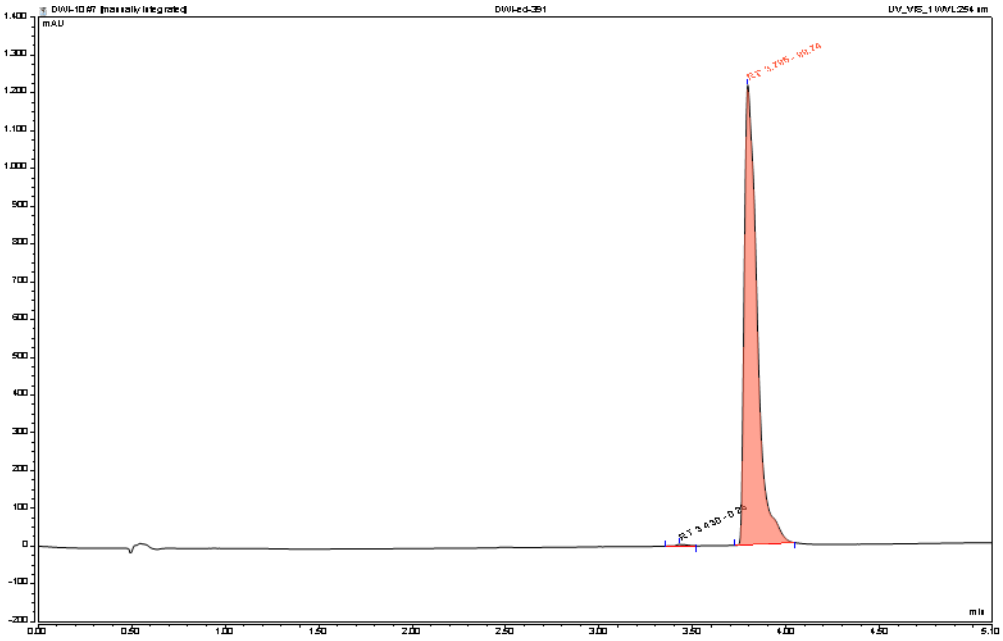

15

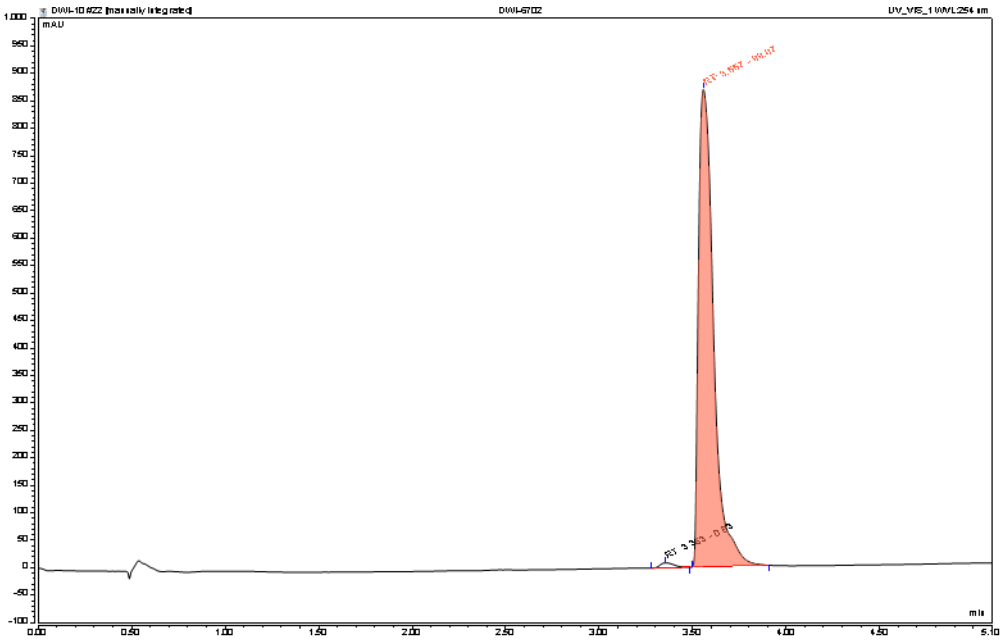

16

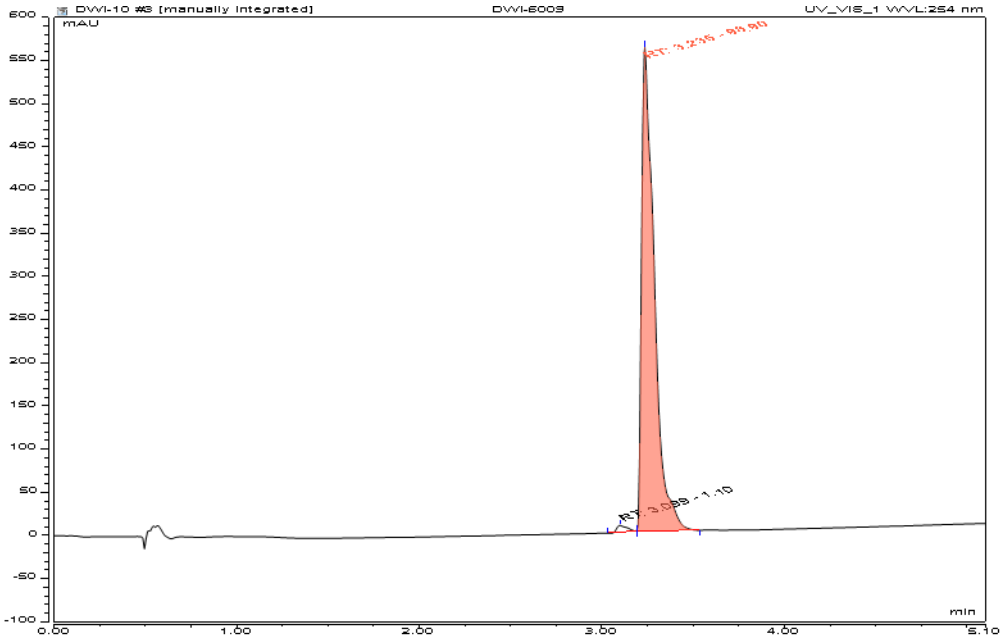
DWI-10 #3 [manually integrated]
DWI-6009
UV_VIS_1 WVL:254 nm
mAU
RT: 3.235 - 1.10
min

17

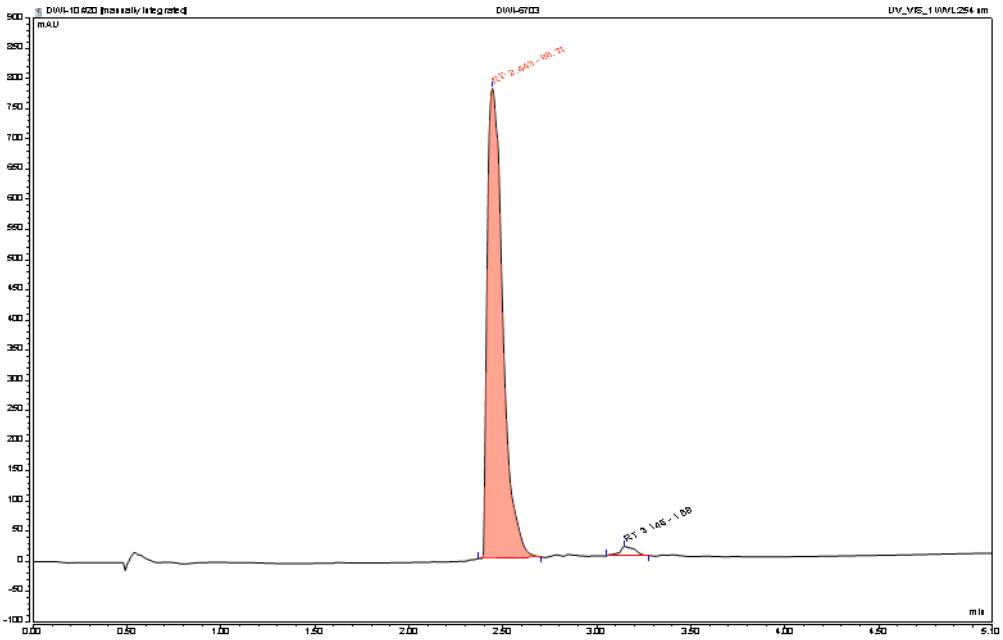
DWI-6703
mAU
min

18

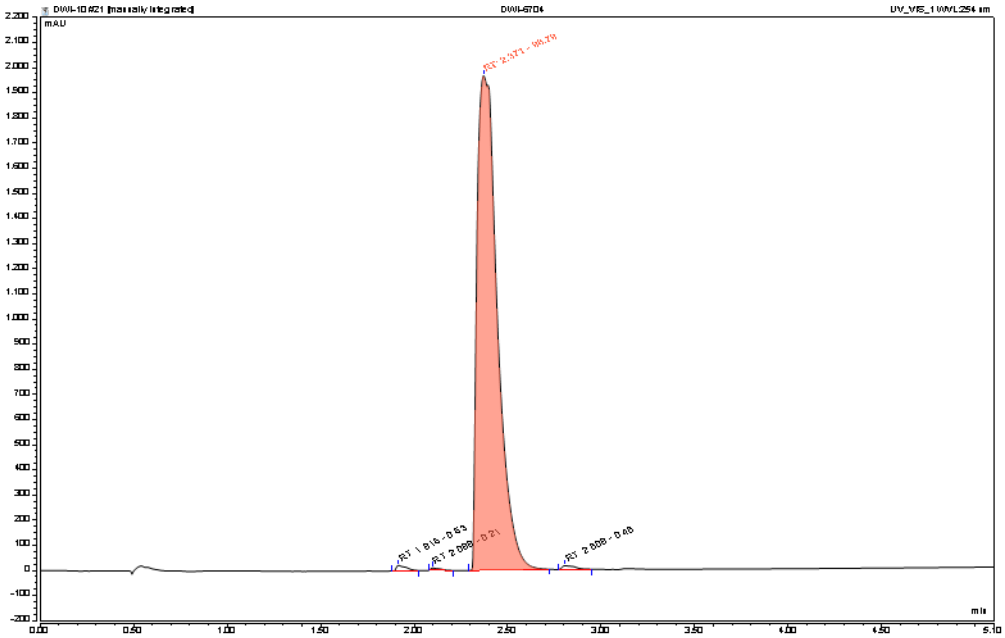

19

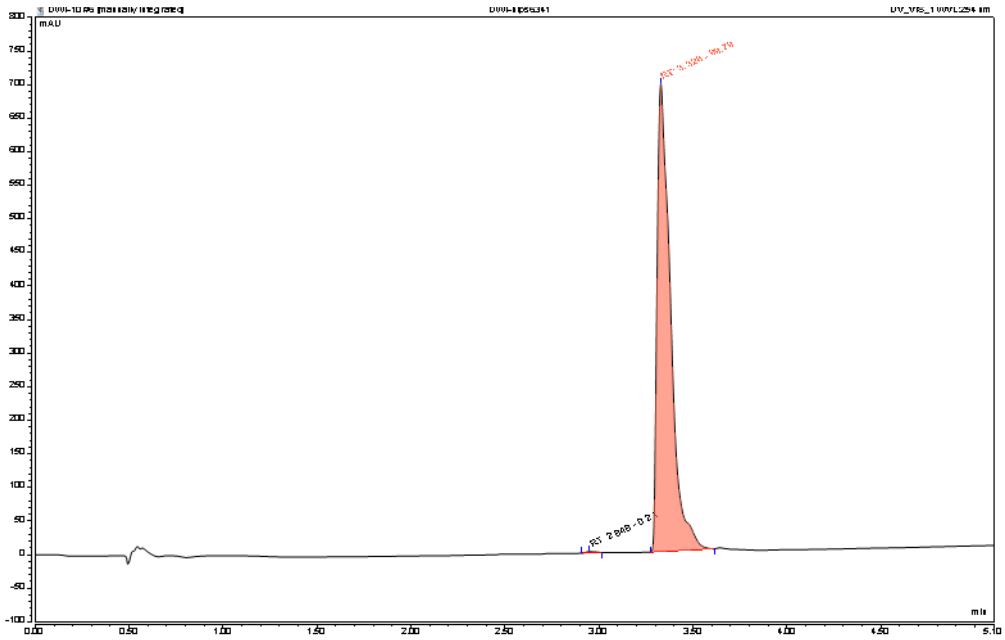

20

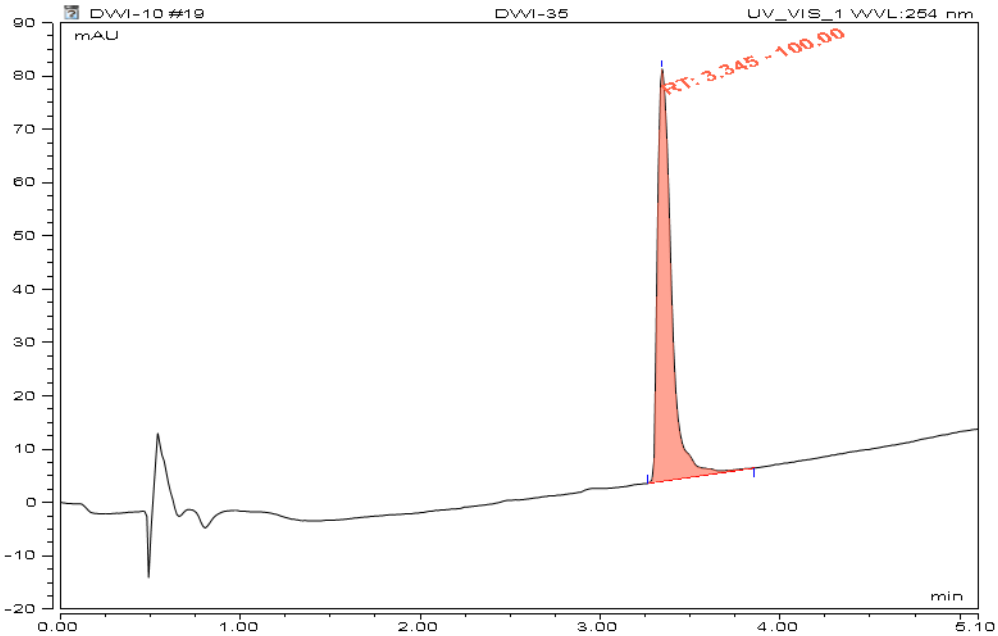
DWI-10 #19
DWI-35
UV_VIS_1 WVL:254 nm
mAU
RT: 3.345 - 100.00
min

21

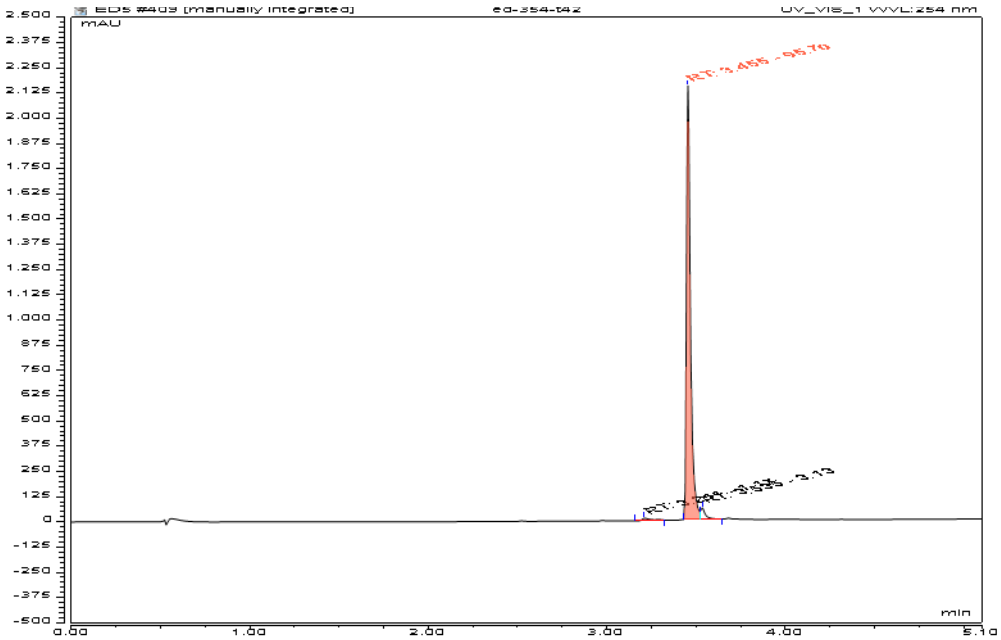
UV_VIS_1 WVL:254 nm
mAU
RT: 3.456 - 95.70
min

22

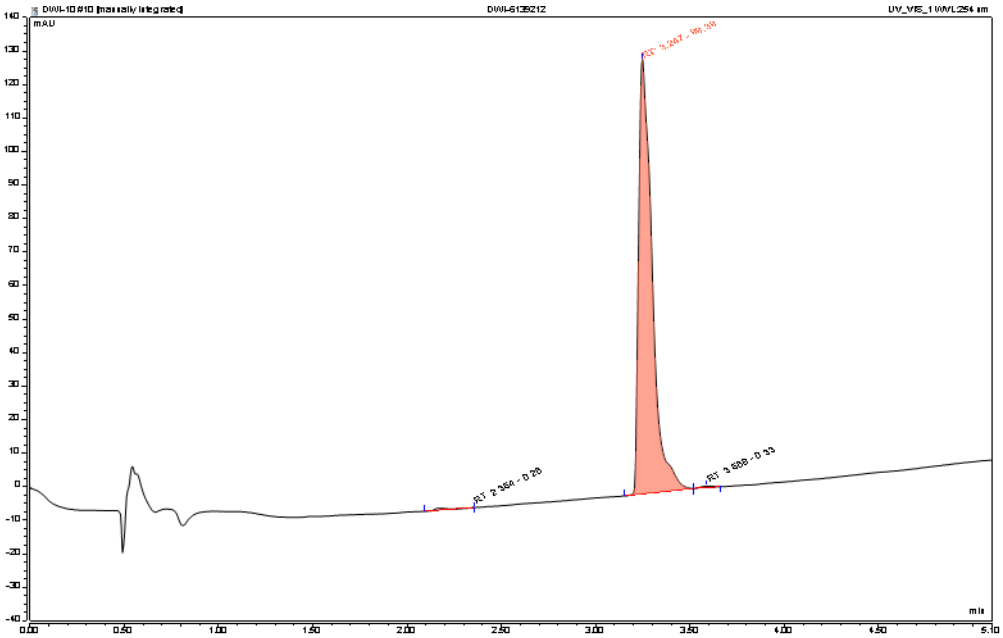
DWU-10 #10 [manually integrated]
DWU-6125212
UV_VIS_1 WVL:254 nm
mAU
RT 2.364 - 0.28
RT 3.608 - 0.33
min

23

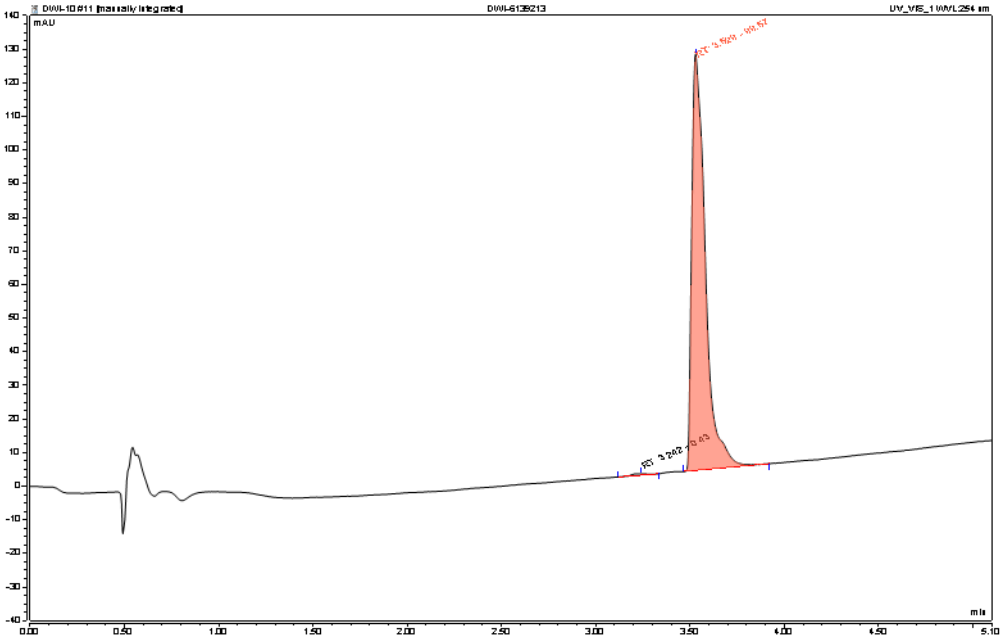
DWU-10 #11 [manually integrated]
DWU-6125213
UV_VIS_1 WVL:254 nm
mAU
RT 3.202 - 0.03
min

24

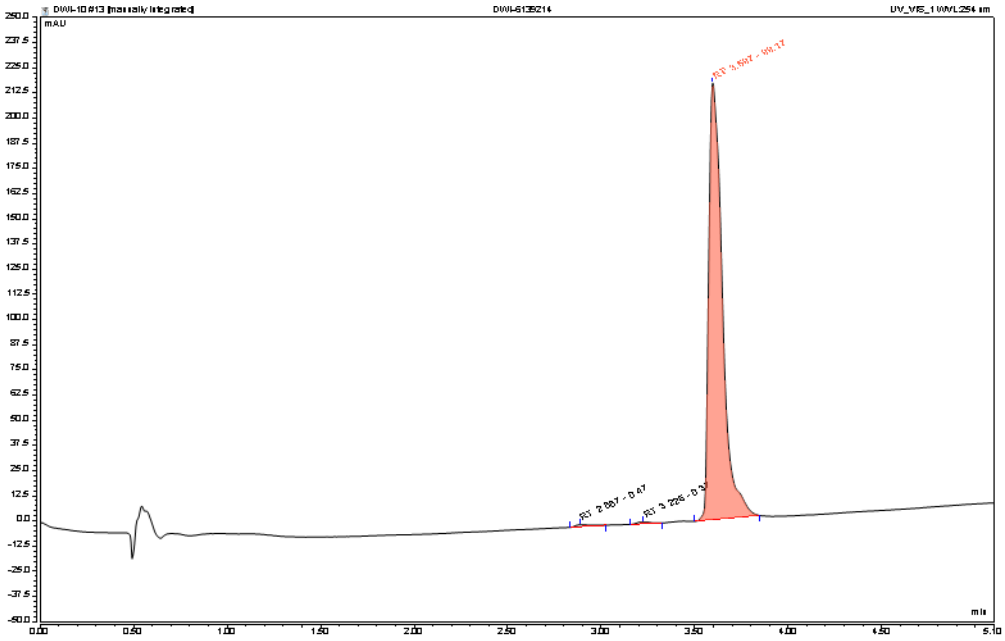

25

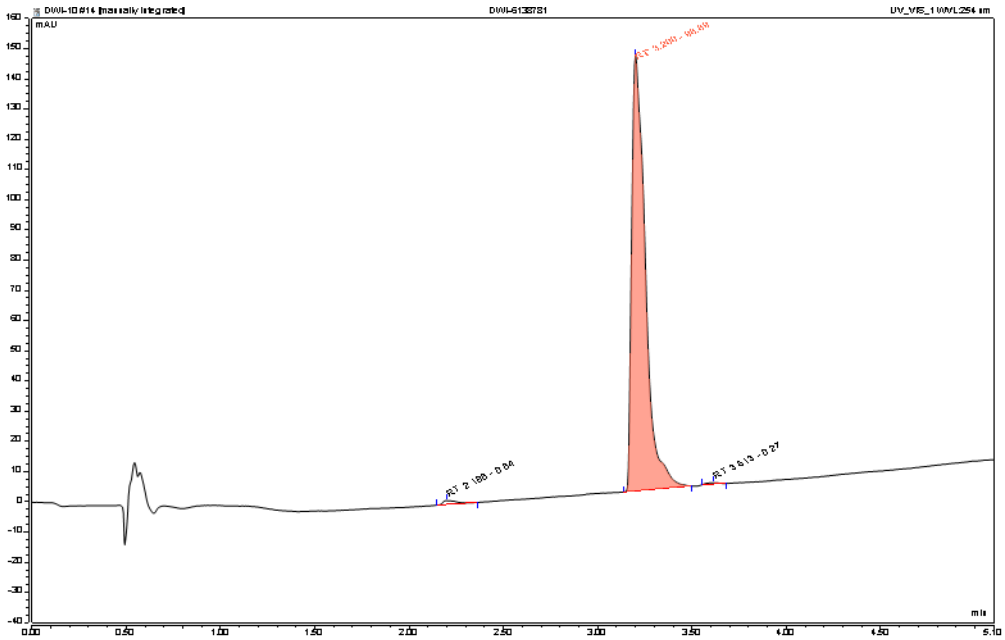

26

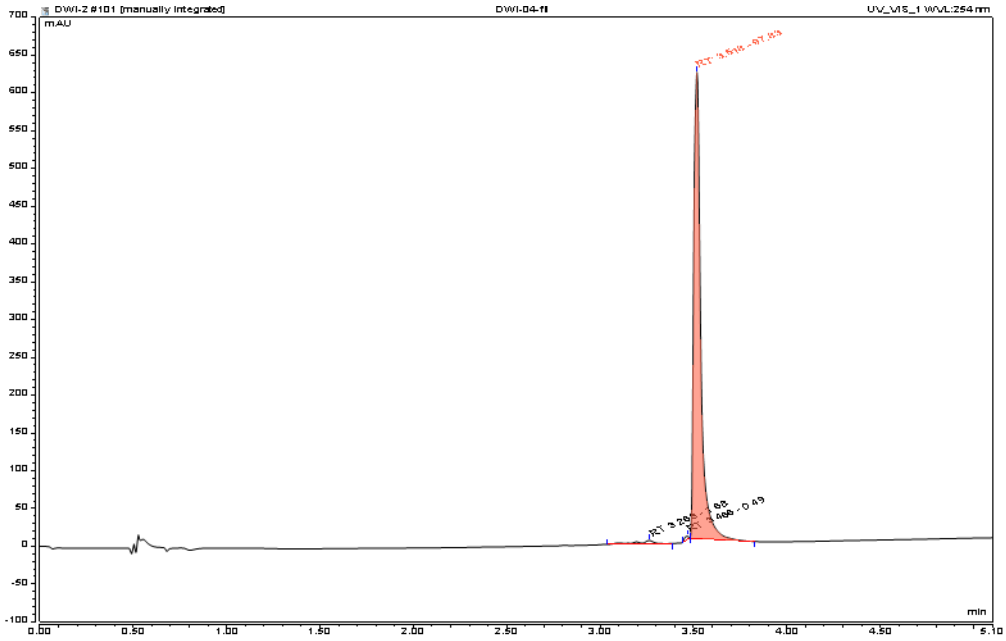
DWI-Z #101 [manually integrated]
DWI-04-fil
UV_VIS_1 WVL:254 nm
mAU
min

27

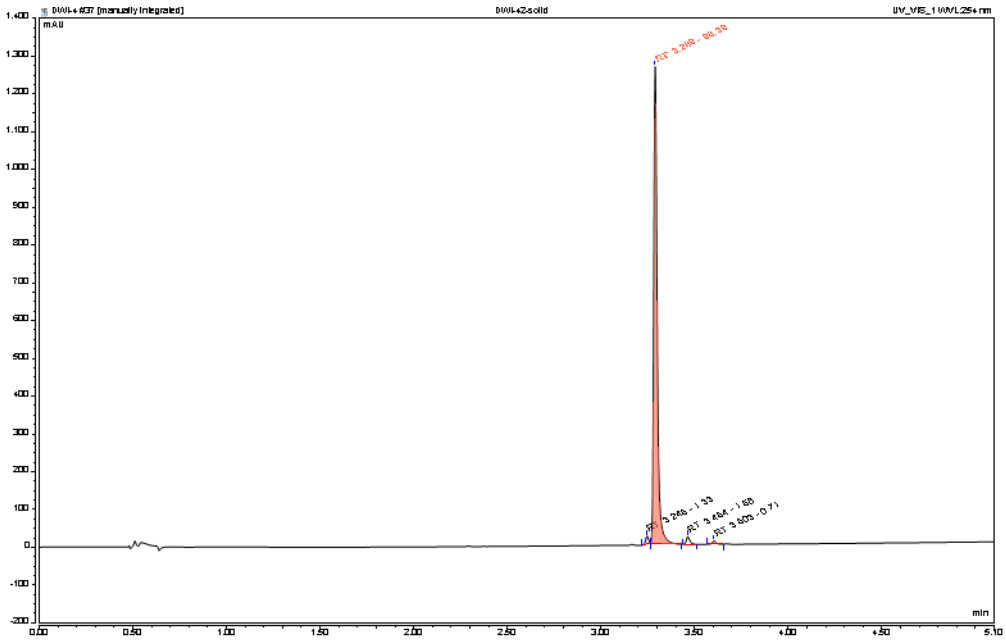
DWI-4 #37 [manually integrated]
DWI-4Z-solid
UV_VIS_1 WVL:254 nm
mAU
min

28

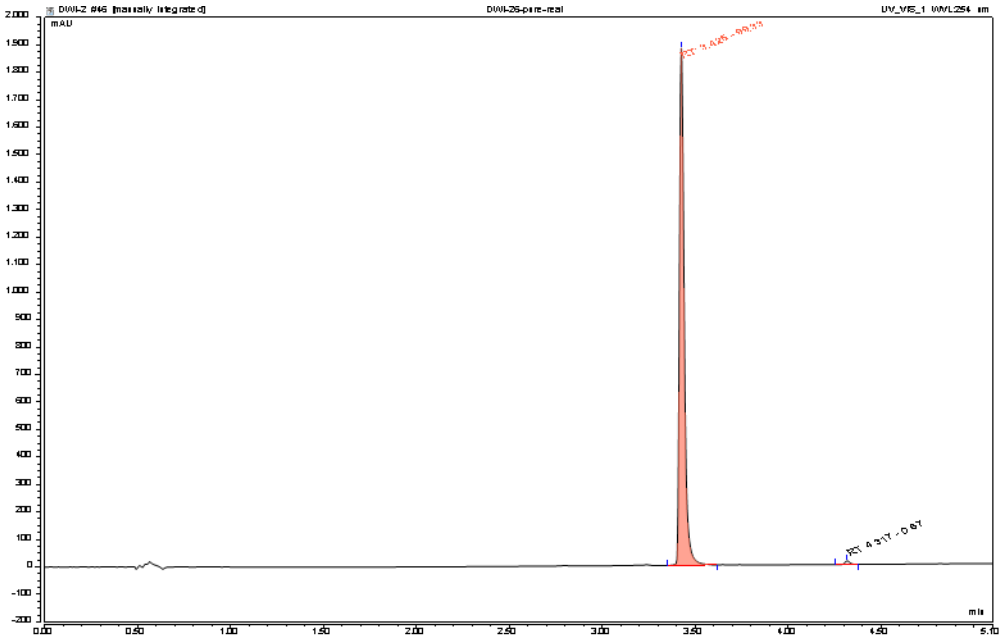
mAU
min

29

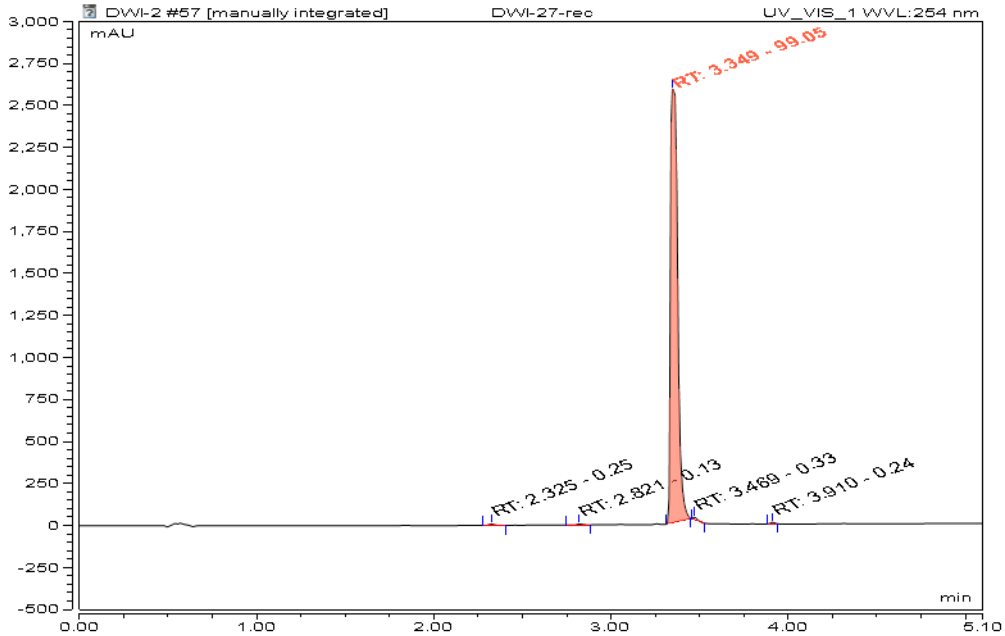
DWI-2 #57 [manually integrated]
DWI-27-rec
UV_VIS_1 WVL:254 nm
mAU
RT: 3.349 - 99.05
RT: 2.325 - 0.25
RT: 2.821 - 0.13
RT: 3.469 - 0.33
RT: 3.910 - 0.24
min

30

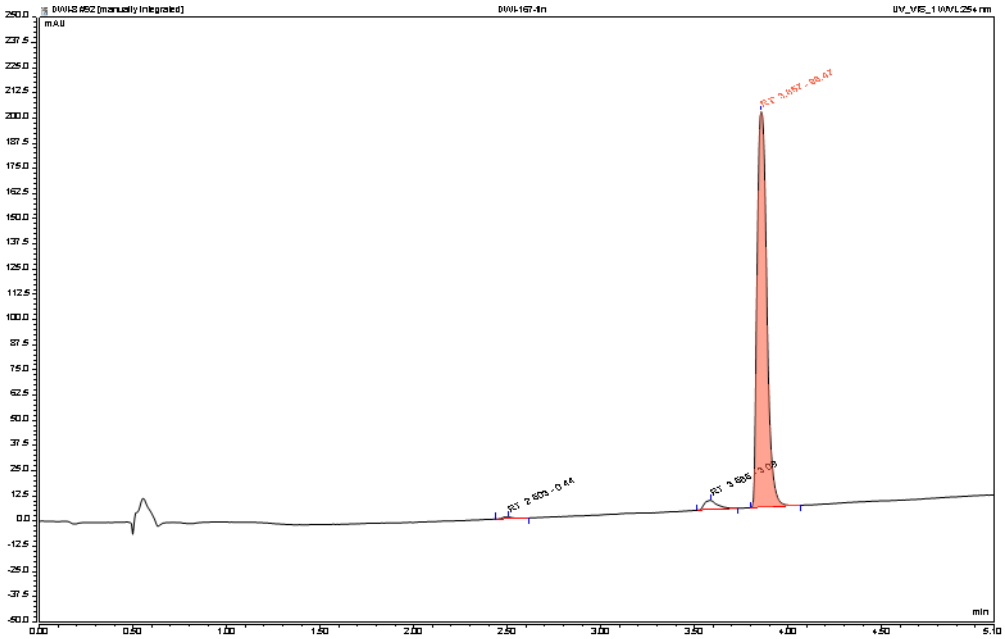
mAU
min

31

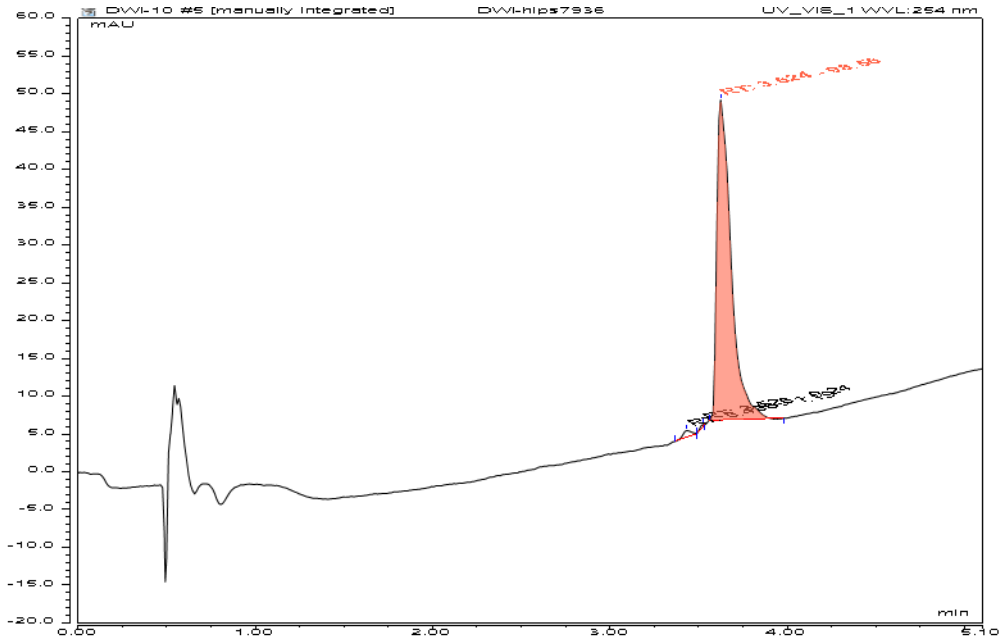
DWI-10 #5 [manually integrated]
DWI-hlps7936
UV_VIS_1 WVL:254 nm
mAU
min

32

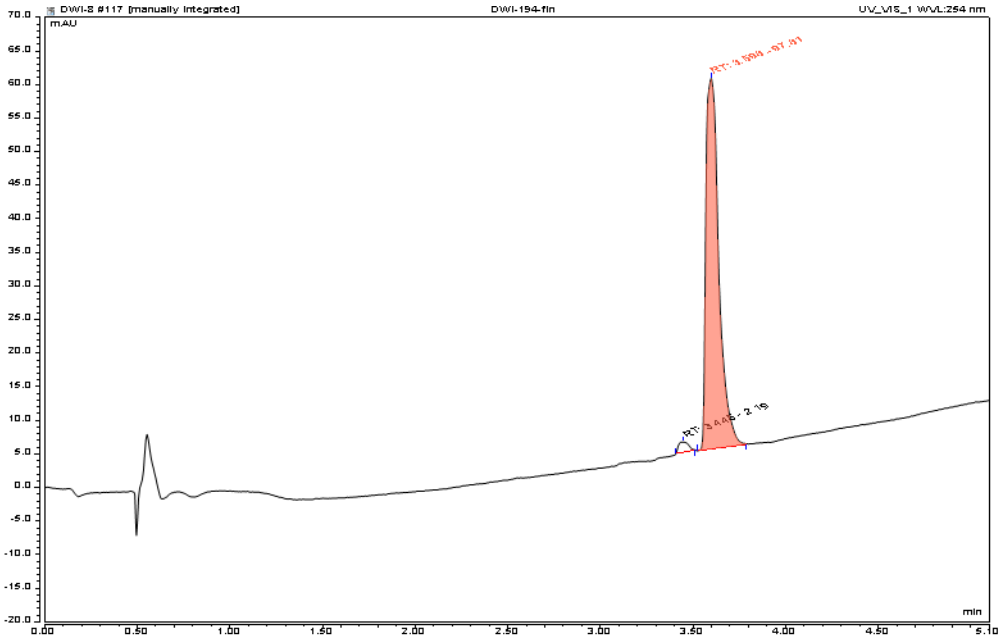
DWI-8 #117 [manually integrated]
DWI-194-fin
UV_VIS_1 WVL:254 nm
mAU
min

33

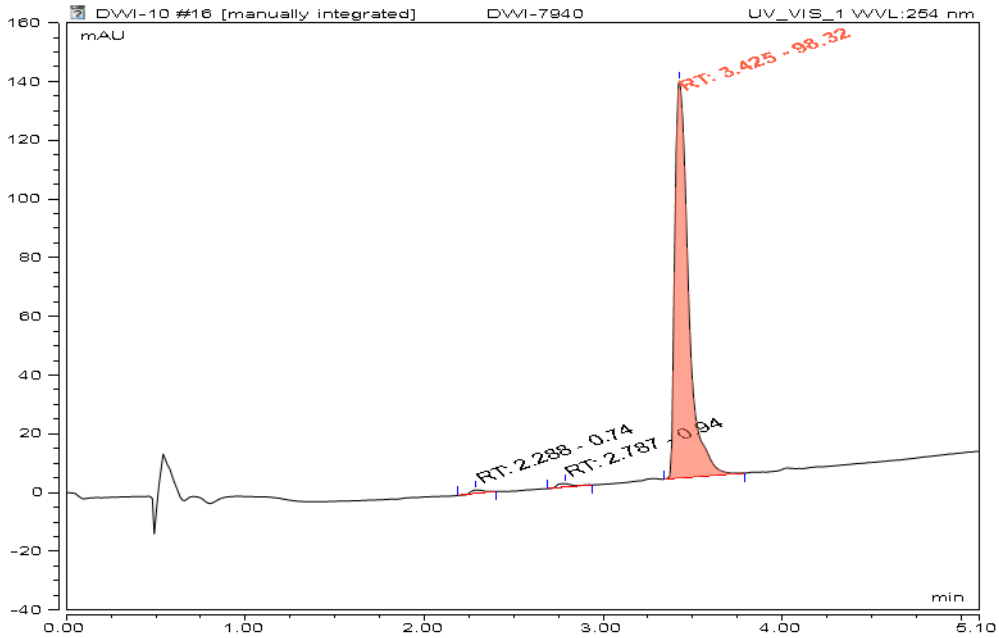
DWI-10 #16 [manually integrated]
DWI-7940
UV_VIS_1 WVL:254 nm
mAU
RT: 3.425 - 98.32
RT: 2.288 - 0.74
RT: 2.787 - 0.94
min

34

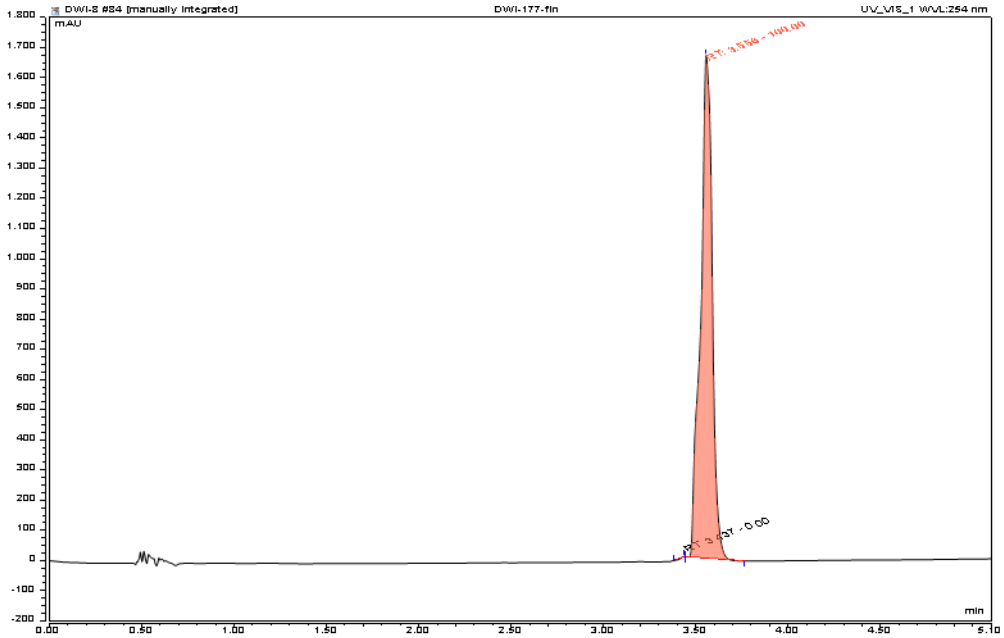
DWI-8 #84 [manually integrated]
DWI-177-fin
UV_VIS_1 WVL:254 nm
mAU
RT: 3.558 - 100.00
RT: 3.437 - 0.00
min

35

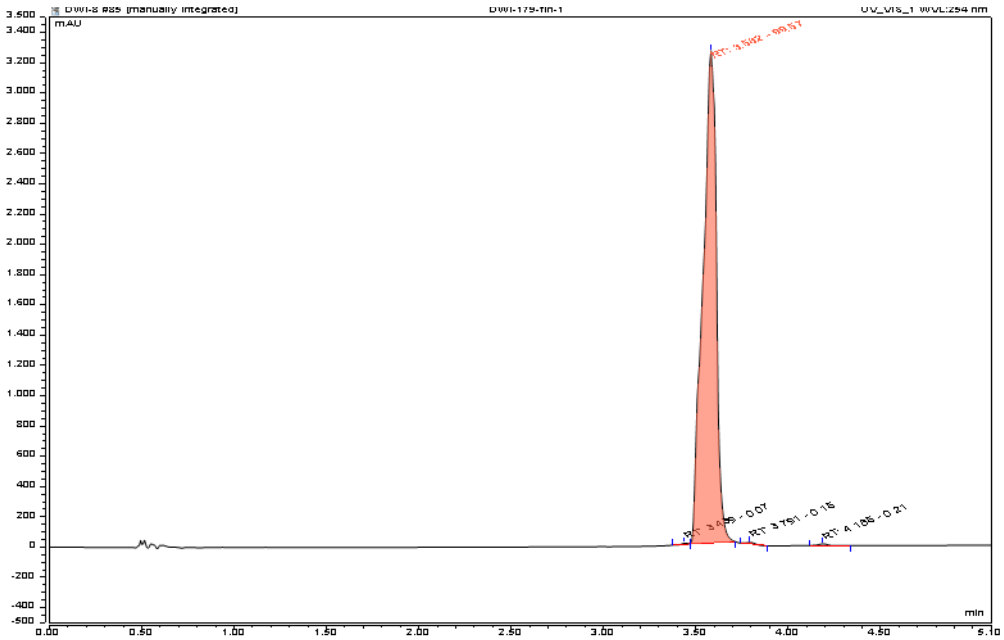
DWI-8 #85 [manually integrated]
DWI-179-fin-1
UV_VIS_1 WVL:254 nm
mAU
RT: 3.502 - 99.57
RT: 3.751 - 0.15
RT: 4.185 - 0.21
min

36

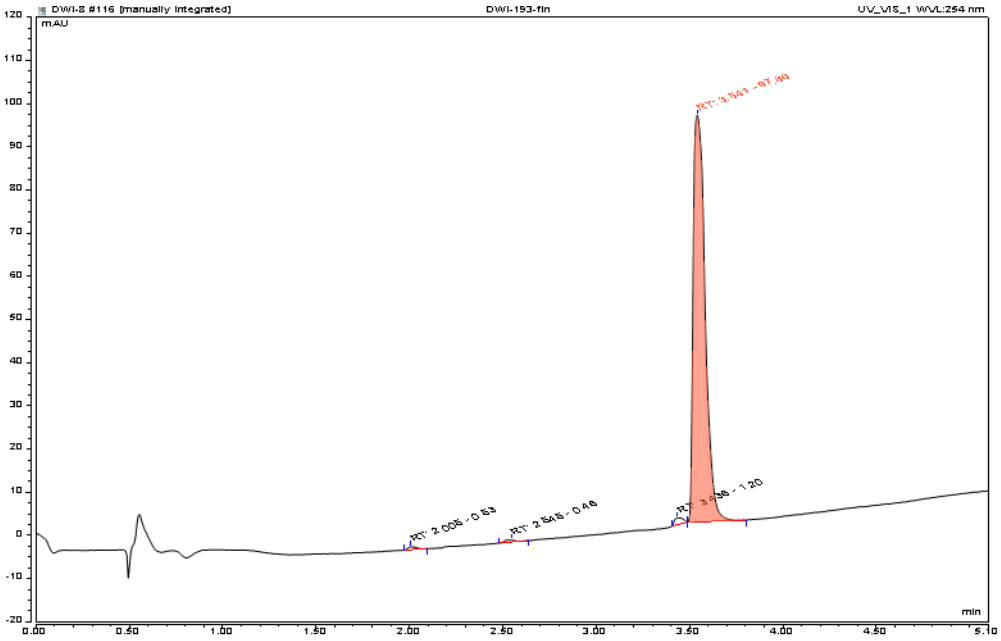
DWI-8 #116 [manually integrated]
DWI-193-fin
UV_VIS_1 WVL:254 nm
mAU
RT: 3.541 - 97.00
RT: 2.005 - 0.53
RT: 2.545 - 0.46
RT: 3.336 - 1.20
min

3.2 Chapter 2: Discovery of fragment by X-ray crystallographic screening targeting the CTP binding site of *Pseudomonas aeruginosa* IspD

Daan Willocx, Lucia D'Auria, Franck Borel, Mostafa M. Hamed, Eleonora Diamanti, Anna K. H. Hirsch

Contributions: Daan Willocx, Eleonora Diamanti, Mostafa M. Hamed, and Anna K. H. Hirsch conceived the project; Crystallographic screening as well as crystallization and obtaining co-crystals was performed by Franck Borel and Lucia D'Auria; Synthesis and characterization of the compounds and ^{1}H-STD-NMR was performed by Daan Willocx; Daan Willocx wrote the manuscript with contributions of all authors. Eleonora Diamanti and Anna K. H. Hirsch coordinated the project.

All authors have given approval to the final version of the manuscript.

This chapter will be submitted to the *Angewandte Chemie* (Wiley-VCH) without or with minor modifications.

Discovery of fragment by X-ray crystallographic screening targeting the CTP binding site of *Pseudomonas aeruginosa* IspD

Daan Willocx,[a] Lucia D'Auria,[b] Franck Borel,[b] Mostafa M. Hamed,[c] Eleonora Diamanti,*[c] Anna K. H. Hirsch*[a]

[a] D.Willocx, Prof. A. K. H. Hirsch
Helmholtz Institute for Pharmaceutical Research Saarland (HIPS)-Helmholtz Centre for Infection Research (HZI)
Campus E8.1,66123 Saarbrücken (Germany)
and
Saarland University, Department of Pharmacy
Campus E8.1,66123 Saarbrücken (Germany)
E-mail: Anna.Hirsch@helmholtz-hips.de

[b] Dr. F. Borel, Dr. L. D'Auria
Univ. Grenoble Alpes, CEA, CNRS, IBS, F-38000 Grenoble (France)

[c] Dr. E. Diamanti, Dr. M. M. Hamed
Helmholtz Institute for Pharmaceutical Research Saarland (HIPS), Helmholtz Centre for Infection Research (HZI)
Campus E8.1,66123 Saarbrücken (Germany)
E-mail: eleonora.diamanti2@unibo.it

Supporting Information for this article is given via a link at the end of the document.

Abstract: With antimicrobial resistance (AMR) reaching alarming levels, new anti-infectives with unpreceded mechanisms of action are urgently needed. The 2-*C*-methylerythritol-D-erythritol-4-phosphate (MEP) pathway represents an attractive source of drug targets due to its essential role in numerous pathogenic Gram-negative bacteria and *Mycobacterium tuberculosis* (*Mt*), whilst being absent in human cells. Here, we present the discovery of a fragment-based compound class identified through crystallographic screening of *Pseudomonas aeruginosa* (*Pa*) IspD, the third enzyme in the MEP pathway. The initial fragment was found to occupy the CTP binding cavity within the active site. Confirmation of fragment–protein interactions was achieved through ^{1}H saturation–transfer difference nuclear magnetic resonance (^{1}H-STD-NMR). Building upon these findings and insights from the co-crystal structures, we identified the optimal growth vectors for fragment growing. Initial fragment growing efforts yielded derivatives capable of inhibiting IspD originating from *Pa*, *Klebsiella pneumoniae*, and *Escherichia coli*, with IC_{50} values around 150 µM. Furthermore, these compounds exhibited promising activity against *Mt*IspD. Lastly, co-crystallization of our most promising derivatives provided insights into further optimization of the fragment class. These findings highlight the potential of this fragment class as a promising avenue for combating AMR.

There have been few medical discoveries as influential to present-day life as the discovery of anti-infectives. Not only do they allow cheap and straightforward treatment of infectious diseases, the confidence that infections could be treated enabled major leaps forward in other medical fields, including surgery and transplantations.[1, 2] However, we might find ourselves lacking potent anti-infectives in the midst of the current antimicrobial resistance (AMR) crisis.[3] Moreover, the clinical pipeline for new anti-infectives has mostly dried up and most of the new antibiotics that do reach the market are modified agents of commercialized antibiotic classes, facing rapid resistance development.[2] Furthermore, the vast majority of these new anti-infectives are ineffective against infections caused by Gram-negative bacteria, which make up a substantial fraction of hospital-acquired infections.[4] Therefore, there is an urgent need for new anti-infectives with innovative modes of action, especially those able

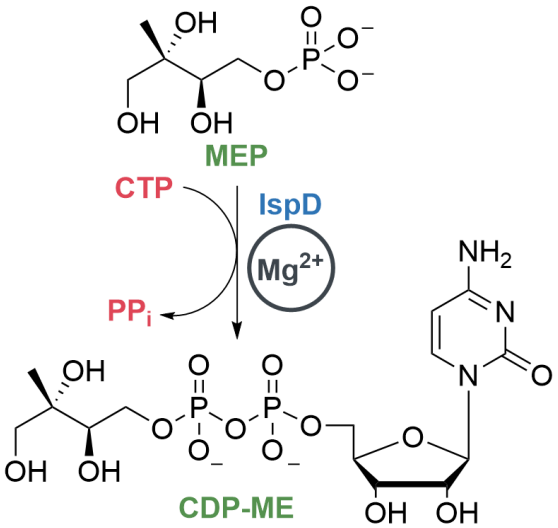

Scheme 1. The reaction between 2-*C*-methylerythritol-D-erythritol-4-phosphate (MEP) and CTP catalyzed by IspD. Mg^{2+} is the presumed cofactor in this reaction.

to target Gram-negative bacteria. The 2-*C*-methylerythritol-D-erythritol-4-phosphate (MEP) pathway for the biosynthesis of the isoprenoid precursors isopentenyl diphosphate (IDP) and dimethylallyl diphosphate (DMADP) is a promising source of drug targets. The pathway is essential for a wide variety of Gram-negative pathogens, including *Pseudomonas aeruginosa* (*Pa*), *Klebsiella pneumoniae* (*Kp*), and, *Mycobacterium tuberculosis* (*Mt*) and is absent in human cells, minimizing the risk of off-target side effects.[5]

In the present work, we set our focus on the third enzyme in the MEP pathway, namely IspD, catalyzing the formation of 4-diphosphocytidyl-2-*C*-methylerythritol (CDP-ME) from MEP and

CTP in the presence of Mg^{2+}, releasing inorganic diphosphate (PP_i) (Scheme 1). To this day, the number of IspD inhibitors reported in literature is limited; moreover, the majority of these inhibitors focus on either *Plasmodial* or botanically derived IspD.[6, 7] Consequently, there remains a considerable gap in our knowledge on inhibitors targeting bacterial homologues of IspD. Notably, one such unexplored variant is IspD originating from *Pa* (*Pa*IspD). In this study, we unveil, for the first time, the crystal structure of this enzyme, which enabled us to embark on a crystallographic screening endeavor, leading to the identification of a co- crystal structure in complex with a fragment. Subsequently, we confirmed interactions using ^{1}H-saturation-transfer difference nuclear magnetic resonance (^{1}H-STD-NMR) and initiated fragment growing resulting in enhanced inhibitory activity. Given the significant conservation of the active site of IspD among bacterial species, we assessed the potency of our hit against IspD originating from other bacterial species such as *K. pneumoniae, Escherichia coli* and *M. tuberculosis*. [8, 9]

After establishing protein expression and purification conditions, we commenced our investigation by obtaining an apo crystal structure of *Pa*IspD, as no previous structures of *Pa*IspD were available in the RCSB Protein Data Bank (PDB). The structure was solved by molecular replacement using the previously published apo crystal structure of *Ec*IspD (PDB: 1INJ) as a template.[10] The solved *Pa*IspD structure belongs to the same space group (C2) and shows similar lattice parameters. The asymmetric units contain only one molecule and about 47% solvent. Several IspD structures from various organisms are already present in the PDB and all these structures are highly conserved. As expected, *Pa*IspD exhibits the standard IspD fold, characterized by a single-domain structure in an α/β conformation composed of a seven-stranded β-sheet with interconnected loops and α-helices, which are connected to a subdomain known as the β-arm of the protein (See Figure S1 in the Supporting Information). This β-arm is primarily responsible for the dimerization of two IspD subunits by forming a hook-like structure that connects the two monomers; the interface between the two constitutes the protein's active site, which remains exposed to solvent. Next, we embarked on a screening campaign of a library containing 192 fragments obtained from Edelris (Lyon, France). In total, we collected crystals for 51 fragments, from which we

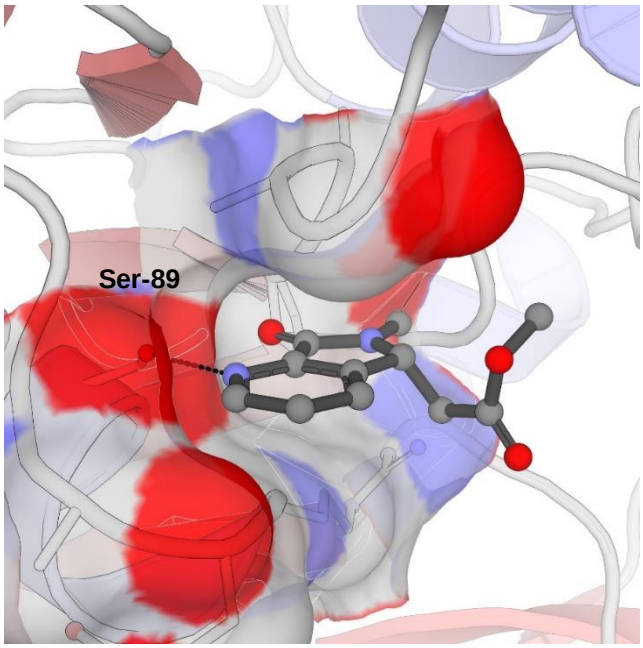

Figure 1. Co-crystal structure of **1** within the active site of *Pa*IspD displaying its interaction with Ser-89

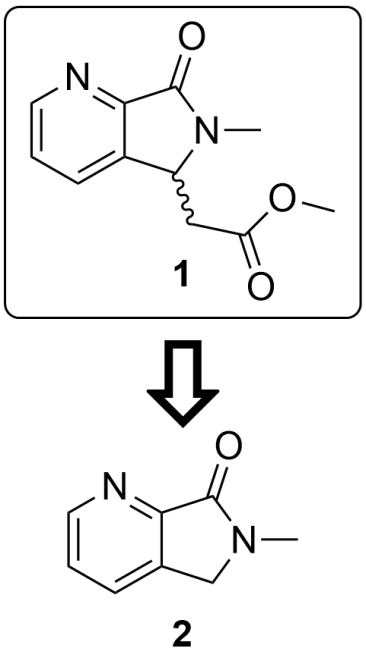

Figure 2. Chemical structure of **1** and its simplified derivative **2**.

obtained a handful of co-crystal structures. Among these, we identified 3 fragments which were in complex with the protein (see Supporting Information). From these fragments, **1** immediately caught our attention as the fragment exhibited the most promising structure for further development (Figure 1). Upon closer inspection, we noticed that the fragment occupied a tight pocket that was previously assigned to the cytosine of CTP in the co-crystal structure of *Ec*IspD with CTP (PDB:1I52).[10] Since all residues involved in CTP binding are conserved between both homologues, we assumed that the cavity had the same function in *Pa*IspD. Within this cavity, the main interaction between **1** and the protein seems to be a hydrogen bond formed between the pyridyl nitrogen atom and the side chain hydroxyl group of Ser-89 (distance = 2.6 Å, Figure 1). Interestingly, this hydroxyl group undergoes a similar interaction with one of the nitrogen atoms of the cytosine of CTP. The rest of the atoms comprising **1** do not seem to undergo any other obvious interactions, with the acetate tail of **1** being mostly solvent-exposed (Figure 1). Based on that, we hypothesized that a similar binding mode could be obtained by excluding this part of the fragment. Nevertheless, to experimentally confirm our hypothesis, we synthesized **2** (Figure 2, Scheme S2 in the Supporting Information) and co-crystallized it with *Pa*IspD under identical conditions. Importantly, as seen in Figure 3, a matching binding mode was observed, thus confirming our hypothesis.

To further validate the occurrence of interactions taking place between the fragment and *Pa*IspD , we referred to ^{1}H-STD-NMR, a commonly used technique for this purpose.[11] For this experiment, we prepared a HEPES buffer in D_2O with a 100-fold excess of **2** compared to *Pa*IspD. In the corresponding difference spectrum, we identified all hydrogen signals previously observed in the ^{1}H-NMR spectrum of **2** (see Figure S2 and S3 in the Supporting Information). This observation suggests that **2** came into close proximity of the protein, thereby affirming the potential interaction between them. We further noted the magnitude of amplification of the signals as the efficiency of saturation transfer scales with distance, enabling us to gain an idea about the proximity of each proton to the protein surface.[12]. Among all

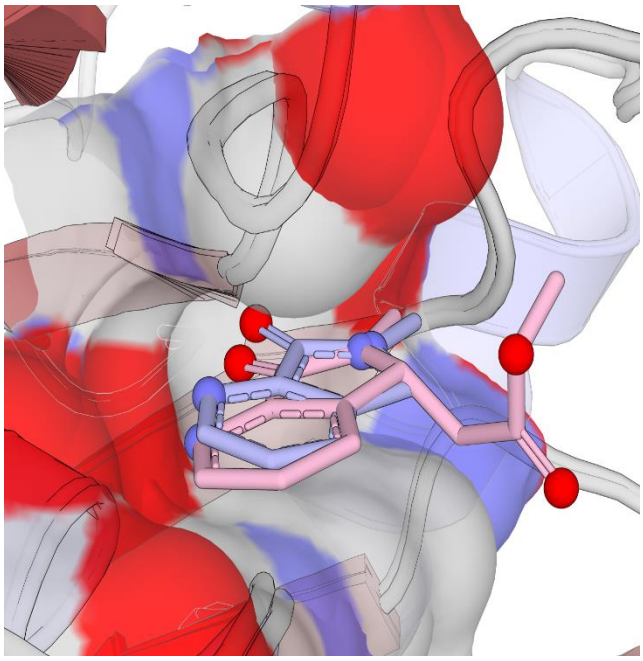

Figure 3. Comparison of the binding pose of **1** (pink) and **2** (light blue) in the active site of *Pa*IspD.

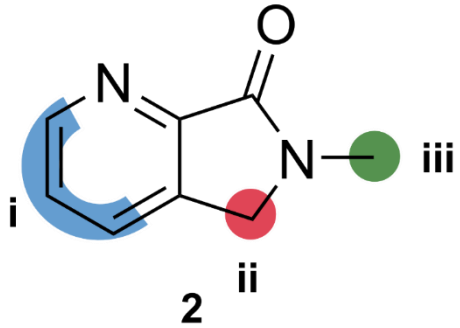

Figure 4. Indication of the area's that received saturation transfer during the ^{1}H saturation transfer difference NMR experiment. Blue: region **i**; Red: region **ii**; Green: region **iii**.

protons, the ones at position **iii** (Figure 4) clearly received a surplus in saturation transfer relative to the other ones, whereas the hydrogens positioned on the pyridyl (**i,** Figure 4) and the protons at position **ii** (Figure 4) received both less amplification with the latter receiving the least amount (Figure 4). These observations correlate reasonably well with the pose observed inside the co-crystal structure, although, based on the crystal structure, we expected to see a difference in amplification between the protons residing on the pyridine ring, with the proton next to the pyridyl nitrogen atom receiving more saturation than the other protons present on the ring. We might explain the observed difference with the static environment of co-crystal structures in comparison with the dynamic environment in a ^{1}H-STD-NMR experiment.

Having validated the binding mode of our optimized fragment hit **2**, we next evaluated its inhibitory activity using our previously established LC-MS based assay.[7] Unfortunately, no inhibition was detectable up to 1 mM for **2**. Nevertheless, we continued our study and we embarked on a rational fragment growing campaign. The analysis both of the co-crystal structure and the ^{1}H-STD-NMR spectrum, suggested two potential growth vectors. Based on the co-crystal structure, modifications at position **iii** (Figure 4) seemed most straightforward, as this would extend the fragment inside the active site towards the location where the ribose of CTP would reside. However, the proton at this position received significant amplification in the ^{1}H-STD-NMR spectrum, implying that the methyl p is in close proximity to the protein surface. On the other hand, from the perspective of the ^{1}H-STD-NMR spectrum, modifications at position **ii** (Figure 4) seems most logical as the associated protons only received limited amplification. However, we previously stated that modifications at this position point towards the solvent in the co-crystal structure. Therefore, aiming to improve the potency of our hit and considering our early stage of the fragment growing work, we moved in both directions.

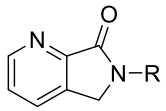

#	Structure, R=	% inhibition of *Pa*IspD at 1000 µM
3	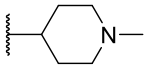	TBD
4	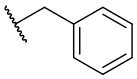	TBD
5	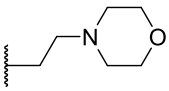	TBD
6	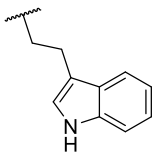	TBD

[a] Assays were performed in replicate as independent experiments ($n \geq 2$). Values are shown as mean ± SD. TBD= to be determined

Table 2. In vitro inhibitory activities against *Pa*IspD for **7**–**12** bearing modifications at position **ii**.

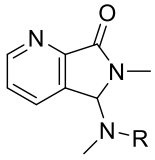

#	Structure, R=	% inhibition *Pa*IspD at 500 µM[a]	#	Structure, R=	% inhibition *Pa*IspD at 500 µM[a]
7	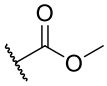	TBD	**10**	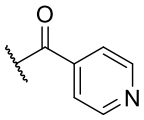	TBD
8	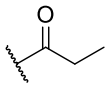	TBD	**11**	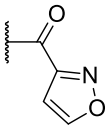	TBD
9	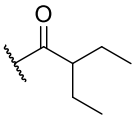	TBD	**12**	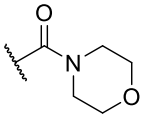	TBD

[a] Assays were performed in replicate as independent experiments ($n \geq 2$). Values are shown as mean ± SD. TBD = to be determined

With these considerations in mind, we designed and synthesized a focused subset of derivatives containing modifications at both positions (Tables 1 and 2). To address potential clashes with the protein surface when growing at position **iii** (Figure 4), we attached most derivatives with an alkane linker to allow some flexibility (Table 1). For modifications at position **ii** (Figure 4), we opted to use methylamine as a linker between the core of the fragment and tail instead of a methyl (see Scheme S2 in the Supporting Information). This linker not only has the ability to form hydrogen bonds with the protein itself, but also enables straightforward modifications via nucleophilic addition or substitution reactions. At first, we synthesized the methylcarbamate starting from the methylamine in an attempt to closely resemble **1** (Table 2 and Scheme S3 in the Supporting Information). Next, we obtained the amide derivative of **7** to gain insights into the influence of the oxygen atom of the carbamate on the activity. Replacement of this moiety by an amide would allow for more straightforward derivatization. Lastly, we synthesized compounds **9**–**12** (see Scheme S3 and Scheme S4 in the Supporting Information). Biological evaluation of the compound class is ongoing.

Lastly, we explored the activity of the fragments against IspD originating from other Gram-negative bacterial species. For this exploration, we established a protocol to obtain IspD from *K. pneumoniae* and utilized earlier protocols to obtain *E. coli IspD* as the active site homology among these species exhibits a high degree of similarity.[9] Moreover, we determined the % inhibition at 500 µM of these three molecules against *Mt*IspD (Table 3).

Table 3. In vitro activities of **10**–**12** against *Pa*, *Kp*, *Ec* and *Mt*IspD.

#	*Pa*IspD IC_{50} (µM)[a]	*Kp*IspD IC_{50} (µM)[a]	*Ec*IspD IC_{50} (µM)[a]	%inhibition *Mt*IspD at 500 µM[a]
10	TBD	TBD	TBD	TBD
11	TBD	TBD	TBD	TBD
12	TBD	TBD	TBD	TBD

[a] Assays were performed in replicate as independent experiments (n ≥ 2). values are shown as mean ± SD.

In summary, we report on the discovery of a fragment-based compound class uncovered during a crystallographic screening using *Pa*IspD. We confirmed interactions between the protein and the fragment by employing ^{1}H-STD-NMR spectroscopy. We combined these results with the insights obtained from the co-crystal structure to identify the most logical sites for growing the fragment.

Acknowledgments

The authors would like to thank Simone Amann, Jeannine Jung and Jannine Seelbach for performing the *in vitro* assays. IBS acknowledges integration into the Interdisciplinary Research Institute of Grenoble (IRIG, CEA)

Keywords: • Drug discovery • Fragment-based drug design • IspD • Medicinal chemistry • MEP pathway

[1] L. B. Rice, *The Journal of Infectious Diseases* **2008**, *197*, 1079-1081; J. Stephen, F. Salam, M. Lekshmi, S. H. Kumar, M. F. Varela, *Antibiotics* **2023**, *12*, 343.

[2] S. Walesch, J. Birkelbach, G. Jézéquel, F. P. J. Haeckl, J. D. Hegemann, T. Hesterkamp, A. K. H. Hirsch, P. Hammann, R. Müller, *EMBO reports* **2023**, *24*, e56033.

[3] C. J. L. Murray, K. S. Ikuta, F. Sharara, L. Swetschinski, G. Robles Aguilar, A. Gray, C. Han, C. Bisignano, P. Rao, E. Wool, S. C. Johnson, A. J. Browne, M. G. Chipeta, F. Fell, S. Hackett, G. Haines-Woodhouse, B. H. Kashef Hamadani, E. A. P. Kumaran, B. McManigal, S. Achalapong, R. Agarwal, S. Akech, S. Albertson, J. Amuasi, J. Andrews, A. Aravkin, E. Ashley, F.-X. Babin, F. Bailey, S. Baker, B. Basnyat, A. Bekker, R. Bender, J. A. Berkley, A. Bethou, J. Bielicki, S. Boonkasidecha, J. Bukosia, C. Carvalheiro, C. Castañeda-Orjuela, V. Chansamouth, S. Chaurasia, S. Chiurchiù, F. Chowdhury, R. Clotaire Donatien, A. J. Cook, B. Cooper, T. R. Cressey, E. Criollo-Mora, M. Cunningham, S. Darboe, N. P. J. Day, M. De Luca, K. Dokova, A. Dramowski, S. J. Dunachie, T. Duong Bich, T. Eckmanns, D. Eibach, A. Emami, N. Feasey, N. Fisher-Pearson, K. Forrest, C. Garcia, D. Garrett, P. Gastmeier, A. Z. Giref, R. C. Greer, V. Gupta, S. Haller, A. Haselbeck, S. I. Hay, M. Holm, S. Hopkins, Y. Hsia, K. C. Iregbu, J. Jacobs, D. Jarovsky, F. Javanmardi, A. W. J. Jenney, M. Khorana, S. Khusuwan, N. Kissoon, E. Kobeissi, T. Kostyanev, F. Krapp, R. Krumkamp, A. Kumar, H. H. Kyu, C. Lim, K. Lim, D. Limmathurotsakul, M. J. Loftus, M. Lunn, J. Ma, A. Manoharan, F. Marks, J. May, M. Mayxay, N. Mturi, et al., *The Lancet* **2022**, *399*, 629-655.

[4] Z. Yu, J. Tang, T. Khare, V. Kumar, *Fitoterapia* **2020**, *140*, 104433; M. S. Butler, I. R. Henderson, R. J. Capon, M. A. T. Blaskovich, *The Journal of Antibiotics* **2023**, *76*, 431-473; M. S. Butler, M. A. T. Blaskovich, M. A. Cooper, *The Journal of Antibiotics* **2017**, *70*, 3-24; G. W. H. Organization, *Vol. WHO/EMP/IAU/2017.12*, **2017**.

[5] A. Frank, M. Groll, *Chemical Reviews* **2017**, *117*, 5675-5703; T. Masini, B. S. Kroezen, A. K. H. Hirsch, *Drug Discovery Today* **2013**, *18*, 1256-1262; T. Masini, A. K. H. Hirsch, *Journal of Medicinal Chemistry* **2014**, *57*, 9740-9763; M. Gabrielsen, J. Kaiser, F. Rohdich, W. Eisenreich, R. Laupitz, A. Bacher, C. S. Bond, W. N. Hunter, *FEBS Journal* **2006**, *273*, 1065-1073.

[6] K. E. Price, C. M. Armstrong, L. S. Imlay, D. M. Hodge, C. Pidathala, N. J. Roberts, J. Park, M. Mikati, R. Sharma, A. S. Lawrenson, N. H. Tolia, N. G. Berry, P. M. O'Neill, A. R. O. John, *Sci Rep* **2016**, *6*, 12; L. S. Imlay, C. M. Armstrong, M. C. Masters, T. Li, K. E. Price, R. L. Edwards, K. M. Mann, L. X. Li, C. L. Stallings, N. G. Berry, P. M. O'Neill, A. R. Odom, *ACS Infect. Dis.* **2015**, *1*, 157-167; D. Reker, M. Seet, M. Pillong, C. P. Koch, P. Schneider, M. C. Witschel, M. Rottmann, C. Freymond, R. Brun, B. Schweizer, B. Illarionov, A. Bacher, M. Fischer, F. Diederich, G. Schneider, *Angewandte Chemie International Edition* **2014**, *53*, 7079-7084; M. Witschel, F. Röhl, R. Niggeweg, T. Newton, *Pest Management Science* **2013**, *69*, 559-563; A. Schwab, B. Illarionov, A. Frank, A. Kunfermann, M. Seet, A. Bacher, M. C. Witschel, M. Fischer, M. Groll, F. Diederich, *ACS Chemical Biology* **2017**, *12*, 2132-2138; A. Kunfermann, M. Witschel, B. Illarionov, R. Martin, M. Rottmann, H. W. Höffken, M. Seet, W. Eisenreich, H.-J. Knölker, M. Fischer, A. Bacher, M. Groll, F. Diederich, *Angewandte Chemie International Edition* **2014**, *53*, 2235-2239; E. Diamanti, M. M. Hamed, A. Lacour, P. Bravo, B. Illarionov, M. Fischer, M. Rottmann, M. Witschel, A. K. H. Hirsch, *ChemMedChem* **2022**.

[7] D. Willocx, L. Bizzarri, A. Alhayek, P. Bravo, B. Illarionov, K. Rox, J. Lohse, M. Fischer, A. M. Kany, H. Hahne, M. Rottmann, M. Witschel, M. M. Hamed, E. Diamanti, A. K. H. Hirsch, *ChemRxiv.* **2024**.

[8] S. B. Richard, A. M. Lillo, C. N. Tetzlaff, M. E. Bowman, J. P. Noel, D. E. Cane, *Biochemistry* **2004**, *43*, 12189-12197; Y. Jin, Z. Liu, Y. Li, W. Liu, Y. Tao, G. Wang, *Sci Rep* **2016**, *6*, 36379; C. Bjorkelid, T. Bergfors, L. M. Henriksson, A. L. Stern, T. Unge, S. L. Mowbray, T. A. Jones, *Acta Crystallographica Section D* **2011**, *67*, 403-414.

[9] L. E. Kemp, C. S. Bond, W. N. Hunter, *Acta Crystallographica Section D Biological Crystallography* **2003**, *59*, 607-610.

[10] S. B. Richard, M. E. Bowman, W. Kwiatkowski, I. Kang, C. Chow, A. M. Lillo, D. E. Cane, J. P. Noel, *Nature Structural Biology* **2001**, *8*, 641-648.

[11] Q. Li, *Frontiers in Molecular Biosciences* **2020**, *7*; C. W. Murray, D. C. Rees, *Nature Chemistry* **2009**, *1*, 187-192.

[12] A. Viegas, J. Manso, F. L. Nobrega, E. J. Cabrita, *Journal of Chemical Education* **2011**, *88*, 990-994; T. Haselhorst, A.-C. Lamerz, M. v. Itzstein, in *Glycomics: Methods and Protocols* (Eds.: N. H. Packer, N. G. Karlsson), Humana Press, Totowa, NJ, **2009**, pp. 375-396.

Entry for the Table of Contents

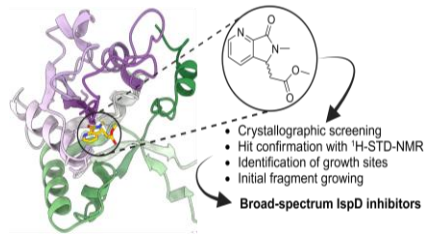

During a crystallographic screening with IspD from *Pseudomonas aeruginosa*, we identified a fragment residing inside the active site. We confirmed its interactions with the protein by ^{1}H saturation-transfer difference-NMR spectroscopy. Initial fragment growing yielded derivatives capable of inhibiting IspD originating from multiple Gram-negative pathogens and *Mycobacterium tuberculosis*.

Supporting Information

Discovery of fragment by X-ray crystallographic screening targeting the CTP binding site of *Pseudomonas aeruginosa* IspD

Daan Willocx,[a] Lucia D'Auria,[b] Franck Borel,[b] Mostafa M. Hamed,[c] Eleonora Diamanti,*[c] Anna K. H. Hirsch*[a]

[a] D.Willocx, Prof. A. K. H. Hirsch
Helmholtz Institute for Pharmaceutical Research Saarland (HIPS)-Helmholtz Centre for Infection Research (HZI)
Campus E8.1,66123 Saarbrücken (Germany)
and
Saarland University, Department of Pharmacy
Campus E8.1,66123 Saarbrücken (Germany)
E-mail: Anna.Hirsch@helmholtz-hips.de

[b] Dr. F. Borel, Dr. L. D'Auria
Univ. Grenoble Alpes, CEA, CNRS, IBS, F-38000 Grenoble (France)

[c] Dr. M. M. Hamed, Dr. E. Diamanti,
Helmholtz Institute for Pharmaceutical Research Saarland (HIPS), Helmholtz Centre for Infection Research (HZI)
Campus E8.1,66123 Saarbrücken (Germany)
E-mail: eleonora.diamanti2@unibo.it

Table of Contents

Crystallization conditions

***Pa*IspD expression and purification.** The *Pseudomonas aeruginosa* IspD (*Pa*IspD) synthetic gene was cloned into pET28 expression plasmid. *Pa*IspD, fused to an *N*-termimal His6 -tag, was expressed in *Escherichia coli* BL21 (DE3) strain. Cell cultures were grown in LB medium at 37 °C until an optical density (A600) of 0.7; then protein expression was induced by adding isopropyl β-D-thiogalactopyranoside to a final concentration of 1 mM. Expression was carried out for four hours at 37 °C. Cells were pelleted by centrifugation, resuspended in 50 mM NaH_2PO_4 pH 8.0, 300 mM NaCl, 1% tween-20, 20 mM imidazole, 10 mM β-mercaptoethanol,10% glycerol and Complete EDTA-free antiprotease (Roche Diagnostics, Meylan, France) (1 tablet Complete in 50 mL buffer), and lysed by sonication. Cellular debris were removed by centrifugation (60 min, 15 000 g). After centrifugation, the supernatant was applied on Nickel beads (Ni-NTA, Qiagen) previously equilibrated in the lysis buffer. The column was washed with 50 mM NaH_2PO_4 pH 8.0, 300 mM NaCl, 40 mM imidazole, 10% glycerol, 10 mM β-mercaptoethanol. *Pa*IspD was eluted with 250 mM imidazole. Incubation with thrombin during overnight dialysis at 4 °C against lysis buffer minus tween-20 removed the amino terminal His-tag. Dialyzed protein was reloaded on a Ni-NTA column. The flow-through was depleted of thrombin using a benzamidine-sepharose column. The protein was further purified by gel filtration on a HiLoad 16/60 Superdex-200 prep grade column equilibrated and eluted with 50 mM Hepes pH 7.5, 100 mM NaCl and 2 mM DTT. Fractions containing *Pa*IspD were pooled, concentrated to 15 mg/mL and stored at –80 °C.

(Co)-crystallization of the fragments with *Pa*IspD. The co-crystallization of *Pa*IspD with the chemical compounds of interest was carried out using "dry" coated crystallization plates. Prior to crystallization, the DropGuard supports of the 15-well EasyXtal® tools (Nextal) were filled with 1 or 2 µL of the chemical compounds to be co-crystallized (20–50 mM in DMSO) and then left in the open air until the DMSO had completely evaporated. The crystallization drops were then prepared by mixing 1 µL of the reservoir with 1 µL of the protein solution on the dried compound. IspD complex were crystallized by the hanging drop vapor diffusion method at 20 °C using either 26% PEG 500 MME or 26 % PEG 400, 0.1 M MES pH 6.5 and a protein concentration of 15 mg mL^{-1}. Native data sets were collected on BL13 XALOC at Alba synchrotron (Barcelona, Spain) and ID30A-3 beamline at ESRF (Grenoble, France). The diffraction data were processed using XDS. Crystals belong to the C2 space group and contain one molecule per asymmetric unit. The structures were solved by molecular replacement using Phaser and *E. coli* IspD structure (Protein Data Bank entry 1INJ)[1] as a search model. Model building was made using Coot and refinements were carried out with Phenix refine. Data and refinement statistics are summarized in table S1. The coordinates and the structure factors will be! deposited in the Protein Data Bank in Europe (http://www.pdbe.org).

Saturation-Transfer Difference (STD)-NMR spectroscopy.

The ^{1}H-STD-NMR experiment was recorded at 25 ºC with 512 scans on a Bruker Avance Neo 500 MHz spectrometer with prodigy cryoprobe system. The on-resonance irradiation was set at –4 ppm, while the off-resonance was set to –40 ppm. Samples contained a concentration of 1 mM of **2** and 10 µM of *Pa*IspD resulting in a 100:1 ratio regarding the enzyme. Spectra were processed using Topspin 4.2.0, Bruker's NMR Data Analysis software.

Biological evaluation

IspD inhibition assay. The *in vitro* inhibition assay against all homologues of IspD was performed as described previously.[2]

Chemistry

General chemistry. Starting materials and solvents were purchased from commercial suppliers, and used without further purification. All chemical yields refer to purified compounds and were not optimized. Column chromatography was performed using the automated flash chromatography system CombiFlash®Rf (Teledyne Isco) equipped with RediSepRf silica columns. Preparative RP-HPLC was performed either using an UltiMate 3000 Semi-Preparative System (Thermo Fisher Scientific) equipped with nucleodur®C18 Gravity (250 mm × 16 mm, 5 µm) column or using a Pure C-850 Flash/Prep (Buchi) equipped with Nucleodur C18 HTec (250 mm x 40 mm, particle size 5 µm). Low resolution mass spectrometry and purity control of final compounds was carried out using an Ultimate 3000-MSQ LCMS system (Thermo Fisher Scientific) consisting of a pump, an autosampler, MWD detector and an ESI quadrupole mass spectrometer. ^{1}H and ^{13}C NMR spectra were recorded as indicated on a Bruker Avance Neo 500 MHz (^{1}H, 500 MHz; ^{13}C, 126 MHz) with a prodigy cryoprobe system. Chemical shifts were recorded as δ values in ppm units and referenced against the residual solvent peak (DMSO-d_6, δ= 2.50, 39.52 and $CDCl_3$-*d1*: δ=7.26, 77.16). Splitting patterns describe apparent multiplicities and are designated as s (singlet), br s (broad singlet), d (doublet), dd (doublet of doublet), t (triplet), q (quartet), m (multiplet). Coupling constants (*J*) are given in Hertz (Hz). High-resolution mass spectra were recorded on a ThermoFisher Scientific (TF, Dreieich, Germany) Q Exactive Focus system equipped with heated electrospray ionization (HESI)-II source.

General procedure (GP-1): Synthesis of Derivatives 2–6

To a crimp vial, methyl 3-(bromomethyl)picolinate (1.0 equiv), the respective primary amine (1.2 equiv) and THF (175 equiv) were added, the vial was capped off, heated to 80 °C and stirred for 2.5 h. Next, water (20 mL) was added, and the resulting solution was extracted with a 3:1 mixture of $CHCl_3$ and propanol (5x 15 mL), the combined organic layers were dried over $MgSO_4$, filtered, concentrated *in vacuo*, and purified by preparative HPLC.

General procedure (GP-2): Synthesis of Derivatives 8–11

To a flask were added, 6-methyl-5-(methylamino)-5,6-dihydro-7*H*-pyrrolo[3,4-β]pyridin-7-one (1.0 equiv), the respective carboxylic acid (1.2 equiv), trimethylamine (2 equiv), and DCM (140 equiv). The resulting solution was stirred at room temperature for 10 min, after which, propanephosphonic acid anhydride (1.5 equiv) was added, and the resulting mixture was stirred at room temperature overnight. Next, water (20 mL) was added and the resulting solution was extracted with a 3:1 mixture of $CHCl_3$ and propanol (5x 15 mL), the organic fractions were dried over $MgSO_4$, filtered, and the solvent was removed *in vacuo*. The residue was purified using preparative HPLC.

6-Methyl-5,6-dihydro-7*H*-pyrrolo[3,4-β]pyridin-7-one (2)

According to **GP-1**, using methylamine (0.04 g, 0.48 mmol), afforded after purification by preparative HPLC, using H_2O and ACN as solvent in a gradient (0% to 100% ACN), **2** as a white powder (0.01 g, 18% yield). ^{1}H NMR (500 MHz, DMSO-d_6, ppm) δ = 8.69 (d, *J* = 4.6 Hz, 1H), 8.05 (d, *J* = 7.6 Hz, 1H), 7.55 (dd, *J* = 7.7, 4.8 Hz, 1H), 4.48 (s, 2H), 3.12 (s, 3H). ^{13}C NMR (126 MHz, DMSO-d_6, ppm) 165.6, 150.3, 150.0, 136.0, 131.8, 125.1, 49.1, 29.4. HRMS (ESI$^+$) calculated for $C_8H_9N_2O$ $[M+H]^+$ 149.06366, found 149.07069.

6-(1-Methylpiperidin-4-yl)-5,6-dihydro-7*H*-pyrrolo[3,4-β]pyridin-7-one (3)

According to **GP-1**, using 4-amino-1-methylpiperidine (0.04 g, 0.26 mmol), afforded after purification by preparative HPLC, **3** as a white powder (0.01 g, 16% yield). ^{1}H NMR (500 MHz, $CDCl_3$-*d*, ppm) δ = 8.80 (d, *J* = 4.4 Hz, 1H), 7.88 – 7.84 (m, 1H), 7.46 (dd, *J* = 7.7, 4.8 Hz, 1H), 4.61 (tt, *J* = 12.2, 4.1 Hz, 1H), 4.46 (s, 2H), 3.43 (br d, *J* = 12.1 Hz, 2H), 2.75 – 2.67 (m, 2H), 2.66 (s, 3H), 2.44 (qd, *J* = 12.8, 3.7 Hz, 2H), 1.99 (br dd, *J* = 12.7, 1.5 Hz, 2H). ^{13}C NMR (126 MHz, $CDCl_3$-*d*, ppm) δ = 167.6, 166.6, 151.3, 150.7, 135.4, 131.7, 125.6, 54.4, 47.1, 44.4, 44.0, 28.0. HRMS (ESI$^+$) calculated for $C_{13}H_{18}N_3O$ $[M+H]^+$ 232.13716, found 232.14404.

6-Benzyl-5,6-dihydro-7*H*-pyrrolo[3,4-β]pyridin-7-one (4)

According to **GP-1**, using benzylamine (0.03 g, 0.26 mmol), afforded after purification by preparative HPLC **4** as a white powder (0.02 g, 48% yield).^{1}H NMR (500 MHz, $CDCl_3$-*d*, ppm) *δ* = 8.81 (br s, 1H), 7.84 – 7.70 (m, 1H), 7.43 (br s, 1H), 7.38 – 7.28 (m, 5H), 4.88 (s, 2H), 4.28 (br s, 2H). ^{13}C NMR (126 MHz, $CDCl_3$-*d*, ppm) *δ* = 165.8, 150.3, 150.2, 136.3, 135.4, 131.9, 128.9, 128.4, 128.0, 125.4, 47.2, 46.9. HRMS (ESI$^+$) calculated for $C_{14}H_{13}N_2O$ [M+H]$^+$ 225.09496, found 225.10170.

6-(2-Morpholinoethyl)-5,6-dihydro-7*H*-pyrrolo[3,4-β]pyridin-7-one (**5**)

According to **GP-1**, using 4-(2-aminoethyl)morpholine (0.03 g, 0.26 mmol), afforded after purification by preparative HPLC **5** as a white powder (0.01 g, 18% yield). ^{1}H NMR (500 MHz, $CDCl_3$-*d*, ppm) δ = 8.80 (d, *J* = 4.7 Hz, 1H), 7.85 (d, *J* = 7.6 Hz, 1H), 7.45 (dd, *J* = 7.7, 4.8 Hz, 1H), 4.61 (s, 2H), 3.95 (br s, 2H), 3.81 (br s, 4H), 2.90 (br s, 2H), 2.75 (br s, 4H). ^{13}C NMR (126 MHz, $CDCl_3$-*d*, ppm) δ = 166.6, 150.6, 150.3, 135.1, 130.9, 125.0, 66.0, 56.0, 53.0, 48.4, 38.8. HRMS (ESI$^+$) calculated for $C_{13}H_{18}N_3O_2$ [M+H]$^+$ 248.13208, found 248.13901.

6-(2-(1*H*-Indol-3-yl)ethyl)-5,6-dihydro-7*H*-pyrrolo[3,4-β]pyridin-7-one (**6**)

According to **GP-1**, using tryptamine (0.04 g, 0.26 mmol), afforded after purification by preparative HPLC **6** as a white solid (0.01g, 23% yield). ^{1}H NMR (500 MHz, $CDCl_3$-*d*, ppm) *δ* = 8.78 (d, *J* = 4.7 Hz, 1H), 8.15 (br s, 1H), 7.71 (d, *J* = 7.8 Hz, 1H), 7.63 (d, *J* = 7.8 Hz, 1H), 7.43 – 7.34 (m, 2H), 7.23 – 7.18 (m, 1H), 7.14 – 7.08 (m, 2H), 4.22 (s, 2H), 4.08 (t, *J* = 6.9 Hz, 2H), 3.22 (t, *J* = 6.9 Hz, 2H). ^{13}C NMR (126 MHz, $CDCl_3$-*d*, ppm) δ = 166.5, 151.0, 150.7, 136.3, 135.0, 131.0, 127.2, 124.9, 119.5, 118.5, 112.5, 111.3, 48.2, 43.1, 24.3. HRMS (ESI$^+$) calculated for $C_{17}H_{16}N_3O$ [M+H]$^+$ 278.12151, found 278.12811.

6-Methyl-5-(methylamino)-5,6-dihydro-7*H*-pyrrolo[3,4-β]pyridin-7-one (**I**)

To a crimp vial, methyl 3-methylpicolinate (1.0 g, 6.6 mmol), 1-bromopyrrolidine-2,5-dione (2.60 g, 14.6 mmol),*di*benzoylperoxide (0.01 g, 0.2 mmol), and $CHCl_3$ (10 mL) were added. The vail was sealed and stirred at 80 °C overnight, after which, water (20 mL) was added, and the resulting solution was extracted with CH_2Cl_2 (3x 15 mL). The combined organic layers were dried over $MgSO_4$, filtered, concentrated *in vacuo*, and purified by flash chromatography using CH_2Cl_2 as solvent. Then, the combined fractions were concentrated *in vacuo* and resolubilized in water (50 mL) to which an excess of methylamine (40% w/v water) was added and, the resulting mixture was stirred at 80 °C overnight. The reaction mixture was extracted using a 3:1 mixture of $CHCl_3$ and propanol (5x 15 mL). The combined organic layers were dried over $MgSO_4$, filtered, and concentrated *in vacuo* to afford **I** as an off-white solid (0.74 g, 63% crude yield). ^{1}H NMR (500 MHz, $CDCl_3$-*d*, ppm) *δ* = 8.82 – 8.78 (m, 1H), 7.94 – 7.86 (m, 1H), 7.49 – 7.42 (m, 1H), 5.33 (s, 1H), 3.16 – 3.10 (m, 3H), 2.01 (s, 3H).

Methyl methyl(6-methyl-7-oxo-6,7-dihydro-5*H*-pyrrolo[3,4-β]pyridin-5-yl)carbamate (**7**).

To a flask containing **I** (0.05 g, 0.28 mmol), trimethylamine (0.06 g, 0.62 mmol), and DMF (2 mL), methylchloroformate (0.04 g, 0.42 mmol) was added at 0 °C. The resulting solution was stirred at 0 °C for 2 h, after which, water (15 mL) was added, and the resulting solution was extracted using a 3:1 mixture of $CHCl_3$ and propanol (5x 15 mL). The combined organic layers were dried over $MgSO_4$, filtered, concentrated *in vacuo*, and purified by preparative HPLC, affording **7** as a white solid (0.02 g, 33% yield). ^{1}H NMR (500 MHz, $CDCl_3$-*d*, ppm) *δ* = 8.85 (br d, *J* = 4.1 Hz, 1H), 7.80 (br d, *J* = 7.8 Hz, 1H), 7.53 – 7.44 (m, *J* = 5.0 Hz, 1H), 6.76 (s, 1H), 3.96 – 3.81 (m, 3H), 3.08 (s, 3H), 2.45 – 2.31 (m, 3H). ^{13}C NMR (126 MHz, $CDCl_3$-*d*) δ = 166.1, 158.0, 152.6, 151.6, 135.1, 131.4, 126.0, 69.5, 53.8, 27.5, 27.1. HRMS (ESI$^+$) calculated for $C_{11}H_{14}N_3O_3$ [M+H]$^+$ 236.09569, found 236.10240.

***N*-Methyl-*N*-(6-methyl-7-oxo-6,7-dihydro-5*H*-pyrrolo[3,4-β]pyridin-5-yl)propionamide** (**8**).

According to **GP-2**, using propionic acid (0.03 g, 0.34 mmol), afforded after purification by preparative HPLC, **8** as a white powder (0.03 g, 45% yield). ^{1}H NMR (500 MHz, $CDCl_3$-*d*, ppm) *δ* = 8.83 (d, *J* = 4.7 Hz, 1H), 7.75 (d, *J* = 7.6 Hz, 1H), 7.47 (dd, *J* = 7.7, 4.8 Hz, 1H), 7.19 (s, 1H), 3.09 – 3.02 (m, 3H), 2.59 – 2.46 (m, 2H), 2.44 (s, 3H), 1.26 (t, *J* = 7.4 Hz, 3H). ^{13}C NMR (126 MHz, $CDCl_3$-*d*, ppm) *δ* = 176.0, 166.1, 152.2, 151.5, 135.2, 131.1, 125.7, 66.4, 28.1, 27.4, 26.9, 9.0. HRMS (ESI$^+$) calculated for $C_{12}H_{16}N_3O_2$ [M+H]$^+$ 234.11643, found 234.12293.

2-Ethyl-*N*-methyl-*N*-(6-methyl-7-oxo-6,7-dihydro-5*H*-pyrrolo[3,4-β]pyridin-5-yl)butanamide (**9**).

According to **GP-2**, using 2-ethylbutanoic acid (0.04 g, 0.34 mmol), afforded after purification by preparative HPLC, **9** as a white powder (0.01 g, 4% yield). ^{1}H NMR (500 MHz, $CDCl_3$-*d*, ppm) δ = 8.87 – 8.83 (m, 1H), 7.71 (d, *J* = 7.3 Hz, 1H), 7.48 (dd, *J* = 7.6, 4.9 Hz, 1H), 7.06 (s, 1H), 3.11 – 3.04 (m, 3H), 2.69 – 2.62 (m, 1H), 2.49 (m, 3H), 1.85 – 1.73 (m, 2H), 1.68 – 1.56 (m, 2H), 1.03 – 0.94 (m, 6H). ^{13}C NMR (126 MHz, $CDCl_3$-d) δ = 178.5, 166.1, 152.2, 151.6, 135.4, 131.0, 125.8, 66.4, 45.7, 28.4, 27.0, 26.0, 25.7, 12.1. HRMS (ESI$^+$) calculated for $C_{15}H_{22}N_3O_2$ [M+H]$^+$ 276.16338, found 276.17015.

***N*-Methyl-*N*-(6-methyl-7-oxo-6,7-dihydro-5*H*-pyrrolo[3,4-β]pyridin-5-yl)isonicotinamide** (**10**). According to **GP-2**, using isonicotinic acid (0.04 g, 0.34 mmol), afforded after purification by preparative HPLC, **10** as a white powder (0.04 g, 45% yield). ^{1}H NMR (500 MHz, $CDCl_3$-*d*, ppm) δ = 8.90 (d, *J* = 4.6 Hz, 1H), 8.80 (br d, *J* = 4.4 Hz, 2H), 7.92 (br d, *J* = 7.6 Hz, 1H), 7.59 – 7.51 (m, 1H), 7.47 – 7.37 (m, 2H), 7.21 (s, 1H), 3.23 – 3.04 (m, 2H), 2.62 – 2.38 (m, 2H). ^{13}C NMR (126 MHz, $CDCl_3$-*d*, ppm) δ = 171.6, 166.3, 152.9, 150.9, 142.4, 134.7, 131.4, 126.3, 121.3, 67.1, 30.7, 27.5. HRMS (ESI$^+$) calculated for $C_{15}H_{15}N_4O_2$ [M+H]$^+$ 283.11168, found 283.11870.

***N*-Methyl-*N*-(6-methyl-7-oxo-6,7-dihydro-5*H*-pyrrolo[3,4-β]pyridin-5-yl)isoxazole-3-carboxamide** (**11**).

According to GP-2, using isoxazole-3-carboxylic acid (0.04 g, 0.34 mmol), afforded after purification by preparative HPLC, **11** as a white powder (0.06, 75% yield). ^{1}H NMR (500 MHz, DMSO-d_6) δ = 9.21 (s, 1H), 8.83 – 8.82 (m, 1H), 8.20 – 8.15 (m, 1H), 7.71 – 7.67 (m, 1H), 7.07 (s, 1H), 7.02 (s, 1H), 6.57 – 6.51 (m, 1H), 2.92 (s, 3H), 2.46 (s, 3H). ^{13}C NMR (126 MHz, DMSO-d_6, ppm) δ = 161.6, 161.2, 160.7, 157.0, 151.9, 134.9, 131.7, 126.2, 105.4, 70.8, 26.1. HRMS (ESI$^+$) calculated for $C_{13}H_{13}N_4O_3$ [M+H]$^+$ 273.09094, found 273.09814.

***N*-Methyl-*N*-(6-methyl-7-oxo-6,7-dihydro-5*H*-pyrrolo[3,4-β]pyridin-5-yl)morpholine-4-carboxamide (12).**

To a flask at 0 °C containing, **I** (0.05 g, 0.28mmol), trimethylamine (0.06 g, 0.62 mmol), and CH_2Cl_2 (3 mL), morpholine-4-carbonyl chloride (0.06 g, 0.42 mmol) was added. The resulting solution was stirred at 0 °C for 2 h, after which, water (15 mL) was added, and the resulting solution was extracted using a 3:1 mixture of $CHCl_3$ and propanol (5x 15 mL), combined organic layers were dried over $MgSO_4$, filtered, concentrated *in vacuo,* and purified by preparative HPLC, affording **12** as a gray solid (0.02 g, 26% yield). ^{1}H NMR (500 MHz, $CDCl_3$-*d*, ppm) δ = 8.84 (d, *J* = 4.0 Hz, 1H), 7.90 (d, *J* = 7.6 Hz, 1H), 7.47 (dd, *J* = 7.7, 4.8 Hz, 1H), 6.45 (s, 1H), 3.79 – 3.74 (m, 4H), 3.45 – 3.37 (m, 4H), 3.13 (s, 3H), 2.38 – 2.33 (m, 3H). ^{13}C NMR (126 MHz, $CDCl_3$-*d*, ppm) δ = 166.2, 164.0, 152.3, 151.4, 135.7, 131.8, 125.9, 70.3, 66.5, 47.2, 30.6, 27.2. HRMS (ESI$^+$) calculated for $C_{14}H_{19}N_4O_3$ [M+H]$^+$ 291.13789, found 291.14486.

Figures, Schemes and Tables

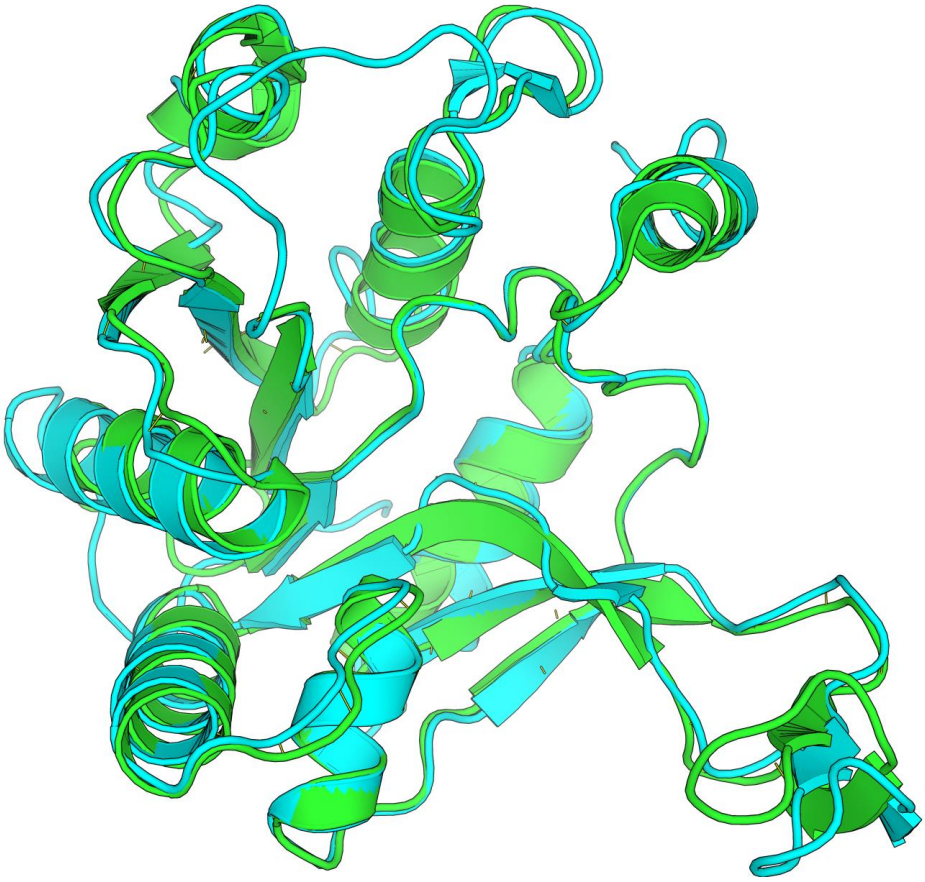

Figure S1. Overlay of the apo crystal structures of both *Pseudomonas aeruginosa* and *Escherichia coli* IspD (Protein Data Bank entry 1INJ); Cyan: *Pa*IspD; green: *Ec*IspD

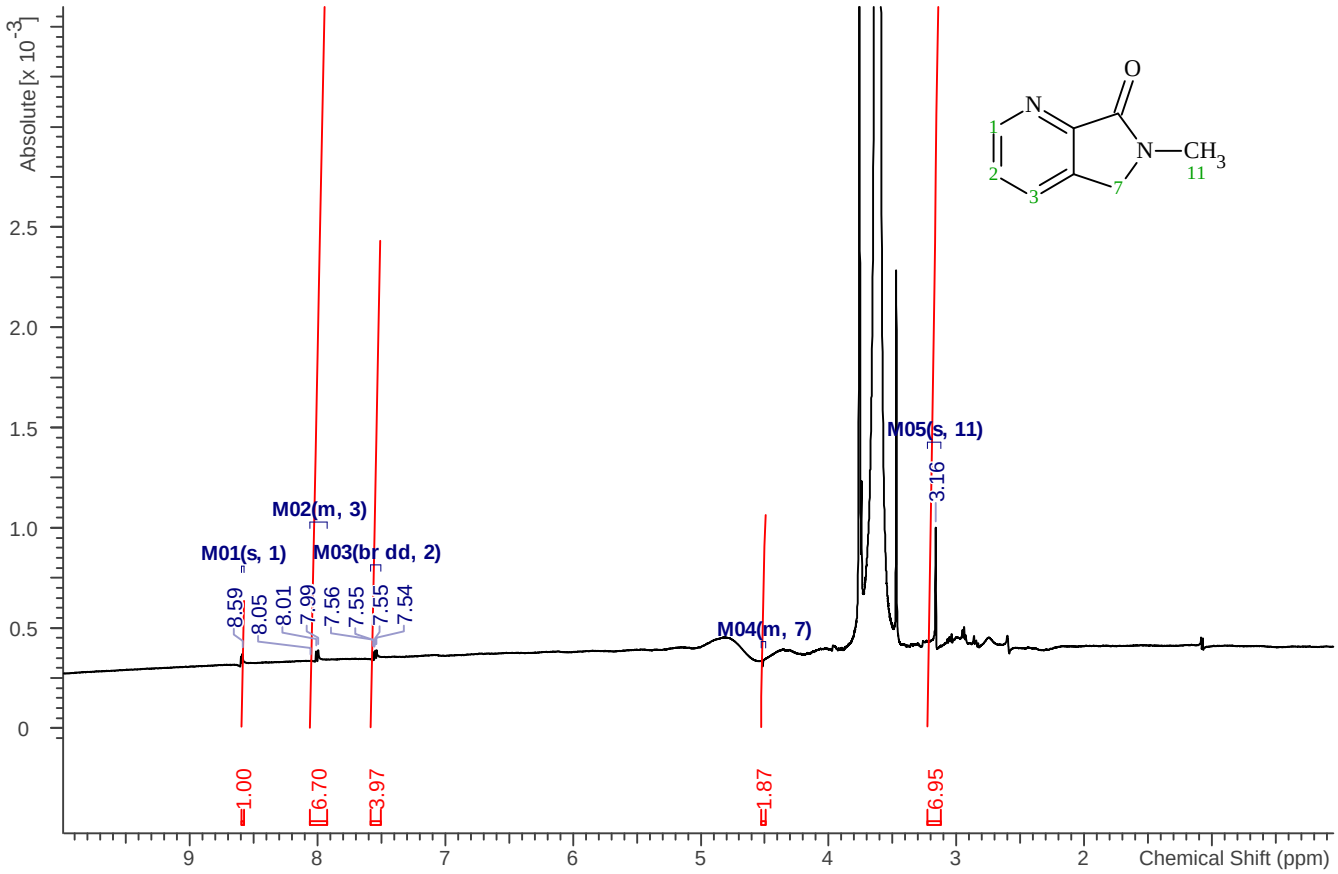

Figure S2. ^{1}H-STD-NMR spectrum of **2** with *Pa*-IspD.

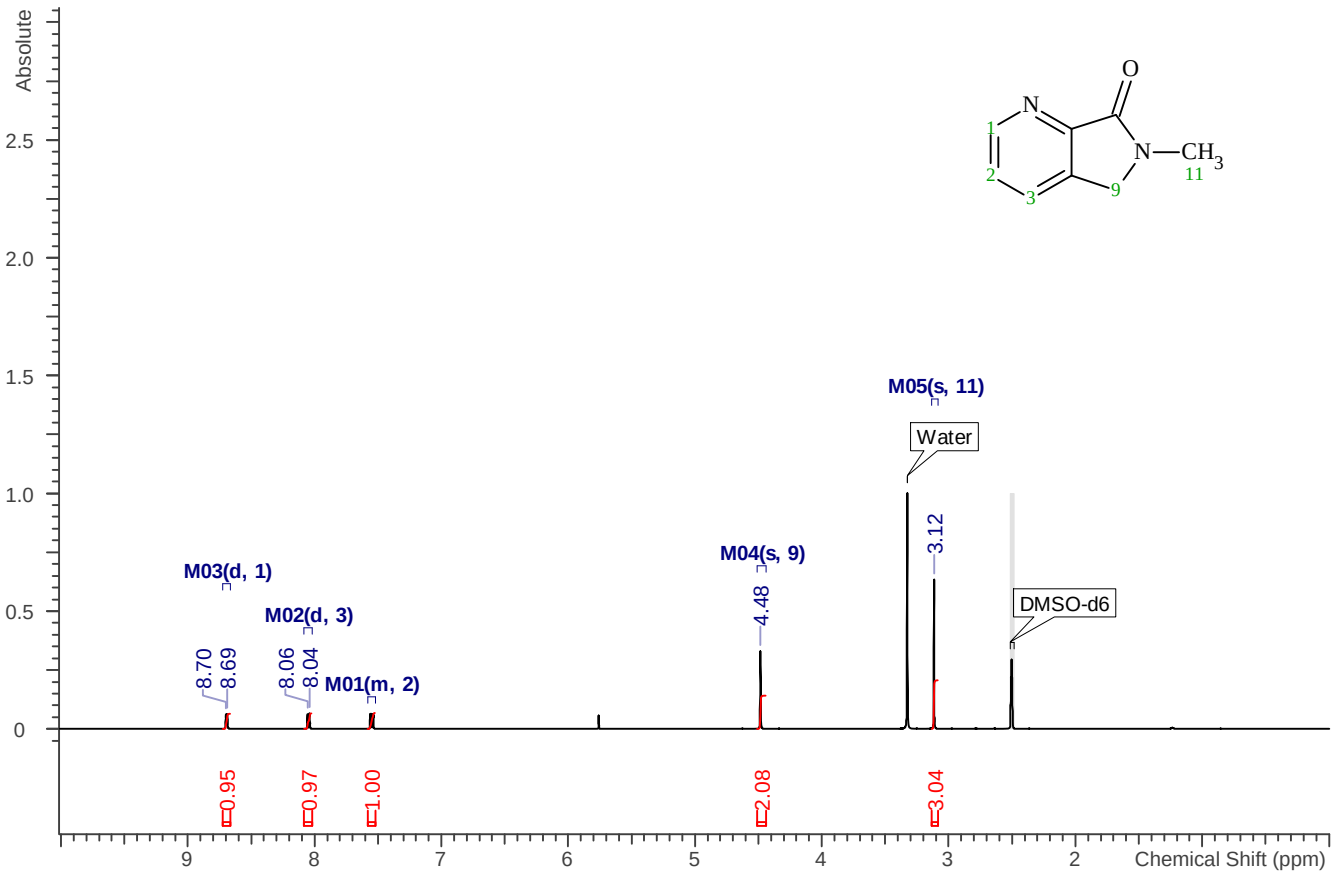

Figure S3. ^{1}H-NMR spectrum of **2**.

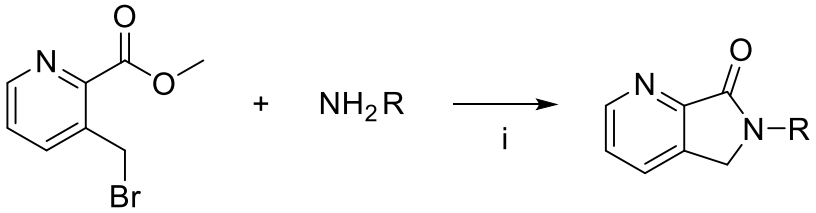

Scheme S1. Synthetic route for the synthesis of **2**–**6**. Reagents and conditions: (i) methyl 3-(bromomethyl)picolinate, the respective primary amine, THF, 80 °C, 2.5 h, 16–48% yield.

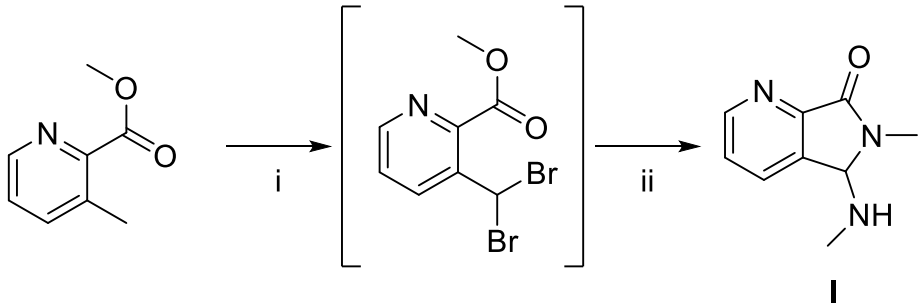

Scheme S2. Synthetic route for the synthesis of **I**. Reagents and conditions: (i) methyl 3-methylpicolinate, 1-bromopyrrolidine-2,5-dione, dibenzoylperoxide, $CHCl_3$, 80 °C, overnight. (ii) methylamine (40% w/v water), water, 80 °C, overnight, 64% crude yield.

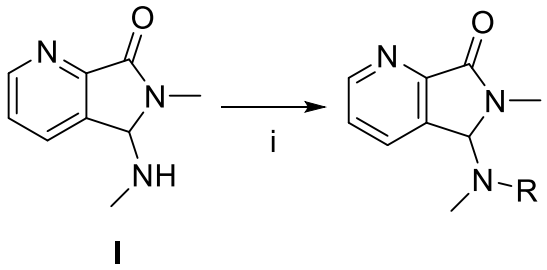

Scheme S3. Synthetic route for the synthesis of **7** and **12**. Reagents and conditions: (i) 6-methyl-5-(methylamino)-5,6-dihydro-7*H*-pyrrolo[3,4-β]pyridin-7-one (**I**), the respective acid chloride, trimethylamine, DMF (**7**) / CH_2Cl_2 (**12**) , 0 °C, 2 h, 26–33% yield.

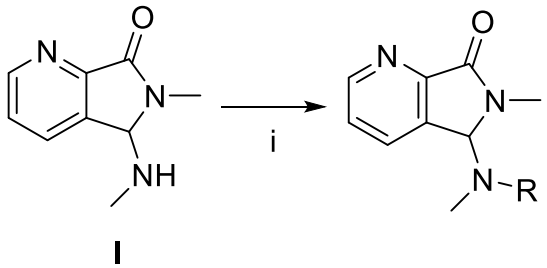

Scheme S4. Synthetic route for the synthesis of **8**–**11**. Reagents and conditions: (i) 6-methyl-5-(methylamino)-5,6-dihydro-7*H*-pyrrolo[3,4-β]pyridin-7-one (**I**), the respective carboxylic acid, trimethylamine, propanephosphonic acid anhydride, CH_2Cl_2, room temperature, overnight, 4–75% yield.

Table S1. Data collection and refinement statistics.

	***Pa*lspD with 1**	***Pa*lspD with 2**
Crystallization		
Crystallization condition	26% PEG 400 100 mM MES pH 6.5	26% PEG 500MME 100 mM MES pH 6.5
Ligand	**1**	**2**
Data collection		
X-ray Source	BL13 XALOC (Alba)	ID30A-3 (ESRF)
wavelength Å	0.979	0.968
Resolution (last shell) (Å)	44.70-1.95 (2.02 -1.95)	44.2 -2.17 (2.248 -2.17)
Total reflections	60026 (6231)	45866 (4132)
Unique reflections	18161 (1818)	12741 (1239)
Multiplicity (last shell)	3.3 (3.4)	3.6 (3.3)
Completeness (last shell) (%)	98.78 (98.96)	95.98 (94.47)
R-merge (last shell) (%)	5.04 (110.2)	6.13 (89.74)
Mean I/σ (last shell)	10.93 (1.27)	11.23 (1.05)
Space group	C2	C2
Cell parameters		
Dimensions *a, b,c* (Å)	92.15, 75.63, 37.63	91.41, 75.59, 37.8
Angle (°)	β = 104.04	β = 104.76
Refinement		
Reflections in refinement	18111 (1807)	12711 (1229)
R-work (last shell) (%)	19.88 (35.54)	0.2003 (0.5580)
R-free (last shell) (%)	22.72 (37.48)	23.50 (53.70)
R.m.s.d bonds (Å)	0.004	0.003
R.m.s.d angles (°)	0.63	0.57
Average B factor ($Å^2$)	56.93	56.29
Water molecules	62	50
Ramachandran plot quality (%)		
Most favoured	97.36	97.36
Additionally allowed	2.64	2.64

^{1}H NMR, ^{13}C NMR and LC-MS Spectra of Final Compounds

2

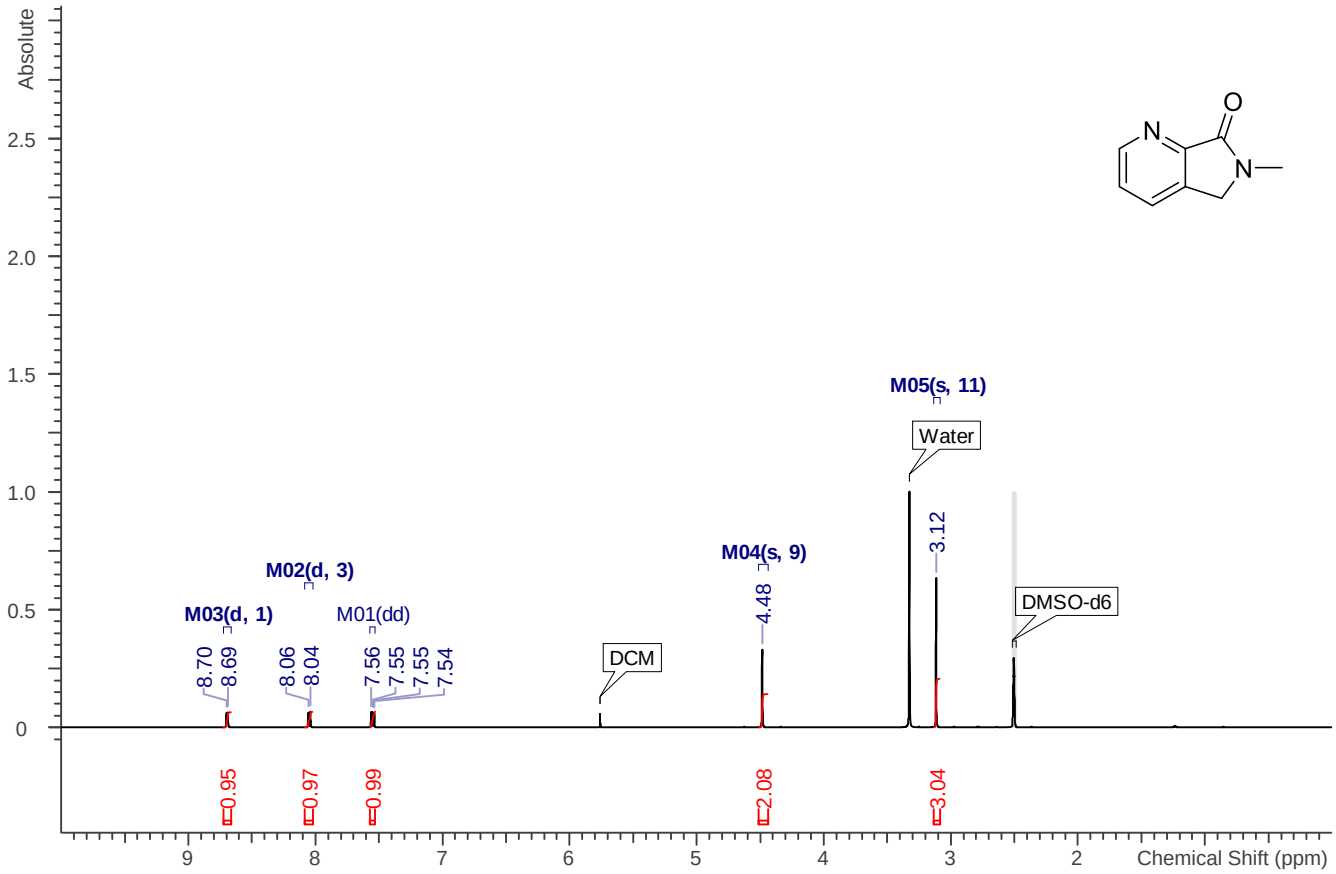

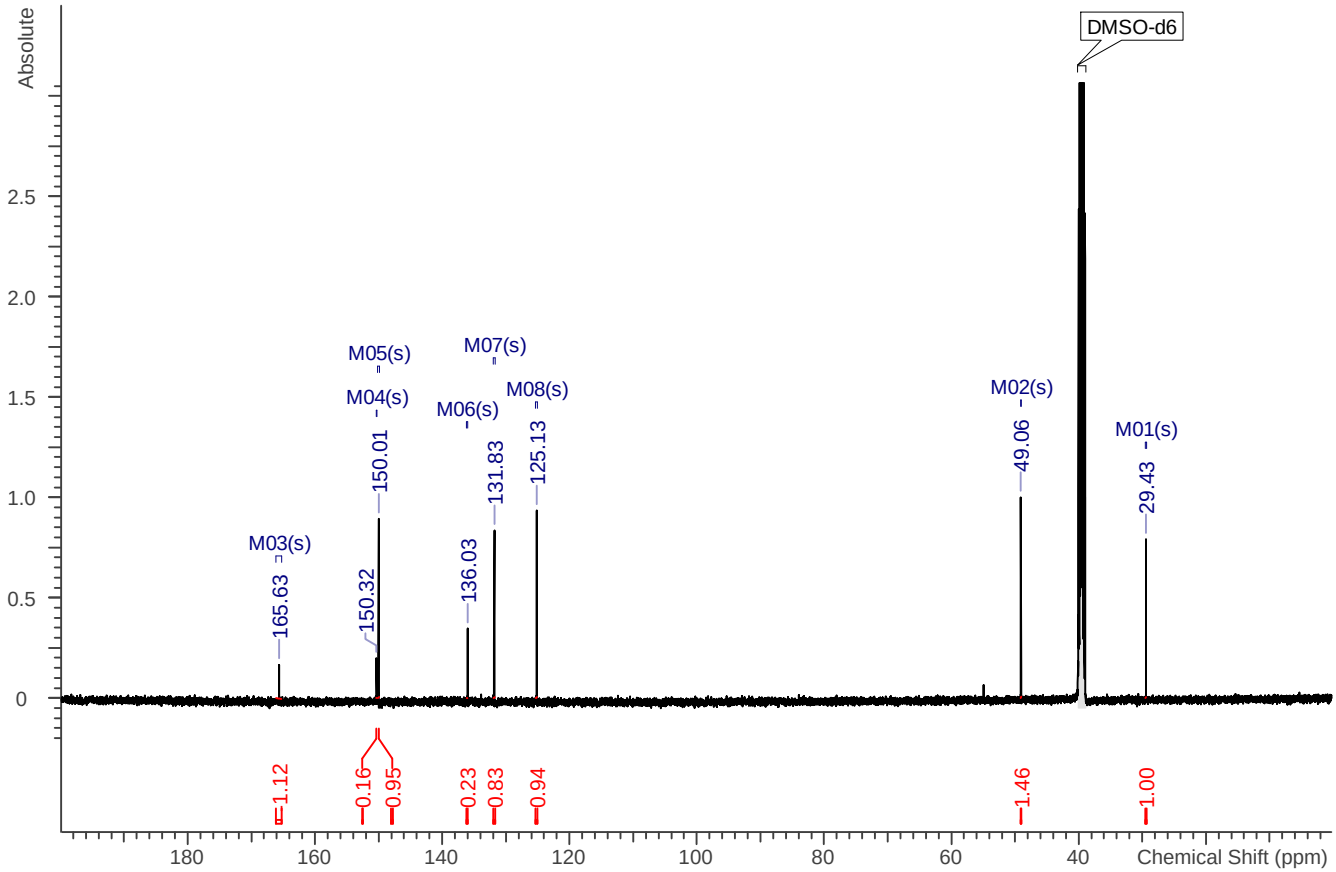

3

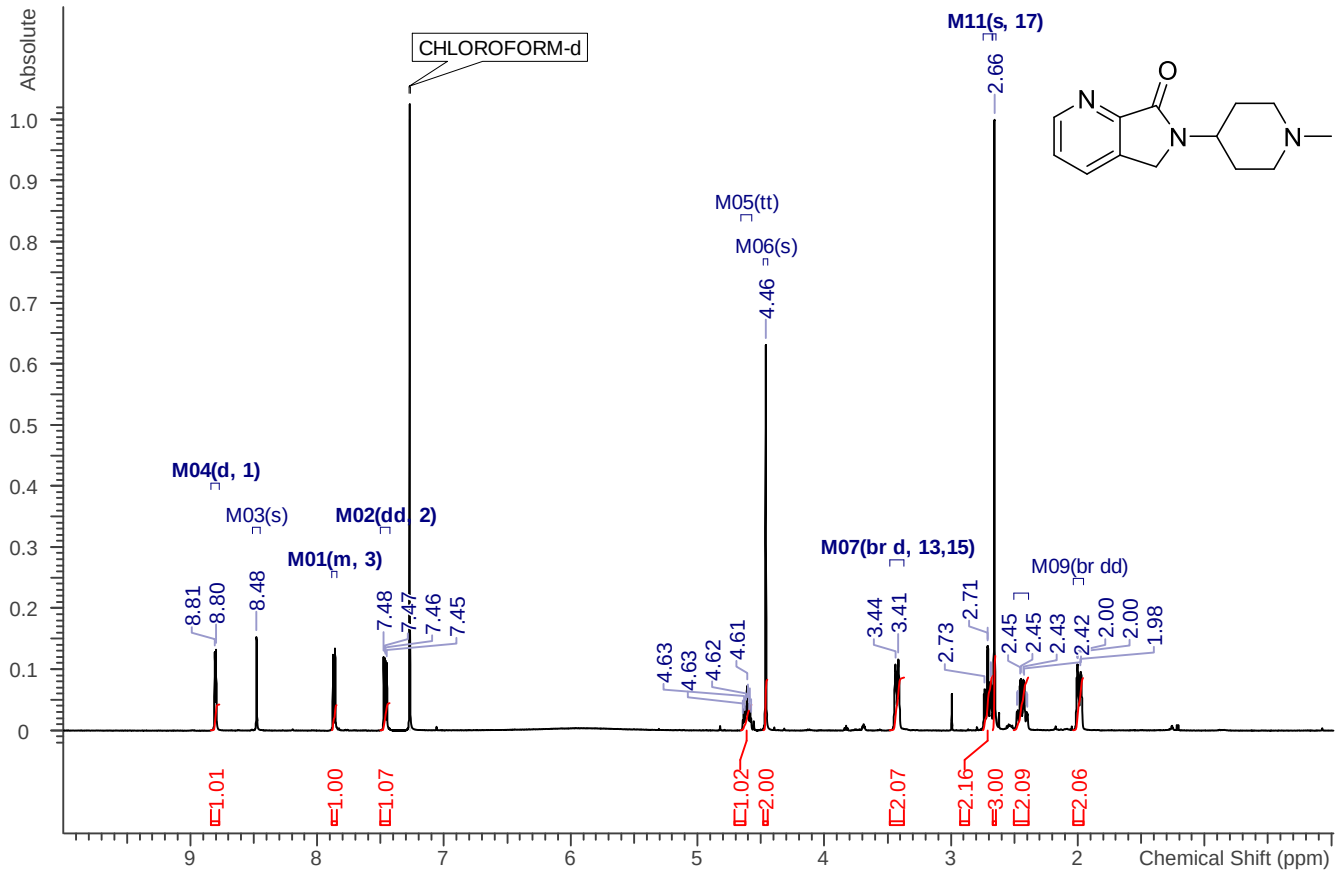
Absolute
CHLOROFORM-d
M11(s, 17)
2.66
M05(tt)
M06(s)
4.46
M04(d, 1)
M03(s)
M02(dd, 2)
M01(m, 3)
M07(br d, 13,15)
M09(br dd)
8.81
8.80
8.48
7.48
7.47
7.46
7.45
4.63
4.63
4.62
4.61
3.44
3.41
2.73
2.71
2.45
2.45
2.43
2.42
2.00
2.00
1.98
1.01
1.00
1.07
1.02
2.00
2.07
2.16
3.00
2.09
2.06
Chemical Shift (ppm)

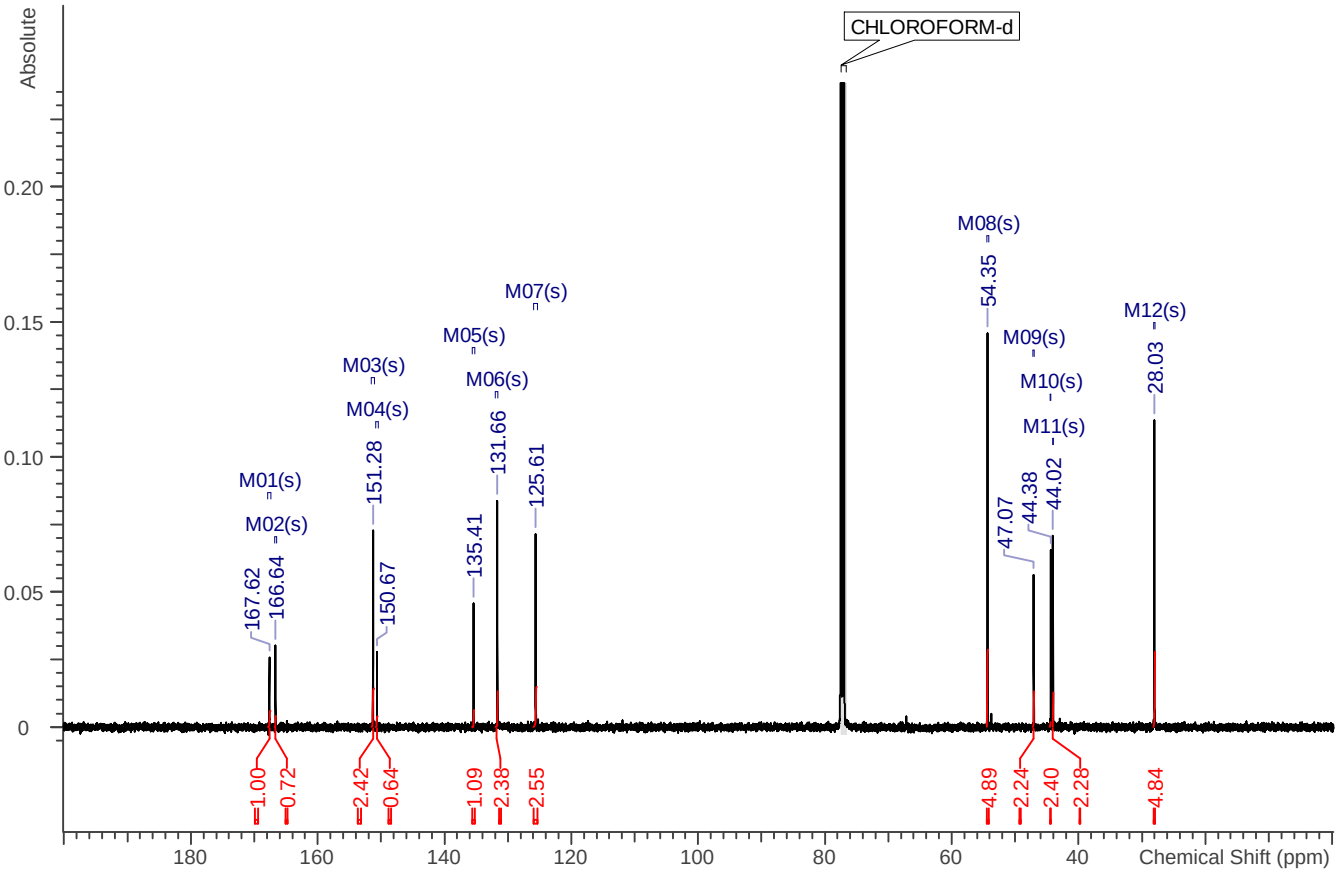
Absolute
CHLOROFORM-d
M08(s)
54.35
M07(s)
M05(s)
M06(s)
M03(s)
M04(s)
M01(s)
M02(s)
M09(s)
M10(s)
M11(s)
M12(s)
28.03
151.28
131.66
125.61
135.41
150.67
167.62
166.64
47.07
44.38
44.02
1.00
0.72
2.42
0.64
1.09
2.38
2.55
4.89
2.24
2.40
2.28
4.84
Chemical Shift (ppm)

4

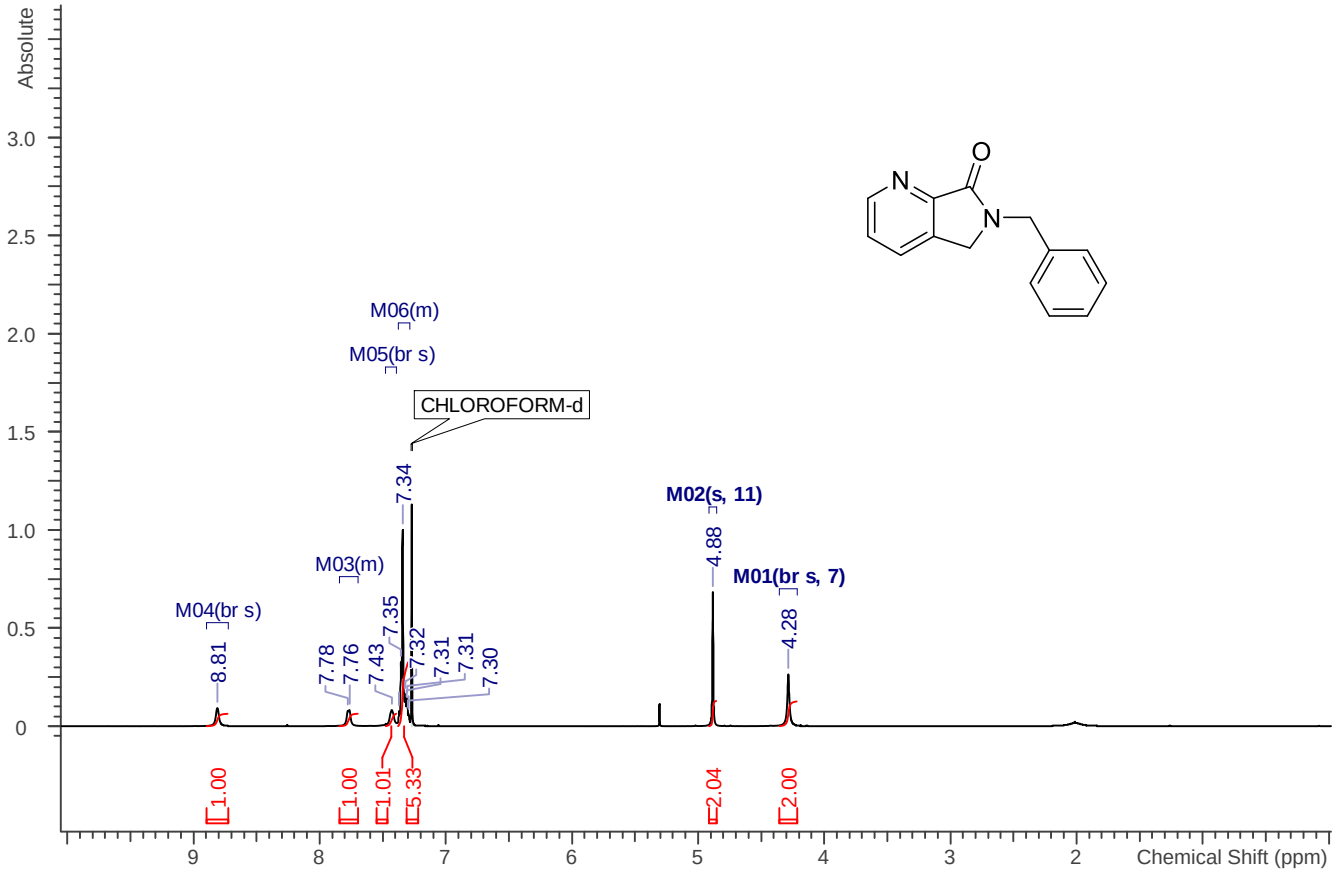
Absolute
3.0
2.5
2.0
1.5
1.0
0.5
0
M06(m)
M05(br s)
CHLOROFORM-d
7.34
M02(s, 11)
4.88
M01(br s, 7)
4.28
M03(m)
M04(br s)
8.81
7.78
7.76
7.43
7.35
7.32
7.31
7.31
7.30
1.00
1.00
1.01
5.33
2.04
2.00
9
8
7
6
5
4
3
2
Chemical Shift (ppm)

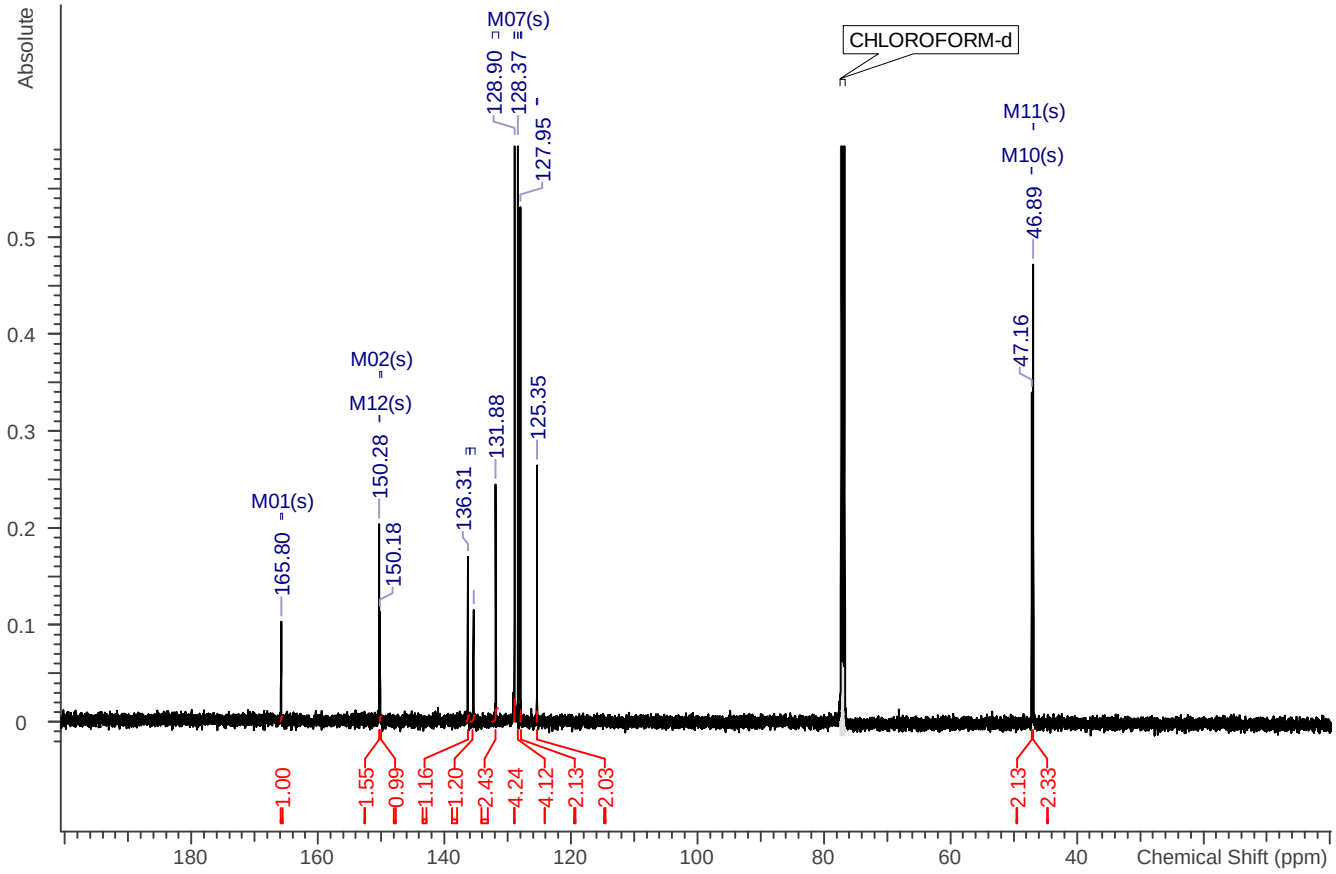
Absolute
0.5
0.4
0.3
0.2
0.1
0
M07(s)
128.90
128.37
127.95
CHLOROFORM-d
M11(s)
M10(s)
46.89
47.16
M02(s)
M12(s)
150.28
150.18
136.31
131.88
125.35
M01(s)
165.80
1.00
1.55
0.99
1.16
1.20
2.43
4.24
4.12
2.13
2.03
2.13
2.33
180
160
140
120
100
80
60
40
Chemical Shift (ppm)

5

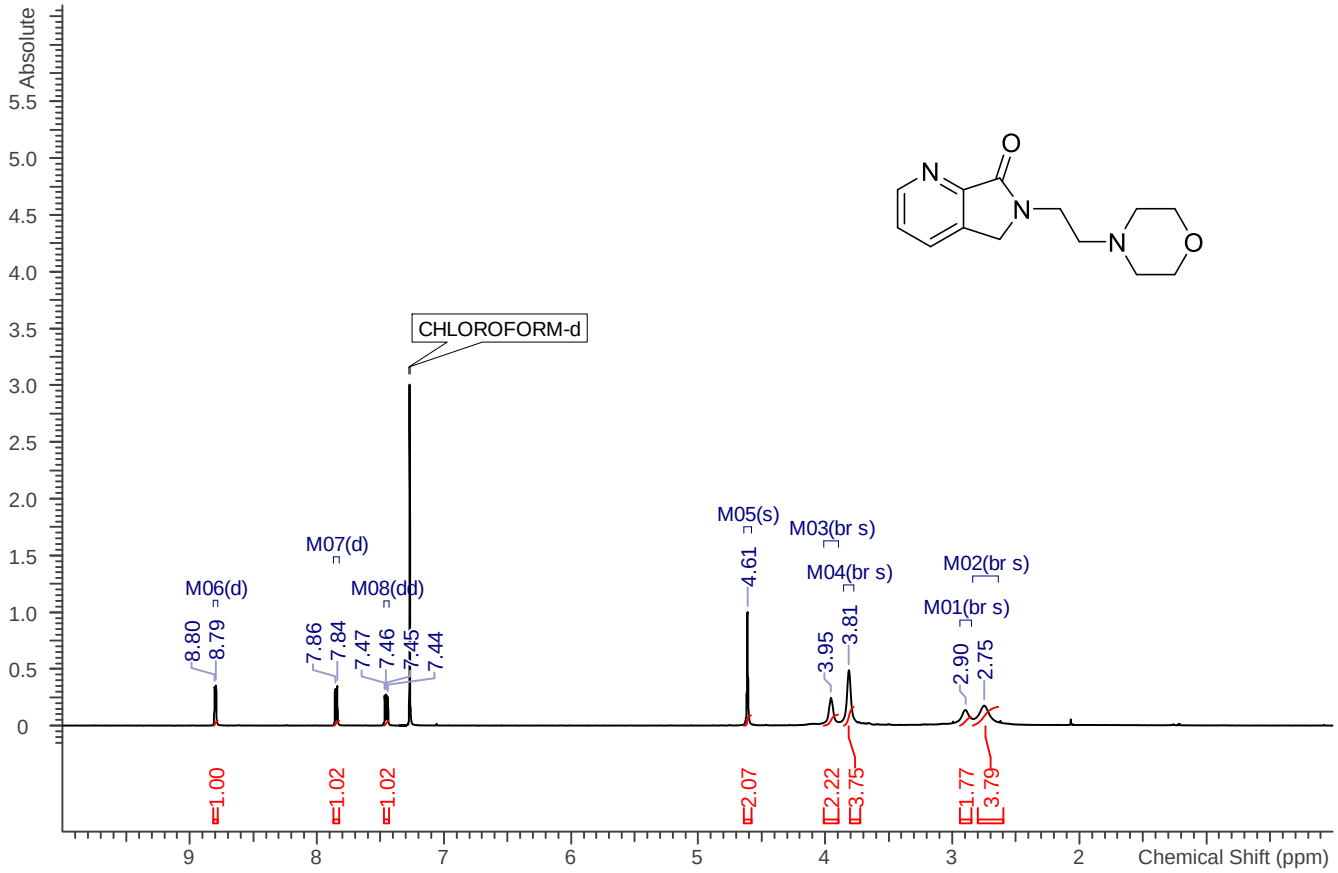
Absolute
CHLOROFORM-d
M06(d)
8.80
8.79
M07(d)
7.86
7.84
M08(dd)
7.47
7.46
7.45
7.44
M05(s)
4.61
M03(br s)
3.95
M04(br s)
3.81
M02(br s)
2.90
M01(br s)
2.75
1.00
1.02
1.02
2.07
2.22
3.75
1.77
3.79
Chemical Shift (ppm)

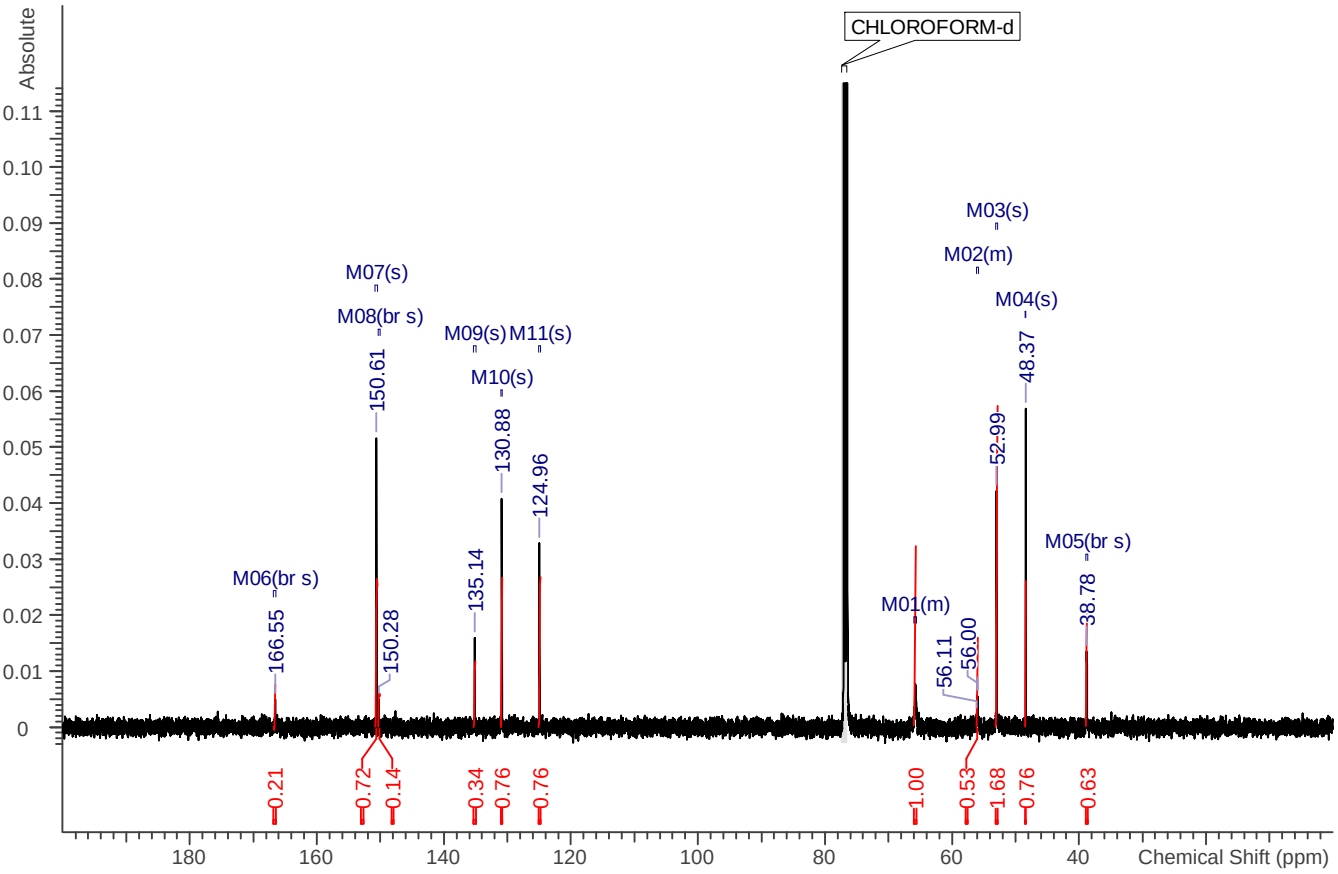
Absolute
CHLOROFORM-d
M06(br s)
166.55
M07(s)
150.61
150.28
M08(br s)
M09(s)
135.14
M10(s)
130.88
M11(s)
124.96
M01(m)
56.11
56.00
M03(s)
52.99
M02(m)
M04(s)
48.37
M05(br s)
38.78
0.21
0.72
0.14
0.34
0.76
0.76
1.00
0.53
1.68
0.76
0.63
Chemical Shift (ppm)

6

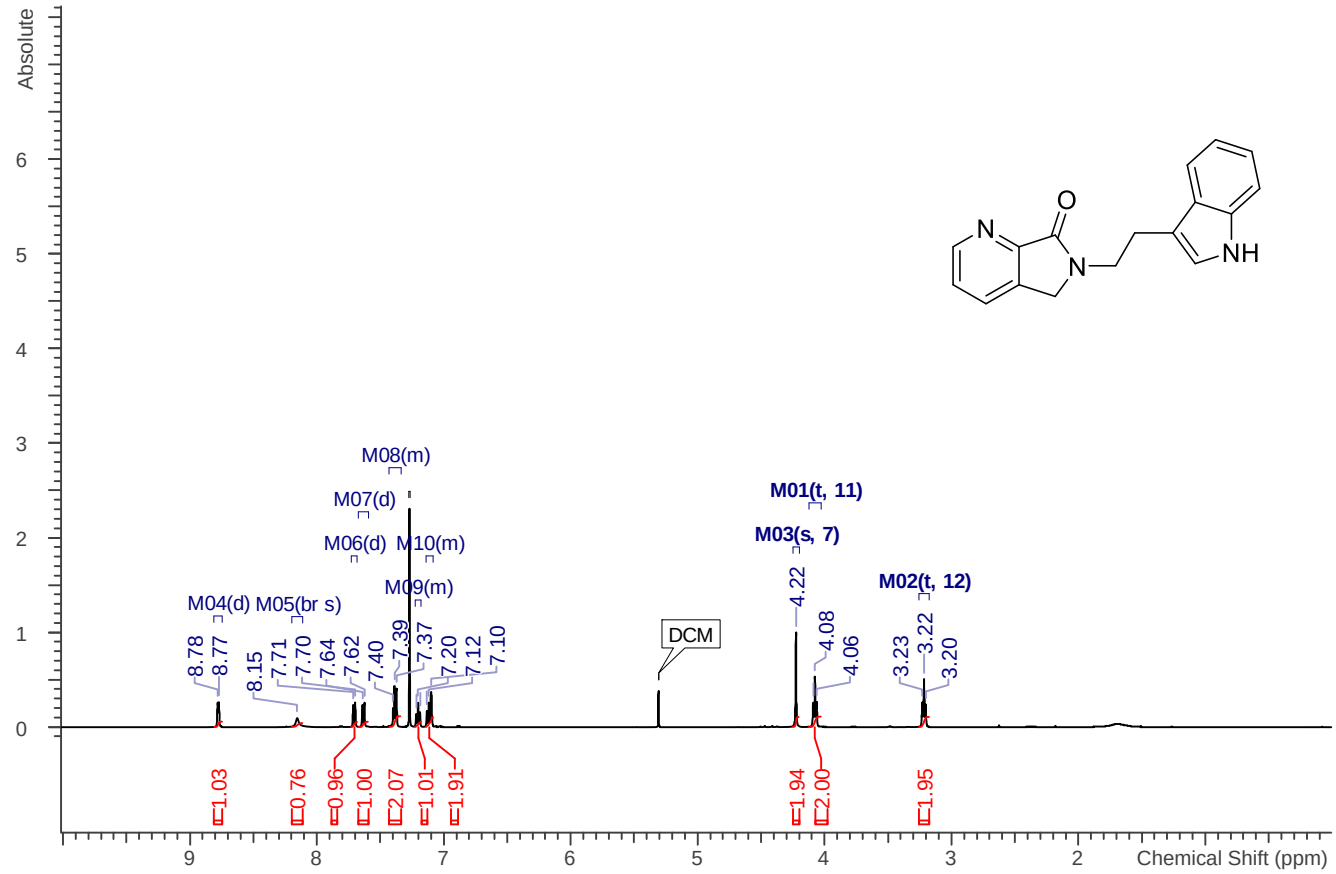
Absolute
M08(m)
M07(d)
M06(d) M10(m)
M09(m)
M04(d) M05(br s)
M01(t, 11)
M03(s, 7)
M02(t, 12)
DCM
8.78
8.77
8.15
7.71
7.70
7.64
7.62
7.40
7.39
7.37
7.20
7.12
7.10
4.22
4.08
4.06
3.23
3.22
3.20
1.03
0.76
0.96
1.00
2.07
1.01
1.91
1.94
2.00
1.95
Chemical Shift (ppm)

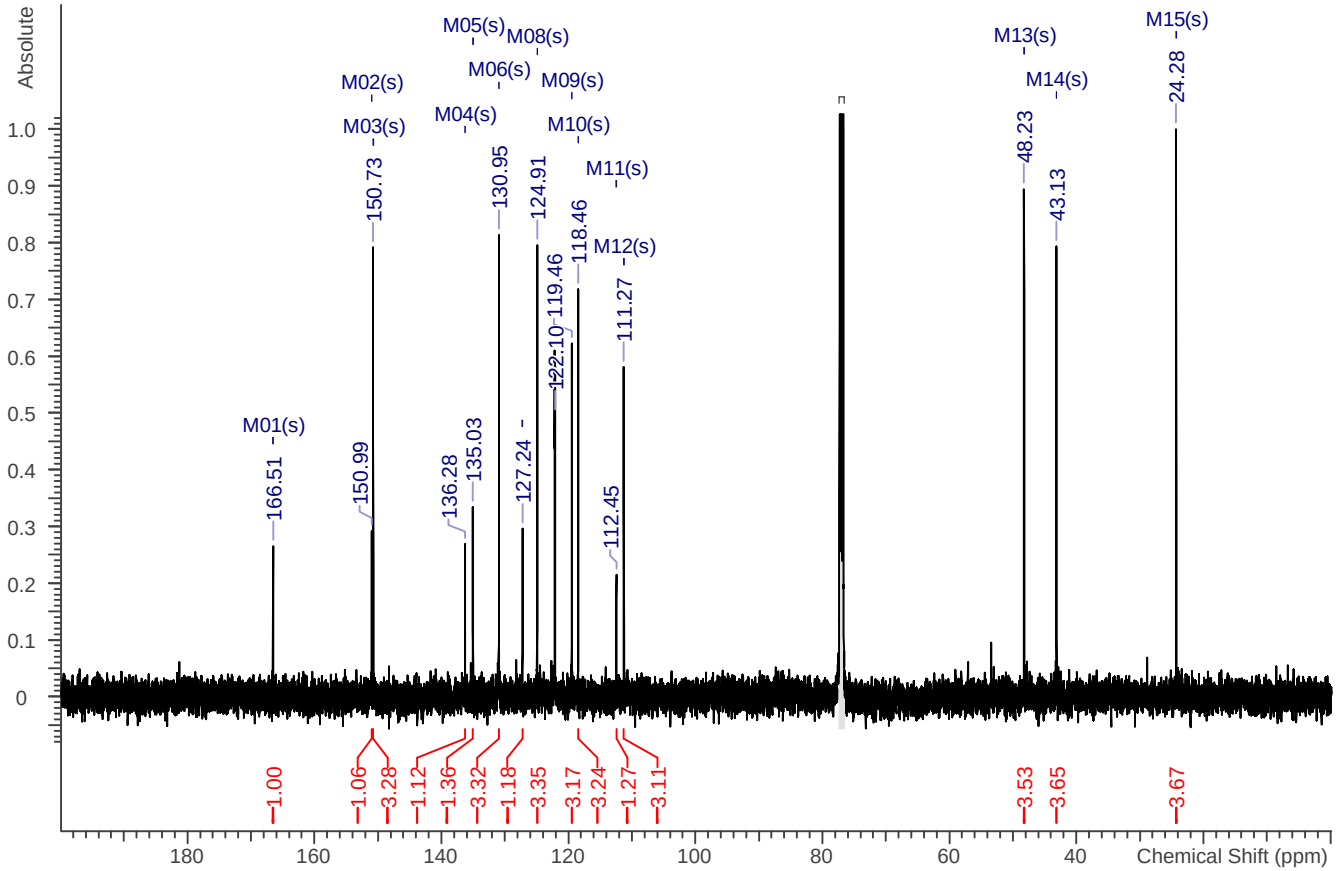
Absolute
M05(s)
M08(s)
M06(s)
M09(s)
M02(s)
M03(s)
M04(s)
M10(s)
M11(s)
M12(s)
M13(s)
M14(s)
M15(s)
M01(s)
166.51
150.99
150.73
136.28
135.03
130.95
127.24
124.91
122.10
119.46
118.46
112.45
111.27
48.23
43.13
24.28
1.00
1.06
3.28
1.12
1.36
3.32
1.18
3.35
3.17
3.24
1.27
3.11
3.53
3.65
3.67
Chemical Shift (ppm)

7

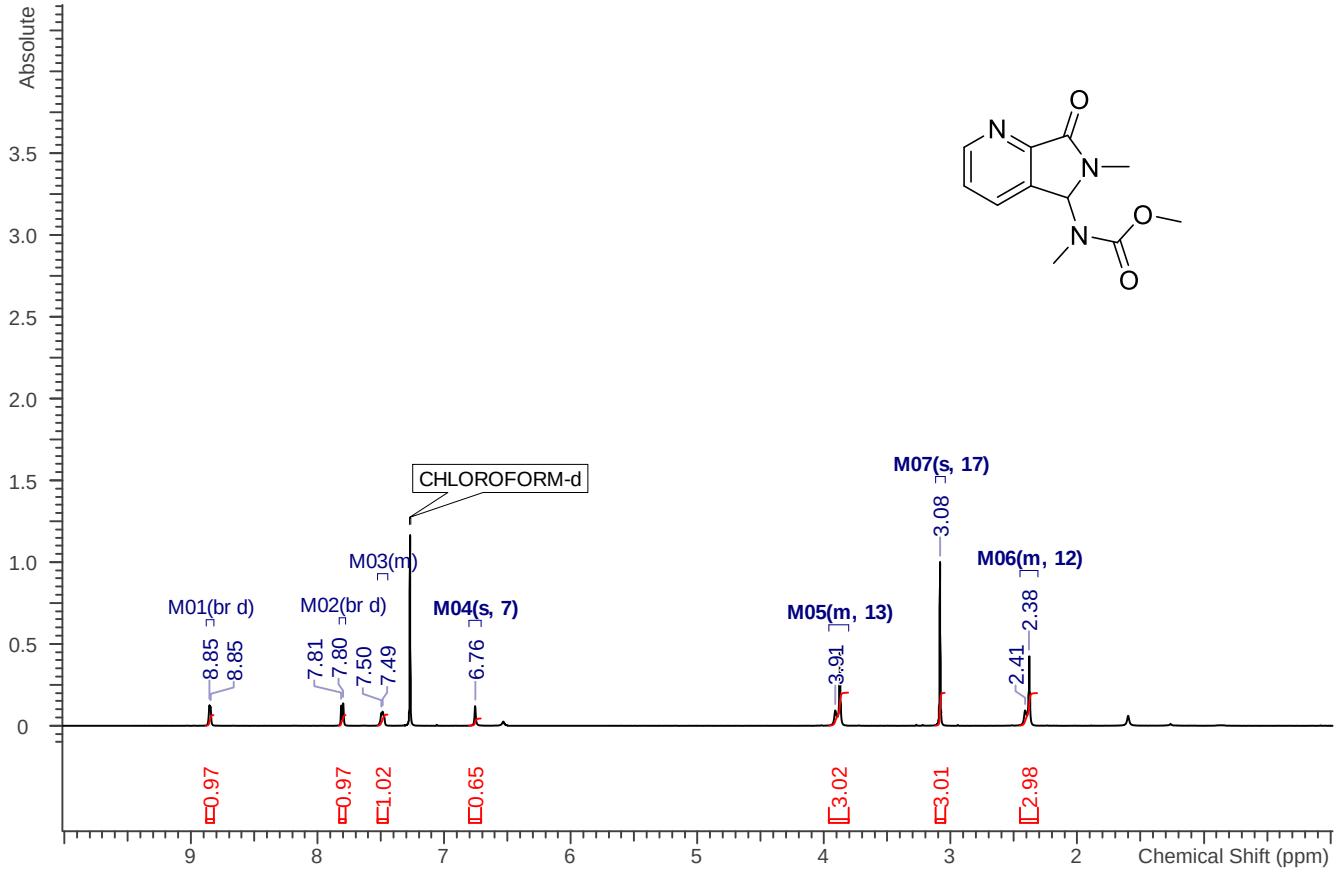
Absolute
3.5
3.0
2.5
2.0
1.5
1.0
0.5
0
CHLOROFORM-d
M01(br d)
8.85
8.85
M02(br d)
7.81
7.80
7.50
7.49
M03(m)
M04(s, 7)
6.76
M05(m, 13)
3.91
M07(s, 17)
3.08
M06(m, 12)
2.38
2.41
0.97
0.97
1.02
0.65
3.02
3.01
2.98
9
8
7
6
5
4
3
2
Chemical Shift (ppm)

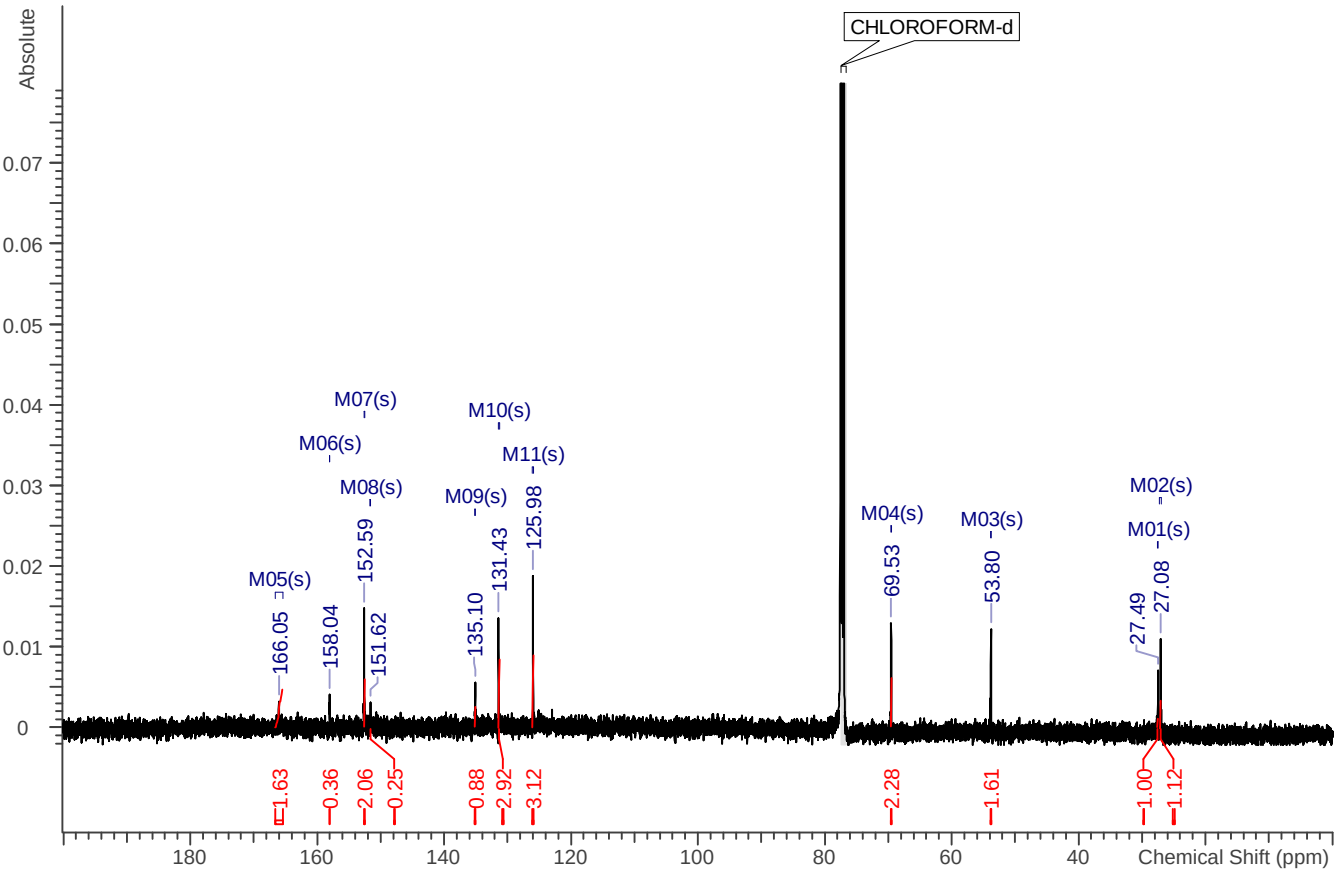
Absolute
0.07
0.06
0.05
0.04
0.03
0.02
0.01
0
CHLOROFORM-d
M07(s)
M06(s)
M08(s)
M10(s)
M11(s)
M09(s)
M05(s)
166.05
158.04
152.59
151.62
135.10
131.43
125.98
M04(s)
69.53
M03(s)
53.80
M02(s)
M01(s)
27.49
27.08
1.63
0.36
2.06
0.25
0.88
2.92
3.12
2.28
1.61
1.00
1.12
180
160
140
120
100
80
60
40
Chemical Shift (ppm)

8

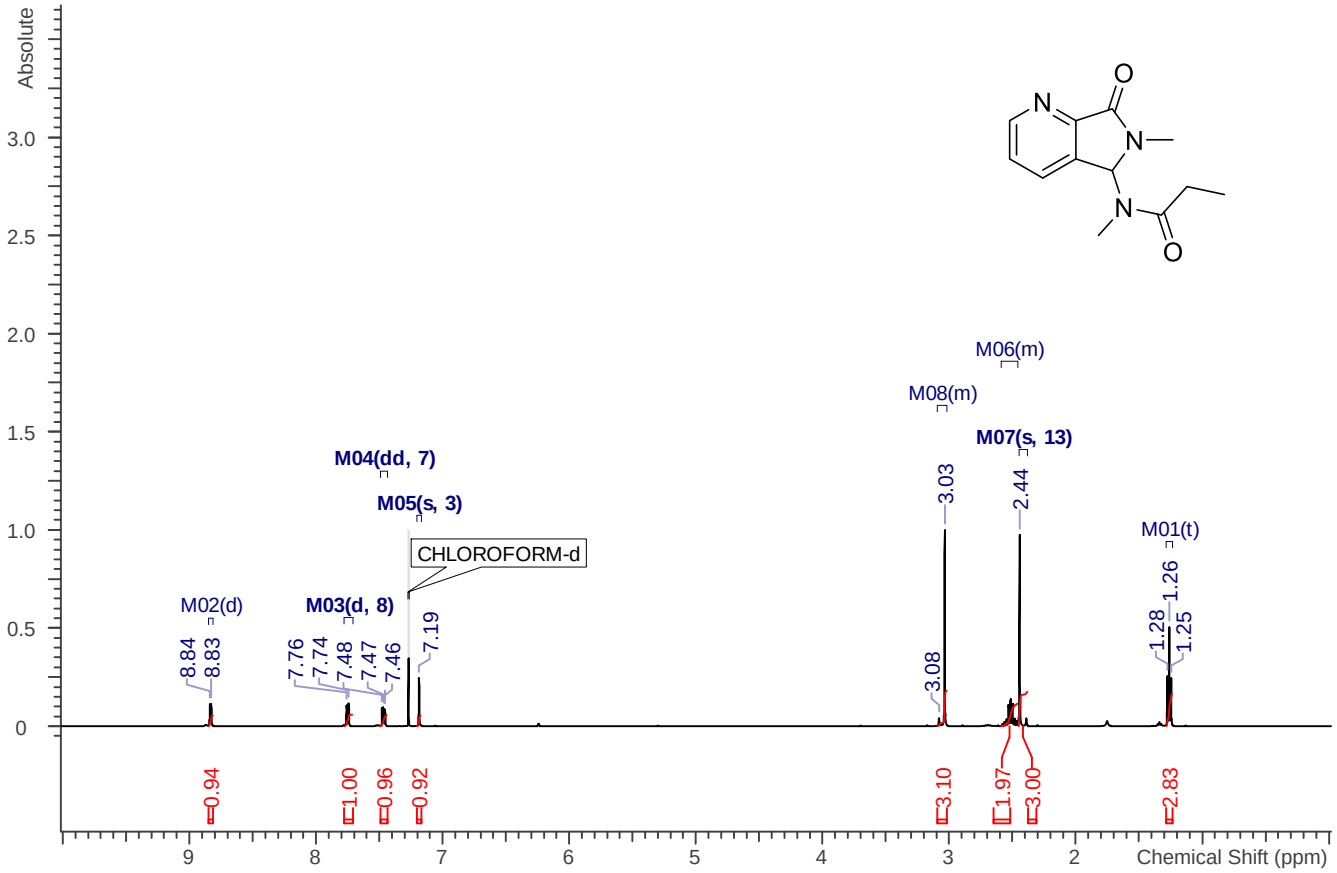
Absolute
3.0
2.5
2.0
1.5
1.0
0.5
0
M02(d)
8.84
8.83
M03(d, 8)
7.76
7.74
7.48
7.47
7.46
M04(dd, 7)
M05(s, 3)
CHLOROFORM-d
7.19
3.08
3.03
M08(m)
M06(m)
M07(s, 13)
2.44
M01(t)
1.28
1.26
1.25
0.94
1.00
0.96
0.92
3.10
1.97
3.00
2.83
9
8
7
6
5
4
3
2
Chemical Shift (ppm)

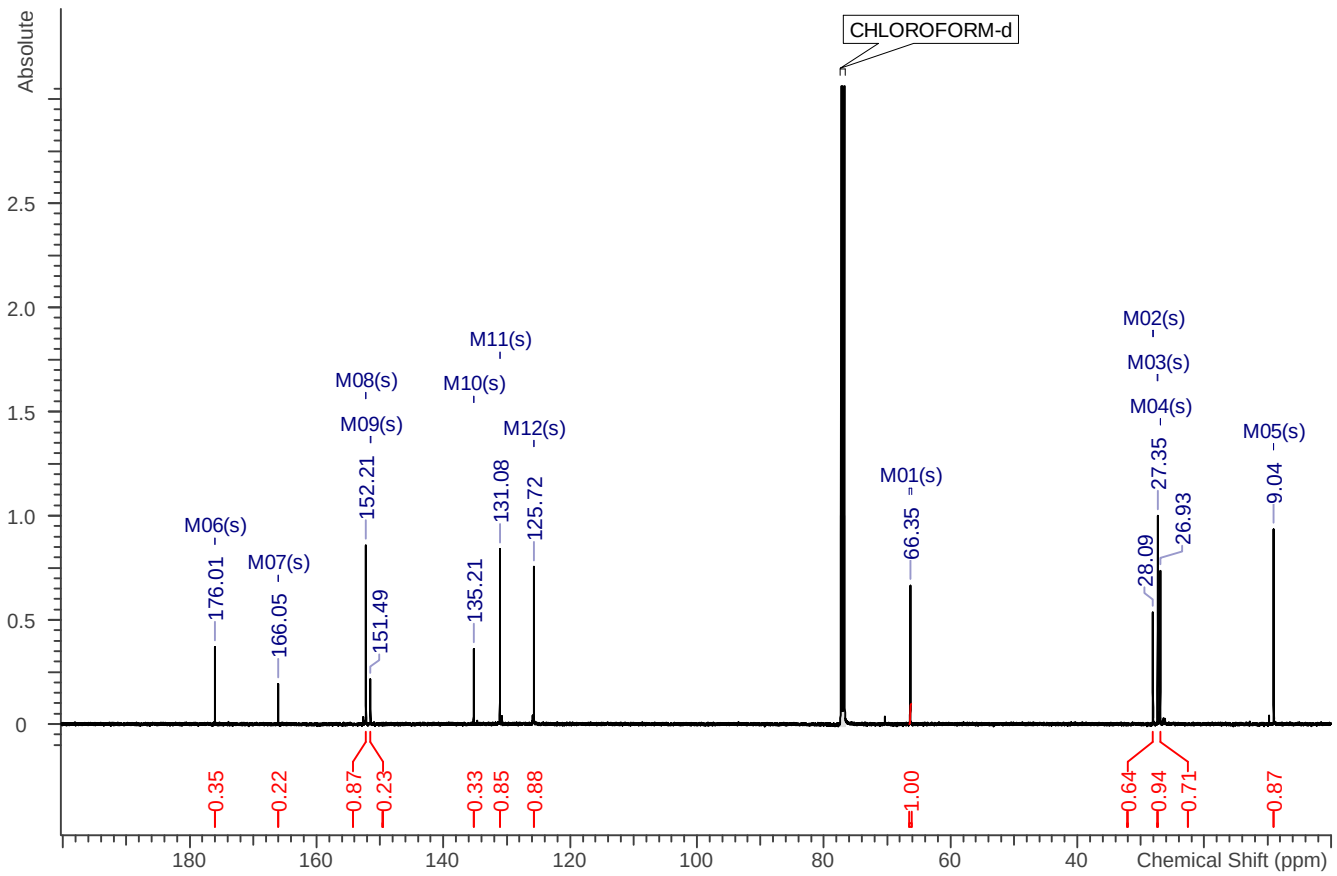
Absolute
2.5
2.0
1.5
1.0
0.5
0
CHLOROFORM-d
M06(s)
176.01
M07(s)
166.05
M08(s)
M09(s)
152.21
151.49
135.21
M11(s)
M10(s)
131.08
M12(s)
125.72
M01(s)
66.35
M02(s)
M03(s)
M04(s)
28.09
27.35
26.93
M05(s)
9.04
0.35
0.22
0.87
0.23
0.33
0.85
0.88
1.00
0.64
0.94
0.71
0.87
180
160
140
120
100
80
60
40
Chemical Shift (ppm)

9

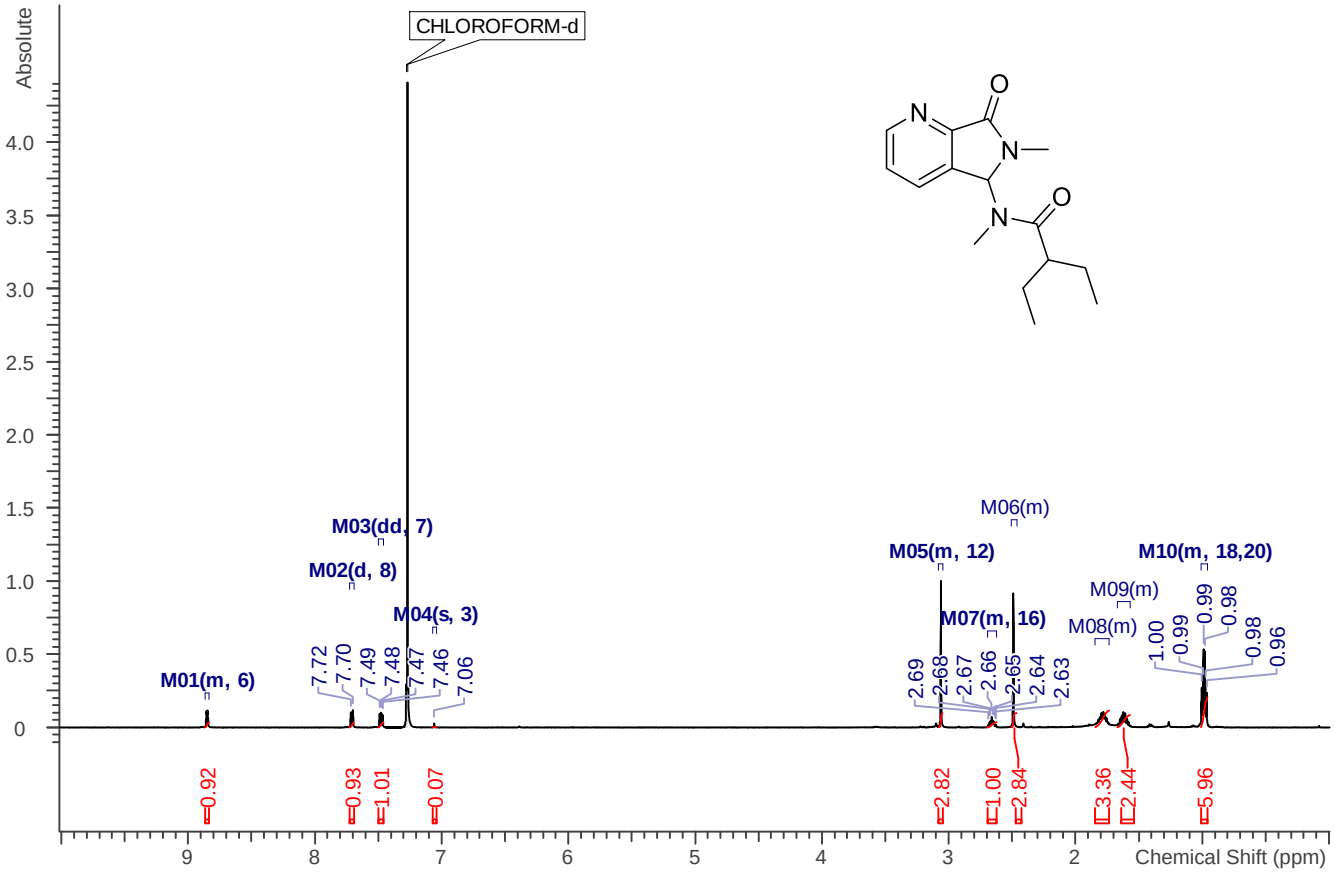
Absolute
CHLOROFORM-d
M01(m, 6)
M02(d, 8)
M03(dd, 7)
M04(s, 3)
M05(m, 12)
M06(m)
M07(m, 16)
M08(m)
M09(m)
M10(m, 18,20)
7.72
7.70
7.49
7.48
7.47
7.46
7.06
2.69
2.68
2.67
2.66
2.65
2.64
2.63
1.00
0.99
0.99
0.98
0.98
0.96
0.92
0.93
1.01
0.07
2.82
1.00
2.84
3.36
2.44
5.96
Chemical Shift (ppm)

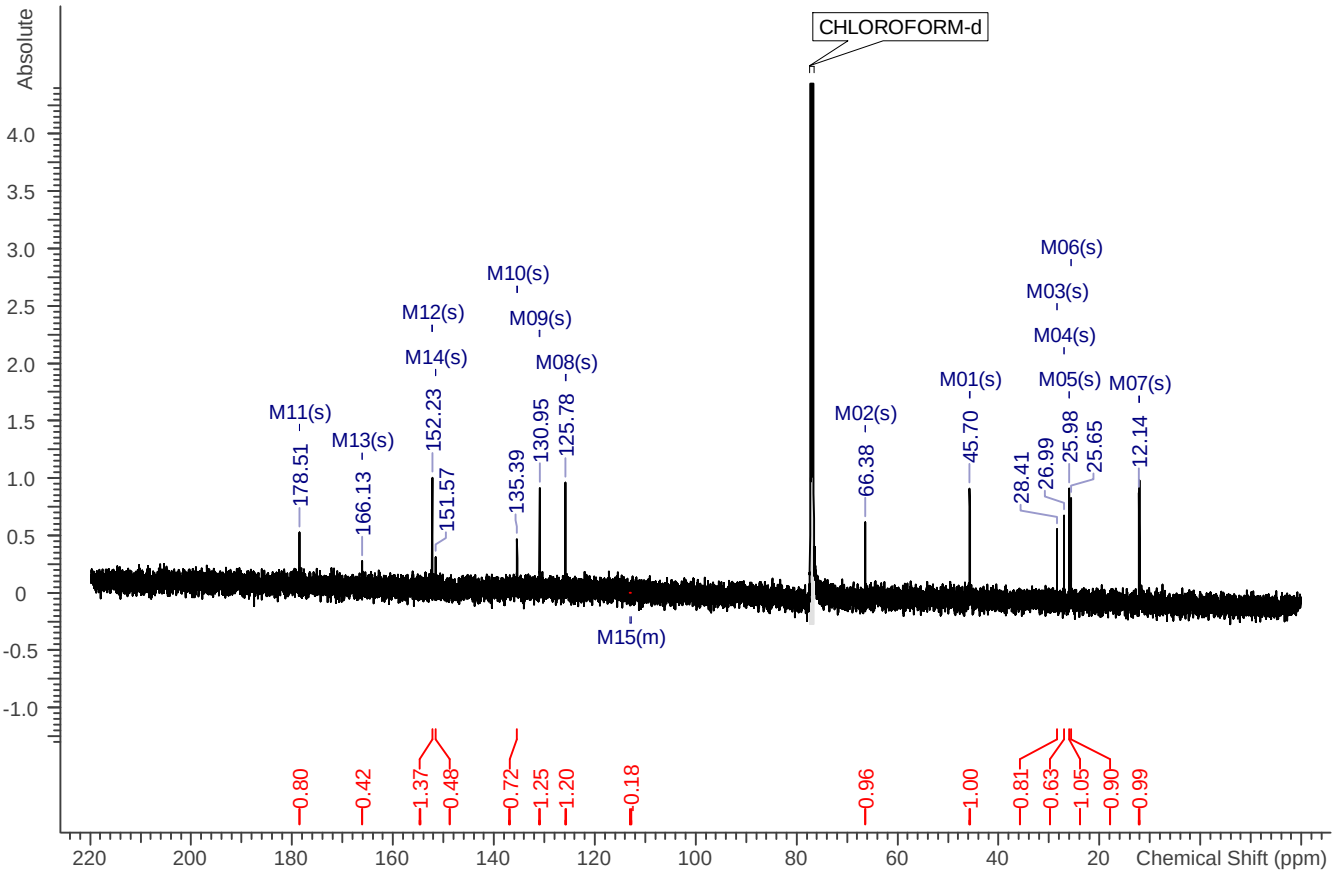
Absolute
CHLOROFORM-d
M01(s)
M02(s)
M03(s)
M04(s)
M05(s)
M06(s)
M07(s)
M08(s)
M09(s)
M10(s)
M11(s)
M12(s)
M13(s)
M14(s)
M15(m)
178.51
166.13
152.23
151.57
135.39
130.95
125.78
66.38
45.70
28.41
26.99
25.98
25.65
12.14
0.80
0.42
1.37
0.48
0.72
1.25
1.20
0.18
0.96
1.00
0.81
0.63
1.05
0.90
0.99
Chemical Shift (ppm)

10

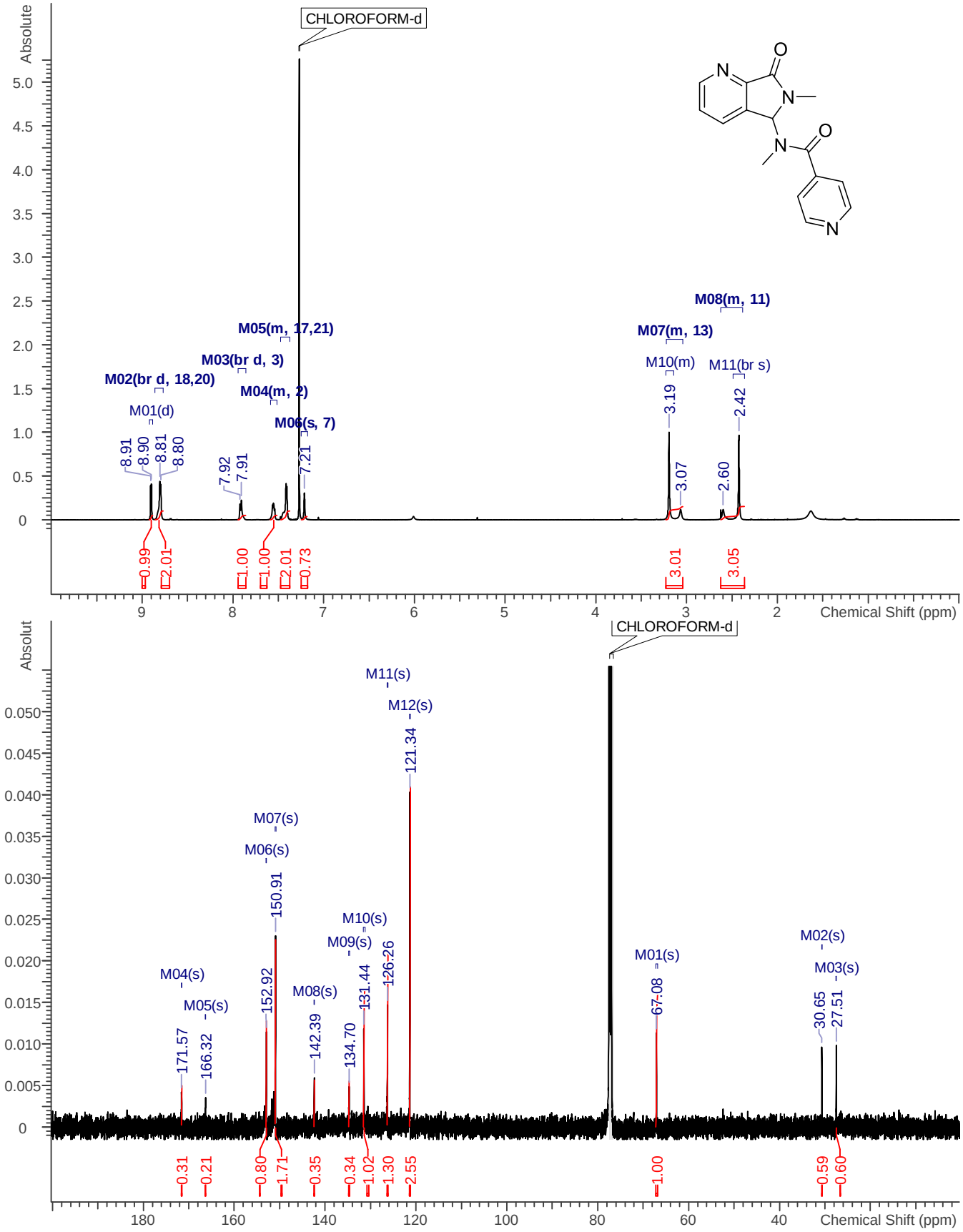
CHLOROFORM-d
Absolute
M02(br d, 18,20)
M01(d)
M03(br d, 3)
M05(m, 17,21)
M04(m, 2)
M06(s, 7)
M07(m, 13)
M08(m, 11)
M10(m)
M11(br s)
8.91
8.90
8.81
8.80
7.92
7.91
7.21
3.19
3.07
2.60
2.42
0.99
2.01
1.00
1.00
2.01
0.73
3.01
3.05
Chemical Shift (ppm)
CHLOROFORM-d
M11(s)
M12(s)
121.34
M07(s)
M06(s)
150.91
M10(s)
M09(s)
126.26
131.44
M08(s)
142.39
134.70
152.92
M04(s)
M05(s)
171.57
166.32
M01(s)
67.08
M02(s)
M03(s)
30.65
27.51
0.31
0.21
0.80
1.71
0.35
0.34
1.02
1.30
2.55
1.00
0.59
0.60
Chemical Shift (ppm)

11 (please refer to Heated ^{1}H and ^{13}C NMR Spectra of 11)

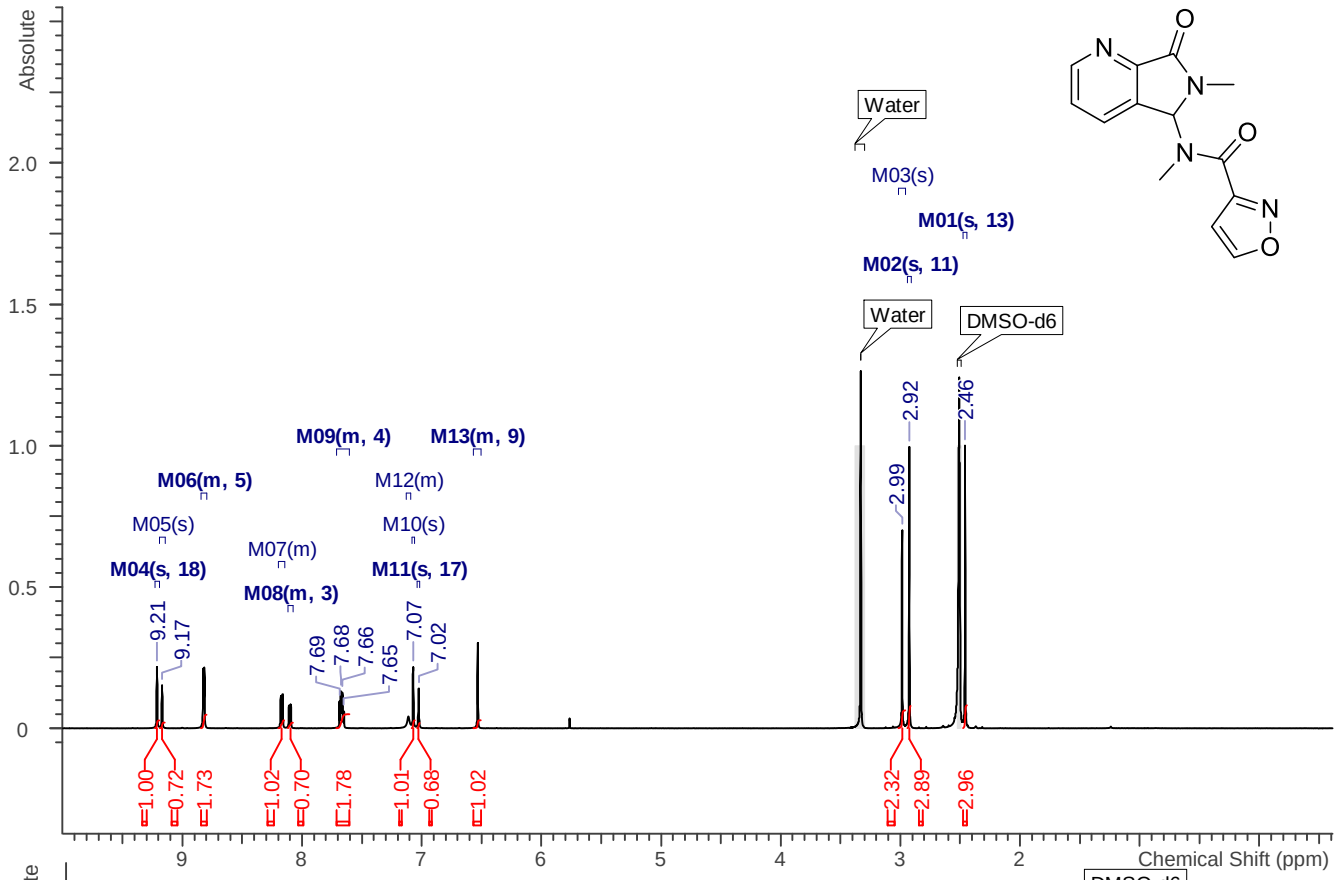

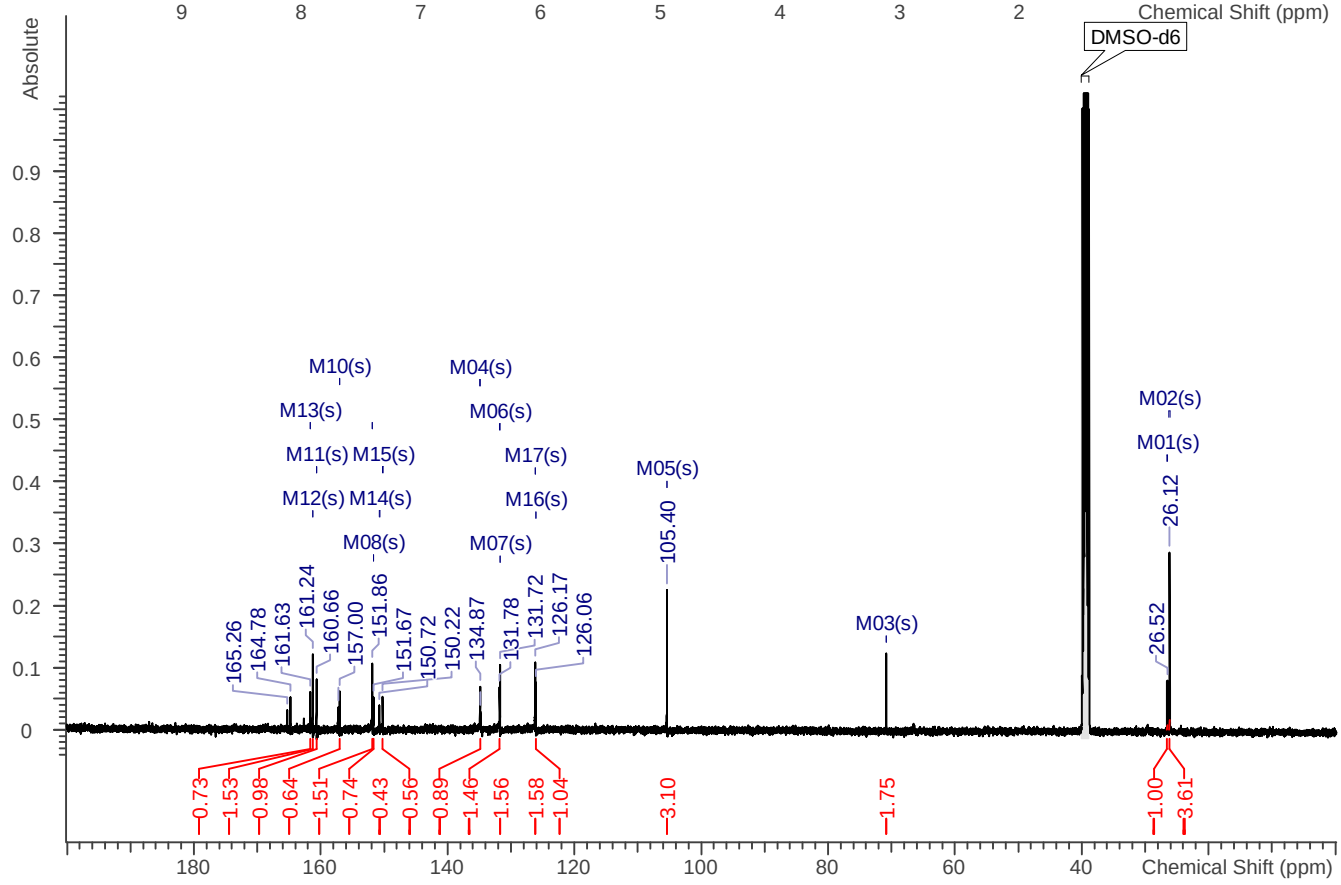

12

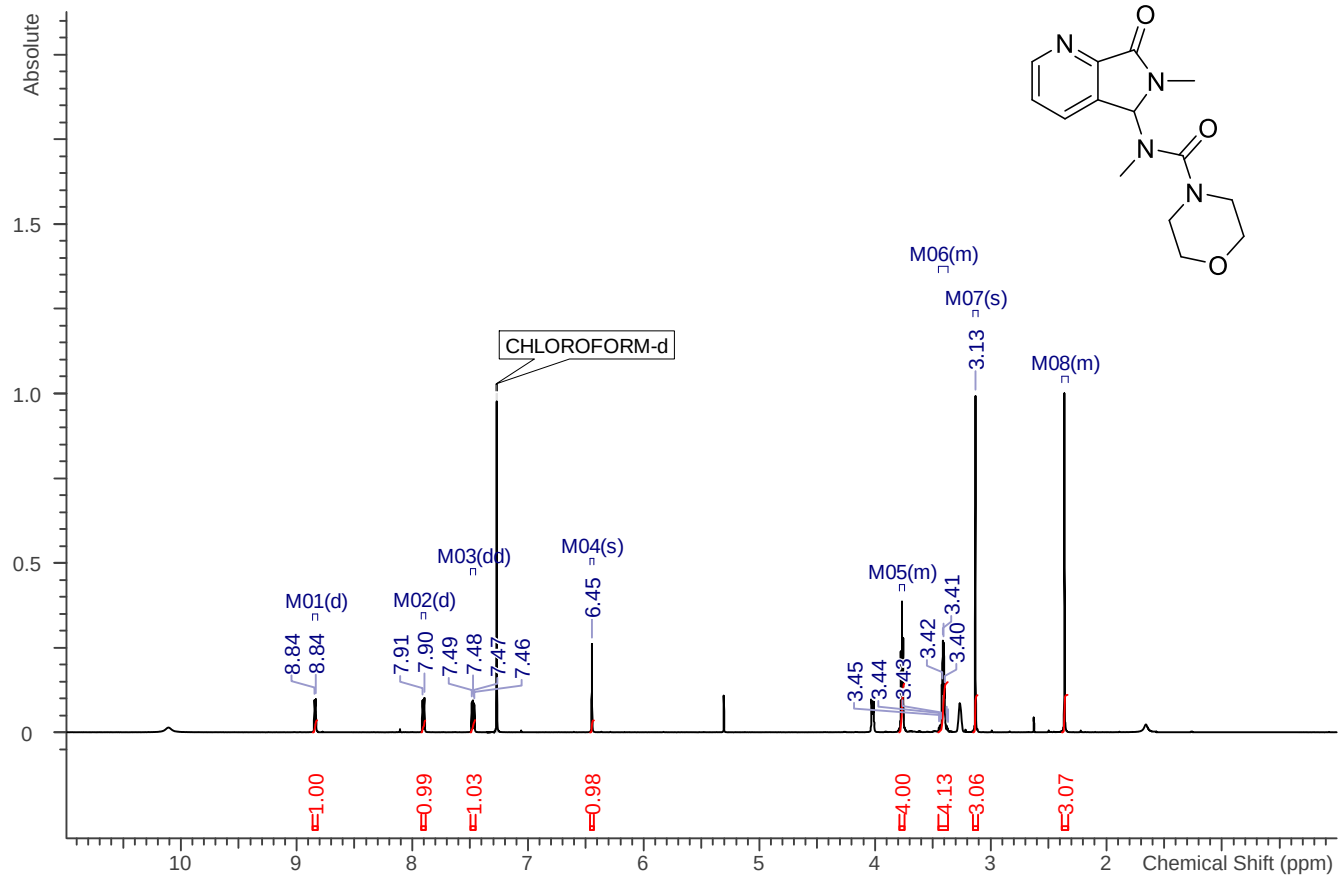
Absolute
1.5
1.0
0.5
0
CHLOROFORM-d
M01(d)
8.84
8.84
M02(d)
7.91
7.90
7.49
7.48
7.47
7.46
M03(dd)
M04(s)
6.45
M05(m)
3.45
3.44
3.43
3.42
3.40
3.41
M06(m)
M07(s)
3.13
M08(m)
1.00
0.99
1.03
0.98
4.00
4.13
3.06
3.07
10
9
8
7
6
5
4
3
2
Chemical Shift (ppm)

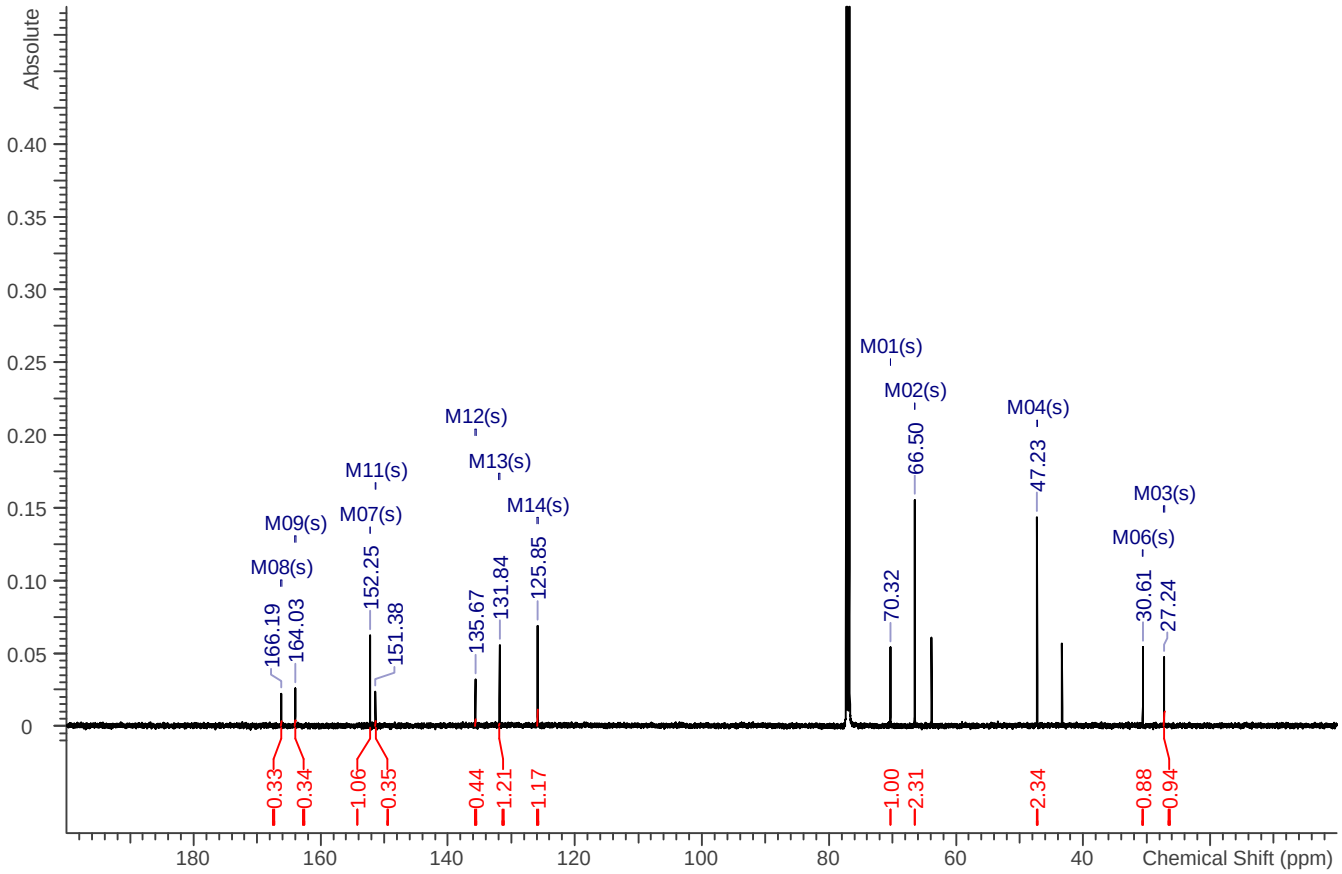
Absolute
0.40
0.35
0.30
0.25
0.20
0.15
0.10
0.05
0
M01(s)
70.32
M02(s)
66.50
M04(s)
47.23
M03(s)
30.61
M06(s)
27.24
M12(s)
135.67
M13(s)
131.84
M14(s)
125.85
M11(s)
152.25
M07(s)
151.38
M09(s)
166.19
M08(s)
164.03
0.33
0.34
1.06
0.35
0.44
1.21
1.17
1.00
2.31
2.34
0.88
0.94
180
160
140
120
100
80
60
40
Chemical Shift (ppm)

I

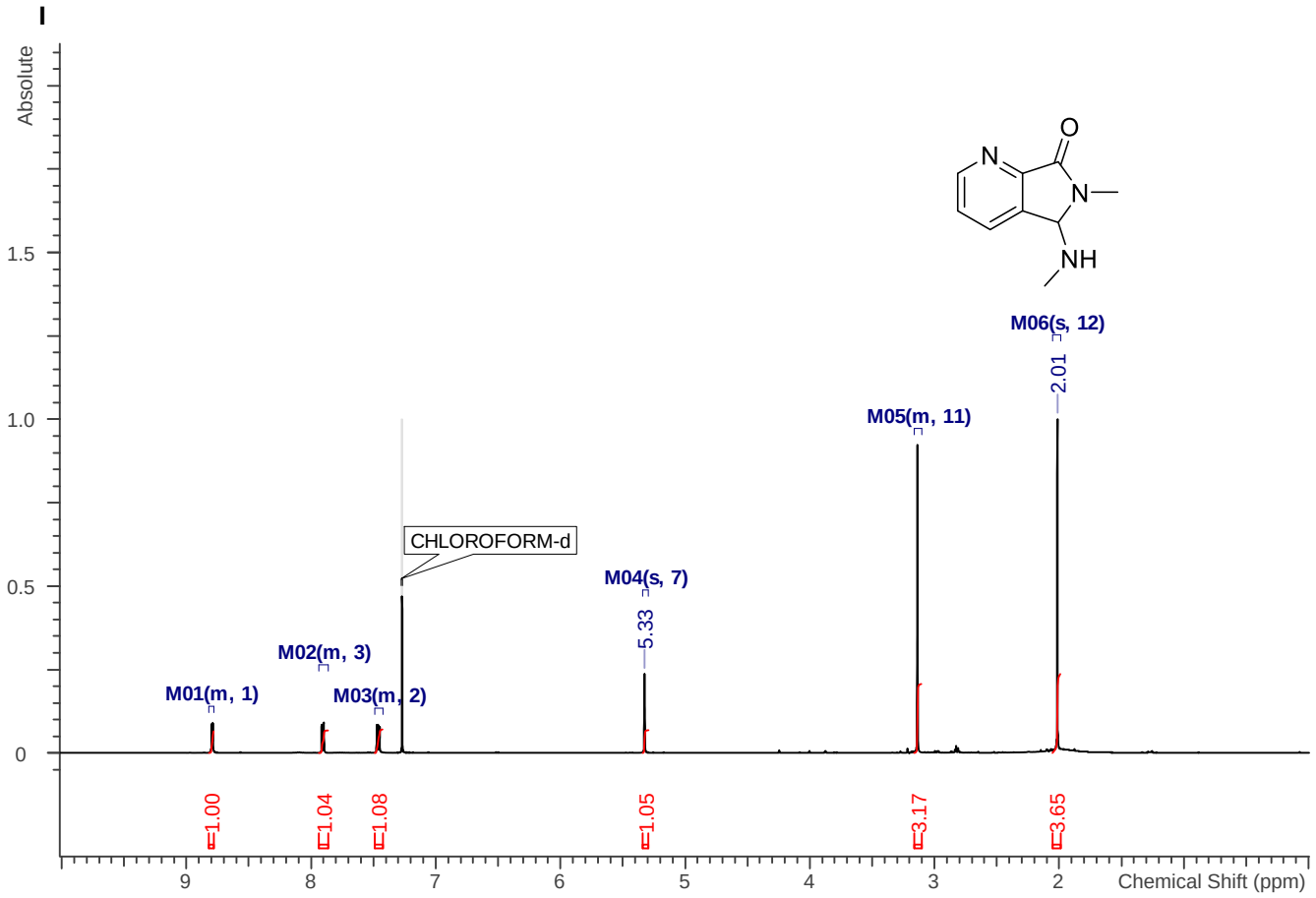
I
Absolute
1.5
1.0
0.5
0
O
N
N
NH
M06(s, 12)
2.01
M05(m, 11)
CHLOROFORM-d
M04(s, 7)
5.33
M02(m, 3)
M01(m, 1)
M03(m, 2)
1.00
1.04
1.08
1.05
3.17
3.65
9
8
7
6
5
4
3
2
Chemical Shift (ppm)

2

Mass Spectrum and Results

Injection Details

Injection Name:	**DWI-HIPS-8083**	*Run Time (min):*	**5,10**
Vial Number:	**GB8**	*Injection Volume:*	**2,00**
Injection Type:	**Unknown**	*Channel:*	**UV_VIS_1**
Calibration Level:		*Wavelength:*	**254**
Instrument Method:	**0.6ml_+ve_-ve_100-600**	*Bandwidth:*	**2**
Processing Method:	**Processing Method - New (190-380)**	*Dilution Factor:*	**1,0000**
Injection Date/Time:	**23.Jan.24 09:56**	*Sample Weight:*	**1,0000**

Integration Results

No.	Peak Name	Retention Time min	Area mAU*min	Height mAU	Relative Area %	Relative Height %	Amount n.a.
1		1,355	22,194	157,168	99,78	99,26	n.a.
2		2,244	0,050	1,173	0,22	0,74	n.a.
Total:			**22,244**	**158,341**	**100,00**	**100,00**	

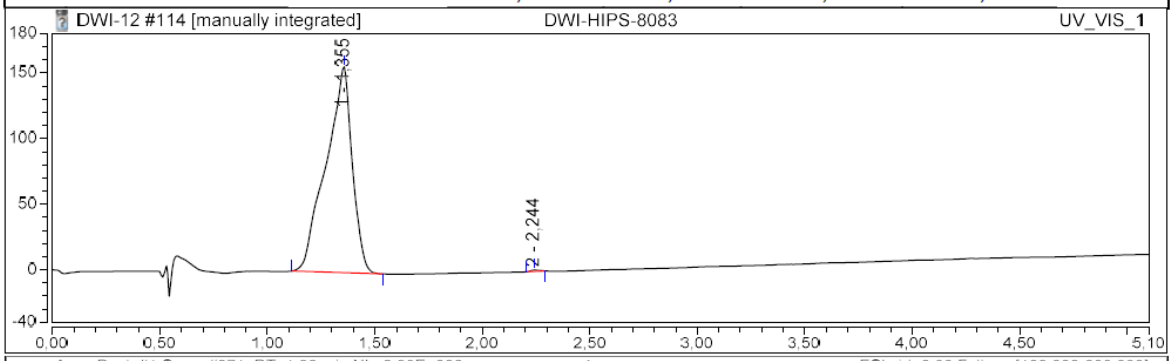

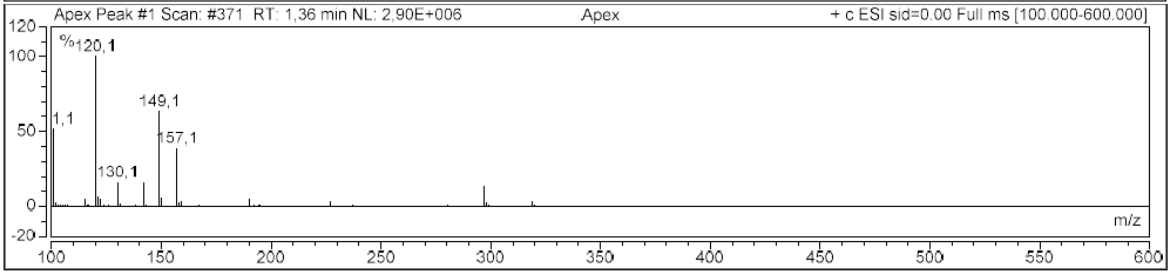

3

Mass Spectrum and Results

Injection Details

Injection Name:	**DWI-HIPS-7860**	*Run Time (min):*	**5.10**
Vial Number:	**GB6**	*Injection Volume:*	**2.00**
Injection Type:	**Unknown**	*Channel:*	**UV_VIS_1**
Calibration Level:		*Wavelength:*	**254**
Instrument Method:	**0.6ml_+ve_-ve_100-600**	*Bandwidth:*	**2**
Processing Method:	**Processing Method - New (190-380)**	*Dilution Factor:*	**1.0000**
Injection Date/Time:	**16/Jan/24 15:21**	*Sample Weight:*	**1.0000**

Integration Results

No.	Peak Name	Retention Time min	Area mAU*min	Height mAU	Relative Area %	Relative Height %	Amount n.a.
1		0.466	60.394	3609.390	96.83	98.28	n.a.
2		0.569	1.977	63.330	3.17	1.72	n.a.
Total:			**62.372**	**3672.720**	**100.00**	**100.00**	

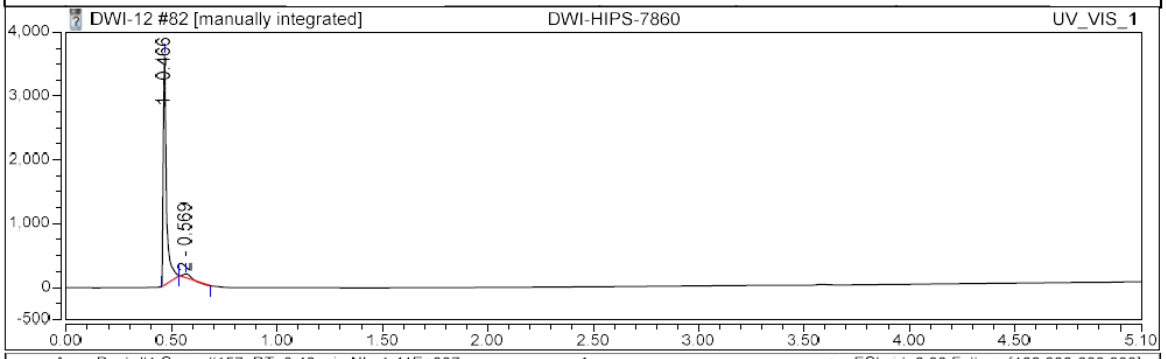

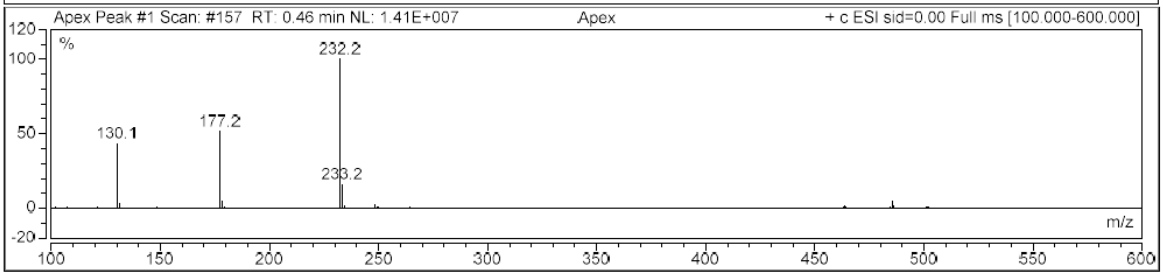

4

Mass Spectrum and Results

Injection Details

Injection Name:	**DWI-HIPS-7859**	*Run Time (min):*	**5.10**
Vial Number:	**GB6**	*Injection Volume:*	**2.00**
Injection Type:	**Unknown**	*Channel:*	**UV_VIS_1**
Calibration Level:		*Wavelength:*	**254**
Instrument Method:	**0.6ml_+ve_-ve_100-600**	*Bandwidth:*	**2**
Processing Method:	**Processing Method - 210-310nm**	*Dilution Factor:*	**1.0000**
Injection Date/Time:	**07/Mar/23 09:59**	*Sample Weight:*	**1.0000**

Integration Results

No.	Peak Name	Retention Time min	Area mAU*min	Height mAU	Relative Area %	Relative Height %	Amount n.a.
1		2.509	82.274	787.577	100.00	100.00	n.a.
Total:			**82.274**	**787.577**	**100.00**	**100.00**	

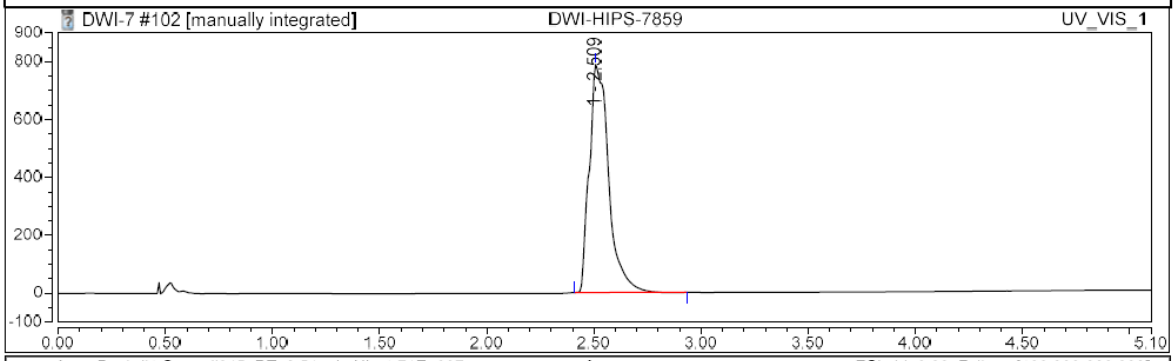

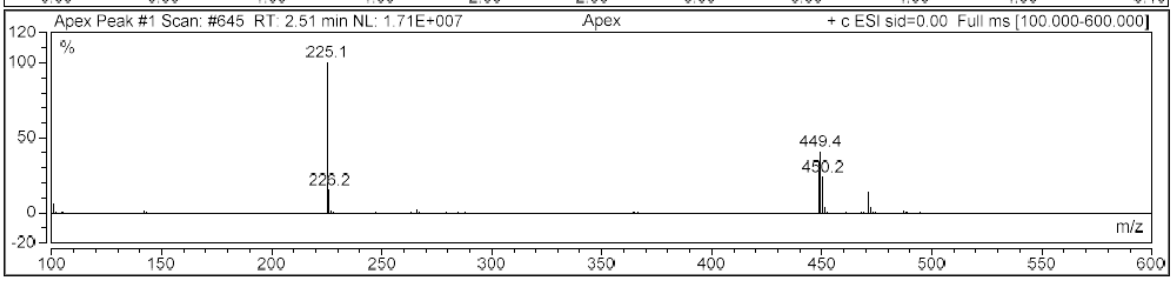

5

Mass Spectrum and Results

Injection Details

Injection Name:	**DWI-HIPS-7861**	*Run Time (min):*	**5.10**
Vial Number:	**GB7**	*Injection Volume:*	**2.00**
Injection Type:	**Unknown**	*Channel:*	**UV_VIS_1**
Calibration Level:		*Wavelength:*	**254**
Instrument Method:	**0.6ml_+ve_-ve_100-600**	*Bandwidth:*	**2**
Processing Method:	**Processing Method - New (190-380)**	*Dilution Factor:*	**1.0000**
Injection Date/Time:	**16/Jan/24 15:28**	*Sample Weight:*	**1.0000**

Integration Results

No.	Peak Name	Retention Time min	Area mAU*min	Height mAU	Relative Area %	Relative Height %	Amount n.a.
1		0.413	1.530	26.433	1.36	0.65	n.a.
2		0.462	111.278	4062.504	98.64	99.35	n.a.
Total:			**112.807**	**4088.937**	**100.00**	**100.00**	

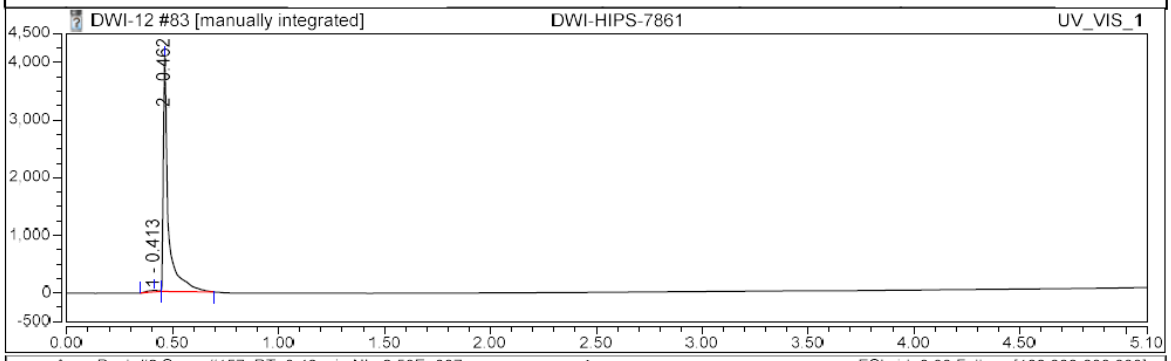

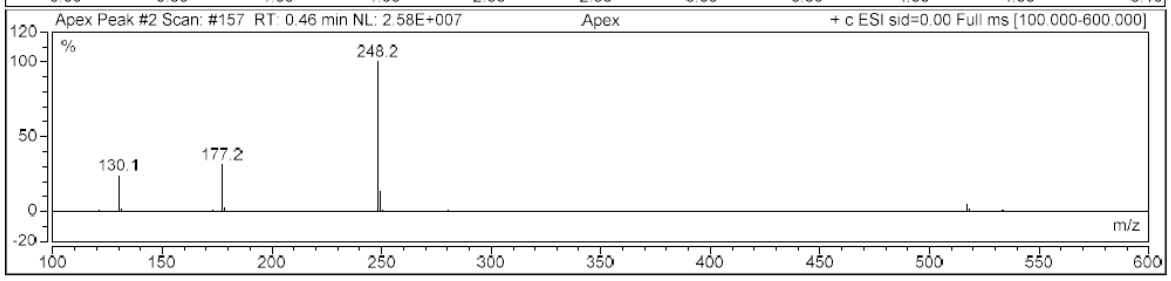

6

Mass Spectrum and Results

Injection Details

Injection Name:	**DWI-HIPS-7858**	*Run Time (min):*	**5.10**
Vial Number:	**GB5**	*Injection Volume:*	**2.00**
Injection Type:	**Unknown**	*Channel:*	**UV_VIS_1**
Calibration Level:		*Wavelength:*	**254**
Instrument Method:	**0.6ml_+ve_-ve_100-600**	*Bandwidth:*	**2**
Processing Method:	**Processing Method - New (190-380)**	*Dilution Factor:*	**1.0000**
Injection Date/Time:	**16/Jan/24 15:14**	*Sample Weight:*	**1.0000**

Integration Results

No.	Peak Name	Retention Time min	Area mAU*min	Height mAU	Relative Area %	Relative Height %	Amount n.a.
1		2.435	36.513	675.647	97.25	98.17	n.a.
2		2.617	1.032	12.625	2.75	1.83	n.a.
Total:			**37.546**	**688.272**	**100.00**	**100.00**	

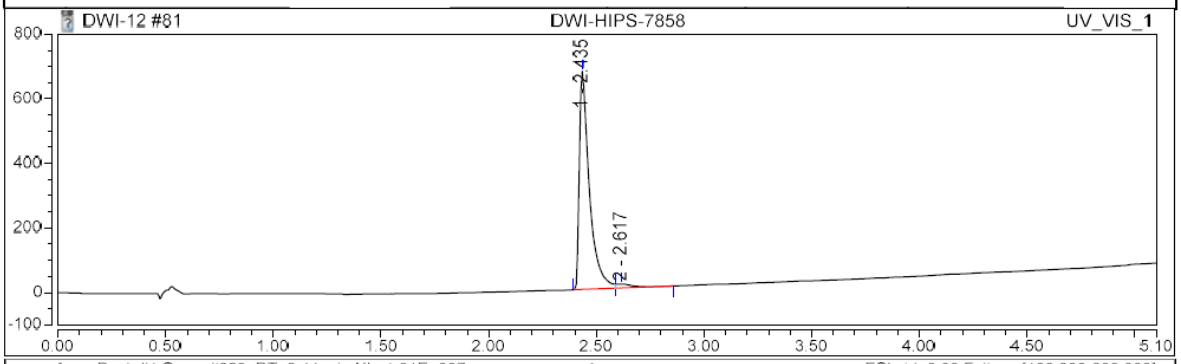

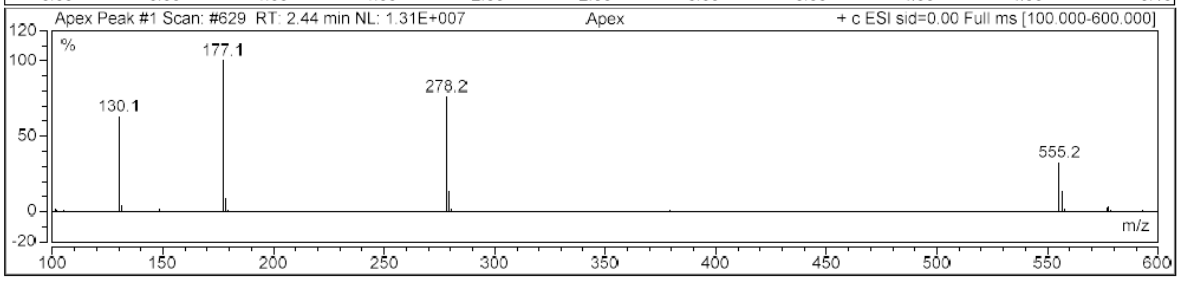

7

Mass Spectrum and Results

Injection Details

Injection Name:	**DWI-HIPS-8134**	*Run Time (min):*	**5,10**
Vial Number:	**GB6**	*Injection Volume:*	**2,00**
Injection Type:	**Unknown**	*Channel:*	**UV_VIS_1**
Calibration Level:		*Wavelength:*	**254**
Instrument Method:	**0.6ml_+ve_-ve_100-600**	*Bandwidth:*	**2**
Processing Method:	**Processing Method - New (190-380)**	*Dilution Factor:*	**1,0000**
Injection Date/Time:	**23.Jan.24 08:59**	*Sample Weight:*	**1,0000**

Integration Results

No.	Peak Name	Retention Time min	Area mAU*min	Height mAU	Relative Area %	Relative Height %	Amount n.a.
1		1,905	1,043	17,348	96,37	97,92	n.a.
2		3,648	0,039	0,369	3,63	2,08	n.a.
Total:			**1,082**	**17,716**	**100,00**	**100,00**	

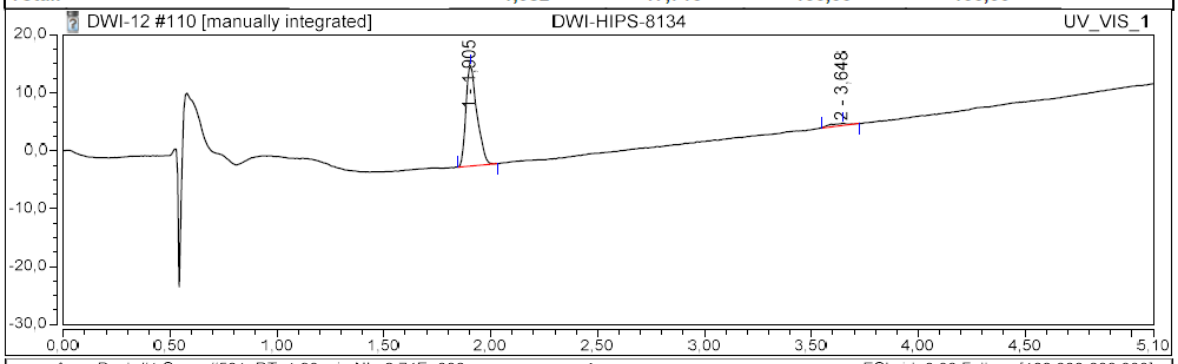

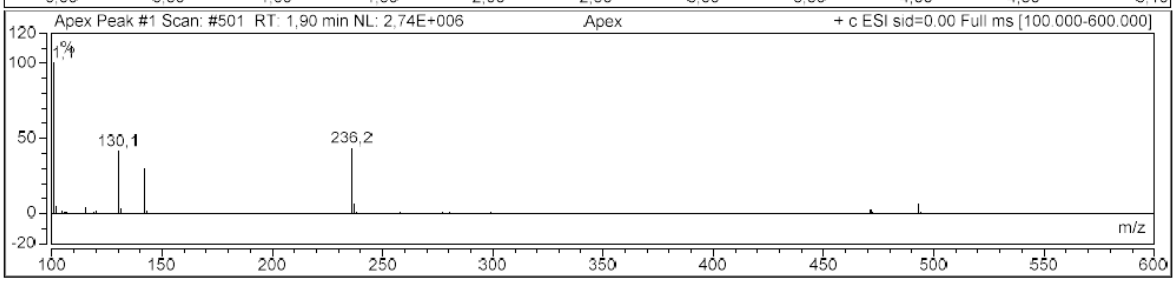

8

Mass Spectrum and Results

Injection Details

Injection Name:	**DWI-HIPS-8208**	*Run Time (min):*	**5.10**
Vial Number:	**GB5**	*Injection Volume:*	**2.00**
Injection Type:	**Unknown**	*Channel:*	**UV_VIS_1**
Calibration Level:		*Wavelength:*	**254**
Instrument Method:	**0.6ml_+ve_-ve_100-600**	*Bandwidth:*	**2**
Processing Method:	**Processing Method - New (190-380)**	*Dilution Factor:*	**1.0000**
Injection Date/Time:	**22/Jan/24 11:57**	*Sample Weight:*	**1.0000**

Integration Results

No.	Peak Name	Retention Time min	Area mAU*min	Height mAU	Relative Area %	Relative Height %	Amount n.a.
1		1.805	13.394	252.073	100.00	100.00	n.a.
Total:			**13.394**	**252.073**	**100.00**	**100.00**	

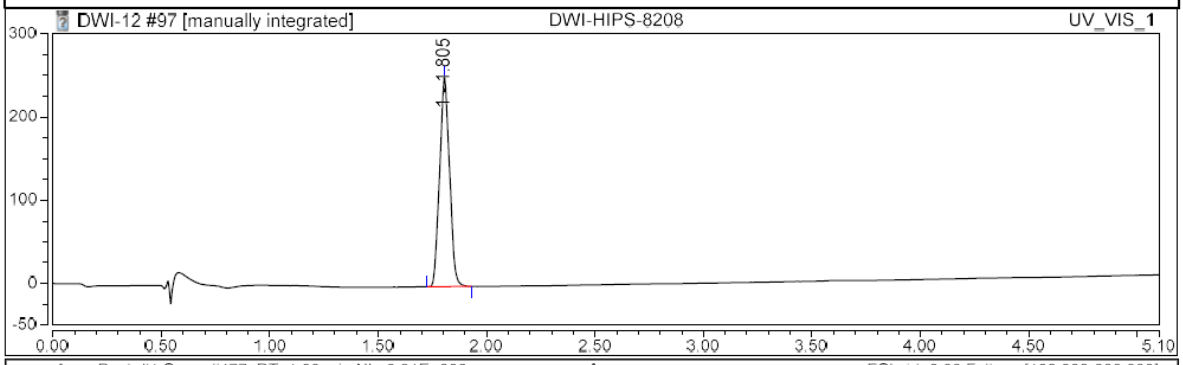

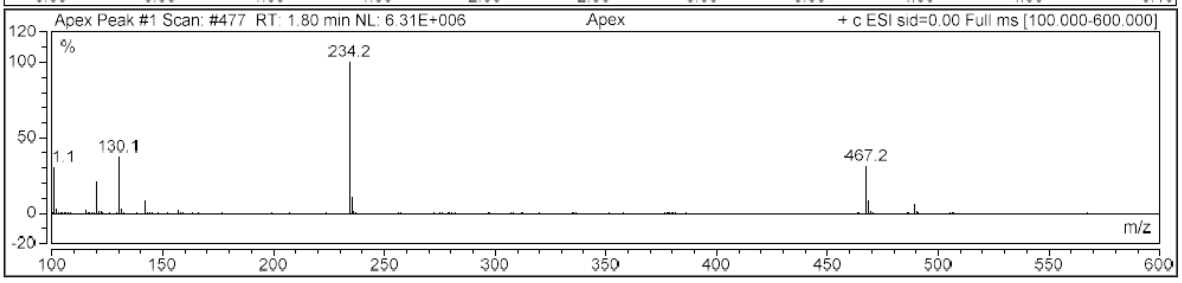

9

Mass Spectrum and Results

Injection Details

Injection Name:	**DWI-HIPS-8209**	*Run Time (min):*	**5.10**
Vial Number:	**GB6**	*Injection Volume:*	**2.00**
Injection Type:	**Unknown**	*Channel:*	**UV_VIS_1**
Calibration Level:		*Wavelength:*	**254**
Instrument Method:	**0.6ml_+ve_-ve_100-600**	*Bandwidth:*	**2**
Processing Method:	**Processing Method - New (190-380)**	*Dilution Factor:*	**1.0000**
Injection Date/Time:	**22/Jan/24 12:04**	*Sample Weight:*	**1.0000**

Integration Results

No.	Peak Name	Retention Time min	Area mAU*min	Height mAU	Relative Area %	Relative Height %	Amount n.a.
1		2.590	8.239	174.745	100.00	100.00	n.a.
Total:			**8.239**	**174.745**	**100.00**	**100.00**	

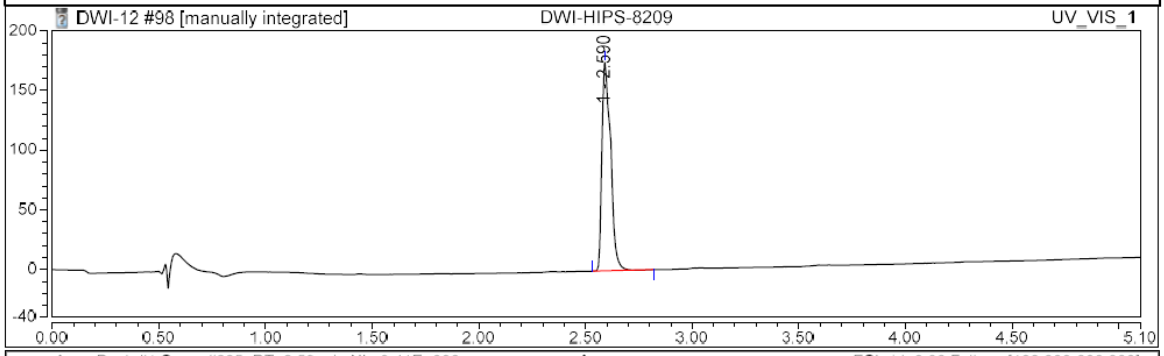

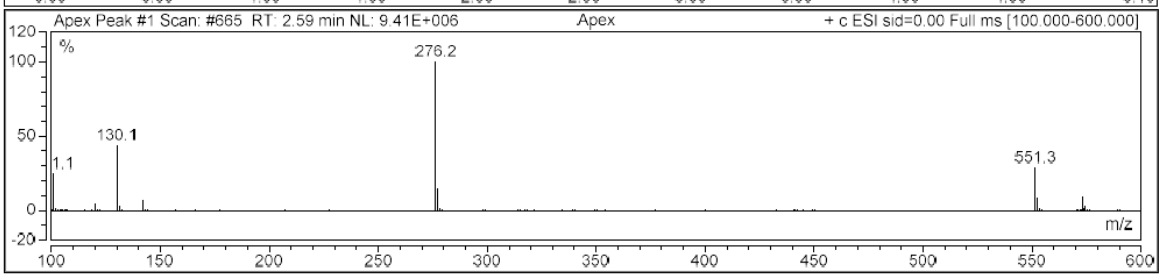

10

Mass Spectrum and Results

Injection Details

Injection Name:	**DWI-HIPS-8211**	*Run Time (min):*	**5.10**
Vial Number:	**GB7**	*Injection Volume:*	**2.00**
Injection Type:	**Unknown**	*Channel:*	**UV_VIS_1**
Calibration Level:		*Wavelength:*	**254**
Instrument Method:	**0.6ml_+ve_-ve_100-600**	*Bandwidth:*	**2**
Processing Method:	**Processing Method - New (190-380)**	*Dilution Factor:*	**1.0000**
Injection Date/Time:	**22/Jan/24 12:11**	*Sample Weight:*	**1.0000**

Integration Results

No.	Peak Name	Retention Time min	Area mAU*min	Height mAU	Relative Area %	Relative Height %	Amount n.a.
1		1.528	25.435	291.262	100.00	100.00	n.a.
Total:			**25.435**	**291.262**	**100.00**	**100.00**	

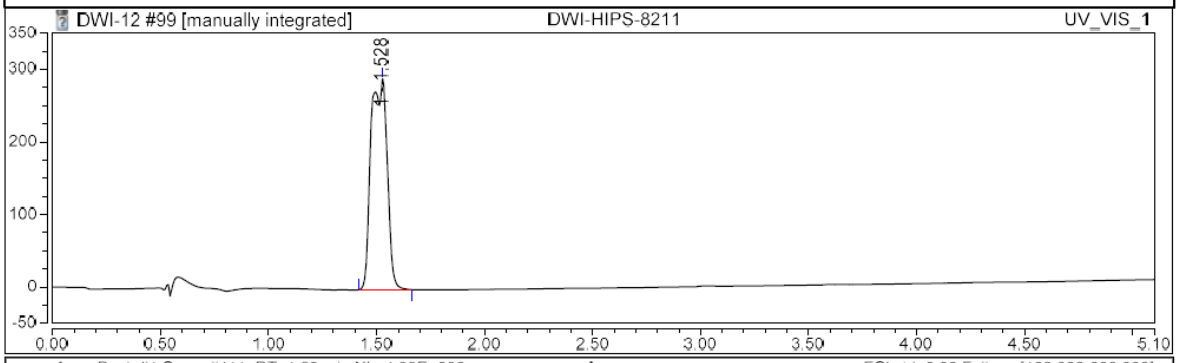

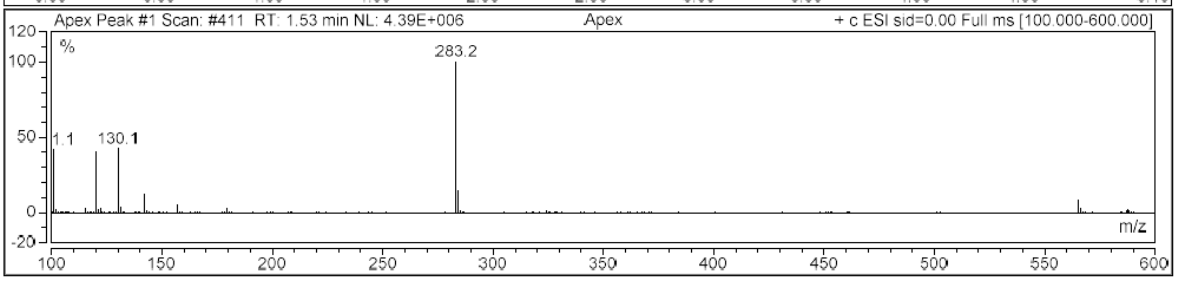

11

Mass Spectrum and Results

Injection Details			
Injection Name:	**DWI-HIPS-8213**	*Run Time (min):*	**5.10**
Vial Number:	**GB5**	*Injection Volume:*	**2.00**
Injection Type:	**Unknown**	*Channel:*	**UV_VIS_1**
Calibration Level:		*Wavelength:*	**254**
Instrument Method:	**0.6ml_+ve_-ve_100-600**	*Bandwidth:*	**2**
Processing Method:	**Processing Method - New (190-380)**	*Dilution Factor:*	**1.0000**
Injection Date/Time:	**22/Jan/24 13:05**	*Sample Weight:*	**1.0000**

Integration Results

No.	Peak Name	Retention Time min	Area mAU*min	Height mAU	Relative Area %	Relative Height %	Amount n.a.
1		2.408	12.451	266.984	100.00	100.00	n.a.
Total:			**12.451**	**266.984**	**100.00**	**100.00**	

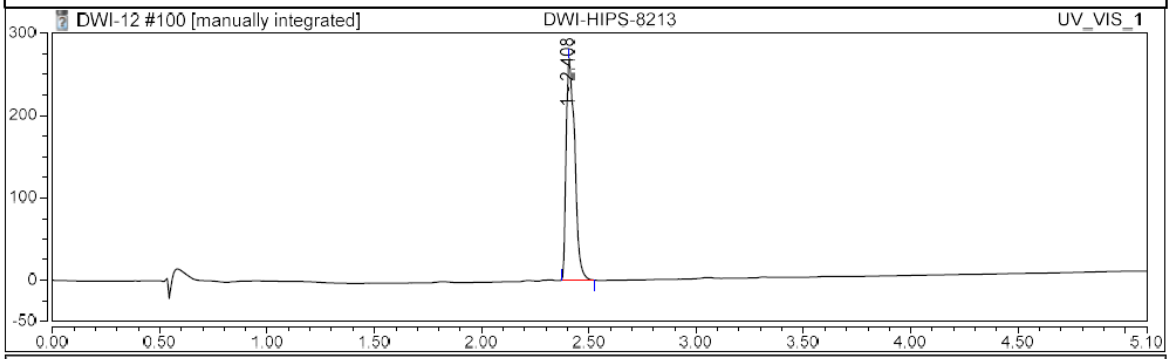

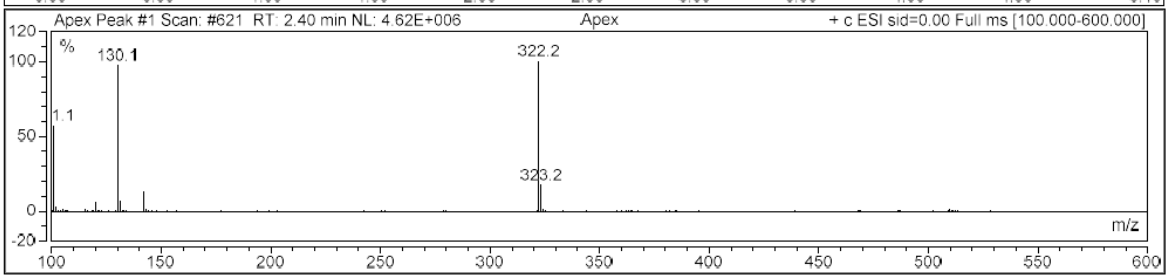

12

Mass Spectrum and Results

Injection Details

Injection Name:	**DWI-HIPS-8246**	*Run Time (min):*	**5.10**
Vial Number:	**GB7**	*Injection Volume:*	**2.00**
Injection Type:	**Unknown**	*Channel:*	**UV_VIS_1**
Calibration Level:		*Wavelength:*	**254**
Instrument Method:	**0.6ml_+ve_-ve_100-600**	*Bandwidth:*	**2**
Processing Method:	**Processing Method - New (190-380)**	*Dilution Factor:*	**1.0000**
Injection Date/Time:	**22/Jan/24 13:19**	*Sample Weight:*	**1.0000**

Integration Results

No.	Peak Name	Retention Time min	Area mAU*min	Height mAU	Relative Area %	Relative Height %	Amount n.a.
1		1.830	5.528	108.041	98.01	98.06	n.a.
2		3.043	0.090	1.543	1.59	1.40	n.a.
3		3.310	0.023	0.599	0.41	0.54	n.a.
Total:			**5.641**	**110.182**	**100.00**	**100.00**	

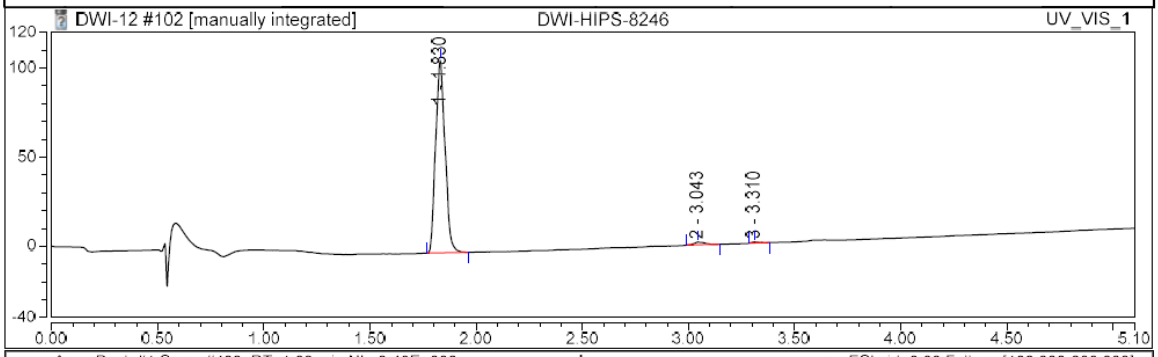

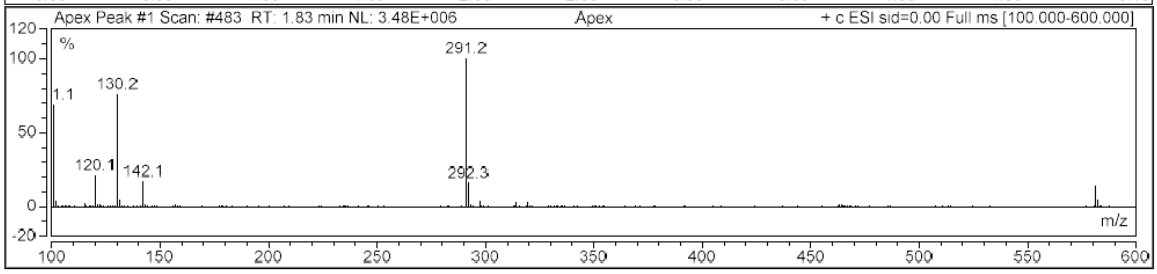

I

Mass Spectrum and Results

Injection Details			
Injection Name:	**DWI-HIPS-8133**	*Run Time (min):*	**5.10**
Vial Number:	**GB8**	*Injection Volume:*	**2.00**
Injection Type:	**Unknown**	*Channel:*	**UV_VIS_1**
Calibration Level:		*Wavelength:*	**254**
Instrument Method:	**0.6ml_+ve_-ve_100-600**	*Bandwidth:*	**2**
Processing Method:	**Processing Method - New (190-380)**	*Dilution Factor:*	**1.0000**
Injection Date/Time:	**10/Jan/24 11:40**	*Sample Weight:*	**1.0000**

Integration Results

No.	Peak Name	Retention Time min	Area mAU*min	Height mAU	Relative Area %	Relative Height %	Amount n.a.
1		0.483	21.783	1492.236	75.82	87.82	n.a.
2		0.635	6.946	207.045	24.18	12.18	n.a.
Total:			**28.729**	**1699.281**	**100.00**	**100.00**	

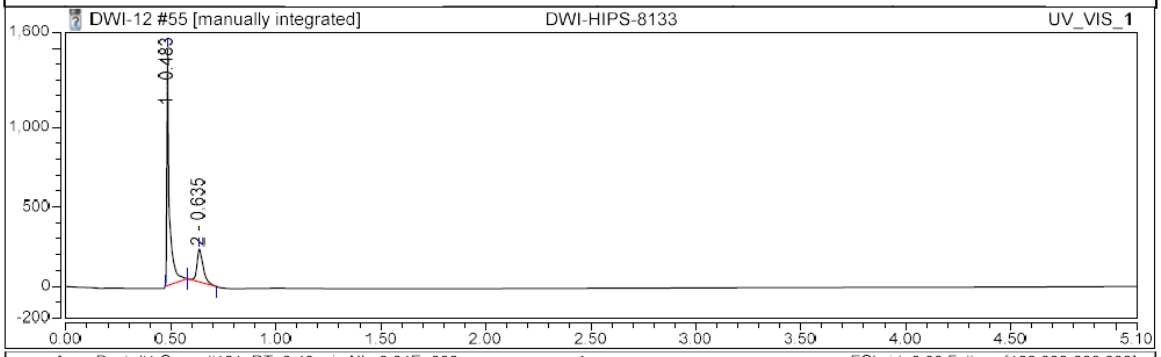

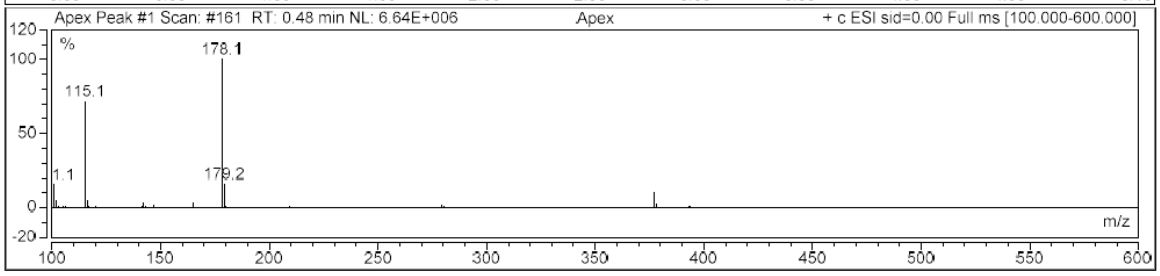

Heated ^{1}H and ^{13}C NMR Spectra of 11

To validate our suspicion that the extra peaks in the NMR spectrum of **11** are due to rotamerization, we measured both ^{1}H and ^{13}C at elevated temperatures (60 and 80 °C). As can be seen below, the "double peaks" converge at elevated temperatures, confirming our hypothesis.

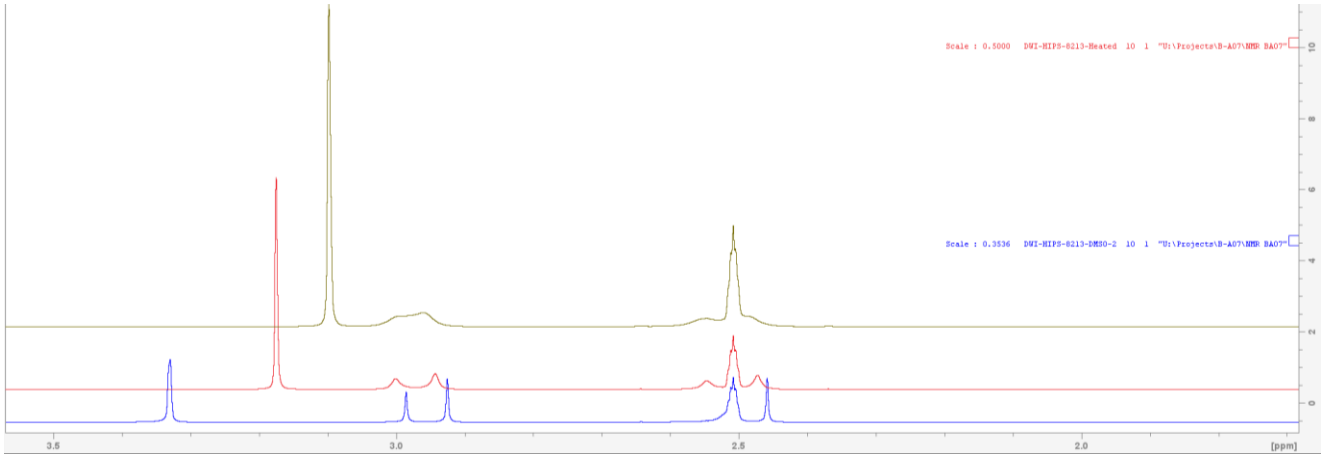

Figure S4 Comparison of ^{1}H NMR spectra of **11** at various temperatures from 1.5 to 3.5 ppm. Bottom: Spectrum measured at 25 °C. Middle: Spectrum measured at 60 °C. ¨Top: Spectrum measured at 80 °C

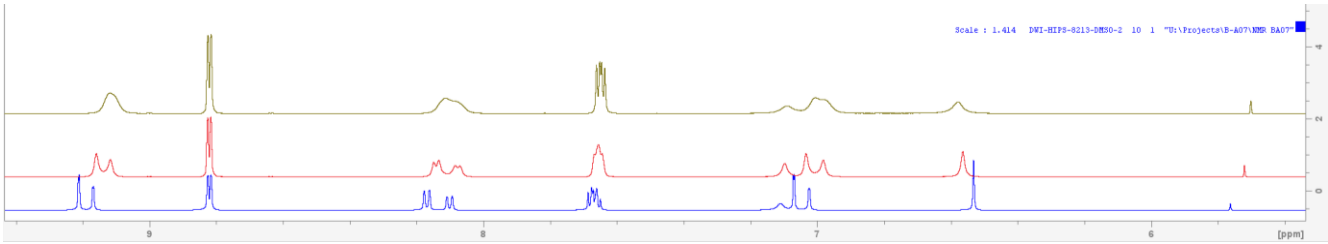

Figure S5 Comparison of ^{1}H NMR spectra of **11** at various temperatures from 5.5 to 9.5 ppm. Bottom: Spectrum measured at 25 °C. Middle: Spectrum measured at 60 °C. ¨Top: Spectrum measured at 80 °C

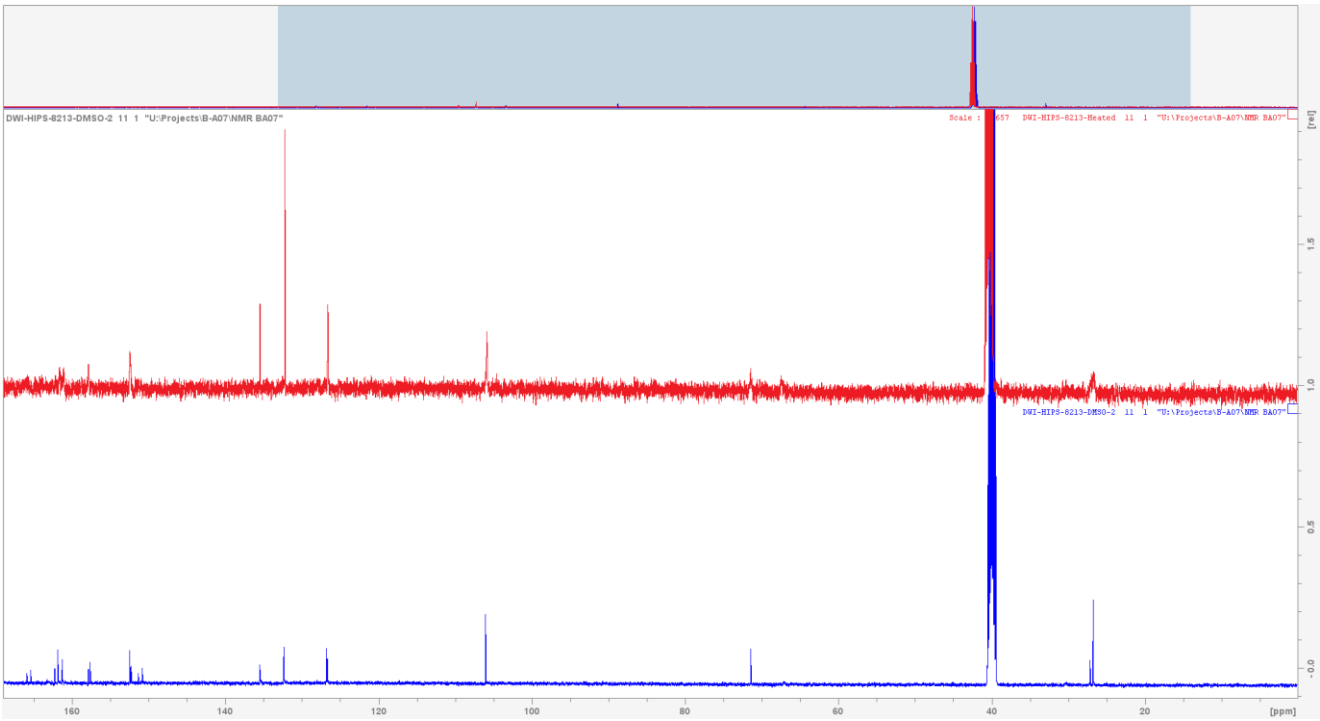

Figure S6 Comparison of ^{13}C NMR spectra of **11** at various temperatures. Bottom: Spectrum measured at 25 °C. Top: Spectrum measured at 80 °C

References

[1] S. B. Richard, M. E. Bowman, W. Kwiatkowski, I. Kang, C. Chow, A. M. Lillo, D. E. Cane, J. P. Noel, *Nature Structural Biology* **2001**, *8*, 641-648.

[2] D. Willocx, L. Bizzarri, A. Alhayek, P. Bravo, B. Illarionov, K. Rox, J. Lohse, M. Fischer, A. M. Kany, H. Hahne, M. Rottmann, M. Witschel, M. M. Hamed, E. Diamanti, A. K. H. Hirsch, *ChemRxiv.* **2024**.

3.3 Chapter 3: Oxaprozine Derivatives as Anti-Gram-Positive Agents Targeting Bacterial Energy-Coupling Factor Transporters

Daan Willocx, Felix F. Lillich, Aleksei Tsarenko, Dirk J. Slotboom, Ewgenij Proschak, Mostafa M. Hamed, Anna K. H. Hirsch

Contributions: Daan Willocx, Mostafa Hamed, Ewgenij Proschak and Anna K. H. Hirsch conceived the project; Synthesis and characterization of the compounds was performed by Daan Willocx and Felix F. Lillich; Biochemical evaluation of derivatives regarding inhibitory activity was performed by Aleksei Tsarenko; Whole-cell assays were performed by Jeannine Jung. Screenings against Gram-positive bacteria were performed by Viktoria George. Daan Willocx wrote the manuscript with contributions of all authors. Anna K. H. Hirsch coordinated the project.

All authors have given approval to the final version of the manuscript.

This chapter will be submitted to the *European Journal of Medicinal Chemistry* (Elsevier) without or with minor modifications.

Title: Oxaprozine Derivatives as Anti-Gram-Positive Agents Targeting Bacterial Energy-Coupling Factor Transporters

Author names and affiliations: Daan Willocx,[a,b] Felix F. Lillich,[c] Aleksei Tsarenko,[d] Dirk J. Slotboom,[d] Ewgenij Proschak,[c] Mostafa M. Hamed,[a] Anna K. H. Hirsch[a,b,*]

[a]Helmholtz Institute for Pharmaceutical Research Saarland (HIPS)-Helmholtz Centre for Infection Research (HZI), Saarland University, Campus E8.1, 66123 Saarbrücken, Germany.

[b]Saarland University, Department of Pharmacy, Campus E8.1, 66123 Saarbrucken, Germany.

[c]Institute of Pharmaceutical Chemistry, Goethe-University Frankfurt, Max-von-Laue-Strasse 9, 60438 Frankfurt am Main, Germany

[d]Biomolecular Sciences and Biotechnology Institute, University of Groningen, Nijenborgh 4, 9747AG Groningen, The Netherlands

*Corresponding author: Anna.Hirsch@helmholtz-hips.de

Highlights

Please refer to additional document named Highlights

Keywords

Antimicrobial resistance

Drug design

Energy-coupling factor transporters inhibitors

Medicinal chemistry

Structure–activity relationships

Transmembrane protein

Abstract

With antimicrobial resistance reaching alarming levels globally, there is an urgent need for the development of novel anti-infectives featuring underexplored modes of action, such as the energy-coupling factor (ECF) transporters. These transmembrane proteins are mostly prevalent among Gram-positive bacteria and facilitate the uptake of various water-soluble B-type vitamins and metal cations. In this study, we report on the discovery of a compound class derived from oxaprozin that inhibits the ECF transporters. Through optimization of our initial hit, we identified a frontrunner compound demonstrating low micromolar activity in our whole-cell and proteoliposome-based uptake assays. Furthermore, our frontrunner exhibited potent antimicrobial activity against a panel of clinically relevant Gram-positive pathogens.

1. Introduction

Development of antimicrobial resistance (AMR) is a natural process that has been going on since the advent of life. For example, D'Costa *et al*. discovered genes encoding for resistance towards β-lactam, tetracycline and glycopeptide antibiotics in 30,000-year-old Beringian permafrost samples by metagenomic analysis.[1, 2] Following the introduction of penicillin in the 1940s, however, resistance development has significantly amplified and reached alarming levels today. Misuse and overuse of anti-infectives in both healthcare and agriculture predominantly stimulate the emergence of multidrug-resistant organisms.[3-5] To ensure effective treatment of infectious diseases in the future, new modes of action for anti-infectives have to be explored. The energy-coupling factor (ECF) transporters are a class of transmembrane proteins and a subfamily of the ATP-binding cassette (ABC) transporters, representing an underexplored target to address AMR. These transmembrane proteins mediate the uptake of various water-soluble vitamins, for instance folate and thiamine, and metal cations such as Ni^{2+} and Co^{2+}. ECF transporters are present in a wide range of pathogens, but are mainly found in Gram-

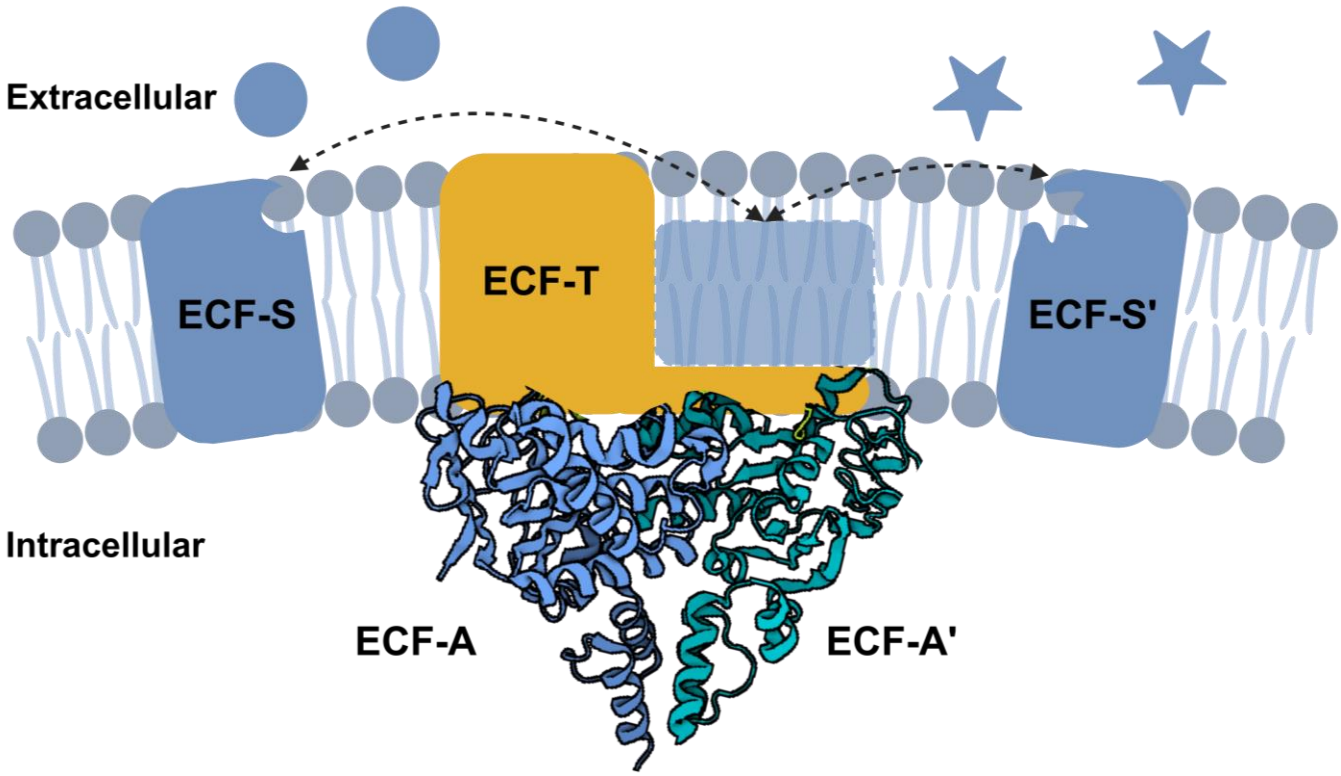

Fig. 1. Visual representation of the energy-coupling factor (ECF) transporter. Structure of ECF-A and A' is adapted from RCSB Protein Data Bank structure 5JSZ.

positive bacteria, including *Streptococcus pneumoniae* and *Staphylococcus aureus*. Interestingly, ECF transporters are absent in human cells, minimizing the risk of off-target side effects.[6-8] These transmembrane proteins are generally comprised of two modules, the ECF module and a substrate-specific binding protein (the S-component) (Fig. 1). The ECF module itself consists of two ATPase subunits (EcfA and EcfA'), located in the cytosol, and one integral membrane protein (ECF-T) (Fig. 1). It is postulated that when a specific substrate is captured by the S-component, the complex will topple over in the membrane where it will interact with the ECF-T module and release the substrate into the cytosol. Lastly, ATP hydrolysis mediated by the ATPase subunits, drives structural changes ultimately leading to the reorientation of the S-component towards the extracellular environment.[9, 10] ECF transporters can be categorized into two different groups. Whereas ECF modules in group I interact with one "dedicated" S-component, ECF modules in group-II interact with several different S-components, making them ideal targets to disrupt the uptake of multiple nutrients concomitantly. Therefore, inhibition of these transporters can have detrimental effects on the growth and survival of bacterial species, especially on those that are auxotrophic for one or multiple vitamins. Furthermore, preventing uptake might also impose great metabolic stress as *de novo* synthesis of vitamins is energetically considerably more demanding.[7]

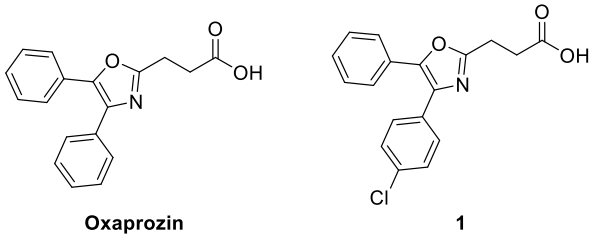

Oxaprozin **1**

ECF-T %inhibition at 50 μM = 21.1 ± 0.7

Fig. 2. Comparison between Oxaprozin (left) and our initial hit **1** (right).

In this study, we present the identification of an oxaprozin-based compound as an inhibitor of the ECF transporters. Oxaprozin is an FDA-approved nonsteroidal antirheumatic. We discovered hit **1** (Fig. 2, ECF-T %inhibition at 50 μM = 21.1 ± 0.7) by examination of a proprietary compound library

predominately containing molecules bearing a carboxylic acid moiety. Based on our experience, carboxylic acids appear to be pivotal for inhibitory activity of ECF-T.[10-12] With our hit in hand, we commenced a structure–activity relationship (SAR) study, ultimately leading to low-micromolar inhibitors of ECF-T in a whole-cell and proteoliposome-based assays. Additionally, the most promising compound was tested against a panel of clinically relevant Gram-positive pathogens.

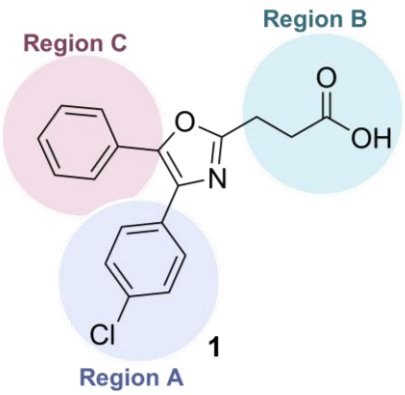

Fig. 3. Structure–activity relationship study focusing on the optimization of regions within hit **1.**

2. Results and discussion

2.1 Chemistry

To make the SAR study as efficient as possible, we decided to subdivide **1** into three regions (Figure 3) and optimize each region sequentially. Initially, we optimized region A, followed by region B and lastly C, as we recognized this was the most straightforward route. All derivatives were synthesized *via* two previously reported synthetic routes (Schemes 1 and 2).[13, 14] For derivatives of regions A and B, both routes were used, whereas, for derivatives of region C only the second synthetic route was employed. The first route starts from the respective 1,2-diphenylethan-1-one (**I**), either synthesized *via* a previously published method [13] or commercially obtained, which was then brominated in the presence of Br_2 (**II**). The resulting brominated intermediate was then mixed, without prior purification, with the respective

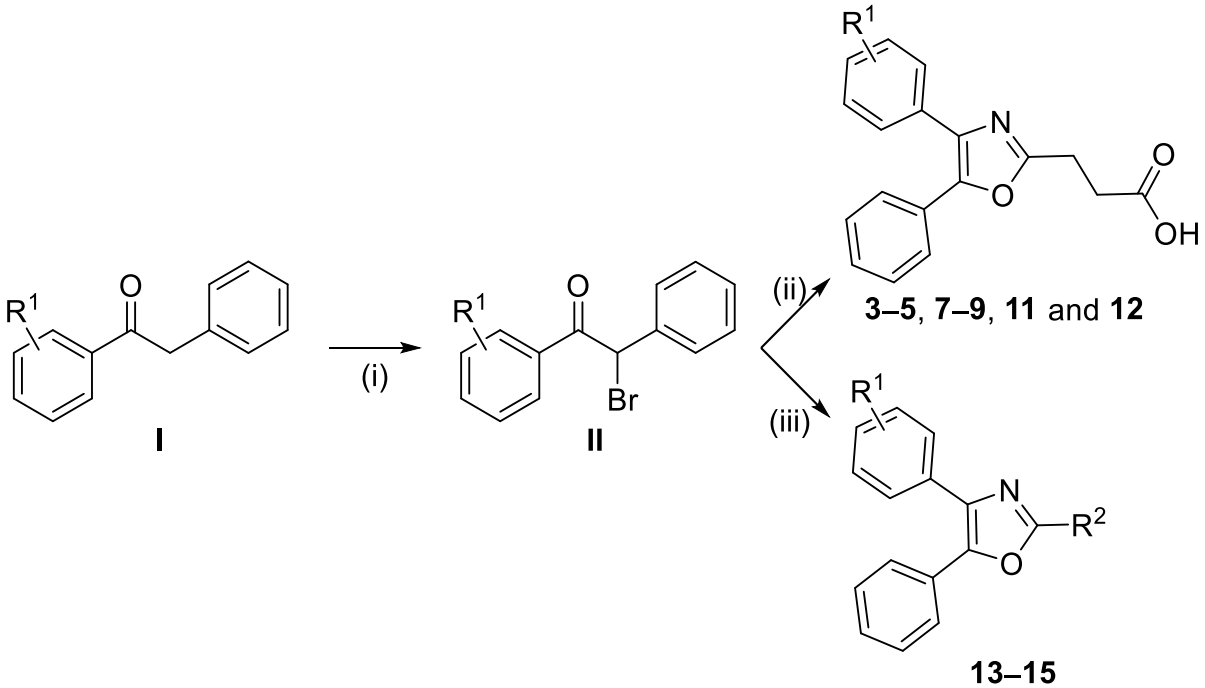

Scheme 1. Synthetic route towards (**3**–**5**, **7**–**9**, **11**–**15**). Reagents and conditions: (i) Br_2, $CHCl_3$, reflux, 2 h; (ii) 1. Et_3N, MeCN, 45 °C, 6 h; 2. NH_4OAc, reflux, 3 h, 11–34% yield (over two steps) (**3**–**5**, **7**–**9**, **11** and **12**); (iii) 1. Et_3N, MeCN, 45 °C, 6 h; 2. NH_4OAc, reflux, 3 h, 11–27% yield (over two steps) (**13**–**15**).

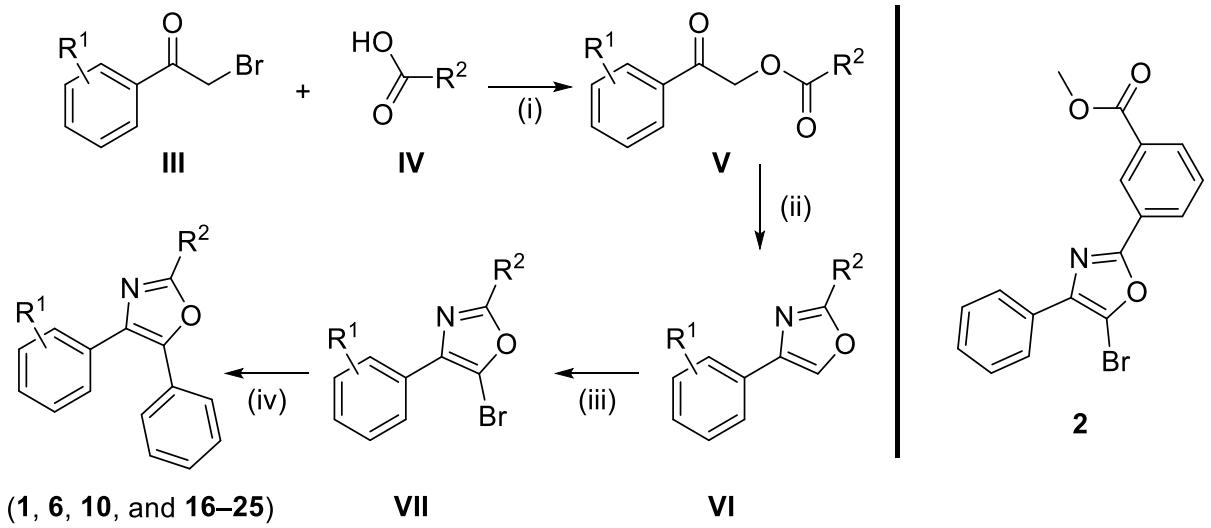

Scheme 2. Synthetic route to (**1**, **6**, **10,** and **16**–**25**). Reagents and conditions, Et_3N, acetone, room temperature, overnight; (ii), $BF_3{\cdot}Et_2O$, acetamide, MeCN, 120 °C, overnight; (iii), *N*-bromosuccinimide, acetic acid, 80 °C, 2 h; (iv), 1. Respective boronic acid, Cs_2CO_3, Pd(dppf)Cl_2, 1,4-dioxane/water (9/1), 110 °C, 1 h, microwave; 2. LiOH (2 M), 1,4-dioxane/water (9:1), room temperature, overnight. 1–4 % yield (over all steps)

carboxylic acid and the mixture was heated to 45 °C for 6 h and refluxed for 3 h to form the oxazole and afford the final product (Scheme 1). The second synthetic route commences from the respective 2-bromo-1-phenylethan-1-one (**III**), which was added to a basic solution containing the corresponding carboxylic acid **IV**, affording the related 2-oxo-2-phenylethyl acetate (**V**). Heating this intermediate to 120 °C in a solution containing $BF_3{\cdot}Et_2O$ and acetamide generated the oxazole **VI**, which was selectively brominated at the 5-position (**VII**) using *N*-bromosuccinimide (NBS). Lastly, a Suzuki reaction with phenylboronic acid and subsequent saponification of a potential ester ultimately provided the desired compound (Scheme 2). For the derivatives of region C, intermediate **2** was synthesized on a large scale using the latter synthetic route to enable straightforward synthesis of derivatives **18**–**25** by employing the respective boronic acids in a Suzuki reaction and subsequent saponification.

2.2 SARs

2.2.1 SAR of Region A.

To understand whether a halogen substituent is essential for activity in this region, we synthesized derivatives **3**–**6** (Table 1). Analysis of these compounds revealed a clear preference for halogen atoms at this position of the phenyl ring. Comparable activities to **1** were obtained for fluoro- (**3**) and trifluoromethyl-substituted (**4**) derivatives, while derivatives bearing non-halogenated moieties (**5**, **6**) demonstrated decreased activity. Next, we investigated the influence of the position of the halogen on the phenyl ring (**7**–**9**). It became clear that both *para* (**1**, **3**) and *meta* (**7**) positions are favorable for retaining activity, whereas substitution in the *ortho* position led to a decrease in activity (**8**, **9**). The comparable activity between *meta* and *para* substituted derivatives encouraged us to synthesize di-substituted derivatives with the anticipation that the effect could be cumulative. Fortunately, di-substitution indeed led to an increase in potency, with **12** (ECF-T whole-cell uptake %inhibition at 50 µM = 42.9 ± 12.3) demonstrating double the inhibition at 50 µM compared to the parent compound **1** (ECF-T whole-cell uptake %inhibition at 50 µM = 21.1 ± 0.7).

Table 1. *In vitro* activities for compounds (**1, 3–12**) in ECF-T whole-cell uptake assay

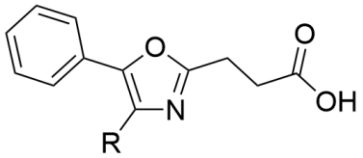

#	Structure, R=	% inhibition at 50 μM[a]	#	Structure, R=	% inhibition at 50 μM[a]
1	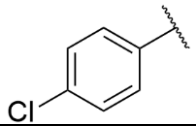	21.1 ± 0.7	**8**	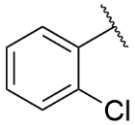	7.5 ± 1.7
3	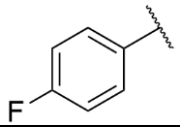	23.8 ± 1.5	**9**	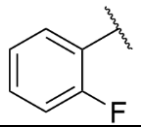	11 ± 1.6
4	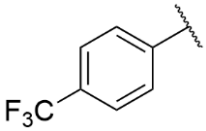	26.2 ± 0.9	**10**	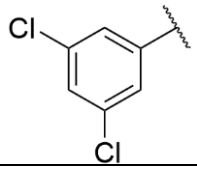	36.6 ± 1.1
5	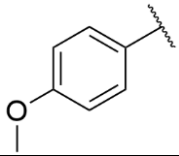	12.1 ± 4.2	**11**	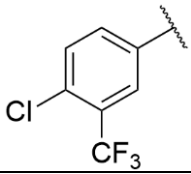	32.6 ± 12.7
6	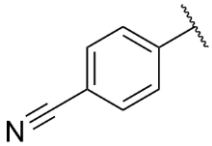	7.7 ± 0.3	**12**	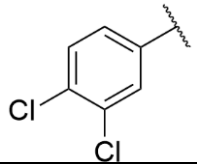	42.9 ± 12.3
7	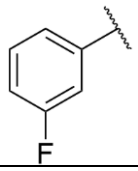	25.4 ± 2.5			

[a]Assays were performed in replicate as independent experiments (*n* = 2); values are shown as mean ± SD; n.d. = not determined.

2.2.2 SAR of Region B.

For the optimization of region B, we used **12** as the starting point. At first, we increased the linker length by one carbon atom (**13**), which unfortunately led to a decrease in activity. We postulated that this decrease in activity might be due to the increased flexibility of the alkyl linker. Therefore, we replaced it with a more rigid phenyl ring (**14**–**16**) and arranged the carboxylic acid in all possible orientations. Here the *meta*-substituted derivative demonstrated superior activity over the other orientations and the parent compound (**12**). To further capitalize on the increase in potency by this replacement, we interchanged the phenyl with a pyridine ring to increase the hydrophilicity. Unfortunately, this exchange ultimately led to a slight decrease in activity (**15**, ECF-T whole-cell uptake IC_{50} = 5.1 ± 2.6 μM; **17** ECF-T whole-cell uptake IC_{50} = 8.2 ± 0.9 μM). Therefore, we selected **15** as the starting point for the optimization of the C region.

Table 2. *In vitro* activities for compounds (**13**–**17**) in ECF-T whole-cell uptake assay

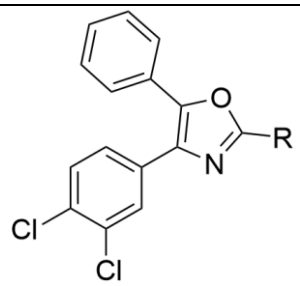

#	Structure, R=	% inhibition at 50 μM	IC_{50} (μM)	#	Structure, R=	% inhibition at 50 μM	IC_{50} (μM)
13	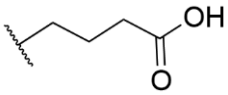	28 ± 3.1	n.d.	**16**	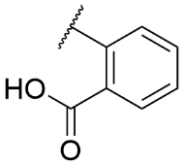	83.4	n.d.
14	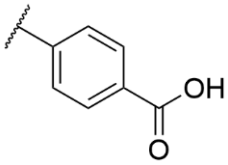	35.6 ± 1.5	n.d.	**17**	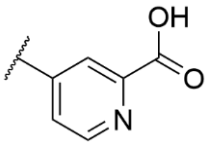	99.6 ± 0.1	8.2 ± 0.9
15	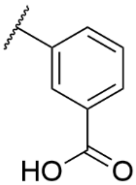	94.8 ± 3.6	5.1 ± 2.6				

[a]Assays were performed in replicate as independent experiments ($n \geq 2$); values are shown as mean ± SD; n.d. = not determined.

2.2.3 SAR of Region C.

Lastly, we shifted our focus to the C region and synthesized several derivatives. Care must be taken when analyzing these results, as inhibitory activities were measured at a lower inhibitor concentration than for previous regions. Despite the diversity, there seemed to be no clear preference for a certain moiety or substitution pattern in this region, with compounds (**20**–**23**) demonstrating comparable inhibitory activities. Additionally, disubstitution of the phenyl ring did not lead to an increase in activity in this case (**24**, **25**). With these results in hand, we assumed that modifications in this region would not have a profound effect on the inhibitory activity of the compound class.

Table 3. *In vitro* activities for compounds (**18**–**25**) in ECF-T whole-cell uptake assay

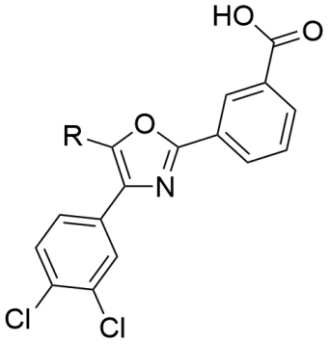

#	Structure, R=	% inhibition at 25 µM	IC_{50} (µM)	#	Structure, R=	% inhibition at 25 µM	IC_{50} (µM)
18	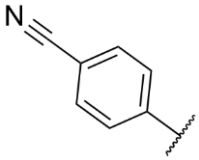	85.5 ± 0.8	n.d.	**22**	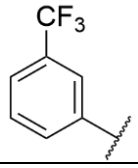	99.9 ± 0.1	2.2 ± 0.5
19	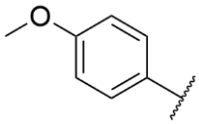	98.8 ± 0.3	3.5 ± 0.1	**23**	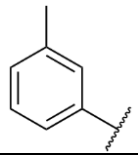	99.1 ± 0.1	2.4 ± 0.3
20	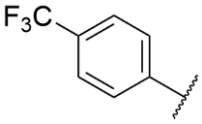	99.7 ± 0.1	2.5 ± 0.4	**24**	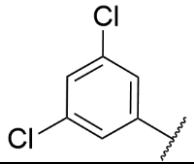	89 ± 2.7	n.d.
21	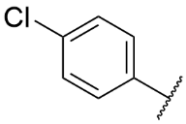	96 ± 2.5	2.4 ± 0.2	**25**	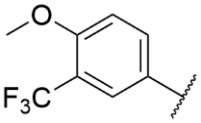	98.1 ± 0.3	2.6 ± 1.4

In summary, we optimized parent hit **1** in three different regions, with modifications in region B resulting

[a]Assays were performed in replicate as independent experiments ($n \geq 2$); values are shown as mean ± SD; n.d. = not determined.

in a significant increase in potency, while adjustments in parts A and C brought about two-fold improvement in activity compared to their respective parent compound. For region A, we found that the 3,4-dichloro substitution pattern (**12**) resulted in the best inhibitory activity. Replacement of the more flexible alkyl linker with a more rigid phenyl ring and positioning the carboxylic acid in *meta* position (**15**) in region B further enhanced the potency to the low micromolar range. Lastly, modifications in region C led to slight improvements, without a clear preference for a certain substituent or substitution pattern. These modifications eventually resulted in **22**, which exhibited the best potency in this series. We

therefore focused on our frontrunner compound **22** for further exploration of the biological potential of the compound class.

2.3 Biological Evaluation

2.3.1. Antimicrobial profiling

We evaluated our frontrunner for its antibacterial activity against a panel of Gram-positive pathogens of relevance. *Enterococcus faecalis* and *E. faecium* are among the most frequent causative agents of hospital-acquired infections, resulting in a wide range of infections, including infections of the urinary tract, bloodstream, and endocardium.[15] While, *Streptococcus pneumonia*e is the leading cause of pneumonia, especially in elderly and children under five years of age, and poses a great threat to public health in low- and middle-income countries. Furthermore, both *E. faecium* and *S. pneumoniae* are on the World Health Organization's priority list for research and development of new antibiotics.[16] Compound **22** demonstrated a minimum inhibitory concentration (MIC) of 4 µM against *E. faecalis* and *E. faecium*. Interestingly, the compound exhibited enhanced potency against a vancomycin-resistant strain of *E. faecium* (MIC = 2 µM). Even more promising results were obtained for *S. pneumoniae*, with **1** demonstrating full inhibition at a concentration ranging between 32 and 16 µM, while **22** achieved the same at a concentration between 0.5 and 1 µM. Additionally, **22** exhibited similar efficacy against a penicillin-resistant strain of *S. pneumoniae*, whereas **1** showed reduced potency against this strain.

In summary, our lead compound **22**, demonstrates significant growth inhibition of relevant strains of Gram-positive bacteria and their resistant variants. The superior activity of **22** compared to **1** suggests that this new class of ECF-T inhibitors has a high potential for further development as antibacterial agents.

Table 4. Whole-cell activity of **1** and **22** against relevant Gran-positive pathogens.

	MIC [µM][a]	
Strain	**1**	**22**
Enterococcus faecalis DSM-20477	>128	4
E. faecium DSM-20478	>128	4
E. faecium DSM-17050[b]	>128	2
Streptococcus pneumoniae DSM-20566	32 – 16	0.5 – 1
S. pneumoniae DSM-11865[c]	>128	0.5 – 1

[a]Assays were performed in replicate as independent experiments (n ≥ 2); values are shown as mean ± SD; [b]Vancomycin-resistant *Enterococcus faecium* strain; [c]Penicillin-resistant *Streptococcus pneumonia* strain; *Enterococcus faecalis*; Minimum inhibitory concentration (MIC).

3. Conclusions

During a screening of a proprietary compound library, we noticed the inhibitory activity of an oxaprozin derivative on folate uptake in *Lactobacillus casei*. With our initial hit in hand, we embarked on an SAR study to optimize the inhibitory activity of our hit and to achieve structural diversity. Ultimately, this led to frontrunner **22**, exhibiting low micromolar activity in the whole-cell and proteoliposome-based assays. Furthermore, **22** demonstrates promising growth inhibition of *E. faecalis*, *E. faecium* and *S. pneumonia*e, as well as of vancomycin-resistant *E. faecium* and penicillin-resistant *S. pneumoniae strains*. In summary, we discovered and optimized a potent inhibitor of ECF-T showing promising activity against a panel of clinically relevant Gram-positive pathogens.

4. Experimental section

4.1. General information

Starting materials and solvents were purchased from commercial suppliers, and used without further purification. All chemical yields refer to purified compounds and were not optimized. Column chromatography was performed using the automated flash chromatography system CombiFlash®Rf (Teledyne Isco) equipped with RediSepRf silica columns. Preparative RP-HPLC was performed either using an UltiMate 3000 Semi-Preparative System (Thermo Fisher Scientific) equipped with nucleodur®C18 Gravity (250 mm × 16 mm, 5 µm) column or using a Pure C-850 Flash/Prep (Buchi) equipped with Nucleodur C18 HTec (250 mm x 40 mm, particle size 5 µm). Low-resolution mass spectrometry and purity control of final compounds was carried out using an Ultimate 3000-MSQ LCMS system (Thermo Fisher Scientific) consisting of a pump, an autosampler, an MWD detector and an ESI quadrupole mass spectrometer. ^{1}H and ^{13}C NMR spectra were recorded as indicated on a Bruker Avance Neo 500 MHz (^{1}H, 500 MHz; ^{13}C, 126 MHz) with prodigy cryoprobe system. Chemical shifts were recorded as δ values in ppm units and referenced against the residual solvent peak (DMSO-*d6*, *δ*= 2.50, 39.52 and $CDCl_3$-*d1*: *δ*=7.26, 77.16). Splitting patterns describe apparent multiplicities and are designated as s (singlet), br s (broad singlet), d (doublet), dd (doublet of doublet), t (triplet), q (quartet), m (multiplet). Coupling constants (J) are given in Hertz (Hz). High-resolution mass spectra were recorded on a ThermoFisher Scientific (TF, Dreieich, Germany) Q Exactive Focus system equipped with heated electrospray ionization (HESI)-II source.

4.2. Chemistry

The synthesis and analysis of compounds (**3**–**5**, **7**–**9**, **11**–**15**) was reported elsewhere [13, 14].

Synthetic conditions of intermediate (**2**) can be found in the supporting information.

*4.2.1. General procedure 1 (GP-1) for the synthesis of **6** and **10***

To a round-bottomed flask, 4-methoxy-4-oxobutanoic acid (1.5 equiv), trimethylamine (2.2 equiv) and acetone were added (100 mL). The solution was stirred at room temperature for 15 min, after which, the respective 2-bromo-1-phenylethan-1-one (1 equiv) was added, and the solution was stirred at room temperature overnight. Subsequently, the solvent was removed *in vacuo*, the residue dissolved in CH_2Cl_2, washed with water (3x), dried over $MgSO_4$, filtered, and the solvent was removed *in vacuo*. Next, the solid was added to a dry crimp tube, which was charged with acetamide (7 equiv), boron trifluoride diethyl etherate (1.2 equiv) and dry ACN (15 mL). Next, the vial was capped, and the solution was stirred at 120 °C overnight. Afterwards, H_2O (20 mL) was added, and the resulting solution was extracted with a mixture of $CHCl_3$/propanol (3:1, 3x15 mL). The organic fractions were combined, dried over $MgSO_4$, filtered, and the solvent removed *in vacuo*. The residue was partially purified using flash chromatography using DCM/MeOH as eluent in a gradient (100% to 95% CH_2Cl_2). The combined fractions were dried, and the solid was added to a flask containing acetic acid (15 mL) and *N*-bromosuccinimide (1.2 equiv). The resulting solution was stirred at 80 °C for 2 h. Next, water (20 mL) was added, and the mixture was filtered. The collected precipitate was washed with water (3x) and dried at room temperature overnight. The residue was then added to a microwave vial containing phenylboronic acid (1.2 equiv) and $CsCO_3$ (2.2 equiv) in a degassed solution of 1,4-dioxane and water (9/1). Next, [Pd(dppf)Cl_2] (0.01 equiv) was added, and the resulting solution was stirred in the microwave at 110 °C for 45 min, after which, more phenylboronic acid (1.2 equiv) was added. The mixture was stirred at 110 °C in the microwave for 45 min. Subsequently, the solution was filtered; to the filtrate, an aqueous solution of LiOH was added (0.5 mL, 2 N), and the resulting solution was stirred at room temperature overnight. Next, the solution was neutralized by the addition of an aqueous solution of HCl (1 N). Water (20 mL) was added, and the resulting mixture was extracted with DCM (3x, 15 mL), dried over $MgSO_4$, filtered, solvent removed *in vacuo*, and the residue was purified by preparative HPLC affording the title compound.

*4.2.2. General procedure 2 (GP-2) for the synthesis of **16** and **17***

To a round-bottomed flask, the respective carboxylic acid (1 equiv), trimethylamine (2.2 equiv) and acetone were added (100 mL). The solution was stirred at room temperature for 15 min, after which, 2-bromo-1-(3,4-dichlorophenyl)ethan-1-one (1.2 equiv) was added, and the solution was stirred at room

temperature overnight. Subsequently, the solvent was removed *in vacuo*, the residue dissolved with CH_2Cl_2, washed with water (3x) dried over $MgSO_4$, filtered, and the solvent was removed *in vacuo*. Next, the solid was added to a dry crimp tube and acetamide (7 equiv), boron trifluoride diethyl etherate (1.2 equiv) and dry ACN (15 mL) were added. Next, the vial was capped, and the solution was stirred at 120 °C overnight. H_2O (20 mL) was added, and the resulting solution was extracted with a mixture of $CHCl_3$/propanol (3:1, 3x15 mL). The organic fractions were combined, dried over $MgSO_4$, filtered, and the solvent removed *in vacuo*. The combined fractions were dried, and the solid was added to a flask containing acetic acid (15 mL) and *N*-bromosuccinimide (1.2 equiv). The resulting solution was stirred at 80 °C for 2 h, after which, water (20 mL) was added, and the mixture was filtered. The collected precipitate was washed with water (3x), and dried at room temperature overnight. The residue was then added to a microwave vial containing phenylboronic acid (1.2 equiv) and $CsCO_3$ (2.2 equiv) in a degassed solution of 1,4-dioxane and water (9:1, 5 mL). Next, [Pd(dppf)Cl_2] (0.01 equiv) was added, and the resulting solution was stirred in the microwave at 110 °C for 45 min, after which, more phenylboronic acid (1.2 equiv) was added. The mixture was stirred at 110 °C in the microwave for 45 min. Subsequently, the solution was filtered; to the filtrate, an aqueous solution of LiOH was added (0.5 mL, 2 N), and the resulting solution was stirred at room temperature overnight. Next, the solution was neutralized by the addition of an aqueous solution of HCl (1 N). Water (20 mL) was added, and the resulting mixture was extracted with DCM (3x, 15 mL), dried over $MgSO_4$, filtered, the solvent removed *in vacuo*, and the residue was purified by preparative HPLC affording the title compound.

*4.2.3. General procedure 3 (GP-3) for the synthesis of **18–25***

To a microwave vial containing **II** (1 equiv), Cs_2CO_3 (2.2 equiv) and a degassed solution of 1,4-dioxane/water (9/1, 5 mL), the respective boronic acid was added (1.2 equiv). Next, [Pd(dppf)Cl_2] (0.01 equiv) was added, and the resulting solution was stirred in the microwave at 110 °C for 30 min, after which, more boronic acid (1.2 equiv) was added, and the mixture was again stirred at 110 °C in the microwave for 45 min. Subsequently, the solution was filtered; to the filtrate, an aqueous solution of LiOH was added (0.5 mL, 2 N), and the resulting solution was stirred at room temperature overnight. Next, the solution was neutralized by the addition of an aqueous solution of HCl (1 N). Water (20 mL) was added, and the resulting mixture was extracted with CH_2Cl_2 (3x15 mL), dried over $MgSO_4$, filtered, and the solvent removed *in vacuo*. The residue was purified by preparative HPLC affording the title compound.

4.2.4. 3-(4-(4-Chlorophenyl)-5-phenyloxazol-2-yl)propanoic acid (**1**)

A flask was charged with succinic acid (0.2 g, 1.7 mmol), trimethylamine (0.5 g, 5.1 mmol) and acetone (20 mL), and the resulting solution was stirred at room temperature for 30 min, after which, 2-bromo-4'-chloroacetophenone (0.4 g, 1.7 mmol) was added. The mixture was stirred at room temperature for 3 h, after which, water (20 mL) was added, and the solution was made slightly basic by the addition of an aqueous solution of NaOH (1N, 2 mL). Next, CH_2Cl_2 (20 mL) was added, and the resulting mixture was extracted (3x), the water fraction was acidified by the addition of an aqueous solution of HCl (1N, 10 mL) and was extracted (3x) by a mixture of $CHCl_3$/propanol (3:1, 3x15 mL). The resulting organic fractions were washed with saturated aqueous NaCl solution, dried over $MgSO_4$, filtered, and solvent was removed *in vacuo*. The residue was then added to a crimp vail containing acetamide (0.5 g, 8.6 mmol) and boron trifluoride diethyl etherate (0.2 g, 1.7 mmol). The tube was capped and mixed under neat conditions overnight at 100 °C. Next, water was added, and the solution was made slightly basic by the addition of an aqueous solution of NaOH (1N, 2 mL). Next CH_2Cl_2 was added, and the resulting mixture was extracted (3x), the water fraction was acidified by the addition of an aqueous solution of HCl (1 N, 10 mL) and was extracted with a mixture of $CHCl_3$/propanol (3:1, 3x15 mL). The resulting organic fractions were washed with saturated aqueous NaCl solution, dried over $MgSO_4$, filtered, and the solvent was removed *in vacuo*. Next, chloroform (3 mL) and *N*-bromosuccinimide (0.1 g, 0.6 mmol) were added, and the resulting mixture was stirred at reflux for 2 h after which, water was added. The resulting mixture was made slightly basic by the addition of an aqueous solution of NaOH (1 N, 2 mL). Next, EtOAc was added, and the resulting mixture was extracted (3x), the water fraction was acidified by the addition of an aqueous solution of HCl (1 N, 10 mL) and was extracted (3x) by a mixture of $CHCl_3$/propanol (3:1, 3x15 mL). The resulting organic fractions were washed with saturated aqueous NaCl solution, dried over $MgSO_4$, filtered, and the solvent was removed *in vacuo*. The solid was added to a degassed solution of 1,4-dioxane/H_2O (4:1, 20 mL) containing Na_2CO_3 (0.1 g, 1.3 mmol) and

phenylboronic acid (0.1 g, 0.4 mmol). Polymer-bound [Pd[(C_6H_5)$_3$P]$_4$] (0.01 g) was added, and the reaction mixture was stirred overnight at 100 °C. Next, an aqueous solution of HCl (1 N, 25 mL) was added, and the resulting mixture was extracted (3x) with a mixture of $CHCl_3$/propanol (3:1, 3x15 mL). The combined organic fractions were washed with saturated aqueous NaCl solution, dried over $MgSO_4$, filtered, and dried *in vacuo*. The residue was purified using preparative RP-HPLC, affording **1** as a white solid (0.01 g, 2% yield). ^{1}H NMR (500 MHz, DMSO-*d6*) δ = 12.35 (br s, 1H), 7.88 (d, *J* = 8.5 Hz, 1H), 7.56 (d, *J* = 8.5 Hz, 1H), 7.58 – 7.54 (m, 1H), 3.04 – 2.99 (m, 1H), 2.76 – 2.72 (m, 1H). ^{13}C NMR (126 MHz, DMSO-*d6*) δ = 173.5, 163, 145.3, 133.5, 133, 131.2, 129.4, 129.3, 129.1, 128.5, 126.9, 30.6, 23.3. HRMS (ESI+) calculated for $C_{18}H_{15}ClNO_3$ [M+H]$^+$ 328.06622, found 328.07302. Purity by HPLC = 100%.

4.2.4. 3-(5-(4-Cyanophenyl)-4-phenyloxazol-2-yl)propanoic acid. (**6**)**.**

According to GP-1, using 4-(2-bromoacetyl)benzonitrile (0.4 g, 1.79 mmol) afforded after purification by preparative HPLC **6** as a white solid (0.01g, 2% yield). ^{1}H NMR (500 MHz, $CDCl_3$-*d*) δ = 7.77 (d, *J* = 8.2 Hz, 2H), 7.63 (d, *J* = 8.2 Hz, 2H), 7.57 – 7.52 (m, 2H), 7.44 – 7.39 (m, 3H), 3.25 – 3.16 (m, 2H), 3.03 – 2.93 (m, 2H). ^{13}C NMR (126 MHz, $CDCl_3$-*d*) δ = 176.5, 162.5, 147.6, 137, 133.5, 132.6, 129.7, 129.2, 128.4, 128.3, 127.3, 119, 111.6, 30.8, 23.4. HRMS (ESI+) calculated for $C_{19}H_{15}N_2O_3$ [M+H]$^+$ 319.10044, found 319.10768. Purity by HPLC = 100%.

4.2.5. 3-(4-(3,5-Dichlorophenyl)-5-phenyloxazol-2-yl)propanoic acid (**10**).

According to GP-1, using 2-bromo-1-(3,5-dichlorophenyl)ethan-1-one (0.45 g, 1.68 mmol), affording after purification by preparative HPLC **10** as a white solid (0.01g, 2% yield). ^{1}H NMR (500 MHz, $CDCl_3$-*d*) δ = 7.56 (d, *J* = 1.8 Hz, 1H), 7.55 – 7.53 (m, 3H), 7.44 – 7.39 (m, 3H), 7.31 (t, *J* = 1.8 Hz, 1H), 3.24 – 3.16 (m, 2H), 3.02 – 2.95 (m, 2H). ^{13}C NMR (126 MHz, $CDCl_3$-*d*) δ = 176.9, 162.2, 147, 135.4, 132.7, 129.6, 129.2, 128.3, 127.1, 126.2, 30.8, 23.4. HRMS (ESI+) calculated for $C_{18}H_{14}Cl_2NO_3$ [M+H]$^+$ 362.02725, found 362.01485. Purity by HPLC = 99%.

4.2.6. 2-(4-(3,4-Dichlorophenyl)-5-phenyloxazol-2-yl)benzoic acid (**16**)

According to GP-2, using 2-(methoxycarbonyl)benzoic acid (0.4 g, 1.49 mmol), affording after purification by preparative HPLC **16** as a white solid (0.01 g, 2% yield). ^{1}H NMR (500 MHz, $CDCl_3$-*d*) δ = 8.48 (dd, *J* = 7.7, 1.0 Hz, 1H), 8.23 (dd, *J* = 7.8, 1.1 Hz, 1H), 7.80 (d, *J* = 1.8 Hz, 1H), 7.74 – 7.70 (m, 1H), 7.69 – 7.63 (m, 3H), 7.62 – 7.62 (m, 1H), 7.54 – 7.50 (m, 1H), 7.49 – 7.45 (m, 4H). ^{13}C NMR (126 MHz, $CDCl_3$-*d*) δ = 167.3, 159.6, 147.3, 134.5, 133.3, 133.1, 132.4, 132.4–132.3 (m, 1C), 131.5, 130.9, 130.4, 130.3, 130.2, 129.4, 129.3, 129.2, 127.1, 127, 126.8, 123.9. HRMS (ESI+) calculated for $C_{22}H_{14}Cl_2NO_3$ [M+H]$^+$ 410.02725, found 410.003459. Purity by HPLC: 100%

4.2.7. 4-(4-(3,4-Dichlorophenyl)-5-phenyloxazol-2-yl)picolinic acid (**17**)

According to GP-2, using 2-(methoxycarbonyl)isonicotinic acid (0.5 g, 2.76 mmol), affording after purification by preparative HPLC **17** as a yellowish solid (0.1 g, 1% yield). ^{1}H NMR (500 MHz, $CDCl_3$-*d*) δ = 8.91 – 8.87 (m, 1H), 8.79 (br d, J = 4.9 Hz, 1H), 8.29 (br d, J = 4.4 Hz, 1H), 7.90 (d, J = 1.2 Hz, 1H), 7.72 – 7.65 (m, 2H), 7.56 (dd, J = 8.3, 1.4 Hz, 1H), 7.53 – 7.45 (m, 4H). ^{13}C NMR (126 MHz, $CDCl_3$-*d*) δ = 163.7, 156.8, 149, 136.6, 135.5, 133.1, 132.8, 131.6, 130.7, 130.1, 129.8, 129.2, 127.4, 127.2, 126.9, 123.9, 120.1. HRMS (ESI+) calculated for $C_{21}H_{13}Cl_2N_2O_3$ [M+H]$^+$ 411.02250, found 411.03005. Purity by HPLC: 100%.

4.2.8. 3-(5-(4-Cyanophenyl)-4-(3,4-dichlorophenyl)oxazol-2-yl)benzoic acid (**18**).

According to GP-3, using (4-cyanophenyl)boronic acid (0.02g, 0.14 mmol), affording after purification by preparative HPLC **18** as a white solid (0.01 g, 15% yield). ^{1}H NMR (500 MHz, DMSO-*d6*) δ = 8.65 – 8.62 (m, 1H), 8.38 (d, *J* = 7.8 Hz, 1H), 8.14 (d, *J* = 7.6 Hz, 1H), 7.99 – 7.96 (m, 2H), 7.93 (d, *J* = 1.8 Hz, 1H), 7.89 (d, *J* = 8.2 Hz, 2H), 7.78 – 7.71 (m, 2H), 7.63 (dd, *J* = 8.4, 1.7 Hz, 1H). ^{13}C NMR (126 MHz, DMSO-*d6*) δ = 166.2, 159.5, 144.5, 135.8, 132.8, 131.6, 131.6, 131.5, 131.4, 131.3, 131, 129.4, 127.7, 126.8, 126.6, 118.1, 111.1, 54.6. HRMS (ESI+) calculated for $C_{23}H_{13}Cl_2N_2O_3$ [M+H]$^+$ 435.02250, found 435.02912. Purity by HPLC: 98%.

4.2.9. 3-(4-(3,4-Dichlorophenyl)-5-(4-methoxyphenyl)oxazol-2-yl)benzoic acid (**19**).

According to GP-3, using (4-methoxyphenyl)boronic acid (0.03 g, 0.21 mmol), affording after purification by preparative HPLC **19** as a white solid (0.1 g, 27% yield). ^{1}H NMR (500 MHz, DMSO-*d6*) δ = 8.59 (s, 1H), 8.32 (d, *J* = 7.8 Hz, 1H), 8.11 (d, *J* = 7.8 Hz, 1H), 7.89 (d, *J* = 2.0 Hz, 1H), 7.74 – 7.69 (m, 2H), 7.64 (d, *J* = 8.7 Hz, 2H), 7.63 – 7.60 (m, 1H), 7.10 (d, *J* = 8.9 Hz, 2H), 3.83 (s, 3H). ^{13}C NMR (126 MHz, DMSO-*d6*) δ = 167.3–166.9 (m, 1C), 159, 147.4, 133, 132.1, 131.9, 131.6, 131.2, 130.6, 130.3, 129.4, 127.7, 127.2, 127.1, 120.2, 115.2. HRMS (ESI+) calculated for $C_{23}H_{16}Cl_2NO_4$ $[M+H]^+$ 440.03781, found 440.04358. Purity by HPLC: 100%.

4.2.10. 3-(4-(3,4-Dichlorophenyl)-5-(4-(trifluoromethyl)phenyl)oxazol-2-yl)benzoic acid (**20**).

According to GP-3, using (4-(trifluoromethyl)phenyl)boronic acid (0.03g, 0.14 mmol), affording after purification by preparative HPLC **20** as a white solid (0.01 g, 8% yield). ^{1}H NMR (500 MHz, DMSO-*d6*) δ = 8.63 (s, 1H), 8.34 (br d, *J* = 7.6 Hz, 1H), 8.13 (d, *J* = 7.8 Hz, 1H), 7.94 – 7.90 (m, 3H), 7.90 – 7.86 (m, 2H), 7.76 (d, *J* = 8.4 Hz, 1H), 7.73 – 7.69 (m, 1H), 7.64 (dd, *J* = 8.4, 1.8 Hz, 1H). ^{13}C NMR (126 MHz, DMSO-*d6*) δ = 166.8, 160, 135.7, 132.2, 132, 131.9, 131.7, 131.6, 131.4, 129.8, 129.8, 128.1, 127.5, 127.1, 126.4, 126.3, 55.1. ^{19}F NMR (470 MHz, DMSO-*d6*) δ = -61.3 (s). HRMS (ESI+) calculated for $C_{23}H_{13}Cl_2F_3NO_3$ $[M+H]^+$ 478.01463, found 478.02262. Purity by HPLC: 98%.

4.2.11. 3-(5-(4-Chlorophenyl)-4-(3,4-dichlorophenyl)oxazol-2-yl)benzoic acid (**21**).

According to GP-3, using (4-chlorophenyl)boronic acid (0.03 g, 0.21 mmol), affording after purification by preparative HPLC **21** as a white solid (0.01 g, 12% yield). ^{1}H NMR (500 MHz, DMSO-*d6*) δ = 8.62 – 8.60 (m, 1H), 8.35 – 8.32 (m, 1H), 8.14 – 8.10 (m, 1H), 7.91 – 7.89 (m, 1H), 7.75 – 7.70 (m, 4H), 7.63 – 7.58 (m, 3H). ^{13}C NMR (126 MHz, DMSO-*d6*) δ = 167.1, 159.7, 146, 134.8, 134.7, 132.6, 132.2, 132.1, 131.7, 131.7, 130.6, 130.2, 129.8, 129.8, 129.2, 128.1, 127.2, 126.9, 126.8. HRMS (ESI+) calculated for $C_{22}H_{13}Cl_3NO_3$ $[M+H]^+$ 443.98828, found 443.99533. Purity by HPLC: 95%

4.2.12. 3-(4-(3,4-Dichlorophenyl)-5-(3-(trifluoromethyl)phenyl)oxazol-2-yl)benzoic acid (**22**).

According to GP-3, using (3-(trifluoromethyl)phenyl)boronic acid (0.03 g, 0.14 mmol), affording after purification by preparative HPLC **22** as a white solid (0.02 g, 35% yield). ^{1}H NMR (500 MHz, DMSO-*d6*) δ = 8.63 (s, 1H), 8.39 (d, *J* = 7.8 Hz, 1H), 8.13 (d, *J* = 7.8 Hz, 1H), 8.04 (s, 1H), 7.99 (d, *J* = 7.8 Hz, 1H), 7.91 (d, *J* = 1.8 Hz, 1H), 7.86 (d, *J* = 7.9 Hz, 1H), 7.78 – 7.71 (m, 3H), 7.63 (dd, *J* = 8.4, 1.8 Hz, 1H). ^{13}C NMR (126 MHz, DMSO-*d6*) δ = 166.2, 159.2, 144.7, 134.6, 131.6, 131.4, 131.4, 131, 130.9, 130.5, 130.1, 130.1, 129.5, 128.9, 128.2, 127.4, 126.6, 126.1, 54.6. ^{19}F NMR (470 MHz, DMSO-*d6*) δ = -61.39 (s). HRMS (ESI+) calculated for $C_{23}H_{13}Cl_2F_3NO_3$ $[M+H]^+$ 478.01463, found 478.02030. Purity by HPLC: 100%.

4.2.13. 3-(4-(3,4-Dichlorophenyl)-5-(m-tolyl)oxazol-2-yl)benzoic acid (**23**).

According to GP-3, using *m*-tolylboronic acid (0.02 g, 0.14 mmol), affording after purification by preparative HPLC **23** as a white solid (0.02 g, 30% yield). ^{1}H NMR (500 MHz, DMSO-*d6*) δ = 8.60 (s, 1H), 8.34 (d, *J* = 7.8 Hz, 1H), 8.12 (d, *J* = 7.8 Hz, 1H), 7.90 (d, *J* = 2.0 Hz, 1H), 7.74 – 7.70 (m, 2H), 7.63 (dd, *J* = 8.5, 1.9 Hz, 1H), 7.57 (s, 1H), 7.48 – 7.45 (m, 1H), 7.43 – 7.39 (m, 1H), 7.34 – 7.31 (m, 1H), 2.39 – 2.36 (m, 3H). ^{13}C NMR (126 MHz, DMSO-*d6*) δ = 166.6, 158.9, 146.8, 138.7, 133.6, 132.4, 131.5, 131.1, 130.9, 130.5, 130.2, 129.8, 129.1, 129, 127.5, 127.4, 127.4, 126.7, 126.6, 124.3, 54.9, 20.9 HRMS (ESI+) calculated for $C_{23}H_{16}Cl_2NO_3$ $[M+H]^+$ 424.04290, found 424.04891. Purity by HPLC: 99%.

4.2.14. 3-(4-(3,4-Dichlorophenyl)-5-(3,5-dichlorophenyl)oxazol-2-yl)benzoic acid (**24**).

According to GP-3, using 3,5-dichlorophenyl)boronic acid (0.03 g, 0.14 mmol), affording after purification by preparative HPLC **24** as a white solid (0.01 g, 4% yield). ^{1}H NMR (500 MHz, DMSO-*d6*) δ =13.40 (br s, 1H), 8.64 (s, 1H), 8.41 (br d, *J* = 7.6 Hz, 1H), 8.14 (br d, *J* = 7.8 Hz, 1H), 7.96 – 7.90 (m, 1H), 7.80 – 7.69 (m, 5H), 7.69 – 7.58 (m, 1H), 7.58 – 7.58 (m, 1H). ^{13}C NMR (126 MHz, DMSO-*d6*) δ = 167.1, 160.2 – 160.1 (m, 1C), 144.2, 136.1, 135.4, 132.4, 132.2, 132.2, 132, 131.7, 131.3, 131, 130.3, 130, 129.4, 128.3, 127.5, 126.8, 125.8. HRMS (ESI+) calculated for $C_{22}H_{12}Cl_4NO_3$ $[M+H]^+$ 479.94635, found: 479.95290. Purity by HPLC: 100%.

4.2.15. 3-(4-(3,4-Dichlorophenyl)-5-(4-methoxy-3-(trifluoromethyl)phenyl)oxazol-2-yl)benzoic acid (**25**).

According to GP-3, using (4-methoxy-3-(trifluoromethyl)phenyl)boronic acid (0.03 g, 0.14 mmol), affording after purification by preparative HPLC **25** as a white solid (0.03 g, 57% yield). ^{1}H NMR (500 MHz, DMSO-*d6*) δ = 8.61 (s, 1H), 8.35 (d, *J* = 7.8 Hz, 1H), 8.12 (d, *J* = 7.8 Hz, 1H), 7.96 – 7.88 (m, 3H), 7.74 – 7.69 (m, 2H), 7.61 (dd, *J* = 8.3, 1.9 Hz, 1H), 7.43 (d, *J* = 8.7 Hz, 1H), 3.97 (s, 3H) ^{13}C NMR (126 MHz, DMSO-*d6*) δ = 166.8, 159.1, 158, 145.6, 133.7, 133.3, 132.3, 132.1, 131.8, 131.7, 131.3, 131.2, 130.4, 130, 129.2, 127.6, 127.6, 126.9, 126.7, 125.8, 125.7, 119.8, 114, 56.7, 55.1. ^{19}F NMR (470 MHz, DMSO-*d6*) δ = -61.25 (s). HRMS (ESI+) calculated for $C_{24}H_{15}Cl_2F_3NO_4$ $[M+H]^+$ 508.02520, found 508.03169. Purity by HPLC: 98%.

4.3. Biological assays

4.3.1. ECF-FolT inhibition assay.

This assay was performed based on the protocol reported by Bousis *et al.* with minor modifications. [8]

4.3.2. *Uptake assay into proteoliposome*

This assay was performed based on the protocol reported by Swier *et al.* with minor modifications. [17]

4.3.3. Screening against clinically relevant Gram-positive pathogens.

All microorganisms were obtained from the German Collection of Microorganisms and Cell Cultures (DSMZ) and were handled according to standard procedures. Bacteria were inoculated into tryptic soy broth (TSB) to obtain a final inoculum of 105 colony-forming units (CFU)/mL. The tested compounds were prepared as DMSO stocks (20 mM). Serial dilutions of derivatives in the growth medium (0.06 to 128 µM) were prepared in sterile 96-well plates, and the bacterial suspensions were added. Growth inhibition was assessed after static incubation at 37 °C for 24 h. *S. pneumoniae* was grown at 5% CO_2. MIC values are defined as the lowest compound concentration where no visible growth is observed.

Author's contributions:

Daan Willocx, Mostafa Hamed, Ewgenij Proschak and Anna K. H. Hirsch coordinated the project; Synthesis and characterization of the compounds was performed by Daan Willocx and Felix F. Lillich. Biochemical evaluation of derivatives regarding inhibitory activity was performed by Aleksei Tsarenko; Whole-cell assay was performed by Jeannine Jung. Screenings against Gram-positive bacteria were performed by Viktoria George. Daan Willocx wrote the manuscript. The manuscript was written through contributions of all authors. All authors have given approval to the final version of the manuscript.

Declaration of competing interest

The authors declare no conflicts of interest.

Acknowledgements

We gratefully acknowledge funding from the European Union's Horizon 2020 research and innovation programme under the Marie Skłodowska-Curie grant agreement No 860816 MepAnti (to A.K.H.Hirsch). we acknowledge Simone Amann, Jeannine Jung, Jannine Seelbach, and Viktoria George for performing the biological evaluation of the compounds

Appendix A. Supplementary data.

Supplementary data to this article can be found online

Abbreviations

ABC, ATP-binding cassette; AMR, antimicrobial resistance; ECF, energy-coupling factor; MIC, minimum inhibitory concentration; NBS, *N*-Bromosuccinimide; SAR, structure–activity relationship.

References

[1] H.D. Marston, D.M. Dixon, J.M. Knisely, T.N. Palmore, A.S. Fauci, Antimicrobial Resistance, JAMA, 316 (2016) 1193.
[2] V.M. D'Costa, C.E. King, L. Kalan, M. Morar, W.W.L. Sung, C. Schwarz, D. Froese, G. Zazula, F. Calmels, R. Debruyne, G.B. Golding, H.N. Poinar, G.D. Wright, Antibiotic resistance is ancient, Nature, 477 (2011) 457-461.
[3] M.A. Salam, M.Y. Al-Amin, M.T. Salam, J.S. Pawar, N. Akhter, A.A. Rabaan, M.A.A. Alqumber, Antimicrobial Resistance: A Growing Serious Threat for Global Public Health, Healthcare, 11 (2023) 1946.
[4] K.W.K. Tang, B.C. Millar, J.E. Moore, Antimicrobial Resistance (AMR), British Journal of Biomedical Science, 80 (2023).
[5] A. Cassini, L.D. Högberg, D. Plachouras, A. Quattrocchi, A. Hoxha, G.S. Simonsen, M. Colomb-Cotinat, M.E. Kretzschmar, B. Devleesschauwer, M. Cecchini, D.A. Ouakrim, T.C. Oliveira, M.J. Struelens, C. Suetens, D.L. Monnet, R. Strauss, K. Mertens, T. Struyf, B. Catry, K. Latour, I.N. Ivanov, E.G. Dobreva, A. Tambic Andraševic, S. Soprek, A. Budimir, N. Paphitou, H. Žemlicková, S. Schytte Olsen, U. Wolff Sönksen, P. Märtin, M. Ivanova, O. Lyytikäinen, J. Jalava, B. Coignard, T. Eckmanns, M. Abu Sin, S. Haller, G.L. Daikos, A. Gikas, S. Tsiodras, F. Kontopidou, Á. Tóth, Á. Hajdu, Ó. Guólaugsson, K.G. Kristinsson, S. Murchan, K. Burns, P. Pezzotti, C. Gagliotti, U. Dumpis, A. Liuimiene, M. Perrin, M.A. Borg, S.C. De Greeff, J.C. Monen, M.B. Koek, P. Elstrøm, D. Zabicka, A. Deptula, W. Hryniewicz, M. Caniça, P.J. Nogueira, P.A. Fernandes, V. Manageiro, G.A. Popescu, R.I. Serban, E. Schréterová, S. Litvová, M. Štefkovicová, J. Kolman, I. Klavs, A. Korošec, B. Aracil, A. Asensio, M. Pérez-Vázquez, H. Billström, S. Larsson, J.S. Reilly, A. Johnson, S. Hopkins, Attributable deaths and disability-adjusted life-years caused by infections with antibiotic-resistant bacteria in the EU and the European Economic Area in 2015: a population-level modelling analysis, The Lancet Infectious Diseases, 19 (2019) 56-66.
[6] D.G. Rudmann, On-target and Off-target-based Toxicologic Effects, Toxicologic Pathology, 41 (2013) 310-314.
[7] S. Bousis, I. Setyawati, E. Diamanti, D.J. Slotboom, A.K.H. Hirsch, Energy-Coupling Factor Transporters as Novel Antimicrobial Targets, Advanced Therapeutics, 2 (2019) 1800066.
[8] S. Bousis, S. Winkler, J. Haupenthal, F. Fulco, E. Diamanti, A.K.H. Hirsch, An Efficient Way to Screen Inhibitors of Energy-Coupling Factor (ECF) Transporters in a Bacterial Uptake Assay, in: International Journal of Molecular Sciences, 2022.
[9] D.J. Slotboom, Structural and mechanistic insights into prokaryotic energy-coupling factor transporters, Nature Reviews Microbiology, 12 (2014) 79-87.
[10] E. Diamanti, I. Setyawati, S. Bousis, L. Mojas, L. Swier, J. Haupenthal, P. Gibson, C. Volz, W. Stanek, M. Jaeger, J. Herrmann, J.-W. Veening, R. Müller, D.J. Slotboom, A.K.H. Hirsch, Discovery of Antibacterial Agents Inhibiting the Energy-Coupling Factor (ECF) Transporters by Structure-Based Virtual Screening, in, American Chemical Society (ACS), 2020.
[11] A.F. Kiefer, S. Bousis, M.M. Hamed, E. Diamanti, J. Haupenthal, A.K.H. Hirsch, Structure-Guided Optimization of Small-Molecule Folate Uptake Inhibitors Targeting the Energy-Coupling Factor Transporters, Journal of Medicinal Chemistry, 65 (2022) 8869-8880.
[12] E. Diamanti, I. Setyawati, S. Bousis, P.C.T. Souza, L. Mojas, L. Swier, J. Haupenthal, P. Gibson, C. Volz, W. Stanek, M. Jaeger, J. Herrmann, S. Marrink, J.-W. Veening, R. Müller, D.J. Slotboom, A.K.H. Hirsch, Targeting the energy-coupling factor (ECF) transporters: identification of new tool compounds, in, American Chemical Society (ACS), 2021.
[13] J.S. Kramer, S. Woltersdorf, T. Duflot, K. Hiesinger, F.F. Lillich, F. Knöll, S.K. Wittmann, F.-M. Klingler, S. Brunst, A. Chaikuad, C. Morisseau, B.D. Hammock, C. Buccellati, A. Sala, G.E. Rovati, M. Leuillier, S. Fraineau, J. Rondeaux, V. Hernandez-Olmos, J. Heering, D. Merk, D. Pogoryelov, D. Steinhilber, S. Knapp, J. Bellien, E. Proschak, Discovery of the First in Vivo Active Inhibitors of the Soluble Epoxide Hydrolase Phosphatase Domain, Journal of Medicinal Chemistry, 62 (2019) 8443-8460.
[14] S. Schierle, A. Chaikuad, F.F. Lillich, X. Ni, S. Woltersdorf, E. Schallmayer, B. Renelt, R. Ronchetti, S. Knapp, E. Proschak, D. Merk, Oxaprozin Analogues as Selective RXR Agonists with Superior Properties and Pharmacokinetics, Journal of Medicinal Chemistry, 64 (2021) 5123-5136.

[15] S. Brinkwirth, O. Ayobami, T. Eckmanns, R. Markwart, Hospital-acquired infections caused by enterococci: a systematic review and meta-analysis, WHO European Region, 1 January 2010 to 4 February 2020, Eurosurveillance, 26 (2021) 2001628.
[16] G.W.H. Organization, Prioritization of pathogens to guide discovery, research and development of new antibiotics for drug-resistant bacterial infections, including tuberculosis, in, 2017.
[17] L.J.Y.M. Swier, A. Guskov, D.J. Slotboom, Structural insight in the toppling mechanism of an energy-coupling factor transporter, Nature Communications, 7 (2016) 11072.

Graphical abstract

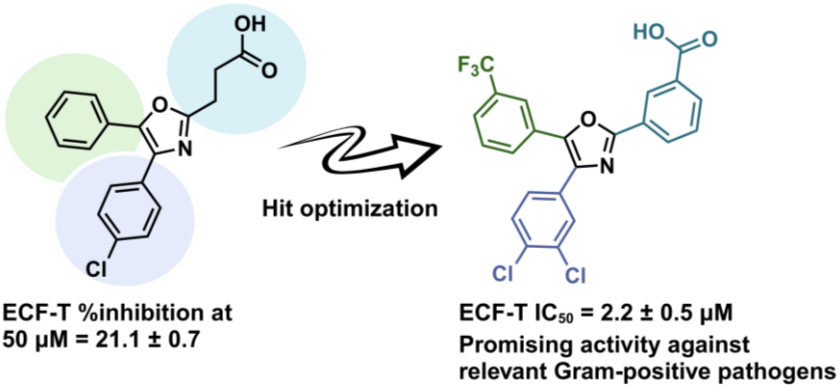

Supporting information

Oxaprozine Derivatives as Anti-Gram-Positive Agents Targeting Bacterial Energy-Coupling Factor Transporters

Daan Willocx,[a,b] Felix F. Lillich,[c] Ewgenij Proschak,[c] Aleksei Tsarenko,[d] Dirk J. Slotboom,[d] Mostafa M. Hamed,[a] Anna K. H. Hirsch[a,b,*]

[a]Helmholtz Institute for Pharmaceutical Research Saarland (HIPS)-Helmholtz Centre for Infection Research (HZI), Saarland University, Campus E8.1, 66123 Saarbrücken, Germany.

[b]Saarland University, Department of Pharmacy, Campus E8.1, 66123 Saarbrucken, Germany.

[c]Institute of Pharmaceutical Chemistry, Goethe-University Frankfurt, Max-von-Laue-Strasse 9, 60438 Frankfurt am Main, Germany

[d]Biomolecular Sciences and Biotechnology Institute, University of Groningen, Nijenborgh 4, 9747AG Groningen, The Netherlands

*Corresponding author: Anna.Hirsch@helmholtz-hips.de

Table of contents

Syntheses of intermediates

Methyl 3-(5-bromo-4-(3,4-dichlorophenyl)oxazol-2-yl)benzoate (**2**). A flask was charged with 3-(methoxycarbonyl)benzoic acid (1.0 g, 5.55 mmol), trimethylamine (1.24 g, 12.21 mmol) and acetone (20 mL), the resulting solution was stirred at room temperature for 30 min. Then, 2-bromo-1-(3,4-dichlorophenyl)ethan-1-one (1.78 g, 6.66 mmol) was added, and the mixture was stirred at room temperature overnight. The solvent was then removed *in vacuo*, and the residue was solubilized with CH_2Cl_2 (25 mL). Next, the solution was washed with water (3x 15 mL), dried over $MgSO_4$, filtered, and the solvent was removed *in vacuo*. The residue was then added to a crimp vail containing acetamide (0.82 g, 13.89 mmol), boron trifluoride diethyl etherate (0.47 g, 3.33 mmol) and acetonitrile (10 mL). The tube was capped and stirred at 120 °C overnight, after which, water was added, and the resulting solution was filtered. The precipitated was washed with water (3x 15 mL), dissolved in CH_2Cl_2 (25 mL) dried over $MgSO_4$, filtered, and the solvent was removed *in vacuo*, affording methyl 3-(4-(3,4-dichlorophenyl)oxazol-2-yl)benzoate as a brown solid (0.99 g, 51% crude yield). To a crimp vail containing methyl 3-(4-(3,4-dichlorophenyl)oxazol-2-yl)benzoate (0.99 g, 2.83 mmol) and acetic acid (10 mL), *N*-bromosuccinimide (0.66 g, 3.69 mmol) was added. The vial was capped, and the resulting solution was stirred at 80 °C for 2 h, after which, water (10 mL) was added, and the resulting mixture was filtered. The precipitate was washed with water (3x 15 mL), dissolved in CH_2Cl_2 (25 mL), dried over $MgSO_4$, filtered, and the solvent was removed *in vacuo* affording **2** as a light brown solid (0.96 g, 41% crude yield). ^{1}H NMR (500 MHz, CHLOROFORM-*d*) δ = 8.76–8.69 (m, 1H), 8.30–8.26 (m, 1H), 8.22–8.13 (m, 2H), 7.93 (dd, *J* = 8.4, 2.1 Hz, 1H), 7.64–7.57 (m, 1H), 7.54 (d, *J* = 8.4 Hz, 1H), 4.00 (s, 3H).

Uptake assay into proteoliposome

In this assay, the ECF transporter for folate (ECF-FolT2) from *Lactobacillus delbrueckii* was used and reconstituted into lipid vesicles known as proteoliposomes. Figure S exhibits the percentage of inhibition for each compound at 150 µM. In Figure S, folic acid uptake traces are shown. Mg-ATP and Mg-ADP were used as positive and negative controls, respectively. The differences in the uptake patterns for the 5 mM Mg-ATP control can be explained by how recently we purified the protein, as over time, the protein tends to lose its activity.[1]

^{1}H-NMR, ^{13}C-NMR Spectrum

1

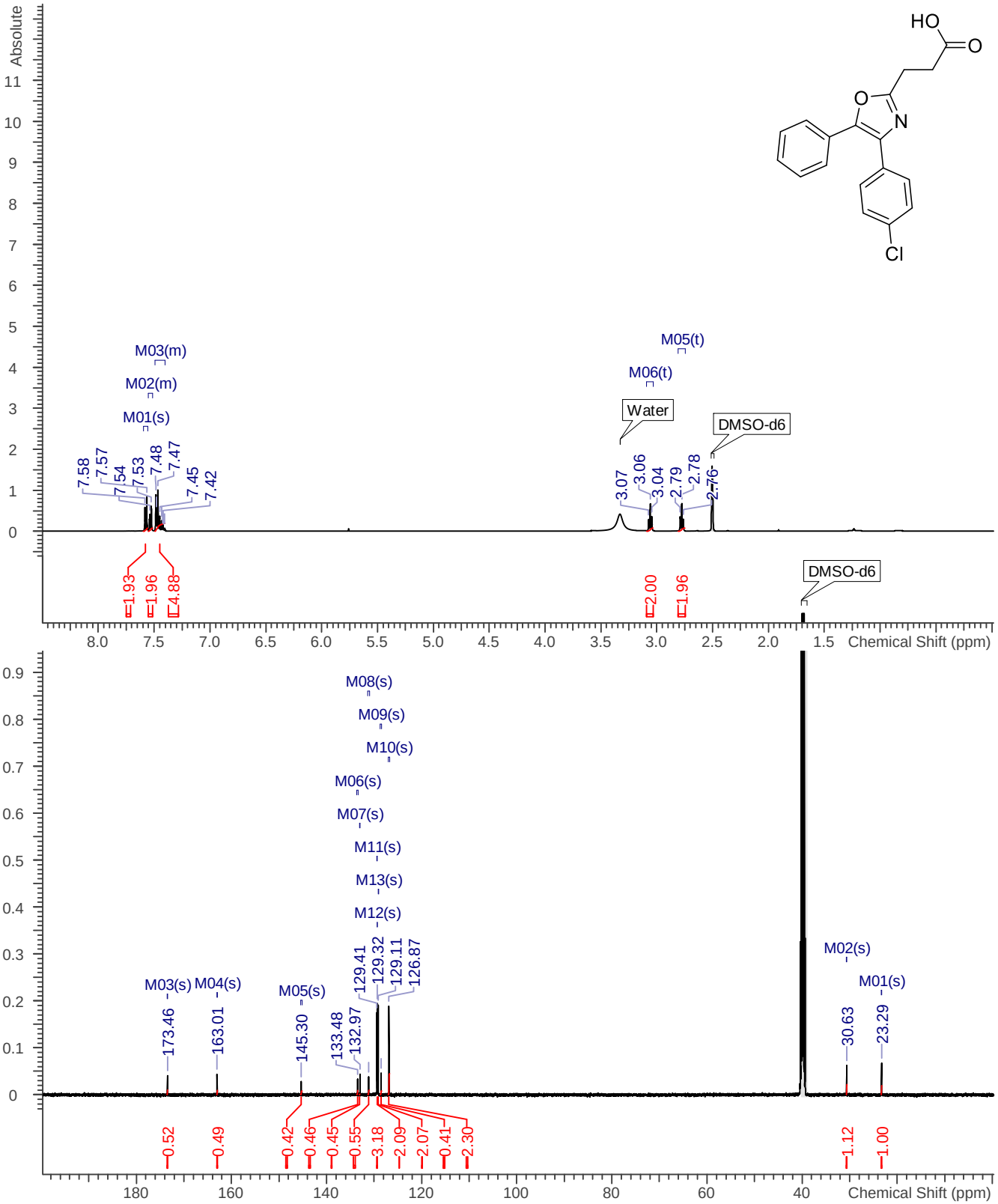

2

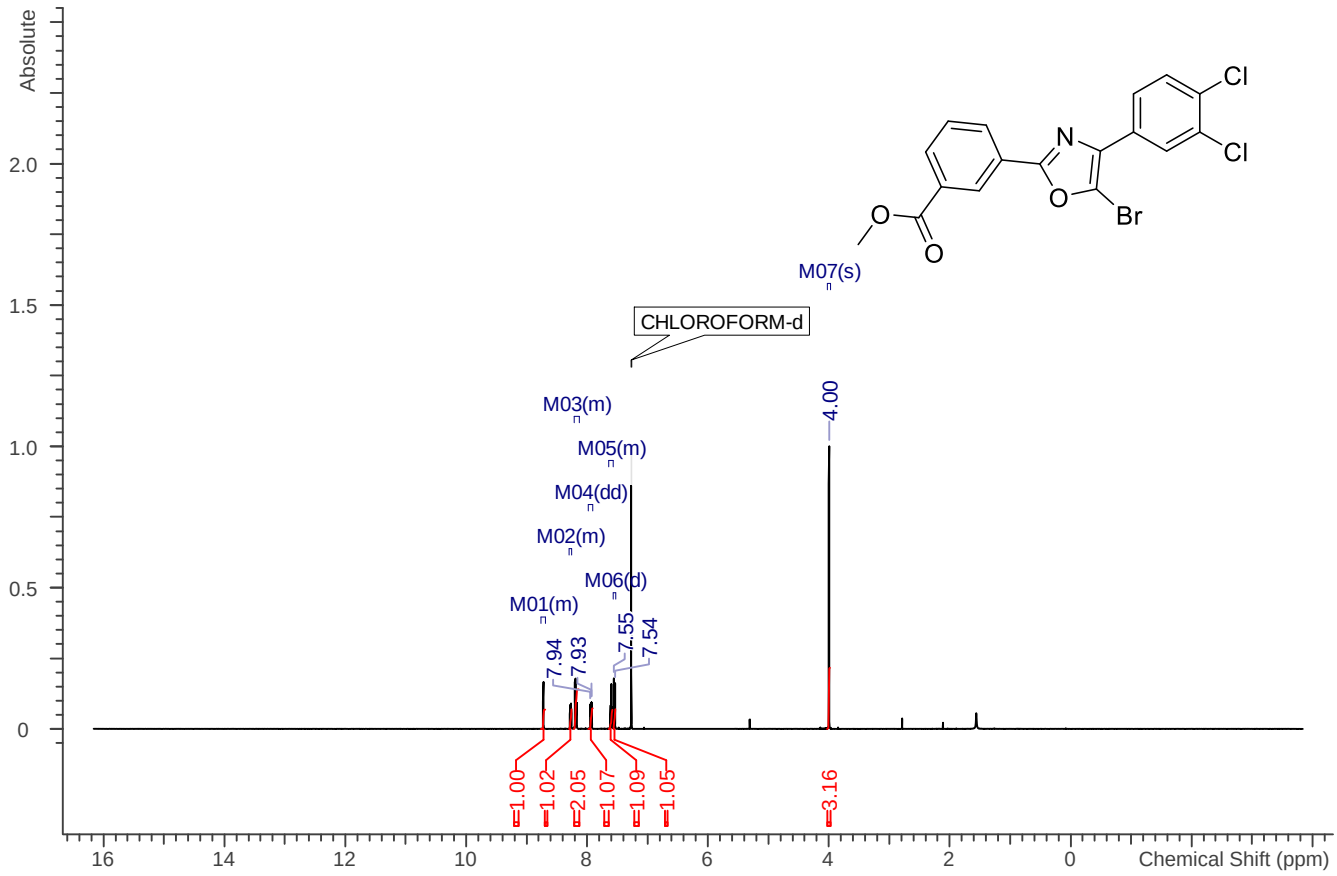
Absolute
2.0
1.5
1.0
0.5
0
16
14
12
10
8
6
4
2
0
Chemical Shift (ppm)
CHLOROFORM-d
M07(s)
M03(m)
M05(m)
M04(dd)
M02(m)
M06(d)
M01(m)
7.94
7.93
7.55
7.54
4.00
1.00
1.02
2.05
1.07
1.09
1.05
3.16
Cl
Cl
N
O
Br
O
O

6

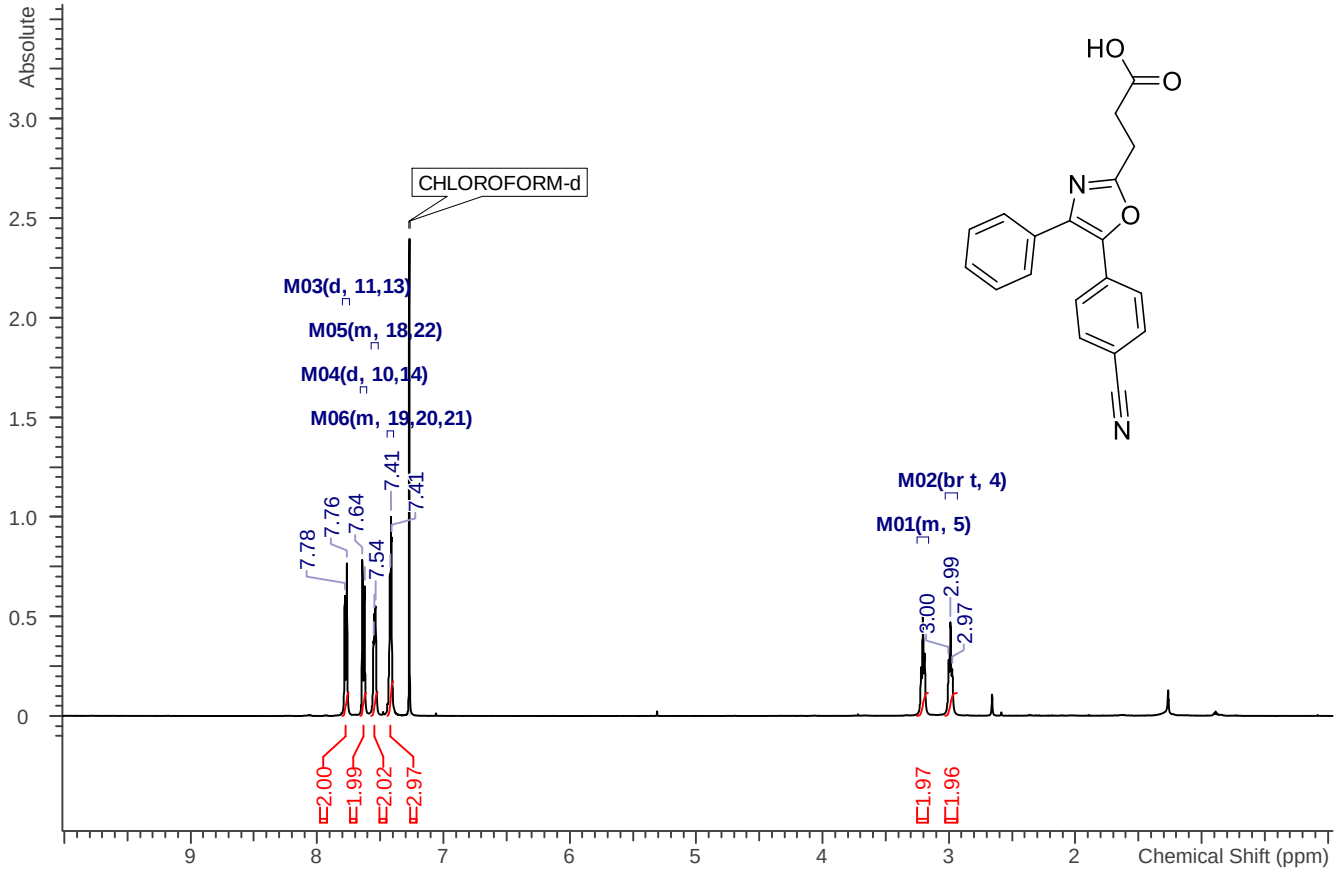
Absolute
CHLOROFORM-d
M03(d, 11,13)
M05(m, 18,22)
M04(d, 10,14)
M06(m, 19,20,21)
M02(br t, 4)
M01(m, 5)
7.78
7.76
7.64
7.54
7.41
7.41
3.00
2.99
2.97
2.00
1.99
2.02
2.97
1.97
1.96
Chemical Shift (ppm)
HO
O
N
O
N

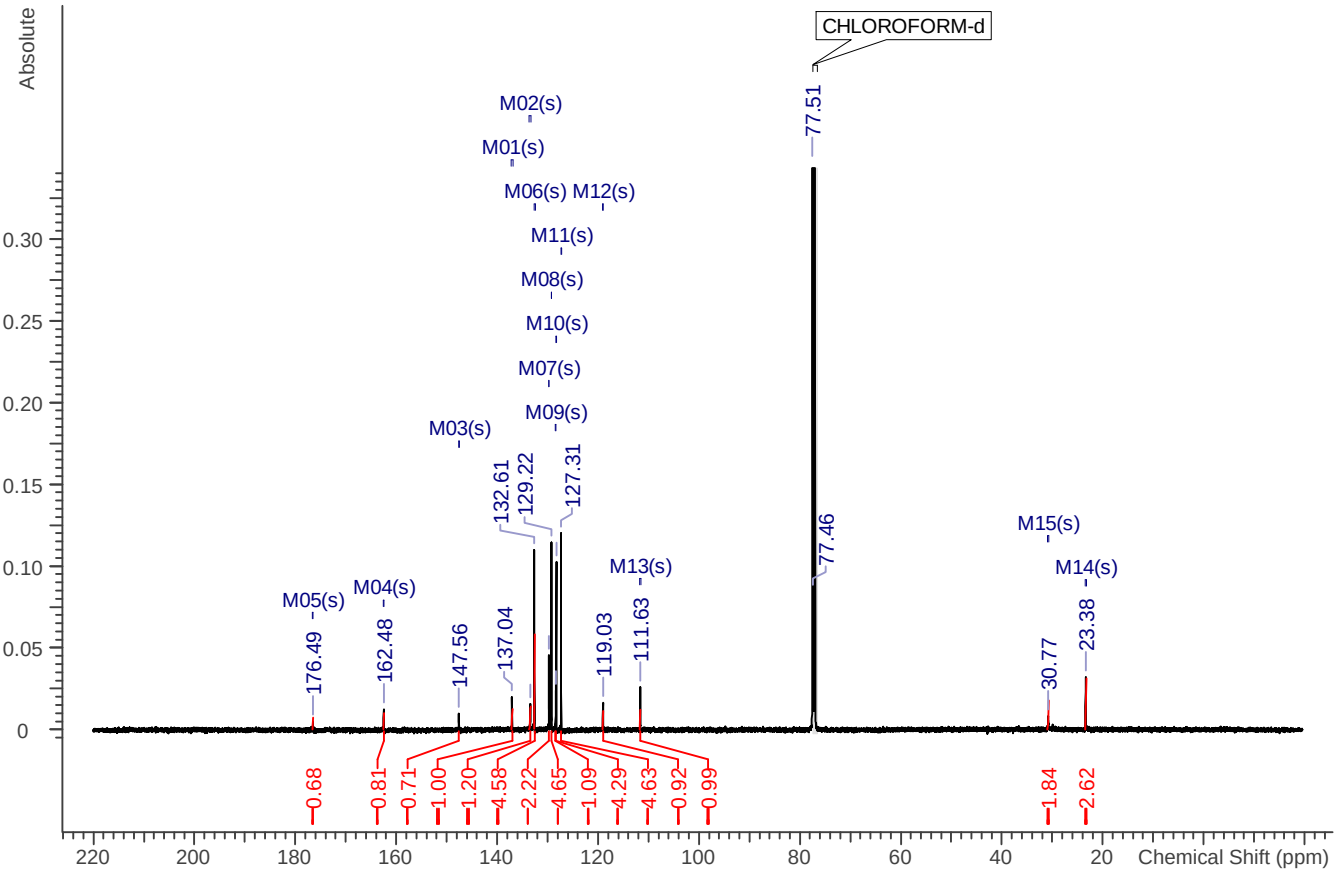
Absolute
CHLOROFORM-d
M02(s)
M01(s)
M06(s) M12(s)
M11(s)
M08(s)
M10(s)
M07(s)
M09(s)
M03(s)
M05(s)
M04(s)
M13(s)
M15(s)
M14(s)
77.51
77.46
132.61
129.22
127.31
176.49
162.48
147.56
137.04
119.03
111.63
30.77
23.38
0.68
0.81
0.71
1.00
1.20
4.58
2.22
4.65
1.09
4.29
4.63
0.92
0.99
1.84
2.62
Chemical Shift (ppm)

10

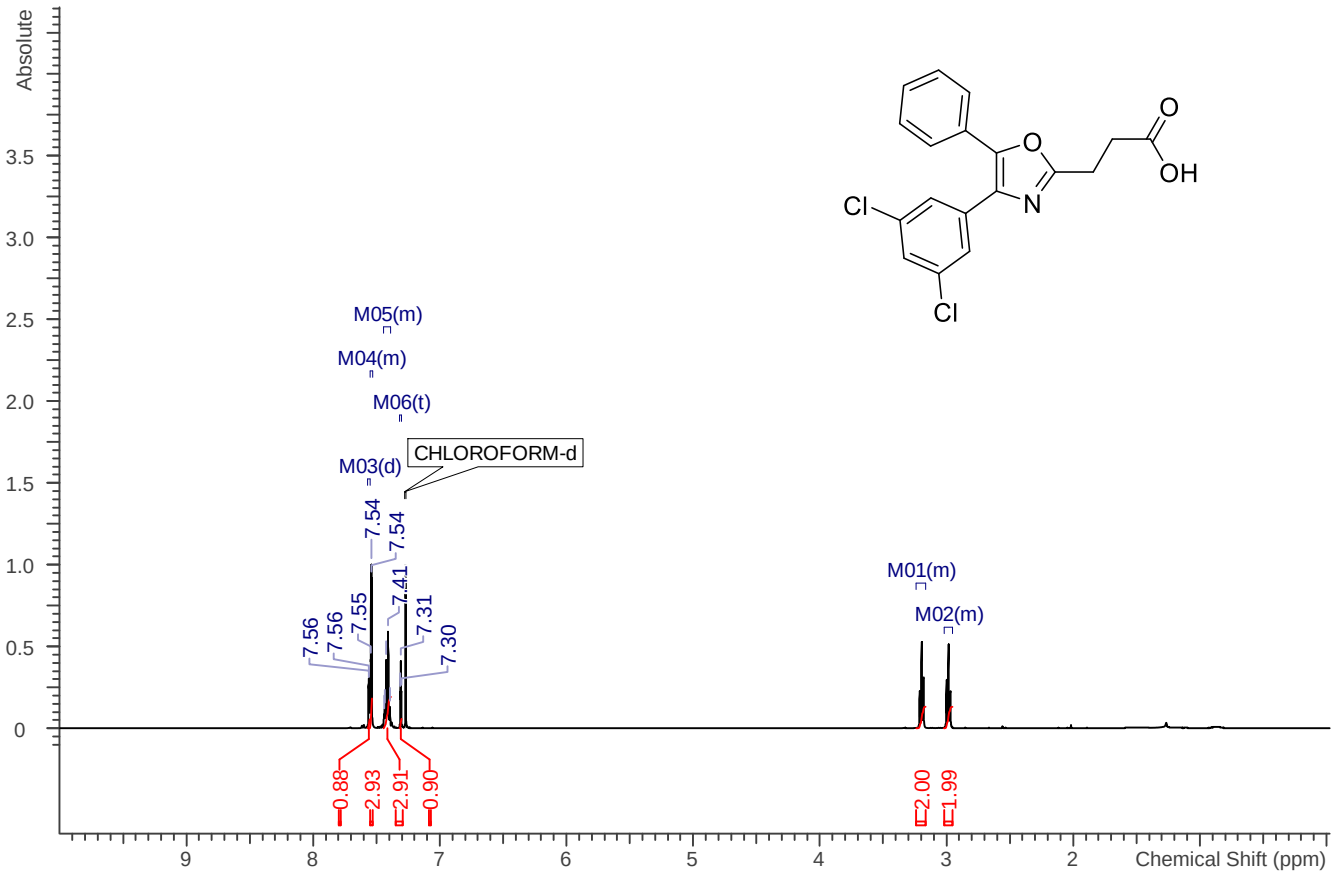
Absolute
3.5
3.0
2.5
2.0
1.5
1.0
0.5
0
M05(m)
M04(m)
M06(t)
M03(d)
CHLOROFORM-d
7.54
7.54
7.56
7.56
7.55
7.41
7.31
7.30
M01(m)
M02(m)
0.88
2.93
2.91
0.90
2.00
1.99
9
8
7
6
5
4
3
2
Chemical Shift (ppm)
O
OH
O
N
Cl
Cl

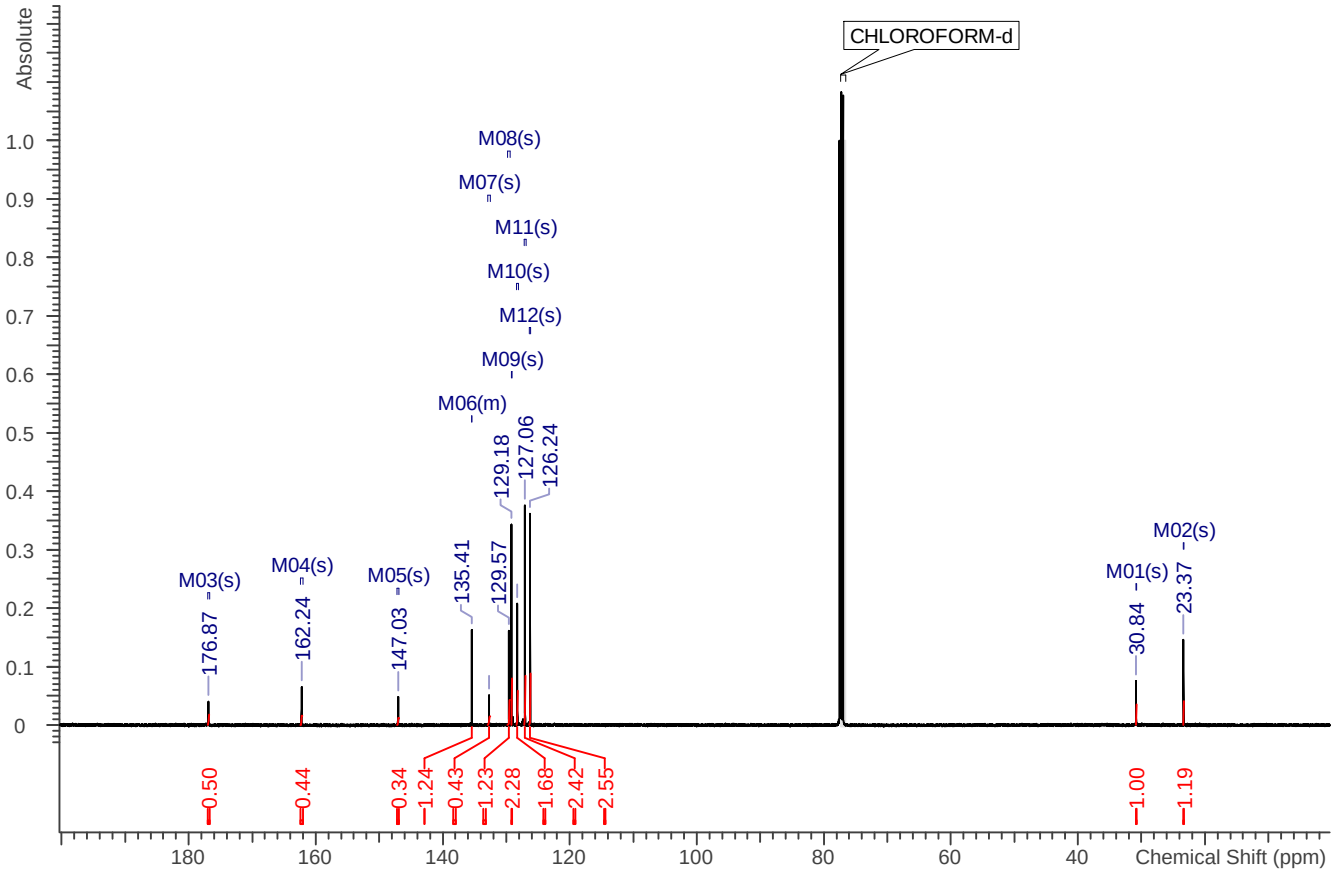
Absolute
1.0
0.9
0.8
0.7
0.6
0.5
0.4
0.3
0.2
0.1
0
CHLOROFORM-d
M08(s)
M07(s)
M11(s)
M10(s)
M12(s)
M09(s)
M06(m)
129.18
127.06
126.24
M03(s)
M04(s)
M05(s)
135.41
129.57
M02(s)
M01(s)
176.87
162.24
147.03
30.84
23.37
0.50
0.44
0.34
1.24
0.43
1.23
2.28
1.68
2.42
2.55
1.00
1.19
180
160
140
120
100
80
60
40
Chemical Shift (ppm)

16

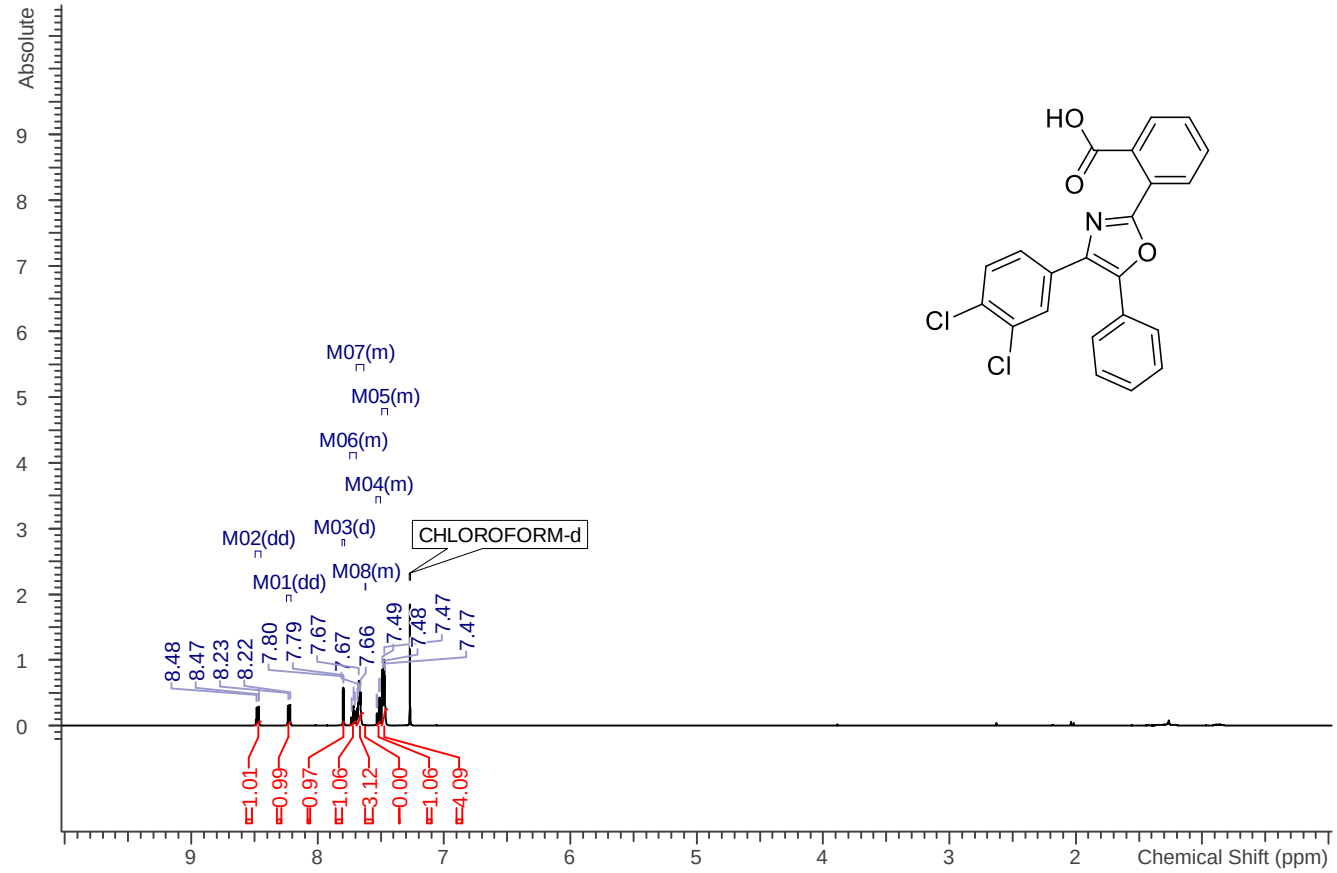
Absolute
HO
O
N
O
Cl
Cl
M07(m)
M05(m)
M06(m)
M04(m)
M03(d)
M02(dd)
M01(dd)
M08(m)
CHLOROFORM-d
8.48
8.47
8.23
8.22
7.80
7.79
7.67
7.67
7.66
7.49
7.48
7.47
7.47
1.01
0.99
0.97
1.06
3.12
0.00
1.06
4.09
Chemical Shift (ppm)

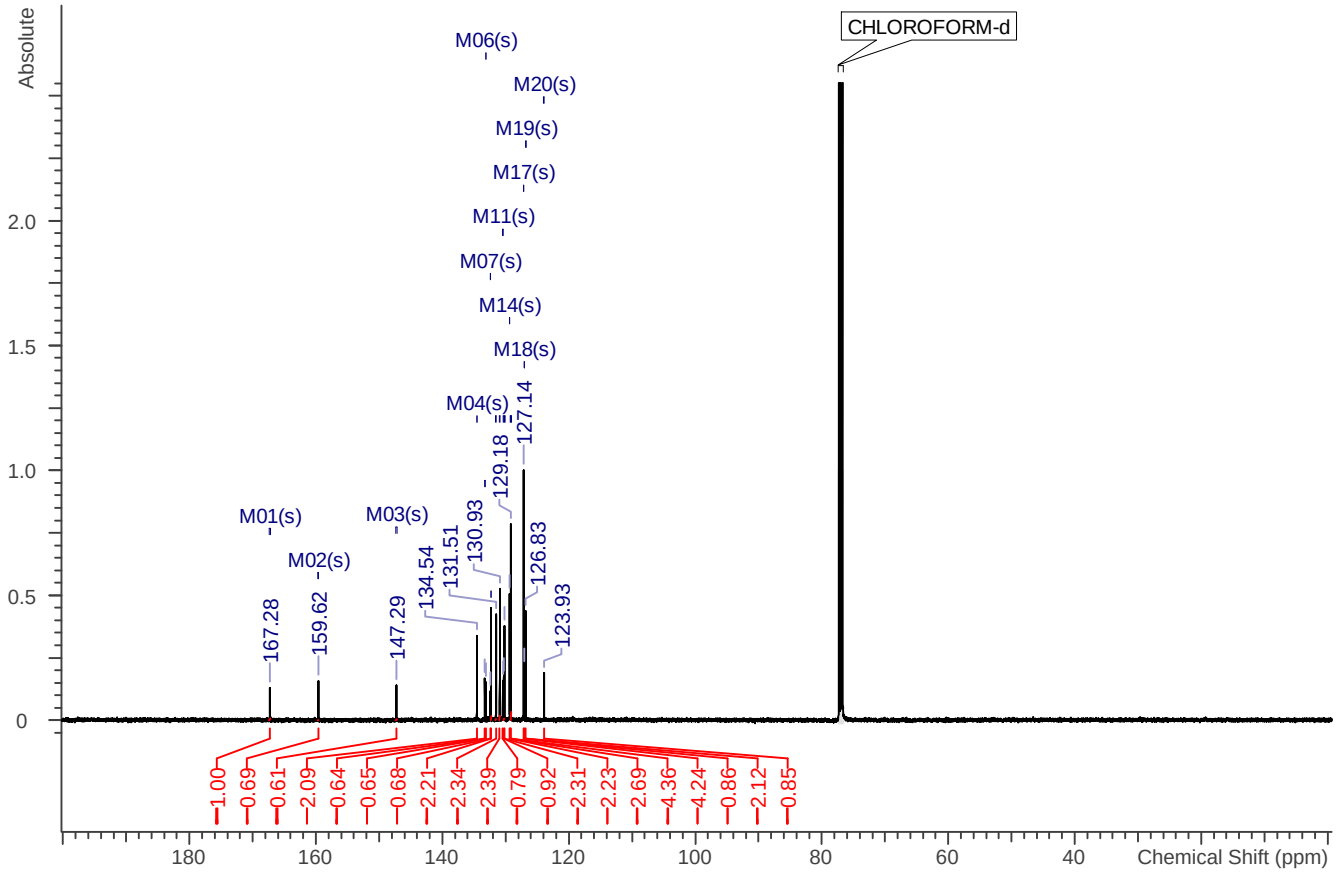
Absolute
CHLOROFORM-d
M06(s)
M20(s)
M19(s)
M17(s)
M11(s)
M07(s)
M14(s)
M18(s)
M04(s)
127.14
129.18
130.93
131.51
134.54
126.83
123.93
M01(s)
M03(s)
M02(s)
167.28
159.62
147.29
1.00
0.69
0.61
2.09
0.64
0.65
0.68
2.21
2.34
2.39
0.79
0.92
2.31
2.23
2.69
4.36
4.24
0.86
2.12
0.85
Chemical Shift (ppm)

17

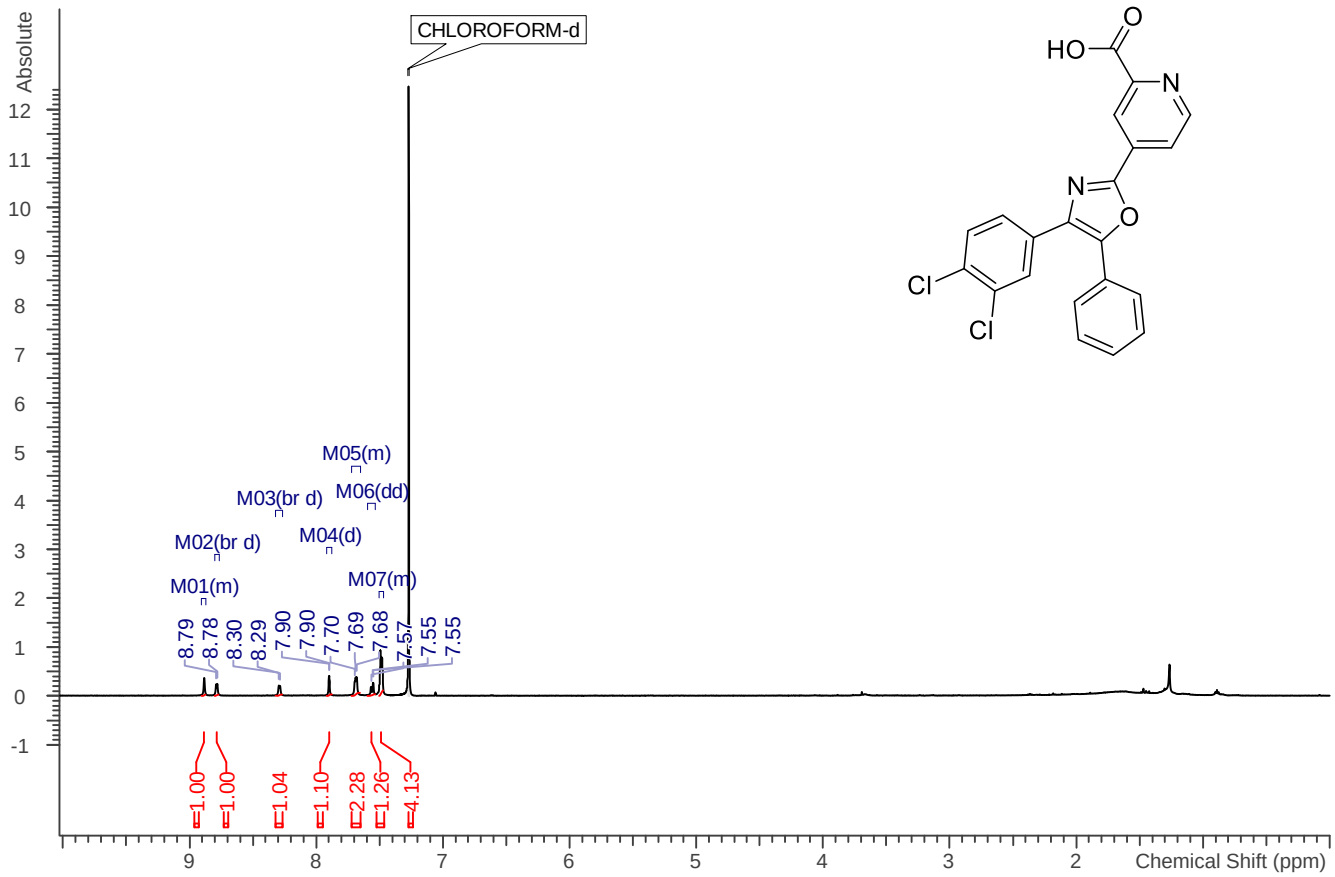
CHLOROFORM-d
Absolute
M01(m)
M02(br d)
M03(br d)
M04(d)
M05(m)
M06(dd)
M07(m)
8.79
8.78
8.30
8.29
7.90
7.90
7.70
7.69
7.68
7.57
7.55
7.55
1.00
1.00
1.04
1.10
2.28
1.26
4.13
Chemical Shift (ppm)

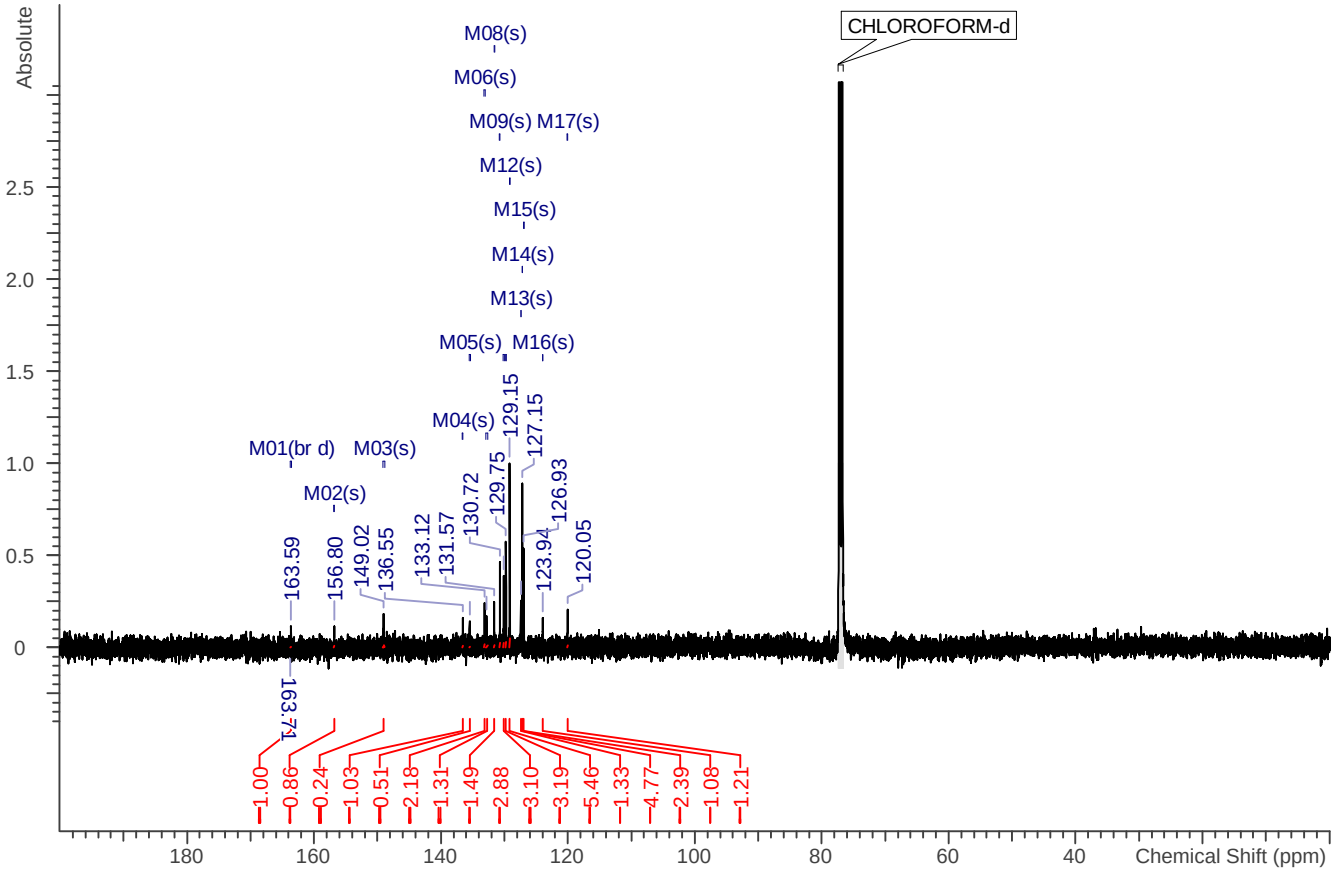
CHLOROFORM-d
Absolute
M08(s)
M06(s)
M09(s)
M17(s)
M12(s)
M15(s)
M14(s)
M13(s)
M05(s)
M16(s)
M04(s)
M01(br d)
M03(s)
M02(s)
163.59
156.80
149.02
136.55
133.12
131.57
130.72
129.75
129.15
127.15
126.93
123.94
120.05
163.74
1.00
0.86
0.24
1.03
0.51
2.18
1.31
1.49
2.88
3.10
3.19
5.46
1.33
4.77
2.39
1.08
1.21
Chemical Shift (ppm)

18

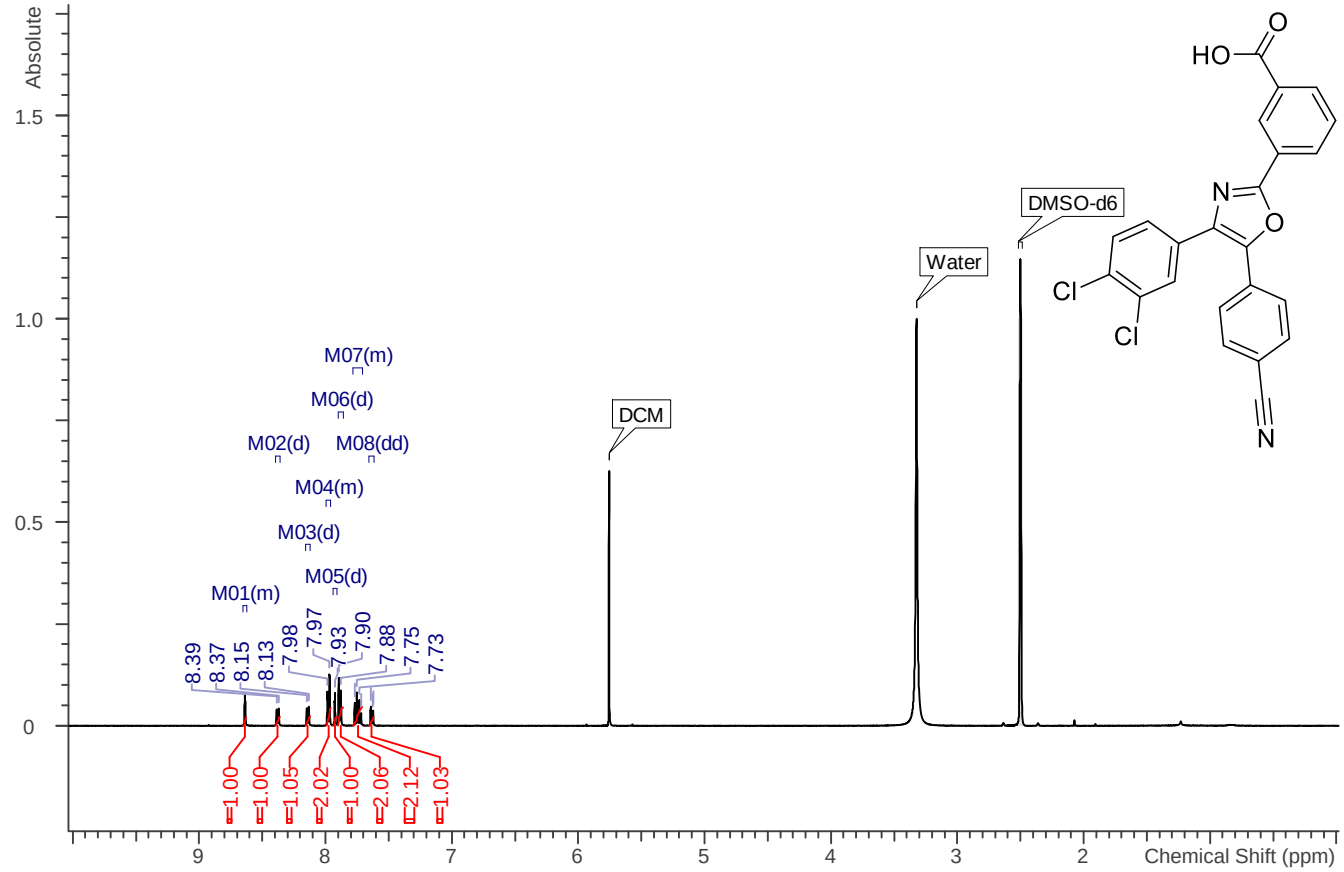
Absolute
1.5
1.0
0.5
0
M07(m)
M06(d)
M02(d)
M08(dd)
M04(m)
M03(d)
M05(d)
M01(m)
8.39
8.37
8.15
8.13
7.98
7.97
7.93
7.90
7.88
7.75
7.73
DCM
Water
DMSO-d6
1.00
1.00
1.05
2.02
1.00
2.06
2.12
1.03
9
8
7
6
5
4
3
2
Chemical Shift (ppm)
HO
O
N
O
Cl
Cl
N

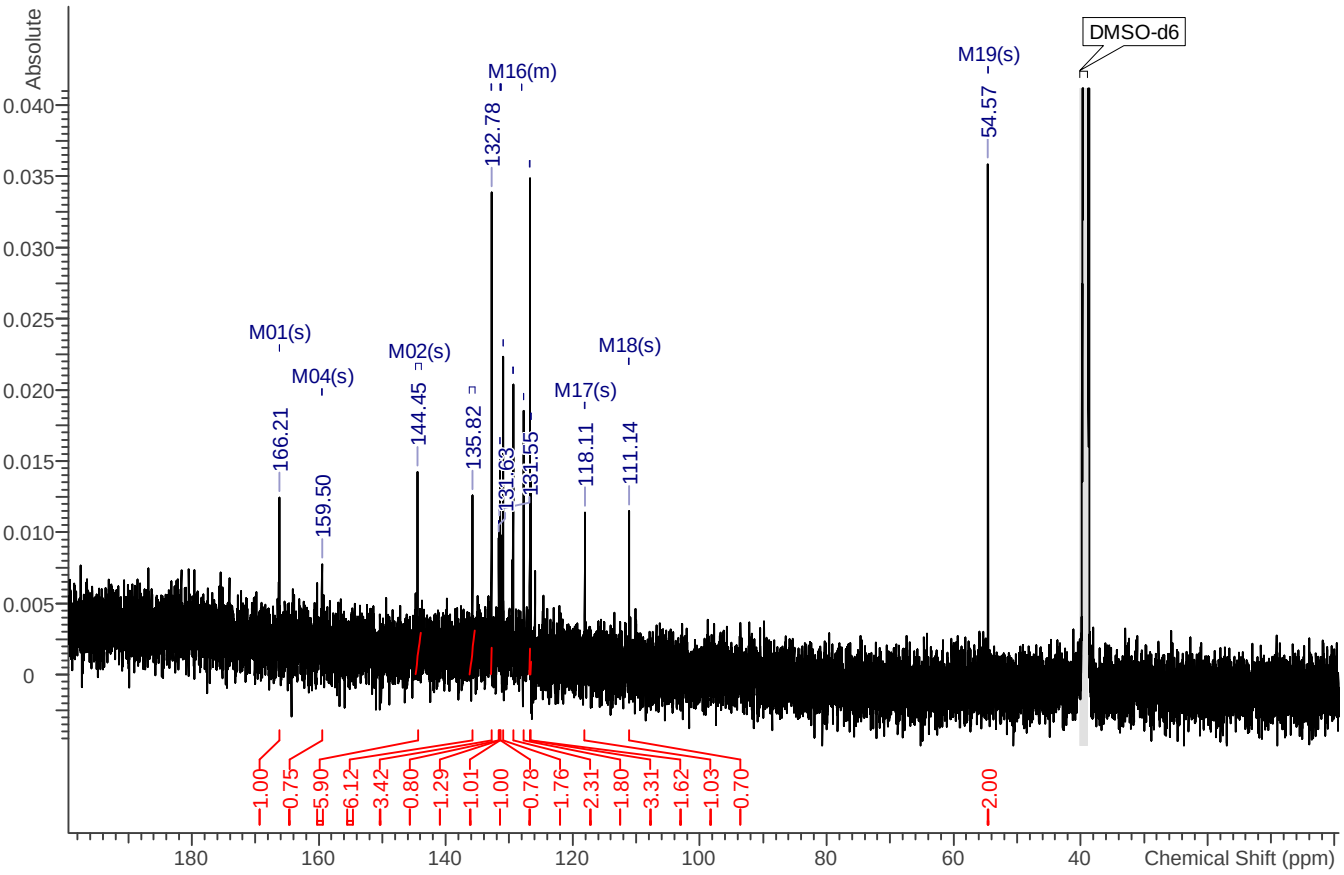
Absolute
0.040
0.035
0.030
0.025
0.020
0.015
0.010
0.005
0
M16(m)
132.78
M19(s)
54.57
DMSO-d6
M01(s)
M04(s)
166.21
159.50
M02(s)
144.45
135.82
131.63
131.55
M17(s)
118.11
M18(s)
111.14
1.00
0.75
5.90
6.12
3.42
0.80
1.29
1.01
1.00
0.78
1.76
2.31
1.80
3.31
1.62
1.03
0.70
2.00
180
160
140
120
100
80
60
40
Chemical Shift (ppm)

19

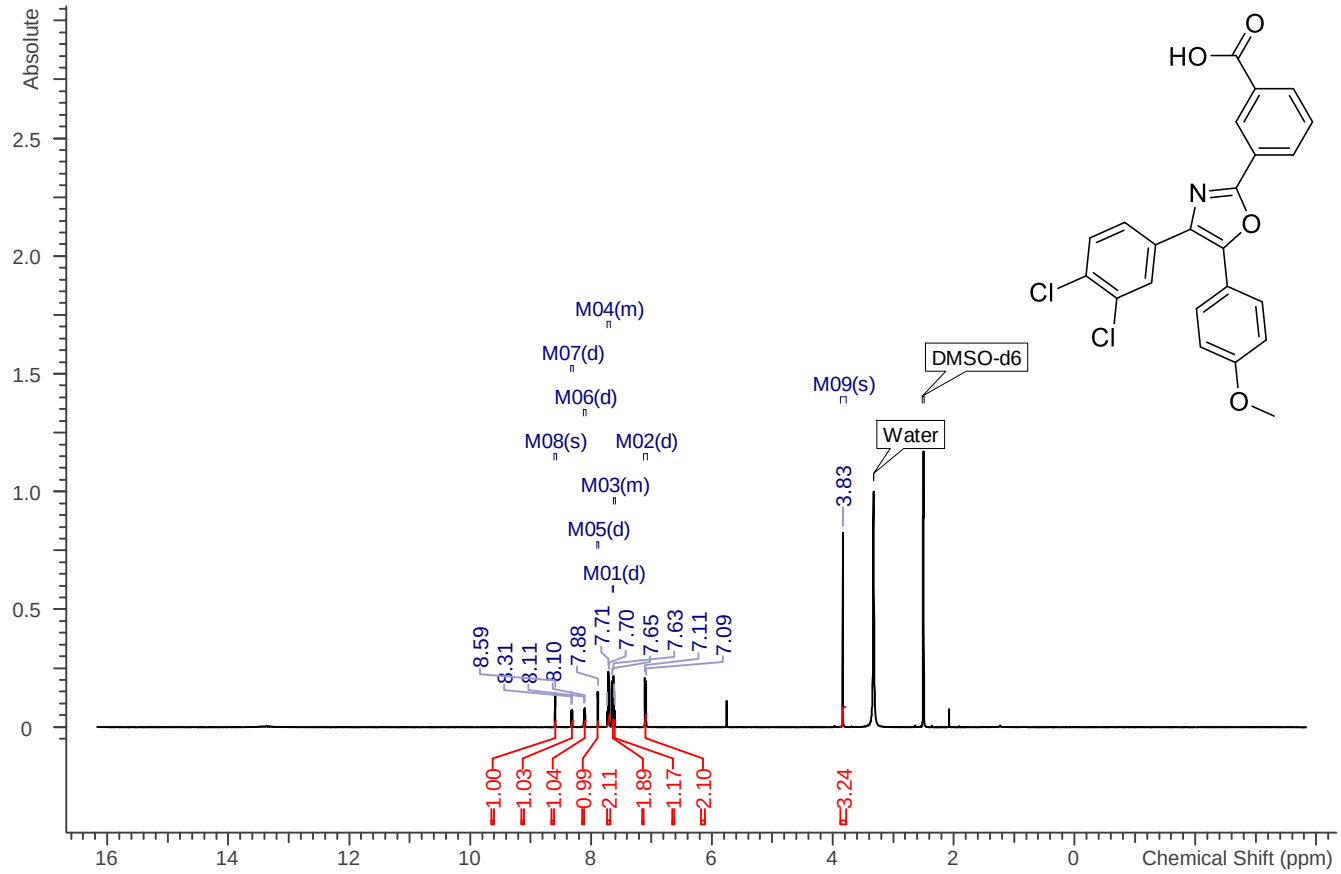
Absolute
2.5
2.0
1.5
1.0
0.5
0
M04(m)
M07(d)
M06(d)
M08(s)
M02(d)
M03(m)
M05(d)
M01(d)
M09(s)
DMSO-d6
Water
3.83
8.59
8.31
8.11
8.10
7.88
7.71
7.70
7.65
7.63
7.11
7.09
1.00
1.03
1.04
0.99
2.11
1.89
1.17
2.10
3.24
16
14
12
10
8
6
4
2
0
Chemical Shift (ppm)

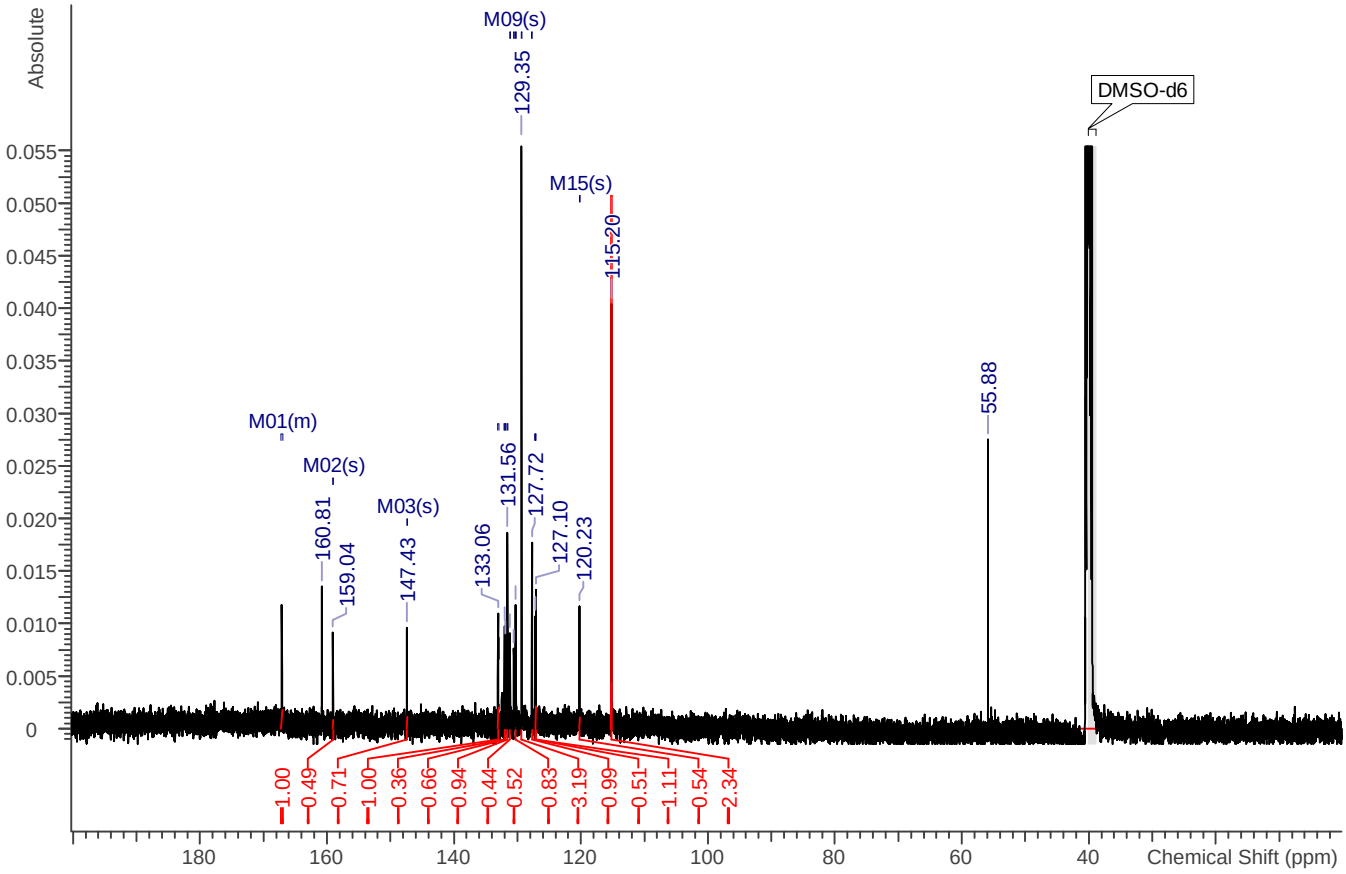
Absolute
0.055
0.050
0.045
0.040
0.035
0.030
0.025
0.020
0.015
0.010
0.005
0
M09(s)
129.35
M15(s)
115.20
DMSO-d6
55.88
M01(m)
M02(s)
160.81
159.04
M03(s)
147.43
133.06
131.56
127.72
127.10
120.23
1.00
0.49
0.71
1.00
0.36
0.66
0.94
0.44
0.52
0.83
3.19
0.99
0.51
1.11
0.54
2.34
180
160
140
120
100
80
60
40
Chemical Shift (ppm)

20

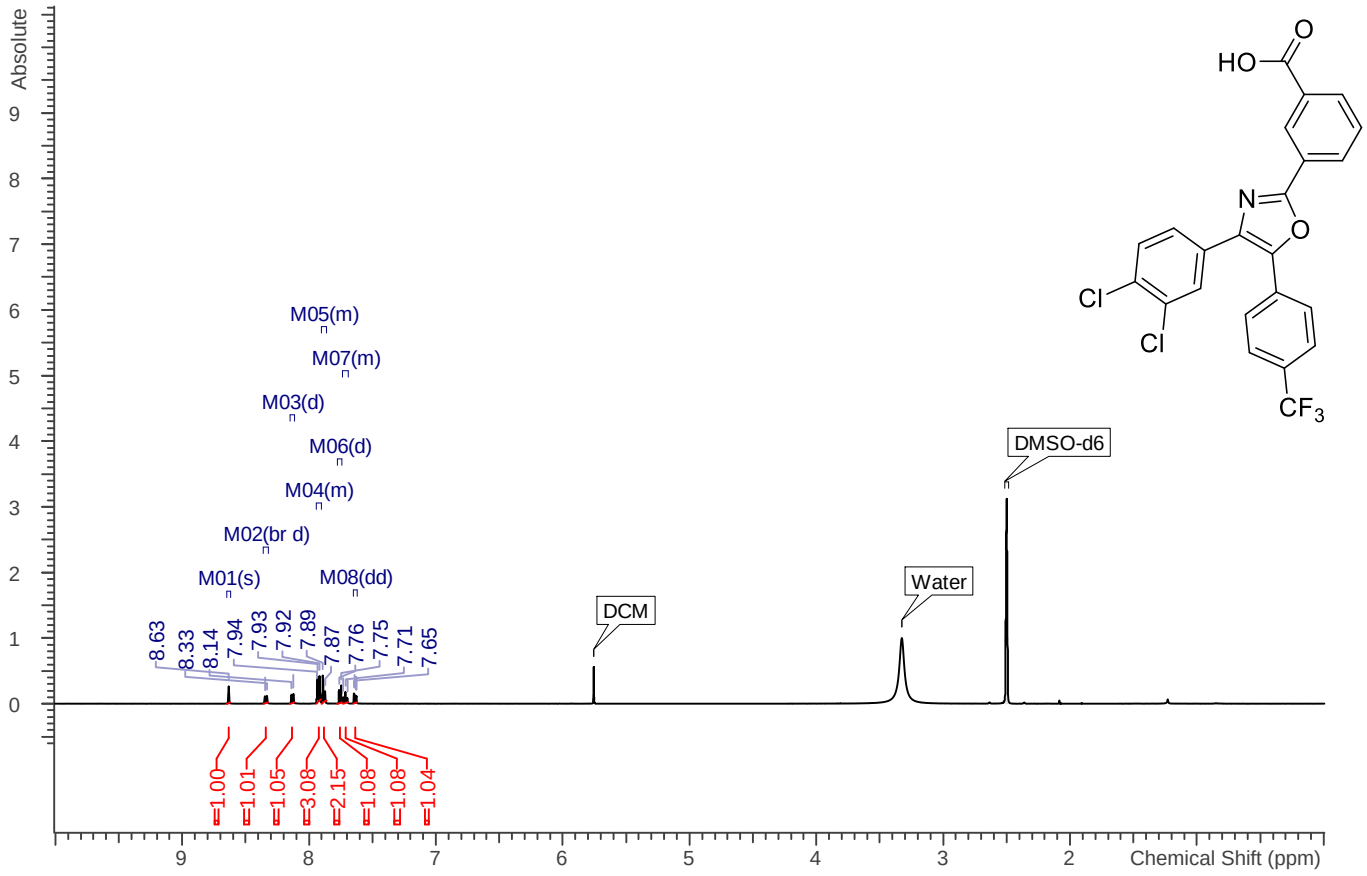
Absolute
M05(m)
M07(m)
M03(d)
M06(d)
M04(m)
M02(br d)
M01(s)
M08(dd)
8.63
8.33
8.14
7.94
7.93
7.92
7.89
7.87
7.76
7.75
7.71
7.65
DCM
Water
DMSO-d6
1.00
1.01
1.05
3.08
2.15
1.08
1.08
1.04
Chemical Shift (ppm)
HO
O
N
O
Cl
Cl
CF3

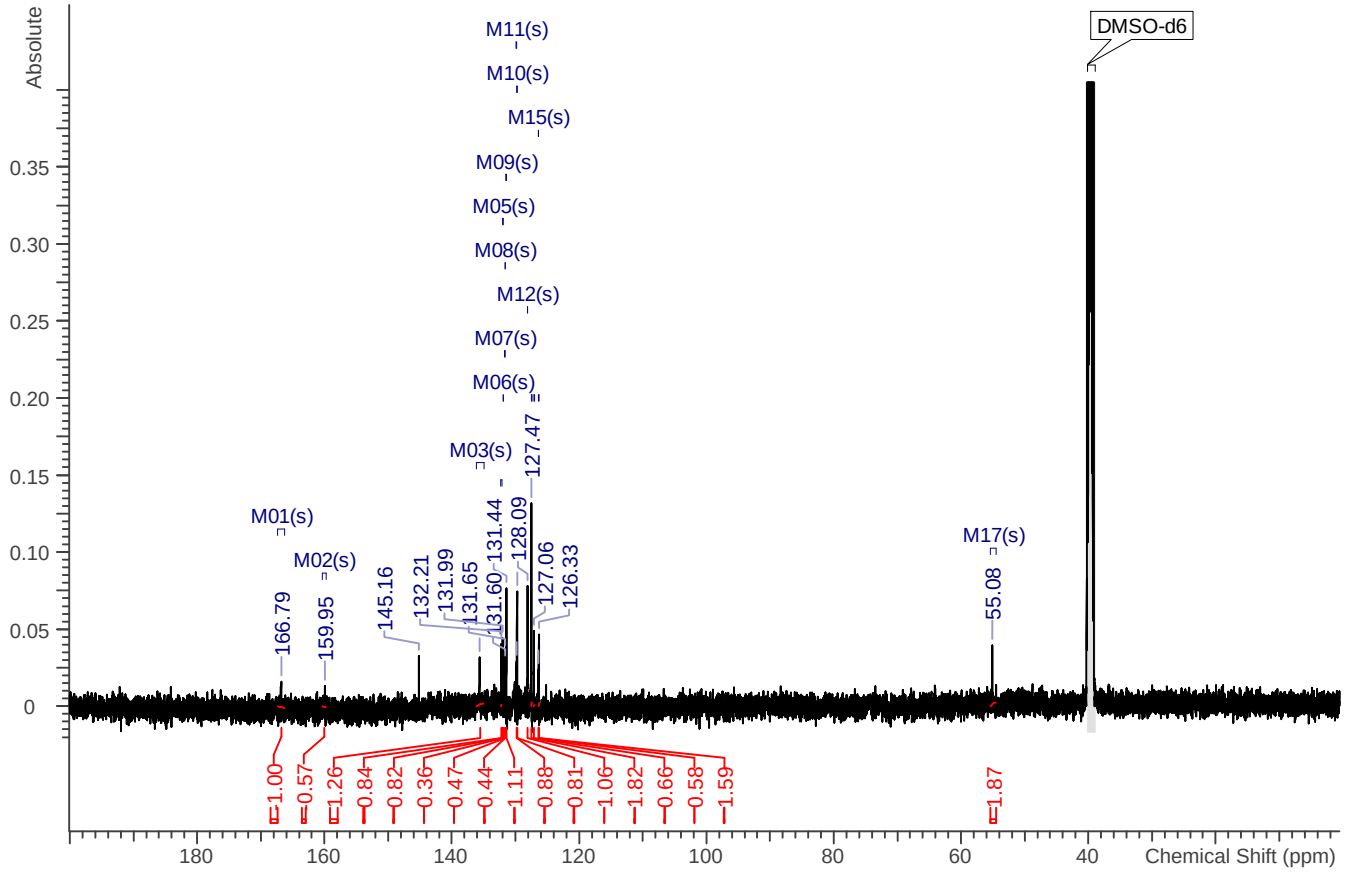
Absolute
M11(s)
M10(s)
M15(s)
M09(s)
M05(s)
M08(s)
M12(s)
M07(s)
M06(s)
M03(s)
M01(s)
M02(s)
M17(s)
DMSO-d6
166.79
159.95
145.16
132.21
131.99
131.65
131.60
131.44
128.09
127.47
127.06
126.33
55.08
1.00
0.57
1.26
0.84
0.82
0.36
0.47
0.44
1.11
0.88
0.81
1.06
1.82
0.66
0.58
1.59
1.87
Chemical Shift (ppm)

21

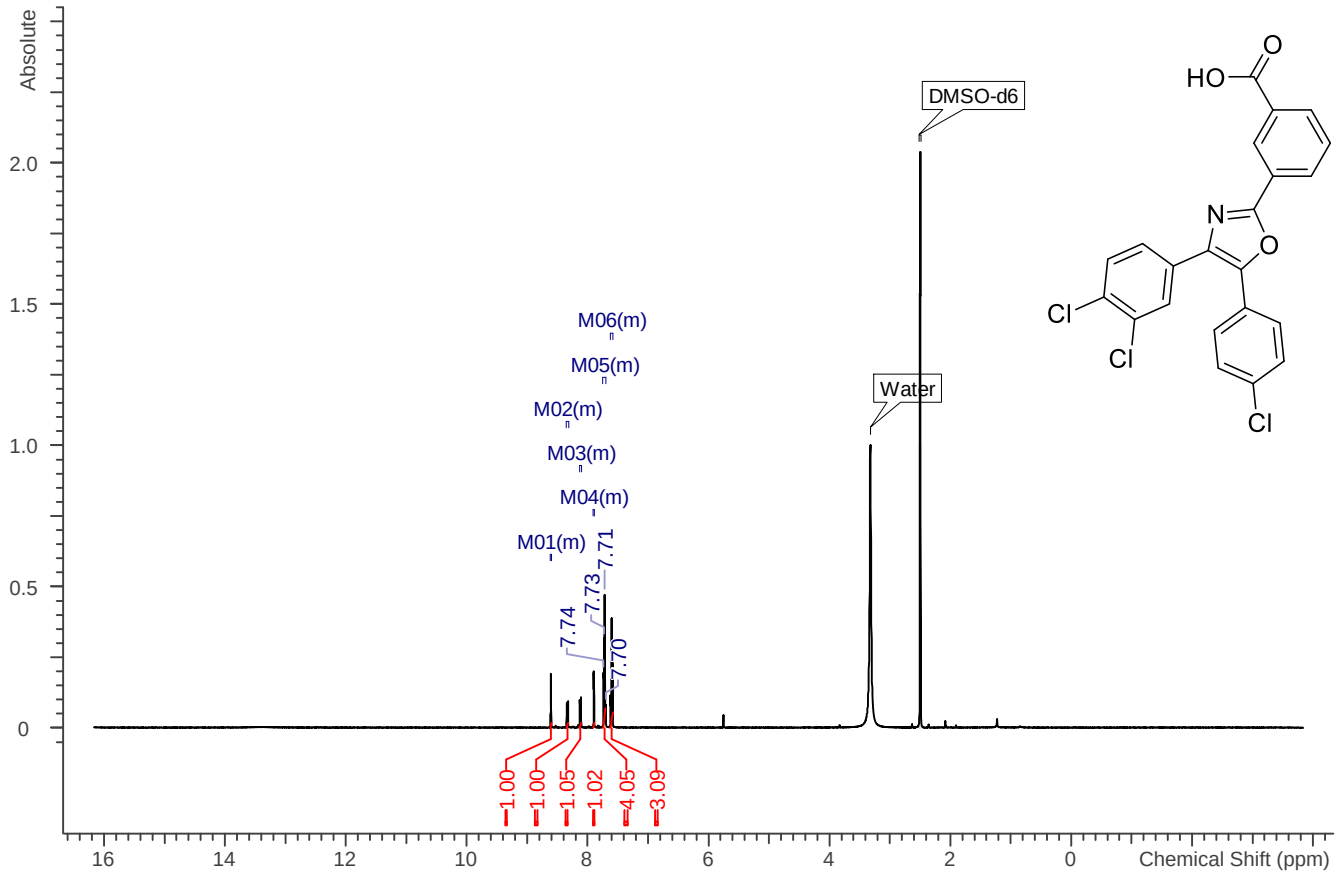
Absolute
2.0
1.5
1.0
0.5
0
DMSO-d6
Water
M06(m)
M05(m)
M02(m)
M03(m)
M04(m)
M01(m)
7.71
7.73
7.74
7.70
1.00
1.00
1.05
1.02
4.05
3.09
16
14
12
10
8
6
4
2
0
Chemical Shift (ppm)
HO
O
N
O
Cl
Cl
Cl

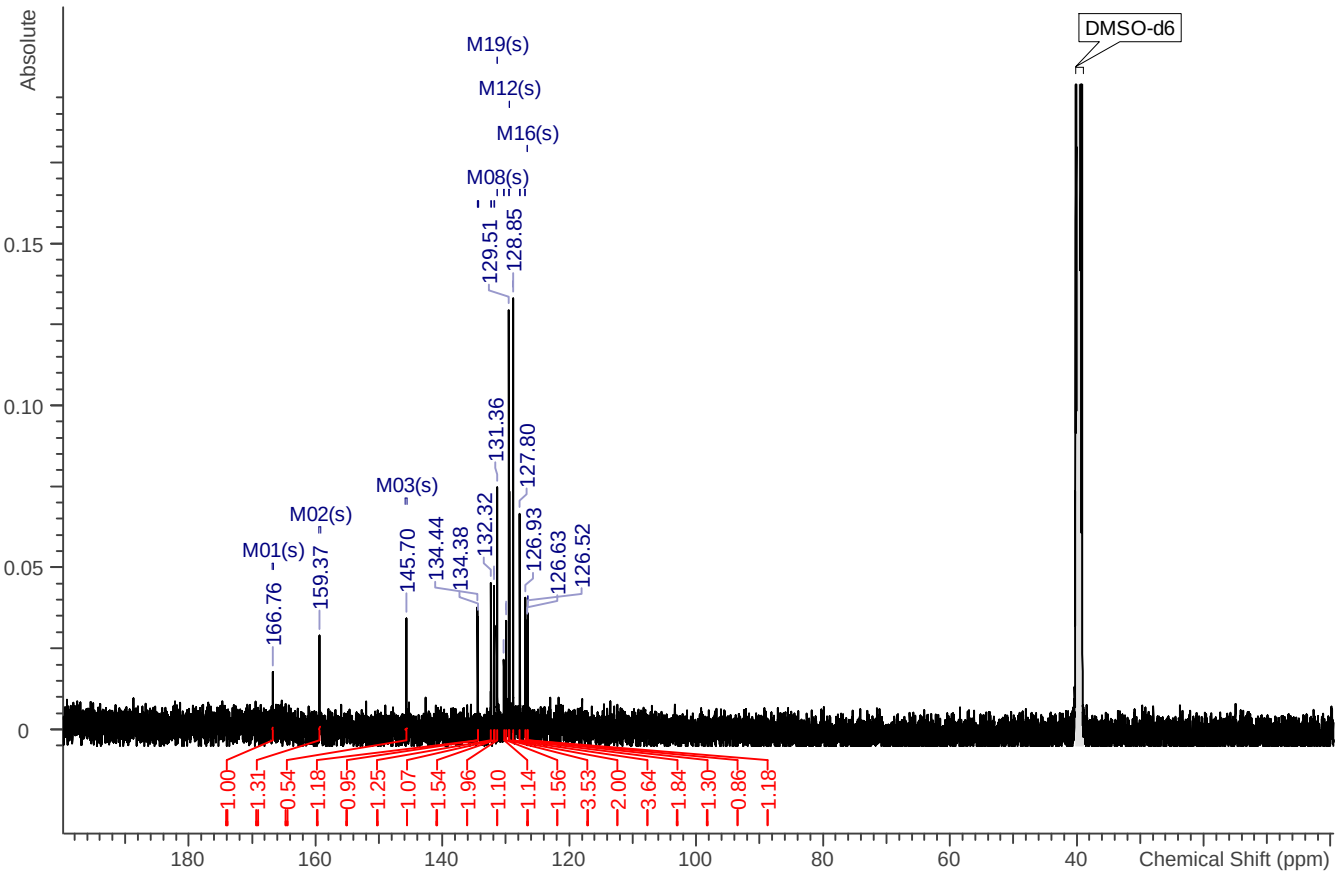
Absolute
0.15
0.10
0.05
0
DMSO-d6
M19(s)
M12(s)
M16(s)
M08(s)
M03(s)
M02(s)
M01(s)
166.76
159.37
145.70
134.44
134.38
132.32
131.36
129.51
128.85
127.80
126.93
126.63
126.52
1.00
1.31
0.54
1.18
0.95
1.25
1.07
1.54
1.96
1.10
1.14
1.56
3.53
2.00
3.64
1.84
1.30
0.86
1.18
180
160
140
120
100
80
60
40
Chemical Shift (ppm)

22

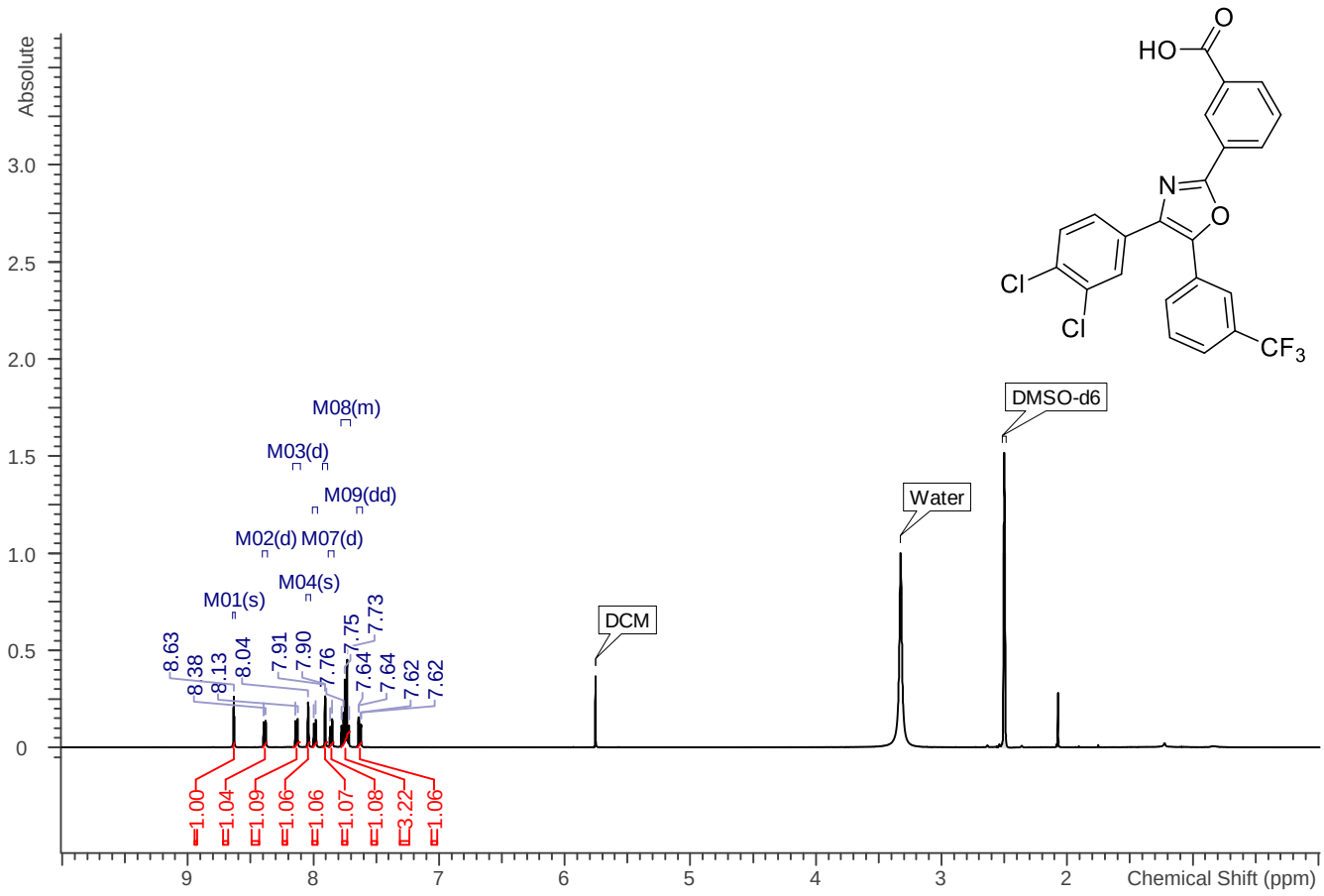
Absolute
3.0
2.5
2.0
1.5
1.0
0.5
0
HO
O
N
O
Cl
Cl
CF3
M08(m)
M03(d)
M09(dd)
M02(d) M07(d)
M04(s)
M01(s)
8.63
8.38
8.13
8.04
7.91
7.90
7.76
7.75
7.73
7.64
7.64
7.62
7.62
DCM
Water
DMSO-d6
1.00
1.04
1.09
1.06
1.06
1.07
1.08
3.22
1.06
9
8
7
6
5
4
3
2
Chemical Shift (ppm)

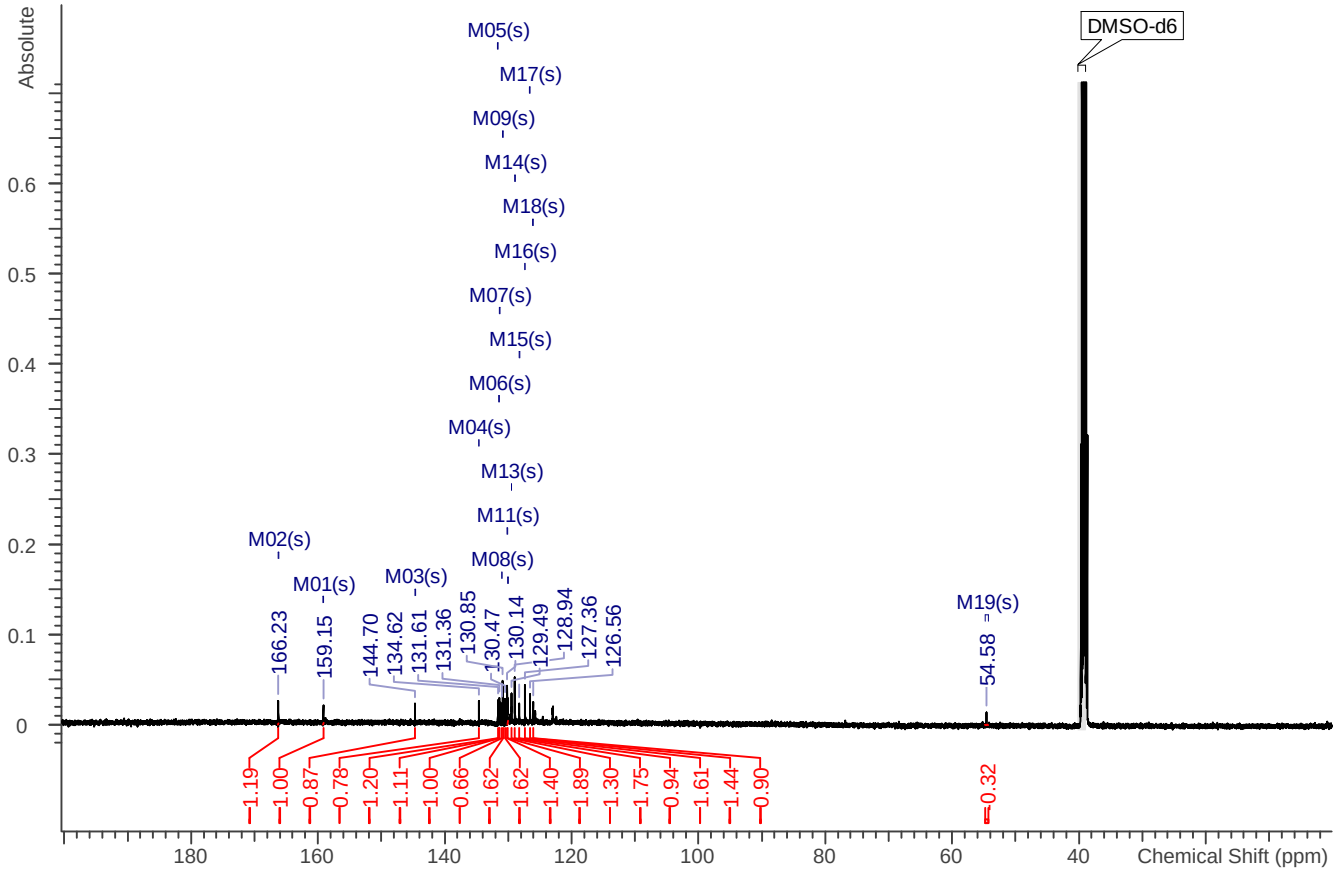
Absolute
0.6
0.5
0.4
0.3
0.2
0.1
0
M05(s)
M17(s)
M09(s)
M14(s)
M18(s)
M16(s)
M07(s)
M15(s)
M06(s)
M04(s)
M13(s)
M11(s)
M08(s)
M02(s)
M01(s)
M03(s)
M19(s)
DMSO-d6
166.23
159.15
144.70
134.62
131.61
131.36
130.85
130.47
130.14
129.49
128.94
127.36
126.56
54.58
1.19
1.00
0.87
0.78
1.20
1.11
1.00
0.66
1.62
1.62
1.40
1.89
1.30
1.75
0.94
1.61
1.44
0.90
0.32
180
160
140
120
100
80
60
40
Chemical Shift (ppm)

23

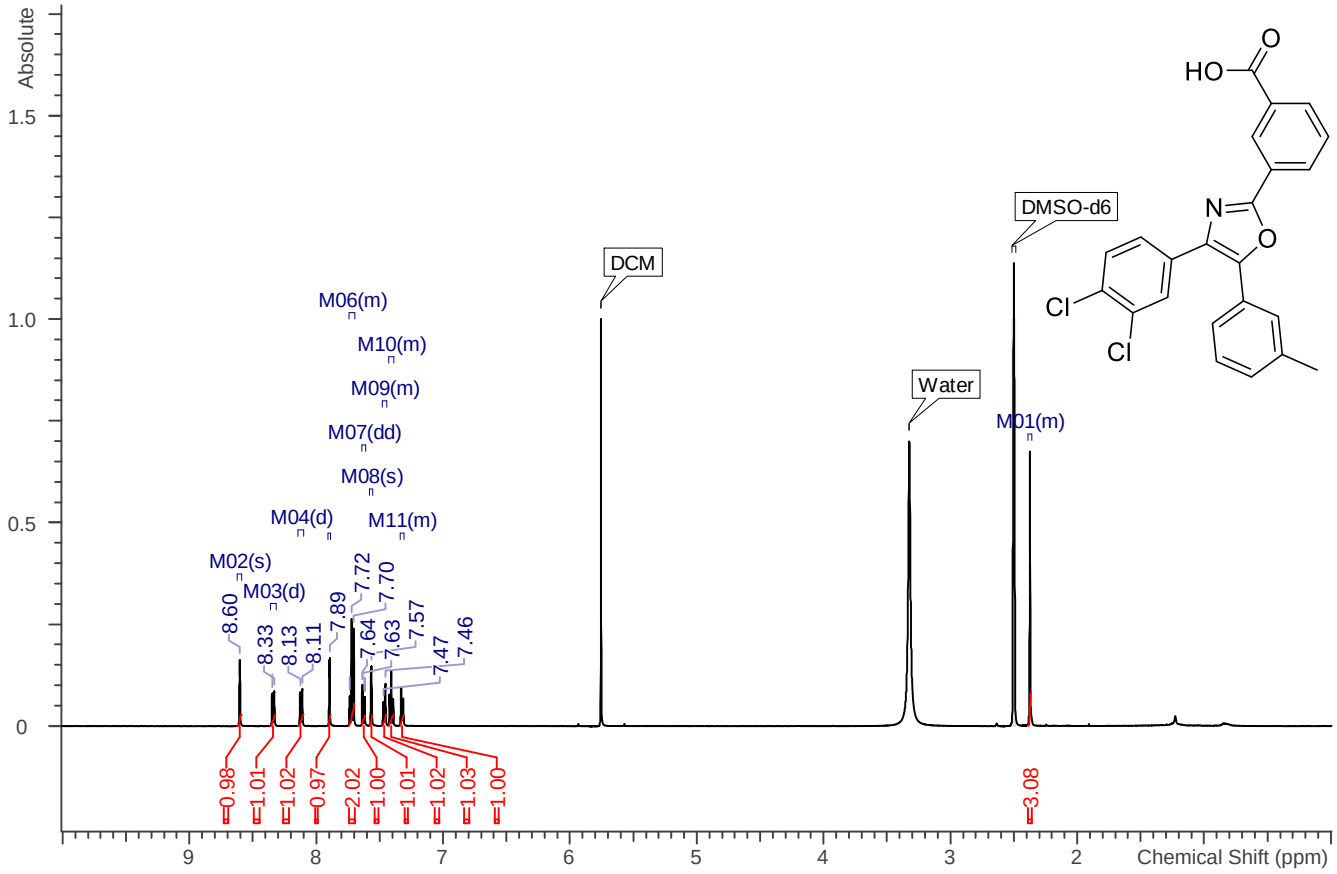
Absolute
1.5
1.0
0.5
0
DCM
Water
DMSO-d6
M06(m)
M10(m)
M09(m)
M07(dd)
M08(s)
M04(d)
M11(m)
M02(s)
M03(d)
M01(m)
8.60
8.33
8.13
8.11
7.89
7.72
7.70
7.64
7.63
7.57
7.47
7.46
0.98
1.01
1.02
0.97
2.02
1.00
1.01
1.02
1.03
1.00
3.08
9
8
7
6
5
4
3
2
Chemical Shift (ppm)
HO
O
N
O
Cl
Cl

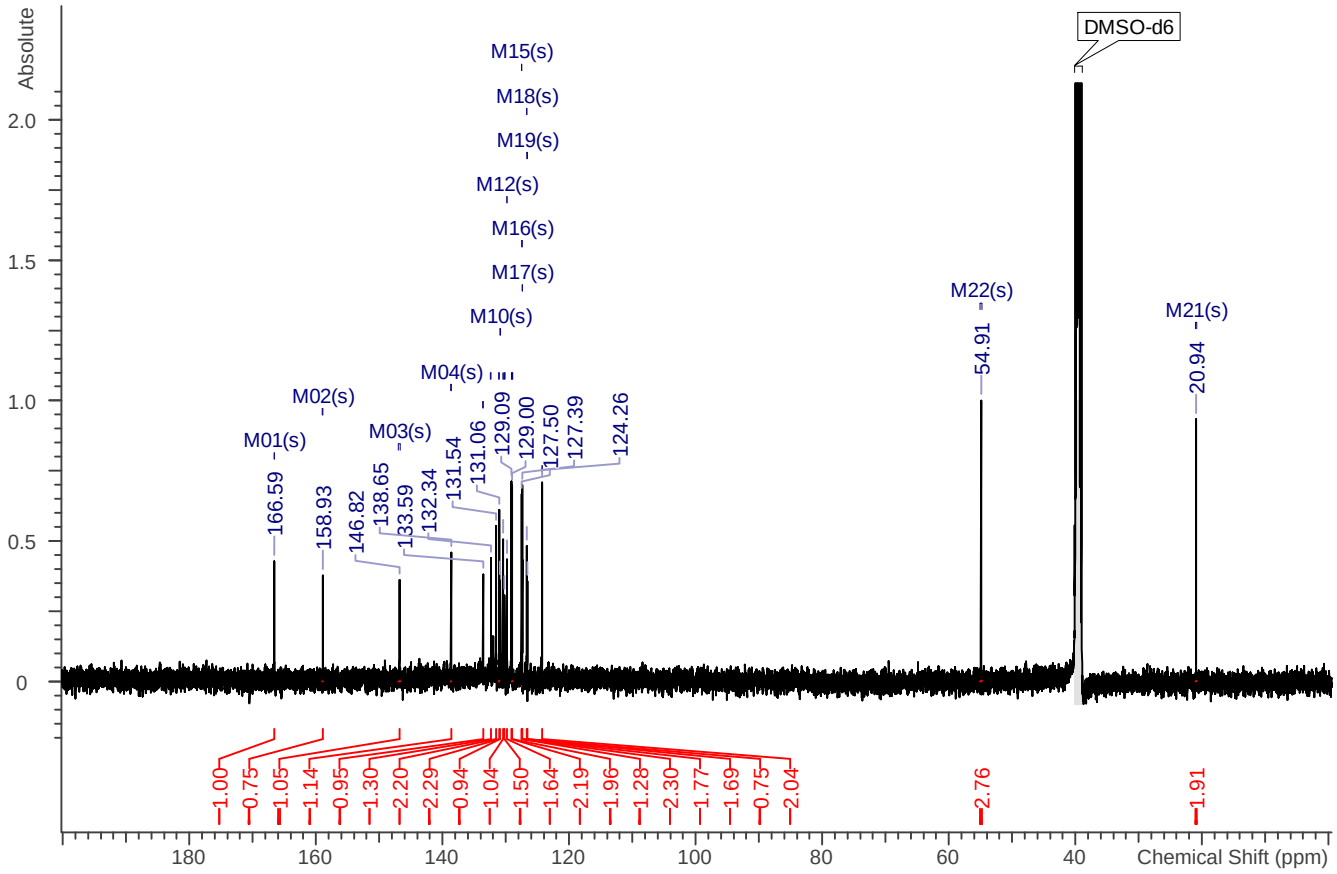
Absolute
2.0
1.5
1.0
0.5
0
DMSO-d6
M15(s)
M18(s)
M19(s)
M12(s)
M16(s)
M17(s)
M10(s)
M04(s)
M02(s)
M01(s)
M03(s)
M22(s)
M21(s)
166.59
158.93
146.82
138.65
133.59
132.34
131.54
131.06
129.09
129.00
127.50
127.39
124.26
54.91
20.94
1.00
0.75
1.05
1.14
0.95
1.30
2.20
2.29
0.94
1.04
1.50
1.64
2.19
1.96
1.28
2.30
1.77
1.69
0.75
2.04
2.76
1.91
180
160
140
120
100
80
60
40
Chemical Shift (ppm)

24

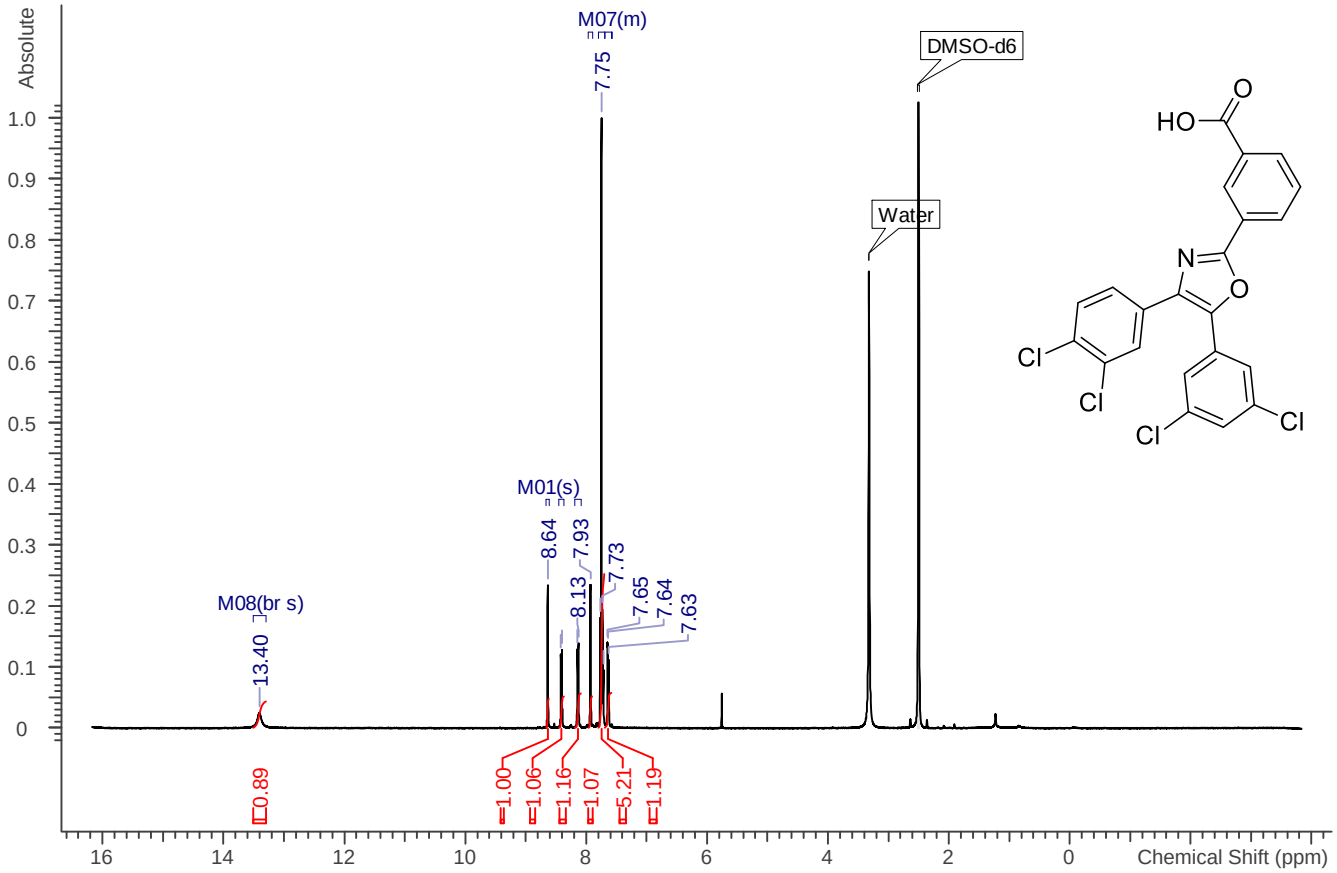
Absolute
M07(m)
7.75
DMSO-d6
Water
M01(s)
8.64
7.93
8.13
7.73
7.65
7.64
7.63
M08(br s)
13.40
0.89
1.00
1.06
1.16
1.07
5.21
1.19
Chemical Shift (ppm)
HO
O
N
O
Cl
Cl
Cl
Cl

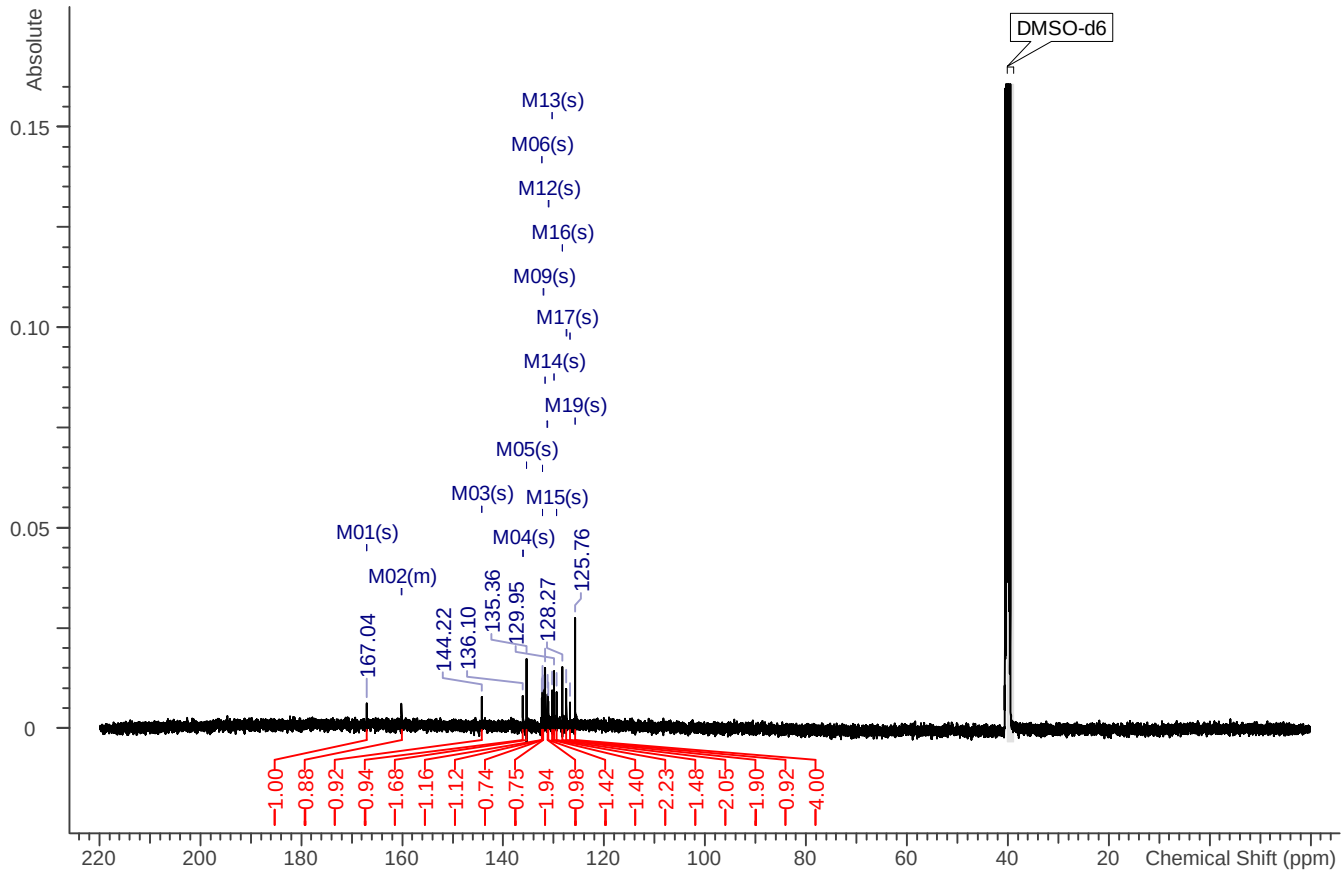
Absolute
DMSO-d6
M13(s)
M06(s)
M12(s)
M16(s)
M09(s)
M17(s)
M14(s)
M19(s)
M05(s)
M03(s)
M15(s)
M01(s)
M04(s)
M02(m)
125.76
135.36
129.95
128.27
167.04
144.22
136.10
1.00
0.88
0.92
0.94
1.68
1.16
1.12
0.74
0.75
1.94
0.98
1.42
1.40
2.23
1.48
2.05
1.90
0.92
4.00
Chemical Shift (ppm)

25

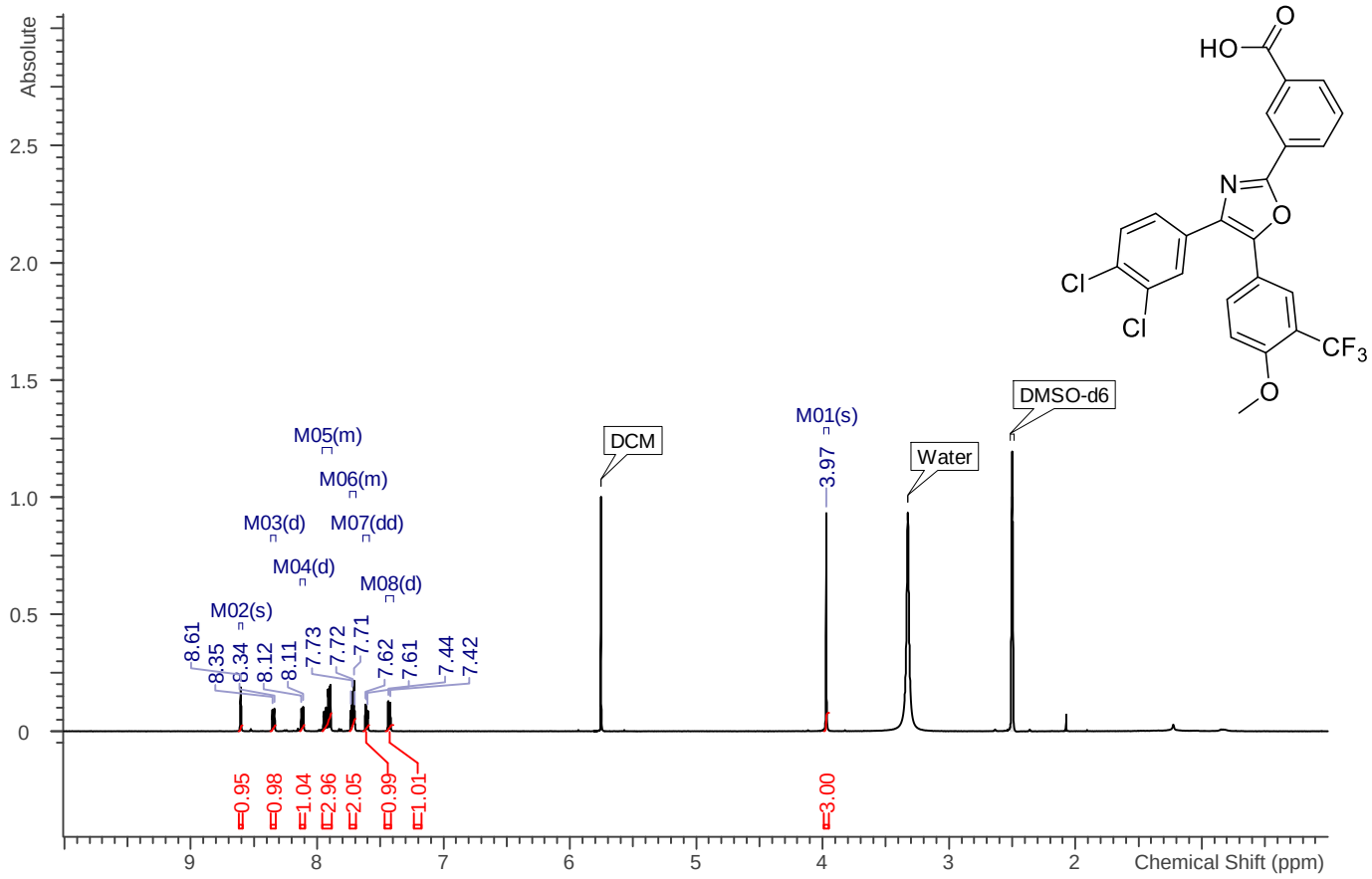
Absolute
Chemical Shift (ppm)
DCM
Water
DMSO-d6
M01(s)
3.97
M02(s)
M03(d)
M04(d)
M05(m)
M06(m)
M07(dd)
M08(d)
8.61
8.35
8.34
8.12
8.11
7.73
7.72
7.71
7.62
7.61
7.44
7.42
0.95
0.98
1.04
2.96
2.05
0.99
1.01
3.00
HO
O
N
O
Cl
Cl
CF3
O

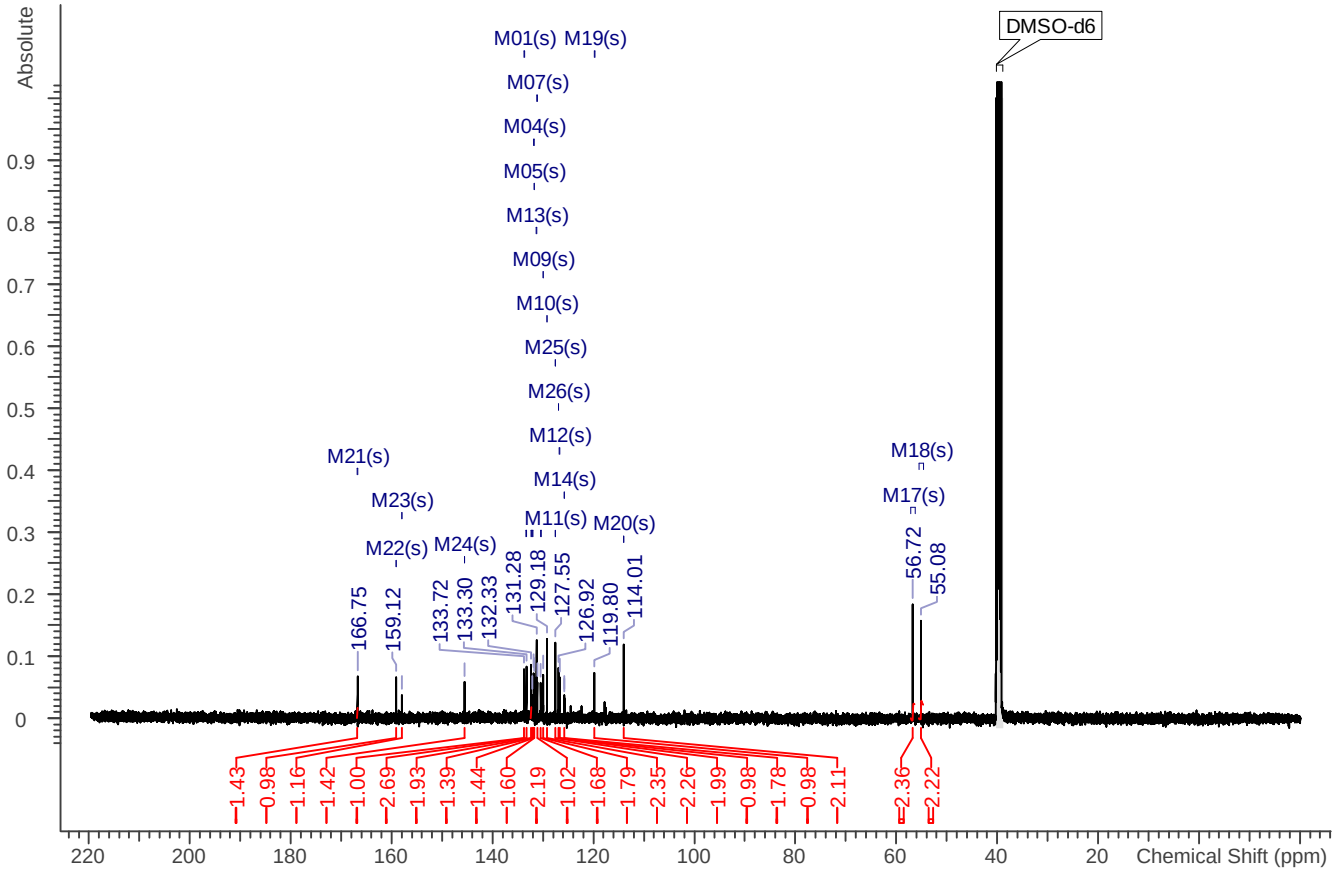
Absolute
Chemical Shift (ppm)
DMSO-d6
M01(s)
M19(s)
M07(s)
M04(s)
M05(s)
M13(s)
M09(s)
M10(s)
M25(s)
M26(s)
M12(s)
M14(s)
M11(s)
M20(s)
M21(s)
M23(s)
M22(s)
M24(s)
M18(s)
M17(s)
166.75
159.12
133.72
133.30
132.33
131.28
129.18
127.55
126.92
119.80
114.01
56.72
55.08
1.43
0.98
1.16
1.42
1.00
2.69
1.93
1.39
1.44
1.60
2.19
1.02
1.68
1.79
2.35
2.26
1.99
0.98
1.78
0.98
2.11
2.36
2.22

LC-MS traces

HPLC traces ECF compounds

1

Mass Spectrum and Results

Injection Details

Injection Name:	**HIPS-8082**	*Run Time (min):*	**5.10**
Vial Number:	**GB6**	*Injection Volume:*	**1.00**
Injection Type:	**Unknown**	*Channel:*	**UV_VIS_1**
Calibration Level:		*Wavelength:*	**254**
Instrument Method:	**0.6ml_+ve_-ve_100-600 new machine name**	*Bandwidth:*	**2**
Processing Method:	**Processing Method - 210-310nm**	*Dilution Factor:*	**1.0000**
Injection Date/Time:	**18/Jul/23 13:29**	*Sample Weight:*	**1.0000**

Integration Results

No.	Peak Name	Retention Time min	Area mAU*min	Height mAU	Relative Area %	Relative Height %	Amount n.a.
1		3.735	22.678	263.557	100.00	100.00	n.a.
Total:			**22.678**	**263.557**	**100.00**	**100.00**	

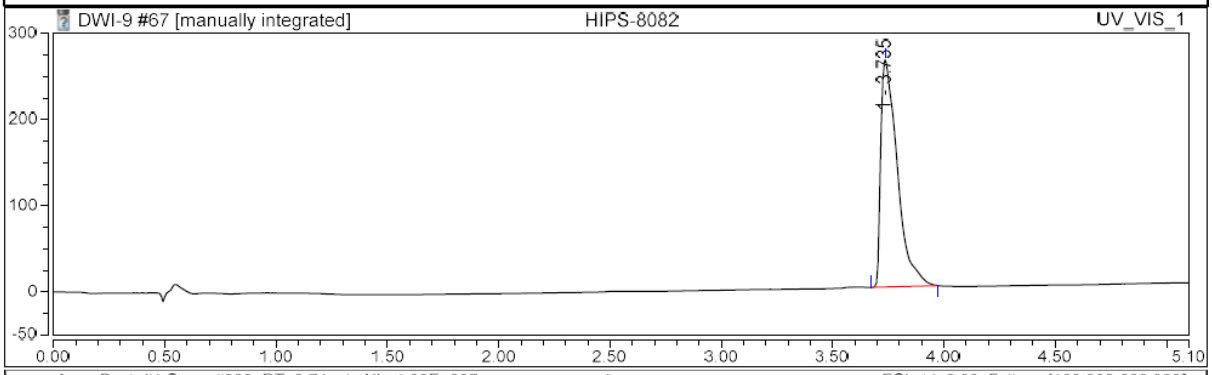

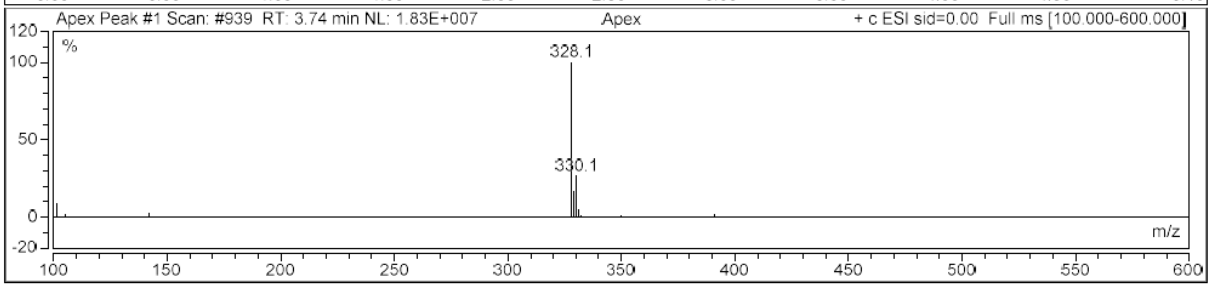

6

Mass Spectrum and Results

Injection Details

Injection Name:	**DWI-HIPS-8206**	*Run Time (min):*	**5.10**
Vial Number:	**GB5**	*Injection Volume:*	**2.00**
Injection Type:	**Unknown**	*Channel:*	**UV_VIS_1**
Calibration Level:		*Wavelength:*	**254**
Instrument Method:	**0.6ml_+ve_-ve_100-600**	*Bandwidth:*	**2**
Processing Method:	**Processing Method - New (190-380)**	*Dilution Factor:*	**1.0000**
Injection Date/Time:	**24/Nov/23 12:20**	*Sample Weight:*	**1.0000**

Integration Results

No.	Peak Name	Retention Time min	Area mAU*min	Height mAU	Relative Area %	Relative Height %	Amount n.a.
1		3.336	27.075	602.416	100.00	100.00	n.a.
Total:			**27.075**	**602.416**	**100.00**	**100.00**	

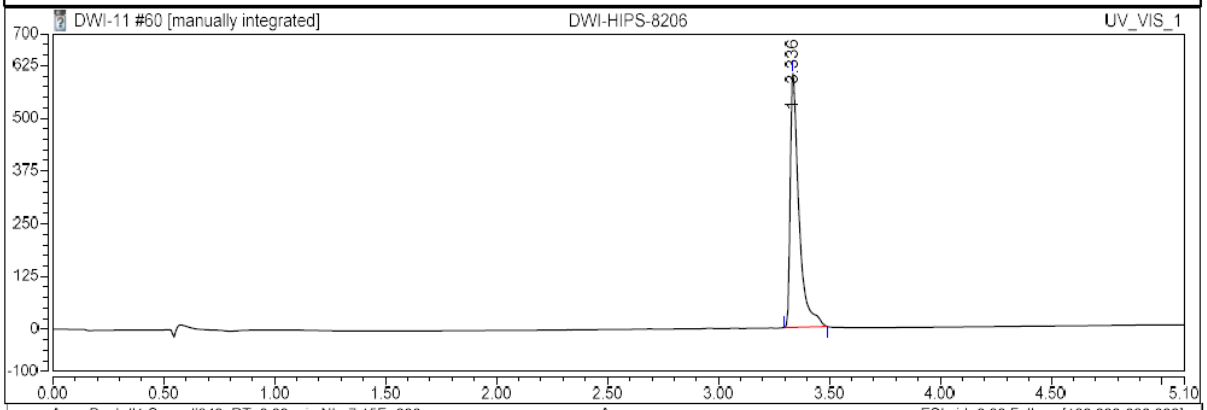

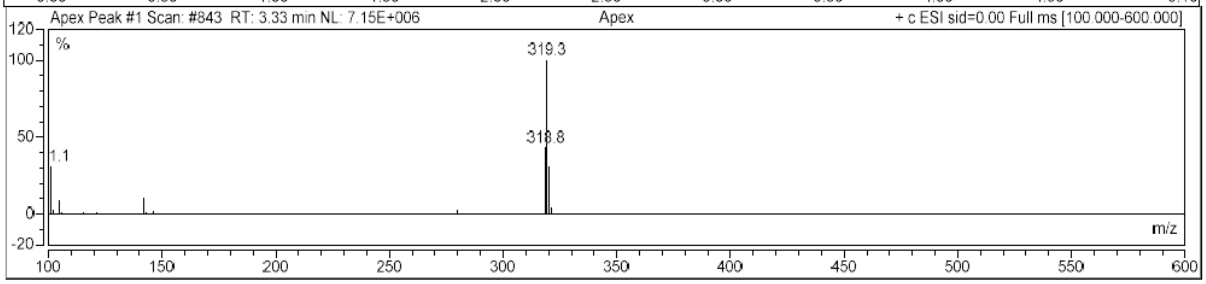

10

Mass Spectrum and Results

Injection Details

Injection Name:	**HIPS-8207**	*Run Time (min):*	**5.10**
Vial Number:	**GB6**	*Injection Volume:*	**2.00**
Injection Type:	**Unknown**	*Channel:*	**UV_VIS_1**
Calibration Level:		*Wavelength:*	**254**
Instrument Method:	**0.6ml_+ve_-ve_100-600**	*Bandwidth:*	**2**
Processing Method:	**Processing Method - New (190-380)**	*Dilution Factor:*	**1.0000**
Injection Date/Time:	**15/Dec/23 11:35**	*Sample Weight:*	**1.0000**

Integration Results

No.	Peak Name	Retention Time min	Area mAU*min	Height mAU	Relative Area %	Relative Height %	Amount n.a.
1		4.045	0.117	3.720	0.96	1.50	n.a.
2		4.257	12.022	243.759	99.04	98.50	n.a.
Total:			**12.140**	**247.480**	**100.00**	**100.00**	

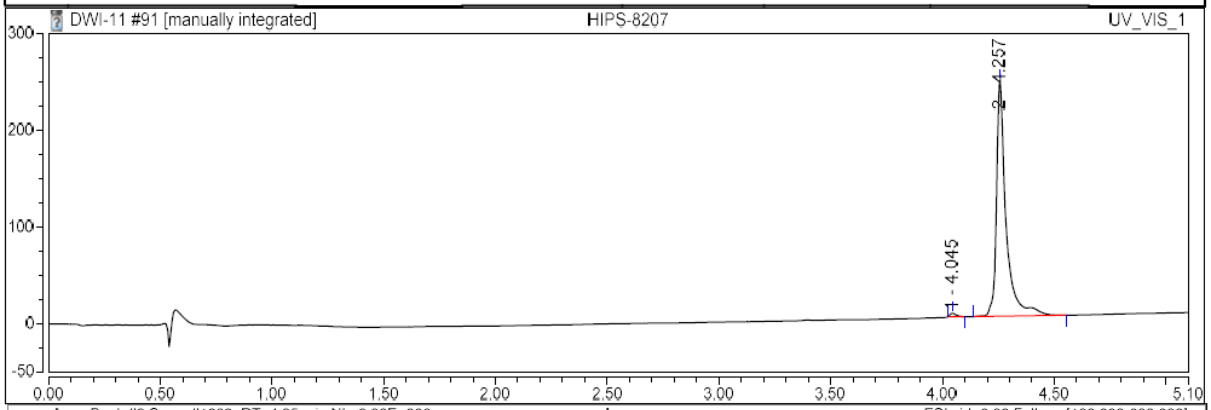

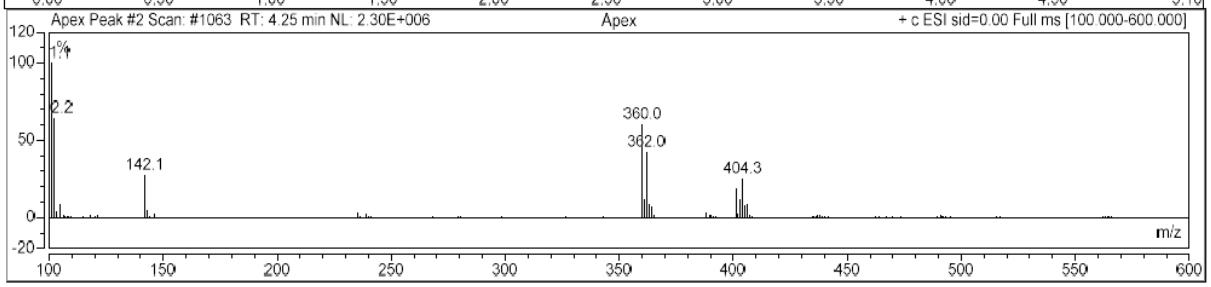

16

Mass Spectrum and Results

Injection Details

Injection Name:	**DWI-HIPS-8229**	*Run Time (min):*	**5.10**
Vial Number:	**GB5**	*Injection Volume:*	**2.00**
Injection Type:	**Unknown**	*Channel:*	**UV_VIS_1**
Calibration Level:		*Wavelength:*	**254**
Instrument Method:	**0.6ml_+ve_-ve_100-600**	*Bandwidth:*	**2**
Processing Method:	**Processing Method - New (190-380)**	*Dilution Factor:*	**1.0000**
Injection Date/Time:	**22/Dec/23 09:44**	*Sample Weight:*	**1.0000**

Integration Results

No.	Peak Name	Retention Time min	Area mAU*min	Height mAU	Relative Area %	Relative Height %	Amount n.a.
1		4.257	148.548	2274.788	100.00	100.00	n.a.
Total:			**148.548**	**2274.788**	**100.00**	**100.00**	

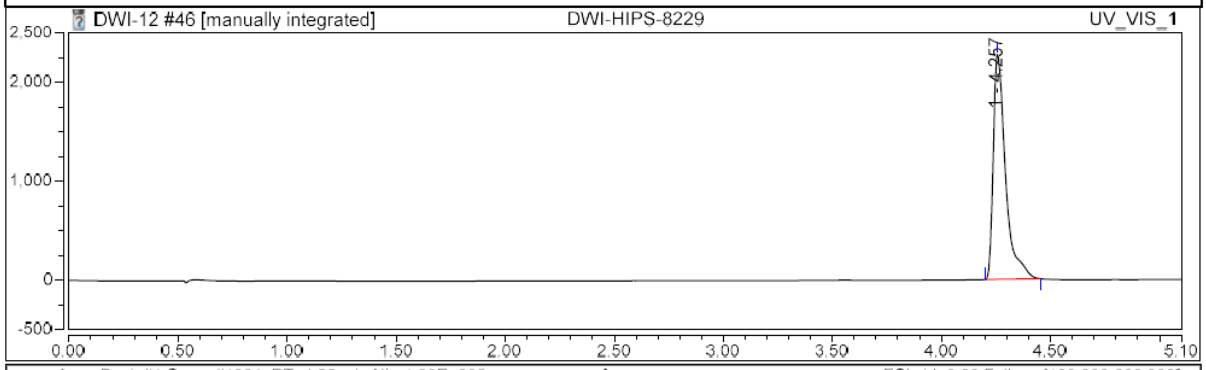

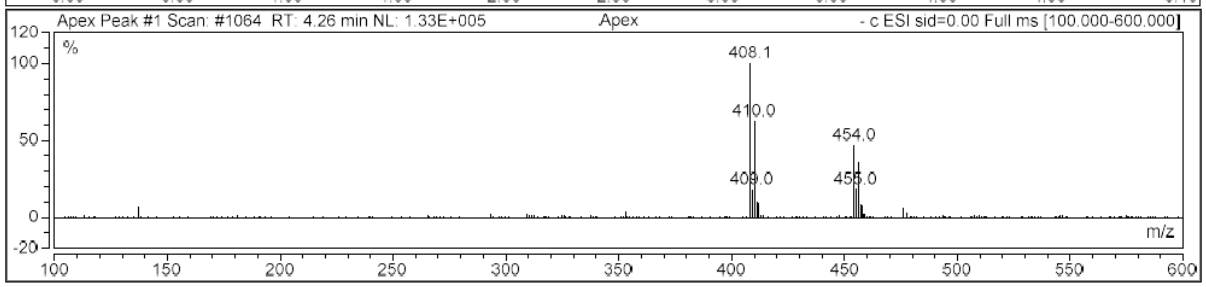

17

Mass Spectrum and Results

Injection Details

Injection Name:	**DWI-HIPS-8154**	*Run Time (min):*	**5.10**
Vial Number:	**GB5**	*Injection Volume:*	**2.00**
Injection Type:	**Unknown**	*Channel:*	**UV_VIS_1**
Calibration Level:		*Wavelength:*	**254**
Instrument Method:	**0.6ml_+ve_-ve_100-600**	*Bandwidth:*	**2**
Processing Method:	**Processing Method - New (190-380)**	*Dilution Factor:*	**1.0000**
Injection Date/Time:	**24/Nov/23 10:20**	*Sample Weight:*	**1.0000**

Integration Results

No.	Peak Name	Retention Time min	Area mAU*min	Height mAU	Relative Area %	Relative Height %	Amount n.a.
1		4.149	8.212	76.735	100.00	100.00	n.a.
Total:			**8.212**	**76.735**	**100.00**	**100.00**	

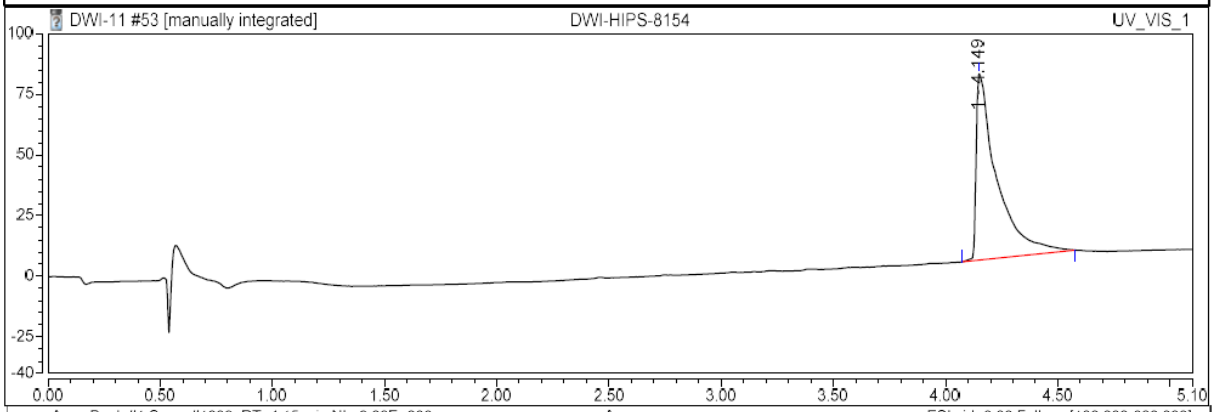

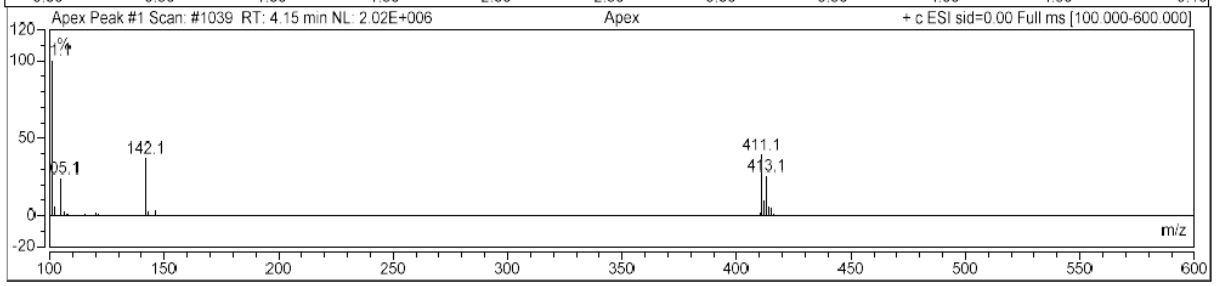

18

Mass Spectrum and Results

Injection Details

Injection Name:	**DWI-HIPS-8233**	*Run Time (min):*	**5.10**
Vial Number:	**GB6**	*Injection Volume:*	**2.00**
Injection Type:	**Unknown**	*Channel:*	**UV_VIS_1**
Calibration Level:		*Wavelength:*	**254**
Instrument Method:	**0.6ml_+ve_-ve_100-600**	*Bandwidth:*	**2**
Processing Method:	**Processing Method - New (190-380)**	*Dilution Factor:*	**1.0000**
Injection Date/Time:	**21/Dec/23 20:01**	*Sample Weight:*	**1.0000**

Integration Results

No.	Peak Name	Retention Time min	Area mAU*min	Height mAU	Relative Area %	Relative Height %	Amount n.a.
1		3.411	0.021	0.384	0.42	0.54	n.a.
2		4.065	0.088	1.796	1.76	2.52	n.a.
3		4.275	4.878	69.187	97.82	96.94	n.a.
Total:			**4.987**	**71.367**	**100.00**	**100.00**	

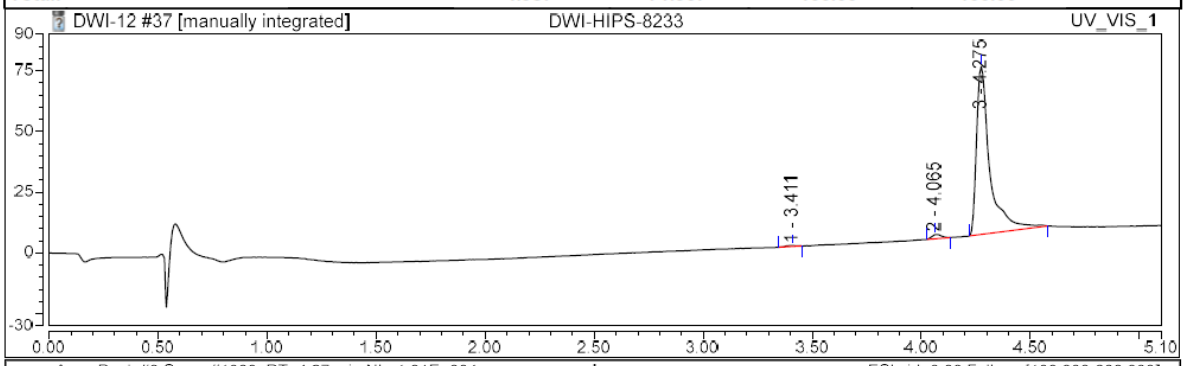

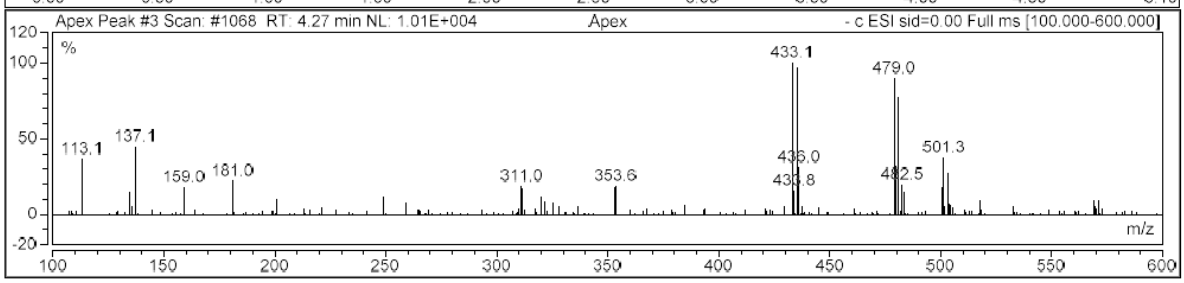

19

Mass Spectrum and Results

Injection Details

Injection Name:	**DWI-HIPS-8230**	*Run Time (min):*	**5.10**
Vial Number:	**GB6**	*Injection Volume:*	**2.00**
Injection Type:	**Unknown**	*Channel:*	**UV_VIS_1**
Calibration Level:		*Wavelength:*	**254**
Instrument Method:	**0.6ml_+ve_-ve_100-600**	*Bandwidth:*	**2**
Processing Method:	**Processing Method - New (190-380)**	*Dilution Factor:*	**1.0000**
Injection Date/Time:	**22/Dec/23 10:44**	*Sample Weight:*	**1.0000**

Integration Results

No.	Peak Name	Retention Time min	Area mAU*min	Height mAU	Relative Area %	Relative Height %	Amount n.a.
1		4.500	7.968	118.849	100.00	100.00	n.a.
Total:			**7.968**	**118.849**	**100.00**	**100.00**	

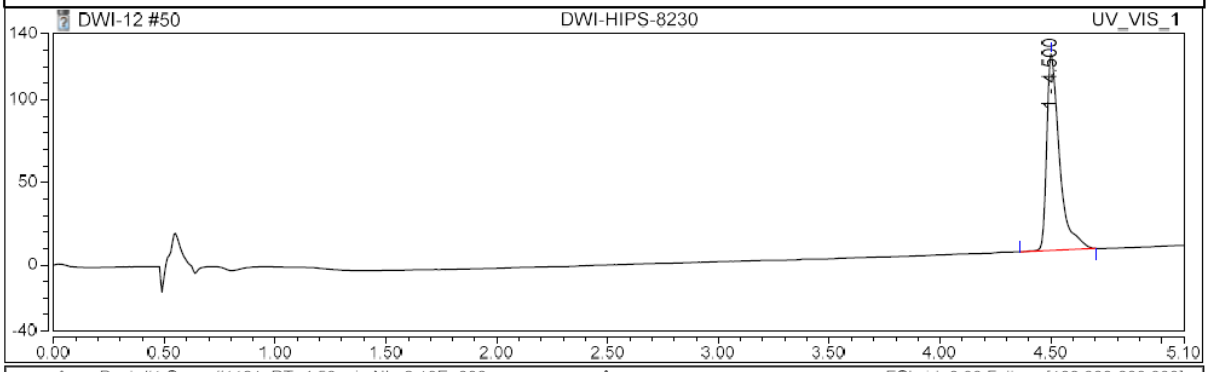

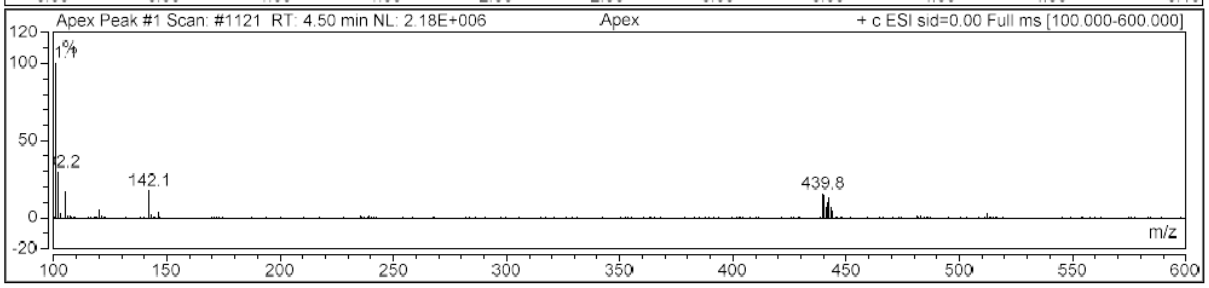

20

Mass Spectrum and Results

Injection Details

Injection Name:	**DWI-HIPS-8232**	*Run Time (min):*	**5.10**
Vial Number:	**GB6**	*Injection Volume:*	**2.00**
Injection Type:	**Unknown**	*Channel:*	**UV_VIS_1**
Calibration Level:		*Wavelength:*	**254**
Instrument Method:	**0.6ml_+ve_-ve_100-600**	*Bandwidth:*	**2**
Processing Method:	**Processing Method - New (190-380)**	*Dilution Factor:*	**1.0000**
Injection Date/Time:	**22/Dec/23 12:15**	*Sample Weight:*	**1.0000**

Integration Results

No.	Peak Name	Retention Time min	Area mAU*min	Height mAU	Relative Area %	Relative Height %	Amount n.a.
1		2.044	0.236	5.612	2.15	4.23	n.a.
2		4.673	10.736	127.094	97.85	95.77	n.a.
Total:			**10.972**	**132.706**	**100.00**	**100.00**	

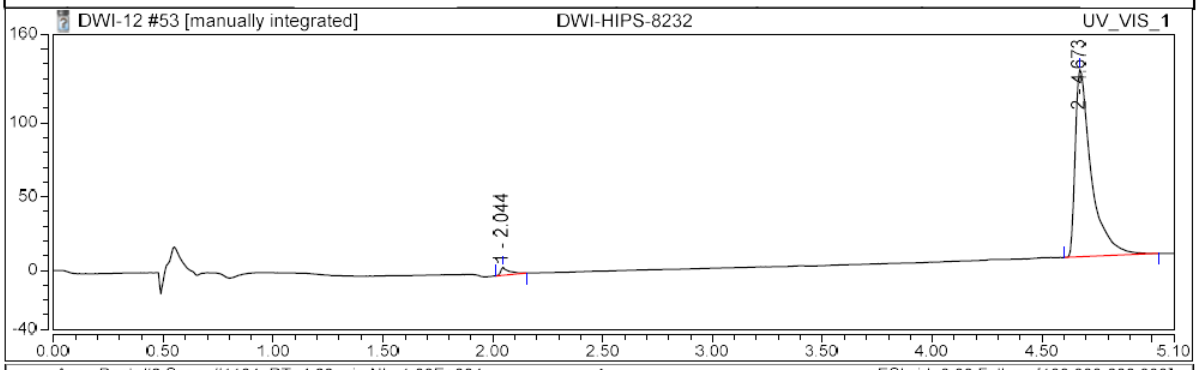

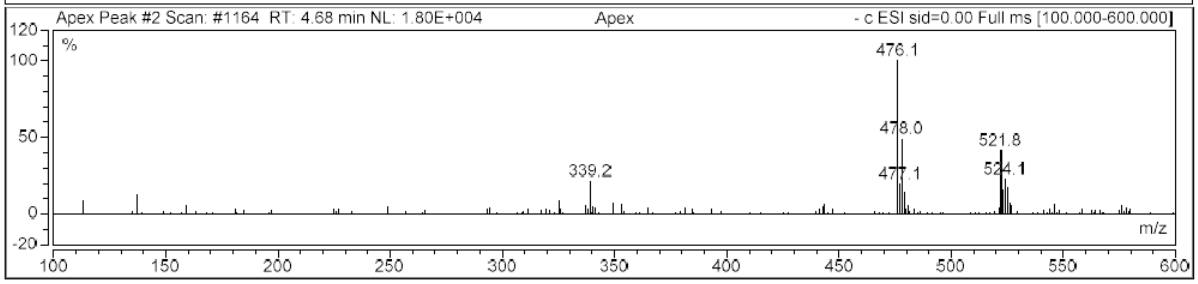

21

Mass Spectrum and Results

Injection Details

Injection Name:	**DWI-HIPS-8231**	*Run Time (min):*	**5.10**
Vial Number:	**GB5**	*Injection Volume:*	**2.00**
Injection Type:	**Unknown**	*Channel:*	**UV_VIS_1**
Calibration Level:		*Wavelength:*	**254**
Instrument Method:	**0.6ml_+ve_-ve_100-600**	*Bandwidth:*	**2**
Processing Method:	**Processing Method - New (190-380)**	*Dilution Factor:*	**1.0000**
Injection Date/Time:	**22/Dec/23 12:08**	*Sample Weight:*	**1.0000**

Integration Results

No.	Peak Name	Retention Time min	Area mAU*min	Height mAU	Relative Area %	Relative Height %	Amount n.a.
1		4.488	0.818	9.846	4.25	3.44	n.a.
2		4.725	18.453	276.436	95.75	96.56	n.a.
Total:			**19.272**	**286.282**	**100.00**	**100.00**	

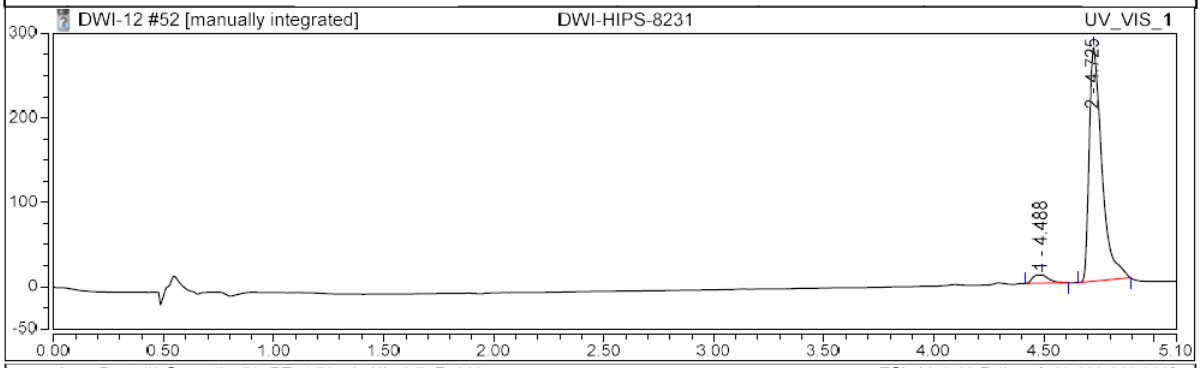

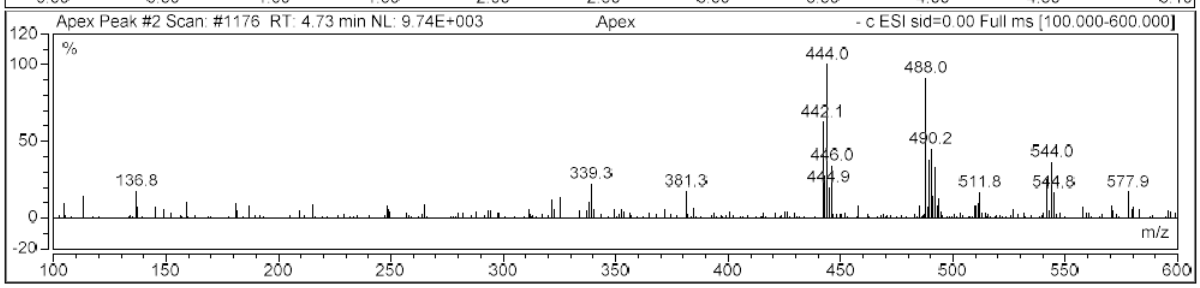

22

Mass Spectrum and Results

Injection Details

Injection Name:	**DWI-HIPS-8235**	*Run Time (min):*	**5.10**
Vial Number:	**GB7**	*Injection Volume:*	**2.00**
Injection Type:	**Unknown**	*Channel:*	**UV_VIS_1**
Calibration Level:		*Wavelength:*	**254**
Instrument Method:	**0.6ml_+ve_-ve_100-600**	*Bandwidth:*	**2**
Processing Method:	**Processing Method - New (190-380)**	*Dilution Factor:*	**1.0000**
Injection Date/Time:	**21/Dec/23 21:27**	*Sample Weight:*	**1.0000**

Integration Results

No.	Peak Name	Retention Time min	Area mAU*min	Height mAU	Relative Area %	Relative Height %	Amount n.a.
1		4.641	17.890	286.556	99.85	99.77	n.a.
2		4.819	0.027	0.673	0.15	0.23	n.a.
Total:			**17.917**	**287.229**	**100.00**	**100.00**	

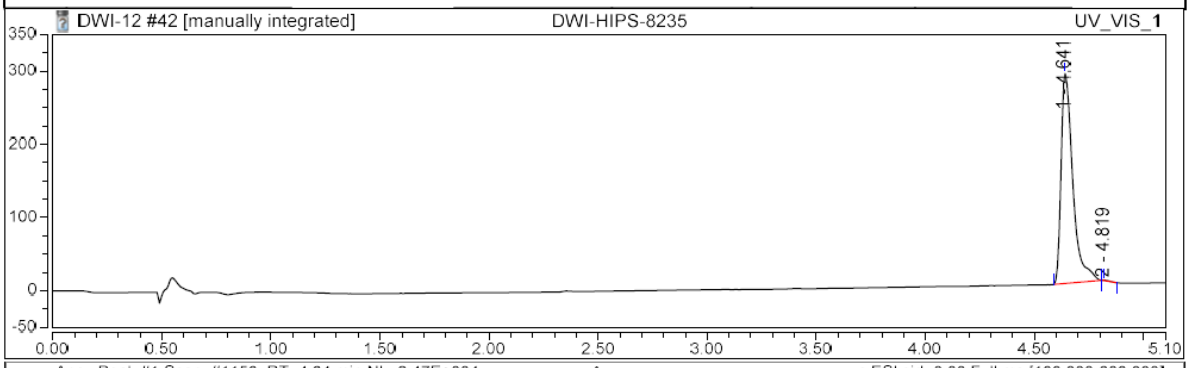

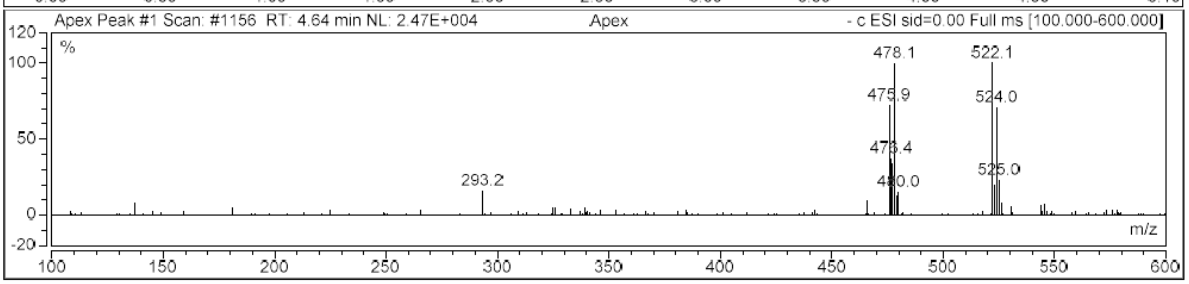

23

Mass Spectrum and Results

Injection Details

Injection Name:	**DWI-HIPS-8234**	*Run Time (min):*	**5.10**
Vial Number:	**GB8**	*Injection Volume:*	**2.00**
Injection Type:	**Unknown**	*Channel:*	**UV_VIS_1**
Calibration Level:		*Wavelength:*	**254**
Instrument Method:	**0.6ml_+ve_-ve_100-600**	*Bandwidth:*	**2**
Processing Method:	**Processing Method - New (190-380)**	*Dilution Factor:*	**1.0000**
Injection Date/Time:	**21/Dec/23 20:15**	*Sample Weight:*	**1.0000**

Integration Results

No.	Peak Name	Retention Time min	Area mAU*min	Height mAU	Relative Area %	Relative Height %	Amount n.a.
1		4.281	0.040	0.756	0.77	0.97	n.a.
2		4.718	5.152	77.021	99.23	99.03	n.a.
Total:			**5.192**	**77.777**	**100.00**	**100.00**	

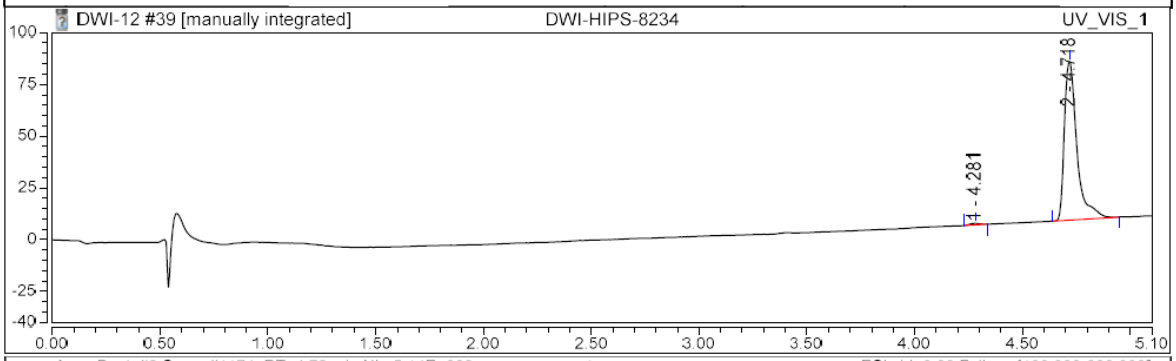

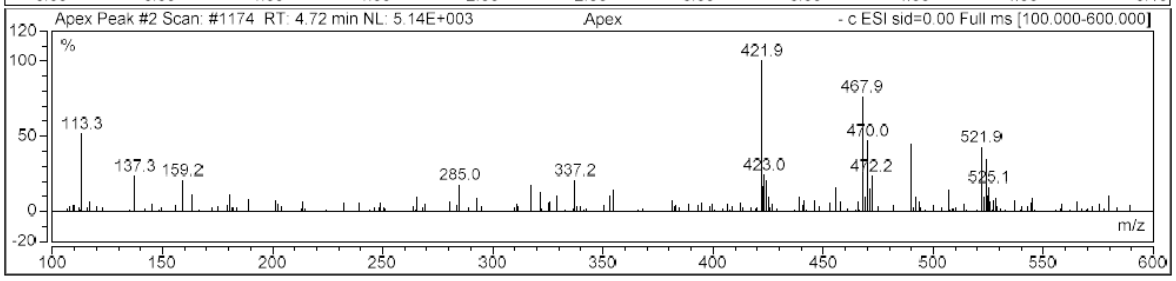

24

Mass Spectrum and Results

Injection Details

Injection Name:	**DWI-HIPS-8237**	*Run Time (min):*	**5.10**
Vial Number:	**GB7**	*Injection Volume:*	**2.00**
Injection Type:	**Unknown**	*Channel:*	**UV_VIS_1**
Calibration Level:		*Wavelength:*	**254**
Instrument Method:	**0.6ml_+ve_-ve_100-600**	*Bandwidth:*	**2**
Processing Method:	**Processing Method - New (190-380)**	*Dilution Factor:*	**1.0000**
Injection Date/Time:	**16/Jan/24 14:02**	*Sample Weight:*	**1.0000**

Integration Results

No.	Peak Name	Retention Time min	Area mAU*min	Height mAU	Relative Area %	Relative Height %	Amount n.a.
1		4.603	11.234	143.218	100.00	100.00	n.a.
Total:			**11.234**	**143.218**	**100.00**	**100.00**	

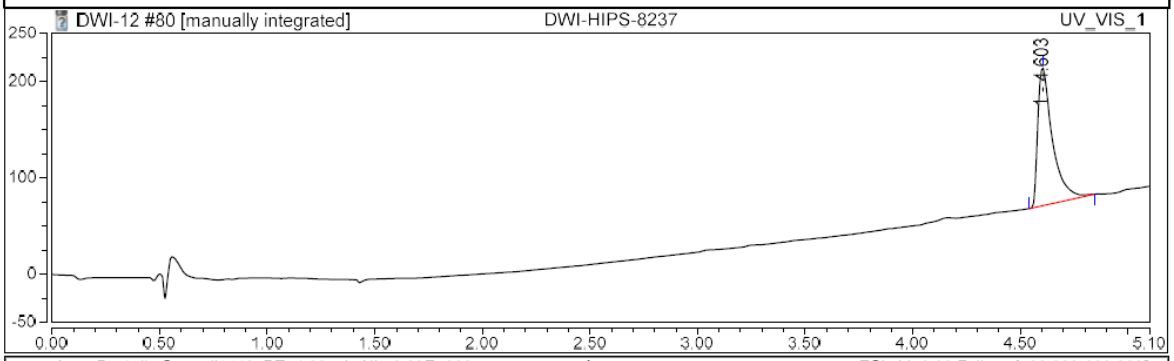

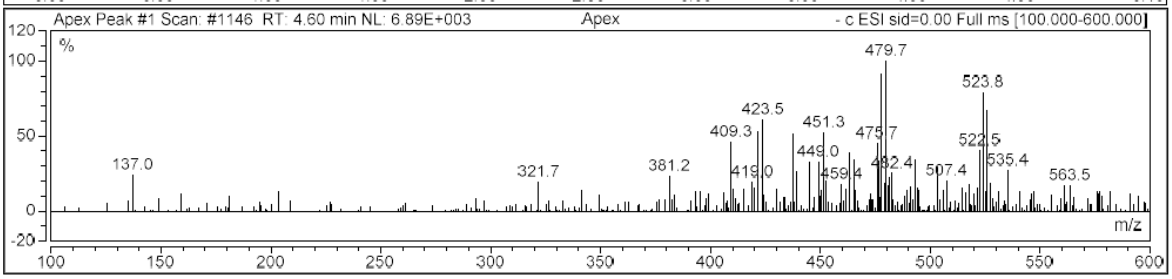

25

Mass Spectrum and Results

Injection Details

Injection Name:	**DWI-HIPS-8236**	*Run Time (min):*	**5.10**
Vial Number:	**GB6**	*Injection Volume:*	**2.00**
Injection Type:	**Unknown**	*Channel:*	**UV_VIS_1**
Calibration Level:		*Wavelength:*	**254**
Instrument Method:	**0.6ml_+ve_-ve_100-600**	*Bandwidth:*	**2**
Processing Method:	**Processing Method - New (190-380)**	*Dilution Factor:*	**1.0000**
Injection Date/Time:	**16/Jan/24 13:54**	*Sample Weight:*	**1.0000**

Integration Results

No.	Peak Name	Retention Time min	Area mAU*min	Height mAU	Relative Area %	Relative Height %	Amount n.a.
1		4.161	0.235	4.709	2.33	2.90	n.a.
2		4.264	9.865	157.911	97.67	97.10	n.a.
Total:			**10.101**	**162.620**	**100.00**	**100.00**	

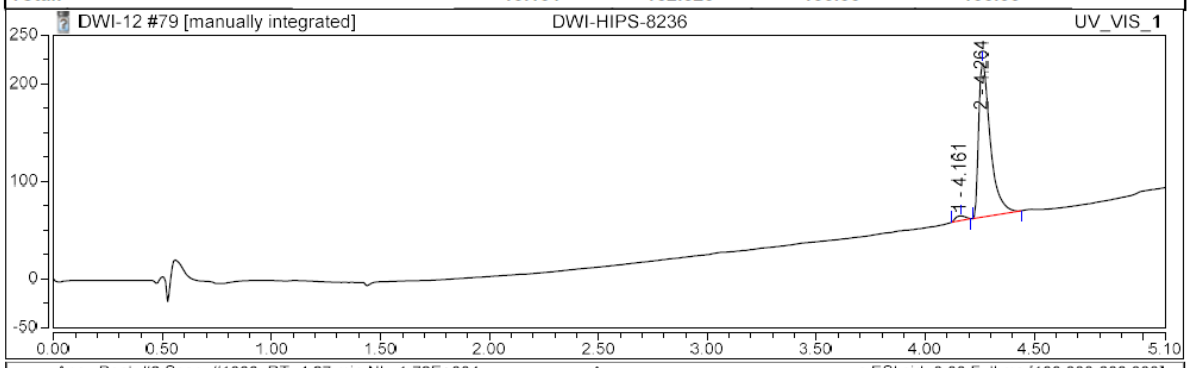

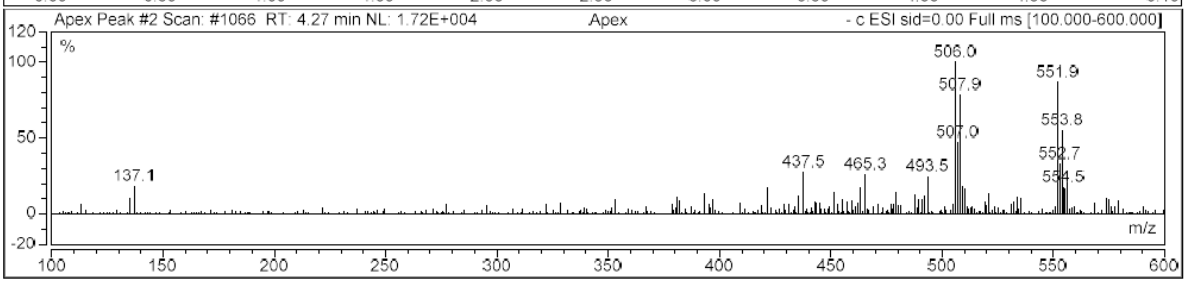

References

[1] L.J.Y.M. Swier, A. Guskov, D.J. Slotboom, Structural insight in the toppling mechanism of an energy-coupling factor transporter, Nature Communications, 7 (2016) 11072.

4. Conclusions and Outlook

With antimicrobial resistance reaching alarming levels globally, there is an urgent need to expand the anti-infective arsenal with new agents targeting unexploited drug targets. Both the MEP pathway, and by extension IspD, and the ECF transporters emerge as promising candidates in this endeavor due to their underexplored nature, widespread presence across pathogens, essentiality for pathogen survival and absence in human cells. Within this work, we attempted to address the lack of inhibitors targeting both targets.

Our efforts directed at IspD led to the discovery of two hits, one targeting IspD from *Plasmodium falciparum* (*Pf*) and the other from *Pseudomonas aeruginosa* (*Pa*). While previous inhibitors targeting *Pf*IspD are complex to synthesize or lacked whole-cell activity, our hit is readily synthesizable from commonly available starting materials and displays promising whole-cell activity. An SAR study conducted with the hit compound, resulted in derivatives showing a remarkable 400-fold increase in *in vitro* activity compared to the initial hit compound. However, this enhancement did not translate to the whole-cell activity of the compound class, with the reason remaining elusive during the scope of this PhD project. Ongoing investigations aim to address this issue. Despite this, we assessed the metabolic, and plasma stability, and *in vivo* pharmacokinetic profile of selected derivatives, revealing promising results for future advancement. Additionally, we developed a mass spectrometry-based IspD activity assay, eliminating the need for auxiliary enzymes present in previously reported IspD assays. We used this assay to determine the binding mode of this new compound class, circumventing potential interference of the auxiliary enzymes.

Discovery of the second inhibitor class was achieved through a fragment-based crystallographic screening directed at *Pa*IspD. To our knowledge, the crystal structure of *Pa*IspD and an inhibitor targeting *Pa*IspD have never been reported before. We used ^{1}H-STD-NMR to confirm interactions taking place between the hit and the protein, yielding results that closely match the observed co-crystal structure. Initial fragment growing resulted in derivatives, which are able to inhibit *Pa*IspD with IC_{50} values around 150 µM. The presence of the compound inside the active site of the protein, in combination with the high active site similarity among IspD homologues, motivated us to assess the most promising derivatives against various IspD homologues. To our delight, the fragments displayed similar activities across the different homologues, displaying the broad potential of the fragment class.

During our screening of a compound library against the ECF transporter, one hit, an oxaprozin derivative, caught our attention. Similar to before, we commenced an SAR study to systematically improve all parts of the compound to ultimately yield a frontrunner, displaying superior activity in both the whole-cell and proteoliposome-based assay. Furthermore, we screened the frontrunner against a panel of clinically relevant Gram-positive pathogens, yielding promising results.

Whereas promising results were obtained for all inhibitors, they are still far away from being lead compounds. For the urea class (Chapter 1), the first step to further progress should be to determine the cause for the discrepancy between *in vitro* and whole-cell activity. Once this is known, it could be addressed and the potency further improved, with an eye on simultaneously improving the ADMET properties as well. For the fragment discussed in Chapter 2, obtaining co-crystal structures of the best derivatives should be prioritized as this would afford valuable insights on how to proceed fragment growing. Lastly, for the oxaprozin-derived compound class described in Chapter 3, ideally either a co-crystal structure is obtained or docking studies are performed to identify the most ideal growth vector to further enhance the potency of the compound class. Alternatively, site-directed mutagenesis studies could be used to determine the binding site of the compound class, which could be used to further enhance the compound. In a next phase, pharmacokinetic properties should be determined and optimized if needed.